JOURNAL OF THE MECHANICS AND PHYSICS OF SOLIDS

EDITORIAL ADVISORY BOARD

J. F. BAKER—Cambridge W. M. BALDWIN—Cleveland
E. BRANDENBERGER—Zürich G. BUSCH—Zürich
A. H. COTTRELL—Harwell C. CRUSSARD—Paris M. J. DRUYVESTEYN—Delft
A. KOCHENDÖRFER—Düsseldorf N. F. MOTT—Cambridge
A. NADAI—Pittsburgh, Pa. G. SACHS—Syracuse, N.Y. E. SIEBEL—Stuttgart
V. V. SOKOLOVSKY—Moscow

EDITOR-IN-CHIEF

R. HILL
University of Nottingham

Volume 5
1956—57

PERGAMON PRESS · LONDON · NEW YORK · PARIS · LOS ANGELES

Contents of Volume 5

Number 1

PAGE

R. Hill: On the problem of uniqueness in the theory of a rigid-plastic solid—II 1

A. H. Chilver: Corrected discontinuities in structural stability problems .. 9

A. H. Chilver: Buckling of a simple portal frame 18

J. H. Hoke and R. Maddin: The deformation of molybdenum single crystals in compressing 26

P. B. Mellor: Stretch forming under fluid pressure 41

Martin Lessen: Thermoelasticity and thermal shock 57

F. A. Gaydon and H. Nuttall: The elastic-plastic bending of a circular plate by an all-round couple 62

R. Hill: New horizons in the mechanics of solids 66

Book Reviews:

"Numerical Analysis," by Z. Kopal (reviewed by R. Hill) 75

"Solid State Physics: Advances in Research and Applications, Vol. I," edited by Frederick Seitz and David Turnbull (reviewed by J. M. Ziman) 75

"Quantum Theory of Solids," by R. E. Peierls (reviewed by L. Rosenfled) .. 76

Number 2

G. Horvay: Some aspects of Saint Venant's principle 77

B. Jaoul: Étude de la forme des courbes de déformation plastique .. 95

J. W. Craggs: The propagation of infinitesimal plane waves in elastic-plastic materials 115

L. E. Samuels and T. O. Mulhearn: An experimental investigation of the deformed zone associated with indentation hardness impressions .. 125

Bekir Tekinalp: Elastic-plastic bending of a built-in circular plate under a uniformly distributed load 135

T. H. Lin: Analysis of elastic and plastic strains of a face-centred cubic crystal 143

Research Note:

N. J. Hoff: On primary creep 150

Book Review:

"Introduction to Plasticity," by A. Phillips (reviewed by A. P. Green) 152

Number 3

R. Hill: On the problem of uniqueness in the theory of a rigid-plastic solid—III 153

S. C. Hunter: Energy absorbed by elastic waves during impact 162

A. W. Magnusson and W. M. Baldwin, Jr.: Low temperature brittleness .. 172

N. E. Frost and D. S. Dugdale: Fatigue tests on notched mild steel plates with measurements of fatigue cracks 182

W. Johnson: Partial sideways extrusion from a smooth container .. 193

NUMBER 3 (*continued*) PAGE

W. JOHNSON: The plane strain extrusion of short slugs 202

G. LIANIS and H. FORD: An experimental investigation of the yield criterion and the stress-strain law 215

Book Review: 233

" Progress in Metal Physics, Vol. 6," edited by B. CHALMERS and R. KING (reviewed by A. H. Cottrell) .. ..

" Analysis of Deformation III—Fluidity," by K. SWAINGER (reviewed by R. Hill) ..

" Mathematical Theory of Elasticity," by I. S. SOKOLNIKOFF (reviewed by R. Hill) ..

" Solid State Physics, Vol. 2," edited by F. SEITZ and D. TURNBULL (reviewed by K. W. H. Stevens) .. ..

" Solid State Physics, Vol. 3," edited by F. SEITZ and D. TURNBULL (reviewed by K. W. H. Stevens) .. ..

" Order-Disorder Phenomena," by E. W. ELCOCK (reviewed by K. W. H. Stevens)

" International Symposium on the non-destructive testing of materials and structures," (reviewed by R. C. Coates) .. ..

Books Received: 228

NUMBER 4

R. HILL: On uniqueness and stability in the theory of finite elastic strain .. 229

P. G. HODGE, JR.: A general theory of piecewise linear plasticity based on maximum shear 242

L. MAUNDER and E. REISSNER: Pure bending of pretwisted rectangular plates 261

L. C. DODEJA and W. JOHNSON: On the multiple hole extrusion of sheets of equal thickness 267

L. C. DODEJA and W. JOHNSON: The cold extrusion of circular rods through square multiple hole dies 281

W. M. SHEPHERD and F. A. GAYDON: Plastic bending of a ring sector by end couples 296

R. HILL: On the problem of uniqueness in the theory of a rigid-plastic solid—IV 302

Book Review: 308

" Fatigue in Aircraft Structures," edited by A. M. FREUDENTHAL (reviewed by F. Sherratt)

Books Received: 308

Author Index

(B) denotes a book review

BALDWIN, W. M. JR. p. 172.
CHILVER, A. H. pp. 9, 18.
COATES, R. C. p. 227 (B).
COTTRELL, A. H. p. 223 (B).
CRAGGS, J. W. p. 115.
DODEJA, L. C. pp. 267, 281.
DUGDALE, D. S. p. 182.
FORD, H. p. 215.
FROST, N. E. p. 182.
GAYDON, F. A. pp. 62, 296.
GREEN, A. P. p. 152 (B).
HILL, R. pp. 1, 66, 75 (B), 153, 223 (B), 224 (B), 229, 302.
HODGE, P. G. JR. p. 242.
HOFF, N. J. p. 150.
HOKE, J. H. p. 26.
HORWAY, G. p. 77.
HUNTER, S. C. p. 162.
JAOUL, B. p. 95.
JOHNSON, W. pp. 193, 202, 267, 281.
LESSEN, M. p. 57.
LIANIS, G. p. 215.
LIN, T. H. p. 143.
MADDIN, R. p. 26.
MAGNUSSON, A. W. p. 172.
MAUNDER, L. p. 261.
MELLOR, P. B. p. 41.
MULHEARN, T. O. p. 125.
NUTTALL, H. p. 62.
REISSNER, E. p. 261.
ROSENFELD, L. p. 76 (B).
SAMUELS, L. E. p. 125.
SHEPHERD, W. M. p. 296.
SHERRATT, F. p. 308 (B).
STEVENS, K. W. H. pp. 225 (B), 226 (B).
TEKINALP, B. p. 135.
ZIMAN, J. M. p. 75 (B).

Journal of the Mechanics and Physics of Solids, 1956, Vol. 5, pp. 1 to 8. Pergamon Press Ltd., London.

ON THE PROBLEM OF UNIQUENESS IN THE THEORY OF A RIGID-PLASTIC SOLID—II

By R. Hill.
Department of Mathematics, University of Nottingham

(*Received 30th April*, 1956)

Summary

The theory of plastic torsion of prismatic bars with work-hardening is reviewed and developed. Uniqueness and extremum principles proved in Part I (Hill 1956) for a general state of stress are here illustrated in relation to the torsion of a bar of hollow section.

1. Résumé of Part I

A rigid-plastic work-hardening solid is considered, with essential properties as stated in equation (1) of Part I (Hill 1956). When the existing hardness distribution is given, the specification of the traction $\boldsymbol{F}$ over a part S_F of the surface, together with the velocity $\boldsymbol{v}$ over the remainder S_v, uniquely determines the state of stress in a certain zone forming part (or sometimes all) of the plastic region. The instantaneous mode of deformation may, however, not be uniquely determined by these boundary conditions. If it is not, a set of modes, called virtual, can be found satisfying I (3). It has been proved (with certain continuity restrictions) that only one of these modes is actual and that this is defined when the traction-rate $\dot{\boldsymbol{F}}$ is specified over S_F. The actual mode is associated through the law I (1) with one or more equilibrium distributions of stress-rate satisfying this boundary-condition; if $S_v \neq 0$, the actual distribution is defined only when, in addition, $\boldsymbol{v}$ is given on S_v. The actual mode can alternatively be characterized by the complementary extremum principles I (4) and I (9).

These results are now illustrated by application to the torsion of a prismatic bar. The boundary conditions here are mixed, the tangential component of $\boldsymbol{v}$ and the normal component of $\boldsymbol{F}$ being prescribed on the plane ends while $\boldsymbol{F}$ is given on the cylindrical surface; the boundary conditions on $\dot{\boldsymbol{F}}$ and $\boldsymbol{v}$ must be similarly mixed. The notation S_F and S_v cannot be retained, so that the statements and proofs of the above theorems require corresponding slight modification.

2. Torsion: Virtual Modes

(i) *State of stress.* Each element is supposed to be isotropic but the bar may be inhomogeneously hardened so that k, the yield stress in shear, is some given continuous function of x, y (the axis of z being parallel to the generators). Initially the cylindrical surface is traction-free and the ends are given relative rigid-body rotations in their planes with freedom to warp (the axial component of $\boldsymbol{F}$ being zero). Whatever the shape of section there is a virtual mode with velocity components of form

$$u = -yz, \qquad v = xz, \qquad w \equiv w(x, y), \tag{1}$$

where the rate of twist per unit length is taken as unity for convenience. The

stress at each point is a pure shear of magnitude τ acting over the transverse section, with (x, y) components denoted by (τ_x, τ_y) where

$$\tau^2 = \tau_x^2 + \tau_y^2 = k^2(x, y) \tag{2}$$

and

$$\frac{\partial \tau_x}{\partial x} + \frac{\partial \tau_y}{\partial y} = 0. \tag{3}$$

Denote by ds the element of arc-length in the direction of the shearing-stress vector and let ϕ be its anticlockwise orientation to the x axis. Equations (2) and (3) are replaced by

$$\tau_x = k \cos \phi, \qquad \tau_y = k \sin \phi, \tag{4}$$

and

$$\left(-\sin\phi \frac{\partial}{\partial x} + \cos\phi \frac{\partial}{\partial y}\right)\phi + \frac{1}{k}\left(\cos\phi \frac{\partial}{\partial x} + \sin\phi \frac{\partial}{\partial y}\right)k = 0, \tag{5}$$

or

$$\frac{\partial \phi}{\partial c} + \frac{1}{k}\frac{\partial k}{\partial s} = 0 \tag{6}$$

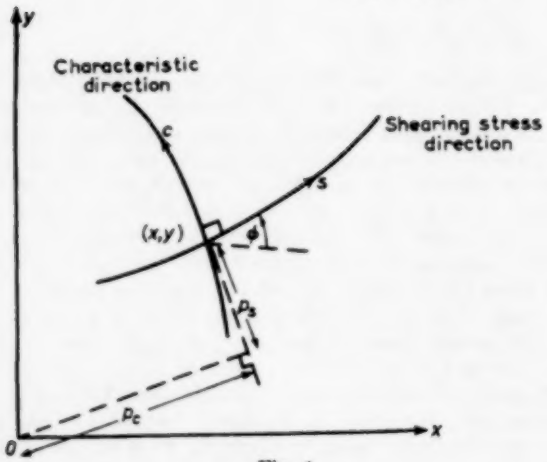

Fig. 1.

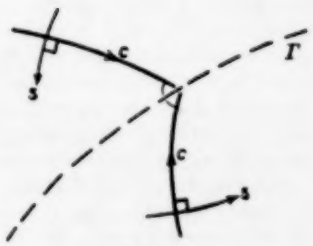

Fig. 2.

where dc is the element of arc-length perpendicular to the shearing-stress vector, obtained by rotating ds through 90° anticlockwise (Fig. 1). This direction is, indeed, that of the characteristic of (5). The curvature of the characteristic is specified by (6) in terms of the existing distribution of hardness $k(x, y)$. At any regular point of the section contour (i.e. where the tangent turns continuously) ds coincides with the tangent and dc with the normal; the sense of ds and dc cannot be decided from purely local considerations but depends on the solution as a whole (as explained later). However, the shape of any characteristic found by integrating (6) from a regular boundary-point is unaffected by this ambiguity at the outset.

The entire section is covered by a field of characteristics by continuing them inward from the boundary until they intersect (exceptionally some may pass unobstructed right across the section). The locus of the points of intersection,

Γ say, is defined by the property that it bisects the angles between intersecting pairs of characteristics (Fig. 2). This ensures that the component shear stress perpendicular to Γ (and hence the traction on Γ) changes continuously in passing from one side to the other. The component parallel to the tangent changes sign, however, and is discontinuous. It is shown later that the condition for the plastic work-rate to be positive on both sides of Γ requires that the directions dc on either side should point *towards* Γ (this restriction does not appear to have been remarked before). In this way the sense of dc (and hence ds) is determined along all characteristics that intersect Γ; it follows that dc must be the *inward* normal on the contour. On other characteristics, if any, the sense is established by continuous variation.

A branch of Γ originates at every projecting angle of the contour. Through a re-entrant angle, on the other hand, there can pass either a branch of Γ or a fan of characteristics. The geometry of the characteristic field elsewhere may decide which alternative is possible in the circumstances, but, where it does not, the indeterminacy is removed by the necessity for there to be an associated warp-rate w which is continuous across Γ (discontinuities of w across any curve except a characteristic are purely formal and must be rejected; cf. Section 5 of Part I). This is ensured by requiring that the field of characteristics is such that none cuts Γ twice (see below).

(ii) *Warping.* The state of stress being known everywhere, the warp-rate is calculable as follows. Since the material is isotropic the strain-rate at each point must be a pure shear over the transverse section, in the direction and sense of the shear stress. The warp-rate therefore satisfies

$$\left.\begin{aligned} \frac{\partial w}{\partial x} - y &= \lambda \cos\phi \\ \frac{\partial w}{\partial y} + x &= \lambda \sin\phi \end{aligned}\right\} \quad (\lambda \geqslant 0) \tag{7}$$

which is in the form I (3) (except that $\frac{1}{2}\lambda$ is now written in place of the original λ). Eliminating λ:

$$\left(-\sin\phi\,\frac{\partial}{\partial x} + \cos\phi\,\frac{\partial}{\partial y}\right) w + (x\cos\phi + y\sin\phi) = 0.$$

This equation has the same family of characteristics as (5) has, and is equivalent to the relation

$$\frac{\partial w}{\partial c} \pm p_c = 0 \tag{8}$$

along them, where $p_c = |x\cos\phi + y\sin\phi|$ is the length of the perpendicular from the origin to the tangent to the characteristic (Fig. 1). The upper sign is to be taken when the direction dc has a positive (anticlockwise) moment about the origin, and otherwise the lower sign. This equation has the interpretation that the component of shear strain-rate in a characteristic direction is zero; the p_c term is the part due to the twisting and the w term that due to the warping. Since the resultant shear strain-rate has the same direction and sense as the shearing-stress vector it must vanish on Γ; for otherwise, as is clear from Fig. 2, the strain-rate component

and derivative of w along the tangent to Γ would have a discontinuity and this is impossible since w must be continuous across Γ*. Thus, equation (8) holds also along Γ, with dc interpreted as the arc-element of Γ and p_c as the perpendicular on to the tangent to Γ. The value of w at every point on Γ is thereby determined by integration once it has been arbitrarily chosen at any one point (on each branch if separate). A further application of (8) then uniquely determines w on those characteristics that intersect Γ. As already stated, the field must be such that no characteristics cut Γ twice since the terminal value of w on any of these would be incompatible‡ (other contra-reasons are that dc could not be directed towards Γ at both ends, or that equation (12) could not be satisfied with both terminal values of λ zero).

When all characteristics cut Γ we conclude that there exists a virtual mode of type (1), and that it is the only mode of this type (the proof that the work-rate is positive everywhere is given later). Moreover, since the strain-rate in this mode does not vanish except at points of the section forming a *curve* (which includes Γ)†, the yield-point distribution of stress in the whole bar is unique (HILL 1951). Hence there exists no yield-point distribution other than that already described, and it is easily verified that all modes associated with this state and the stipulated boundary-conditions on v must be of type (1). In this case, then, there is no problem of selection.

When there are characteristics that do not cut Γ, but pass right across the section, w can be arbitrarily assigned at one of the endpoints of every such characteristic, subject to the work-rate being positive. There is thus a single infinity of virtual modes of type (1), and the same argument as before shows that no others exist. An analogous situation occurs in a twisted circular ring sector (FREIBERGER and PRAGER, 1955).

The selection of the actual mode is described in the following Section and illustrated in Section 4.

3. SELECTION OF ACTUAL MODE

(i) *Calculation of strain-rate.* The actual mode is uniquely distinguished by the property that

$$\tfrac{1}{2}\lambda = \boldsymbol{n}\,\dot{\boldsymbol{\sigma}}/h \tag{9}$$

in the notation of Part I, where $\dot{\boldsymbol{\sigma}}$ is an equilibrium distribution of stress-rate satisfying the boundary conditions on $\boldsymbol{F}$, and h is the local rate of hardening. In the present problem

$$\boldsymbol{n}\,\dot{\boldsymbol{\sigma}} = \dot{\tau}_x \cos\phi + \dot{\tau}_y \sin\phi = \dot{\tau} \tag{10}$$

where τ^2 continues to mean $\tau_x^{\,2} + \tau_y^{\,2}$. The other components of $\dot{\boldsymbol{\sigma}}$ are, of course, not necessarily zero.

As a preliminary, then, to obtaining the actual mode we calculate $\lambda(x, y)$ for each virtual mode; note that λ is here equal to the resultant shear strain-rate. We could calculate w first and then

*This method of proof is due to HILL (1952, p. 26) and GEIRINGER (1953, p. 276).

‡Equation (8), with w continuous, cannot hold everywhere on a closed circuit formed by two characteristics and two arcs of Γ since the integral of p_c round the circuit is equal to twice the area enclosed by it and so could not vanish.

†For there is clearly no function w such that $\partial w/\partial x - y$ and $\partial w/\partial y + x$ simultaneously vanish over an *area*.

$$\lambda = \frac{\partial w}{\partial s} \pm p_s \tag{11}$$

with the same sign convention as in (8), where p_s is the length of the perpendicular from the origin on to the tangent to a shearing-stress contour. However, it is simpler to proceed as follows. The elimination of w from (7) leads to a linear first-order partial differential equation for λ with the same characteristics as before, the relation along them being

$$-\frac{\partial \lambda}{\partial c} + \lambda \frac{\partial \phi}{\partial s} = 2. \tag{12}$$

We have seen that λ is zero on Γ and that each virtual mode is distinguished by the values of λ assigned at one point of each of the characteristics that do not cut Γ. The values of λ elsewhere are then uniquely found from (12) (an equation which appears to be new, despite the extensive literature on plastic torsion). Note that λ is discontinuous across a characteristic if the curvature of the shearing-stress contours is.

According to (12) $\partial\lambda/\partial c$ has the value -2 immediately on each side of Γ. If the direction dc were towards Γ λ would be positive in the neighbourhood of Γ, while if the direction dc were away from Γ λ would be negative. Since λ is required to be positive, dc must be towards Γ (proving a statement in Section 2). With this choice of the sense of dc, the equation shows that λ then remains positive all along the characteristics, so completing the justification of the expressions (1) for possible virtual modes (this has been taken for granted in the literature).

(ii) *Calculation of stress-rate.* Suppose that the boundary conditions on $\dot{\boldsymbol{F}}$ and $\dot{\boldsymbol{v}}$ are such that $\dot{\tau}_x$ and $\dot{\tau}_y$ are the only nonvanishing components of $\dot{\boldsymbol{\sigma}}$: i.e., on the ends $\dot{u}$, $\dot{v}$, and the z component of $\dot{\boldsymbol{F}}$ are zero, and on the cylindrical surface the x, y components of $\dot{\boldsymbol{F}}$ are zero. In this case (and not in general otherwise) $\dot{\tau}$ is equal to $\dot{k}$ and (10) becomes

$$\boldsymbol{n}\,\dot{\boldsymbol{\sigma}} = \dot{k}, \tag{13}$$

k retaining its meaning of the yield stress in pure shear. From (9) and (13) :

$$\dot{k} = \tfrac{1}{2} h \lambda \tag{14}$$

in the actual mode ; this is otherwise obvious since h is the slope of the stress-curve in pure shear while $\frac{1}{2}\lambda$ is equal to the (tensor) shear strain-rate.

The equilibrium equation for the stress-rate is

$$\frac{\partial \dot{\tau}_x}{\partial x} + \frac{\partial \dot{\tau}_y}{\partial y} = 0.$$

On substituting from (4) and transforming as before, there results

$$\frac{\partial \dot{\phi}}{\partial c} + \left(\frac{1}{k}\frac{\partial k}{\partial c} - \frac{\partial \phi}{\partial s}\right)\dot{\phi} + \frac{\partial}{\partial s}\left(\frac{\dot{k}}{k}\right) = 0 \tag{15}$$

with the use of (6). The boundary values of $\dot{\phi}$ are known when $\dot{\boldsymbol{F}}$ is given on the cylindrical surface ; the most likely boundary condition is $\dot{\phi} = 0$, the surface remaining free from traction. When all characteristics intersect Γ (15) can be integrated along them from the external contour ; the stress-rate is thus uniquely determined

over the whole section. $\dot{\phi}$, and hence $\dot{\tau}_x$ and $\dot{\tau}_y$, will generally be discontinuous across Γ, implying that Γ moves (cf. the discussion in Section (2) of Part I). ϕ is also discontinuous across a characteristic if $\partial(\dot{k}/k)/\partial s$ is.

Along characteristics that do not cut Γ the boundary values of $\dot{\phi}$ are specified at both ends. The condition that these should be compatible imposes restrictions on the distribution of $\dot{k}$ (through the last term in equation 15) and hence on the hitherto arbitrary values of w and λ at a point of each characteristic. By the uniqueness theorem of Part I, the mode so determined would also be the actual mode if nonzero values of $\dot{u}$ and $\dot{v}$ were prescribed on the ends, but the actual stress-rate would be different from that calculated here.

4. ILLUSTRATION

Consider a hollow section of uniform wall thickness t with smooth boundaries (Fig. 3). If the bar is uniformly hard initially, the shearing stress contours are involutes of the same family and can be identified by their distance c from the outer

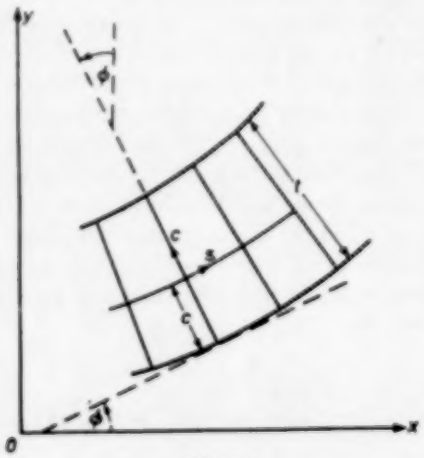

Fig. 3.

boundary. The radius of curvature of the latter is denoted by ρ_0 and is some given function of ϕ, which is here equal to the anti-clockwise orientation of a normal to the y axis. It is assumed that the curvature changes continuously*.

Let $\lambda_0(\phi)$ be the values of λ on the outer boundary. These are arbitrarily chosen in the first instance, subject only to their being continuous* and positive, and such that

$$\int_0^{2\pi} \rho_0 \lambda_0 \, d\phi = 2A_0 \tag{16}$$

where A_0 is the area enclosed by the outer boundary. This follows from (11) if the warp-rate is required to be continuous and single-valued.*.

*If the restriction that both λ and w are continuous is dropped, or if the boundary curvature is discontinuous, virtual modes could be constructed that do not come within the scope of the uniqueness theorem as formulated in Part I.

In (12) substitute $\rho_0 - \rho$ for c, where ρ is the local radius of curvature of a stress contour, and integrate :

$$\rho\,(\rho - \lambda) = \rho_0\,(\rho_0 - \lambda_0) \tag{17}$$

or

$$\lambda = \frac{c^2 - 2\,\rho_0\,c + \rho_0\,\lambda_0}{\rho_0 - c} \tag{18}$$

This is positive everywhere provided $\lambda_0\,(\phi)$ is chosen so that

$$\lambda_0 \geqslant t\,(2 - t/\rho_0) \qquad \text{or} \qquad \rho_0\,(\rho_0 - \lambda_0) \leqslant (\rho_0 - t)^2. \tag{19}$$

Hence

$$\int_0^{2\pi} \rho_0\,\lambda_0\,d\phi \geqslant \int_0^{2\pi} \{\rho_0^{\,2} - (\rho_0 - t)^2\}\,d\phi = 2\,(A_0 - A_i)$$

where A_i is the area enclosed by the inner boundary. The conditions (16) and (19) are thus mutually consistent (16 enforces the equality in 19 when $A_i = 0$, the bar being solid and circular). Equations (16), (17), and (19) define the set of (continuous) virtual modes.

When ϕ and c are taken as the independent variables (15) becomes

$$\frac{\partial}{\partial c}\,(\rho\dot{\phi}) + \frac{\partial}{\partial \phi}\left(\frac{\dot{k}}{k}\right) = 0,$$

remembering that k is assumed uniform. The requirement that $\dot{\phi} = 0$ on both boundaries is therefore met if

$$\int_0^t \dot{k}\,dc = \text{const.} \tag{20}$$

If h is uniform, (14), (18) and (20) combine to give

$$\rho_0\,(\rho_0 - \lambda_0) = \frac{\rho_0\,t - \alpha\,t^2}{\log\{\rho_0/(\rho_0 - t)\}} \tag{21}$$

where α is a dimensionless constant whose value is determined by (16). Equations (17) and (21) give the strain-rate λ at any point of the section. This is the actual mode in a bar in which h has any uniform value, in particular zero (cf. the discussion in Section 4 of Part I).

Alternatively, (21) can be established directly by the extremum principle (equation 5 of Part I). Here we have to minimize

$$\int\int \rho\,\lambda^2\,d\rho\,d\phi$$

where λ depends on λ_0 through (17) and $\lambda_0\,(\phi)$ is any continuous function satisfying (16) and (19). The integral becomes

$$\int_0^{2\pi} \left[\tfrac{1}{4}\,\rho^4 - \rho^2\,\rho_0(\rho_0 - \lambda_0) + \rho_0^{\,2}\,(\rho_0 - \lambda_0)^2 \log \rho\right] d\phi$$

where the square brackets denote the difference of the terminal values of the integrand on a characteristic (ρ being given the values ρ_0 and $\rho_0 - t$). The condition

that this is a minimum subject to (16) is immediately seen to be (21) with αt^2 as the Lagrangian multiplier.

In particular, when the boundaries are circles, ρ_0 and hence λ_0 are constant. From (16) we find that $\lambda_0 = \rho_0$ (so that $\alpha = \rho_0/t$) and from (17) that $\lambda = \rho$, the radius from the bar axis. Hence $w = 0$ in the actual mode, in agreement with the conventional treatment.

Another particular case is that of a thin-walled section, Equation (21) yields the constant value $(\alpha + \frac{1}{2})t$ for λ (the subscript can now be dropped). Then, from (16),

$$\lambda = 2A/l \tag{22}$$

where l is the length of the perimeter. Since the hardness distribution remains uniform, the rate of increase of torque is $2kAt$, or $2hA^2t/l$ from (14) and (22).

REFERENCES

FREIBERGER, W. and PRAGER, W.	1953	*A.S.M.E. Preprint* No. 55-A. 85.
GEIRINGER, H.	1953	*Advances in Applied Mechanics* **3**, pp. 197-292 (Academic Press, N.Y.).
HILL, R.	1951	*Phil. Mag.*, **42**, 868.
	1952	*J. Mech. Phys. Solids*, **1**, 19.
	1956	*J. Mech. Phys. Solids*, **4**, 247.

Journal of the Mechanics and Physics of Solids, 1956, Vol. 5, pp. 9 to 17. Pergamon Press Ltd., London.

CORRECTED DISCONTINUITIES IN STRUCTURAL STABILITY PROBLEMS

By A. H. Chilver
Department of Engineering, University of Cambridge

(*Received 26th June*, 1956)

Summary

A method is described for the derivation of the basic differential equations of a structural stability problem. It is suggested that this method is rather different in concept from the conventional equilibrium-strain-compatibility approach. In its simplest form the method has been used by Timoshenko (1945) and others. In deriving the basic differential equations of a stability problem the method makes direct use of the linear-elastic properties of the structure. This is illustrated by a discussion of the torsional-flexural buckling of an axially loaded strut.

1. Introduction

The basic differential equations of a structural stability problem are derived usually by one of two well-known methods. In simple problems interest centres generally on a condition of elastic neutral equilibrium. The first method – which we shall describe as the 'conventional' approach – consists in a discussion of the equilibrium and strain-compatibility of an isolated element of the structure; this approach has been widely used by Timoshenko (1936), and other writers, in studying the Euler buckling of columns. The second method – which we might describe as the energy approach – consists in setting up the equation of total potential energy of the system and minimizing this relation; this method is outlined by Bleich (1952), and the general basis is discussed by Morice (1955). Both methods are powerful; the conventional approach, however, becomes involved in dealing with complex problems, as, for example, torsional-flexural buckling of a compressed strut. The energy method offers a general approach to all elastic stability problems; in practice, however, it is perhaps most useful in giving approximate solutions to complex stability problems.

The approach discussed in this paper makes use of the concept of a correct discontinuity; this involves an analysis similar to the conventional method, but it has the advantage that the basic differential equations for certain problems may be derived more easily. In this alternative method the structure is reduced initially to a set of *disconnected* elements; for any buckled form the external forces required for equilibrium of the elements are evaluated. A second system of external forces is then found to give a *continuous* structure with the same displaced form. If the two systems of external forces are in equilibrium with each other the buckled form can be maintained without external forces; this corresponds to the required condition of neutral equilibrium. The method consists essentially

in *correcting* an arbitrary set of *discontinuities*. It can be shown that this approach has been used in its simplest form by earlier writers; this aspect is discussed in the examples studied.

2. Solution of the Simple Strut Problem

The differences between the conventional approach and the method of corrected discontinuities can be demonstrated by reference to the simple strut problem.

Fig. 1.

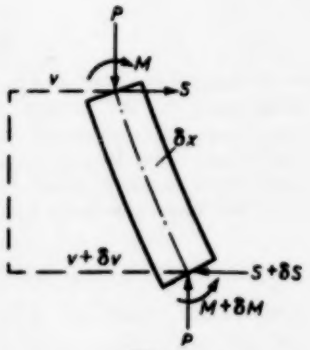

Fig. 2.

A straight uniform strut has a cross-sectional form with two axes of symmetry; the strut is loaded with compression forces on its longitudinal centroidal axis Ox (Fig. 1). For flexural buckling of the strut the relevant flexural stiffness is EI. In the buckled mode the lateral deflection of any point parallel to Oy is v. The conditions of support at the ends of the strut are taken to be quite arbitrary.

In the conventional method of deriving the differential equation of equilibrium, we discuss the equilibrium and strain-compatibility of a displaced longitudinal element of length δx (Fig. 2); it is in equilibrium under the action of end compression loads P, lateral shear forces S, and bending moments M. The two equations of statical equilibrium for the element are

$$\delta M + P\,\delta v - S\,\delta x = 0, \qquad \delta S = 0.$$

On eliminating S, we have

$$\frac{d^2 M}{dx^2} + P\frac{d^2 v}{dx^2} = 0. \tag{1}$$

But the bending-moment-curvature relation is

$$M = EI\frac{d^2 v}{dx^2},$$

so that, on eliminating M from equation (1),

$$\frac{d^2}{dx^2}\left(EI\frac{d^2v}{dx^2}\right) + P\frac{d^2v}{dx^2} = 0. \tag{2}$$

This is the well-known differential equation governing the buckling of an axially-compressed strut.

Now consider an alternative approach to the problem; suppose the elemental length δx of the strut is disconnected from the rest of the structure (Fig. 3a). If this element is to be in equilibrium in the displaced form under the action of end compression forces P, a possible system of restraining forces consists of lateral loads Pv' at the ends of the element, together with a distributed lateral

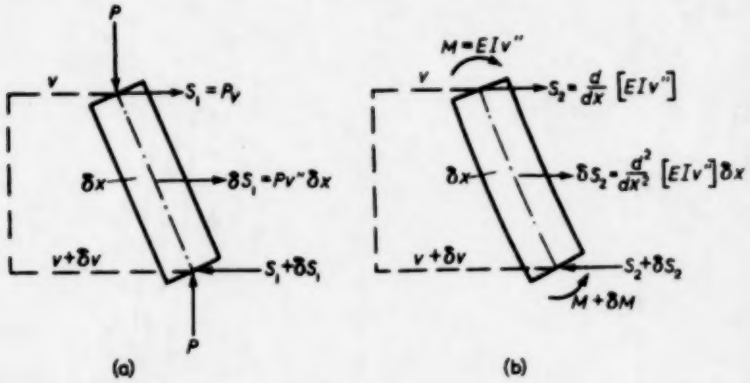

Fig. 3.

force of intensity Pv'', (primes refer to differentiation with respect to x). The ends of the element may be treated as pinned, and discontinuities are present therefore at the ends of adjacent elements. A system of lateral forces and bending moments which would correct the assumed discontinuities is shown in Fig. 3 (b); these consist of bending moments EIv'' and a lateral shear force of intensity $d^2(EIv'')/dx^2$, if the element is assumed to bend linearly. Superposition of the loads indicated in Fig. 3 (b) on the element of Fig. 3 (a) results in the correction of the discontinuities of Fig. 3 (a); moreover – and here the method gives its important result – the resulting intensity of lateral load is zero if

$$\frac{d^2}{dx^2}\left(EI\frac{d^2v}{dx^2}\right) + P\frac{d^2v}{dx^2} = 0. \tag{3}$$

This, of course, corresponds to the buckled condition of the strut.

In this particular problem the two methods of analysis are equally simple; this, however, is not true of all problems, as the examples discussed later will illustrate. The second method – using correct discontinuities – suggests that buckling of a strut is equivalent to a lateral force of intensity Pv'', as implied by Figs. 3 (a) and 3 (b). This concept is often used to explain instability problems; it is, however, misleading, for there is no variation of lateral shear force in a buckled strut, as is obvious from Fig. 2, in which $\delta S = 0$. It is strictly more correct to argue that a lateral force of intensity Pv'' is required to eliminate an arbitrary set of discontinuities in the strut.

3. TORSIONAL BUCKLING OF A COMPRESSED STRIP

A stability problem of a more involved nature is that of a long thin uniform strip, simply-supported on one longitudinal edge, free on the other, and loaded with a uniform compression stress σ on its ends (Fig. 4). In the torsional mode of buckling it is assumed that all points in a cross-section of the strip have the same angular displacement θ about the simply supported axis of twist. The width of the strip is b, and the uniform thickness is t.

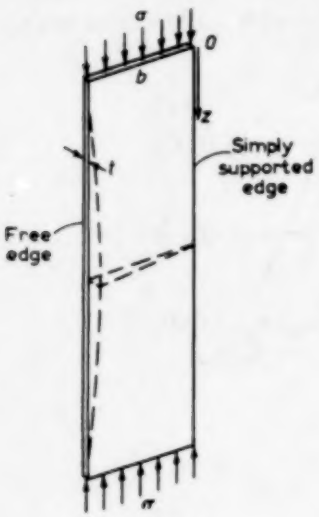

Fig. 4.

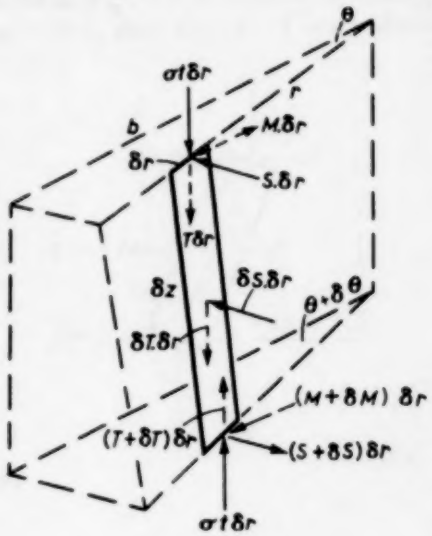

Fig. 5.

In the conventional treatment of this problem we consider the equilibrium and strain compatibility of a displaced element (Fig. 5), of length δz and width δr, located a distance r from the axis of twist. The element withstands end compression loads $\sigma t\,\delta r$ together with end shear forces, moments and torques of lineal intensities S, M and T, respectively. For equilibrium the element also withstands a lateral shear force of areal intensity S', and a torque of areal intensity T', (where primes refer to differentiation with respect to z only). There are two equations of statical equilibirum for the element; firstly, for bending actions

$$\sigma t\, r\theta' + S + M' = 0. \tag{4}$$

The shear forces and torques, S' and T', respectively, are transmitted from one element to another in the cross-section; if there is no external moment about the axis of twist, we have secondly

$$\int_0^b S'\, r\,dr + \int_0^b T'\,dr = 0. \tag{5}$$

On eliminating S between equations (4) and (5), we have

$$\int_0^b T'\,dr - \int_0^b (M'' + \sigma t\, r\theta'')\, r\,dr = 0. \tag{6}$$

It remains to substitute for M and T in terms of the displaced form ; now

$$M = EI_1 r\theta'', \qquad T = GJ_1\theta',$$

in which EI_1 and GJ_1 are the flexural and torsional stiffnesses, respectively, of a unit width of the plate. Then equation (6) becomes

$$\tfrac{1}{3}\tfrac{1}{6} b^3 t^3 E\theta'''' + (\sigma J_0 - GJ)\theta'' = 0, \tag{7}$$

in which J_0 is the polar second moment of area of the cross-section about the axis of twist, and GJ is the pure torsional stiffness of the whole strip. Equation (7) governs the stability of the strip ; when the first term is negligible we have the well-known approximate result

$$\sigma = G\left(\frac{J}{J_0}\right) = G\left(\frac{t}{b}\right)^2,$$

given by TIMOSHENKO (1945).

An interesting feature in the derivation of equation (7) is that we have not used directly the torsional properties of the composite strip, but only the pure torsional properties of the separate elements.

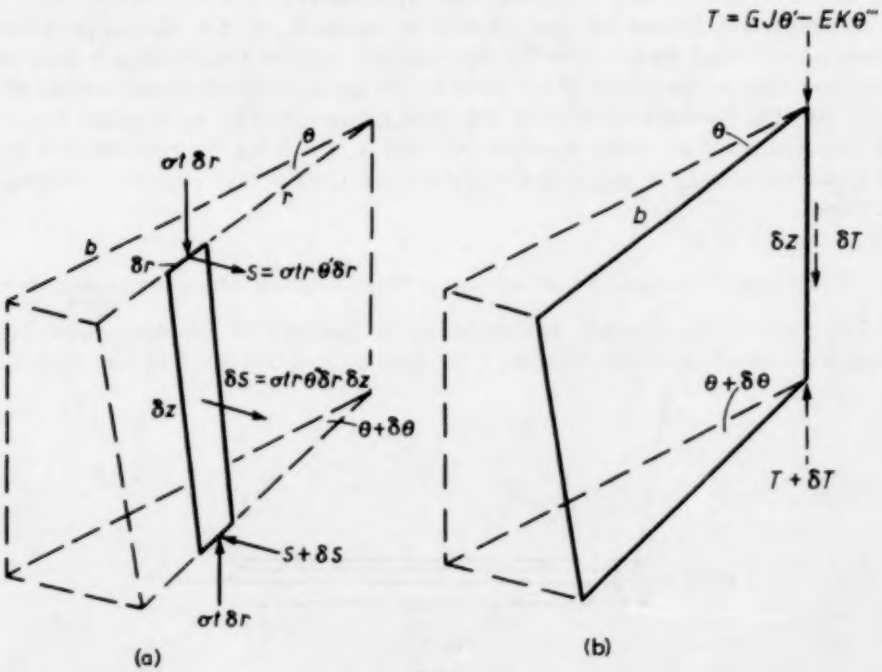

Fig. 6.

In the alternative approach we consider, firstly, a loaded element disconnected from all other elements in the strip (Fig. 6a). This element could be maintained in equilibrium with a lateral force of areal intensity $\sigma t r\theta''$; r is again the distance of the element from the centre of twist, and θ is the angle of twist of the cross-section. Consider, secondly, a system of torques giving continuity of all elements

throughout the cross-section and length of the strip (Fig. 6b). A torque at any cross-section of

$$T = GJ\theta' - EK\theta''', \tag{8}$$

where GJ is the pure torsional stiffness of the strip, and EK is its warping stiffness about the axis of twist, provides longitudinal continuity at all sections and twists all elements in a cross-section by the same amount, θ. But the variation of T along the length of the strip implies an external torque of lineal intensity

$$T' = GJ\theta'' - EK\theta'''' \tag{9}$$

If this system of *correcting* torques is applied to the original set of *discontinuous* elements no external torque is required to maintain equilibrium if

$$GJ\theta'' - EK\theta'''' - \int_0^b \sigma t\, \theta''\, r^2\, dr = 0.$$

This gives the differential equation

$$EK\theta'''' + (\sigma J_0 - GJ)\,\theta'' = 0. \tag{10}$$

In fact $K = \frac{1}{3}\frac{1}{6}\, b^3 t^3$, and this reduces to equation (7).

An important feature of this alternative approach is that the torque-twist relation (8) is used directly. In the conventional solution this relation is derived fundamentally in the course of the analysis. In using corrected discontinuities we may say that the buckled form of the strip is equivalent to an external torque of lineal intensity given by equation (9); this is essentially the method used by TIMOSHENKO (1945) in studying the stability of a strip with negligible warping stiffness.

4. TORSIONAL-FLEXURAL STABILITY OF A THIN-WALLED OPEN-SECTION STRUT

The method of corrected discontinuities is powerful in problems involving complex linear-elastic relations of the type given by equation (8). The conventional

Fig. 7.

approach would imply the simultaneous derivation of these relations; it is simpler, however, to derive these relations independently, and then to solve the stability problem making use of corrected discontinuities.

Consider, for example, the buckling of a uniform strut of thin-walled open cross-section, under a uniform end compression stress, σ (Fig. 7). Suppose Cx, Cy are the principal centroidal axes of the cross-section, and that (x_0, y_0) are the

co-ordinates of the shear centre, O (Fig. 8). On buckling, the cross-section of the strut is displaced laterally and twisted (Fig. 8). Suppose u, v are the displacements of any point in the wall of the strut parallel to Cx, Cy, respectively. These displacements may be considered to be compounded of general lateral displacements along the axes Cx, Cy, together with a general rotation about some arbitrary point

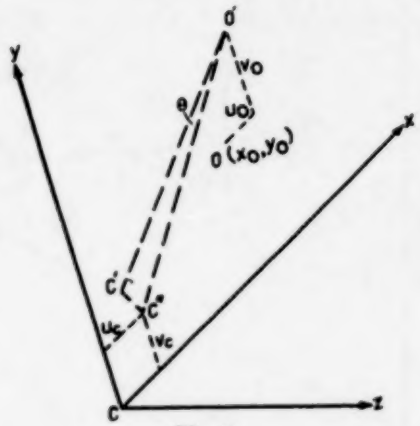

Fig. 8.

which, for convenience, we take as the shear centre. Suppose u_0, v_0 are the lateral displacements of the shear centre parallel to Cx, Cy, respectively, and that the cross-section as a whole twists an amount θ about the shear centre. Then the lateral displacements of the centroid C, to the required degree of accuracy, are

$$u_c = u_0 + y_0\,\theta, \qquad v_c = v_0 - x_0\,\theta.$$

The lateral displacements of any point (x, y) of the centre-line of the wall are

$$u = u_0 + (y_0 - y)\,\theta, \qquad v = v_0 - (x_0 - x)\,\theta.$$

Now consider an element of the wall of length δz, width δs, and thickness t (Fig. 9a); s is measured from a convenient origin round the centre line of the wall. If the element were quite detached from all other elements of the strut, a possible system of equilibrating forces consists of lateral shear forces parallel to Cx and Cy (Fig. 9a). The total lateral shear force parallel to Cx for all elements is

$$\int_A \sigma t\, u''\, \delta z\, ds = \sigma\, \delta z \int_A t\left[u_0'' + (y_0 - y)\,\theta''\right] ds = P\,\delta z\,(u_0'' + y_0\,\theta''),$$

where P is the total end load, and the integration is carried out over the whole cross-sectional area A of the strut. Similarly the total shear force parallel to Cy for all elements is

$$\int_A \sigma t v''\, \delta z\, ds = P\delta z\,(v_0'' - x_0\,\theta'').$$

The total torque about the shear centre of these forces is

$$\int_A \sigma t\, u''\,(y_0 - y)\,\delta z\, ds + \int_A \sigma t\, v''\,(x - x_0)\,\delta z\, ds$$
$$= P\,(y_0\, u_0'' - x_0\, v_0'' + r_0^2\, \theta'')\,\delta z,$$

in which r_0 is the polar radius of gyration of the cross-section about the shear-

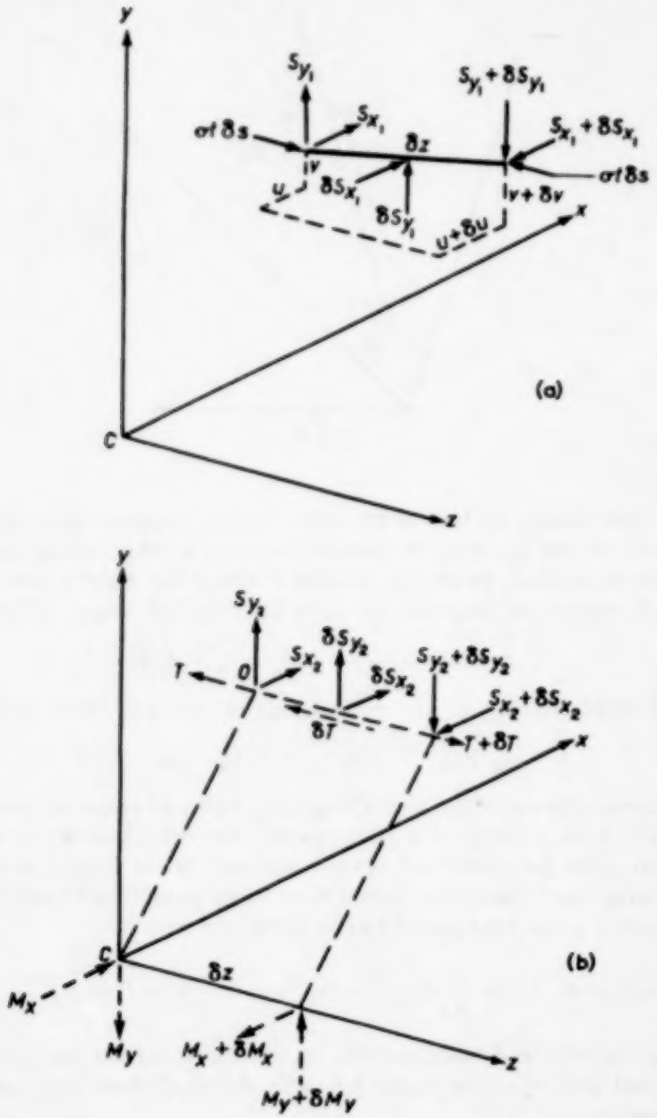

Fig. 9.

centre axis, given by

$$A r_0^2 = I_x + I_y + A\,(x_0^2 + y_0^2),$$

where A is the area of the cross-section, and I_x, I_y are the principal second moments of area of the cross-section about Cx, Cy, respectively.

Now consider an elemental length of strut acted upon by bending and torque actions alone (Fig. 9b). Bending moments M_x, M_y, are applied about the centroidal axis, and shear forces S_x, S_y, at the shear centre; the element is also subject to a torque T. The distorted form u_0, v_0, can be maintained by external shear forces of lineal intensity

$$EI_y\, u_0'''', \qquad EI_x\, v_0'''',$$

parallel to Cx, Cy, respectively, and an external torque of lineal intensity

$$GJ\theta'' - EK\theta'''',$$

where GJ is the pure torsional stiffness and EK the warping stiffness of the strut. The original set of disconnected elements could be formed into a continuous system by the application of these forces and torque. Moreover, no external forces would be required in the buckled mode if

$$\left.\begin{aligned} &EI_y\, u_0'''' + P\,(u_0'' + y_0\,\theta'') = 0, \\ &EI_x\, v_0'''' + P\,(v_0'' - x_0\,\theta'') = 0, \\ &(GJ\theta'' - EK\theta'''') - P\,(y_0\,u_0'' - x_0\,v_0'' + r_0^2\,\theta'') = 0. \end{aligned}\right\} \qquad (11)$$

These basic differential equations of the problem are in a more general form than those given by Timoshenko (1945).

5. Conclusions

It is suggested that the concept of corrected discontinuities may be of some value in deriving the differential equations of an elastic stability problem. Their use in the problem of torsional flexural buckling of a thin-walled open-section strut eliminates the need to discuss the basic torsional properties of the strut. In more general terms an advantage of the method is that buckling of the disconnected elements on the one hand and the linear-elastic properties of the structure on the other can be discussed independently. In this respect the method may be useful in giving a rational approach to other types of stability problems.

References

Bleich, F.	1952	*Buckling Strength of Metal Structures* (McGraw-Hill, New York).
Morice, P. B.	1955	*Structural Engineer*, June.
Timoshenko, S. P.	1936	*Theory of Elastic Stability* (McGraw-Hill, New York).
	1945	*J. Franklin Inst.* **239**, 3, 4, 5.

Journal of the Mechanics and Physics of Solids, 1956, Vol. 5, pp. 18 to 25. Pergamon Press Ltd., London

BUCKLING OF A SIMPLE PORTAL FRAME

By A. H. Chilver
Department of Engineering, University of Cambridge

(*Received 26th June*, 1956)

Summary

An interesting characteristic of portal frames noted by Chwalla (1938) is that lateral buckling loads may be influenced by the presence of initial bending effects. A simple model portal frame is introduced, and an exact elastic stability analysis shows that symmetric buckling loads are affected appreciably by initial bending effects. An exact treatment is also given for small antisymmetric displacements; the buckling loads are influenced again by initial bending effects, but not so seriously. For antisymmetric distortions the behaviour is reasonably linear until the onset of buckling.

1. Introduction

In recent years there has been a revived interest in problems of the stability of rigidly jointed framed structures; this has been brought about by the need for careful design of steel framed buildings, in which there are no substantial walls to give the skeleton additional bracing stiffness. Merchant (1955) and his associates have recently considered the stability of portal frames, tall buildings, and trusses; Livesley (1956) and Bolton (1955) have discussed iterative and relaxation methods of solving the small deflection equations in problems of this type. More recently Horne (1956), in an excellent treatment of the stanchion problem, has considered a column as an isolated element of the steel skeleton; he discusses the strength and stability of this column under various end conditions.

It is important, however, to appreciate in the portal frame problem that buckling may not in general occur in a simple condition of neutral equilibrium, as is the case in many simple strut problems. The elastic stability of a single strut is governed largely by the Euler critical load; an interesting feature of strut behaviour is that the elastic critical load – corresponding to the development of large lateral deflections in the elastic condition of the material – is not affected by eccentric application of the load, by the presence of lateral forces or end moments, or by initial imperfections.

As early as 1938 Chwalla showed that simple portal frames may have somewhat different buckling characteristics; he found that when vertical loads are applied to the cross-beam of a simple portal frame the critical value of these loads for lateral instability of the whole frame may be slightly smaller than the critical value of loads applied to the tops of the stanchions; this reduction in critical load is due to the presence of an appreciable thrust in the cross-beam of the frame when vertical loads are applied to the cross-beam. The reduction in critical load noted by Chwalla (1938) is small – of the order of 3% or so – for the particular cases studied.

2. A Simple Model Portal Frame

In studying the buckling of portal frames, it is difficult to generalize from the results of Chwalla's necessarily complicated analysis. It is interesting at this stage to study the elastic stability of the model portal frame shown in Fig. 1, under the action of a symmetrical system of vertical loads. Two rigid columns, AB and GF, are hinged to rigid foundations at A and G; at B and F the columns are hinged to rigid triangular members, BCD and FED, which are hinged to each other at D. At B and F rotations at the hinges are resisted by linear-elastic springs of stiffness λ; the hinge D is unrestrained. The corners C and E of the model correspond to the rigid corners of a simple portal frame. The main dimensions of the frame are indicated in Fig. 1.

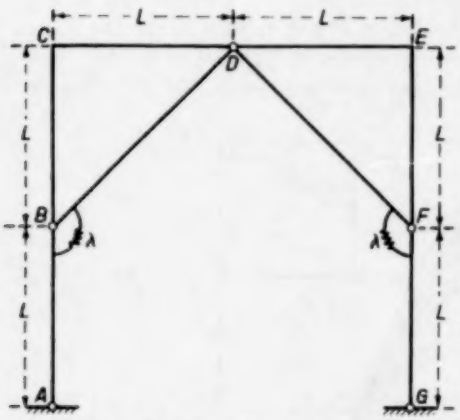

Fig. 1. Simple model portal frame.

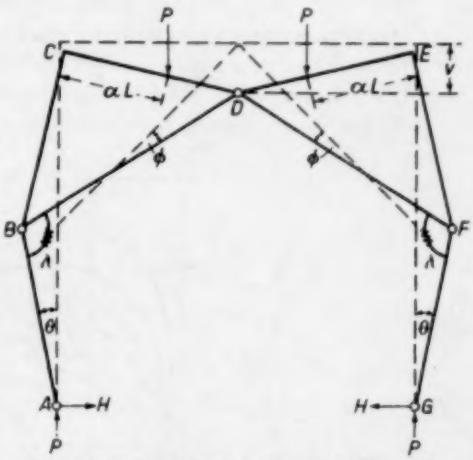

Fig. 2. Symmetric distortions of the model under the action of vertical loads P.

3. Symmetric Distortions

Vertical loads P are now applied to the cross-member CDE at distances αL from C and E; consider, firstly, symmetric distortions of the frame as shown in Fig. 2; we imagine that lateral forces could be brought into action to prevent lateral buckling of the frame. Suppose that hinge D moves vertically an amount v, that AB and GF rotate through angles θ, that BD and FD rotate through angles ϕ, and that horizontal thrusts H are induced at A and G.

On discussing the exact geometry of the frame we have that

$$\cos\phi + \sin\phi = 1 + \sin\theta, \tag{1}$$

$$2 - \frac{v}{L} = (\cos\phi - \sin\phi) + \cos\theta. \tag{2}$$

Furthermore, for statical equilibrium of the frame, we have

$$H = \frac{P\left[1 - (1-\alpha)\cos\phi\right]}{2 - \dfrac{v}{L}}, \tag{3}$$

$$\lambda(\theta + \phi) = PL \sin\theta + HL \cos\theta. \tag{4}$$

On eliminating H from (4) and substituting for (v/L) from (2), we have

$$\lambda(\theta + \phi) = PL\left\{\sin\theta + \frac{[1 - (1 - \alpha)\cos\phi]\cos\theta}{\cos\theta + (\cos\phi - \sin\phi)}\right\}. \tag{5}$$

The simplest method of solving these exact equations is as follows : give ϕ any particular value, and deduce the corresponding value of θ from equation (1) ; then substitute these values of θ and ϕ into equation (2) to deduce the value of (v/L) ; finally, substitute the values of θ and ϕ into equation (5), and hence calculate the corresponding value of (PL/λ), i.e. the load parameter corresponding to any displaced form θ, ϕ.

The variation of (v/L), a parameter defining the vertical deflection of the hinge D, with increasing values of the load parameter (PL/λ) is shown in Fig. 3 for various values of α ; when $\alpha = 0$ the vertical loads P are applied along the axes of the columns AB, GF ; symmetric buckling occurs at $(PL/\lambda) = 2$; but the condition of equilibrium is unstable, and the continued application of $(PL/\lambda) = 2$

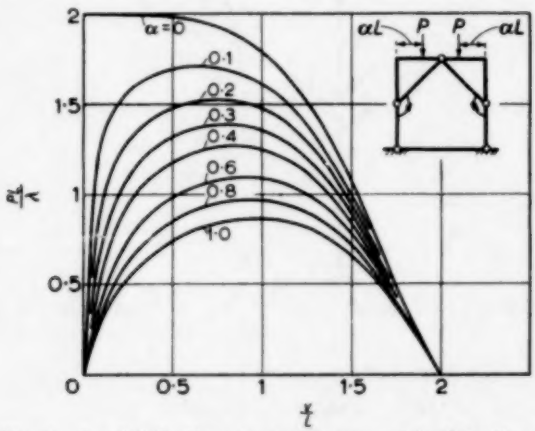

Fig. 3. Load-deflection curves for symmetric distortions.

leads to a " snap-through " in which the frame is geometrically inverted ; theoretically no vertical loads are required to maintain the hinge D at the level of hinges A and G. When $0 < \alpha < 1$, the vertical loads P are applied at some intermediate positions between C, D and E ; vertical deflection of the hinge D occurs from the onset of loading. Initially, when deflections are small, we have the approximate linear relation

$$\theta = \tfrac{1}{4}\alpha\left(\frac{PL}{\lambda}\right), \tag{6}$$

which is easily derived from equation (5) on making θ and ϕ small quantities. But as the vertical loads increase in magnitude linearity is not maintained ; in fact the stiffness of the frame diminishes appreciably until a certain value of (v/L) is attained at which the vertical loads can be increased no further. The maximum value of (PL/λ) which can be attained depends largely on the position

of the loads P; when both loads are applied directly to the hinge D, i.e. when $\alpha = 1$, the maximum load which the frame withstands is only 0·87 (PL/λ), or about 43·5% of the buckling load for $\alpha = 0$. Maximum values of (PL/λ) for symmetric distortions are shown in Fig. 4, for values of α from 0 to 1.

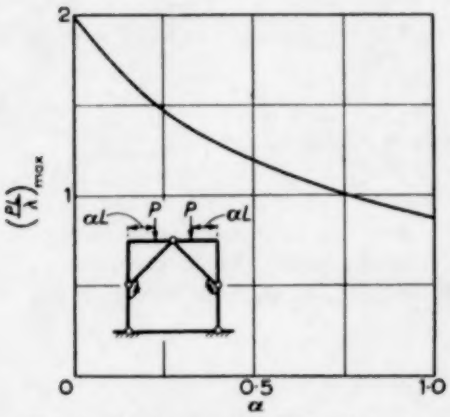

Fig. 4. Maximum attainable values of (PL/λ) for different values of α and symmetric distortions.

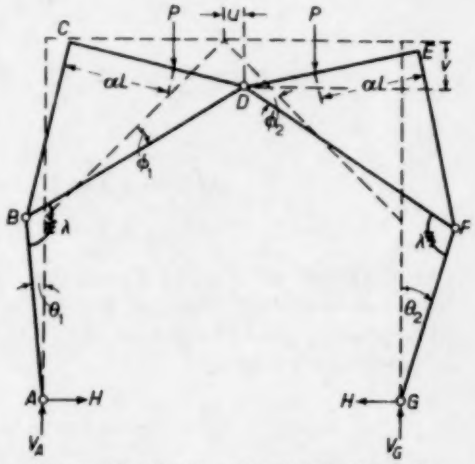

Fig. 5. Model with a lateral deflection of the hinge D.

4. Antisymmetric Mode of Buckling

In discussing symmetric distortions of the frame it was assumed that no lateral displacements of the hinge D occur when vertical loads are applied. Consider now the possibility of a small lateral movement of the hinge D during the loading process.

In Fig. 5 the frame, under the action of vertical loads P only, is shown in any displaced form of equilibrium in which u and v are the horizontal and vertical displacements of the hinge D; in addition, θ_1, ϕ_1 are the angular displacements of the members AB, BD, respectively, while θ_2, ϕ_2 are the angular displacements of the members GF, FD, respectively.

The conditions of geometrical compatibility are

$$\left.\begin{aligned} 2 - \frac{v}{L} &= (\cos\phi_1 - \sin\phi_1) + \cos\theta_1, \\ 2 - \frac{v}{L} &= (\cos\phi_2 - \sin\phi_2) + \cos\theta_2, \end{aligned}\right\} \tag{7}$$

$$\left.\begin{aligned} 1 + \frac{u}{L} &= (\cos\phi_1 + \sin\phi_1) - \sin\theta_1, \\ 1 - \frac{u}{L} &= (\cos\phi_2 + \sin\phi_2) - \sin\theta_2. \end{aligned}\right\} \tag{8}$$

For statical equilibrium of the frame in the laterally displaced form we have

$$\left.\begin{aligned} V_A &= P\left[1 - \frac{u}{L} + \tfrac{1}{2}(1-\alpha)(\cos\phi_1 - \cos\phi_2)\right], \\ V_G &= P\left[1 + \frac{u}{L} - \tfrac{1}{2}(1-\alpha)(\cos\phi_1 - \cos\phi_2)\right], \end{aligned}\right\} \tag{9}$$

$$\left.\begin{aligned} H\left(2 - \frac{v}{L}\right) &= V_A\left(1 + \frac{u}{L}\right) - P(1-\alpha)\cos\phi_1, \\ H\left(2 - \frac{v}{L}\right) &= V_G\left(1 - \frac{u}{L}\right) - P(1-\alpha)\cos\phi_2, \end{aligned}\right\} \tag{10}$$

and

$$\left.\begin{aligned} \lambda(\theta_1 + \phi_1) &= V_A L \sin\theta_1 + HL\cos\theta_1, \\ \lambda(\theta_2 + \phi_2) &= V_G L \sin\theta_2 + HL\cos\theta_2. \end{aligned}\right\} \tag{11}$$

In these equations V_A and V_G are the vertical reactions at A and G, respectively. Now consider small changes δu, δv, in u, v, respectively, which give rise to corresponding small changes $\delta\theta_1$, $\delta\theta_2$, $\delta\phi_1$, $\delta\phi_2$, in θ_1, θ_2, ϕ_1, ϕ_2, respectively. From equation (7) we have

$$\left.\begin{aligned} \frac{\delta v}{L} &= (\cos\phi_1 + \sin\phi_1)\,\delta\phi_1 + \sin\theta_1\,\delta\theta_1, \\ \frac{\delta v}{L} &= (\cos\phi_2 + \sin\phi_2)\,\delta\phi_2 + \sin\theta_2\,\delta\theta_2, \end{aligned}\right\} \tag{12}$$

and from equations (8),

$$\left.\begin{aligned} \frac{\delta u}{L} &= (\cos\phi_1 - \sin\phi_1)\,\delta\phi_1 - \cos\theta_1\,\delta\theta_1, \\ -\frac{\delta u}{L} &= (\cos\phi_2 - \sin\phi_2)\,\delta\phi_2 - \cos\theta_2\,\delta\theta_2. \end{aligned}\right\} \tag{13}$$

We are interested in the critical load at which lateral displacements first commence; for a small lateral movement δu from the symmetric form of distortion we put $u = 0$ in equations (12) and (13); we can also put $\theta_1 = \theta_2 = \theta$, (say), and $\phi_1 = \phi_2 = \phi$, (say). Then we have

$$\left.\begin{aligned} (\cos\phi + \sin\phi)(\delta\phi_1 - \delta\phi_2) + \sin\theta(\delta\theta_1 - \delta\theta_2) &= 0, \\ (\cos\phi - \sin\phi)(\delta\phi_1 - \delta\phi_2) - \cos\theta(\delta\theta_1 - \delta\theta_2) &= 2\frac{\delta u}{L}. \end{aligned}\right\} \tag{14}$$

On solving for $(\delta\phi_1 - \delta\phi_2)$ and $(\delta\theta_1 - \delta\theta_2)$ we have

$$\left.\begin{aligned} (\delta\phi_1 - \delta\phi_2) &= \frac{2\delta u}{L} \cdot \frac{\sin\theta}{\cos(\theta + \phi) + \sin(\theta + \phi)}, \\ (\delta\theta_1 - \delta\theta_2) &= -\frac{2\delta u}{L} \cdot \frac{\cos\phi + \sin\phi}{\cos(\theta + \phi) + \sin(\theta + \phi)}. \end{aligned}\right\} \tag{15}$$

We must also study the effect of small changes δu, δv, on the equations of statical equilibrium; suppose δV_A, δV_G, δH, are the corresponding small changes in V_A,

V_G, H, respectively. Now equations (11) give

$$\lambda(\theta_1 - \theta_2) + \lambda(\phi_1 - \phi_2) = L\left[V_A \sin\theta_1 - V_G \sin\theta_2\right] + HL\left[\cos\theta_1 - \cos\theta_2\right]. \quad (16)$$

so that for small changes δu, δv, we have

$$\lambda(\delta\theta_1 - \delta\theta_2) + \lambda(\delta\phi_1 - \delta\phi_2) = L\left[\delta V_A \sin\theta_1 + V_A \cos\theta_1\,\delta\theta_1 - \delta V_G \sin\theta_2 - V_G \cos\theta_2\,\delta\theta_2\right] + \delta H \,.\, L\left[\cos\theta_1 - \cos\theta_2\right] - HL\left[\sin\theta_1\,\delta\theta_1 - \sin\theta_2\,\delta\theta_2\right]. \quad (17)$$

For a small change δu from the symmetric form of distortion with $u = 0$, $\theta_1 = \theta_2 = \theta$, $\phi_1 = \phi_2 = \phi$, as before, and we have

$$\lambda(\delta\theta_1 - \delta\theta_2) + \lambda(\delta\phi_1 - \delta\phi_2) = L\sin\theta\,(\delta V_A - \delta V_G) + (PL\cos\theta - HL\sin\theta)(\delta\theta_1 - \delta\theta_2), \quad (18)$$

since $V_A = V_G = P$ when $u = 0$. Now from equations (9) we have

$$\delta V_A - \delta V_G = -P\left[\frac{2\delta u}{L} + (1-\alpha)\sin\phi\,(\delta\phi_1 - \delta\phi_2)\right], \quad (19)$$

for the particular case where $u = 0$. From equations (10) we have

$$H = \frac{P}{2 - \dfrac{v}{L}}\left[1 - (1-\alpha)\cos\phi\right] \quad (20)$$

when $u = 0$. On substituting for $(\delta V_A - \delta V_G)$ and H in equation (18) we have

$$\lambda(\delta\theta_1 - \delta\theta_2) + \lambda(\delta\phi_1 - \delta\phi_2) = -PL\sin\theta\left[2\frac{\delta u}{L} + (1-\alpha)\sin\phi\,(\delta\phi_1 - \delta\phi_2)\right] + PL\left[\cos\theta - \frac{\sin\theta}{2 - \dfrac{v}{L}}\left\{1 - (1-\alpha)\cos\phi\right\}\right](\delta\theta_1 - \delta\theta_2). \quad (21)$$

Finally, on introducing equations (15) we can express $(\delta\theta_1 - \delta\theta_2)$ and $(\delta\phi_1 - \delta\phi_2)$ in terms of $(2\,\delta u/L)$; equation (21) then gives either $(2\,\delta u/L) = 0$, corresponding to no antisymmetric distortions, or

$$\frac{\lambda}{PL} = \left[\cos\theta - \frac{\sin\theta}{2 - \dfrac{v}{L}}\left\{1 - (1-\alpha)\cos\phi\right\}\right](\cos\phi + \sin\phi) + \sin\theta\left[\cos(\theta + \phi) + \sin(\theta + \phi)\right] + (1-\alpha)\sin^2\theta\sin\phi, \quad (22)$$

which defines the value of P at which antisymmetric distortions can occur; in this sense the solution of equation (22) is the lateral buckling load.

From the analysis of the symmetric distortions we have corresponding values of θ and ϕ; lateral buckling of the frame is possible when equations (5) and (22) give the same value of (PL/λ) for corresponding values of θ and ϕ. Values of the loading parameter (PL/λ) at which lateral instability can occur are shown in Fig. 6; consider the particular case $\alpha = 0{\cdot}4$: when loads P are applied distortions are initially of the symmetric type, and these are easily reproduced from Fig. 3; the relation between (PL/λ) and (v/L) deviates slightly from linearity; when (PL/λ)

is equal to about 0·79, any further increase in P may give rise to lateral anti-symmetric distortions, and $P = 0{\cdot}79\ \lambda/L$ may be taken as the critical lateral buckling load; the remaining part of the curve for $\alpha = 0{\cdot}4$ in Fig. 3, defining large symmetric distortions of the frame, is only attainable if lateral buckling is prevented. When $\alpha = 0$ the loads P are applied along the columns ABC, GEF;

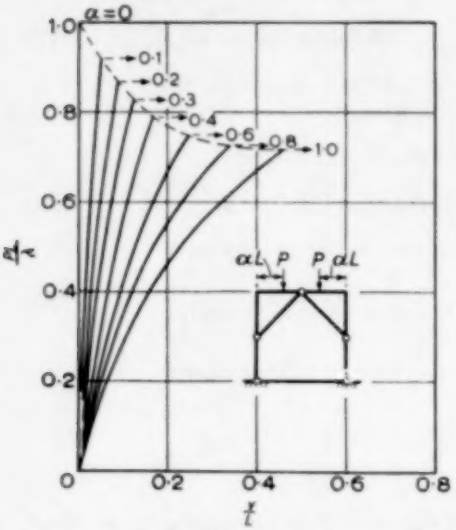

Fig. 6. Load-deflection curves for symmetric distortions, showing the critical lateral buckling loads.

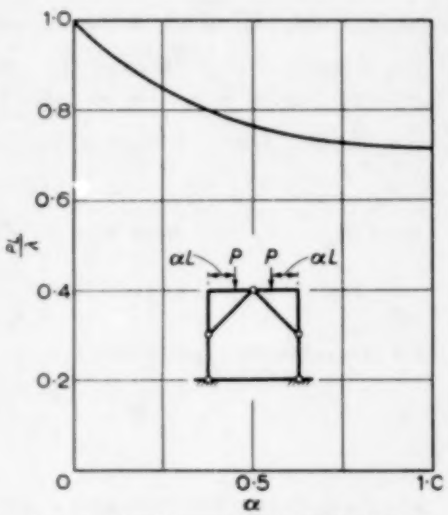

Fig. 7. Anti-symmetric buckling loads for different values of α.

in this case lateral buckling of the frame occurs when $(PL/\lambda) = 1$. When both loads P are applied at the hinge D, $\alpha = 1$, and for lateral instability we have $(PL/\lambda) = 0{\cdot}72$, which is 28% lower than that for $\alpha = 0$. Lateral buckling loads for different values of α are shown in Fig. 7; an interesting feature is the relatively sudden reduction in (PL/λ) for small values of α.

5. Approximate Solution for Antisymmetric Buckling

For most values of α, antisymmetric buckling of the frame occurs for small values of v/L; this suggests that an approximate solution of equations (5) and (22) may be of interest. When θ and ϕ are small, equation (5) gives for the symmetric distortions

$$2\lambda\theta \cdot =. PL\left(\theta + \frac{\alpha}{2-\theta}\right), \tag{23}$$

since $\theta \cdot =. \phi$. This gives approximately

$$\theta = \frac{\frac{1}{2}\alpha\left(\frac{PL}{\lambda}\right)}{1 - \frac{1}{2}(1 + \frac{1}{4}\alpha)\left(\frac{PL}{\lambda}\right)}. \tag{24}$$

For very small values of (PL/λ) we deduce the approximate linear relation $\theta = \frac{1}{4}\alpha\left(\frac{PL}{\lambda}\right)$. For small values of θ and ϕ, equation (22), governing the onset of lateral instability, gives

$$\frac{\lambda}{PL} \cdot = . 1 + \tfrac{1}{2}(4 - \alpha)\theta. \tag{25}$$

On substituting for θ from equation (24) we have

$$(4 - 3\alpha + \alpha^2)\left(\frac{PL}{\lambda}\right)^2 - (12 + \alpha)\left(\frac{PL}{\lambda}\right) + 8 = 0. \tag{26}$$

Solutions of this quadratic equation give critical loads to within about 2% of the exact values of Fig. 7, and equation (26) is useful in defining the curve of Fig. 7 in an approximate analytic form.

6. Conclusions

The " model " portal frame shows firstly that for symmetric distortions the maximum attainable vertical load diminishes appreciably as the loads are placed nearer to the central hinge D; in fact, when both loads P are applied at the hinge D, the maximum attainable value of P is $0{\cdot}87\ \lambda/L$, compared with $2\lambda/L$ when the loads are applied at C and E; this represents a marked reduction in maximum load, and is accounted for by the appreciable thrust in CDE and the development of large distortions in the early stages of loading.

The model shows clearly and simply the variation of lateral buckling loads with different positions of the applied loads P. The critical value of P varies from λ/L when $\alpha = 0$ to $0{\cdot}72\ \lambda/L$ when $\alpha = 1$; the model therefore demonstrates the reductions in critical load noted by Chwalla (1938).

Obviously the model could be modified to give a more practical type of portal frame, although with a more complicated model an exact analysis of symmetric and antisymmetric distortions might prove formidable. There are many limitations to the model – as, for example, the idealized system of vertical loads, and the linear-elastic stiffness of the joints B and F. In spite of these shortcomings the model is useful in demonstrating in a simple fashion the influence of initial bending distortions on the lateral buckling of a simple portal frame.

References

Bolton, A.	1955	*Structural Engineer*, August.
Chwalla, E.	1938	*Der Bauingenieur*, **19**, 69.
Horne, M. R.	1956	*Proc. Inst. Civ. Engrs.* Part III, Vol 5.
Livesley, R. K.	1956	*Structural Engineer*, January.
Merchant, M.	1955	*Structural Engineer*, March.

Journal of the Mechanics and Physics of Solids, 1956, Vol. 5, pp. 26 to 40. Pergamon Press Ltd., London.

THE DEFORMATION OF MOLYBDENUM SINGLE CRYSTALS IN COMPRESSION*

By J. H. Hoke† and R. Maddin‡

(*Received 8th August*, 1956)

Summary

The results from the compression of 43 molybdenum single crystals are presented. They indicate that the slip process may be considered to occur in < 111 > directions along zones of weakness which generally do not define a low indices plane. The position of this zone is influenced by external variables such as extraneous grains, prior deformation and anvil or grip effect. Axis migration is toward the pole of the gross slip plane responsible for the slip traces only when one set of slip traces is present. No correlation is found between properties as defined by the proportional limit and crystal orientation. However, the strain hardening rate is orientational dependent.

1. The Deformation of Molybdenum Single Crystals in Compression

Crystallographically, the shear process of deformation in body-centred cubic metals is not fully understood and has been a matter of dispute for many years. The situation is different from that of the face-centred cubic and hexagonal close-packed metals where the mechanics of the deformation or slip process have been worked out specifically with very consistent results. Of these three structures most common in metallic materials, the face-centred cubic and hexagonal are close-packed structures with close-packed planes and directions present. Deformation or slip has been found to take place preferentially on a close-packed plane and in a close-packed direction, the specific system operating depending upon the maximum resolved shear stress. However, for body-centred cubic materials there is no close packed plane of atoms present even though there are four close-packed directions. Thus it is seen that the simple rule of slip in the close-packed plane and in the close-packed direction of maximum shear stress must be modified in some manner. This modification is one of considerable controversy, even though it is generally accepted that the deformation process is semicrystallographic in that shear does take place in one of the close-packed directions.

There are four general points of view found in the literature on the subject of slip in body-centred cubic metals :

(1) Slip takes place in the octahedral or < 111 > direction, but not necessarily on planes of low indices.

*This is part of a Dissertation submitted by Mr. John H. Hoke in 1955 to the Advisory Board of the School of Engineering of The Johns Hopkins University in partial fulfilment of the requirements for the degree of Doctor of Engineering.

†Research Metallurgist, The Babcock & Wilcox Co., Research and Development Center, Alliance, Ohio.

‡Formerly Associate Professor Metallurgy, The Johns Hopkins University ; now Professor of Metallurgy, School of Metallurgical Engineering, The University of Pennsylvania, Philadelphia 4, Pennsylvania.

(2) Slip takes place in the $< 111 >$ direction and is limited to the {110}, {112} or {123} planes.

(3) Deformation in body-centred cubic metals is composite shear on non-parallel {110} or {110} – {112} planes.

(4) Slip will occur in those directions and on those planes for which the β parameter – the ratio of the BURGER's vector to the interplanar distance – is a minimum.

The early works on body-centred cubic metals by TAYLOR and ELAM (1926) and ELAM (1936) supported the first theory, as well as recent results by VOGEL and BRICK (1953) and STEJN and BRICK (1954) from which it appears that glide can take place on any plane along the $< 111 >$ zone, depending on the variation of the relative strengths of planes in the zone and orientation with respect to the applied stress. However, much of the intermediate work was based on the assumption that body-centred cubic crystals have a plane of shear which is one of rational indices specifically the {110}, {112} or {123} planes, the choice of which may be influenced by temperature or composition. This view is discussed critically by VOGEL and BRICK (1953).

The third view suggested earlier by TAYLOR and ELAM (1926) and GRENINGER (1938) and more recently by CHEN and MADDIN (1951) proposes that all slip in body-centred cubic metals is {110} slip, and {112}, {123} and noncrystallographic slip is spurious and can always be resolved into slip on {110} planes. In addition, STEIJN and BRICK (1954) using a hard sphere model showed that {110} slip involves only one particular movement per atom while {112} slip also involved only one but a quite different type of atomic movement. Thus the slip process on intermediate planes in the $< 111 >$ zone would require only a definite relative proportion of the two types of movements and may be likened to a co-operative {110} – {112} process.

Some discrepancy exists for the fourth view, proposed by CHALMERS and MARTIUS (1952) with respect to body-centred cubic metals, because additional slip directions other than the $< 111 >$ are predicted which have never been identified experimentally. However, CHEN and MADDIN (1954) derived modified values of the CHALMERS and MARTIUS parameters β, assuming an alternative {110} slip process which are in good agreement with the general theory in that the additional slip system correspond to the next lowest values of β.

The present investigation was undertaken to study the behaviour of molybdenum single crystals in compression, since the specimen axis migration should indicate the glide plane poles in the same manner that the specimen axis migration in tension indicates the direction of glide. Thus this additional information would supplement the slip line analysis in the identification of the active slip planes.

EXPERIMENTAL PROCEDURE

Molybdenum single crystals were grown by a modified strain-anneal technique developed by CHEN, MADDIN and POND (1951) from sintered rods. This material had a purity of 99·9 + per cent, of which the principal impurities were found to be approximately 0·01-0·02 per cent chromium, 0·01 per cent copper, and 0·03 per cent carbon. The treatment, when successful, produced large cylindrical grains of $\frac{1}{2}$ to $1\frac{1}{2}$ inches in length, which were cut into samples for compression studies from the rods by a jeweller's saw, ends ground flat and parallel, and then polished electrolytically in a stainless-steel crucible. Because of the rather limited range of specimen orientations obtainable

TABLE 1. *Summary of results.*

Specimen	*Code*	*Type*	*Number of loadings*	*Total compression %*	*Proportional limit kg/mm²*	*Strain hardening rate*	*Approximate slip plane poles*	*Remarks*
1	Mo-6	Cylindrical	10	6·6	13·1	Medium	1. SW (112) 2. ($\bar{1}$23) 3. ($\bar{1}$12)	Major With increasing deformation Poorly defined
2	Mo-16	Cylindrical Shell, Polycrystalline Core	5	13·0	12·3	Medium	1. (213) 2. ($\bar{1}$12) 3. (12$\bar{3}$) 4. —	Major – not sharply defined Quite extensive also Minor Indication of others that disappeared with increasing deformation
3	Mo-11B	Cylindrical Bicrystal Grain B	6	12·3	11·0	Medium	1. (112) 2. SE ($\bar{1}$01) 3. NE (0$\bar{1}$1)	Slip plane poles poorly defined
4	Mo-5	Cylindrical	5	9·0	14·6	Medium	1. (112)-(213) 2. ($\bar{1}$01) 3. (0$\bar{1}$1)	Primary set, but pole poorly defined Extensive cross markings With increasing deformation
5	Mo-11A	Cylindrical Bicrystal Grain A	6	12·3	11·0	Medium	1. ($\bar{1}$01) 2. (101)-(213)	Fairly well defined Minor and considerable scatter
6	Mo-7	Cylindrical	6	8·9	17·7	Medium	1. SE ($\bar{1}$01) 2. NW (101) 3. (123) 4. (0$\bar{1}$1)	Well defined Much scatter. These two most well-defined in all the scatter Latecomer
7	Mo-19	Cylindrical Shell, Polycrystalline Core	4	16·8	17·9	Medium	1. ($\bar{1}$01)-($\bar{3}$12) 2. Between (101) & (213)	Scatter Secondary – more sharply defined
8	Mo-28A	Rectangular SA/CA	3	17·8	10·3	Medium	1. ($\bar{1}$01) 2. (0$\bar{1}$1) Slightly NW	Both quite extensive
9	Mo-28B	Rectangular	3	12·0	20·4	High	1. ($\bar{3}$12) 2. (1$\bar{3}$2)	Both about equal intensity

TABLE 1. *Summary of results—continued.*

Specimen	*Code*	*Type*	*Number of loadings*	*Total compression %*	*Proportional limit kg/mm²*	*Strain hardening rate*	*Approximate slip plane poles*	*Remarks*
10	Mo-28C	Rectangular	4	14·0	12·6	Low	1. $(\bar{1}01)$ 2. $(1\bar{2}1)$-$(2\bar{3}1)$	Both quite extensive
11	Mo-22A	Cylindrical	5	21·8	6·3	Medium	1. $(\bar{1}01)$ 2. (101) 3. $(0\bar{1}1)$	Primary plane depends upon position of observation surface Hint
12	Mo-22B	Rectangular	3	12·0	17·2	Medium	1. $(\bar{1}01)$ Slightly NW 2. $(0\bar{1}1)$ Approximately	Both of equal intensity
13	Mo-22C	Rectangular	4	16·4	10·9	Medium	1. $(\bar{3}12)$ 2. SW (101)	Widely scattered
14	Mo-22D	Hexagonal	3	13·0	8·2	Medium	1. $(\bar{1}01)$ 2. (101)	Slightly NW Slightly NE
15	Mo-22E	Septagonal	3	10·1	12·1	Medium	1. $(\bar{3}12)$ to $(\bar{1}01)$ 2. $(0\bar{1}1)$	Scatter – primary Secondary – more sharply defined
16	Mo-22F	Rectangular	3	12·0	15·8	Low	1. $(\bar{2}\bar{1}1)$	Wide scatter – poorly defined
17	Mo-27-1A	Cylindrical	3	11·1	9·8	Medium	1. $(\bar{1}01)$ 2. (101)	Both quite extensive
18	Mo-27-1B	Rectangular	3	11·8	9·8	High	1. $(\bar{2}\bar{1}1)$ 2. $(0\bar{1}1)$	Wide scatter Secondary
19	Mo-27-1D	Rectangular	2	8·5	10·3	High	1. $(\bar{2}\bar{1}1)$ 2. $(0\bar{1}1)$	Wide scatter Secondary
20	Mo-27-1E	Rectangular	2	7·3	11·1	Low	1. $(\bar{2}\bar{1}1)$	Wide scatter
21	Mo-27-2	Cylindrical	3	8·5	8·7	Medium	1. $(\bar{1}01)$ Slightly NW 2. $(0\bar{1}1)$	Both Primary

TABLE 1. *Summary of results—continued.*

Specimen	*Code*	*Type*	*Number of loadings*	*Total compression %*	*Proportional limit kg/mm²*	*Strain hardening rate*	*Approximate slip plane poles*	*Remarks*
22	Mo-27-3	Cylindrical	3	8·7	5·9	Low	1. $(\bar{2}\bar{1}1)$ 2. $(2\bar{1}1)$-$(3\bar{1}2)$	Primary Secondary
23	Mo-30A	Octagonal	2	6·8	12·3	Low	1. $(\bar{1}01)$ Slightly NW 2. (101) Slightly SW	Both quite extensive
24	Mo-30B	Octagonal	2	7·4	8·6	Low	1. $(\bar{2}\bar{1}1)$ 2. $(2\bar{1}1)$-$(3\bar{2}1)$	Primary Secondary
25	Mo-30C	Octagonal	2	7·4	12·0	Low	1. $(\bar{3}\bar{1}2)$ 2. $(1\bar{1}0)$-$(2\bar{3}1)$	Primary Poorly defined – secondary
26	Mo-21A	Cylindrical	3	9·0	6·3	Medium	1. $(\bar{1}01)$ and NW 2. NW (101)	Scatter major Fairly well established
27	Mo-25A-1	Octagonal	2	6·7	6·2	Medium	1. NW $(\bar{1}01)$ 2. SE $(0\bar{1}1)$	Primary Fairly well established
28	Mo-25A-2	Octagonal	2	7·5	8·8	Medium	1. $(\bar{3}\bar{1}2)$ 2. SW $(0\bar{1}1)$ 3. SW (101)	Primary Secondary Secondary
29	Mo-25B-1	Octagonal	2	8·3	7·2	Medium	1. SW $(\bar{1}01)$ 2. (101)	Primary Minor, poorly defined
30	Mo-25B-2	Octagonal	2	8·0	9·8	Medium	1. NW $(\bar{1}01)$ 2. SW (101)	Primary Secondary, but definite
31	Mo-23B	Octagonal	2	8·9	7·9	Medium	1. $(\bar{1}01)$-$(\bar{2}13)$ 2. (101)	Both of about equal intensity
32	Mo-23D	Octagonal	2	7·6	10·9	Medium	1. $(\bar{1}01)$-$(\bar{3}\bar{1}2)$ 2. Near $(0\bar{1}1)$	Primary Secondary, but quite prevalent

TABLE 1. *Summary of results—continued.*

Specimen	*Code*	*Type*	*Number of loadings*	*Total compression %*	*Proportional limit kg/mm²*	*Strain hardening rate*	*Approximate slip plane poles*	*Remarks*
33	Mo-23E	Octagonal	1	6·7	11·3	High	1. $(\bar{1}01)$ to $(\bar{2}\bar{1}1)$ 2. $(0\bar{1}1)$	Poorly defined More sharply defined – prevalent
34	Mo-27S	Cylindrical	6	7·5	—	Medium	1. SE $(\bar{1}01)$ 2. NE (101)	Primary With increasing deformation
35	Mo-23A	Cylindrical	2	16·0	5·1	Medium	1. (213) 2. NW $(\bar{2}13)$ 3. (112)	Scatter } Both More sharply defined } extensive Considerable scatter – Minor
36	Mo-32A	Octagonal	1	8·5	9·9	Low	1. $(\bar{2}\bar{1}1)$ 2. $(2\bar{1}1)$	Both quite extensive
37	Mo-32B	Octagonal	1	6·9	10·0	High	1. $(\bar{1}01)$ 2. $(0\bar{1}1)$	Considerable scatter – both quite extensive
38	Mo-29A	Rectangular	1	8·6	9·8	High	1. (112) 2. $(\bar{1}01)$-$(\bar{2}13)$ 3. $(1\bar{2}3)$	Primary Secondary Secondary
39	Mo-26A	Octagonal	1	8·0	14·1	Medium	1. $(3\bar{1}2)$	
40	Mo-26B	Octagonal	1	8·6	12·0	Low	1. $(3\bar{1}2)$ 2. $(2\bar{3}1)$	Primary Secondary
41	Mo-23C	Octagonal	1	8·2	8·4	Low	1. NW $(\bar{1}01)$ 2. $(2\bar{1}1)$-(101)	Scatter
42	Mo-21B	Rectangular	1	4·3	11·0	Medium	1. SE $(\bar{1}01)$ 2. (213)	Wide scatter
43	Mo-21C	Cylindrical	1	7·8	9·3	Medium	1. $(\bar{1}01)$ 2. $(0\bar{1}1)$	Primary Slightly NW – Secondary

in the crystals as grown, it was necessary to cut new orientations from samples grown in duplicate orientations. The single crystals as grown had a marked preference for specimen orientation in the cube apex of the stereographic unit triangle. The new orientations were cut from the ¼-inch-diameter crystals with the new specimen axis perpendicular to the original. Such samples were ground from the original material using a Dremel Moto-tool. Since rectangular specimens produce only two unique planes of observation, additional faces were ground on the samples when possible. After grinding, the faces of the specimens were abraded through 400-grit silicon-carbide abrasive paper followed by polishing electrolytically until all traces of cold work were removed as indicated by the appearance of Laue spots on photograms taken after polishing. A total of 43 molybdenum single-crystal specimens were tested in compression. Table 1 includes the pertinent information on these specimens and Fig. 2 shows by stereographic projection the initial orientation.

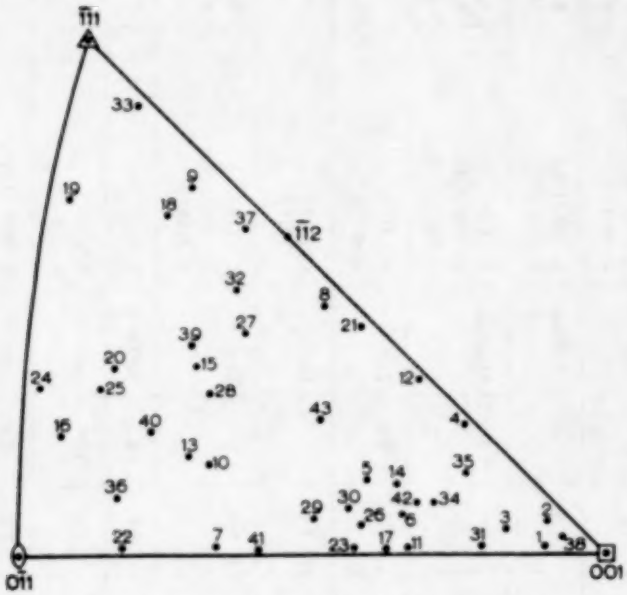

Fig. 2. Initial orientation of molybdenum crystals.

A special jig was constructed for testing small samples in compression as shown in Fig. 1 (a). Fig. 1 (d) shows the compression jig in conjunction with a universal testing machine and a SR-4 strain indicator. The applied load is transmitted to the moveable cross head from the spherically seated compression plate of the testing machine through a *T*-shaped adapter and ball bearing, as illustrated. Strain was measured by a SR-4 strain indicator or recorder using a calibrated clip-gauge arrangement activated by the upper compression cone. The design is such that the compression jig also acts as the specimen holder for Laue X-ray diffraction photograms (Fig. 1 c) as well as for microscopic examinations (Fig. 1 b) in conjunction with a research metallograph. The details of construction are such that a specimen may be placed in the holder or jig, and X-rayed before deformation at any desired position. The jig with specimen is then removed to an appropriate load-applying device where it is compressed, returned for X-ray diffraction exposures at the same or additional locations on the cylindrical surface, and then transferred to the metallograph where the complete surface can be examined in detail for the study of deformation markings. This complete programme is carried out without any direct handling of the specimen after insertion in the compression jig. Such an arrangement eliminates many of the experimental difficulties, particularly with respect to the handling of small specimens and maintaining of alignment during the several operations.

The compression cones were hard chrome plated, and greased with a high-pressure lubricant in order to eliminate frictional complications as much as possible. The specimens were compressed at rates of approximately $2{\cdot}0 \times 10^{-5}$ inch per second. Analysis of the slip trace measurements was carried out using a modified version of Barrett's method for determination of slip plane poles from slip trace normals. To evaluate the technique, the apparatus was applied to the compression of a series of aluminium crystals with results which were consistent with those of other investigators on aluminium crystals.

Results

The results from this investigation are summarized as much as possible in Table I, which includes information on the number of loadings, total compression, proportional limit, and the position of the slip plane poles as identified by slip trace analysis. General or typical behaviour for the several variations of results studied, such as slip lines, axis migration, stress-strain curves, Laue reflections, etc., was observed, and is presented in the following sections.

(a) *Slip Lines.* The general appearance of the slip lines was quite variable and was a function of the position of the observation surface with respect to the glide ellipse. This is illustrated in Fig. 3 for Specimen No. 26 (Mo-21A) after 9·0 per cent compression. Here it is seen that at approximately 90 degrees to either side of the head of the glide ellipse the slip lines are relatively straight, but that when the observation surface moves toward the head or tail of the glide ellipse the lines tend to become very wavy and irregular in appearance. This is emphasized in Fig. 3 (d) at higher magnification for an unusually well defined area on the specimen surface. The slip line photographs included herein are so arranged that the subject specimen axis is approximately perpendicular to the figure captions. Identification of the observation surface is based on the position of the head of the glide ellipse, as determined from the slip line measurements.

The presence of duplex slip marking was very typical for most of the specimens. The sharpness and intensity of these markings depended to a certain extent on the position of the specimen axis in the stereographic unit triangle. Those specimens located near any of the symmetry boundaries or in the vicinity of the cube apex exhibited very predominant duplex slip, while those more within the triangle showed it to a lesser degree. These observations indicate that the grip effect, even though precautions were taken to minimize it, influences the appearance of secondary slip lines in this work, as well as specimen orientation, since duplex slip becomes very evident even before specimen axis migrations reach a symmetry position. Reference to Table 1 will emphasize the prevalence of more than one slip system. Fig. 4 further illustrates the typical appearance of slip lines as observed for various specimens and positions. Duplex slip may be observed readily, even for specimens orientated well within the stereographic unit triangle. When the orientations are near a symmetry boundary, duplex slip markings are usually very extensive. Most frequently, the duplex slip markings were completely interleaved with one another, but occasionally the two sets alternate in intensity, sometimes on a microscale giving a patchy appearance, and sometimes on a macro scale. In this case opposite sides of the specimen slipped on different planes and the specimen, being near the (001)-($0\bar{1}1$) boundary acted essentially as a bicrystal. Three sets of slip markings were even observed infrequently and were identified for many of the specimens, but usually only two sets of markings

were observed in any one particular field of observation. Frequently, the secondary systems would increase in intensity with deformation, apparently being encouraged by favourable specimen axis migration. By contrast, occasionally the secondary systems observed after small deformations would fade away with increasing deformation as some other system became more and more pronounced.

The appearance and direction of these slip lines were easily influenced by extraneous variables, particularly when observed at a position where they appeared wavy. The presence of extraneous grains causes these lines to curve or change direction, and to change in intensity. The presence of superficial cold working, produced by abrasion or scratches, is also a factor. As commonly observed, the slip lines become very intense and well defined when crossing such a region, and

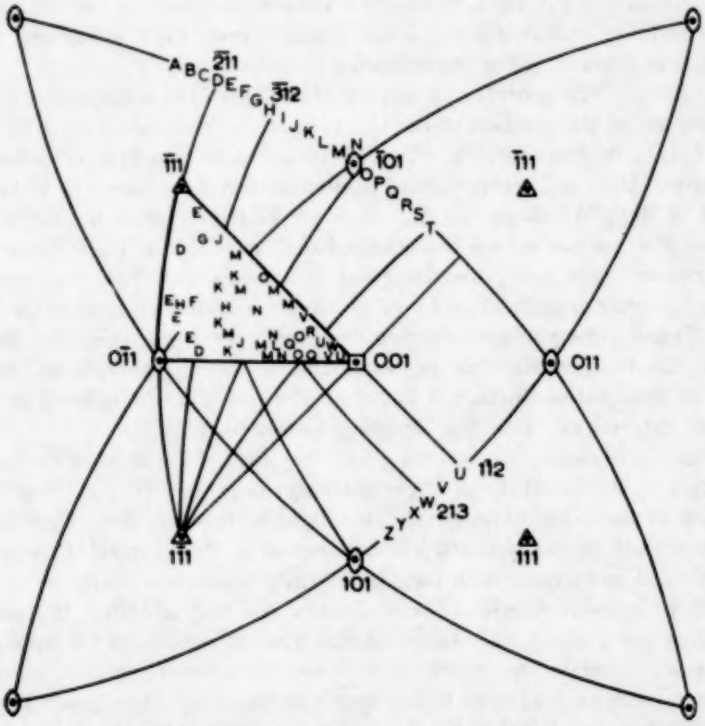

Fig. 5. Summary plot showing effect of orientation on location of primary slip-plane poles. The various letters in the unit triangle, representing specimen axis positions, correspond to similar letters on the < 111 > zones, which are the general positions of the respective slip-plane poles.

have a tendency to change direction so that they cross more nearly at right angles to the direction of the scratches. Other regions frequently showed such variations, particularly those near the ends of the specimens showing an anvil or grip effect and occasionally near the corners of ground samples. Such observations indicate that the slip traces are produced by not-very-well-defined planes.

(b) *Glide-Plane Poles.* The poles of the slip planes responsible for the surface markings or slip lines were determined stereographically from measurements

of these markings at various positions about the specimens surface. As described above, several sets of slip lines were frequently encountered, so the total number of poles that were identified are included in Table 1 along with brief information as to their relative importance. Fig. 5 is a summary plot, showing stereographically the effect of specimen orientation on the primary slip plane observed. As may be noted, the slip plane poles cannot be sharply defined. Letters are spaced along the $< 111 >$ zones and the initial orientation positions are also represented by letters; thus a particular letter in the unit triangle means that for that orientation the experimentally determined slip plane pole was in the vicinity of the corresponding letter on the $< 111 >$ zones. There is no one-one correspondence between letters in the triangle and those on the zones; the plot is to be used to convey the range or spread in poles. Here it appears that orientation is very much of a factor in determining the position of the operative slip plane pole and that there is some relation with the plane of maximum shear. Note that orientations in the cube apex showed primary slip on planes whose poles were in the $< \bar{1}11 >$ zone rather than the $< 1\bar{1}1 >$.

Specimens 2 and 7, consisting of single crystalline shells with polycrystalline cores, were studied with the idea that the restriction of the core would induce all potential slip planes to operate and be identified. However, this idea worked too well in that there were so many different and overlapping systems operating that only a couple of the more predominant ones could be identified with any degree of certainty.

As determined, the slip plane poles were not sharply defined, but due to the scatter of data, were areas frequently of several degrees diameter or more. This is in marked contrast to results found for face-centered cubic metals. This scatter is due to the waviness of the slip lines at certain positions, making accurate measurements difficult as well as to a general scatter in the angular measurements apparently due to variations in the inclination of the slip plane itself. Such variations detract from the reliability of slip-plane-pole determinations for the samples cut from cylindrical single crystals, particularly those of rectangular cross-section, due to the limited number of observation surfaces.

No attempt was made to determine the slip directions directly, but indirectly, from the position of the slip-plane-poles on or near a $< 111 >$ zone, it appears that slip in molybdenum takes place in a $< 111 >$ direction. Infrequently, the pole of a secondary slip plane was located slightly off the proper zone, indicating that perhaps the slip direction is not rigorously $< 111 >$.

(c) *Laue Reflections.* Typical changes in the appearance of X-ray Laue photograms with deformation are illustrated in Fig. 6 and 7. Such series were taken for determination of initial orientation and axis migrations with deformation. As seen from these figures, the undeformed crystals produce round, sharply defined series of spots on the Lauegrams, but with increasing deformation, these spots become more and more distorted. The distortion depends upon the number of slip planes acting. For example, Specimen 17, represented by the series in Fig. 6 was oriented on the (001)-($0\bar{1}1$) boundary, and slip was of a decidedly duplex nature. The distortion of the Laue spots was two dimensional. Specimen No. 15 was oriented in the centre of the sterographic triangle and sheared mainly on one slip plane. The spots on the resulting series of photograms (Fig. 7) tend to be

elongated rather than smeared out. As mentioned above, the distribution of duplex slip was occasionally on a macro scale, and in such cases the appearance of the spots was dependent upon the specific area covered by the beam. Two dimensional distortion of these spots also became more prevalent with increasing deformation as additional slip systems became operative and increased in intensity. It was also observed in many cases that, after considerable specimen deformation, the resulting deformed Laue spots appeared to be separating into subspots or regions of varying intensity. The heterogeneous distortion in the Laue reflections with increasing amounts of compression is indirect evidence of duplex or triplex slip-system activity and correlates well with specimen orientation and slip line observations.

(d) *Axis Migration.* The progress of specimen axis migration with deformation was followed in order to help identify the active slip planes, since, during compression, the specimen axis migration is supposed to be toward the pole of the active slip plane. Such migration was followed by means of Laue photograms taken after increments of deformation. However, such information was not so enlightening as anticipated. As long as only one slip plane was operating for the region covered by the X-ray beam, the migration was toward the pole of this plane. However, when duplex slip set in with increasing deformation it was found that the migration now took place in some new direction that was apparently a resultant due to the relative intensity of the two planes operating. Specimens so oriented that extensive duplex or triplex slip occurred from the start of deformation did not show any clear-cut migration toward any pole, but merely wandered or remained stationary. This was particularly true for specimens oriented within the cube apex of the unit triangle. Specimens located along one of the symmetry boundaries and showing duplex slip frequently had a slight resultant migration. These results, though rather inconclusive, do indicate that during compression the specimen axis tends to migrate toward the pole of the gross slip plane operating. This point is further emphasized by Specimen No. 11 which slipped on different planes on opposite sides of the specimen, thus acting essentially as a bicrystal. Here the specimen axis migration occurred in different directions on opposite sides, being toward the pole of the slip plane acting at any particular position.

(e) *Stress-Strain Relations.* The stress-strain characteristics were observed during the several loadings of the individual specimens. The proportional limit was used as a measure of the strength of the various specimens, the value of stress reported being that at which the stress-strain curve was first observed to deviate from a straight line. These values of proportional limit are also included in Table 1. No apparent correlation of specimen orientation and proportional limit was found. Since the total deformation of the various specimens was accomplished in several stages in order to follow the specimen axis migration and the development of slip systems, the overall stress-strain diagram for each specimen actually consists of as many portions as there were loading cycles. In general, stress was proportional to strain until some value of stress, termed the proportional limit, was reached after which a gradual and increasing amount of deviation occurred with increasing stress. There was a marked tendency for the stress-strain curves to assume a constant slope in the plastic region after several per cent compression.

Difficulty was encountered in reproducing the strain rates with the hydraulic

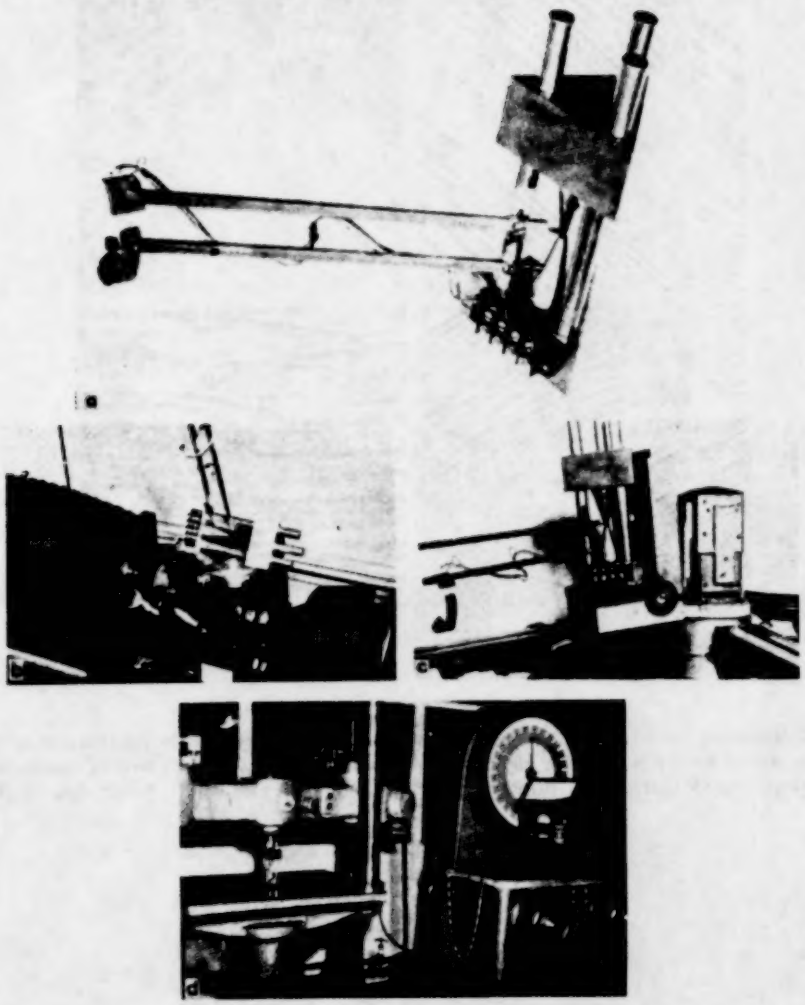

Fig. 1. Illustration of experimental technique and details. (a) Compression jig. (b) Microscopic examinations. (c) X-ray diffraction lauegrams. (d) Compression testing.

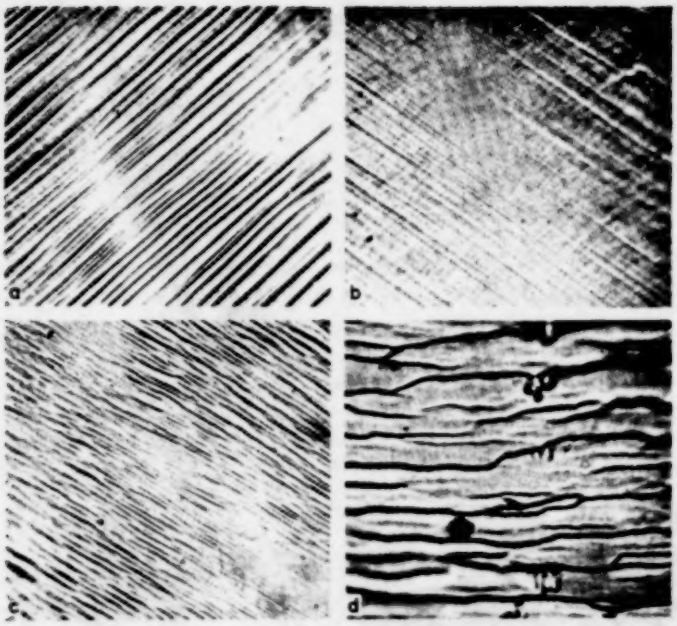

Fig. 3. Specimen No. 26 (Mo-21A), 9·0% compression. Identification of the observation surface is with respect to the head of the glide ellipse when facing the specimen. Axis of compression is vertical. (a) 85° left 330 X. (b) 86° right 330 X. (c) 46° right 330 X. (e) 6° right 1130 X.

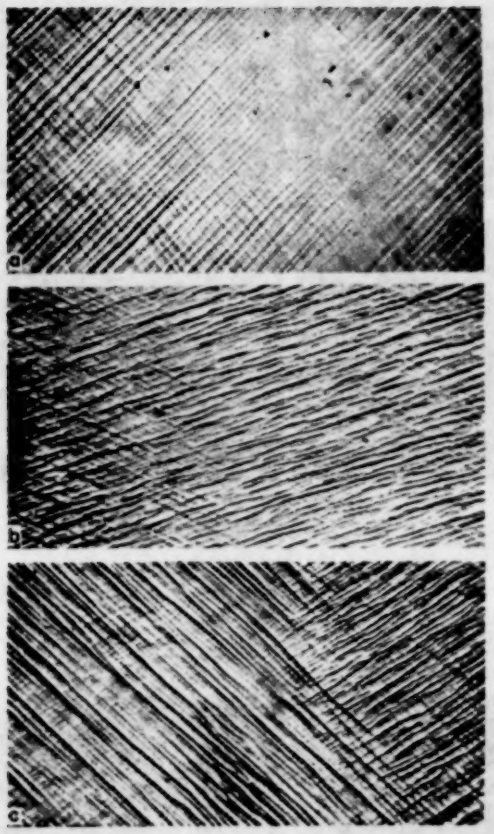

Fig. 4. Duplex slip markings in specimens oriented near symmetry boundaries. Axis of compression is vertical. 200X. (a) Specimen No. 41 (Mo-23C), 8·2% compression. 103° right (Set 1); 81° left (Set 2). (b) Specimen No. 21 (Mo-27-2), 8·5% compression. 87° right (Set 1-faint); 142° left (Set 2-wavy). (c) Specimen No. 11 (Mo-22A), 21·8% compression. 101° right (Set 1); 118° left (Set 2).

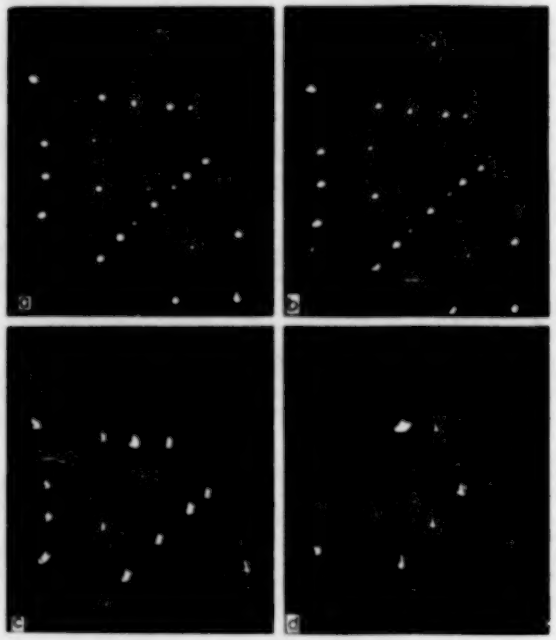

Fig. 6. Lauegrams after various steps in the compression of specimen No. 17 (Mo-27-1A). (a) 0% compression. (b) 3·7% compression. (c) 7·4% compression. (d) 11·1% compression.

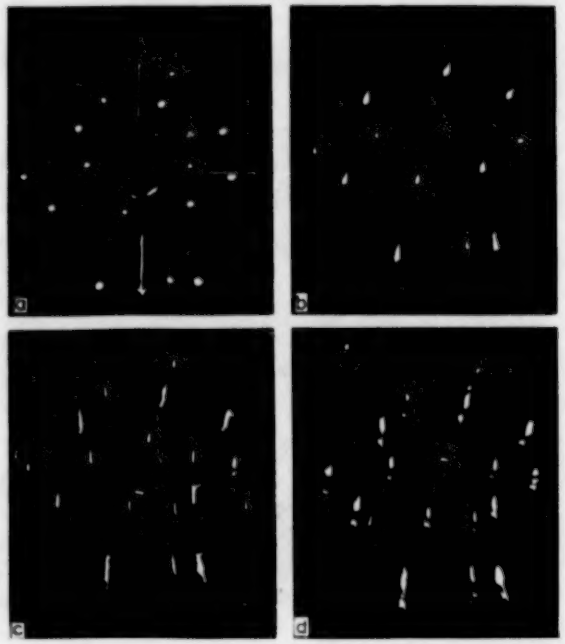

Fig. 7. Lauegrams after various steps in the compression of specimen No. 15 (Mo-22E). (a) 0% compression. (b) 3·1% compression. (c) 6·6% compression. (d) 10·1% compression.

machine since the rate of cross-head travel desired was very low and also since there was a tendency for slowing down with increasing load at such low rates, it was frequently necessary to adjust the rate during the progress of the test. Such manipulations showed that these molybdenum samples were very strain-rate sensitive. It was found that increasing the strain rate mainly causes deformation at these faster rates to occur at higher stress levels, thus affecting greatly the early parts of the curves but having much less effect on the strain-hardening rate. An increase in the rate of deformation during test would cause a sudden shift in stress to higher values with relatively little deformation.

In general, the molybdenum single crystals also showed a marked tendency for recovery after deformation. This was observed to occur between loadings while the specimens were being X-rayed and examined microscopically. Following such an interval upon reloading the stress strain curve deviated from linearity at stress values well below the previous maximum. This deviation or measured proportional limit for the various loadings was also highly influenced by strain rate, which undoubtedly contributed greatly to the wide range of scatter of values. Unfortunately no study was made of the rate of recovery.

It was observed from the stress-strain data that although all specimens showed strain hardening, there was a considerable variation in these rates of strain hardening. Qualitatively these rates were broken down into classifications of low, moderate and high rates of strain hardening at approximately equal values of strain (0·05 strain). A definite orientational effect was found for this breakdown. There is a definite tendency for samples in the $(0\bar{1}1)$ apex of the stereographic triangle to show low and those in the $(\bar{1}\bar{1}1)$ apex high rates of strain hardening. The strain-hardening rates involved were of the order of magnitude of 1·5 to $10{\cdot}0 \times 10^{-5}$ psi.

4. Discussion of Results

Crystal orientation within the stereographic unit triangle appears to be very much of a factor in determining the position of the primary glide plane pole as shown in Fig. 5. Such a possibility was not considered by many of the previous investigators studying the deformation of body-centred cubic metals and probably led to premature conclusions due to incomplete evidence. The slip planes observed in the present work are not restricted to any specific plane or planes of rational indices. From observed positions and degree of scatter they seem to be non-crystallographic or semicrystallographic in that their poles may occur at any position along one of the four $< 111 >$ zones. According to Opinsky and Smoluchouski's calculations (1951), two slip directions are predicted – $(1\bar{1}1)$ and $(\bar{1}\bar{1}1)$ for samples in the unit triangle depending upon orientation. Orientation in the cube apex should shear in the $(\bar{1}\bar{1}1)$ instead of the more common $(1\bar{1}1)$ direction, which was observed as seen in Fig. 5. The effect of orientation on the position of the primary slip plane pole is such that the pole migrates along the $< 1\bar{1}1 >$ zone roughly parallelling that of the minimum shear plane. However, when considering individual samples, rather seldom does that slip plane coincide with the maximum shear plane. If the critical resolved shear stress for slip for planes in this zone varies as postulated by Opinsky and Smoluchouski, Brick, and others, there should be an observed clustering of the slip plane poles about

the position of the plane of minimum shear strength. Such a preference was little evident except perhaps for a position slightly northwest of ($\bar{1}01$). There is the possibility that in the present work of compression testing, the restriction of the anvils or grip effect may have tended to mask such boundaries particularly if such variations of shear strength along a $< 111 >$ zone are slight.

Well-defined slip planes were not observed. There was always a considerable degree of scatter or variation in the position of the slip plane poles as determined from slip trace measurements. Thus the slip plane is not very rigorously defined and its position should be easily influenced by external variables. This was found to be the case, as illustrated by the influence of extraneous grains and prior deformation and also similar variations frequently observed near the ends due to anvil or grip effect and edges of cut samples. Such observations and measurements indicate strongly that the slip planes in molybdenum are noncrystallographic in that they cannot be completely defined by rational indices. However, these observations do not indicate whether or not the bulk slip traces may be caused by co-operative {110} or {112}-{110} slip.

In general, duplex slip and the appearance of secondary slip systems were very evident throughout this investigation. Such systems were frequently observed, even though their resolved shear stress was low, and the specimen axis had not migrated to a symmetry position. Apparently, the occurrence of these additional systems was premature and mainly due to a grip or anvil effect associated with compression testing. Precautions were taken to minimize such factors by the use of chrome-plated anvils and a high-pressure lubricant. It was impossible to isolate the grip effect further by the use of longer specimens due to buckling which was observed in specimens with a length-to-diameter ratio greater than two. Thus, the unit triangle could not be divided into sharply defined regions according to the active slip planes observed. From the discussion above however, it appears that such well-defined boundaries do not exist.

Study and measurements of slip traces will not, of course, define the slip directions completely, but the repeated occurrence of the slip-plane poles on $< 111 >$ zones is excellent indirect evidence that slip does take place in the $< 111 >$ direction In almost all cases, even for secondary and tertiary systems, the slip-plane poles fell on one of the four $< 111 >$ zones. However, since the poles themselves are not sharply defined as discussed above, it is still possible that the slip directions are not uniquely $< 111 >$.

It appears that the term slip plane is a misnomer, because shear does not take place along any such well-defined region as a plane, but rather along some general zone of weakness containing the $< 111 >$ direction, the choice of which depends upon the position of the maximum shear stress plane, the variation of shear strength along the $< 111 >$ zone, and the possible influence of extraneous variables. These observations are in good agreement with early work reported by Elam and co-workers, as well as with some of the general results reported by Brick and co-workers with respect to the first theory listed in the early part of this paper. However, no direct evidence was found to discredit the theory that slip may be due to some co-operative arrangement of shear on nonparallel planes containing a mutual slip direction.

From the shape of the various stress-strain diagrams, it was seen that the general reactions of the various specimens to stress was quite similar. None of the specimens was compressed to failure, though they were compressed varying amounts up to 22 per cent, illustrating that these single crystals have considerable ductility. The proportional limit was used as a strength criterion, but no correlation with orientation was observed, however, though there should be a measurable variation, when considered on the basis of equal values of critical resolved shear stress on the maximum shear stress planes containing the $< 111 >$ direction. The maximum strength predicted would be in the octahedral apex of the unit triangle. The scatter in values measured was considerably greater than that predicted by variations in the shear-stress factor, and there appears to be no correlation with orientation. This scatter in the measured values of proportional limit was apparently due to variations in strain rate, since the crystals were found to be very strain rate sensitive, and also showed a marked tendency toward recovery. That is, if duplicate samples were loaded at different rates, the stress-strain curve for the one loaded at the faster rate would be displaced in the stress direction, and yield higher values for the various strength criteria. Such strain-rate and recovery effects may not be unusual for commercial pure molybdenum. The material used in this investigation did show a trace of carbon, and no analyses were made for gaseous elements such as oxygen and nitrogen, which may well be responsible for such observations.

During plastic deformation, the stress-strain curves were frequently found to decrease in slope to a constant value after several per cent strain. The slope of this straight-line portion is taken as a measure of the strain-hardening rate, while the tangent at comparative values of strain is used for other specimens. As mentioned above, strength values were greatly influenced by strain rates, but strain-hardening rates were much less affected, and values of strain-hardening rates are a more intrinsic property of the specimens than strength values. These strain-hardening rates were also observed to vary considerably from specimen to specimen and were orientational dependent as previously described. From the slip-trace observations, the reason for such a distribution appears rather obscure. There was no observed correlation with the number of identified slip systems operating, for if such were the case, samples orientated in the cube apex and along the boundaries would be expected to show the high rates of strain hardening. Also, there is no correlation with the position of the primary slip plane, for, if such were the case, both the high and low regions would be expected to have the same strain-hardening rate. Also no correlation was observed with the combination of planes or slip directions for the primary and secondary slip systems. Possibly some relation exists with respect to separation of the duplex slip-plane poles as measured stereographically. When the separation of the duplex slip-plane poles tends to be a minimum such as along the northwest sections of the $< 1\bar{1}1 >$ and $< \bar{1}11 >$ zone, high strain-hardening rates were observed, while low rates were observed when the separation was a maximum, such as along the northwest section of the $< 1\bar{1}1 >$ and southwest section of $< \bar{1}\bar{1}1 >$ zones. In other words, it appears that when the duplex planes make small angles with the stress axis, strain-hardening rates are low, and if these angles are large, strain-hardening rates are high.

5. CONCLUSIONS

The results from the compression of the body-centred cubic metal molybdenum indicate that deformation does not occur by shearing on any specific plane of rational indices. Instead, the slip process may be considered semicrystallographic in that slip takes place in a $< 111 >$ direction, but on no specific plane of rational, or even irrational, indices. The so-called slip planes can hardly be considered as planes, as shown by the scatter of results, variable appearance of slip traces, and susceptibility to external influences. Thus, deformation takes place in $< 111 >$ directions along generally defined zones of weakness which are determined by such factors as stress axis orientation or position of the maximum shear-stress plane containing a $< 111 >$ direction, some unknown distribution of shear strengths of planes containing this $< 111 >$ direction, and the presence of external influences such as extraneous grains, specimen geometry, grip or anvil effects, and prior deformation.

During compression, specimen axis migration is toward the pole of the gross slip plane responsible for the slip markings. Duplex slip produces a rotation which is some resultant of the two directions toward the respective poles. The degree of distortion of the Laue reflections with compression is increased by the presence of additional slip systems, and is by no means homogeneous, the Laue spots showing a considerable amount of structure.

Molybdenum single crystals have considerable ductility and their reactions to deformation show a high degree of strain-rate sensitivity and a considerable tendency toward relaxation at room temperature after deformation. Strain hardening rates are orientational dependent, being highest in the octahedral and lowest in the dodecahedral apices of the stereographic unit triangle.

ACKNOWLEDGMENTS

The discussions and help of Professors N. K. CHEN and R. B. POND are gratefully acknowledged, as was the aid of Miss D. SHAEFFER in growing the crystals. This research was sponsored by the Office of Naval Research.

REFERENCES

CHALMERS, B. and MARTIUS, U. M. 1952 *Proc. Roy. Soc.* **A213**, 176.
CHEN, N. K. and MADDIN, R. 1951 *Trans.* AIME, **197**, 1131.
CHEN, N. K., MADDIN, R. and POND, R. B. 1951 *Trans.* AIME, **191**, 461.
ELAM, C. F. 1936 *Proc. Roy. Soc.* **153**, 273.
GRENINGER, A. B. 1938 *Metals Tech.* **5**, 892.
OPINSKY, A. J. and SMOLUCHOWSKI, 1951 *J. Appl. Phys.* **22**, 1380 and 1488.
STEIJN, R. P. and BRICK, R. M. 1954 *Trans.* ASM, **46**, 1406.
TAYLOR, G. I. and ELAM, C. F. 1926 *Proc. Roy. Soc.*, **A112**, 337.
VOGEL, F. L. and BRICK, R. M. 1953 *Trans.* AIME, **197**, 700.

Journal of the Mechanics and Physics of Solids, 1956, Vol., 5 pp. 41 to 56. Pergamon Press Ltd., London.

STRETCH FORMING UNDER FLUID PRESSURE

By P. B. Mellor
Department of Mechanical Engineering, The University of Sheffield

(*Received 30th July*, 1956)

Summary

An account is given of an experimental investigation into the hydrostatic bulging of circular metal diaphragms. The development of strain and of instability is studied, and a strain-hardening characteristic is derived for each of the materials tested. Experimental results are correlated with theoretical predictions of instability, and in the case of half-hard aluminium with theoretical predictions of the general strain geometry of the bulge.

1. Introduction

The stretch forming of a thin circular sheet of metal by fluid pressure provides a means of studying strains under biaxial tensile conditions and also, if measurements are taken over the strained surface, of obtaining a strain-hardening characteristic of the material. This manner of stretch forming sheet metal is one of the simplest to be found in practice and the most amenable to mathematical solution.

A large volume of experimental work on this subject was carried out by American investigators (Brown and Sachs 1948; Brown and Thompson 1949 and others) during and after the war, but no detailed comparison was made between strain-hardening characteristics of the same material obtained by different methods of straining, nor were mathematical solutions based on the theory of plasticity available at that time.

Hill (1950) developed a theory which predicts the strain development across the bulge for a material with a linear strain-hardening characteristic, and Swift (1952) obtained a solution for the strain at instability. In the present paper experimental results are correlated with these theories.

The purposes of the present investigation have been :

1. To examine the credentials of a potentially new means for obtaining a strain-hardening characteristic for sheet metal.
2. To examine the validity, over its applicable range, of Hill's theory for the general strain geometry of the bulge.
3. To ascertain to what extent theory is capable of predicting the condition of instability under biaxial tension.

The following assumptions and limitations have been made in interpreting the experimental results :

1. The normal principal stress is negligible compared with the principal

stresses in the plane of the sheet. In other words straining takes place under conditions of plane stress.

2. The flexural effect of the peripheral clamping may be neglected, i.e. the stiffness of the sheet is negligible.
3. The material is isotropic initially and remains so throughout the deformation.
4. The material is incompressible, i.e. there is no volumetric change during straining.

2. APPARATUS AND PROCEDURE

The apparatus (Fig. 1) was designed to produce a 10-in.-diameter bulge on sheet metal of approximately 20 s.w.g. and to withstand working pressures up to 1500 lb. per sq. in. The design was intended to allow a small thickness-to-diameter ratio, thus reducing the effects of flexural stiffness and keeping the experimental pressures as low as possible for a given gauge of material. Precautions were taken in the design of the apparatus and in the methods of measurement, to ensure precision and especially consistency in the results, since their significance depends on small increments, and the standards of measurement in some of the earlier American work were scarcely commensurate with its purpose. For this reason the methods of measurements are here described in some detail.

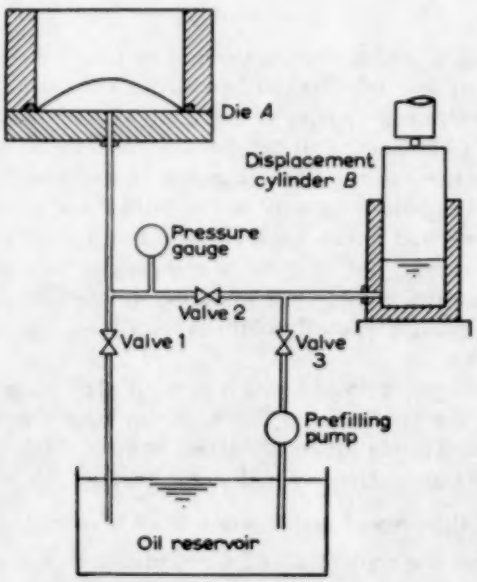

Fig. 1. Layout of apparatus.

The die is of simple but robust construction. The upper portion consists of a hollow steel girder of 2½ in. wall thickness. The material to be tested is securely clamped between this upper cylinder and the steel base-plate by means of twelve 1-in.-diameter studs and bolts. Oil is supplied, under pressure from a displacement cylinder, through a hole in the centre of the base-plate, and an oil-tight joint is ensured by a clamping ring on the baseplate and a mating groove in the cylindrical body. The die ring is a push fit in the body and has a profile radius of ¼ in., which was found to be the suitable minimum radius which would obviate shearing on the profile of the die of all the metals tested.

In preliminary tests the oil under pressure was supplied from a large hydraulic accumulator through a reducing valve, and a smaller (pressure-gauge-testing) type of hydraulic accumulator was included in the oil feed line between the reducing valve and the test sheet to enable predetermined constant pressures to be maintained for a convenient length of time. It was found that even at loads much smaller than that known to induce failure, excessive creep occurred. This is clearly seen from Fig. 2, which shows the effect of creep, with the duration of load application, on the bulge profile of a half-hard aluminium specimen subjected to a pressure of 126 lb. per sq. in., which is 75 per cent of the load known to induce failure.

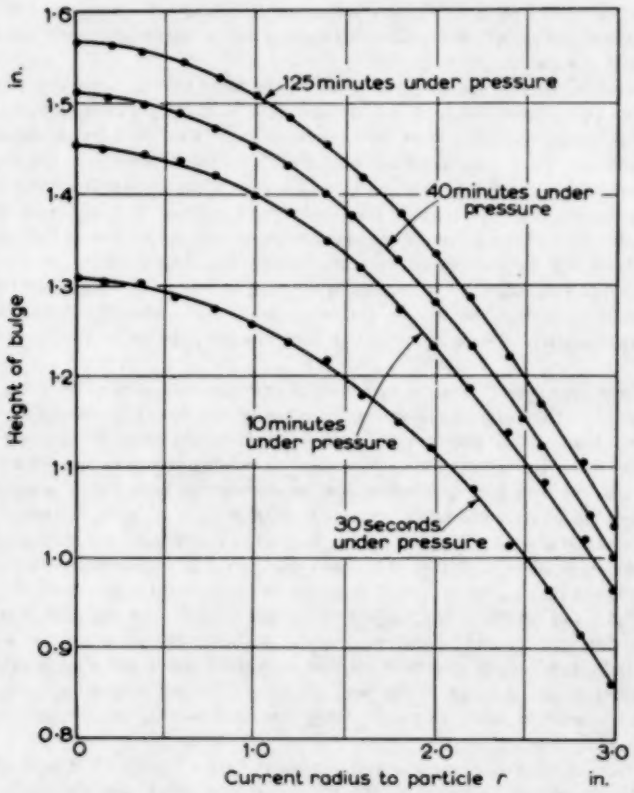

Fig. 2. Effect of creep on bulge profile.

In order to reduce creep to a minimum and to allow closer control of the oil feed, the large hydraulic accumulator was dispensed with and a small oil-displacement cylinder, fitted into a universal multilever testing machine, used in its stead. With this arrangement the oil pressure, for a given rate of testing, depended entirely on the resistance of the sheet metal to deformation. An oil flow of 11·3 cu. in. per minute was chosen as giving a convenient period for the completion of the test, allowing time for simultaneous readings of oil pressure and polar height, and being comparable with the possible rate of straining in the tensile tests on the material. The time taken to fracture any specimen therefore depended only on the material, varying from nine minutes for half-hard aluminium to twenty-one minutes for softened stainless steel.

Four sets of measurements were made in this work : oil pressure, circumferential (hoop) strain, thickness strain across the bulge, and profile. This last included radius and depth from the centre or pole of the specimens. Before any measurements were taken the oil pressure was released. This of course enabled measurements to be made without fear of creep, and it was shown by taking

readings for both continuous and interrupted tests that it made no appreciable difference in the results. The oil pressure was measured by a pressure gauge set near to the die. To ensure accurate readings of pressure four calibrated gauges were used to cover the range 0-1,500 lb. per sq. in.

The datum lines for the hoop strains were concentric ink circles drawn from the centre of the blank at radial intervals of approximately 0·2 in. Special care was taken in locating the geometric centre of the blank when mounted in the apparatus, and a patch of perspex was used to protect this centre from indentation while the circles were being drawn.

The surfaces of the blanks were cleaned with trichlorethylene, and it was found that, if the cleaned surface was faintly smeared with ink, the ink circles could be drawn easily on this base. This simple method produced satisfactory results, and since the total number of blanks required was not large, it was considered unnecessary to have recourse to the photogrid method (BREWER and GLASSCO 1941 ; JACKSON 1948).

If r_0 is the initial horizontal distance of a point on the test piece from the centre and r its final distance, then the logarithmic hoop strain is defined as $\epsilon_h = \ln (r/r_0)$. Hoop-strain measurements at any stage of bulging were taken over the upper surface of the blank by means of a travelling microscope, graduated to 10^{-4} in., positioned by dowels on the top surface of the upper portion of the die. Measurements were taken on the outside edges of the ink circles along two diameters at right angles, one diameter lying along the direction of rolling. Measurements were taken on the original blank before straining and at as many intermediate stages during bulging as required. The four sets of readings were averaged, to minimize any anisotropic effect, and the mean curves were plotted for half the bulge, a typical example being shown in Fig. 4. Since the bulge is intrinsically symmetrical about the centre, the hoop-strain curve should cut the prime ordinate of the graph orthogonally. Use is made of this fact in extrapolation of the hoop strains to the pole.

Measurements of thickness were made by means of a simple dial-gauge micrometer jig graduated to 10^{-4} in. The mean thickness of the undeformed blank was found by taking eight readings at points around the blank ; the difference between readings on any sheet never exceeded 0·0005 in. To measure the thickness strains at a given stage of bulging the pressings were removed from the apparatus and cut into four quadrants, and measurements were taken along the same two diameters as for hoop strain. Thickness strain is defined as $\epsilon_0 = -\ln (t_0/t)$ where t_0 is the initial and t the current thickness of the sheet (where it is more convenient the absolute magnitude of the thickness strain is plotted). It will be seen that a set of thickness measurements at any intermediate stage of bulging involves the destruction of the sheet under test.

The polar height and profile of the bulge were measured with the aid of a depth micrometer mounted on a saddle which could be traversed across the bulge by means of a 20 t.p.i. micrometer screw. When the pointer made electrical contact with the bulge surface an indicator lamp was lit and this obviated any damage to the test specimen. Height recordings were taken across the bulge, at horizontal intervals of 0·2 in., along the same two perpendicular diameters as the strain measurements.

To measure the radius of curvature at the pole and to show the trend of radii of curvature at other points, the general method used by BROWN and SACHS (1948) was adopted. Average radii of curvature were measured for various chord lengths, and the radius at the pole was obtained by extrapolation. Each of these radii was calculated from the chord length and its corresponding sagitta, neglecting any deviation of the arc from a circle. If d is the vertical distance of a point from the pole and r its horizontal distance from the pole, then it is easily shown that the radius of the circle passing through the pole and the given point and having its centre on the axis of symmetry is $\rho = (r^2 + d^2)/2d$ (Fig. 5).

3. EXPERIMENTAL WORK

(1) *Variation of Polar Height with Oil Pressure.* Before any detailed tests, the capabilities of each material were ascertained by examining the behaviour of an unscribed blank under continuous loading up to the point of fracture. The polar height was measured by means of a dial gauge with 2 in. travel, fitted with extension pieces, mounted vertically and in a central position over the bulge. Simultaneous

readings of polar height and oil pressure were taken. The results are shown plotted in Fig. 3 and give some idea of the wide range of physical properties of the materials tested.

Instability of the material is said to occur if straining in any region is able to continue at constant or decreasing oil pressure. From Fig. 3 it is seen that only the annealed materials and half-hard copper developed such a condition of instability; the other materials fractured while the hydrostatic pressure was still increasing.

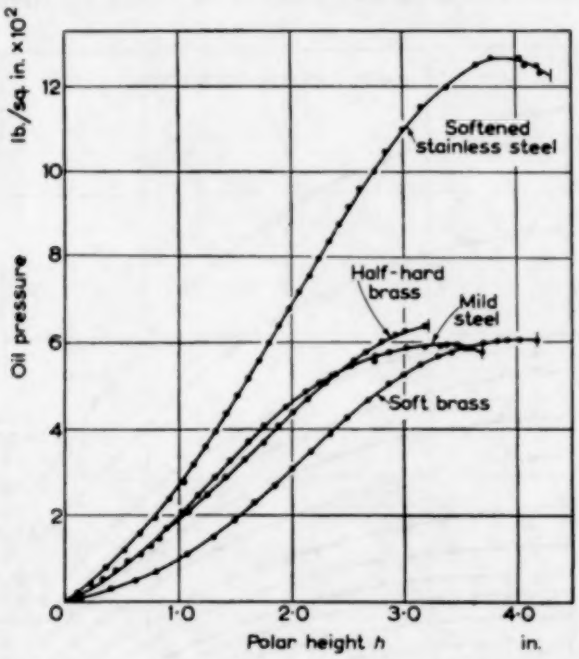

Fig. 3. Oil pressure – polar height diagrams : continuous testing to fracture.

For an isotropic blank of uniform thickness the maximum thinning would be at the pole of the bulge, and it would be expected that fracture would occur at this point. In practice the fracture was found to occur within a region up to 1·5 in. from the pole, and to extend in the direction of rolling for approximately equal distances on either side of the pole. Some of the copper and brass pressings exhibited a pin-hole fracture, the cause of which was ascribed to initial defects in the material. Where such failures took place the results were ignored and repeat tests were made on other specimens.

(2) *Distribution of Strains.* Typical curves showing the distribution of hoop strains for half-hard brass are plotted in Fig. 4. Measurements are taken up to a radial distance of approximately 3·6 in. from the pole, and it will be noticed that the strain increases from the die edge and is maximum at the pole. Also, the curves are of the same general form at all stages of the test. In a limited number of cases hoop and thickness measurements were made across the entire pressing. The curves of results for annealed copper, killed steel, and lead, present a similar appearance.

It was observed that for all these metals there was an appreciable thickness strain in the region of the die. These results differed from those for a severely cold-worked material such as half-hard aluminium (Fig. 13) where the thickness strain at the die is exceedingly small.

Considerable scatter was found in the thickness-strain measurements for the lead bulge, because the metal developed an ' orange peel ' effect during the straining. This roughening of the surface, which was not obtained with killed mild steel and soft copper, was reflected in the consistency of their thickness strains.

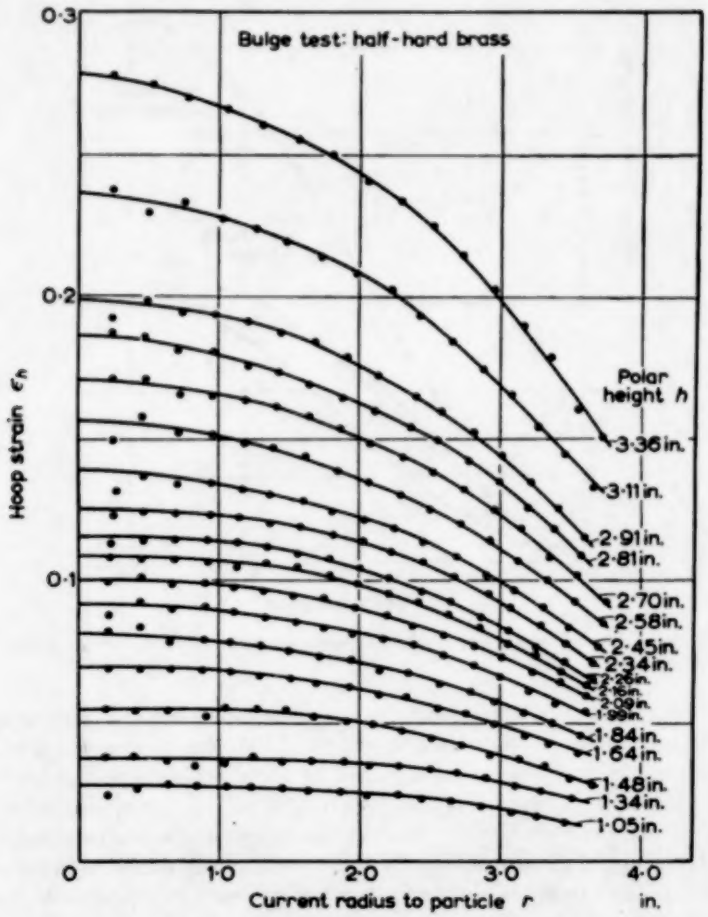

Fig. 4. Distribution of hoop strain for half-hard brass.

Because of the symmetrical nature of the bulge there is a state of balanced biaxial tension at the pole, which means in effect that the hoop strain ϵ_h is equal to the radial strain ϵ_r, and to half the thickness strain, $-\epsilon_t$. Therefore, taking into account the scales on which the hoop and thickness strains are plotted, each pair of curves in Fig. 13 should coincide at the pole (i.e., when $r = 0$). Part of the discrepancy is no doubt due to experimental error in determining the strains, but

it must be remembered that the effect of anisotropy may not have been taken fully into account by averaging of the strains in different directions.

3. *The Geometry of the Bulge.* The shape of a hydrostatic bulge depends mainly on the ratio between metal thickness and die diameter, but it may be modified by the profile radius of the die, which has the effect of slightly decreasing the effective diameter of the blank as the polar height increases. From the plot of the profile it would appear that, except in the proximity of the die edge, the bulge is spherical in shape, but by taking values of computed radii of curvature it is possible to detect a divergence in shape from the truly spherical.

This is shown in Fig. 5 for the case of half-hard 70/30 brass. It is seen that at small strains the curves have negative slopes, indicating that the radius of curvature decreases from the pole. With increasing strain the slope gradually approaches zero, indicating uniform curvature, and with still further strain the slope of the curves increases in a positive direction, showing that the radius of curvature is least at the pole. This behaviour is identical for all materials and may be caused by the clamping conditions. Similar results were noted by Brown and Thompson (1949).

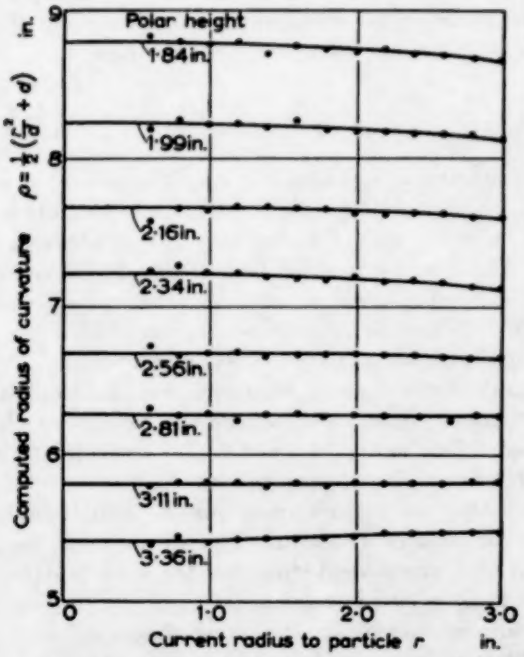

Fig. 5. Determination of polar radius of curvature for half-hard brass.

Within a distance of 2·0 in. from the pole the derived radius of curvature is constant for a given height, and the polar radius of curvature could be estimated with some confidence by extrapolating the measurements in this region to zero radius. On grounds of consistency it is thought that the values obtained for polar radii of curvature less than 10 in. are correct to within 0·2 in.

(4) *Strain-hardening Characteristics.* At the pole of the bulge the relationship between the internal pressure p, the hoop stress σ_h, the radius of curvature ρ and the current thickness t is given by $p = 2\sigma_h t/\rho$ where p is measured directly, and ρ and t are derived from the profile and hoop strain measurements respectively. Hence the biaxial stress σ_h can be derived. By correlating this with a representative strain based on measured hoop and thickness strains we can obtain a strain-hardening characteristic for the material in the vicinity of the pole.

By adopting an appropriate system of representative stress and strain the strain-hardening characteristics obtained in the above manner can be compared with strain-hardening characteristics of the same material obtained under different stress systems. It has been suggested (Swift 1946) that all stress-strain data should be evaluated in terms of q, the root-mean-square shear stress, and ψ, its natural strain analogue defined by the relations

$$q^2 = \tfrac{1}{12}\Sigma(\sigma_1 - \sigma_2)^2, \qquad (\delta\psi)^2 = \tfrac{1}{12}\Sigma(\delta\epsilon_1 - \delta\epsilon_2)^2.$$

If the principal stresses are taken in descending algebraic order, in plane stress $\sigma_3 = 0$ and $\sigma_2 = x\sigma_1$ where the stress ratio x is a proper fraction. In cases where x is constant during straining (e.g. in a tensile test to necking or at the pole of a circular bulge) the assumptions of constancy of volume and the Lévy-Mises law lead to the following relations between the total strains :

$$\frac{\psi}{\sqrt{3(1 - x + x^2)/2}} = \frac{\epsilon_1}{2 - x} = \frac{\epsilon_2}{2x - 1} = \frac{-\epsilon_3}{1 + x}.$$

In the normal tensile test $q = \sigma_1/\sqrt{6}$ and $\psi = \epsilon_1\sqrt{(3/8)}$ where σ_1 is the longitudinal stress and ϵ_1 the longitudinal logarithmic strain. Under biaxial tension at the pole of a circular bulge $q = \sigma_h/\sqrt{6}$ and $\psi = \epsilon_h\sqrt{(3/2)}$ where σ_h is the hoop stress and ϵ_h the hoop strain, which is equal to half the thickness strain ϵ_t; i.e. $\psi = \epsilon_t\sqrt{(3/8)}$. In the case of cold rolling with inhibited spread (that is, deformation under plane strain) q cannot be determined directly, but $\psi = \epsilon_1\sqrt{2}$ where ϵ_1 is the longitudinal strain (equal to the thickness strain $-\epsilon_3$).

With this method of stress-strain representation the strain-hardening characteristics of 70/30 brass, copper, and aluminium have been obtained from the ' bulge test ' and are shown in Figs. 6, 7 and 8. The strain-hardening characteristics for the half-hard tempers were superimposed on the curves for the respective annealed materials and, making allowance for the initial strain, the two curves have in each case the same general form. This signifies that the plastic properties of these materials at a given yield-stress are the same whether they have been cold-worked by rolling or biaxial tension.

These curves are compared, in the same diagrams, with strain-hardening characteristics obtained from tensile tests taken to the point of necking. It is seen that, although the tensile tests on the annealed materials show a very similar characteristic to stretch forming, the necking point in simple tension occurs at a far lower strain than is the case in stretch forming. In order to obtain some comparison beyond the point of tensile necking, the materials were first strain hardened by rolling and then tested in tension (Ford 1948). The technique adopted was as follows : 3-in.-wide strips of the material were cut from the parent sheet in the direction of rolling, and rolled successively in approximately 10 per cent

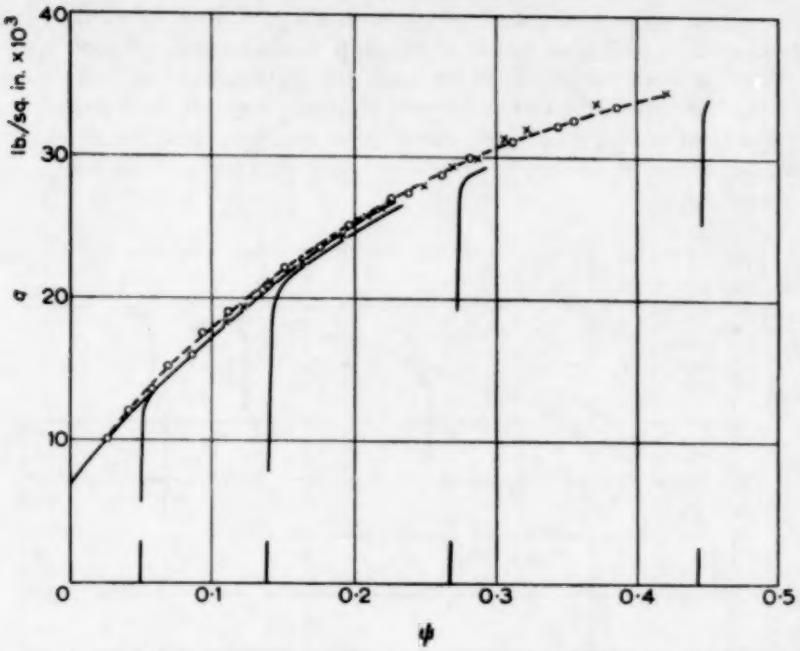

Fig. 6. Strain-hardening characteristics for 70/30 brass. O – soft brass, X – half-hard brass, from bulge test. Full-line curves obtained by rolling and testing in tension.

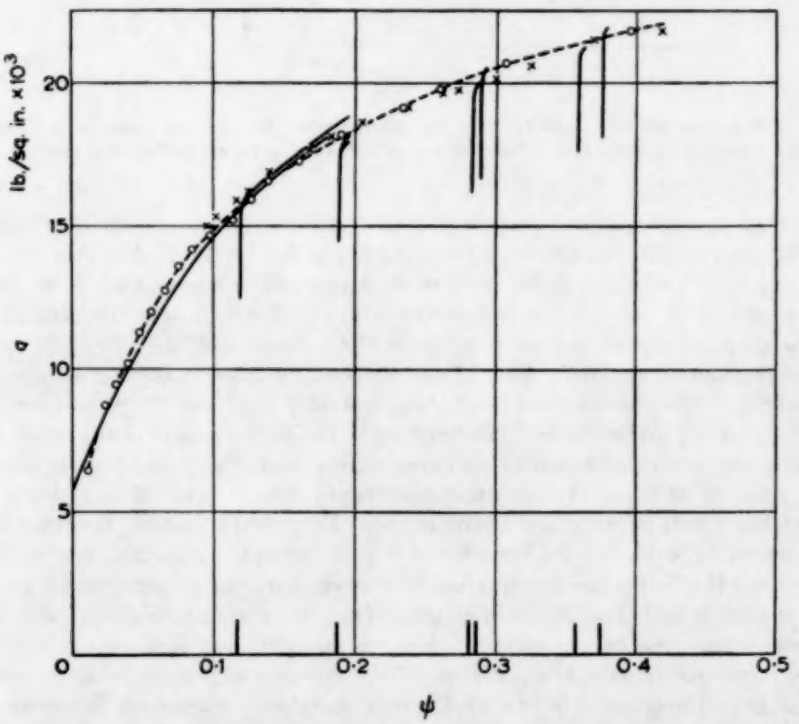

Fig. 7. Strain-hardening characteristics for copper. O – soft copper, X – half-hard copper, from bulge test. Full-line curves obtained by rolling and testing in tension.

reductions, one strip being taken out of the batch after every reduction. (It was ascertained that the lateral spread of the strip was negligible.) Tensile specimens were then cut from the centre of the strip and tested in the normal manner, at least two specimens being tested for each temper. It will be seen from Figs. 6, 7 and 8 that there is quite good agreement between the stress-strain relations obtained by biaxial tension and plane compression plus tension for 70 30 brass, copper, and aluminium.

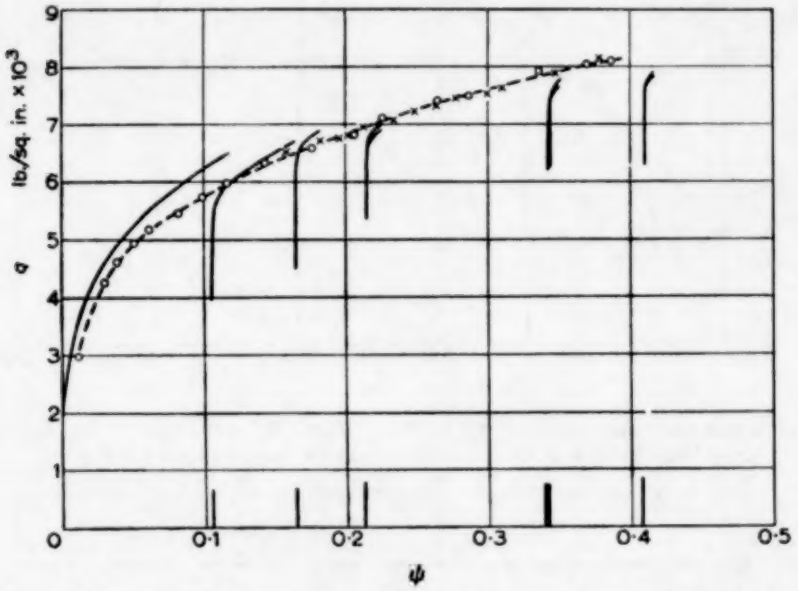

Fig. 8. Strain-hardening characteristics for aluminium. O – soft aluminium, X – half-hard aluminium from bulge test. Full-line curves obtained by rolling and testing in tension.

For the purpose of easy analysis it is convenient to fit some empirical equation to the curves. A suitable equation, suggested by SWIFT (1952), has the form $q = c\,(a + \psi)^n$ where q is the root-mean-square shear stress and ψ its natural strain analogue. In this expression for strain-hardening c sets the general scale of the relation, n is an inverse measure of the decrement of the rate of hardening, and a depends on the initial state of the material, its value increasing with previous overstrain. The method of fitting the equation $q = c\,(a + \psi)^n$ to a stress-strain curve is an approximate one intended to give the best result over the whole range of straining. A comparison of an experimental and empirical curve is shown in Fig. 9 for 70/30 brass. The greatest discrepancy is in the case of annealed copper, which has a well-rounded stress-strain curve. Empirical equations for other metals are shown in Table 1. In the case of a fully annealed material, $a = 0$ and we then have the better-known equation to a strain-hardening characteristic $q = c\psi^n$. By plotting q and ψ on logarithmic scales (Fig. 10) the empirical equations in the annealed form can be represented simply as straight lines of slope n.

(5) *Experimental Instability Strains.* The instability of plastic strain under plane stress is of importance in stretch-forming operations because it determines the

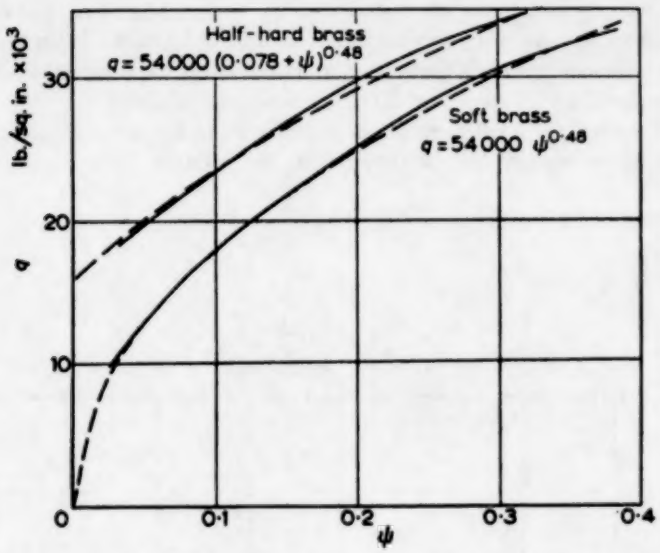

Fig. 9. Empirical strain-hardening characteristics for 70/30 brass. ———— from bulge test, – – – – – – – $q = c\,(a + \psi)^n$

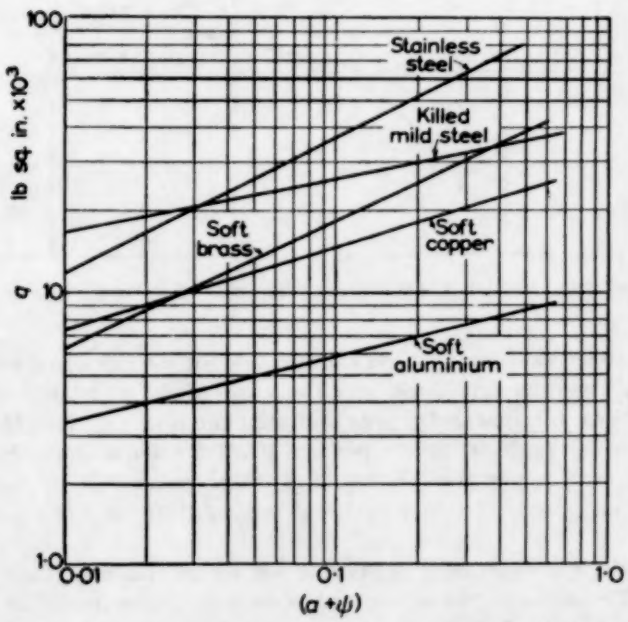

Fig. 10. Empirical curves $q = c\,(a + \psi)^n$, expressed logarithmically.

degree of thinning which the sheet can undergo before fracture. Values of polar-thickness strain at instability can be determined from a graph of this strain against oil pressure. However, since this method gives only approximate values, a graphical solution proposed by BROWN and SACHS (1948) was adopted.

As stated earlier, the conditions at the pole are given by the equation $p = 2\sigma_h t/\rho$. The instability condition $dp = 0$ then yields the relation

$$\frac{d\sigma_h}{\sigma_h} - \frac{d\rho}{\rho} + \frac{dt}{t} = 0$$

which may be written

$$\frac{1}{\sigma_h} \cdot \frac{d\sigma_h}{d\epsilon_t} = \frac{1}{\rho} \cdot \frac{d\rho}{d\epsilon_t} - 1$$

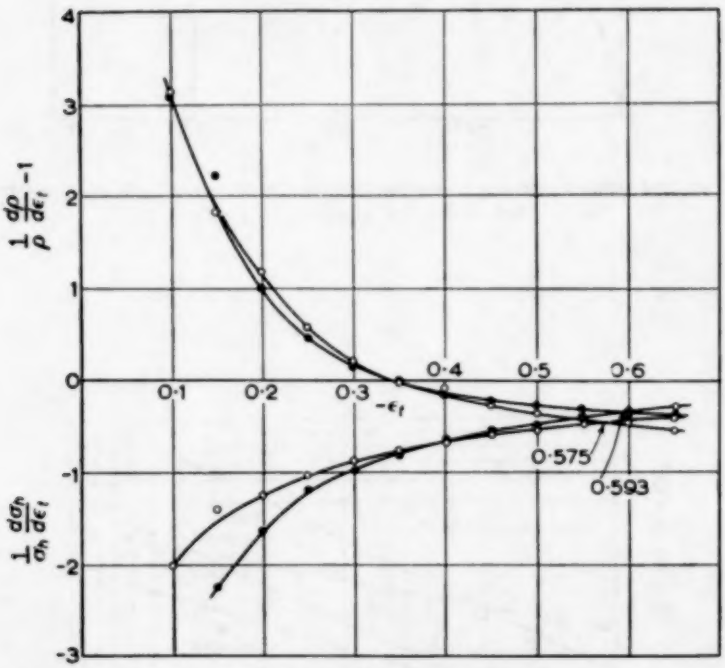

Fig. 11. Experimental instability strains from bulge test. ● soft copper, ○ soft aluminium.

where ϵ_t is defined as $-\ln(t_0/t)$. If the two sides of the last equation are plotted in terms of ϵ_t the intersection will give the value of the instability strain. Such curves are shown for annealed copper and aluminium in Fig. 11. The instability strain is shown to be 0·593 for copper and 0·575 for aluminium. Failure of the curves to intersect before fracture would of course mean that no instability had occurred. This was so for annealed and half-hard 70/30 brass and half-hard aluminium.

Values of the experimental instability strain for all materials tested are shown in Table 1. The strain is represented as the ratio of t, the current thickness of the sheet at the pole, to t_0, the initial thickness of the sheet. The experimental thickness

ratios at fracture are also shown tabulated. By comparing these ratios at instability and fracture it will be noticed, as might be expected, that there is more straining after instability with the annealed materials than with the tempered materials (also, of course, in the tensile test after the start of necking).

4. Correlation of Results with Theory

Swift (1952) has put forward a theory predicting the instability strains in a deformed circular membrane and has demonstrated that the instability occurs at the pole of the bulge. The strain-hardening characteristic adopted was of the form $q = c\,(a + \psi)^n$. It was concluded that the polar strain ϵ_0 at instability was the appropriate root of the equation

$$\epsilon_0^3 - \epsilon_0^2\left(\tfrac{33}{20} + \frac{n}{2} - a\sqrt{\tfrac{1}{3}}\right) + \epsilon_0\left(\tfrac{9}{40} + \tfrac{9}{10}\,n - a\,\tfrac{33}{40}\sqrt{\tfrac{1}{3}}\right) + a\,\tfrac{9}{40}\sqrt{\tfrac{1}{3}} = 0$$

The corresponding reduction in thickness at the pole is then given by $\ln(t/t_0) = 2\epsilon_0$. The equation has been solved graphically for all the materials tested, their stress-strain curves having been represented by the empirical relation proposed above. A comparison between the experimental and predicted critical thickness ratio is given in Table 1. In all cases the theoretical values are higher than the experimental values, so that the theory seems to underestimate the stretch forming capabilities of the materials. On the other hand, the theory does place the materials in the correct order of merit.

Table 1.

Metal	$q = c\,(a + \psi)^n$	*Experimental Thickness ratio*		*Theoretical critical Thickness ratio* t/t_0
		Instability t/t_0	*Fracture* t/t_0	
Copper, soft	$q = 28{,}900\,(0{\cdot}01 + \psi)^{0{\cdot}3}$	0·555	0·50	0·625
Copper, half-hard	$q = 28{,}900\,(0{\cdot}07 + \psi)^{0{\cdot}3}$	0·59	0·58	0·65
Brass, soft	$q = 54{,}000\,\psi^{0{\cdot}48}$	No instability	0·50	0·38
Brass, half-hard	$q = 54{,}000\,(0{\cdot}078 + \psi)^{0{\cdot}48}$	No instability	0·51	0·61
Aluminium, soft	$q = 10{,}300\,\psi^{0{\cdot}25}$	0·565	0·48	0·65
Aluminium, half-hard	$q = 10{,}300\,(0{\cdot}136 + \psi)^{0{\cdot}25}$	No instability	0·65	0·68
Killed steel	$q = 41{,}000\,\psi^{0{\cdot}2}$	0·57	0·48	0·66
Stainless steel	$q = 115{,}000\,(0{\cdot}01 + \psi)^{0{\cdot}5}$	0·52	0·50	0·58

In discussing this lack of correlation, it should be kept in mind that, in order to apply the theory, it is necessary to adopt some analytical expression for the strain-hardening characteristic, which has in fact been chosen to cover the whole useful range of deformation. Now the condition of instability is concerned solely with the value of the slope of the characteristic at a particular point, and not otherwise with the general form of this characteristic. A fitted equation which would give accurate values for the slope of an empirical curve at all points involves difficulties of a higher order than are necesssary to reproduce the general form of

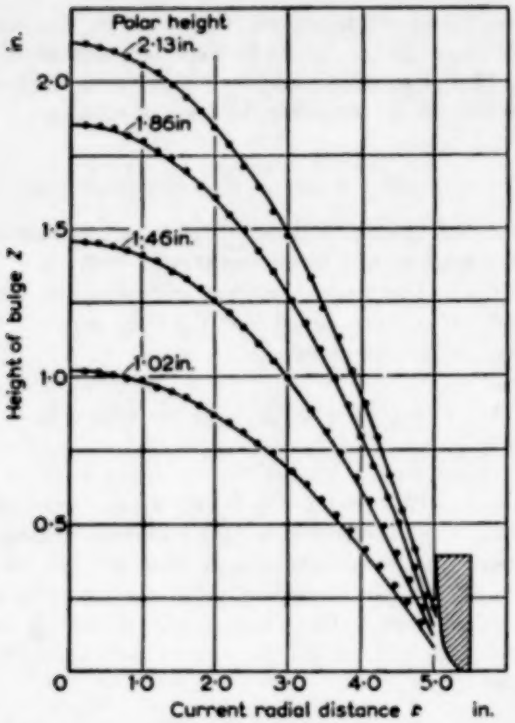

Fig. 12. Profile of bulge for half-hard aluminium. ———— theoretical curve, - - - - - - experimental points.

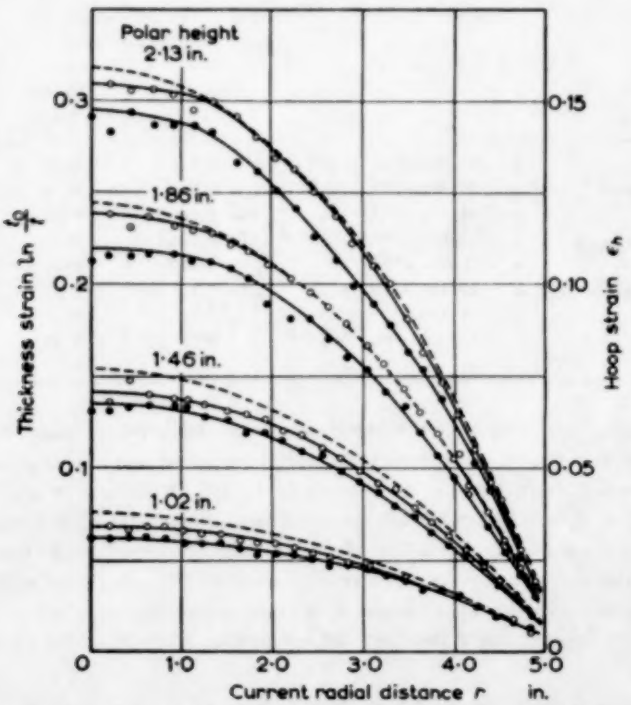

Fig. 13. Strain distribution for half-hard aluminium. ● thickness strain, ○ hoop strain, from bulge test. - - - - - - - theoretical thickness strain.

such a curve, and it may well be that the want of closeness in agreement is in fact due more to imperfection of the empirical strain-hardening expression than to any error in the theory itself.

HILL (1950) obtained a general solution for the geometry of the bulge and the strain distribution in the case of a metal whose stress-strain curve can be approximated by the linear relation $\sigma/Y = 1 + H\epsilon$, where Y is the initial yield stress and H is a nondimensional constant. Such a relation is approximated by a metal in a work-hardened state, but of the materials tested it can only be applied to half-hard aluminium whose strain-hardening characteristic can be expressed in the form $\sigma/15{,}460 = 1 + 0{\cdot}76\,\epsilon$ where the stress is measured in lb. per sq. in.

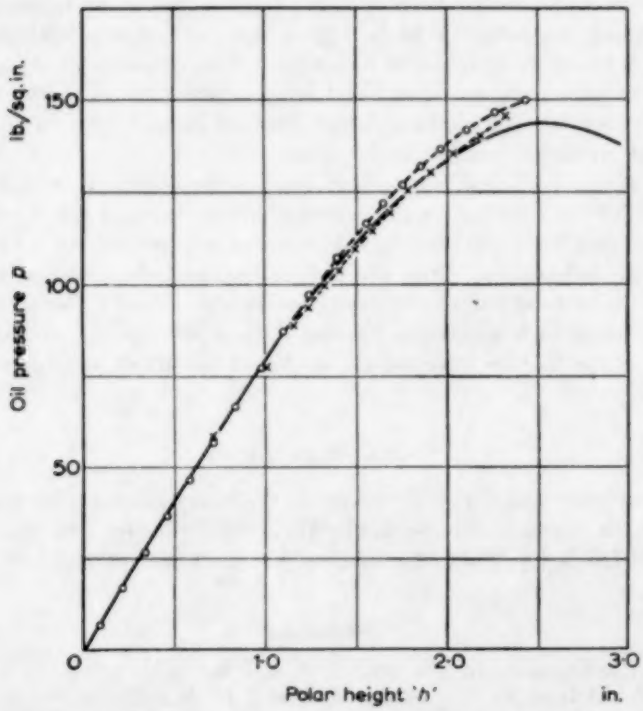

Fig. 14. Theoretical and experimental results for the variation of oil pressure with polar height for half-hard aluminium. ———— theoretical curve ; —O—O—O— experimental points, continuous test ; —X—X—X— experimental points, interrupted test.

Comparison between experiment and HILL's theory are given in Figs. 12 to 14. The correlation of results for the profile of the bulge (Fig. 12) is good except in the region of the clamped edge. The thickness strains are more sensitive than the profile to the value of H, and it will be seen from Fig. 13 that the theoretical strains are greater than the experimental thickness strains and tend to lie rather closer to the experimental hoop strains (which are plotted to twice the scale). There is also fair correlation between the experimental and theoretical values of oil pressure and polar height (Fig. 14) except near maximum pressure. The theory

predicts an instability at a polar height of 2·6 in., but in fact the material fractured under increasing pressure at a polar height of approximately 2·5 in.

Following the work of Hill, Thomas (1954) has taken the particular case of soft copper and has obtained a solution by a method of successive approximations which is in fairly good agreement with the experimental work. But he concluded that the numerical integration entailed in the solution is so lengthy that it is unsuitable for frequent use.

5. Conclusions

The extent of general thinning before the point of instability is reached in the bulge test is so much greater than in simple tension that it can be used to obtain a strain-hardening characteristic to far higher strains than is possible in the tensile test, and it is therefore more useful under conditions of severe plastic deformation. However, the procedure is lengthy and tedious, since the oil pressure, the polar strain, and the polar radius of curvature must all be measured to obtain a single point on the strain-hardening characteristic.

In the case of half-hard aluminium good experimental correlation has been obtained with Hill's theory for the development of straining and for the geometry of the bulge, and Thomas (1954) has shown that it is possible to obtain as good a correlation for soft copper. Thus, this particular stretch-forming operation appears now to be understood sufficiently well to serve as an introduction to the more general problems such as stretch-forming with a solid punch and deep-drawing operations where friction between the tool and the blank has to be taken into account.

Acknowledgments

The author wishes to thank Professor H. W. Swift for his guidance and advice throughout the course of this work, Mr. W. Johnson for his help in preparing the paper and BISRA for which Association this work was carried out.

References

Brewer, G. A. and Glassco, R. B.	1941	*J. Aero. Sci.*, **9**.
Brown, W. F. and Sachs, G.	1948	*Trans. A.S.M.E.* **70**, 241.
Brown, W. F. and Thompson, F. C.	1949	*Trans. A.S.M.E.*, **71**, 575.
Chow, C. C., Dana, A. W. and Sachs, G.	1949	*J. Metals*, **1**, 49.
Ford, H.	1948	*Proc. I. Mech. E.*, **159**, 115.
Gleyzal, A.	1948	*Trans. A.S.M.E.*, **70**, 288.
Hill, R.	1950	*Phil. Mag.*, **41**, 1133.
Lankford, W. T. and Low, J. R.	1947	*Trans. Am. Inst. Min. Met. Engrs.*, **171**, 574.
Mostow, W.	1948	*Plastic Deformation, Symposium edited by* H. H. Hausner, *Chap.* 6, 137 (Mapleton House, NY).
Swift, H. W.	1946	*Engineering*, **162**, 381.
	1952	*J. Mech. Phys. Solids*, **1**, 1.
Thomas, D. G. B.	1954	*B.I.S.R.A. Research Report* MW/B/4/54.

Journal of the Mechanisc and Physics of Solids, 1956, Vol. 5, pp. 57 to 61 Pergamon Press Ltd., London.

THERMOELASTICITY AND THERMAL SHOCK

By Martin Lessen
School of Civil Engineering, University of Pennsylvania

(*Received* 2nd *August*, 1956)

Summary

The relevant equations for a thermoelastic solid are derived from thermodynamical principles. The problem of "initial" thermal shock is formulated and the solution is found to be similar to that of the Fourier equation with a modified diffusivity. The solution of the more general case of thermal shock is expressed as a perturbation expansion about the usual solution.

1. Introduction

The usual treatment of infinitesimal deformation thermoelastic problems considers the following relations :

Equilibrium : $$\rho \frac{\partial^2 u_i}{\partial t^2} = \tau_{ki,k} + Q_i$$

Generalized Stress-Strain-Temperature law : $$\epsilon_{ij} = G_{ij,kl}\, \tau_{kl} + \alpha_{ij}(T - T^{(0)})$$

Generalized Temperature Distribution (Fourier) : $$\frac{\partial T}{\partial t} = D_{mn}\, T_{,mn}$$

where repeated indices are summed and a comma indicates differentiation.

The physical implications of the foregoing ensemble of equations are that, although there is a thermodynamic interaction term in the generalized stress-strain-temperature law that is then felt in the equilibrium equation, the intuitively expected mechanical interaction term in the temperature-distribution equation is absent.

Many years ago, Duhamel (1837) and Neumann (1885) tried to include such an interaction with the argument (for an isotropic substance) that the rate of temperature change was linearly dependent not only on the net rate of heat inflow but also on the rate of dilatation. A generalization of their considerations would yield as a temperature distribution equation

$$\frac{\partial T}{\partial t} = D_{mn}\, T_{,mn} + E_{mn} \frac{\partial \epsilon_{mn}}{\partial t}.$$

The equations of Duhamel and Neumann were correct : an analysis by Lessen and Duke (1953) based on thermodynamic considerations arrived at the same equation as theirs.

In the following analysis, a more direct thermodynamic argument is presented and it is seen for instance that a generalized Hooke's law is a consequence of the

thermodynamic treatment rather than an independent postulate. It should be noted that the internal energy referred to is the thermodynamic property and not the " strain " energy which is utilized in many of the conventional treatments of elasticity.

2. General Analysis

The Gibbs total differential equation for an elastic solid where T, S, U, τ_{ij}, and ϵ_{ij} are properties of a state may be written as

$$TdS = dU - \frac{1}{\rho}\,\tau_{ij}\,d\epsilon_{ij}. \tag{1}$$

If, in an assumed equation of state, U is expressed in terms of S and ϵ_{ij},

$$U = U(S,\ \epsilon_{ij}) \tag{2}$$

the temperature and stress are given directly by

$$T = \frac{\partial U}{\partial S}\,; \qquad \tau_{ij} = \rho\,\frac{\partial U}{\partial \epsilon_{ij}}.$$

Then, expanding U in a Taylor series about a reference state (to second-order terms),

$$U = U^{(0)} + U^{(1)}\,s + A_{ij}\,\epsilon_{ij} + \tfrac{1}{2}\,U^{(2)}\,S^2 + B_{ij}\,s\epsilon_{ij} + \frac{1}{2\rho}\,C_{ijkl}\,\epsilon_{ij}\,\epsilon_{kl}, \tag{3}$$

the temperature and stress are

$$T = U^{(1)} + U^{(2)}\,s + B_{ij}\,\epsilon_{jj}, \tag{4}$$

$$\tau_{ij} = \rho A_{ij} + \rho B_{ij}\,s + C_{ijkl}\,\epsilon_{kl}. \tag{5}$$

$U^{(1)}$ is obviously the reference temperature $T^{(0)}$ while ρA_{ij} is obviously the reference stress $\tau_{ij}^{(0)}$.

By solving for s in (4) and substituting in (5), a generalized Hooke's Law is obtained :

$$\tau_{ij} = \tau_{ij}^{(0)} + \frac{\rho}{U^{(2)}}\,B_{ij}\,(T - T^{(0)}) + \left(C_{ijkl} - \frac{\rho}{U^{(2)}}\,B_{ij}\,B_{kl}\right)\epsilon_{kl}. \tag{6}$$

The first law of thermodynamics for a homogeneous, elastic solid undergoing small deformations may be written as

$$\rho\,\frac{\partial U}{\partial t} = K_{mn}\,T_{,mn} + \tau_{ij}\,\frac{\partial \epsilon_{ij}}{\partial t}. \tag{7}$$

Substituting in (7) from (3), (4), (5) for U, T and τ_{ij} respectively and then substituting from (4) for s, one obtains (to first order)

$$\frac{\partial T}{\partial t} - B_{ij}\,\frac{\partial \epsilon_{ij}}{\partial t} = D_{mn}\,T_{,mn}. \tag{8}$$

If considerations are limited to an isotropic solid, and $\tau_{ij}^{(0)} = 0$, (6) and (8) may be written as

$$\tau_{ij} = -\frac{\rho B}{U^{(2)}}\,\delta_{ij}\,(T - T^{(0)}) + \left(\lambda - \frac{\rho B^2}{U^{(2)}}\right)\delta_{ij}\,\epsilon_{kk} + 2\mu\,\epsilon_{ij}, \tag{9}$$

$$\frac{\partial T}{\partial t} - B\,\frac{\partial \epsilon_{kk}}{\partial t} = D\,T_{,kk}. \tag{10}$$

Equations (9) and (10) together with the equilibrium equation

$$\rho\,\frac{\partial^2 u_i}{\partial t^2} = \tau_{ki\ k} + Q_i \tag{11}$$

and suitable boundary conditions then determine a solution.

3. The Thermal-Shock Problem

We now consider the problem of a homogeneous, elastic body at an initial temperature of $T^{(0)}$ suddenly brought into contact with a surrounding medium such that the surface of the body is immediately brought to and maintained at a temperature of $T^{(1)}$.

Almost immediately, a region (or boundary layer) will form in the body, adjacent to its surface, where the temperature varies from $T^{(1)}$ at the surface to $T^{(0)}$ at the inner edge of the boundary layer. The layer will, of course, thicken with time. At such times that the layer thickness is still small compared to a minimum characteristic dimension of the body, the problem may be reduced to the one-dimensional problem corresponding to a semi-infinite solid bounded by a plane corresponding to the surface at temperature $T^{(1)}$. The material in the boundary layer is then constrained in the directions tangential to the surface but free in the direction normal to the surface. If dynamic effects are neglected, the stress normal to the surface is zero and the equilibrium equations are identically satisfied if the body force is taken as zero.

Since ϵ_{kk} is needed for (10) it is necessary to invert (9) so that $\epsilon_{ij} \equiv \epsilon_{ij}\,(T, \tau_{kl})$. This may be effected by solving for ϵ_{ij} in (9), contracting (9) and substituting for τ_{kk} in terms of ϵ_{kk}, T. The resulting strain-stress-temperature relation is

$$\epsilon_{ij} = \gamma\delta_{ij}\,\tau_{kk} + \eta\tau_{ij} + \alpha\,(T - T^{(0)})\,\delta_{ij}. \tag{12}$$

Considering, now, that the semi-infinite solid at initial temperature $T^{(0)}$ fills space $x_1 < 0$, and that at $t = 0$ the temperature of $x_1 = 0$ is suddenly brought to and maintained at temperature $T^{(1)}$, the solid is so constrained that

$$\epsilon_{22} = \epsilon_{33} = 0, \qquad \tau_{22} = \tau_{33},$$

while (neglecting dynamic effects)

$$\tau_{11} = 0,$$

(12) may be written for ϵ_{11} and ϵ_{kk}:

$$\epsilon_{11} = \gamma\tau_{kk} + \alpha\,(T - T^{(0)}),$$

$$\epsilon_{kk} = (3\gamma + \eta)\,\tau_{kk} + 3\alpha\,(T - T^{(0)}).$$

Since, due to the constraints, $\epsilon_{11} = \epsilon_{kk}$, ϵ_{kk} may be obtained from the above equations as a function of $(T - T^{(0)})$,

$$\epsilon_{kk} = \frac{\alpha\eta}{2\gamma + \eta}(T - T^{(0)}). \tag{13}$$

Substituting (13) into (10) one obtains

$$\frac{\partial T}{\partial t} = \frac{D}{1 - \dfrac{\alpha B\eta}{2\gamma + \eta}} T_{,11} \tag{14}$$

Thus the problem of initial thermal shock is solved by solving the ordinary Fourier heat conduction equation with a modified diffusivity.

The problem of thermal shock, where the thermal boundary layer thickness is no longer small compared to a characteristic body dimension l, may be approached through a perturbation expansion. First, the following dimensionless transformation of variable should be effected in (10), (11), and (12):

$$x_i = lx'_i, \qquad \epsilon_{ij} = \alpha T^{(0)} \epsilon'_{ij},$$

$$T - T^{(0)} = T^{(0)} T', \qquad \tau_{ij} = \frac{\alpha T^{(0)}}{\gamma} \tau'_{ij}, \qquad t = \frac{l^2}{D} t'.$$

These yield respectively (with primes dropped and acceleration effects neglected)

$$\frac{\partial T}{\partial t} - \alpha B \frac{\partial \epsilon_{kk}}{\partial \tau} = T_{,kk}, \tag{15}$$

$$\tau_{ki,k} = 0, \tag{16}$$

$$\epsilon_{ij} = \tau_{kk}\,\delta_{ij} + \frac{\eta}{\gamma}\,\tau_{ij} + T\delta_{ij}. \tag{17}$$

A perturbation series in αB for ϵ_{ij}, τ_{ij}, T, viz.

$$\epsilon_{ij} = \sum_{n=0} (\alpha B)^n \epsilon_{ij}^{(n)},$$

$$\tau_{ij} = \sum_{n=0} (\alpha B)^n \tau_{ij}^{(n)},$$

$$T = \sum_{n=0} (\alpha B)^n T^{(n)},$$

will effect a solution where the initial approximation is the full solution usually given for the problem, and the succeeding solutions are solutions of the same ensemble of equations with a forcing function obtained from previous approximations.

NOTATION

T = temperature
S = specific entropy
U = specific internal energy
Q_i = body force per unit mass
τ_{ij} = stress tensor
ϵ_{ij} = strain tensor
G_{ijkl} = isothermal elasticity tensor
ρ = density
t = time co-ordinate
x_i = space co-ordinate
K_{mn} = thermal conductivity tensor
D_{mn} = thermal diffusivity tensor
λ, μ = Lamé constants corresponding to isotropic C_{ijkl}
u_i = displacement
$S^{(0)}$ = reference specific entropy
$= S - S^{(0)}$

References

Duhamel, J. M. C.	1837	*J. de l'Ecole Polytechnique*, **15**, 1.
Lessen, M.	1953	*J. Aero. Sci.*, **20**, 716.
Lessen, M. and Duke, C. E.	1953	*Proc. 1st Midwest. Conf. on Mechanics of Solids.*
Neumann, F	1885	*Vorlesungen über die Theorie der Elasticität der festen Körper und des Lichtäthers* (Meyer, Breslau).

Journal of the Mechanics and Physics of Solids ,1956, Vol. 5, pp. 62 to 65. Pergamon Press Ltd., London.

THE ELASTIC-PLASTIC BENDING OF A CIRCULAR PLATE BY AN ALL-ROUND COUPLE

By F. A. Gaydon and H. Nuttall
Department of Theoretical Mechanics, University of Bristol

(*Received* 19*th July*, 1956)

Summary

The problem of the elastic-plastic bending of a circular plate by an all-round couple is solved. An ideal elastic-plastic material is assumed.

1. Introduction

In view of the scarcity of solutions to elastic-plastic problems without an assumption that the material is incompressible, it has been thought worthwhile to publish the solution to this relatively simple problem. The solution is *not* in the usual "spirit of thin plates," the only assumption being that the slope of the surface of the plate is sufficiently small for the curvature to be regarded as constant for a given applied couple as in the Euler-Bernoulli theory of bending.

2. The Elastic Problem

Cylindrical co-ordinates (r, θ, z) are used. The origin is taken at the centre of the middle section of the plate, the upper and lower surfaces as $z = \pm h$ and the positive direction of the z-axis upwards. From symmetry the co-ordinate θ will not appear in the equations. With the usual notation u, v, w are the displacements in the r, θ z directions and σ_r, σ_θ are the radial and circumferential stresses.

The solution of the elastic problem is known to be

$$\sigma_r = \sigma_\theta = \frac{E}{1-\nu} \cdot \frac{z}{R} \tag{1}$$

$$u = \frac{rz}{R}, \qquad v = 0, \qquad w = -\frac{\nu z^2}{(1-\nu)R} + \frac{a^2 - r^2}{2R} \tag{2}$$

where ν is Poisson's ratio, E is Young's modulus, a is the radius of the plate and R the radius of curvature of the plate ($\partial w/\partial r$ being assumed small compared with unity, as stated in the Introduction). w is taken to be zero along $z = 0$, $r = a$.

The couple M per unit arc of circumference is

$$M = \frac{2E}{1-\nu} \cdot \frac{h^3}{3R} \tag{3}$$

3. The Elastic-Plastic Problem

The Mises yield criterion in cylindrical co-ordinates is

$$(\sigma_r - \sigma_\theta)^2 + (\sigma_\theta - \sigma_z)^2 + (\sigma_z - \sigma_r)^2 + 6\tau_{rz}^2 + 6\tau_{z\theta}^2 + 6\tau_{r\theta}^2 \leqslant 6k^2 \qquad (4)$$

where k is the yield stress in pure shear and is a constant for a nonhardening material. If the couple given by (3) is increased to $2kh^2/\sqrt{3}$ the plate becomes plastic at $z = \pm h$ and

$$\sigma_r = \sigma_\theta = \sqrt{3}\,k \qquad \text{at} \qquad z = \pm h,$$

these stresses satisfying (4) with the equality sign, all other stresses being zero. The elastic-plastic surface moves into the plate as M increases beyond the critical value.

It is now assumed that $\sigma_r = \sigma_\theta$ throughout the plastic region (this assumption is justified in Section 5). With this assumption it may be proved that all other stresses are zero*. It follows that the elastic-plastic surfaces are spherical with curvature $1/R$ and that the stresses and displacements in the elastic region are given by equations (1) and (2). For $|z| \geqslant c$ the plate is plastic and c is given by

$$c = \frac{\sqrt{3}\,k\,(1-\nu)\,R}{E} = KR, \text{ say,} \qquad (5)$$

and the couple M by

$$M = \sqrt{3}\,k\,h^2 - \frac{\sqrt{3}\,k^3\,(1-\nu)^2\,R^2}{E^2}. \qquad (6)$$

4. The Velocities

If the length c is taken to be the parameter of the progress of the bending, the elastic velocities are

$$\left.\begin{aligned} \frac{\partial u}{\partial c} &= -\frac{rzK}{c^2}, \\ \frac{\partial w}{\partial c} &= \frac{\nu z^2}{1-\nu}\cdot\frac{K}{c^2} - \frac{(a^2 - r^2)}{2}\cdot\frac{K}{c^2}. \end{aligned}\right\} \qquad (7)$$

In the plastic region, the stress remains constant in an element, the elastic strain rate vanishes and the plastic strain rate increments are related by the equations

$$d\left(\frac{\partial u}{\partial r}\right) = \frac{du}{r} = -\tfrac{1}{2}\,d\left(\frac{\partial w}{\partial z}\right), \qquad d\left(\frac{\partial u}{\partial z} + \frac{\partial w}{\partial r}\right) = 0. \qquad (8)$$

From equations (8) it follows that

$$\left.\begin{aligned} \frac{\partial u}{\partial c} &= A\,(z, c)\,.\,r \\ \frac{\partial w}{\partial c} &= -2\int A\,(z, c)\,dz + B\,(r, c) \end{aligned}\right\} \qquad (9)$$

and

$$r\frac{\partial A}{\partial z} + \frac{\partial B}{\partial r} = 0$$

*Cf. Prager and Hodge (1951, p. 51). A similar method may be used in this case.

in the plastic region. At the elastic-plastic boundary $|z| = c$, $\partial u/\partial c$, $\partial w/\partial c$, u and w are now made continuous.

It is found that the equations (9) are satisfied and $\partial u/\partial c$, $\partial w/\partial c$ are continuous if

$$A(z, c) = -Kz/c^2,$$

$$B(r, c) = -\frac{a^2 - r^2}{2} \cdot \frac{K}{c^3} - \frac{1 - 2\nu}{1 - \nu} K.$$

These lead to

$$\frac{\partial u}{\partial c} = -\frac{rzK}{c^3}, \qquad |z| \leqslant h,$$

$$\frac{\partial w}{\partial c} = \frac{z^2 K}{c^3} - \frac{a^2 - r^2}{2} \cdot \frac{K}{c^3} - \frac{1 - 2\nu}{1 - \nu} \cdot K, \qquad h \geqslant |z| \geqslant c,$$

$$\frac{\partial w}{\partial c} = \frac{\nu z^2}{1 - \nu} \cdot \frac{K}{c^3} - \frac{a^2 - r^2}{2} \cdot \frac{K}{c^3}, \qquad |z| \leqslant c.$$

u can be continuous only if

$$u = rzK/c$$

throughout the material. On the other hand,

$$w = -\frac{Kz^2}{c} + \frac{a^2 - r^2}{2} \cdot \frac{K}{c} - \frac{(1 - 2\nu) Kc}{1 - \nu} + C(r, z), \qquad h \geqslant |z| \geqslant c,$$

$$w = -\frac{\nu z^2}{1 - \nu} \cdot \frac{K}{c} + \frac{a^2 - r^2}{2} \cdot \frac{K}{c}, \qquad |z| \leqslant c.$$

It follows immediately that $C(r, z)$ is a function of z only and

$$C(z) = 2K|z|\left(\frac{1 - 2\nu}{1 - \nu}\right), \qquad h \geqslant |z| \geqslant c.$$

The expressions for the displacements are

$$u = rzK/c,$$

$$\left.\begin{aligned} w &= -\frac{\nu z^2}{1 - \nu} \cdot \frac{K}{c} + \frac{a^2 - r^2}{2} \cdot \frac{K}{c}, \qquad |z| \leqslant c \\ w &= -z^2 \cdot \frac{K}{c} + \frac{a^2 - r^2}{2} \frac{K}{c} - \frac{(1 - 2\nu)}{1 - \nu} Kc + 2K|z|\left(\frac{1 - 2\nu}{1 - \nu}\right), \qquad |z| \geqslant c \end{aligned}\right\} \quad (10)$$

where $K = \dfrac{\sqrt{3}\, k (1 - \nu)}{E}$ and $c = \dfrac{\sqrt{3}\, R (1 - \nu)}{E} R.$

From equation (6) the applied couple is

$$M = \sqrt{3}\, k (h^2 - c^2/3).$$

5. Uniqueness of the Solution

Since only small strains are possible it follows from a uniqueness theorem due to GREENBERG (1949) that the stresses found are the correct ones. The uniqueness

of the strain-rates does not follow and each problem has to be considered separately. In the problem under consideration uniqueness has been achieved by making the displacements and velocities continuous at the elastic-plastic boundary. This is justified by the following arguments. The continuity of u, w, $\partial u/\partial r$ and $\partial w/\partial r$ follow from the continuity of the material. Since there is no shear strain at the elastic-plastic boundary $\partial u/\partial z$ must be continuous across the boundary and the continuity of $\partial u/\partial z$ implies that of $\partial u/\partial c$. A discontinuity in $\partial w/\partial z$, implying one in $\partial w/\partial c$, is not immediately ruled out; in fact, it might be expected to occur at an elastic-plastic surface. In the present problem, however, $\partial w/\partial z$ is continuous for the following reason. The cubical dilatation of an element is

$$\frac{\partial w}{\partial z} + \frac{\partial u}{\partial r} + \frac{u}{r}.$$

Since all stress components are unaltered while an element is crossed by the moving elastic-plastic surface, the dilatation is also unchanged. The continuity of $\partial w/\partial z$ now follows from that of $\partial u/\partial r$ and u.

6. Effect of Poisson's Ratio

It is interesting to compare the problem with that of the pure bending of a beam. Since, in the bending of a circular plate, the stress system in every element is biaxial, the principal curvatures are equal and do not involve Poisson's ratio. In consequence, the curvature of an element in the plastic zone is the same as that of an element in the elastic zone at any instant. If the beam problem is approached with the assumption that the only stress is longitudinal then the stress in every element would be uniaxial and the principal curvatures unequal, having the ratio $-\nu$ in an elastic element and $-\frac{1}{2}$ in a plastic element. The elements would therefore not fit together at the elastic-plastic surface except in the special case of $\nu = \frac{1}{2}$. For a fuller discussion of this point see Hill (1950, p. 82).

Acknowledgments

The authors wish to acknowledge helpful discussions with Dr. W. M. Shepherd and Professor R. Hill.

References

Greenberg, H. J. 1949 *Quart. Appl. Math.* **7**, 85.

Prager, W. and Hodge, P. G. 1951 *Theory of Perfectly Plastic Solids* (Wiley).

Hill, R. 1950 *Mathematical Theory of Plasticity* (Clarendon Press, Oxford).

Journal of the Mechanics and Physics of Solids, 1956, Vol. 5, pp. 66 to 74. Pergamon Press Ltd., London.

NEW HORIZONS IN THE MECHANICS OF SOLIDS†

By R. Hill
Department of Mathematics, University of Nottingham

(*Received* 18*th September*, 1956)

Introduction and Summary

At the present time the subject known as mechanics of solids embraces elastic, viscous, viscoelastic, viscoplastic, elastic-plastic and rigid-plastic solids. The list is already lengthy and will assuredly soon become more so. Even now, there is a distinct tendency for the subject to be studied, not as a whole, but in separate compartments. In consequence, progress is uneven and there is unwitting duplication of effort. For these and other reasons there seems to be need for a deliberate study of connexions between theories for different solids (and indeed fluids), at all levels and in whatever degrees of generality. In this paper a number of scattered illustrations are brought together, some of them familiar but most of very recent origin. Although somewhat haphazard, they are sufficiently varied and suggestive to hint at what might be accomplished by systematic investigation.

1. Uniqueness Theorems and Extremum Principles

Here the respective theories have reached markedly different stages of development, and we may infer that it has not been obvious in advance what form the principles should take in any one case. Moreover, existing proofs are ad hoc, and on the face of it have little in common, nor do the results as they stand show much resemblance. It is clearly desirable to see how far the basic theorems can be obtained in some uniform, and preferably simplified and automatic way.*

The relevant unifying concept, so it seems to me, is that of a *convex function*; to fix ideas this will be introduced in connexion with a nonlinear viscous solid (or fluid). Let σ_i and ϵ_i be the components of stress $\boldsymbol{\sigma}$ and strain-rate $\boldsymbol{\epsilon}$, regarded as vectors in a 9-space to simplify the notation. It is supposed that the σ_i's are single-valued functions of the ϵ_i's satisfying $\partial\sigma_i/\partial\epsilon_j = \partial\sigma_j/\partial\epsilon_i$. They can therefore be written as

$$\sigma_i = \partial E/\partial\epsilon_i \tag{1}$$

where E is a function of the ϵ_i's‡ and will be referred to as the *work function*; it is calculable as $\int \boldsymbol{\sigma}\, d\boldsymbol{\epsilon}$. It is supposed further that E is convex, in the sense that

† Except for changes from the spoken to the written word, this is the text of a General Lecture delivered on 7th September, 1956, to the 9th International Congress for Applied Mechanics, Brussels.

* A full account is to be given elsewhere.

‡ Treated as independent, E being symmetrized in the nondiagonal components of the strain-rate tensor.

$$E(\epsilon^*) - E(\epsilon) \geqslant \Sigma(\epsilon_i^* - \epsilon_i)\,\partial E/\partial\epsilon_i \tag{2}$$

for any pair ϵ, ϵ^*. A necessary and sufficient condition is that, for any ϵ, the quadratic form associated with the Hessian matrix $\partial^2 E/\partial\epsilon_i\,\partial\epsilon_j$ (or the Jacobian $\partial\sigma_i/\partial\epsilon_j$) should be non-negative. In particular, if the matrix is positive-definite the strict inequality holds when $\epsilon^* \neq \epsilon$, it is then convenient to say that E is *strictly convex*.

Consider, now, the boundary-value problem for a body on whose surface S the traction $\mathbf{F}$ is given on a part S_F and the velocity $\mathbf{u}$ on the remainder S_u. Let σ, ϵ, $\mathbf{u}$ denote the actual stress, strain-rate, and velocity, and ϵ^* the strain-rate corresponding to some artificial continuous velocity field $\mathbf{u}^*$ such that $\mathbf{u}^* = \mathbf{u}$ on S_u. On the supposition that the straining is quasi-static, it can be shown that

$$\int\{E(\epsilon^*) - \rho\mathbf{g}\mathbf{u}^*\}\,dV - \int\mathbf{F}\mathbf{u}^*\,dS_F \geqslant \int\{E(\epsilon) - \rho\mathbf{g}\mathbf{u}\}\,dV - \int\mathbf{F}\mathbf{u}\,dS_F \tag{3}$$

where $\mathbf{g}$ is the body-force vector per unit mass and ρ is the density. It may also be shown that the solution is uniquely determined at points of the body where E is strictly convex, but not necessarily in all respects elsewhere; the quantity on the right-hand side of (3) is of course always unique.

Similarly, if the ϵ_i's are single-valued functions of the σ_i's such that $\partial\epsilon_i/\partial\sigma_j = \partial\epsilon_j/\partial\sigma_i$, we can write

$$\epsilon_i = \partial E_c/\partial\sigma_i \tag{4}$$

where E_c is a function of the σ_i's, called the *complementary function* and calculable as $\int\epsilon\,d\sigma$. If E_c is a convex function,

$$E_c(\sigma^*) - E_c(\sigma) \geqslant \Sigma(\sigma_i^* - \sigma_i)\,\partial E_c/\partial\sigma_i \tag{5}$$

and

$$\int\mathbf{F}^*\mathbf{u}\,dS_u - \int E_c(\sigma^*)\,dV \leqslant \int\mathbf{F}\mathbf{u}\,dS_u - \int E_c(\sigma)\,dV \tag{6}$$

where σ^* is any equilibrium distribution of stress with the same body-forces and such that $\mathbf{F}^* = \mathbf{F}$ on S_F. The solution is uniquely determined at points of the body where E_c is strictly convex.

If both E and E_c exist (this requires that the relations between σ and ϵ are one-one) and are convex (the convexity of one implies that of the other), all the preceding equations are simultaneously valid. Moreover,

$$E + E_c = \int(\sigma\,d\epsilon + \epsilon\,d\sigma) = \sigma\epsilon \tag{7}$$

and the relations (1) and (4) are seen as a Legendre dual transformation.* In view of (7) the right-hand sides of (3) and (6) are identical, and hence the left-hand sides furnish bounds from above and below. It is evident, moreover, that the first variations of these functionals vanish for an actual state. The extrema in (3) and (6) are therefore *analytic*, and so close bounds can be obtained even from comparatively crude approximations σ^* and $\mathbf{u}^*$.

When the material is incompressible, E_c is a function only of the components

* It may be observed that if two materials are such that the σ (ϵ) relations of one have the same form as the ϵ (σ) relations of the other, then the work function of one has the same form as the complementary function of the other.

of $\mathbf{s}$, the deviator of $\boldsymbol{\sigma}$. Since the physical law defines $\mathbf{s}$ only for deviatoric $\boldsymbol{\epsilon}$, (1) is replaced by

$$s_i = \partial E/\partial \epsilon_i \tag{1'}$$

where the definition of E is formally extended to (virtual) non-deviatoric $\boldsymbol{\epsilon}$ by setting $E(\boldsymbol{\epsilon}) = E(\mathbf{e}) = \int \mathbf{s}\, d\mathbf{e}$, $\mathbf{e}$ being the deviator of $\boldsymbol{\epsilon}$; in the differentiation all ϵ_i's are still treated as independent. In particular, when E_c is a function only of the invariant $s = \sqrt{(\mathbf{s}^2)}$ and E is correspondingly a function only of $e = \sqrt{(\mathbf{e}^2)}$,

$$\mathbf{s} = \frac{E'(e)}{e}\,\mathbf{e}, \qquad \mathbf{e} = \frac{E_c'(s)}{s}\,\mathbf{s}. \tag{8}$$

E and E_c are convex if $s(e)$ is a single-valued increasing function.

An important special case is

$$\mathbf{s} = 2\mu e^{n-1}\,\mathbf{e}, \qquad E = \frac{2\mu}{n+1}\,e^{n+1}, \qquad n \geqslant 0 \tag{9}$$

When $n = 0$, $\mathbf{s} = 2\mu\mathbf{e}/e$ is independent of time and (9) formally defines a Lévy-Mises rigid-plastic solid whose yield condition is $s = 2\mu$. With $E = 2\mu e$, which is convex, the extremum principle (3) for a fully plastic body was obtained by MARKOV (1947). Since $\mathbf{e}$ is not determined in magnitude when $\mathbf{s}$ is given, a complementary function (4) cannot be defined, and in fact (6) is replaced by the maximum-work principle (HILL 1950, p. 66) which depends on an inequality entirely different in character from (5).* When $n = 1$ we have a Newtonian viscous solid. For general values of n, (9) or its inverse has been used to represent secondary creep of metals and quasi-steady flow of ice.

Another special case of (8) is the viscoplastic (BINGHAM) solid

$$2\mu\mathbf{e} = \begin{cases} (1 - s_0/s)\,\mathbf{s} \\ 0 \end{cases}, \qquad E_c = \begin{cases} (s - s_0)^2/4\mu, & s \geqslant s_0 \\ 0, & s \leqslant s_0 \end{cases} \tag{10a}$$

E_c is convex, strictly so for $s \geqslant s_0$. The solution is therefore unique where deformation occurs, but not necessarily elsewhere. The inverse of (10a) is

$$\mathbf{s} = 2(\mu + s_0/e)\,\mathbf{e}, \qquad E = \mu e^2 + 2s_0 e, \qquad e \neq 0. \tag{10b}$$

When $e = 0$ the stress is arbitrary subject to $s \leqslant s_0$, while E has a singularity; this case can be included in the basic theory by an obvious slight extension. Note that the maximum in (6) is here always analytic but that the minimum in (3) is analytic only when the entire body deforms. The extremum principles were derived by PRAGER (1954) by algebraic methods (Schwarz inequality).

Equation (1) can also be regarded as the stress-strain law of a nonlinear elastic solid whose free energy per unit volume is E. The subsequent analysis remains valid with $\mathbf{u}$ as the displacement and either of two interpretations of the other symbols: (a) $\boldsymbol{\epsilon}$ is infinitesimal strain and $\boldsymbol{\sigma}$ true stress, or (b) $\boldsymbol{\epsilon}$ denotes the tensor $\partial u_j/\partial x_i$, where x_i is the initial position, and $\boldsymbol{\sigma}$ denotes the (unsymmetric) nominal-

* For a general yield condition, $E = \mathbf{s}\mathbf{e}$ since the $\mathbf{s}$ corresponding to $\mathbf{e}$ is such that $\mathbf{e}\,d\mathbf{s} = 0$ for neighbouring plastic states. The extremum principle is valid also when only part of the body deforms, but the minimum is no longer analytic; the extremum in the maximum work principle is *never* analytic. This helps to explain the common experience that it is less easy to obtain a good lower bound.

stress tensor (i.e. σ_{ij} is the x_j component of the force, per unit original area, acting on an element initially perpendicular to x_i). It was shown by KIRCHHOFF that (1) is satisfied with these variables. In (a) the difference between the initial and final configurations is neglected; in (b) the integrals are taken over the initial volume and surface, while $\mathbf{F}$ is the nominal traction. In (a) when E is quadratic we return to the classical linear theory, and (3) and (6) coincide with well-known results. When E has the form (8), KACHANOV (1942) has proved the weaker result that the functionals in (3) and (6) attain *local* extrema in the actual state. In (b) the uniqueness theorem and extremum principles appear to be new. Note that E is here assumed convex in the $\partial u_j/\partial x_i$'s and is not necessarily so in other strain variables formed from them.

Finally, consider a class of solids such that the strain-rate $\boldsymbol{\epsilon}$ depends on the stress-rate $\dot{\boldsymbol{\sigma}}$. The latter replaces stress in the general formalism, and the typical boundary-value problem is that presented at each instant by given velocities on S_u and traction-rates on S_F.* Other quantities, such as stress, strain, or parameters depending on strain history, may enter the relations between $\boldsymbol{\epsilon}$ and $\dot{\boldsymbol{\sigma}}$; they are to be regarded as given or previously determined, and are to be treated as passive variables in the Legendre transformation. Suppose that the dependence is linear so that

$$\boldsymbol{\epsilon} = \boldsymbol{\alpha}\dot{\boldsymbol{\sigma}} + \boldsymbol{\eta} \tag{11}$$

where $\boldsymbol{\alpha}$ is a nonsingular symmetric matrix and $\boldsymbol{\eta}$ a vector. Then

$$E = \tfrac{1}{2}\dot{\boldsymbol{\sigma}}(\boldsymbol{\epsilon} - \boldsymbol{\eta}), \qquad E_c = \tfrac{1}{2}\dot{\boldsymbol{\sigma}}(\boldsymbol{\epsilon} + \boldsymbol{\eta}), \tag{12}$$

and both are convex (strictly) when $\boldsymbol{\alpha}$ is positive (definite). A particular case is the viscoelastic solid of Maxwell type where $\boldsymbol{\eta}$ depends only on stress; the corresponding extremum principles seem to be new.† Another particular case is a work-hardening elastic-plastic solid for which $\boldsymbol{\eta} = 0$, while $\boldsymbol{\alpha}$ is positive-definite provided the yield function and plastic potential coincide; $\boldsymbol{\alpha}$ takes different forms in different regions of the $\dot{\boldsymbol{\sigma}}$ and $\boldsymbol{\epsilon}$ spaces according to whether an element is elastic or plastic, loading or unloading. The extremum principles have been obtained before, but less simply (see HILL 1950, pp. 63-66). The effects of viscous creep and thermal expansion can be incorporated by retaining a term $'\boldsymbol{\eta}$ depending on stress and temperature; the extended results were obtained by WANG and PRAGER (1954).

The potentialities of the various extremum principles have hitherto been exploited mainly in the linear elastic context. Here, when for example $\mathbf{F} = 0$ on S_F and $\mathbf{g} = 0$ in V, the quantity bracketed by (3) and (6) is $\frac{1}{2}\int \mathbf{F}\mathbf{u}\, dS$ since $E = E_c = \frac{1}{2}\int \mathbf{F}\mathbf{u}\, dS$ in the actual state. Thus, if the given values of $\mathbf{u}$ constitute a rigid-body translation or rotation on part of S_u, together with fixed constraints elsewhere it is effectively the resultant load or couple that is bracketed; the most thoroughly explored application is the estimation of torsional rigidity. The analogous method for Newtonian viscous flow was first used only recently (HILL and POWER 1956). When the behaviour is nonlinear, however, the possibilities

* Positional changes are neglected, together with the convective component of stress rate.

† Similarly, the Voigt material can be treated as a quasiviscous solid with total strain as a passive variable.

appear to be completely unexplored (apart from the exceptional case $n = 0$ when the solid is rigid-plastic). If E is a homogeneous function of degree $n + 1$, the bracketed quantity is $\int \mathbf{F}\mathbf{u}\, dS/(n+1)$ under the afore-mentioned boundary conditions, since $E = E_c/n = \int \mathbf{F}\mathbf{u}\, dS/(n+1)$ in the actual state. By this method one could, for example, estimate directly the creep-rate of a pressure vessel or the fluid flow through a pipe under a given head. In general, however, we have to proceed indirectly as follows. It can be proved that

$$\int \mathbf{F}\mathbf{u}\, dS = \left[\frac{\partial}{\partial \lambda}\int E_\lambda\, dV\right]_{\lambda=1} \tag{13}$$

where E_λ is the work function in the actual state produced by $\lambda\mathbf{u}$ on $S_{\mathbf{u}}$ and $\mathbf{F} = \mathbf{0}$ on $S_{\mathbf{F}}$. Accordingly, we first use (3) and (6) to approximate E_λ for a range of values of λ and then differentiate the result. Bounds are, however, not known for the eventual error.

2. Exact Correspondences between Field Equations

We have seen that the universality of the extremum principles arises from a certain broad similarity of structure in the different field equations. Let us now inquire what *exact* correspondences exist between the solutions to the boundary-value problems for the various solids; naturally, we can not expect results of such generality. Only a few disconnected illustrations can be given at the present time, but they suggest that this is a field meriting exploration.

The most obvious example, due to Lord Rayleigh, is implicit in what has gone before, namely the correspondence between solutions in linear elasticity and in quasi-static Newtonian viscosity: both media have to be supposed incompressible, and rigidity modulus and displacement in one solution are simply replaced by coefficient of viscosity and velocity in the other. It is surprising how little used this is. For instance, the powerful complex variable methods for plane elastic problems, developed by Muskhelishvili and the Russian school, are immediately available for plane viscous flow, but have not yet been called upon.

Another example, discussed by Hill (1955) and Prager (1956), concerns plane states of deformation in incompressible media. It depends on the circumstance that the equation of continuity in the infinitesimal displacements (or velocities) u, v is similar in form to the equation of equilibrium in the components P, Q of the resultant force acting on any curve joining the point (x, y) to some origin:

$$\partial u/\partial x + \partial v/\partial y = 0, \qquad \partial P/\partial x + \partial Q/\partial y = 0.$$

An equilibrium distribution of stress can therefore be derived from any incompressible displacement (or velocity field), and vice-versa, by the correspondence (in suitable units)

$$P^* = u, \qquad Q^* = v, \tag{14}$$

and then

$$\tau^* = -\partial P^*/\partial x = -\epsilon, \qquad \sigma^* = \tfrac{1}{2}(\partial P^*/\partial y + \partial Q^*/\partial x) = \gamma, \tag{15}$$

where (σ^*, τ^*) and (ϵ, γ) are the normal and shear components of the deviatoric stress and strain (-rate) tensors. Similarly, if

$$u^* = -P, \qquad v^* = -Q, \tag{16}$$

then

$$\epsilon^* = \tau, \qquad \gamma^* = -\sigma. \tag{17}$$

Thus, if two solids have defining laws that transform into one another through the substitutions (15) and (17), the respective classes of all possible plane states can be put into (1, 1) correspondence by (14) and (16); moreover, conjugate states can be recognized *at sight* since their natural boundary conditions satisfy (14) and (16), and if either solution is known the other follows. In particular, a solid with (anisotropic) work function $E(\epsilon, \gamma)$ and complementary function $E_c(\sigma, \tau)$ is conjugate to a solid with work function $E_c(-\gamma^*, \epsilon^*)$ and complementary function $E(\tau^*, -\sigma^*)$. Isotropic linear elastic or Newtonian viscous solids are self-conjugate. Further properties of the correspondence and applications to special problems can be found in the papers mentioned. This seems to be a promising new departure.

The next example is taken from the work of Inoue (1952) and Hill (1954a). The basic idea is that a symmetric tensor can be constructed from the variables characterizing steady flow of inviscid compressible fluid, namely pressure p, density ρ, and velocity components u_i:

$$\sigma_{ij} = (p - p_0)\,\delta_{ij} + \rho u_i u_j \tag{18}$$

where p_0 is an arbitrary constant and δ_{ij} is the Kronecker delta. It can be shown that this tensor satisfies the equations of equilibrium and hence may be regarded as a stress. Its principal values are evidently

$$\sigma_1 = p - p_0 + \rho u^2, \qquad \sigma_2 = \sigma_3 = p - p_0, \tag{19}$$

where u is the velocity magnitude and the first principal axis is in the stream direction. By eliminating p, ρ and u between Bernoulli's integral, the pressure-density law, and (19), a relation bteween σ_1 and σ_2 is obtained. This may be interpreted as the yield condition of a plastic solid. For instance, plastic states in which the maximum shearing stress is constant correspond to supersonic flows of Mach $\sqrt{2}$. The transformation (18) thus provides a means of cross-fertilising the two fields of fluid mechanics and plastic flow. It is, however, subject to rather severe restrictions, but nevertheless appears to merit more attention. For example, the study of elliptic (subsonic) regimes and singularities of various kinds has been much more thorough in the fluid context, and its methods might with advantage be transferred to plastic theory.

3. Partial Correspondences

Mathematical convenience not infrequently prompts the inquiry: in what particulars is the behaviour of a given solid exactly or approximately like the behaviour of one whose properties can be more readily analysed? In the following three cases the question has been answered precisely and in some generality.

The first is due essentially to Alfrey (1944) and relates to the quasi-static loading of an incompressible viscoelastic solid defined by

$$M\mathbf{s} = N\mathbf{e} \tag{20}$$

where M and N are differential operators in the time, with degrees m and n respectively, and $\mathbf{s}$ and $\mathbf{e}$ are the stress and strain deviators. If M and N are linear, $M\mathbf{s}$ satisfies the stress equilibrium equations and $N\mathbf{e}$ the strain compatibility equations. In view of the equality (20) it follows that $M\mathbf{s}$ satisfies the equations $L\mathbf{s}^* = 0$ characterizing the deviatoric stress $\mathbf{s}^*$ in an isotropic incompressible elastic solid (L being a linear operator in the space variables). Thus

$$LM\mathbf{s} = 0 = LM\mathbf{s}^*. \tag{21}$$

The last equation following by operating with M on $L\mathbf{s}^* = 0$. Suppose, now, that the tractions are specified functions of time t everywhere on the surface of our visco-elastic body. The stress $\mathbf{s}^*$ can be calculated at each t for the elastic problem defined by the same (instantaneous) boundary values, and hence so can the time derivatives of $\mathbf{s}^*$ up to order $m-1$ everywhere in the body at $t = 0$. If these are also the initial values specified for the same derivatives of $\mathbf{s}$ in the visco-elastic problem,* then evidently $\mathbf{s} = \mathbf{s}^*$ always, since both satisfy (21) and the same conditions on the surface and initially. Consequently, if only the stress at a certain time is required (and not the strain), one need merely solve the elastic problem defined by the tractions at that instant. (There is, of course, a dual theorem for the strain when the boundary conditions are for displacement.)

The second example concerns a nonhardening elastic-plastic solid which is being strained monotonically; that is, constant velocities $\mathbf{u}$ are maintained on S_u while the tractions $\mathbf{F}$ are held fixed on S_F. In the solution of particular problems it has been found that, when geometry changes are neglected, the tractions on S_u tend asymptotically with increasing strain to the unique values associated with the yield point of a rigid-plastic solid under the same boundary conditions. Moreover, the behaviour of the elastic-plastic solid eventually approaches that of the rigid-plastic solid, in the sense that the elastic part of the strain-rate would vanish everywhere in the limit if the tractions became constant (DRUCKER, PRAGER and GREENBERG 1952). Very often, as in the plastic design of structures, a calculation of the asymptotic loads is of prime interest, and for this purpose the elastic-plastic solid is replaced by the rigid-plastic one. However, a general proof of the asymptotic approach† does not appear in the literature. Surprisingly, the proof is actually very simple, and for that reason can be included here. Remembering that $\dot{\mathbf{F}} = 0$ on S_F and $\dot{\mathbf{u}} = 0$ on S_u,

$$\frac{d}{dt}\int \mathbf{F}\mathbf{u}\, dS_u = \int \dot{\mathbf{F}}\mathbf{u}\, dS_u = \int \dot{\mathbf{F}}\mathbf{u}\, dS = \int \dot{\boldsymbol{\sigma}}\boldsymbol{\epsilon}\, dV > 0$$

unless $\dot{\boldsymbol{\sigma}} \equiv 0$, by a well-known inequality arising from the identity of the yield function and plastic potential. Hence the work-rate W on S_u increases monotonically. Also, according to the maximum work principle, it is bounded above by the work-rate W^* on S_u at the yield point of the rigid-plastic solid. Hence W approaches a limit at which, as already mentioned, the behaviour would be rigid-plastic and so the limit must be W^* itself. It can be shown further that the stress locally

* ALTHEY stated the theorem with the requirement that the tractions should vary in such a way that their derivatives up to order $m-1$ *vanish* when $t = 0$; since the derivatives of $\mathbf{s}^*$ consequently also vanish, the derivatives of $\mathbf{s}$ must be given zero. For other generalizations see LEE (1955).

† This is virtually self-evident when the loads themselves are raised proportionately, with $\mathbf{u} = 0$ on S_u (or $S_u = 0$).

approaches the value it would have in that part of the rigid-plastic body where it is uniquely determined. Nothing is known in general about the relative rapidity of approach in various circumstances (for instance, the influence of initial stresses).

In the third example the properties of the solid are entirely arbitrary except that the strain is insignificant when (and only when) the stress vector in stress space lies inside a certain surface Σ. This must contain the origin and be convex when viewed from outside. It is now supposed that tractions in given ratios are applied to a part S_F of the surface of such a body. We ask : what traction magnitude produces significant distortion of the body, *no matter how* the remainder S_u is loaded ? It is remarkable that a question in such general terms can actually be answered precisely. It turns out that the critical value is that associated with the yield point of a geometrically similar *rigid-plastic* body under the same distribution of tractions on S_F and with rigid constraints maintained over S_u : its yield function and plastic potential must be identical with Σ (HILL 1954b).

4. Removal of Indeterminacy by Generalization

Conversely, it sometimes becomes necessary to regard one solid as a limiting or degenerate case of another, not simply to improve agreement with experiment (as when the perfect fluid of classical hydrodynamics is regarded as having vanishingly small viscosity), but primarily to secure a unique solution. Let us reconsider in this light the notorious difficulty in the theory of a nonhardening rigid-plastic solid, as it has stood for the last five years. The natural boundary conditions have been regarded as specifying traction $\mathbf{F}$ on S_F and velocity $\mathbf{u}$ on S_u, the existing state of hardness being given. In the nonplastic part of the body the stress is strictly indeterminate. In the plastically-stressed part there is usually an infinity of possible modes of deformation ; in the region covered by these the stress itself is unique (HILL 1951). A unique solution in the nonplastic zone could be defined as the limit approached by a nonhardening elastic-plastic solid whose rigidity is made infinitely great, but the indeterminacy in the plastic zone could not usually be removed in this way.

It is natural to turn instead to a work-hardening rigid-plastic solid in which the hardening rate is to be made vanishingly small. The strain-rate is given by

$$\epsilon = \begin{cases} (\mathbf{n}\dot{\sigma})\,\mathbf{n}/h, & \mathbf{n}\dot{\sigma} \geqslant 0 \\ 0 \quad , & \mathbf{n}\dot{\sigma} \leqslant 0 \end{cases} \tag{22}$$

for an element in a plastic state σ, where $\mathbf{n}$ is the corresponding unit outward normal to the current yield surface in stress space ; h is a measure of the rate of hardening and is to be made small in the sequel. When the element is nonplastic, $\epsilon = 0$ for all $\dot{\sigma}$. However, of itself, this step in no way alters the situation since the modes allowed by the stated boundary conditions depend on the existing distribution of hardness and not on the ensuing rate of hardening ; i.e. they satisfy

$$\epsilon^* = \lambda^* \mathbf{n}, \qquad \lambda^* > 0, \tag{23}$$

where deformation occurs. The vital point is that, in addition, the traction-rate $\dot{\mathbf{F}}$ must be specified on S_F (HILL 1956a). Subject to certain continuity restrictions and to the neglect of changes in shape and position, it may be proved that there

is only one mode for which an equilibrium distribution of stress-rate can be found satisfying (22) and the boundary conditions. The actual mode minimizes

$$\tfrac{1}{2}\int h\dot{\epsilon}^{*2}\,dV - \int \dot{\mathbf{F}}\mathbf{u}^*\,dS_F$$

in the class of competing modes (23).†

It is not possible to mention the interesting points connected with the passage to a limit as $h \to 0$, nor the role of velocity discontinuities which have been such a common feature of rigid-plastic solutions, nor the modifications in the preceding theory when positional changes are allowed for. Suffice it to say that, although there are still outstanding difficulties here in certain respects, progress is being made.

REFERENCES

ALFREY, T.	1944	*Qu. Appl. Math.*, **2**, 113.
DRUCKER, D. C., PRAGER, W. and GREENBERG, H. J.	1952	*Qu. Appl. Math.*, **9**, 381.
HILL, R.	1950	*Mathematical Theory of Plasticity* (Clarendon Press)
	1951	*Phil. Mag.*, **42**, 868.
	1954	*J. Mech. Phys. Solids* (a), **2**, 110 ; (b) **2**, 278.
	1955	*J. Mech. Phys. Solids*, **4**, 1.
	1956	*J. Mech. Phys. Solids* (a) **4**, 247 ; (b) **5**, 1.
HILL, R. and POWER, G.	1956	*Quart. J. Mech. Appl. Math.*, **9**, 313.
INOUE, N.	1952	*J. Aero. Sci.*, **19**, 783.
KACHANOV, L. M.	1942	*Prik. Mat. Mekh.*, **6**, 187.
LEE, E. H.	1955	*Quart. Appl. Math.*, **13**, 184
MARKOV, A. A.	1947	*Prik. Mat. Mekh.*, **11**, 339.
PRAGER, W.	1954	*R. von Mises Presentation Volume*, p. 208.
	1956	*J. Mech. Phys. Solids*, **4**, 167.
WANG, A. J. and PRAGER, W.	1954	*J. Aero. Sci.*, **21**, 343.

† These ideas have been applied to the plastic torsion of a hollow bar (HILL 1956b) where, according to the old formulation of the problem, the warping function is indeterminate on any characteristic that passes from one boundary to the other without encountering an internal stress discontinuity.

BOOK REVIEWS

Z. KOPAL : **Numerical Analysis.** Chapman and Hall Ltd., 1955, pp. 556, 63s.

IT WOULD probably be conceded by most applied mathematicians that they undertake with some distaste (or gladly relegate to a junior) the unavoidable complement to their theorizing : the actual calculations without which, to echo Lord KELVIN, they could not feel the numerical magnitude of their formulae. And in these days, as more and more branches of nonlinear mechanics develop, it is becoming rare indeed to encounter a problem with a solution in closed form amenable simply to a slide rule and tables. So such procedures as the numerical integration of two-point differential equations, or the close estimation of an eigenvalue, have to be mastered by every self-respecting applied mathematician. Electronic computers are, it is true, relieving him of the worst drudgery, but they are too inflexible to handle such individual day-to-day calculations as are involved, say, in the trial and modification of successive stages in the development of a theory.

Since the war there have been many good books on numerical analysis, but none so readable as Professor KOPAL's and few that are so eminently *practical*. Here, every formula or process is accompanied by worked examples and helpful advice about its value and proper field of application. The explanation is detailed and many worthwhile refinements are described. There are interesting historical passages, a very full and critical bibliography, and examples for further practice.

The subject matter is closely knit, being mainly concerned with problems of infinitesimal calculus in a single variable. The chapter headings are : Polynomial Interpolation, Numerical Differentiation, Integration of Ordinary Differential Equations, Boundary-Value Problems (Algebraic, Variational, Iterative and other Methods), Mechanical Quadratures, Numerical Solution of Integral and Integro-Differential Equations. It is intended both as an advanced undergraduate text and for use in research. It can be very warmly recommended. The printers are to be congratulated for the setting and type which makes for pleasant and easy reading.

R. HILL

Solid State Physics : Advances in Research and Applications, Volume 1. Edited by FREDERICK SEITZ and DAVID TURNBULL. pp. 469. Academic Press, New York, 1955. 80s.

THIS is the first of a semiannual series of volumes surveying the field which now contains about half of current research in physics. No such survey has been attempted since SEITZ wrote a treatise fifteen years ago. The present volume is concentrated to some extent on the theory of cohesion in metals. Although this is an old subject, one notes with astonishment that almost none of this work had previously been published in book form, or even as extensive review articles. The whole subject has burst out of the covers of a single volume and is now too large for the pen of a single author. In the absence of omniscience, the editors have made the best of it ; it is clear that the authors of the separate articles are thoroughly well qualified, and have succeeded admirably in their main task ; that is, they have so expounded the hundreds of scientific papers which they have read that they have given us confidence that we need not read all those papers ourselves, but may proceed directly from the reviews themselves. In particular, whilst boiling down so much knowledge they have remembered to leave the bones of the logical and mathematical arguments and have avoided, in most instances, those infuriating words " it has been shown, by *X*, that . . . . "

In this volume REITZ discusses the methods of the one-electron theory of solids, setting forth the various modern techniques for energy-band calculation. An elegant paper by WIGNER and SEITZ shows how the cohesion of metals may be analysed qualitatively, stepping back from

niggling numerical calculations on idealized models for a view of the periodic table as a whole. The quantum defect method, described by HAM, is an ingenious trick by which atomic wave functions may be determined in the region outside the core, simply from knowledge of the spectroscopic term values of the free atom. The article by PINES reports on the recent work on electron interaction in metals, where the method of plasma oscillations has recently made great headway.

It has proved impossible for practical reasons to publish the articles in any logical order. There is thus, also, an excellent review, by MUTO and TAKAGI, of the theory of order-disorder transitions in alloys, where the simpler approximation methods are developed from the beginning. FAN's review of the properties of the valence semiconductors, germanium and silicon, will be welcomed by all those who have struggled to keep up with the enormous literature (205 references;) and who wish to know what others know or guess about these important materials.

J. M. ZIMAN

R. E. PEIERLS : **Quantum theory of solids.** Clarendon Press, Oxford 1955. viii-229 pages. 30s.

THIS book has its origin in a course of lectures to advanced students, and it most happily preserves the freshness and terseness which distinguish lecture-room presentation from a more formal textbook treatment. All the main aspects of crystal and metal physics are reviewed, briefly but authoritatively, with the right emphasis on essentials. The physical aspect always comes first and foremost ; mathematics is used skilfully and discreetly to make the discussion precise as well as clear. For students wishing a first introduction into this important subject, and for non-specialists in need of an up-to-date survey, this masterly treatise offers the best possible guidance.

L. ROSENFELD

Journal of the Mechanics and Physics of Solids, 1957, Vol. 5, pp. 77 to 94. Pergamon Press Ltd., London.

SOME ASPECTS OF SAINT VENANT'S PRINCIPLE

By G. Horvay
General Electric Research Laboratory, Schenectady, N.Y.

(*Received* 10*th August*, 1956)

Summary

When self-equilibrating tractions act on an edge of a rectangle, the stresses decay exponentially with distance from the loaded edge. This decay is illustrated for a number of important cases. Results are also given for the half plane loaded by self-equilibrating edge tractions. In this case the stresses decay as integral powers of the distance. The paper concludes with an illustration of the effect on the maximum stress of the rapidity of shear traction variation.

1. Introduction

When self-equilibrating tractions act on a portion of the periphery of a simply connected isotropic, homogeneous, plane elastic figure, the stresses decay as $(r/h)^{-\mu k}$ where $2h$ is the length of the arc over which the tractions act, and r is the distance from the centre of the arc (Horvay, to be published). The subscript k is used to indicate that various characteristic tractions are associated with various decay rates. While this result was established only for the symmetrical wedge (Fig. 1a) loaded on the edge $x = 0$ by self-equilibrating tractions, it is rather plausible that the statement is of general validity. The reference furthermore shows that the decay is slowest for a wedge semiangle $\omega = \pi/2$, and increases to infinity (not necessarily monotonically, but nevertheless continuously) as $\omega \to 0$. When $\omega = 0$ the decay is exponential.

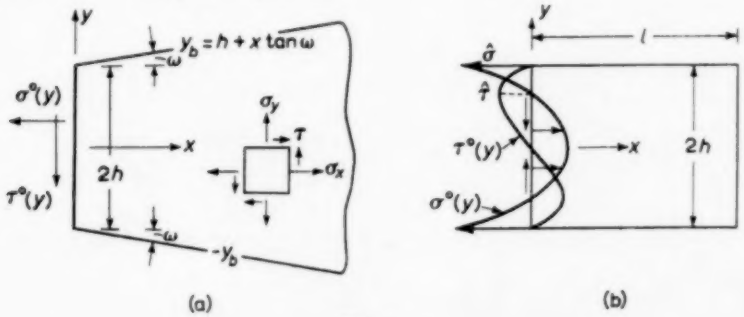

Fig. 1.

The purpose of Sections 2 and 3 of the present paper is to investigate more fully (Figs. 2-8) the stress and displacement distributions that arise in the rectangle (Fig. 1b) when the simplest possible self-equilibrating tractions act on the left edge, namely, the quadratic normal traction

$$\sigma_x^{\circ}(y) = \tfrac{1}{2}\overset{\wedge}{\sigma}\left[-1 + 3y^2/h^2\right], \tag{1a}$$

or the cubic shear traction

$$\tau^{\circ}(y) = \frac{3\sqrt{3}}{2}\overset{\wedge}{\tau}\left[\frac{y}{h} - \left(\frac{y}{h}\right)^3\right]. \tag{1b}$$

The plate is assumed to be of unit thickness. Superscript $^{\circ}$ indicates $x = 0$ location; $\overset{\wedge}{\sigma}$, $\overset{\wedge}{\tau}$ denote the peak values of the edge distributions $\sigma_x^{\circ}(y)$, $\tau^{\circ}(y)$. $\overset{\wedge}{\sigma}$ is assumed at $y = h$, $\overset{\wedge}{\tau}$ at $y = h/\sqrt{3}$.

In Section 4 some comments are made about higher self-equilibrating tractions. Section 5 deals with the semi-infinite plane ($\omega = \pi/2$, see Figs. 9 and 10) which is loaded at $x = 0$, $-h \leqslant y \leqslant h$, by various self-equilibrating tractions. The concluding section illustrates the increase in stress that is brought about in a body when the shear traction gradient is increased, yet the total shear load is kept constant.

2. The Semi-Infinite Rectangle

It was shown in an earlier paper (HORVAY 1953a) that the traction (1a) creates stresses and displacements in a long rectangle which to a very good approximation may be derived from the approximate (variational) stress function

$$\Phi_2 = \frac{2}{3\sqrt{35}}h^2\overset{\wedge}{\sigma}f_2(y)\,g_2(x), \tag{2a}$$

$$f_2(y) = \frac{3\sqrt{35}}{16}(1 - y^2/h^2)^2, \tag{2b}$$

$$g_2(x) = e^{-\alpha_2 x/h}\left[\cos\left(\beta_2\frac{x}{h}\right) + \frac{\alpha_2}{\beta_2}\sin\left(\beta_2\frac{x}{h}\right)\right], \tag{2c}$$

$$\alpha_2 + i\beta_2 = 2{\cdot}0751 + i\,1{\cdot}1429. \tag{2d}$$

i.e., the stresses and displacements may be written in the form (HORVAY 1953b)

$$\sigma_x = \partial^2\Phi/\partial y^2, \qquad \sigma_y = \partial^2\Phi/\partial x^2, \qquad \tau = -\partial^2\Phi/\partial x\,\partial y, \tag{3a}$$

$$Eu = \int_{\infty}^{x}\frac{\partial^2\Phi}{\partial y^2}\,dx - \nu\frac{\partial\Phi}{\partial x}, \qquad Ev = \int_{0}^{y}\frac{\partial^2\Phi}{\partial x^2}\,dy - \nu\frac{\partial\Phi}{\partial y} + K, \tag{3b, c}$$

where

$$hK(x) = 0, \quad \text{or} \quad -\int_{\infty}^{x}\int_{\infty}^{x}\frac{\partial^2\Phi(x,h)}{\partial y^2}\,dx\,dx - \int_{0}^{h}\int_{0}^{y}\frac{\partial^2\Phi(x,y)}{\partial x^2}\,dy\,dy, \tag{3d}$$

according to whether $f_n(y)$ is even or odd (n is even or odd). In particular, for function (2a),

$$\sigma_x(0, y) = \tfrac{1}{2}\overset{\wedge}{\sigma}(-1 + 3y^2/h^2), \qquad \tau(0, y) = 0.$$

The functions $f_k(y)$, $g_k(x)$, and $h_k(x)$ below, are seen to obey the relations

$$\int_{-h}^{h} f^2\,dy = h, \qquad f(\pm h) = f'(\pm h) = 0, \tag{4a}$$

$$g(0) = h'(0) = 1, \qquad g'(0) = h(0) = 0. \tag{4b}$$

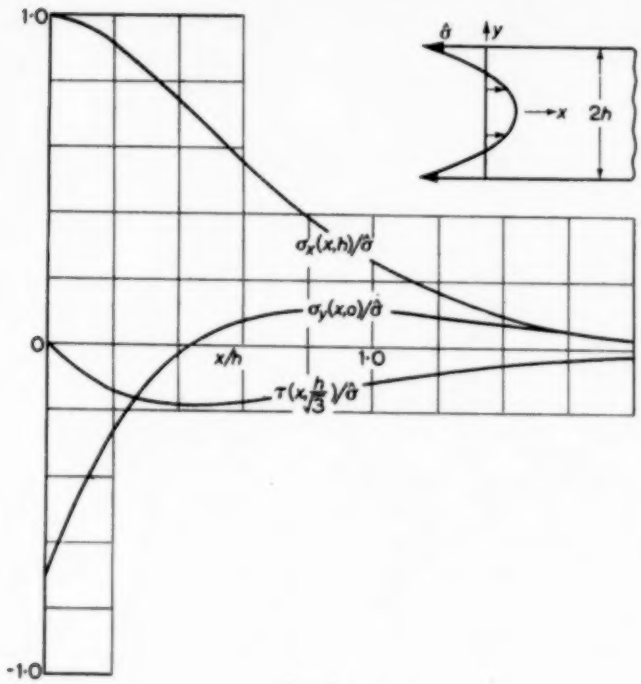
1·0
0
-1·0
$\hat{\sigma}$
y
x
2h
$\sigma_x(x,h)/\hat{\sigma}$
$\sigma_y(x,0)/\hat{\sigma}$
x/h
1·0
$\tau(x,\frac{h}{\sqrt{3}})/\hat{\sigma}$

Fig. 2a.

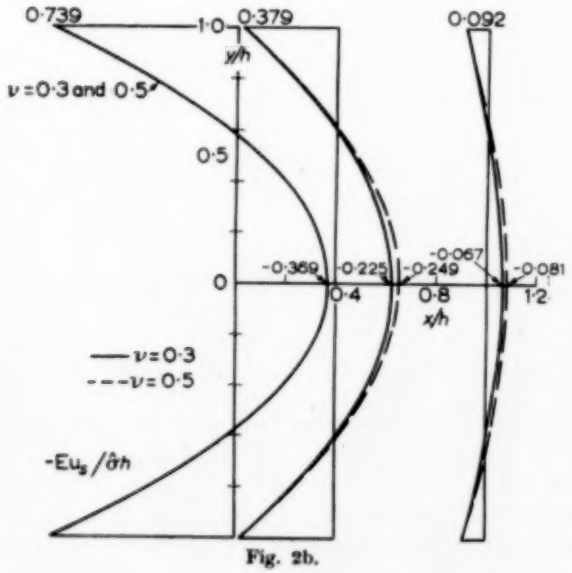
0·739
1·0
0·379
0·092
y/h
ν=0·3 and 0·5
0·5
0
-0·369
-0·225
-0·249
-0·067
-0·081
0·4
0·8
1·2
x/h
ν=0·3
ν=0·5
$-Eu_y/\hat{\sigma}h$

Fig. 2b.

Similarly, the traction distribution (1b) creates stresses and displacements which may be derived, in an identical manner, from the approximate stress function

$$\Phi_\tau = 2\sqrt{\frac{3}{35}}\, h^2\, \hat{\tau} f_2(y)\, h_2(x) \tag{5a}$$

$$h_2(x) = e^{-\alpha_2 x/h} \cdot \frac{\sin(\beta_2 x/h)}{\beta_2} \tag{5b}$$

In Fig. 2 (a) are plotted the stresses $\sigma_x(x, h)/\hat{\sigma}$, $\sigma_y(x, 0)/\hat{\sigma}$, $\tau(x, h/\sqrt{3})/\sigma$ caused by the distribution (1a); the results hold equally for a thin strip or wide slab (a " bar "); in Fig. 2b is plotted, for $\nu = 0{\cdot}3$ and $\nu = 0{\cdot}5$, the thin strip displacement $E u_s(x, y; \nu)/\hat{\sigma}$; and in Fig. 2c is plotted the bar displacement $E u_b(x, y; \nu)/\hat{\sigma}$. It will be recalled (TIMOSHENKO and GOODIER 1951) that

$$E u_b(\nu) = (1 - \nu^2)\, E u_s\left(\frac{\nu}{1-\nu}\right). \tag{6}$$

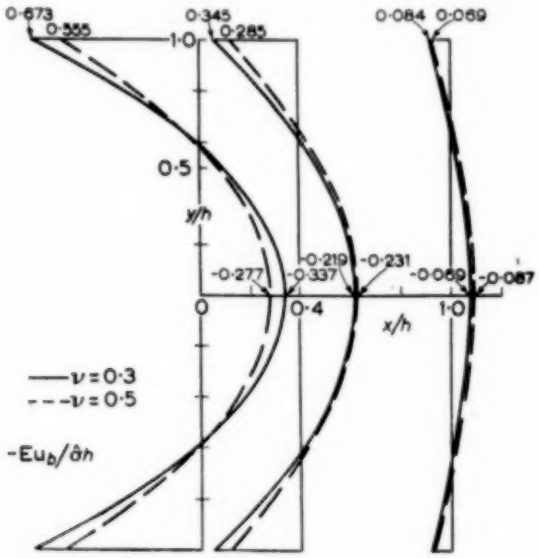

Fig. 2c.

Note that while the stress profiles do not vary with x in the variational approximation (in the rigorous, solution e.g., HORVAY and BORN 1954b, they do vary, but vary very slowly), the displacement profile u does vary with x (a Poisson ratio effect) and therefore complete profiles are shown in the figure.

In Fig. 3 (a, b, c) similar plots are shown for the $\tau^\circ(y)$ loading. There exist some arbitrariness in the displacements; arbitrary rigid body displacements may be added to the solutions (3b, c), and they still remain solutions. In (3b, c) the arbitrariness was eliminated by requiring that the displacement at infinity be zero. This requirement insures that, for $\sigma_x(y)$ loading, the average u displacement of the $x = 0$ end is also zero. In contrast it is seen from Fig. 3 (b, c) that the shear load $\tau^\circ(y)$ causes a net extrusion of the strip (or the bar) to the left. This effect is particularly pronounced for the $\nu = 0{\cdot}5$ case of Fig. 3 (c).

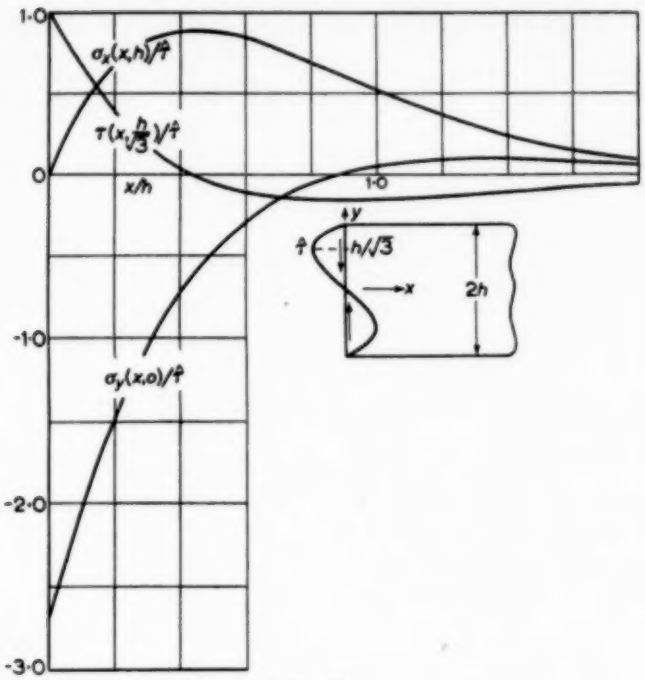
1·0
0
-1·0
-2·0
-3·0
$\sigma_x(x,h)/\hat{T}$
$\tau(x,\frac{h}{\sqrt{3}})/\hat{T}$
x/h
1·0
$\sigma_y(x,0)/\hat{T}$
y
$\hat{T}$
$h/\sqrt{3}$
x
2h

Fig. 3a.

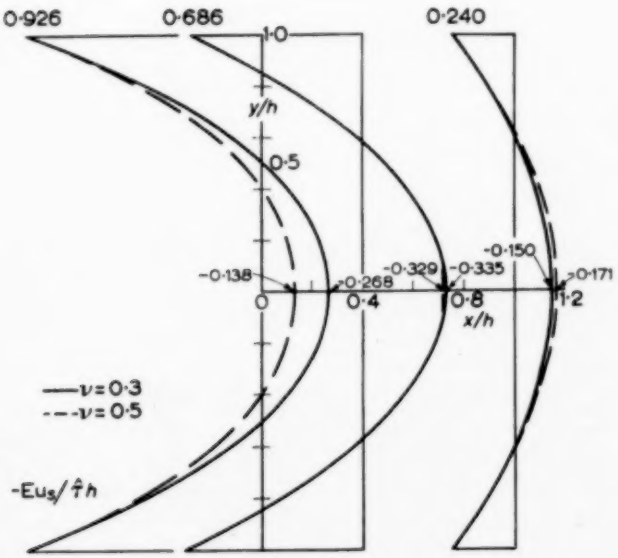
0·926
0·686
1·0
0·240
y/h
0·5
-0·138
0·268
-0·329
-0·335
-0·150
0·171
0
0·4
0·8
1·2
x/h
ν=0·3
ν=0·5
$-Eu_s/\hat{T}h$

Fig. 3b.

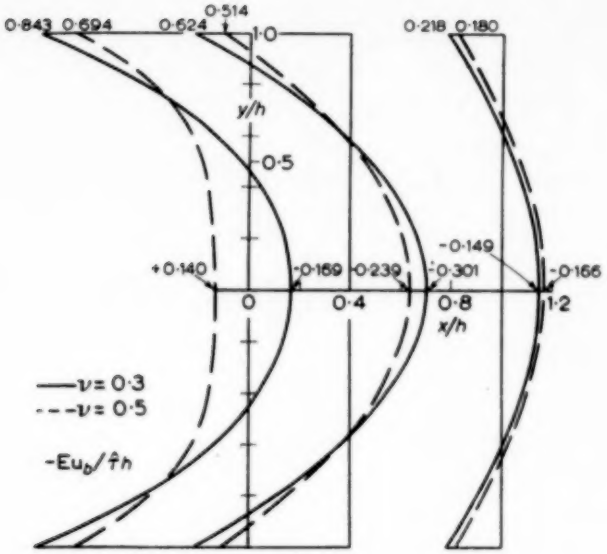

Fig. 3c.

3. THE FINITE RECTANGLE

As the x-length l of the rectangle is gradually shortened the stresses originating at $x = 0$ no longer decay to zero at location $x = l$, but are reflected, so as to ensure a free edge at $x = l$*. The case $l/h = 5$ was plotted in an earlier paper (HORVAY and BORN 1954a); in the present paper (Figs. 4, 5) the stresses pertaining to the more interesting case $l/h = 1$ are plotted. The pertinent variational stress functions now are†

$$\Phi_\sigma = \frac{2}{3\sqrt{35}}\, h^2\, \hat{\sigma}\, f_2(y)\, g_2(x), \qquad \Phi_\tau = 2\sqrt{\frac{3}{35}}\, h^2\, \hat{\tau}\, f_2(y)\, h_2(x), \tag{6a}$$

$$2\, g_2(x), \qquad 2\, h_2(x) = \mathcal{A}_2 \cosh \alpha_2 \xi \cos \beta_2 \xi + \mathcal{B}_2 \cosh \alpha_2 \xi \sin \beta_2 \xi$$

$$+ \mathcal{C}_2 \sinh \alpha_2 \xi \cos \beta_2 \xi + \mathcal{D}_2 \sinh \alpha_2 \xi \sin \beta_2 \xi\,; \qquad \xi \equiv \frac{x}{h} - \tfrac{1}{2}. \tag{6b}$$

*Care must be exercised in regard to the sign of the reflected stresses and displacements. The σ_x stress which arrives at $x = l$ is simply fed back into the rectangle with opposite sign. The case of the shear stress is more complicated. A shear stress which assumes, say, a positive value on the $x = l$ edge of the rectangle, must be regarded as negative when the direction of the x axis is reversed. Therefore, to eliminate the boundary shear, we must apply an equal and opposite compensating shear at $x = l$, i.e., a positive shear with respect to the $-x$ direction. This was overlooked by BORN and HORVAY (1955); correspondingly Fig. 3 of that reference is incorrect.

†Write $g_2(x) = \frac{1}{2}(g_{2e} - g_{2o})$, $h_2(x) = \frac{1}{2}(-h_{2e} + h_{2o})$ where $g_{2e}, \ldots, h_{2o}$ are given in (9) of the reference, and $k = \frac{1}{2}$ is used. Since in the reference x is measured from the centre of the strip, in the present paper x is measured from the left face of the strip; moreover the strip width is now $2h$ while previously it was 2, the symbol x of the reference is now replaced by $x/h - \frac{1}{2}$.

	g_2	h_2
$\mathcal{A}_2$	0·932411	0·209608
$\mathcal{B}_2$	1·55041	0·800814
$\mathcal{C}_2$	− 2·24663	− 0·662792
$\mathcal{D}_2$	− 0·368094	− 0·419565

(6c)

One notes from the Figures that while in the semi-infinite case the maximum tensile σ_y developed, around $x \simeq h$, was trifling, in the present finite rectangle case, the tensile σ_y at $x = h$ builds up to a considerable magnitude, because of repeated

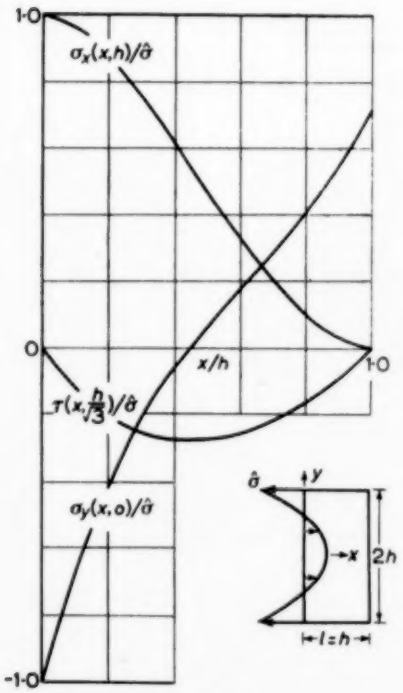

Fig. 4.

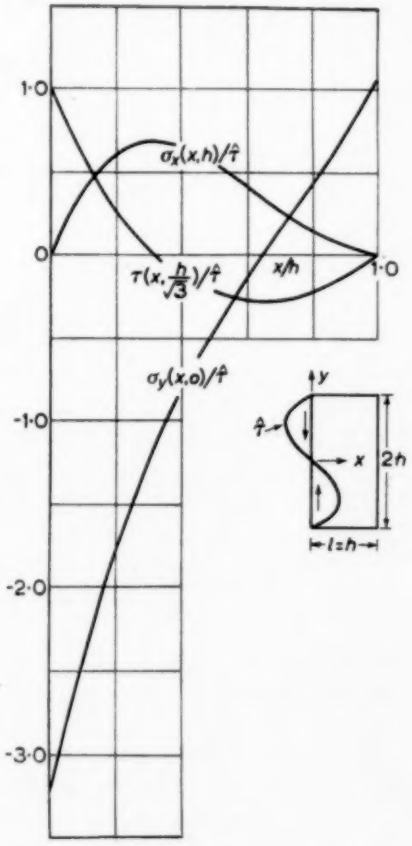

Fig. 5.

reflections at the free edge. (The $x = 0$ value of σ_y also increases, but more moderately). As l/h is further reduced, the self-equilibrating loads acting at $x = 0$ take on the aspect of simple bending, and of combined bending and tension, respectively, as illustrated in Fig. 6 (a, b), where

$$M = \int_0^h \sigma_x^{\circ}\, y dy = \tfrac{1}{8} h^2 \overset{\wedge}{\sigma} \tag{7a}$$

and

$$V = \int_0^h \tau^{\circ}\, dy = \frac{3\sqrt{3}}{8} h \overset{\wedge}{\tau}, \qquad M = \tfrac{1}{2} lV \tag{7b}$$

respectively.

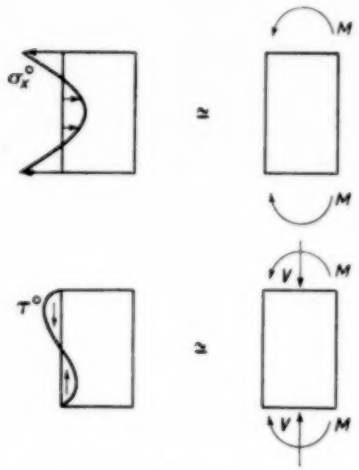

Fig. 6.

In Fig. 7 (a, b, c) are plotted $\sigma_y(0, 0)/\overset{\wedge}{\sigma}$, $\sigma_y(l, 0)/\overset{\wedge}{\sigma}$, $Eu(0, h)/\overset{\wedge}{\sigma}h$, $Eu(0, 0)/\overset{\wedge}{\sigma}h$, $Eu(l, h)/\overset{\wedge}{\sigma}h$ and $Eu(l, 0)/\overset{\wedge}{\sigma}h$ vs. l/h. It is seen that in so far as the σ_y stress is concerned, the rectangle behaves for $l/h > 2$ essentially as a semi-infinite strip, for $l/h < 1$ it behaves essentially as a narrow beam with stresses

$$\sigma_y(0, y)/\overset{\wedge}{\sigma} = -\tfrac{3}{4}(h/l)^2, \qquad \sigma_y(l, y)/\overset{\wedge}{\sigma} = \tfrac{3}{4}(h/l)^2, \tag{8}$$

appropriate to the (7a) loading. The narrow-beam displacement formulas

$$\frac{Eu(0, y)}{\overset{\wedge}{\sigma}h} = \frac{Eu(l, y)}{\overset{\wedge}{\sigma}h} = \tfrac{1}{4}\left(\frac{h}{l}\right)^3\left(1 - 3\frac{y^2}{h^2}\right) = \begin{cases} -\tfrac{1}{2}(h/l)^3, & y = h \\ \tfrac{1}{4}(h/l)^3, & y = 0 \end{cases} \tag{9}$$

are, as seen from Fig. 7 (b), much more laggard in asserting themselves. The strip displacements (9) are converted into the bar displacements of Fig. (7c) by formula (6).

Fig. 8 (a, b, c) shows the corresponding results for the boundary shear traction (1b). For the case of the narrow beam the asymptotic relations are*

$$\frac{\sigma_y(0, y)}{\overset{\wedge}{\tau}} = -\frac{3\sqrt{3}}{2}\frac{h}{l} = -2{\cdot}60\,\frac{h}{l}, \qquad \frac{\sigma_y(l, y)}{\overset{\wedge}{\tau}} = \frac{3\sqrt{3}}{4}\frac{h}{l} = 1{\cdot}30\,\frac{h}{l}, \tag{10}$$

$$\frac{Eu(0, y)}{\overset{\wedge}{\tau}h} = \frac{3\sqrt{3}}{8}\left[\left(\frac{h}{l}\right)^2\left(1 - 3\frac{y^2}{h^2}\right) - \nu\right] = \begin{cases} -1{\cdot}30\,(h^2/l^2 + \nu/2), & y = h \\ 0{\cdot}65\,(h^2/l^2 - \nu), & y = 0 \end{cases} \tag{11a}$$

*The equations (25) of HORVAY and BORN (1954a) contain a misprint: the factors k^2 which divide the second terms should be replaced by first powers k. The second of (23b) of the reference is also in error; it should read $M = -k$; and (15b) should read $\sigma_{y,\max} = 2/k$. These errors do not affect the figures or the remainder of the paper.

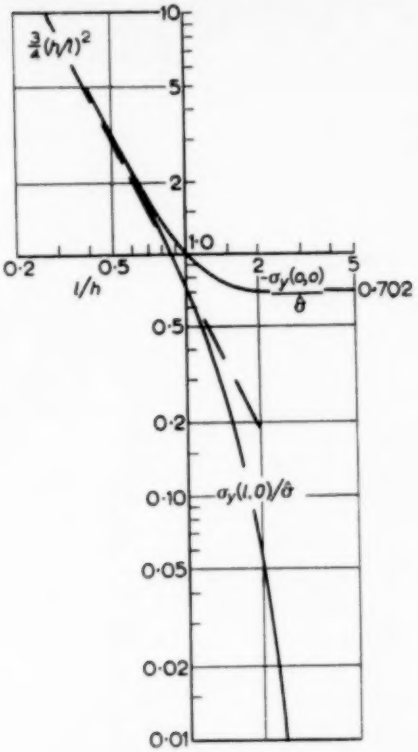

Fig. 7a.

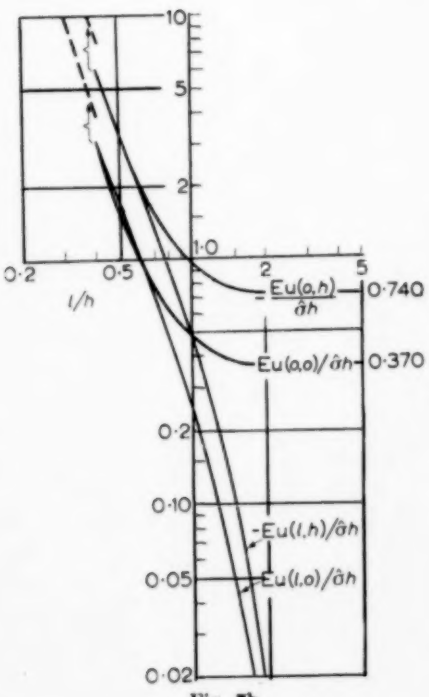

Fig. 7b.

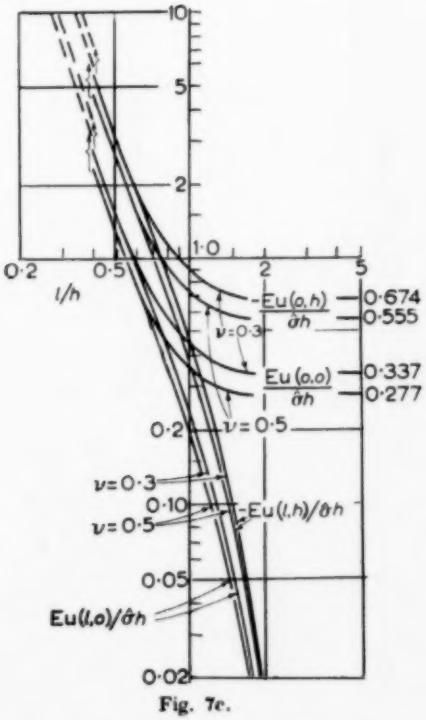

Fig. 7c.

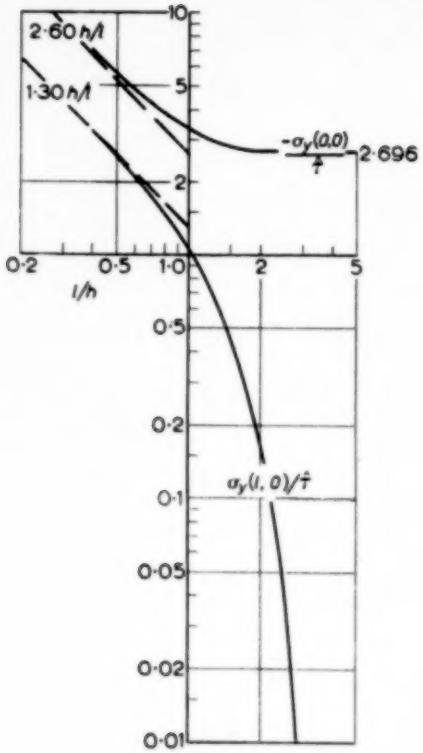

Fig. 8a.

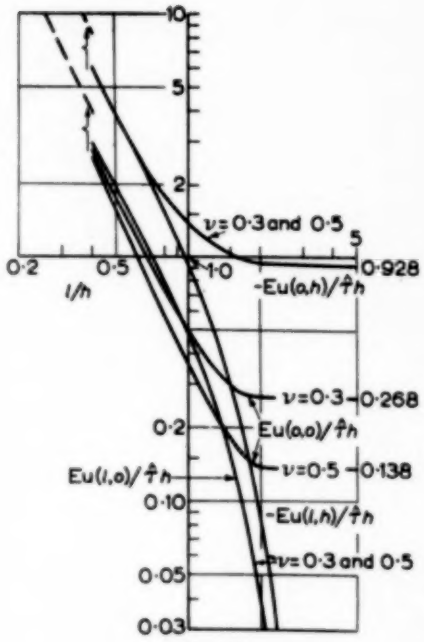

Fig. 8b.

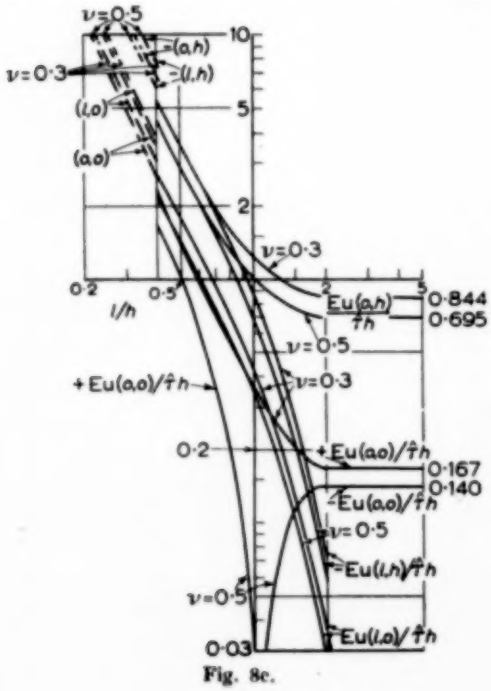

Fig. 8c.

$$\frac{Eu\,(l,\,y)}{\overset{\wedge}{\tau} h} = \frac{3\sqrt{3}}{8}\left(\frac{h}{l}\right)^2\left(1 - 3\,\frac{y^2}{h^2}\right) = \begin{cases} -\,1{\cdot}30\,h^2/l^2, & y = h \\ 0{\cdot}65\,h^2/l^2, & y = 0 \end{cases} \tag{11b}$$

Note that the ν portion of the displacement $Eu\,(0, y)$ is due to the Poisson ratio effect that results from the squashing of the strip by shear forces V of Fig. 6 (b). It would probably be more logical to assign to the cross-section $x = l/2$ the displacement u with zero average than to the cross-section $x = l$, as is done in Fig. 8 (b, c). However, the latter choice avoids the necessity of calculating $Eu\,(l/2,\,y)$. The conversion of the strip displacements of Fig. 8 (b) into the bar displacements of Fig. 8 (c) is carried out as before.

4. Higher Tractions

The parabolic normal traction (1a) and the cubic shear traction (1b) are the simplest possible self-equilibrating tractions that may be prescribed. As was shown (Horvay 1953a) any given self-equilibrating traction $\sigma_x^{\circ}\,(y)$ may be represented as a linear combination of the tractions $f_2''\,(y)$, $f_3''\,(y)$, $f_4''\,(y)\,\ldots$ and any given self-equilibrating traction $\tau^{\circ}\,(y)$ may be represented as a linear combination of the tractions $f_2'\,(y)$, $f_3'\,(y)$, $f_4'\,(y)\,\ldots$, where $f_2\,(y)$,

$$f_3\,(y) = \frac{3\sqrt{385}}{16}\,(1 - y^2/h^2)^2\,(y/h),$$

$$f_4\,(y) = \frac{3\sqrt{91}}{32}\,(1 - y^2/h^2)^2\,(-\,1 + 11\,y^2/h^2),\ \text{etc.}, \tag{12}$$

are orthonormal polynomials, defined by (2b), (4a). Associated with these higher degree polynomials are the more rapidly decaying longitudinal factors $g_k\,(x)$, $h_k\,(x)$, retaining the form (2c), (5b) but having now parameters

$$\begin{aligned} \alpha_3 + \beta_3\,i &= 3{\cdot}656 + 1{\cdot}538\,i, \\ \alpha_4 + \beta_4\,i &= 5{\cdot}259 + 2{\cdot}062\,i, \qquad \text{etc.} \end{aligned} \tag{13}$$

Figures similar to Figs. 2-5, 7, 8 may be plotted also for these higher tractions. No such plots are given in this paper, since the higher tractions are usually of interest only in the exceptional cases where the f_2'', f_2' components are precisely absent from the applied traction distributions.

5. The Semi-infinite Plane

It was pointed out (Horvay, to be published) that the slowest decay (namely for given self-equilibrating tractions σ_x°, τ° applied to edge $x = 0$ at $-\,h \leqslant y \leqslant h$) occurs when the wedge semi-angle ω is $\pi/2$. Assuming for simplicity that $h = 1$, and introducing the notation

$$Z = -\,iz = y - ix, \qquad \bar{P}_k\,(y) = \int_{-1}^{y} P_k\,(y)\,dy, \tag{14}$$

we find, more specifically, that when tractions

$$\sigma_k^{\circ}\,(y) = P_k\,(y), \qquad \tau_k^{\circ}\,(y) = -\,\bar{P}_k\,(y), \tag{15}$$

$$2P_2 = -1 + 3y^2 \qquad -2\bar{P}_2 = y - y^3$$
$$2P_3 = -3y + 5y^3 \qquad -8\bar{P}_3 = -1 + 6y^2 - 5y^4 \tag{16}$$
$$8P_4 = 3 - 30y^2 + 35y^4 \qquad -8\bar{P}_4 = -3y + 10y^3 - 7y^5, \quad \text{etc.}$$

act on the portion $|y| \leqslant 1$ of the edge (and no tractions act on $|y| > 1$) the MUSKHELISVILI potentials Φ and Ψ are (see Appendix) given by

$\sigma_2^{\circ}(y)$:

$$2\pi i\,\Phi = \frac{1-3Z^2}{2}\ln\frac{Z-1}{Z+1} - 3Z = \tfrac{4}{15}Z^{-3} + \tfrac{8}{35}Z^{-5} + \dots$$

$$2\pi i\,\Psi = \frac{2Z}{Z^2-1} + 3Z^2\ln\frac{Z-1}{Z+1} + 6Z = \tfrac{4}{3}Z^{-3} + \tfrac{8}{7}Z^{-5} + \dots$$

$\sigma_3^{\circ}(y)$:

$$2\pi i\,\Phi = \frac{3Z-5Z^3}{2}\ln\frac{Z-1}{Z+1} + \tfrac{4}{3} - 5Z^2 = \tfrac{4}{35}Z^{-4} + \tfrac{8}{63}Z^{-6} + \dots$$

$$2\pi i\,\Psi = \frac{2}{Z^2-1} + \frac{-3Z+15Z^3}{2}\ln\frac{Z-1}{Z+1} + 2 + 15Z^2 = \tfrac{16}{35}Z^{-4} + \tfrac{16}{81}Z^{-6} + \dots \tag{17}$$

$\sigma_4^{\circ}(y)$:

$$2\pi i\,\Phi = \tfrac{1}{8}(-3 + 30Z^2 - 35Z^4)\ln\frac{Z-1}{Z+1} + \tfrac{46}{15}Z - \tfrac{35}{4}Z^3 = \tfrac{16}{315}Z^{-5} + \tfrac{16}{231}Z^{-7} + \dots$$

$$2\pi i\,\Psi = \frac{2Z}{Z^2-1} + \tfrac{1}{2}(-15Z^2 + 35Z^4)\ln\frac{Z-1}{Z+1} - \tfrac{10}{3}Z + 35Z^3 = \tfrac{16}{63}Z^{-5} + \tfrac{16}{33}Z^{-7} + \dots$$

$\tau_2^{\circ}(y)$:

$$2\pi\,\Phi = \frac{-Z+Z^3}{2}\ln\frac{Z-1}{Z+1} - \tfrac{2}{3} + Z^2 = \tfrac{2}{15}Z^{-2} + \tfrac{2}{35}Z^{-4} + \dots$$

$$2\pi\,\Psi = \frac{3Z-5Z^3}{2}\ln\frac{Z-1}{Z+1} + \tfrac{4}{3} - 5Z^2 = \tfrac{4}{35}Z^{-4} + \tfrac{8}{63}Z^{-6} + \dots$$

$\tau_3^{\circ}(y)$:

$$2\pi\,\Phi = \tfrac{1}{4}(1 - 6Z^2 + 5Z^4)\ln\frac{Z-1}{Z+1} - \tfrac{13}{12}Z + \tfrac{5}{4}Z^3 = \tfrac{4}{105}Z^{-3} + \tfrac{8}{315}Z^{-5} + \dots \tag{18}$$

$$2\pi\,\Psi = \tfrac{1}{4}(-1 + 12Z^2 - 15Z^4)\ln\frac{Z-1}{Z+1} + \tfrac{7}{4}Z - \tfrac{15}{2}Z^3 = \tfrac{4}{105}Z^{-3} + \tfrac{8}{105}Z^{-5} + \dots$$

$\tau_4^{\circ}(y)$:

$$2\pi\,\Phi = \tfrac{1}{8}(3Z - 10Z^3 + 7Z^5)\ln\frac{Z-1}{Z+1} + \tfrac{4}{15} - \tfrac{23}{12}Z^2 + \tfrac{7}{4}Z^4 = \tfrac{44}{735}Z^{-4} + \tfrac{8}{147}Z^{-6} + \dots$$

$$2\pi\,\Psi = \tfrac{1}{8}(-9Z + 50Z^3 - 49Z^5)\ln\frac{Z-1}{Z+1} - \tfrac{8}{15} + \tfrac{101}{12}Z^2 - \tfrac{49}{4}Z^4 = \tfrac{88}{735}Z^{-4} + \tfrac{32}{147}Z^{-6} + \dots$$

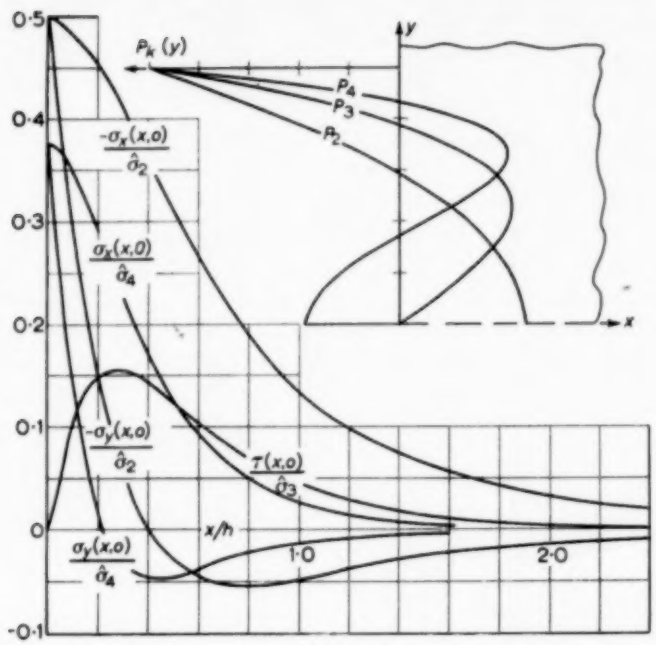
0·5
0·4
0·3
0·2
0·1
0
-0·1
$P_k(y)$
P_4
P_3
P_2
y
x
$\frac{-\sigma_x(x,0)}{\hat{\sigma}_2}$
$\frac{\sigma_x(x,0)}{\hat{\sigma}_4}$
$\frac{-\sigma_y(x,0)}{\hat{\sigma}_2}$
$\frac{\tau(x,0)}{\hat{\sigma}_3}$
$\frac{\sigma_y(x,0)}{\hat{\sigma}_4}$
x/h
1·0
2·0

Fig. 9.

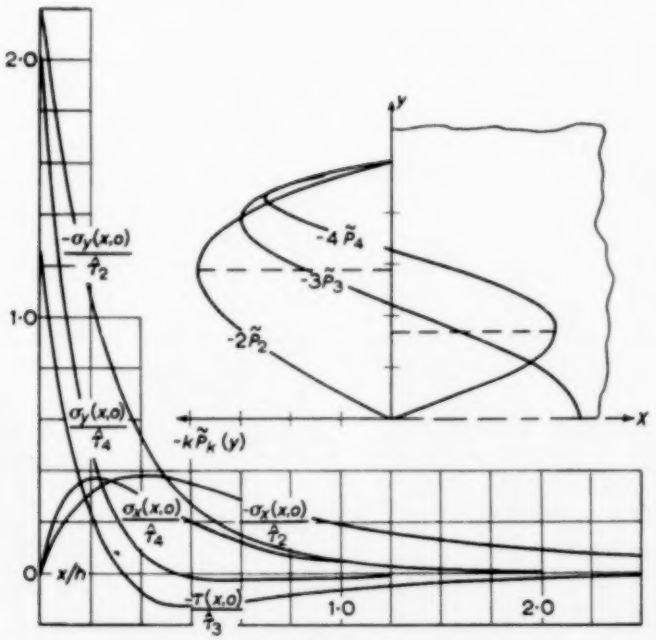
2·0
1·0
0
$\frac{-\sigma_y(x,0)}{\hat{\tau}_2}$
$\frac{\sigma_y(x,0)}{\hat{\tau}_4}$
$\frac{\sigma_x(x,0)}{\hat{\tau}_4}$
$\frac{-\sigma_x(x,0)}{\hat{\tau}_2}$
$\frac{-\tau(x,0)}{\hat{\tau}_3}$
$-4\tilde{P}_4$
$-3\tilde{P}_3$
$-2\tilde{P}_2$
$-k\tilde{P}_k(y)$
y
x
x/h
1·0
2·0

Fig. 10.

From these expressions the stresses are obtained in the form ($\mathcal{R}$ = real part of)

$$\begin{aligned} \sigma_x + \sigma_y &= 4\,\mathcal{R}\,\Phi(Z), \\ \sigma_x - \sigma_y - 2i\,\tau_{xy} &= 2\left[Z\,\Phi'(Z) + \Psi(Z)\right]. \end{aligned} \tag{19}$$

It is clear from the expansions in (17) and (18) that the stresses decay as r^{-3}, r^{-4}, r^{-5}, ... and r^{-2}, r^{-3}, r^{-4}, ... respectively, with distance r from the loaded edge. In Figs. 9 and 10 are plotted the stresses $\sigma_x/\hat{\sigma}_k$, $\sigma_y/\hat{\sigma}_k$, $\tau_{xy}/\hat{\sigma}_k$ (or $\sigma_x/\hat{\tau}_k$, $\sigma_y/\hat{\tau}_k$, $\tau_{xy}/\hat{\tau}_k$) along the x axis. Subscript k attached to $\hat{\sigma}$; $\hat{\tau}$ is used to indicate the traction distribution, $P_k(y)$ or $-\bar{P}_k(y)$, from which the stresses are derived. For even k the shear stresses vanish along $y = 0$, for odd k the normal stresses vanish. It will be noted that the shear traction decays more slowly than the corresponding normal traction. This was explained by v. MISES and STERNBERG as due to lack of " astatic equilibrium " in the case of shear loading (v. MISES 1945 ; STERNBERG 1954). However, as ω is decreased, the two rates of decay get closer to each other, and eventually coalesce. For $k = 2$ this occurs (HORVAY, to be published, Fig. 3a) at about $\omega_{crit} \simeq 56°$. Above this critical wedge angle the decay of the stresses is aperiodic, below ω_{crit} it is sinusoidal. For small angles ω the decay is greatly accelerated by interference due to reflections from the free edges $y = \pm y_b = \pm (h + x \tan \omega)$.

6. Effect of the Shear Traction Gradient

It is well known that a jump in the normal traction acting on the smooth edge of a figure creates only finite stresses in the body ; in contrast a jump in the shear traction – see the insert to Fig. 11 (a) – creates a logarithmically infinite σ_y stress at the point of discontinuity ; see, e.g., FROCHT (1951, equation 2.22). This indicates that shear loadings applied to a body must be controlled with greater care and their variation must be maintained more gradual, if excessive stresses are to be avoided, than is the case for normal loads. Since a quantitative estimate of the required " gradualness," even if obtained only for a special case, is of interest in design, the effect of the shear gradient will be explored for the case illustrated in the Fig. 11 (a) insert.

The traction

$$\tau^{\circ}(y) = \begin{cases} 1 - y, & y > 0 \\ -y - 1, & y < 0 \end{cases} \tag{20}$$

applied to the edge $x = 0$ of the semi-infinite strip $-\leqslant y \leqslant 1$ may be expanded into $f_k'(y)$ polynomials, as follows

$$\begin{aligned} \tau_{(2)}^{\circ} &= -0{\cdot}845105\, f_2' \\ \tau_{(4)}^{\circ} &= -0{\cdot}288761\, f_2' + 0{\cdot}069886\, f_4' \\ \tau_{(6)}^{\circ} &= -0{\cdot}315356\, f_2' + 0{\cdot}063288\, f_4' - 0{\cdot}028701\, f_6' \\ \tau_{(8)}^{\circ} &= -0{\cdot}301074\, f_2' + 0{\cdot}069868\, f_4' - 0{\cdot}029049\, f_6' + 0{\cdot}015409 f_8', \text{ etc.,} \end{aligned} \tag{21}$$

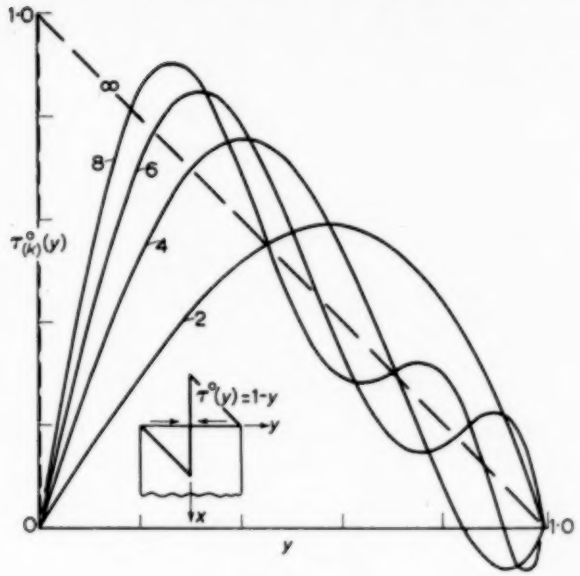

Fig. 11a.

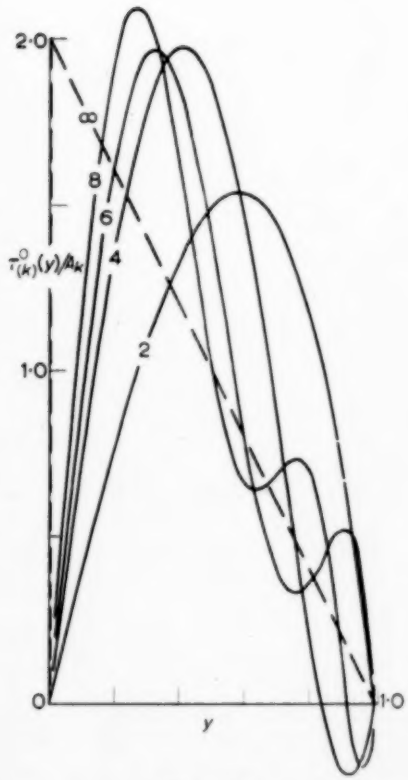

Fig. 11b.

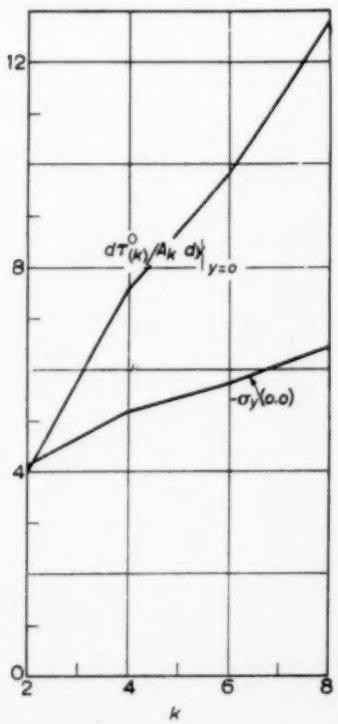

Fig. 11c.

These successive approximations, of type $-\sum_{i=2}^{n} b_{ni} f_i(y)$, are plotted in Fig. 11 (a)*. Dividing by the respective areas

$$A_2 = 0{\cdot}38281, \qquad A_4 = 0{\cdot}38281, \qquad A_6 = 0{\cdot}43075, \qquad A_8 = 0{\cdot}43386, \tag{22}$$

one obtains Fig. 11 (b) in which every curve subtends the same area, 0·5. The stress σ_y at $x = 0$ is finally obtained from the formula $\sum_{i=2}^{n} b_{ni} f_i(y)\, h_i''(0)$, where $f_i(y)$, $h_i''(x)$ are tabulated functions (HORVAY and BORN 1955). In this fashion one arrives at Fig. 11 (c) which indicates that as one increases the order of approximation from $k = 2$ to $k = 8$ and thereby triples the slope $d\tau_{(k)}{}^{\circ}/A_k\, dy$ at $y = 0$, the stress $\sigma_y(0, 0)$ increases by about 50 per cent.

APPENDIX

DETERMINATION OF THE MUSHKHELISVILI FUNCTIONS FOR THE LOADING OF THE SEMI-INFINITE PLANE

The formulas for the complex potentials Φ, Ψ adapted to the notation of Fig. 12, may be written in the form (MUSHKHELISVILI 1953, pp. 385-388)

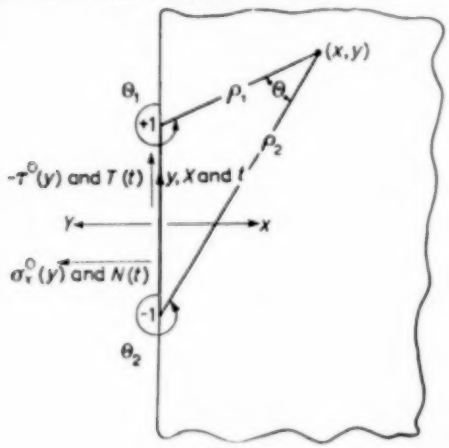

Fig. 12.

$$\Phi(Z) = -\frac{1}{2\pi i}\int_{-\infty}^{\infty} \frac{N(t) - iT(t)}{t - Z}\, dt,$$

$$\Psi(Z) = \begin{cases} -Z\,\Phi'(Z) & \text{for} \quad T = 0 \\ -2\,\Phi(Z) - Z\,\Phi'(Z) & \text{for} \quad N = 0 \end{cases}$$

$$N(t) = \sigma^{\circ}(y), \qquad T(t) = -\tau^{\circ}(y). \tag{24}$$

$$z = x + iy = iZ = iX - Y,$$

$$\sigma_x = \sigma_Y, \qquad \sigma_y = \sigma_X, \qquad \tau_{xy} = -\tau_{YX}.$$

$$\int_{-1}^{1} \frac{dt}{t - Z} = \ln\frac{Z - 1}{Z + 1} = \ln\frac{\rho_1}{\rho_2} + i(\theta_1 - \theta_2) = \ln\frac{\rho_1}{\rho_2} - i\Theta$$

*It is simplest to expand (20) first into the $T_k(y)$ polynomials (HORVAY and BORN, to be published).

$$1 - y = -0{\cdot}597739\, T_2(y) + 0{\cdot}323609\, T_4(y) - 0{\cdot}225662\, T_6(y) + 0{\cdot}0174251\, T_8(y) - \ldots \tag{23}$$

The $T_k(y)$ are the orthonormalized $f_k'(y)$ polynomials. Because of their orthogonality, the coefficients of the expansion (23) do not change as more terms are added. Then one rearranges the partial sums of (23) into the $f_k'(y)$ expansions listed in (21).

These formulas lead immediately to the potentials listed in (17) and (18). Denoting

$$D = (1 + x^2 - y^2)^2 + 4x^2 y^2, \qquad \lambda = \ln \frac{\rho_1}{\rho_2}, \tag{25}$$

one then obtains, by (19), the following stress expressions.

Equations (26) :

$\sigma_2^{\circ} = P_2(y)$:

$$2\pi\sigma_x = (-1 + 3y^2 + 3x^2)\,\Theta - 6x + 4x(1 + x^2 - y^2)/D$$

$$2\pi\sigma_y = (-1 + 3y^2 - 9x^2)\,\Theta + 12xy\,\lambda + 18x - 4x(1 + x^2 - y^2)/D$$

$$2\pi\tau_{xy} = -6xy\,\Theta - 6x^2\,\lambda + 8x^2\,y/D$$

$\sigma_3^{\circ} = P_3(y)$:

$$2\pi\sigma_x = (-3 + 15x^2 + 5y^2)\,y\Theta + 10x^2\,\lambda - 10xy + 4xy(1 - x^2 - y^2)/D$$

$$2\pi\sigma_y = (-3 - 45x^2 + 5y^2)\,y\Theta - (6 + 20x^2 - 30y^2)\,x\lambda + 50xy - 4xy(1 - x^2 - y^2)/D$$

$$2\pi\tau_{xy} = (3 + 15x^2 - 15y^2)\,x\,\Theta - 30x^2\,y\lambda - 30x^2 + 4x^2(1 + x^2 + y^2)/D$$

$\sigma_4^{\circ} = P_4(y)$:

$$4\pi\sigma_x = \left[\tfrac{3}{2} - 15(x^2 + y^2) + \tfrac{35}{2}(-3x^4 + 6x^2y^2 + y^4)\right]\Theta + 140x^3\,y\lambda - 5x(1 - 21x^2 + 7y^2) + 8x(1 + x^2 - y^2)/D$$

$$4\pi\sigma_y = \left[\tfrac{3}{2} + 15(3x^2 - y^2) + \tfrac{35}{2}(5x^4 - 18x^2y^2 + y^4)\right]\Theta - 20(3 + 14x^2 - 7y^2)\,xy\lambda - 5x(\tfrac{19}{3} + 35x^2 - 49y^2) - 8x(1 + x^2 - y^2)/D$$

$$4\pi\tau_{xy} = 10(3 + 21x^2 - 7y^2)\,xy\,\Theta + 10(3 + 7x^2 - 21y^2)\,x^2\,\lambda - 280x^2\,y + 16x^2\,y/D.$$

Equations (27) :

$\tau_2^{\circ} = -\tilde{P}_2(y)$:

$$2\pi\sigma_x = -(1 + 3x^2 - 3y^2)\,x\Theta + 6x^2\,y\,\lambda + 6x^2$$

$$2\pi\sigma_y = (3 + 5x^2 - 9y^2)\,x\Theta - 2(1 + 6x^2 - y^2)\,y\lambda - \tfrac{8}{3} - 10x^2 + 4y^2$$

$$2\pi\tau_{xy} = (1 + 9x^2 - y^2)\,y\Theta + 2(1 + 2x^2 - 3y^2)\,x\,\lambda - 10xy$$

$\tau_3^{\circ} = -\tilde{P}_3(y)$:

$$4\pi\sigma_x = -2(3 + 15x^2 - 5y^2)\,xy\Theta - 2(3 + 5x^2 - 15y^2)\,x^2\,\lambda + 40x^2\,y$$

$$4\pi\sigma_y = 2(9 + 25x^2 - 15y^2)\,xy\Theta + \left[1 + 6(2x^2 - y^2) + 5(3x^4 - 12x^2y^2 + y^4)\right]\lambda - 2y(\tfrac{13}{3} + 35x^2 - 5y^2)$$

$$4\pi\tau_{xy} = \left[-\tfrac{1}{2} - 3(3x^2 - y^2) - \tfrac{5}{2}(5x^4 - 18x^2y^2 + y^4)\right]\Theta + 4(3 + 10x^2 - 5y^2)\,xy\lambda + x(\tfrac{29}{3} + 25x^2 - 35y^2)$$

$\tau_4 = -\tilde{P}_4(y)$:

$$8\pi\sigma_x = \left[3 + 30(x^2 - y^2) + 35(x^4 - 6x^2y^2 + y^4)\right]x\,\Theta - 20(3 + 7x^2 - 7y^2)\,x^2\,y\lambda - 10x^2(\tfrac{11}{3} - 7x^2 + 21y^2)$$

$$8\pi\sigma_y = -\left[9 + 10(5x^2 - 9y^2) + 7(7x^4 - 30x^2y^2 + 15y^4)\right]x\Theta + 2\left[3 + 10(6x^2 - y^2) + 7(15x^4 - 20x^2y^2 + y^4)\right]y\lambda + \tfrac{64}{15} + \tfrac{202}{3}x^2 - \tfrac{92}{3}y^2 + 14(7x^4 - 27x^2y^2 + 2y^4)$$

$$8\pi\tau_{xy} = -\left[3 + 10(9x^2 - y^2) + 7(25x^4 - 30x^2y^2 + y^4)\right]y\Theta - 2\left[3 + 10(2x^2 - 3y^2) + 7(3x^4 - 20x^2y^2 + 5y^4)\right]x\lambda + 2xy(\tfrac{101}{3} + 133x^2 - 63y^2).$$

ACKNOWLEDGMENTS

The author is indebted to Mrs. J. S. BORN for help with analysis and for calculating most of the curves. He wishes to express his appreciation also to Mrs. C. BOHLMAN for curve plotting.

REFERENCES

BORN, J. S. and HORVAY, G.	1955	*J. Appl. Mech.* **22**, 401.
FROCHT, M. M.	1948	*Photoelasticity*, Vol. II (New York, Wiley and Sons, Inc.).
HORVAY, G.	1953a	*J. Appl. Mech.* **20**, 87.
	1953b	Discussion of above paper, *ibid.* **20**, 376.
	1954	*Proc. 2nd. Nat. Cong. Appl. Mech.* ASME, 313.
	1957	To be published.
HORVAY, G. and BORN, J. S.	1954	*Proc. 2nd. Nat. Cong. Appl. Mech.* ASME, 267.
	1955	*J. Math. Phys.* **33**, 360.
	1957	*J. Appl. Mech.* in press.
MISES, R. v.	1945	*Bull. Amer. Math. Soc.* **51**, 555.
MUSHKHELISVILI, N. I.	1953	*Some Basic Problems in the Math. Theory of Elasticity* translated by J. R. M. RADOK (Groningen, P. Noordhoff Ltd.).
STERNBERG, E.	1954	*Quart. Appl. Math.* **11**, 393.
TIMOSHENKO, S. and GOODIER, J. N.	1951	*Theory of Elasticity* (New York, McGraw-Hill Book Co.).

Journal of the Mechanics and Physics of Solids, 1957, Vol. 5, pp. 95 to 114. Pergamon Press Ltd., London.

ETUDE DE LA FORME DES COURBES DE DEFORMATION PLASTIQUE

Par B. JAOUL
Centre de Recherches Métallurgiques de l'Ecole des Mines de Paris

(*Received* 10*th December*, 1956)

SOMMAIRE

L'ANALYSE précise de la forme des courbes de traction des métaux permet de définir, dans le cas le plus général, quatre mécanismes de déformation qui se développent successivement et correspondent à diverses lois d'écrouissage :

(1) Déformation pseudo-élastique, où tous les glissements sont réversibles.

(2) Domaine de consolidation intergranulaire, où quelques glissements sont encore réversibles; l'origine de l'écrouissage est principalement aux joints, car cette portion de la courbe correspond, dans les monocristaux, à la zone de glissement facile.

(3) Domaine d'écrouissage intracristallin linéaire où la consolidation due aux joints ne croit plus. La pente de la courbe est alors égale au centième du module élastique jusqu'au point de transition.

(4) Au delà du point de transition, le taux d'écrouissage diminue par suite d'une diffusion des dislocations bloquées, ce qui entraine une fragmentation progressive des grains.

Les amplitudes respectives de chacun de ces domaines sont fortement influencées par la nature du métal, sa pureté et la température de l'essai ; certains peuvent alors disparaitre et les quatre domaines ne sont observables simultanément sur une même courbe que dans des conditions particulières.

SUMMARY

PRECISE analysis of the shape of tensile test curves of metals enables, in the most general case, the definition of four mechanisms of deformation which appear in succession and correspond to differing laws of strain-hardening :

(1) Pseudo-elastic deformation where all slip is reversible.

(2) Domaine of intergranular hardening where some slip is still reversible ; the origin of the work hardening is principally in the grain boundaries for, in monocrystals, this position of the curve corresponds with the zone of easy glide.

(3) A region of linear intracrystalline strain hardening wherein the hardening due to the grain boundaries does not increase. Then, up to the transition point, the slope of the curve is equal to a hundredth of the modulus of elasticity.

(4) Beyond the transition point the rate of increase of work hardening diminishes due to the diffusion of blocked dislocations which entails the progressive fragmentation of the grains.

The respective ranges of each of these regions is strongly influenced by the nature of the metal, its purity and the testing temperature ; certain regions can then disappear and the four domains are not observable simultaneously on the same curve other than in special conditions.

1. INTRODUCTION

LES courbes de déformation plastique des métaux sont généralement représentées par des relations paraboliques qui rendent assez bien compte de la valeur de la

tension nécessaire pour atteindre un certain allongement. Il existe cependant de nombreux cas où la courbe réelle est très éloignée d'une courbe parabolique simple, par suite de phénomènes particuliers se développant au cours de la déformation ; nous pouvons citer notamment le cas des courbes de traction d'acier doux qui présentent un palier et celui des courbes des monocristaux qui sont caractérisées par la présence d'un " glissement facile " précédent la courbe de consolidation classique.

2. DECOMPOSITION DES COURBES DE DEFORMATION

Ce n'est cependant pas pour rendre compte de tels phénomènes que nous avons recherché avec C. CRUSSARD (CRUSSARD 1950, CRUSSARD et JAOUL 1950) si l'on pouvait admettre d'une manière précise une relation du type de celle de LUDWIK (LUDWIK 1909) :

$$\sigma = \sigma_0 + A\epsilon^m$$

σ étant la tension appliquée, ϵ l'allongement rationnel, σ_0 la limite de proportionnalité, A et m des coefficients. Il s'agissait de déterminer si un mécanisme unique de déformation intervenait tout au long de la déformation plastique.

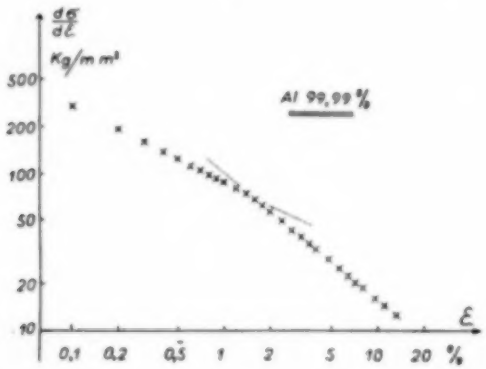

Fig. 1. Variation de la pente d'une courbe de traction en fonction de l'allongement (Al. 99,99 %).

Le tracé continu des courbes de traction, tel qu'il est possible de l'obtenir, par exemple, avec une micromachine Chevenard à enregistrement photographique, peut permettre de saisir de petites variations de forme. Au lieu de représenter l'ensemble de la courbe par une formule du type précédent, on peut essayer de voir, par une méthode différentielle appropriée, si telle ou telle portion où la courbure semble varier de façon continue est représentable par une parabole de LUDWICK ; c'est ce que nous avons fait en étudiant les variations de σ_0, A et m au cours de la déformation (CRUSSARD 1950, CRUSSARD et JAOUL 1950). D'une manière générale, ces coefficients gardent une valeur constante dans un petit domaine d'allongement faisant suite à la limite de proportionnalité, puis présentent une brusque variation pour prender de nouvelles valeurs qu'ils gardent jusqu'à la striction.

Il apparait donc une anomalie dans les courbes de déformation, anomalie que nous avons appelée le " *point de transition des courbes de traction,*" car il correspond

à une transition entre deux mécanismes de déformation. Ce point n'est pas visible sur une courbe de traction normale, car la variation brusque n'est que du second ordre, c'est à dire une variation de courbure : dans le cas de l'aluminium bien recristallisé à grains fins, le rayon de courbure passe brusquement de — 210 à — 140 (valeurs exprimées en kg/mm², comme les tensions) pour un allongement de 1,5% ; pour le cuivre OFHC, il passe de —. 5.800 à — 1.800 kg/mm² pour $\epsilon = 7\%$.

Si l'on porte sur un diagramme doublement logarithmique les valeurs de la pente de la courbe de traction en fonction de l'allongement, les points s'alignent sur deux droites se coupant au point de transition (Fig. 1). Une étude précise de la variation de la pente au voisinage de ce point montre qu'il n'y a pas de zone de raccordement progressif, et qu'il s'agit d'un passage brusque d'un mécanisme de déformation à un autre.

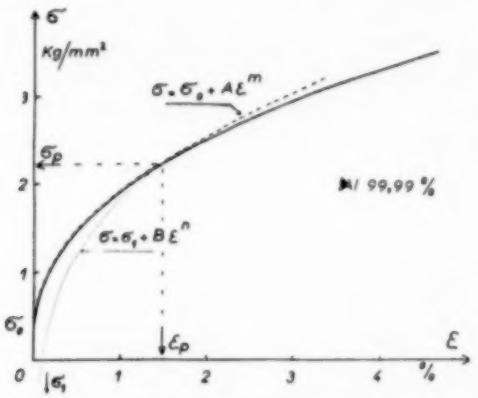

Fig. 2. Décomposition de la courbe de traction d'un aluminium raffiné.

Nous avons alors été conduits à représenter les courbes de traction par deux relations successives :

$$\sigma = \sigma_0 + A\epsilon^m \quad \text{pour} \quad \epsilon < \epsilon_p$$

$$\sigma = \sigma_1 + B\epsilon^n \quad \text{pour} \quad \epsilon > \epsilon_p$$

ϵ_p étant l'allongement au point de transition. Ces deux paraboles sont représentées sur la Fig. 2.

La précision de ces relations trouve une application dans la détermination de la striction ; la relation classique : $d\sigma/d\epsilon = \sigma$ qui détermine l'instabilité de forme conduisant à la striction donne des résultats souvent assez éloignés de la réalité si l'on admet pour la forme de la courbe une relation parabolique unique ; mais si l'on considère l'équation de notre seconde parabole, on détermine des allongements de striction ne différant que de très peu des valeurs expérimentales (Jaoul 1954).

Il est à remarquer que cette décomposition en deux tronçons de parabole successifs permet, ainsi que nous le verrons plus loin, de rendre compte des courbes anormales que nous avons mentionnées : celles du fer et celles des monocristaux.

La forme d'une courbe de traction dépend donc de six paramètres ; ils se réduisent à cinq avec la condition de continuité pour $\epsilon = \epsilon_p$:

σ_0 : limite de proportionnalité

m : coefficient d'écrouissage dans le premier domaine

n : coefficient d'écrouissage dans le second domaine

ϵ_p et σ_p : allongement et tension au point de transition

3. Valeurs des Coefficients dans le Cas de l'aluminium

Nous avons étudié un grand nombre de courbes de traction (environ 300) d'aluminium raffiné à 99,99%. Les éprouvettes (3 mm de diamètre et 25 mm de longueur) avaient été usinées dans des barres tréfilées, puis traitées thermiquement de telle manière que la recristallisation soit totale.

Les essais ont d'abord montré qu'il existait une vitesse critique de déformation en dessous de laquelle une variation de vitesse était sans influence sur la forme des courbes de traction. Aux grandes vitesses surviennent des perturbations dues soit à des effets dynamiques (Crussard et Jaoul 1950), soit à des modifications dans la structure des bandes de glissement analogues à celles signalées par Müller et Leibfried (1955) pour des monocristaux. Pour simplifier, nous ne considérerons que les résultats relatifs à des essais à faible vitesse, c'est à dire inférieure à 10^{-4} sec.

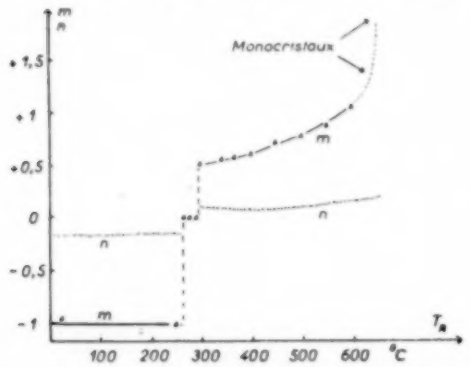

Fig. 3. Variation de l'exposant m en fonction de la température de recuit (aluminium raffiné).

La première particularité est que l'allongement correspondant au point de transition, ϵ_p, reste constant quelle que soit la grosseur du grain : $\epsilon_p = 1{,}6\% \pm 0{,}1\%$ Par contre, cette valeur varie avec la température de l'essai et la pureté du métal, ainsi que nous le verrons plus loin. La tension au point de transition, σ_p, croit quand la densité des joints augmente.

Le deuxième coefficient d'écrouissage, n, varie peu ; il reste compris entre 0,1 et 0,2. Pour certains alliages d'aluminium, il peut cependant être plus faible et même devenir dans certains cas négatif, ce qui correspond alors à une courbe de traction hyperbolique.

Le coefficient m croit régulièrement avec la grosseur du grain ; pour les cristaux très fins, il est égal à 0,5, mais si les grains traversent l'épaisseur de l'éprouvette,

il devient voisin de 1. Enfin, on sait que pour les monocristaux le début de la courbe a sa concavité tournée vers la haut ; m est alors supérieur à 1.

Ces résultats sont relatifs à un métal bien recristallisé ; mais si la température de recuit est insuffisante et l'éprouvette partiellement restaurée, le coefficient m est négatif et égal à -1 ; le point de transition se trouve alors à un allongement plus faible, de l'ordre de 0,3 à 0,4% et l'exposant n est lui aussi négatif. Il existe une température de recuit intermédiare (vers 275° pour l'aluminium raffiné à 99,99%, brut de tréfilage) à laquelle le traitement thermique entraine une structure telle que l'on trouve pour m et n des valeurs nulles, c'est à dire, intermédiaires entre la parabole et l'hyperbole. La courbe de traction peut alors être représentée par une relation logarithmique unique, le point de transition disparaissant ; cette forme est caractéristique de l'état polygonisé.

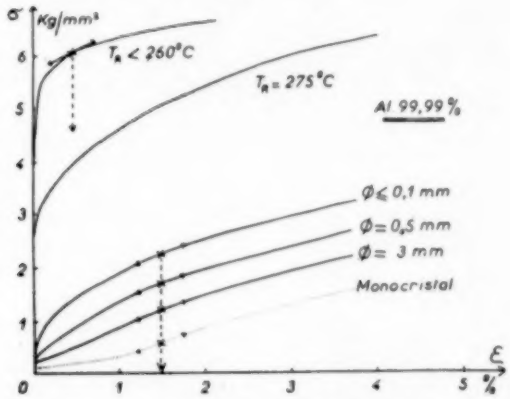

Fig. 4. Divers types de forme de courbe de traction d'aluminium raffiné en fonction de la température de recuit et de la grosseur du grain.

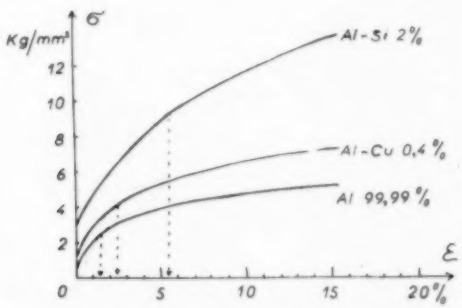

Fig. 5. Influence des éléments d'alliage sur la forme de la courbe de traction de l' aluminium.

La variation de l'exposant m en fonction de la température de recuit est représentée sur la Fig. 3. On voit qu'il est possible de caractériser les différentes étapes de la restauration et du recuit, ainsi que la grosseur du grain, par la forme du début de la courbe de traction. La Fig. 4 représente les divers types de courbe que l'on peut obtenir avec un aluminium raffiné ; les quatre courbes inférieures correspondent à des éprouvettes bien recristallisées, les deux supérieures à des éprouvettes

partiellement restaurées ou polygonisées ; on remarque les variations de l'exposant m, mais on voit qu'au delà du point de transition, les courbes sont toutes sensiblement parallèles.

La présence d'impuretés dans l'aluminium se traduit par une augmentation de l'allongement de transition et aussi une augmentation de résistance. La figure 5 est relative à l'influence du silicium et du cuivre. Nous avons montré que l'allongement ϵ_p croissait comme la puissance $\frac{1}{4}$ de la concentration en atomes dissous (JAOUL, AUBERTIN et CRUSSARD 1952), tandis que la limite élastique et la charge ϵ_p variaient comme la puissance $\frac{3}{4}$ de cette concentration (JAOUL 1954). Cette variation générale de forme mise à part, on retrouve, en fonction de la grosseur du grain et du traitement thermique, les caractéristiques énoncées pour l'aluminium raffiné.

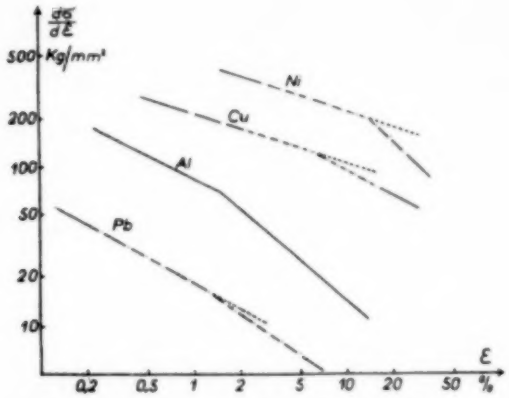

Fig. 6. Variation de la pente en fonction de l'allongement pour des métaux cubiques à faces centrées.

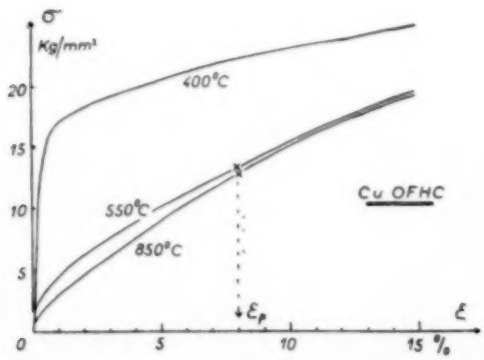

Fig. 7. Divers types de forme de courbe de traction du cuivre OFHC, suivant la température de recuit indiquée.

4. CAS DE METAUX AUTRES QUE L'ALUMINIUM

Nous avons retrouvé cette décomposition de la courbe de traction en deux parties avec de nombreux métaux.

Dans le cas de métaux cubiques à faces centrées, nous l'avons observée sur le cuivre, le nickel et le plomb. Les variations de la pente de la courbe en fonction de l'allongement sont représentées sur la Fig. 6 ; on retrouve les mêmes caractéristiques qu'avec l'aluminium. Notamment, l'influence du traitement thermique et de la grosseur du grain est la même ; la Fig. 7 est relative à des éprouvettes de cuivre OFHC dans divers états.

Le point de transition existe aussi dans les métaux cubiques centrés ; nous l'avons observé sur le fer Armco, l'acier extra-doux (0,1% de carbone) et l'acier mi-dur (0,3% de carbone). Mais, il est généralement masqué par le palier ; on parvient à l'observer en partant d'éprouvettes trempées (trempe γ) que l'on fait vieillir jusqu'à réapparition complète du palier (Fig. 8, sur laquelle nous avons

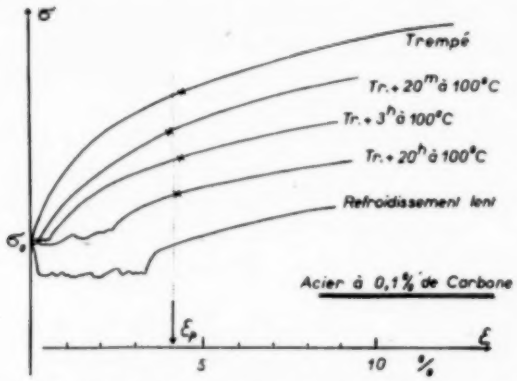

Fig. 8. Forme des courbes de traction de fer, après trempe et vieillissements.

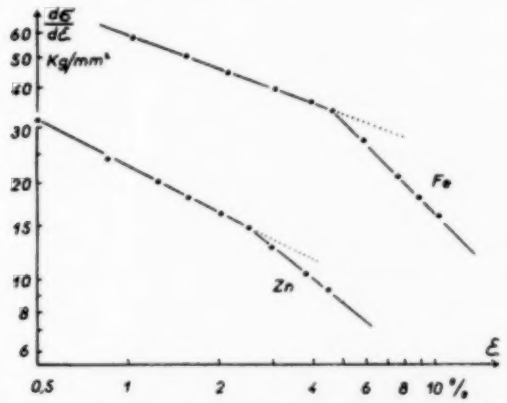

Fig. 9. Variation de la pente de la courbe de traction en fonction de l'allongement (cas du fer et du zinc).

déduit la limite élastique supérieure, afin d'éliminer les phénomènes dus aux nuages d'impuretés, problème qui n'est pas du cadre de cette étude). La trempe ayant supprimé le palier, l'analyse de la courbe révèle deux portions paraboliques séparées par le point de transition ; le vieillissement ne modifie pas la valeur de ϵ_p et le vieillissement complet conduit à un palier qui atteint presque ϵ_p ; d'ailleurs,

presqu'immédiatement après le palier, le coefficient d'écrouissage a une valeur très faible, correspondant à celle de n dans les métaux cubiques à faces centrées. On peut donc considérer que dans le cas du fer dans l'état " normalisé " le palier correspond au premier domaine de déformation ; d'après les essais de BOULANGER (1930) le palier varie avec la température et la pureté comme le premier domaine des courbes de traction de l'aluminium. Donc, on peut encore caractériser les courbes de traction du fer par deux relations successives :

$$\sigma = \sigma_0 \qquad \text{pour} \quad \epsilon < \epsilon_p$$

$$\sigma = \sigma_1 + B\epsilon^n \quad \text{pour} \quad \epsilon > \epsilon_p$$

Les coefficients A et m des relations générales sont alors nuls.

Enfin, nous avons observé les mêmes phénomènes avec les métaux hexagonaux : le magnésium, le zinc, le cadmium et le titane. Mais la faible ductilité de certains, à l'état polycristallin, rend difficile la détermination du point de transition et, surtout, les éléments de la seconde parabole.

En résumé, on peut dire que, d'une manière tout à fait générale, une courbe de traction doit être décomposée en deux parties, quels que soient le système cristallin, la pureté, le traitement thermique et la grosseur du grain. Particulièrement, cette représentation peut s'appliquer aux courbes de traction des monocristaux, cas que nous allons étudier maintenant plus en détail.

5. COURBES DE TRACTION DES EPROUVETTES MONOCRISTALLINES

Dans le cas des monocristaux, un nouveau facteur doit intervenir : l'orientation du cristal par rapport à l'axe de la déformation. Ce facteur est plus ou moins important selon le système cristallin et les éléments de glissement dans le métal. Nous considérerons principalement le cas des métaux cubiques à faces centrées. qui ont été le plus étudiés. et particulièrement celui de l'aluminium.

On sait qu'un cisaillement pur appliqué à un monocristal entraine une déformation de celui-ci par glissement sur une seule famille de plans, avec un taux de consolidation constant, mais faible (SCHMIDT et BOAS 1935). Autrement dit, le développement d'un seul système n'entraine pas d'écrouissage important ; aussi appelle-t-on ce type de déformation " *glissement facile* " ; C'est particulièrement le cas des métaux hexagonaux pour lesquels on peut observer des glissements faciles pouvant atteindre 100% (LÜCKE, MASING et SCHRODER 1955). Mais, quand on étire une éprouvette, le cisaillement n'est pas pur, par suite de la rotation du réseau due aux glissements eux-mêmes, sauf, peut-être, si l'échantillon est long et très mince. Cette rotation entraine alors le développement d'hétérogénéités de déformation dont la nature est responsable de l'allure de l'écrouissage (JAOUL et BRICOT 1955).

Dans le cas de l'aluminium déformé à la température ambiante, ces hétérogénéites peuvent être groupés en deux classes : les bandes de glissement secondaire (Fig. 10) et les pliages (Fig. 11) qui, eux-mêmes, peuvent revêtir plusieurs aspects (JAOUL, BRICOT et LACOMBE 1957). Les uns ou les autres se développent de préférence selon l'orientation du cristal, mais en général pas simultanément. Si ce sont des pliages, la vitesse de consolidation est faible ; elle est plus forte s'il y a des bandes de glissement secondaire ; elle atteint sa valeur maximum si deux systèmes de

Fig. 10. Bandes de glissement secondaire dans l'aluminium raffiné: $G = 150$.

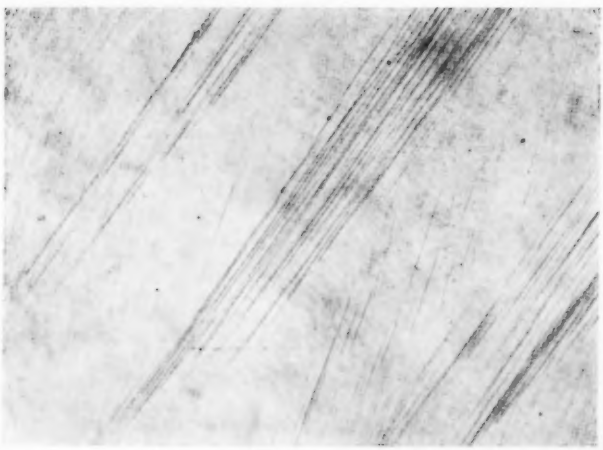

Fig. 11. Pliage dans l'aluminium raffiné : $G = 150$.

Fig. 12. Développement simultané de deux systèmes dans l'aluminium raffiné: $G = 150$.

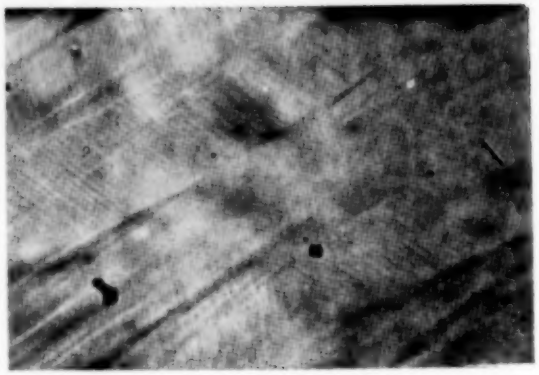

Fig. 14. Aspect de la géométrie de la déformation à basse température; Aluminium raffiné étiré de 5% dans l'air liquide; $G = 150$.

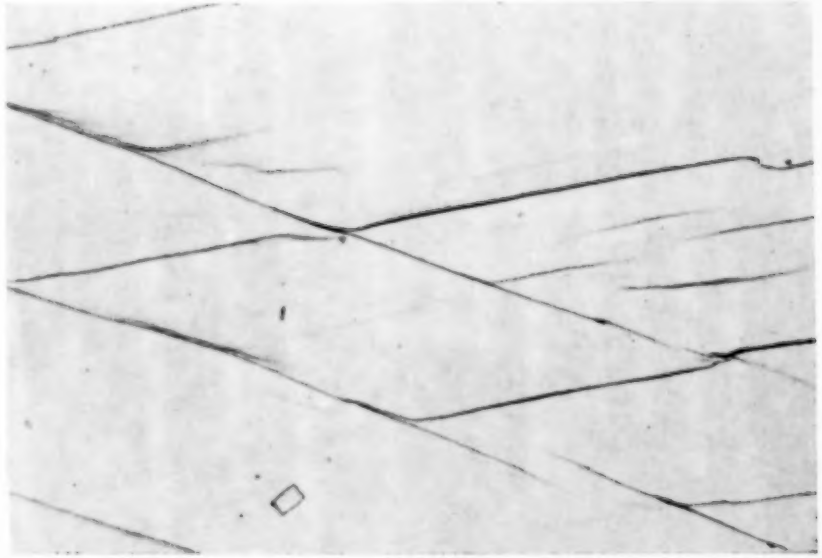

Fig. 17. Aspect des glissements se développant dans la partie linéaire de la courbe de cisaillement à — 195° d'un monocristal d'aluminium raffiné. $G = 4{\cdot}000$. (Micrographie électronique réalisée à l'IRSID).

glissement se développent en même temps (Fig. 12), ce qui correspond à des cas particuliers de l'orientation.

La Fig. 13 représente les courbes de cisaillement (contrainte de cisaillement et glissement dans la direction de glissement) relatives à ces trois types de cristaux. Comme dans le cas des polycristaux, on peut les décomposer en deux parties, donc les caractériser par cinq coefficients :

$$\tau_0,\ m^*,\ \gamma_p,\ \tau_p,\ n$$

Mais on s'aperçoit qu'un seul varie : le glissement au point de transition, γ_p ,et les courbes sont affines par rapport à l'axe des cisaillements ; la loi de SCHMID (SCHMID et BOAS 1935), exprimant la constance du cisaillement critique τ_0 peut alors être étendue au cisaillement au point de transition τ_p. Le nouveau facteur qui intervient dans l'étude des monocristaux se traduit donc sur la forme des courbes de consolidation par une variation du point de transition qui est liée à la géométrie de la déformation.

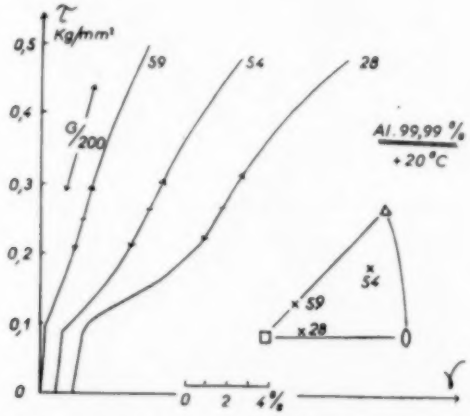

Fig. 13. Forme des courbes de cisaillement de monocristaux d'aluminium raffiné déformés à la température ambiante.

Dans le cas d'essais à plus basse température, par exemple dans l'air liquide, l'observation micrographique des glissements révèle une structure de déformation beaucoup plus complexe (Fig. 14) : pour toutes les orientations, plusieurs systèmes de glissement apparaissent simultanément, même après de très faibles déformations. Là, interviennent problablement le libre parcours des glissements (SUZUKI, IKEDA et TAKEUCHI 1956), qui est plus faible qu'à la température ambiante, et les dimensions des éprouvettes.

Les courbes de cisaillement ne présentent alors plus la variété que l'on avait par déformation à l'ambiante ; elles ont à peu près toutes la même forme (Fig. 15). Le premier domaine est cependant beaucoup plus important et se termine par une portion sensiblement linéaire que certains auteurs distinguent et appellent deuxième domaine (FRIEDEL 1956). BLEWITT (BLEWITT, COLTMAN et REDMAN 1955) a observé que dans le cas du cuivre étiré à très basse température la portion linéaire

* En réalité, la première partie de la courbe n'est pas rigoureusement parabolique ; nous avons montré (JAOUL 1955) qu'il était possible de la représenter avec une bonne précision par une relation logarithmique.

avait une pente bien définie, égale à $G/200$, G étant le module de cisaillement (Fig. 16). C'est aussi la valeur que l'on obtient d'une manière très précise dans le cas de l'aluminium étiré à froid : les valeurs de la pente sont comprises entre $G/205$ et $G/190$.

FRIEDEL (1955) a expliqué ce taux d'écrouissage, dans les métaux cubiques à faces centrées, en supposant que chaque source de dislocations devait être enfermée entre quatre barrières de LOMER-COTTRELL. Les glissements doivent alors être courts et limités aux plans de glissement d'un autre système. C'est effectivement

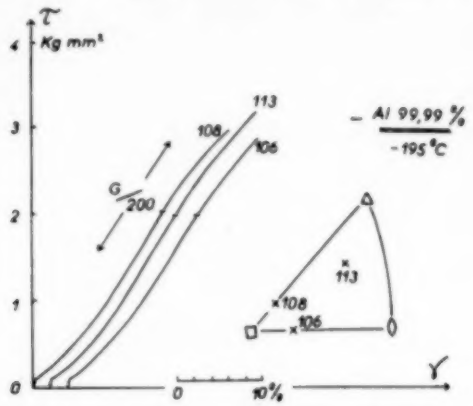

Fig. 15. Forme des courbes de cisaillement de monocristaux d'aluminium raffiné déformés dans l'air liquide.

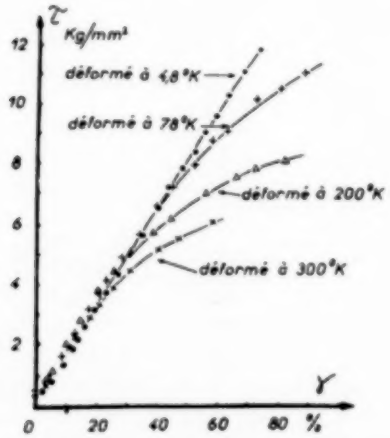

Fig. 16. Courbes de cisaillement de monocristaux de cuivre à diverses températures (BLEWITT *et al.*).

ce que l'on observe sur la Fig. 17, relative à une éprouvette d'aluminium raffinée déformée préalablement de 5% à − 195°, puis repolie et allongée de nouveau de 3% ; la micrographie correspond donc aux lignes se développant dans la portion sensiblement linéaire de la courbe de cisaillement (glissement de 11 à 17%, Fig. 15) et montre un aspect des glissements bloqués sur un autre système ; l'échelle de

ce réseau est inférieure à 10 microns. D'après la forme exacte des courbes, il existe déjà des barrières avant la déformation, car le taux d'écrouissage n'est pas nul à l'origine, mais égal sensiblement à $G/400$ (Jaoul 1955). Ces barrières se développeraient progressivement en même temps que les glissements ; la pente de la courbe croît alors d'une manière continue jusqu'à la valeur $G/200$ qui se conserverait indéfiniment si le mécanisme correspondant au point de transition n'intervenait pas.

Ce dernier apparait pour une valeur bien définie de l'effort ; dans le cas de l'aluminium raffiné à 99,99%, le cisaillement au point où la courbe s'infléchit a les valeurs suivantes :

$$\text{à } + 20^\circ \; : \; \tau_p = 0{,}26 \text{ kg/mm}^2$$

$$\text{à } - 75^\circ \; : \; \tau_p = 0{,}55 \text{ kg/mm}^2$$

$$\text{à } - 195^\circ \; : \; \tau_p = 2{,}0 \text{ kg/mm}^2$$

Il croit en fonction de la teneur en élément d'alliage (Jaoul 1955), ainsi que nous l'avons déjà vu pour les polycristaux, et décroit quand la température croit. Si donc la température de déformation est trop haute, la pente $G/200$ ne sera jamais atteinte.

D'autre part, pour que chaque source puisse être enfermée entre quatre barrières, il faut que plusieurs systèmes de glissement puissent de développer. Nous avons vu que celà était courant à basse température, mais ne correspondait qu'à des orientations particulières pour des déformations à la température ambiante. Effectivement, la pente au point d'inflexion varie, à la température ambiante, de $G/1.000$ à $G/200$ en fonction de la géometrie de la déformation ; mais on voit que pour le cristal présentant le plus de systémes de glissement (courbe 59, Fig. 13) et qui est donc comparable aux cristaux déformés à basse température, la pente a bien la valeur caractéristique $G/200$.

Donc, pour un monocristal se déformant par le jeu de plusieurs systèmes de glissement, la portion de la courbe de cisaillement à concavité tournée vers le haut présente une "branche asymptotique" dont la pente est égale au deux-centième du module de cisaillement. Pour une certaine valeur de l'effort, fonction décroissante de la température, le changement de mécanisme de déformation correspondant au point de transition se traduit par une inflexion de la courbe qui reprend une allure parabolique classique.

Le fait que pour atteindre la valeur $G/200$ il soit nécessaire d'avoir plusieurs systèmes de glissement est intéressant, car c'est une condition parfaitement bien réalisée dans les polycristaux, par suite de la présence des joints.

6. Pente au Point de Transition des Courbes de Traction des Polycristaux

L'étude de l'influence de la grosseur du grain sur la forme des courbes de traction (Crussard 1950, Crussard et Jaoul 1950, Jaoul 1954) nous a montré qu'au delà du point de transition la consolidation est principalement intracristalline, les courbes étant sensiblement parallèles (Fig. 4) ; mais si les joints ne contribuent plus à l'augmentation d'écrouissage, la seconde partie de la courbe des monocristaux

doit être parallèle à celle des polycristaux, la différence d'ordonnée correspondant à la " *consolidation intergranulaire* " qui a atteint une valeur maximum au point de transition *; dans ces conditions, on doit trouver une valeur caractéristique de la pente au point de transition.

Une difficulté surgit du fait qu'il ne s'agit plus de courbe de cisaillement, étant donné toutes les orientations des grains d'un polycristal ; mais, en considérant l'orientation moyenne, on a pour un métal cubique à faces centrées, d'après SACHS (1929) :

$$\tau = \sigma/2{,}24, \qquad \gamma = 2{,}24\,\epsilon$$

σ et ϵ étant la tension et l'allongement parallèlement à l'axe de l'effort. On a alors

$$\frac{d\sigma}{d\epsilon} = (2{,}24)^2 \frac{d\tau}{d\gamma}$$

et la pente des courbes de cisaillement $d\tau/d\gamma = G/200$ devra donner $d\sigma/d\epsilon = G/40$.

On sait que le rapport du module de traction au module de cisaillement est de l'ordre de 2,5. On doit donc trouver sur les courbes de traction des polycristaux la valeur

$$\frac{d\sigma}{d\epsilon} = \frac{E}{100}.$$

Or, c'est précisément la valeur que l'on observe au point de transition de l'aluminium raffiné (Fig. 4) ; pour tous nos essais, nous obtenons, d'après les relations fixant les valeurs des paramètres des courbes (JAOUL 1954) :

$$65 < \left(\frac{d\sigma}{d\epsilon}\right)_p < 80 \text{ kg/mm}^2,$$

soit, d'après la valeur du module de l'aluminium, $E = 7.200$:

$$P = \left(\frac{d\sigma}{d\epsilon}\right)_p = \frac{E}{100} \qquad \text{à } 10\% \text{ près.}$$

Dans la suite, nous désignerons par " P " la valeur de la pente au point de transition.

On retrouve également cette valeur avec les alliages d'aluminium ; la Fig. 18 représente les valeurs de la pente à la courbe de traction corrigée en fonction de l'allongement pour des aluminiums à diverses teneurs en magnésium. Le tableau suivant indique les valeurs de la pente P pour divers alliages d'aluminium :

Al–Cu	0,4% :	$\epsilon_p = 2{,}8\%$	$P = 68$	$E/P = 106$
	1%	$= 5{,}0\%$	$= 62$	$= 116$
	5% :	$= 9\%$	$= 72$	$= 100$
Al–Mg	1,6% :	$= 4{,}7\%$	$= 76$	$= 94$
	3,2% :	$= 7{,}7\%$	$= 71$	$= 101$
	7% :	$= 10\%$	$= 73$	$= 99$
	11% :	$= 12\%$	$= 72$	$= 100$
Al–Mn	0,6% :	$= 2{,}4\%$	$= 63$	$= 114$
	1,1% :	$= 3{,}0\%$	$= 67$	$= 107$

* Le terme " consolidation intergranulaire " indique une augmentation de contrainte qui peut être conséquence directe de la résistance des joints, ou indirecte par la modification des mécanismes intracristallins qu'ils provoquent.

Dans le cas du cuivre OFHC, on trouve aussi au point de transition une pente égale au centième du module élastique, sa valeur étant de l'ordre de 120 kg/mm². Cette propriété se retrouve également avec le plomb, le nickel et les aciers austénitiques (nous reviendrons sur les particularités de ces derniers) ; la valeur caractéristique observée sur les monocristaux se retrouve donc bien sur les polycristaux de métaux cubiques à faces centrées.

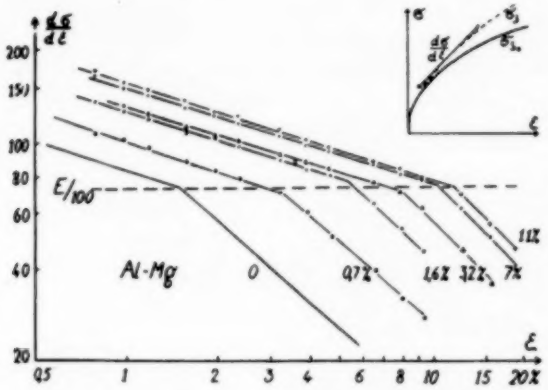

Fig. 18. Variation de la pente des courbes de traction en fonction de l'allongement pour diverses teneurs en magnésium d'alliages d'Al.

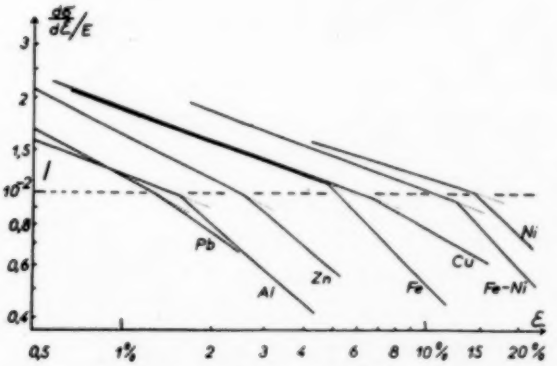

Fig. 19. Variation, pour divers métaux, de la pente de la courbe de traction en fonction de l'allongement, les pentes étant rapportées au module d'élasticité.

Avec les métaux d'un autre système, le calcul de Sachs n'est plus valable ; d'autre part, trop peu d'essais ont été faits pour connaitre avec précision la forme des courbes de traction des monocristaux. Cependent, ainsi que nous l'avons indiqué (Figs. 8 et 9), le point de transition existe sur les courbes de traction des polycristaux et la pente correspondante est toujours égale au centième du module élastique (Fig. 19).

Si l'on considère le cas d'un métal mal recristallisé, comme l'aluminium recuit à moins de 250° (Fig. 4) ou le cuivre recuit à 400° (Fig. 7), on trouve des points

de transition pour des allongements plus faibles, mais la pente P garde la même valeur. Cela peut permettre, dans certains cas, d'assimiler le début d'une courbe de traction à une droite de pente $E/100$.

Le supplément de consolidation dû à la présence des joints n'augmente donc plus après le point de transition. Si l'on essaye d'augmenter la tension au point de transition, par exemple en diminuant la température de l'essai, on doit obtenir une portion de courbe assimilable à une droite, comme dans le cas des monocristaux.

C'est ce que l'on obtient avec l'acier inoxydable 18/10 par simple déformation à l'ambiante. Celui-ci a la même structure que l'aluminium, mais à 20° il est beaucoup plus éloigné de son point de fusion ; on peut donc penser qu'il se comportera comme un aluminium déformé à basse température. D'autre part, l'importante

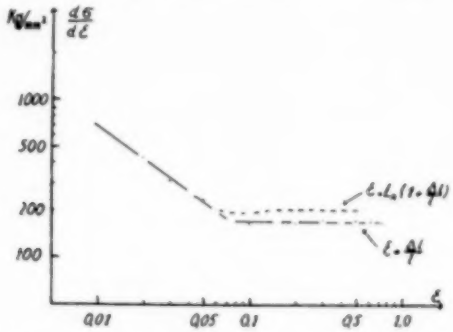

Fig. 20. Variation de la pente d'une courbe de traction d'un acier 18/10 en fonction de l'allongement.

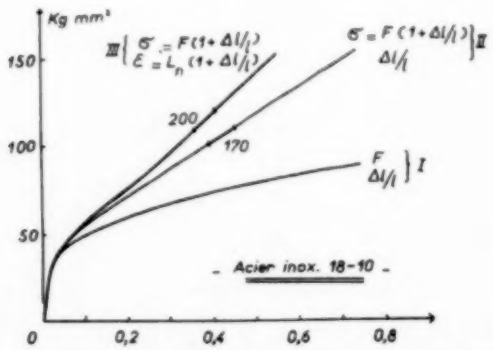

Fig. 21. Acier 18/10 : (I) Courbe expérimentale ; (II) Courbe corrigée de la réduction de section; (III) Allongements naturels.

concentration en éléments d'addition doit faire que le point de transition est rejeté très loin (comme dans les monocristaux de laiton (SCHMID et BOAS 1935) ; nous n'en avons effectivement pas observé, ce qui est en accord avec la difficulté de créer des germes de recristallisation par écrouissage à froid de ce métal. La Fig. 20 représente la variation de la pente de la courbe de traction : elle décroit jusqu'à une valeur de l'ordre de $E/100$, atteinte pour une déformation de 8%, puis reste

constante jusqu'à l'apparition de la striction. La courbe corrigée de la réduction de section (Fig. 21) est donc une droite à partir d'un certain point ; on retrouve la propriété observée par BLEWITT sur le cuivre étiré à très basse température.

Les autre métaux, étirés dans l'air liquide, conduisent à des résultats comparables. La Fig. 22 représente les courbes de traction de divers métaux à — 195° ; les courbes ont une partie relativement plate et sensiblement parallèle à une droite de pente $E/100$ (jusqu'à 10% pour l'aluminium).

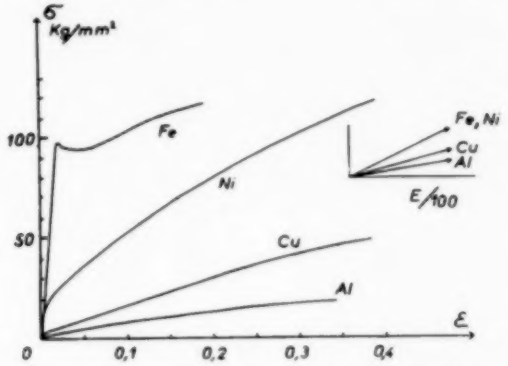

Fig. 22. Courbes de traction de divers métaux dans l'air liquide.

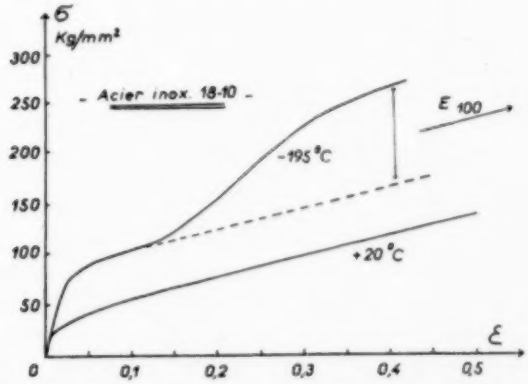

Fig. 23. Courbes de traction de l'acier inoxydable à l'ambiante et à la température de l'air liquide.

La courbe de traction de l'acier inoxydable dans l'air liquide devrait alors être parallèle à celle obtenue à l'ambiante, à la variation du module élastique près. Mais à — 195° l'austénite n'est plus stable et se transforme en martensite sous l'effet de l'écrouissage. La courbe de traction dont le début a l'aspect normal se se redresse au fur et à mesure de la déformation et affecte une forme rappelant celle de la courbe du monocristal. (Fig 23). Quand la transformation est complète, on devrait retrouver une droite de pente $d\sigma/d\epsilon = E/100$; mais les tensions atteintes sont trop fortes (de l'ordre de 250 kg/mm²) et supérieures au centième du module. On se trouve alors en condition d'instabilité et la striction apparait avant la fin de la transformation martensitique.

Les métaux hexagonaux se comportent différemment (Fig. 24) : ils n'ont pas de limite élastique et le début de la courbe de traction est une droite de pente égale à $E/7{,}5$ pour le zinc et à $E/6{,}5$ pour le magnésium ; la rupture apparait à la fin de cette droite. Nous verrons que ces pentes correspondent à peu près aux pentes pseudo-élastiques observées à la température ambiante. En arrêtant l'essai avant la rupture (pour Zn, à 1% d'allongement), ou note que cette déformation est totalement réversible.

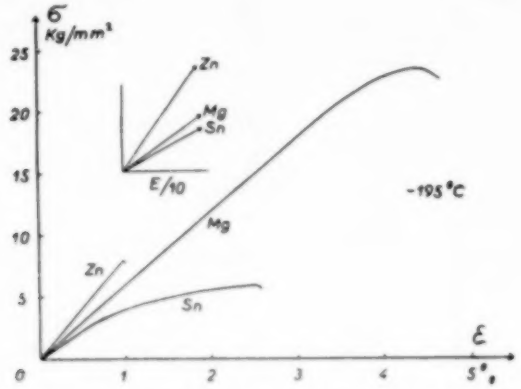

Fig. 24. Courbes de traction de zinc, magnésium et étain à − 195 .

On remarque sur la Fig. 22, que les courbes obtenues à − 195° sont plus plates que celles qui ont été réalisées à la température ambiante ; autrement dit, l'exposant m caractérisant le début de la courbe de consolidation croit quand la température décroit. Dans le cas de l'aluminium rafliné, nous avions relié cette croissance à un grossissement du grain ; l'influence des joints doit donc se faire moins sentir à basse température : la courbe de traction du polycristal se rapproche de celle du monocristal. C'est d'ailleurs ce que l'on peut observer par micrographie : à basse température (Fig. 25) l'échelle des glissements est plus petite qu'à la température ambiante (Fig. 26) ; pour des déformations plus fortes, la distorsion aux joints semble moins importante après déformation à basse température ; d'autre part (Fig. 27) les glissements sont courts et très fins (BLEWITT, COLTMAN et REDMAN 1955). Le blocage des glissements dans les joints est donc relativement moins important à basse température et une variation de température peut donc bien avoir le même effet qu'une variation inverse de la grosseur du grain.

7. ETUDE DES MECANISMES SUCCESSIFS DE DEFORMATION

Si l'on veut donc représenter d'une manière tout à fait générale une courbe de déformation, il faut considérer, avant l'apparition de l'instabilité entrainant la striction, quatre domaines de déformation (Fig. 28) :

(1) Portion réversible : OA

(2) Premier domaine de déformation plastique : AB

(3) Portion linéaire : BC

(4) Domaine des grandes déformations : CD

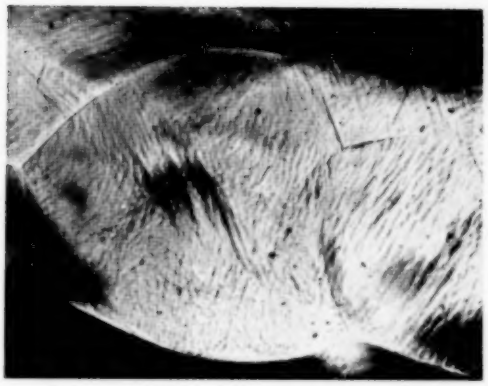

Fig. 25. Aspect des lignes de glissement sur la surface d'un polycristal déformé de 5% à — 195°; $G = 150$ (Aluminium 99,99%).

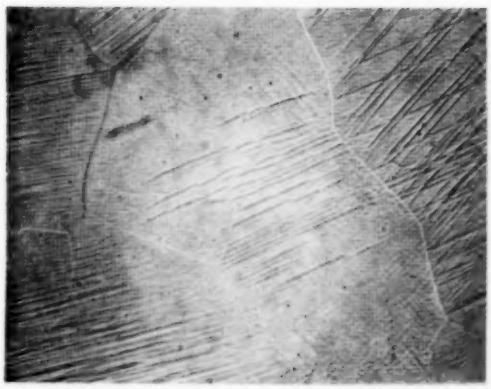

Fig. 26. Aspect des lignes de glissement sur la surface d'un polycristal déformé de 5% à + 20°; $G = 150$ (Aluminium 99,99%).

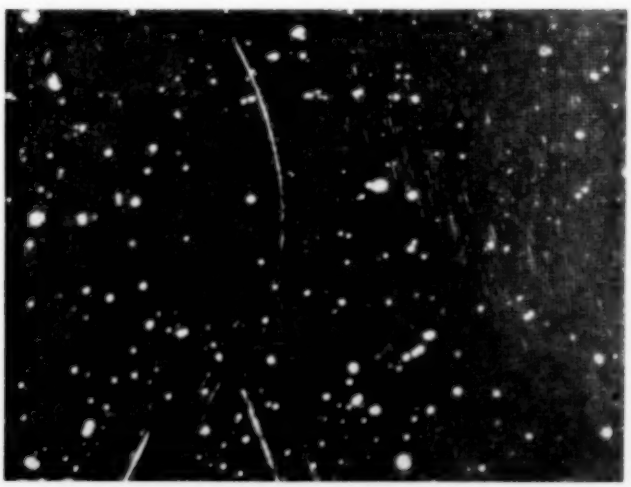

Fig. 27. Même région que sur la Fig. 25, mais éclairée en fond noir pour faire ressortir les glissements fins et courts se développant à — 195°; $G = 300$.

Nous allons étudier successivement le mécanisme de déformation correspondant à chacun.

(i) *Déformation réversible.* Dans le cas des métaux purs et bien recristallisés, la pente de la portion réversible est toujours plus faible que le module élastique théorique : elle est de l'ordre de $E/5$ à $E/10$. Mais la présence d'impuretés à l'état précipité entraine une augmentation du module réel ; par exemple, il croit au cours du vieillissement d'un aluminium-cuivre à 4% ou d'un acier doux trempé.

D'autre part, la présence de tensions internes augmente la valeur de la pente : si une éprouvette bien recristallisée subit des déformations plastiques successives, la pente de la portion réversible de la déformation croit et si la déformation plastique atteint le point de transition, la pente devient égale au module d'élasticité théorique.

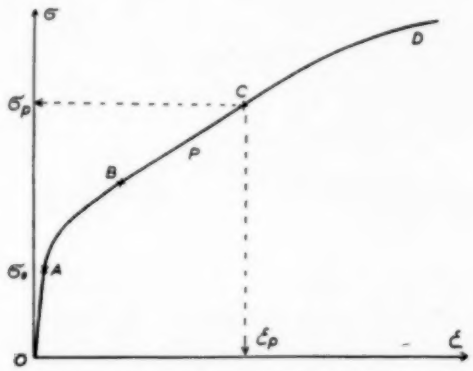

Fig. 28. Décomposition d'une courbe de traction dans le cas le plus général.

Le fait que la déformation réversible soit plus forte que celle que laisseraient prévoir les propriétés élastiques du métal montre qu'il existe des glissements réversibles. La première partie des courbes de traction est donc une portion "*pseudo-élastique.*"

(ii) *Premier domaine de déformation plastique.* Dès que la limite de proportionnalité est dépassée, les glissements commencent à se bloquer sur les barrières de Cottrell et ne sont plus tous réversibles ; la consolidation apparait et varie selon une loi de la forme :

$$\frac{d\sigma}{d\epsilon} = \frac{\alpha}{\epsilon^{(1-m)}}.$$

$(1 - m)$ ayant une valeur négative dans le cas des monocristaux, c'est à dire que le taux de consolidation va en s'accentuant. Avec les polycristaux à grains fins, $(1 - m)$ est de l'ordre de $\frac{1}{2}$.

On peut appeler cette portion "*élastique-plastique*" car, ainsi que nous venons de la voir, il y a une certaine proportion de glissements réversibles. D'après des observations précises de la déformation de tubes par traction, nous avions déduit que le coefficient de contraction transversale n'atteignait la valeur $\frac{1}{2}$ qu'à la fin de ce domaine (Jaoul 1956). Un résultat comparable a été obtenu par Shelton t Ford (1956) par mesure directe du coefficient de contraction transversale sur

divers métaux. On doit donc considérer qu'au cours de cette partie de la déformation, on passe progressivement du type élastique (coefficient de Poisson égal à 0,3) au type plastique (coefficient de contraction transversale égal à 0,5).

Mais la caractéristique principale de ce domaine est le rôle de la consolidation intergranulaire σ_j ; celle-ci, qui croit très rapidement au début de la déformation, atteint son maximum à la fin de ce domaine. Fig. 29 représente les courbes de

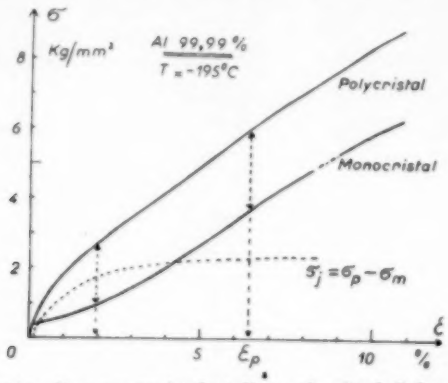

Fig. 29. Courbes de traction d'un monocristal et d'un polycristal d'aluminium ; déformations à − 195°.

traction d'un monocristal et d'un polycristal d'aluminium raffiné, déformés à − 195°. La courbe en pointillé est la différence des ordonnées, donc la partie de la consolidation due aux joints ; on voit que celle-ci tend rapidement vers un maximum qui est de 1,75 kg/mm². Or, c'est également la valeur que l'on observe pour les déformations à la température ambiante (JAOUL 1956) ; *la résistance des joints est donc peu fonction de la température.*

A partir de la fin de ce domaine, toute nouvelle augmentation de consolidation du polycristal est donc seulement intracristalline.

(iii) *Domaine d'écrouissage linéaire.* Les joints n'interviennent plus et le mécanisme de la déformation doit être le même dans le monocristal et le polycristal. Depuis le début de la déformation plastique, les barrières de COTTRELL se sont formées aux intersections des glissements et, selon le mécanisme proposé par FRIEDEL (1955), la consolidation croit selon une droite de pente égale à $G/200$ s'il s'agit d'une courbe de cisaillement, égale à $E/100$ dans une simple courbe de traction. On peut alors définir un " *module de plasticité* ":

$$P = E/100.$$

Ce mécanisme de déformation se poursuit jusqu'à une certaine valeur de la tension, fonction de la température et des impuretés. Sous l'effort correspondant, les dislocations empilées sur les barrières peuvent être arrachées par un mécanisme de cross-slips (MADER 1956)* ou de recomposition des dislocations (FRIEDEL 1956). Cette tension au point de transition est aussi fonction de la stabilité des dislocations décomposées, ce qui peut permettre d'expliquer les différences de tension observées : par exemple, à la température ambiante :

* Nous avions d'ailleurs constaté que l'on ne voyait jamais de cross-slips avant une déformation correspondant au point de transition (JAOUL 1954).

Aluminium 99,99% : $\sigma_p = 2{,}3$ kg/mm^2

Cuivre OFHC : $\sigma_p = 12$ kg/mm^2

Acier 18/10 : $\sigma_p > 140$ kg/mm^2

Il est à remarquer d'autre part que le point de transition est bien un phénomène d'origine intracristalline (Crussard et Jaoul 1950, Jaoul 1954) et que, par suite, il existe aussi bien dans les monocristaux que dans les polycristaux.

(iv) *Domaine des grandes déformations.* A partir du point de transition, les dislocations sont donc arrachées, ce qui permet le développement de nouvelles boucles pour une augmentation de tension plus faible : le taux de consolidation diminue et la courbe s'infléchit. En même temps le réarrangement des dislocations arrachées entraine une fragmentation des grains par formation de parois, ce qui s'observe facilement par les rayons X (Jaoul 1954, Crussard 1953).

Ces quatre mécanismes ne s'observent pas sur toutes les courbes de traction, car ils peuvent empiéter l'un sur l'autre : le domaine de consolidation intergranulaire est sensiblement indépendant de la température et a un étalement de l'ordre de 2% dans l'aluminium raffiné ; le point de transition, par contre, varie beaucoup avec la température : il se situe à un allongement de 1,6% à + 20°, de 6,5% à − 195°. Le domaine d'écrouissage linéaire, important à la température de l'air liquide, disparait donc à la température ambiante. Mais, il est visible sur les courbes de traction du cuivre ou du nickel à la température ambiante où la courbe corrigée de la réduction de section présente un méplat ; enfin il est très développé dans le cas de l'acier inoxydable. Quant au domaine de fragmentation, il peut commencer avant la fin du domaine élastique-plastique, avant que la pente ait atteint la valeur théorique $E/100$.

8. Conclusions

L'observation précise des courbes de traction des monocristaux et des polycristaux de divers métaux étirés à diverses températures permet de définir plusieurs mécanismes successifs intervenant au cours de la déformation plastique.

Dans le cas du monocristal, après une portion réversible pseudo-élastique, car elle comporte déjà quelques glissements ou déplacements de dislocations, le taux de consolidation va en croissant et tend vers une valeur égale au deux-centième du module de cisaillement. Mais, pour une certaine valeur de la tension, correspondant au point de transition et variant en fonction de la température, les dislocations bloquées qui étaient responsables de l'augmentation d'écrouissage sont arrachées et la courbe s'infléchit.

Dans les polycristaux, le mécanisme de la consolidation à l'intérieur des grains est le même, mais la présence des joints entraine une augmentation de consolidation beaucoup plus rapide au début de la déformation plastique. Cependant, cette consolidation intergranulaire atteint vite une valeur maximum ; la courbe du polycristal est alors parallèle à celle du monocristal se déformant avec plusieurs systèmes de glissement.

Si le maximum de consolidation aux joints a lieu avant le point de transition, on verra apparaitre sur les courbes de traction des polycristaux une portion linéaire, comme dans le cas de monocristaux ; la pente de cette portion est la même

et, traduite en coordonnées tension normale – allongement, elle est égale au centième du module élastique. Cette valeur, qui est le taux de consolidation maximum après que la consolidation aux joints ait cessé de croitre, peut être considérée comme un " module de plasticité " pour les déformations à basse température.

REMERCIEMENTS

L'auteur exprime ses remerciements au Professeur C. CRUSSARD, Directeur du Département de Physique de l'Institut de Recherches Sidérurgiques, pour ses discussions et l'aide qu'il a apportée dans la rédaction de ce mémoire.

RÉFÉRENCES BIBLIOGRAPHIQUES

BLEWITT, T. H., COLTMAN, R. R. and REDMAN, J. K.	1955	*Defects in Crystalline Solids*, p. 369, Phys. Soc. London (1955).
BOULANGER, C.	1950	*Rev. Métal.* **47**, 547.
CRUSSARD, C.	1950	*Some recent developments in Rheology*, p. 33 (United Trade Press, London).
CRUSSARD, C. et JAOUL, B.	1950	*Rev. Métal.* **47**, 589.
	1953	*Rev. Métal.* **50**, 697.
FRIEDEL, J.	1955	*Phil. Mag.* **46**, 1169.
	1956	*Les Dislocations*, p. 131 (Ed. Gauthiers-Villars, Paris).
JAOUL, B.	1954	Contribution à l'étude de la déformation plastique, *Pub. Sc. Tech. Ministr. de l'Air*, no. 290.
	1955	*Comptes Rendus Acad. Sci.* **240**, 2532 ; **241**, 161.
JAOUL, B. AUBERTIN, F. et CRUSSARD, C.	1952	*Rev. Métal.* **49**, 633.
JAOUL, B. et BRICOT, I.	1955	*Rev. Métal.* **52**, 629.
	1956	*U.I.T.A.M. Madrid Colloquium*, p. 13 (Springer, Berlin).
JAOUL, B., BRICOT, I. et LACOMBE, P.	1957	Congrès Soc. Fse. de Métallurgie, Paris. *Rev. Métal.* Jan. 57.
LUCKE, K., MASING, G. et SCHRODER, K.	1955	*Zeit. Metallk.* **46**, 792.
LUDWIK, P.	1909	*Elemente der Technologischen Mechanik* (Berlin).
MADER, S.	1956	Thèse, Colloque de Dusseldorf.
MULLER, H. et LIEBFRIED, G.	1955	*Z. Physik.* **142**, 87.
SACHS, G.	1929	V.D.I. **72**, 34.
SCHMID, E. et BOAS, W.	1935	*Kristallplastizität* (Berlin).
SHELTON, A. et FORD, H.	1956	*J. Iron Steel Inst.* **182**, 160.
SUZUKI, H., IKEDA, S. et TAKEUCHI, S.	1956	*J. Phys. Soc. Japan* **11**, 382.

Journal of the Mechanics and Physics of Solids, 1957, Vol. 5, pp. 115 to 124. Pergamon Press Ltd., London.

THE PROPAGATION OF INFINITESIMAL PLANE WAVES IN ELASTIC-PLASTIC MATERIALS

By J. W. Craggs
King's College, University of Durham

(*Received* 16*th October*, 1956)

Summary

The propagation of small discontinuities of stress in a plastic-elastic material is examined. It is shown that plane waves of two types may exist, each involving both dilatation and shear strain, and an equation for the velocities of such waves is given. Possible interactions between plastic (loading) waves and elastic (unloading) waves are discussed and the treatment of such interactions is illustrated by examples.

Introduction

Since the publications of Taylor (1940) and v. Karman (1942) on the propagation of stress and strain in elastic-plastic wires many dynamic problems in the theory of plasticity have been studied. These include uniaxial compression in cylinders (Lee 1953; White and Griffis 1947, 1948), transverse waves in wires and membranes (Craggs 1952, 1954), radial waves in a thin plate (Freiberger 1952) and flexural waves in beams (Conroy 1952; Duwez, Clark and Bohnenblust 1952). In all these papers approximations are used which are based on the assumption that some linear dimension of the system is small.

As an example, consider elastic tension waves in a thin cylindrical wire of radius a. Then, in the approximate method, the integral over the cross section of the tensile stress T, is related to the longitudinal strain ϵ, by Hooke's law $T = \pi E a^2 \epsilon = \pi E a^2 \partial u/\partial x$, where E is Young's modulus and u is the displacement along the wire of a cross-section initially at x. The equation of motion

$$\pi \rho a^2 \frac{\partial^2 u}{\partial t^2} = \frac{\partial T}{\partial x}$$

then leads to a wave equation

$$\frac{\partial^2 u}{\partial x^2} = \frac{1}{c^2} \frac{\partial^2 u}{\partial t^2}$$

where $c^2 = E/\rho$, and a sinusoidal wave is $u = A \sin 2\pi (x - ct)/\lambda$. This approximation, however, is valid only when the wave length λ is sufficiently great, that is when $a/\lambda \to 0$ (see Love 1927, p. 428). It follows that the approximate methods become suspect for precisely those types of loading (impact loads) for which the solutions are most important.

In this present paper an analysis is given of infinitesimal plane waves in an elastic-plastic material, as a necessary preliminary to any more accurate treatment of impact problems for such a material. It is assumed throughout that an infinitesimal plastic wave can propagate, as a plastic wave, only into a material which is exactly at its yield stress.

1. Equations of Plastic Flow

Let rectangular Cartesian coordinates x_i $(i = 1, 2, 3)$ be used and write u_i for the velocity of the material at x_i. Let σ_{ij} be the true stress tensor, and write

$$\dot{\eta}_{ij} = \tfrac{1}{2}\left(\frac{\partial u_i}{\partial x_j} + \frac{\partial u_j}{\partial x_i}\right) \tag{1}$$

for the tensor rate of strain, using the dot consistently to indicate differentiation following the motion. This analysis is of Eulerian type. Note that integration of (1), following the motion of an element, leads to a logarithmic strain, in which an infinitesimal strain increment is referred to the current shape of the element instead of the original shape.

Define an elastic strain-rate tensor $\dot{e}_{ij}$ and a plastic strain-rate tensor $\dot{\epsilon}_{ij}$ by

$$E\dot{e}_{ij} = (1 + \nu)\,\dot{\sigma}_{ij} - \nu\dot{\sigma}_{kk}\,\delta_{ij} \tag{2}$$

and

$$\dot{\epsilon}_{ij} = \dot{\eta}_{ij} - \dot{e}_{ij} \tag{3}$$

where E, ν are Young's modulus and Poisson's ratio, and the repeated suffix implies summation. The definition of elastic strain by integration of (2) then accords with that of infinitesimal elasticity theory for small strains.

Write

$$\dot{W} = \sigma_{ij}\,\dot{\epsilon}_{ij} \tag{4}$$

and let W represent the total plastic work done on an element since last annealing.

Finally, define a "reduced stress" tensor σ'_{ij} by

$$\sigma'_{ij} = \sigma_{ij} - \tfrac{1}{3}\,\sigma_{kk}\,\delta_{ij} \tag{5}$$

and the octahedral stress S by

$$2S^2 = \sigma_{ij}'\,\sigma_{ij}', \qquad S \geqslant 0. \tag{6}$$

Assume a (Reuss) material with the following properties:

For any element of the material there exists a Mises-Hencky yield limit, $k(W)$, depending only on the plastic work W done on that element and such that if either

$$S < k(W)$$

or

$$S = k(W), \qquad \dot{s} \leqslant 0,$$

then

$$\dot{\epsilon}_{ij} = 0, \qquad \dot{\eta}_{ij} = \dot{e}_{ij}; \tag{7}$$

while if

$$S = k(W), \qquad \dot{s} > 0,$$

the plastic strain rate is

$$\dot{\epsilon}_{ij} = \sigma_{ij}' \dot{S} (2k^2 dk/dW)^{-1}. \tag{8}$$

Note that for simple shear strain, with all tensor components vanishing except $i, j = 1, 2$ or $i, j = 2, 1$, (2), (3), (6) and (8) lead to

$$\dot{\eta}_{12} = \frac{\dot{\sigma}_{12}}{2G} + \frac{\dot{\sigma}_{12}}{2kdk/dW}$$

where G is the shear modulus. Half the slope of the stress-strain in shear (the " tangent " shear modulus) is therefore

$$\frac{kdk/dW}{K} \tag{9}$$

where

$$K = 1 + (k/G)\, dk/dW. \tag{10}$$

In a simple tension test, where $\sigma_{ij} = 0$ for $i \neq 1, j \neq 1$, the corresponding result is

$$\dot{\eta}_{11} = \frac{\dot{\sigma}_{11}}{E} + \frac{\dot{\sigma}_{11}}{3kdk/dW}$$

with tangent tensile modulus

$$\frac{3Ek\, dk/dW}{E + 3kdk/dW}. \tag{11}$$

Note also that, for perfect plasticity, $\dot{s}$ and dk/dW tend to zero, and (8) reduces to

$$\dot{\epsilon}_{ij} = \mu\sigma'_{ij} \tag{8a}$$

where μ is indeterminate.

The set of equations for solution is completed by the inclusion of the equations of motion

$$\frac{\partial}{\partial x_i} \sigma_{ij} = \rho\ddot{u}_j \tag{12}$$

where ρ, the density, may be assumed constant, since only elastic volume changes occur.

Note that no strain-rate effect in the stress-strain curve *of an element* is assumed. This simplification has been challenged by Malvern (1951), Sternglass and Stuart (1953), and others, but the experimental evidence is not yet adequate for a final decision on the point, and since no experiment can be performed on an element, the question can only be decided when the complete consequences of the assumption have been examined.

2. Propagation of Infinitesimal Discontinuities

A direct analysis of the characteristic properties of the equations of plastic flow is straightforward but long. It is therefore more satisfactory to approach the problem in a slightly different manner (cf. Love, *loc. cit.*, pp. 295-297).

Consider the propagation of a plane wave-front separating two regions of uniform

stress. Let the wave front be brought to rest by superposition of a suitable constant velocity. Choose axes such that the wave-front is the plane $x_3 = 0$ and the velocity component u_3 is negative and of magnitude λ, and let the stress tensor and velocity vector for $x_3 > 0$ be σ_{ij}, u_i and the infinitesimal discontinuities across the wave front $\Delta\sigma_{ij}$, Δu_i. Assume the tensor σ_{ij} to satisfy the yield condition $S = k$.

Continuity of the material demands

$$\Delta\eta_{11} = \Delta\eta_{12} = \Delta\eta_{22} = 0, \tag{13}$$

$$2\lambda\Delta\eta_{13} = \Delta u_1, \qquad 2\lambda\Delta\eta_{23} = \Delta u_2, \qquad \lambda\Delta\eta_{33} = \Delta u_3, \tag{14}$$

where $\Delta\eta_{ij}$ is the change in strain of an element as it crosses the wave front. Conservation of momentum requires

$$\Delta\sigma_{13} = \rho\lambda\Delta u_1, \qquad \Delta\sigma_{23} = \rho\lambda\Delta u_2, \qquad \Delta\sigma_{33} = \rho\lambda\Delta u_3 \tag{15}$$

and equations (8) are replaced by

$$\Delta\epsilon_{ij} = \sigma_{ij}\,\Delta S\,(2k^2\,dk/dW). \tag{16}$$

Substitute in (16) from (13) and (14). Then

$$\left.\begin{aligned} &\frac{-\Delta\sigma_{11} + \nu\Delta\sigma_{22} + \nu\Delta\sigma_{33}}{\sigma_{11}'} = \frac{-\Delta\sigma_{22} + \nu\Delta\sigma_{33} + \nu\Delta\sigma_{11}}{\sigma_{22}'} = \frac{-(1+\nu)\,\Delta\sigma_{12}}{\sigma_{12}} \\ &= \frac{\Delta\sigma_{33}\left\{E/(2\rho u_3^2) - 1\right\} + \nu\Delta\sigma_{11} + \nu\Delta\sigma_{22}}{\sigma_{33}'} = \frac{\Delta\sigma_{13}\left\{E/(2\rho u_3^2) - (1+\nu)\right\}}{\sigma_{13}} \\ &= \frac{\Delta\sigma_{23}\left\{E\,(2\rho u_3^2) - (1+\nu)\right\}}{\sigma_{23}} = \frac{\Delta S}{2k^2\,(dk/dW)} \end{aligned}\right\} \tag{17}$$

provided that $\Delta S \geqslant 0$.

First choose axes such that $\sigma_{23} = 0$. Then either $\Delta\sigma_{23} = 0$ or

$$\lambda^2 = \frac{E}{2\,(1+\nu)\,\rho} = \frac{G}{\rho} = c_2^2. \tag{18}$$

where c_2 is the velocity of transverse elastic waves. Thus, an infinitesimal transverse wave polarised in a direction of zero shear travels with the velocity of elastic shear-waves. This is to be expected since such a wave entails no first order change in S. Now use the first four fractions to express $\Delta\sigma_{11}$, $\Delta\sigma_{12}$, $\Delta\sigma_{22}$ in terms of $\Delta\sigma_{33}$. Then

$$\left.\begin{aligned} \sigma_{33}'\,\Delta\sigma_{11} &= \left\{\sigma_{11}' - \frac{2G\,(\sigma_{11}' + \nu\sigma_{22}')}{(1-2\nu)\,\rho\,\lambda^2}\right\}\Delta\sigma_{33}, \\ \sigma_{33}'\,\Delta\sigma_{22} &= \left\{\sigma_{22}' - \frac{2G\,(\sigma_{22}' + \nu\sigma_{11}')}{(1-2\nu)\,\rho\,\lambda^2}\right\}\Delta\sigma_{33}, \\ \sigma_{33}'\,\Delta\sigma_{12} &= \sigma_{12}\left\{1 - \frac{2G\,(1-\nu)}{(1-2\nu)\,\rho\,\lambda^2}\right\}\Delta\sigma_{33}. \end{aligned}\right\} \tag{19}$$

Use of the fractions with denominators σ_{13} and σ_{33}' in (17) then gives

$$\sigma_{33}'\,\Delta\sigma_{13}\,(\lambda^2 - c_2^2) - \sigma_{13}\,\Delta\sigma_{33}\,(\lambda^2 - c_1^2) = 0 \tag{20}$$

where $c_1^2 = 2G\,(1-\nu)/(1-2\nu)$ is the square of the velocity of longitudinal

elastic waves, while the use of the fourth and last fractions leads to

$$G\sigma_{33}'\,\sigma_{13}\,\Delta\sigma_{33} + \left[(2k^2\,K)\,(\rho\lambda^2 - G) + 2G\sigma_{13}^2\right]\Delta\sigma_{13} = 0 \tag{21}$$

where K is given by (10). Equations (20) and (21) are compatible provided that

$$A\rho^2\,\lambda^4 - B\rho\,\lambda^2\,G + CG^2 = 0, \tag{22}$$

where

$$\left.\begin{aligned} A &= (1-2\nu)\,Kk^2, \\ B &= (3-4\nu)\,Kk^2 - (1-2\nu)\,(\sigma_{33}'^2 + \sigma_{13}^2), \\ C &= 2\,(1-\nu)\,Kk^2 - (1-2\nu)\,\sigma_{33}'^2 - 2\,(1-\nu)\,\sigma_{13}^2. \end{aligned}\right\} \tag{23}$$

(When $\sigma_{23} \neq 0$ the corresponding expressions may be obtained by writing $\sigma_{13}^2 + \sigma_{23}^2$ instead of σ_{13}^2 in (21) to (23).)

Now A, B, C are essentially positive when $dk/dW > 0$, and the discriminant of (22) is D, given by

$$D = \left\{Kk^2 - (1-2\nu)\,(\sigma_{33}'^2 - \sigma_{13}^2)\right\}^2 + 4\,(1-2\nu)^2\,\sigma_{33}'^2\,\sigma_{13}^2,$$

and is always positive. Equation (22) has therefore two real positive roots for λ, and there are always two basic wave-velocities, though as $\nu \to \frac{1}{2}$ (the incompressible case) one of the velocities tends to infinity.

In two particular cases the equation has rational factors for any value of dk/dW. First, suppose $\sigma_{33}' = 0$. Then the basic waves are a longitudinal wave of velocity c_1, where, as above, c_1 is the velocity of dilatational elastic waves, and a transverse wave whose velocity is given by

$$\lambda^2 = c_2^2\,\frac{Kk^2 - \sigma_{13}^2}{Kk^2} \tag{24}$$

(provided that $\sigma_{13}\,\Delta\sigma_{13} > 0$). When the initial stress is a pure shear, $\sigma_{13} = k$, the velocity reduces to

$$\left(\frac{1}{\rho K}\,\frac{dk}{dW}\right)^{\frac{1}{2}}.$$

This value is, from (9) the wave velocity obtained by using the " tangent modulus " given by the stress-strain curve in pure shear.

Secondly, suppose $\sigma_{13} = 0$, then there is a transverse wave with the same velocity as a transverse elastic wave, and a longitudinal wave with velocity given by

$$\lambda^2 = \frac{G}{\rho}\cdot\frac{2\,(1-\nu)^2\,Kk^2 - (1-2\nu)\,\sigma_{33}'^2}{(1-2\nu)\,K} \tag{25}$$

provided that $\sigma_{33}'\,\Delta\sigma_{33} > 0$, the condition for plastic deformation. Note that in uniaxial stress $\sigma_{33} = \sqrt{3}k$, $\sigma_{ij} = 0$ for $i, j \neq 3$, the right-hand side of (25) reduces to

$$\frac{G}{\rho}\cdot\frac{2\,(1+\nu) + 2\,(1-\nu)\,(k\,dk/dW)/G}{3\,(1-2\nu)\,K}$$

which does not correspond to the tangent modulus, (11), appropriate to uniaxial stress.

For general values of σ_{13}, σ'_{33}, and dk/dW, the roots of (22) cannot be expressed as rational functions, and the two possible waves cannot be distinguished as longitudinal and transverse, since both involve discontinuities in both velocity components. However, it is immediately clear from (22) that the two roots, λ_1, λ_2, for λ (with $\lambda_1^2 > \lambda_2^2$), satisfy the inequalities

$$c_1^2 \geqslant \lambda_1^2 > c_2^2 \geqslant \lambda_2^2 \tag{26}$$

where the inequality $\lambda_1^2 > c_2^2$ depends on the relation $kdk/dW > 0$, and is therefore valid for all strain-hardening materials. It is convenient to call these the fast and slow waves.

Now, $\Delta S > 0$ for any plastic wave, and so, from (17), for a fast plastic wave, $\Delta\sigma_{13}/\sigma_{13} < 0$ and, from (20), $\Delta\sigma_{33}/\sigma_{33}' > 0$. For the slow wave (17) shows that $\Delta\sigma_{13}/\sigma_{13} > 0$ and (20) that $\Delta\sigma_{33}/\sigma_{33}' > 0$. Thus in any plastic wave the change in σ_{33} is of the same sign as σ_{33}'. This gives a convenient criterion for distinguishing between plastic and elastic waves.

3. Direct Interaction of Waves of Different Types

In the linearized theory, appropriate to waves of small amplitude, two plastic waves which interfere remain unchanged and the state of stress or strain is obtained by addition of the corresponding terms for the separate waves. The same is true of the interference of two elastic unloading waves. Interference between an elastic unloading and a plastic wave is a more complicated problem, but may be illustrated by a few examples.

Consider a material at the yield point under uniaxial stress, and suppose all waves are plane waves with direction of propagation at an angle θ to the stress axis, so that, in the previous notation,

$$\sqrt{3}\,\sigma_{33}' = k\,(2\cos^2\theta - \sin^2\theta), \tag{27}$$

$$\sqrt{3}\,\sigma_{13} = -3k\sin\theta\cos\theta. \tag{28}$$

Use c_1, c_2, λ_1, λ_2 for the velocities of fast and slow elastic and plastic waves, and write n_1, n_2 for the ratios $\Delta\sigma_{13}/\Delta\sigma_{33}'$ in the fast and slow plastic waves. It is convenient to suppose $\cos^2\theta < \frac{1}{3}$ so that $\sigma_{33}' > 0$, $\sigma_{13} < 0$, and, from (20) and (25), $n_1 > 0$, $n_2 < 0$. (When $\cos^2\theta > \frac{1}{3}$ certain changes of sign are required in the following analysis, but the corresponding differences in the argument are trivial.) Then any plastic wave increases σ_{33}, a fast elastic wave changes σ_{33} but not σ_{13}, and a slow elastic wave changes σ_{13} but not σ_{33}. Much verbiage is eliminated by use of diagrams, with consistent conventions as follows. The waves are represented by vertical lines, each with an arrow showing the direction of motion, and the velocity, which implies the type of wave, to the right of the line. The figures to the left indicate the differences between the values, on the left and right (left minus right) of the wave-front, of the quantities σ_{33}, σ_{13}, reading downwards. Note that a positive change of σ_{33}, propagating forward (i.e. to the right) implies loading. A negative change of σ_{13} propagating forward also implies loading. Reversal of *either* the direction of propagation *or* the sign of the stress increment implies unloading.

There are in all nine cases to be considered, but we give only three. The others are all more or less similar.

(i) A fast elastic wave overtakes a fast plastic wave. There are initially two wave fronts as shown in Fig. 1a. In order that the elastic wave may cause unloading and the plastic wave loading, the parameters α, δ must both be positive.

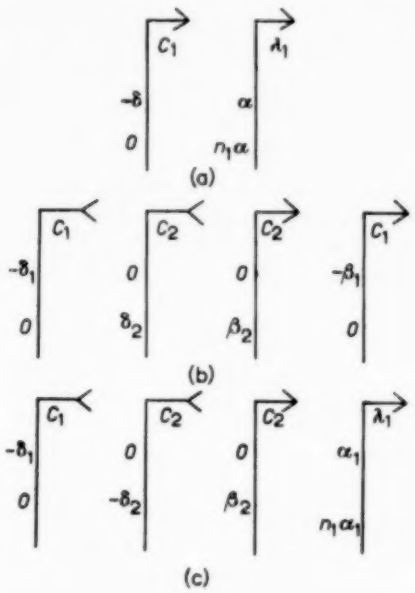

Fig. 1.

Assume first that $\delta > \alpha$, then the plastic wave may be expected to be annihilated, and four elastic waves, one fast and one slow in each direction (Fig. 1 (b)) are needed to satisfy the continuity and momentum conditions. Let the stress discontinuities be as shown; then continuity implies

$$-\delta + \alpha = -\delta_1 - \beta_1, \qquad n_1\alpha = \delta_2 + \beta_2,$$

and conservation of momentum implies

$$-\frac{\delta}{c_1} + \frac{\alpha}{\lambda_1} = \frac{\delta_1}{c_1} - \frac{\beta_1}{c_1}, \qquad \frac{n_1\alpha}{\lambda_1} = -\frac{\delta_2}{c_2} + \frac{\beta_2}{c_2}.$$

The solution of the four equations is given by

$$2\lambda_1\delta_1 = \alpha(c_1 - \lambda_1), \qquad 2\lambda_1\delta_2 = n_1\alpha(\lambda_1 - c_2),$$

$$2\lambda_1\beta_2 = n_1\alpha(\lambda_1 + c_2), \qquad 2\lambda_1\beta_1 = 2\lambda_1\delta - (\lambda_1 + c_1)\alpha.$$

The first three waves are then, reading from left to right, a reloading fast wave of amplitude δ_1, a reloading slow wave of amplitude δ_2, and an unloading slow wave of amplitude β_2. The fourth wave is an unloading wave if

$$\delta \geqslant (\lambda_1 + c_1)\alpha/(2\lambda_1) \tag{29}$$

and since a loading wave travelling into a material at the yield stress is necessarily plastic, the solution is valid only when the inequality holds. Note that since β_1, β_2 give unloading waves the value of S between the slow elastic waves is less than that behind the original α wave. The combined effect of the δ_1, δ_2 waves is therefore not sufficient to load the material to above a previous yield point, and neither of these two waves need be plastic. When the inequality (29) is not satisfied, the fast progressive wave is a loading wave (Fig. 1 (c)) and the amplitudes are given by

$$(c_1 + \lambda_1)\,\delta_1 = (c_1 - \lambda_1)\,\delta, \qquad 2\lambda_1\,\delta_2 = (\lambda_1 - c_2)\,n_1\,(\alpha - \alpha_1),$$

$$2\lambda_1\,\beta_2 = (\lambda_1 + c_2)\,n_1\,(\alpha - \alpha_1), \qquad (\lambda_1 + c_1)\,(\alpha - \alpha_1) = 2\lambda_1\,\delta,$$

and the waves are reloading, reloading, unloading, loading. Again, since $\alpha_1 < \alpha$ and β_2 is unloading the yield stress is not exceeded between the slow waves.

(ii) A fast elastic wave meets a fast plastic wave. Fig. 2 shows the original waves, (a), and the resulting waves for a weak plastic wave, (b), and a strong plastic wave (c).

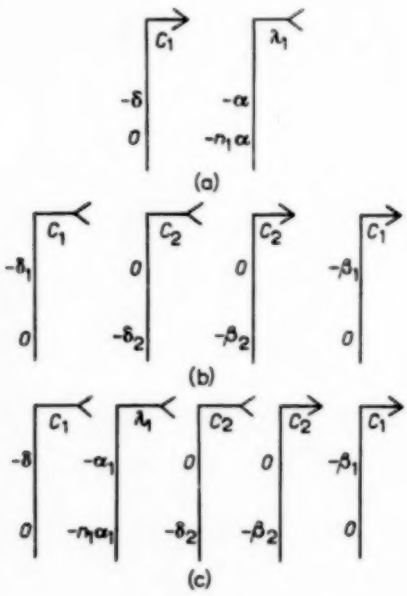

Fig. 2.

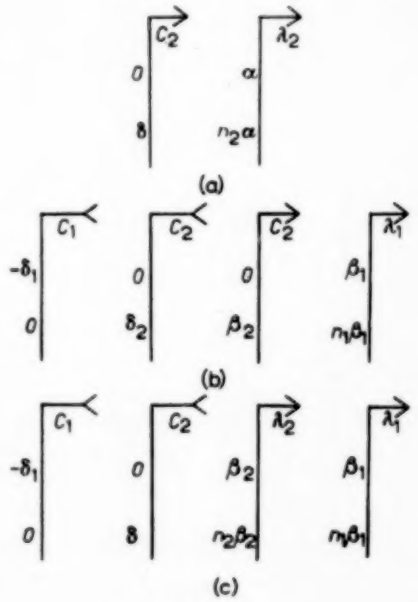

Fig. 3.

In Fig. 2 (b) the amplitudes are given by

$$2\lambda_1\,\delta_1 = (\lambda_1 + c_1)\,\alpha, \qquad 2\lambda_1\,\delta_2 = (\lambda_1 + c_2)\,\alpha,$$

$$2\lambda_1\,\beta_2 = n_1\,(\lambda_1 - c_2)\,\alpha. \qquad 2\lambda_1\,\beta_1 = 2\lambda_1\,\delta - (c_1 - \lambda_1)\,\alpha,$$

and the waves are reloading, unloading, reloading, unloading from left to right. The solution is valid if $\delta_1 < \delta$, i.e. if $2\lambda_1\,\delta > (\lambda_1 + c_1)\,\alpha$. For stronger plastic waves the scheme is shown in Fig. 2 (c). The loading wave δ, is broken up into

an elastic reloading wave of strength δ which brings the material to the yield point, and a plastic loading wave of strength α_1. The amplitudes are given by

$$(\lambda_1 + c_1)\,\alpha_1 = (\lambda_1 + c_1)\,\alpha - 2\lambda_1\,\delta, \qquad (\lambda_1 + c_1)\,\delta_2 = (\lambda_1 + c_2)\,n_1\,\delta$$
$$(\lambda_1 + c_1)\,\beta_2 = n_1\,(\lambda_1 - c_2)\,\delta, \qquad (\lambda_1 + c_1)\,\beta_1 = 2\lambda_1\,\delta.$$

The interference phenomena between fast elastic and slow plastic waves are similar, and need not be given.

(iii) When a slow elastic wave overtakes a slow plastic wave the situation is slightly more complicated. Suppose first that the plastic wave is relatively weak. Then it can be easily deduced that a fast plastic wave is set up, and the configuration of the waves is that shown in Fig. (3b). The amplitudes are given by

$$\lambda_2\,(\lambda_1 + c_1)\,\delta_1 = c_1\,(\lambda_1 - \lambda_2)\,\alpha,$$
$$2\lambda_1\,\lambda_2\,\delta_2 = -\,n_2\,\lambda_1\,(c_2 - \lambda_2)\,\alpha - n_1\,\lambda_2\,(\lambda_1 - c_2)\,\beta_1,$$
$$2\lambda_1\,\lambda_2\,\beta_2 = 2\lambda_1\,\lambda_2\,\delta + \lambda_1\,(\lambda_2 + c_2)\,n_2\,\alpha - \lambda_2\,(\lambda_1 + c_2)\,n_1\,\beta_1,$$
$$\lambda_2\,(\lambda_1 + c_1)\,\beta_1 = \lambda_1\,(\lambda_2 + c_1)\,\alpha,$$

and the waves β_1, δ_1 are loading waves. Also, from (20),

$$n_2/n_1 = -\,(c_1^{\,2} - \lambda_2^{\,2})\,(\lambda_1^{\,2} - c_2^{\,2})/(c_2^{\,2} - \lambda_2^{\,2})\,(c_1^{\,2} - \lambda_1^{\,2})$$

and substitution in the equation for δ_2 shows that $\delta_2 > 0$, and the corresponding wave is a loading wave. The solution is valid provided that $\beta_2 \geqslant 0$ and δ_1, δ_2 do not together load the material beyond the yield point; that is, if

$$2\lambda_2\,(\lambda_1 + c_1)\,(\delta/\alpha) \geqslant (-\,n_2)\,(\lambda_2 + c_2)\,(\lambda_1 + c_1) + n_1\,(\lambda_1 + c_2)\,(\lambda_2 + c_1) \qquad (30)$$

and

$$2c_1\,(\lambda_1 - \lambda_2)\,\sigma_{33}' + (-\,n_2)\,(\lambda_1 + c_1)\,(c_2 - \lambda_2)\,(-\,2\sigma_{13})$$
$$-\,n_1\,(\lambda_2 + c_1)\,(\lambda_1 - c_2)\,(-\,2\sigma_{13}) \leqslant 2\lambda_2\,(\lambda_1 + c_1)\,(\delta/\alpha)\,(-\,2\sigma_{13}). \qquad (31)$$

A value of δ/α can be found which violates (30) but satisfies (31) provided that

$$(-\,2\sigma_{13})\,\{(-\,n_2)\,\lambda_2\,(\lambda_1 + c_2) + n_1\,\lambda_1\,(\lambda_2 + c_1)\} > c_1\,(\lambda_1 - \lambda_2)\,\sigma_{33}'. \qquad (32)$$

For such a value of δ/α the β_2 wave becomes plastic (Fig. 3 (c)) and the amplitudes are given by

$$\frac{\beta_1}{\lambda_1\,(c_1 + \lambda_2)} = \frac{\alpha - \beta_2}{\lambda_2\,(\lambda_1 + c_1)} = \frac{2\delta}{n_1\,(\lambda_1 + c_2)\,(\lambda_2 + c_1) - n_2\,(\lambda_2 + c_2)\,(\lambda_1 + c_1)}$$
$$= \frac{\delta_1}{c_1\,(\lambda_1 - \lambda_2)} = \frac{-\,2\delta_2}{n_1\,(\lambda_1 - c_2)\,(\lambda_2 + c_1) - n_2\,(\lambda_2 - c_2)\,(\lambda_1 + c_1)}.$$

The condition (31) shows that the material behind the wave δ_2 is not required to yield by this solution, and the solution is therefore valid.

But the left-hand side of (32) is greater than

$$(-2\sigma_{13})\,\lambda_1\lambda_2(n_1-n_2)/\{\sigma_{33}'(\lambda_1-\lambda_2)\}$$

$$=\frac{2\sigma_{13}^2\lambda_1\lambda_2}{\sigma_{33}'(\lambda_1-\lambda_2)}\cdot\frac{(c_1^2-\lambda_1^2)(c_2^2-\lambda_2^2)+(\lambda_1^2-c_2^2)(c_1^2-\lambda_2^2)}{(\lambda_1^2+\lambda_2^2)c_2^2-c_2^4-\lambda_1^2\lambda_2^2}$$

$$=\frac{2\sigma_{13}^2\lambda_1\lambda_2}{\sigma_{33}'^2}\cdot\frac{(c_1^2-c_2^2)(1-2\nu)Kk^2(\lambda_1+\lambda_2)}{c_2^4\sigma_{13}^2}$$

$$=\frac{2(c_1^2-c_2^2)\sqrt{BC}}{\sigma_{33}'^2c_2}>\frac{2(c_1^2-c_2^2)k}{\sigma_{33}'c_2}>\frac{\sqrt{6}\,c_2}{1-2\nu}$$

$$>c_1\left[=2^{\frac{1}{2}}c_2(1-\nu)^{\frac{1}{2}}(1-2\nu)^{-\frac{1}{2}}\right]$$

where B, C are given in (23) and the last inequality holds as long as $\nu>\frac{1}{2}$, so the condition is satisfied for all real materials.

Similar reasoning is required to justify the solutions for some of the other cases.

4. Conclusions

It has been shown that the basic waves in an elastic-plastic medium are "fast" and "slow" waves of types and velocities depending on the state of stress of the medium into which they are propagated. In a particular experiment, for example Sternglass and Stuart (1953), in which waves are propagated in a thin strip initially in uniaxial stress, the calculation of the surface displacements as functions of time and position is clearly a programme of considerable magnitude. There is, in the opinion of the present author, only one experimental programme which can in principle give an unequivocal answer to the question of whether strain-rate effects do or do not exist in a given material. This experiment is to follow the propagation of pure torsional waves in a thin tube initially stressed to the yield limit in pure torsion. Only then can the wave-velocity (25) be predicted, from the tangent modulus for torsion of the tube.

References

Conroy, M. F.	1952	*J. Appl. Mech.* **19**, 521.
Craggs, J. W.	1952	*Proc. Roy. Soc. Edin.* **63**, 339.
Duwez, P. E., Clark, D. S. and Bohnenblust, H. F.	1950	*J. Appl. Mech.* **17**, 27.
Freiberger, W.	1952	*Proc. Camb. Phil. Soc.* **48**, 135.
Karman, Th. von	1942	*N.D.R.C.* Rep. A.29.
Lee, E. H.	1953	*Quart. J. Appl. Math.* **10**, 335.
Love, A. H.	1927	*Theory of Elasticity* 4th Edition (Macmillan).
Malvern, L. E.	1951	*Trans. A.S.M.E.* **73**, 263.
Sternglass, E. J. and Stuart, D. A.	1953	*J. Appl. Mech.* **20**, 427.
Taylor, G. I.	1940	*British Official Report R.C.* 70.
White, M. P. and Griffis, Le van	1947	*J. Appl. Mech.* **14**, 337.
	1949	*J. Appl. Mech.* **15**, 256.

Journal of the Mechanics and Physics of Solids, 1957, Vol. 5, pp. 125 to 134. Pergamon Press Ltd., London.

AN EXPERIMENTAL INVESTIGATION OF THE DEFORMED ZONE ASSOCIATED WITH INDENTATION HARDNESS IMPRESSIONS

By L. E. Samuels and T. O. Mulhearn
Defence Standards Laboratories, Sydney, Australia

(*Received 2nd November*, 1956)

Summary

Using a metallographic method and specimens of 70 : 30 brass, experimental determinations have been made of the elastic-plastic and other low-strain boundaries of the deformed zone associated with indentation hardness impressions. Pyramidal impressions in specimens of semi-infinite and finite thickness, pyramidal impressions made close to the edge of the specimen, and ball impressions made under a range of indenting conditions have been investigated. The results suggest that indentation by the standard pyramidal indenter occurs in this particular material by a compression type of mechanism rather than by a cutting type of mechanism on which theoretical treatments of the indentation process have been based. The practical significance of the results is also discussed.

1. Introduction

A basic requirement for an understanding of the mechanism of indentation in hardness testing is a knowledge of the pattern and extent of the deformed zone associated with an impression; this would also provide information concerning the limits of variables in testing practice, such as the spacing of impressions and critical specimen dimensions (the dimensions above which the measured hardness is independent of specimen size). The problem has been treated theoretically by Hill, Lee and Tupper (1947), and by Hill (1950a) but, because of mathematical difficulties, these treatments necessarily have been two-dimensional and confined to an idealized rigid-plastic material. Their results have received a considerable measure of support from the work of Dugdale (1953) who investigated impressions made in cold-worked metals, which approximate to a rigid-plastic material, with a range of wedge indenters. He determined the critical specimen dimensions and found that they agreed well with those predicted by Hill (1950a); he also showed that the shear yield stress deduced from these tests on the basis of rigid-plastic theory was in fair agreement with that obtained from torsion tests. Nevertheless, it would still be of considerable interest to determine experimentally the boundaries of the deformed zone for actual three-dimensional hardness impressions. This was the purpose of the present work.

Previous experimental investigations of this type have been based on one of two experimental techniques: namely, observations of the distortion of markings on a face of the specimen, and hardness exploration of a section through the

impression. An extensive investigation of the second type has been reported recently by Williams and O'Neill (1956). Both of these methods have serious limitations. Firstly, the impression investigated must be comparatively large : in the case of Vickers-type pyramid impressions it must be much larger than in normal hardness testing practice and consequently a standard diamond indenter cannot be used. Secondly, the sensitivity of both methods in detecting deformation is comparatively low and they are suitable only for investigating the more highly strained areas immediately adjacent to the impression.

Methods based on the metallographic examination of sections through the impression might overcome both these limitations if a technique were available which detected prior deformation with sufficient sensitivity. Green and Hundy (1956) have developed a method of this type applicable to specimens of mild steel, but this method does not appear to be suitable for the investigation of pyramid hardness impressions of normal size. The most suitable experimental material for this purpose at present appears to be 70 : 30 brass because a number of metallographic techniques are available with which deformation can be detected with very high sensitivity (see Jacquet (1949) and (1954), Samuels (1954) and Samuels and Hatherly (1955)). These techniques are most suited to the determinations of low-strain boundaries, and would therefore provide information complementary to that obtained in investigations of the type carried out by Williams and O'Neill (1956).

However, 70 : 30 brass has the disadvantage for the present purposes that the stress-strain curve is of a well-rounded form and, in this respect, is far removed from the theoretical rigid-plastic material; consequently, the theoretical models may not be strictly applicable. Nevertheless, it is representative of many common materials in the annealed condition and it is therefore of some importance to determine whether there is any significant departure from the theoretical models.

2. Experimental Methods

The material used was a 0·5-in. hot-rolled commercial brass plate containing 29·9% Zn. and spectrographic traces only of other elements. Specimens of suitable shape were cut from the plate and annealed at 600° C for 2 hr, establishing a grain size of 0·05 mm mean dia.; a grain size of this order was desirable to facilitate the metallographic observations. A test surface was then prepared by methods which are known to produce a strain-free surface (Samuels 1952 and 1956). The impressions made on this test surface were as large as practicable and were always at least an order of magnitude larger than the grain size of the specimen material. As in normal hardness testing practice, the indenter was not lubricated when making the impressions.

Two techniques were used to determine the pattern of the deformation zones. In the first, a series of levels beneath the indented surface was examined by removing successive layers of known thickness from this surface ; in the second, a section cut through the centre of the impression and normal to the indented surface was examined. The first method enabled the zones to be determined with greater certainty and consequently was used in all the exploratory experiments. In either case, the section was metallographically polished to produce a truly representative surface and was then etched by one of the methods chosen to develop the metallographic indications of deformation (Table 1). The limit of the zone in which these indications were developed, which was determined by examination under a metallurgical microscope using a calibrated traversing stage, was taken as a strain boundary and a strain value was ascribed to the boundary according to the threshold sensitivity of the particular etching method used.

Before the latter could be done, it was necessary to make some estimate of the threshold sensitivities of the etching methods employed under the conditions of the present experiment.

Cylinders were therefore cut from the plate, annealed as above and compressed between oiled steel platens at about the same rate as the rate of travel of the indenter in the hardness-testing machine. The cylinders were then sectioned longitudinally, polished and etched, and the compression (percentage reduction in original length) determined at which the metallographic indications were first developed. Threshold values for the first two etching methods listed in Table 1 were determined in this way, together with the compressive stress required in these experiments to produce the threshold strain. This method is not precise enough for determining the sensitivity of the electrolytic thiosulphate etch, but it is reasonable in this case to accept the earlier results of SAMUELS and HATHERLY (1955). For the present purposes, therefore, the boundary determined by this etching method may be regarded as being the elastic-plastic boundary in the sense that it is the boundary between the zone in which slip has occurred in the majority of the grains and the zone in which it has not. The corresponding elastic limit is estimated to be of the order of 1 kg/mm^2. This calibration method assumes that the strains at the levels concerned are of a simple compressive nature, an assumption which may not be fully justified. If not, the absolute value ascribed to the strain boundaries may be in some doubt; however, it is probable that the only boundary likely to be affected to any extent is that referred to as the 7%-strain boundary.

TABLE 1. Etching methods chosen for the determination of the strain boundaries

Etching method	*Threshold Sensitivity* (% *Compression*)	*Corresponding Compressive Stress* (*kg/mm*^{2})
Acid Ferric Chloride Reagent	7	19·5
Electrolytic Thiosulphate Etch. Low-Sensitivity Method	1	10
Electrolytic Thiosulphate Etch. High-Sensitivity Method	$< 0{\cdot}05$	1

NOTE : Details of these etching methods are given by SAMUELS (1954-55).

The boundaries determined as described above may be taken as boundaries of constant strain because the development of the etching effects indicates that a more or less definite amount of slip has occurred in the grain concerned. However, they represent boundaries of constant stress only if the elastic restraint is everywhere uniform and, even then, the stress value will be that listed in Table 1 only if the elastic restraint is negligible (HILL, LEE and TUPPER 1947).

3. SEMI-INFINITE SPECIMENS

In the first series of experiments, impressions were made with Brinell-ball and Vickers-pyramid indenters on disc-shaped specimens (2·5 cm diameter x 1·25 cm thick). The first group of Brinell-ball impressions were made with a 2 mm diameter (D) steel ball indenter and an indenting load (P) of 40 kg, the diameter of the resulting impression (d_b) being 1·021 mm; these conditions correspond to a P/D^2 ratio of 10, a d_b/D ratio of 0·51, and a Brinell hardness number 45·4. This is a standard impression for the material concerned. The pyramid impressions were made with the same indenting load, giving an impression with a mean diagonal (d_p) of 1·288 mm, equivalent to a diamond pyramid hardness number 44·7. Five impressions of the one type were made on each specimen, the impressions being spaced at about 5 mm centres. Under these conditions the specimen can be regarded as being semi-infinite.

These two types of impression are closely equivalent to one another. For example, TABOR (1951) ascribes a " representative strain " (ϵ_r) value of 8% to a pyramidal impression ; the corresponding value for the above ball impression is 10% ($\epsilon_r = 20\, d_b/D$). The strain boundaries of other pyramidal impressions can be expected to be geometrically similar to that determined for the above impression, but this is not so in the case of ball impressions with other d_b/D ratios. Therefore, two non-standard ball impressions were also investigated, both being made with a 2 mm diameter steel ball. The first was made with a 120 kg indenting load giving an impression with the following characteristics : $d_b = 1{\cdot}400$ mm, $d_b/D = 0{\cdot}7$, $P/D^2 = 30$, $\epsilon_r = 14\%$. The second was made with a 5 kg indenting load, the other values being $d_b = 0{\cdot}386$ mm, $d_b/D = 0{\cdot}19$, $P/D^2 = 1{\cdot}25$, $\epsilon_r = 3{\cdot}8\%$.

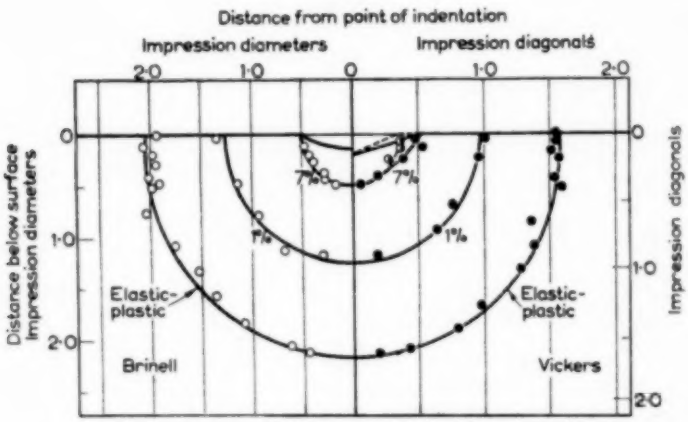

Fig. 1. Strain boundaries for Brinell-ball (left) and Vickers-pyramid (right) impressions in a semi-infinite specimen. Both impressions made with a 40-kg indenting load ; for the ball impression, $d_b/D = 0{\cdot}51$.

(a) *Standard Impressions.* Cross sections of the three boundaries determined for the ball and pyramidal impressions are compared in Fig. 1. The coordinates are given in terms of impression diagonals or diameters, this being the most general method of comparing the results ; however, in these particular cases, the curves have actually been plotted on the same linear scales in order to show that the absolute extents of the boundaries are very similar in the two cases. The only marked difference is that, whereas the strain boundaries are always circular in plan for the ball impression, the 7%-strain boundary for the pyramidal impression is approximately square in plan close to the indented surface, merging gradually into an approximately circular plan at greater depths. Two sections of this boundary are therefore given in Fig. 1, one parallel to the side of the impression and the other parallel to the impression diagonal. In view of the close equivalence of the two types of impression, the similarity in strain boundaries is not unexpected. The strain boundaries for these two impressions all appear to be approximately hemispherical in form, the hemisphere being centred at, or slightly below, the point of indentation. The radii of the elastic-plastic boundaries were about 2·1 d_b

and 1·7 d_p respectively. Although a direct comparison is not possible, the form of the 7%-strain boundary is consistent with the results of WILLIAMS and O'NEILL (1956).

The bulging of the free surface adjacent to the impressions was also investigated by examining the indented surface microscopically under phase-contrast illumination and determining the extent of the zone in which surface slip steps had developed. This zone coincided exactly with the elastic-plastic boundary determined as above, confirming the nature of the latter. DUGDALE (1954) has also investigated the extent of the plastically-deformed area at the free surface adjacent to conical impressions, the specimens being examined microscopically under strongly oblique illumination. The radius of the deformed area for cold-worked steel, copper and aluminium was about 0·8 times the diameter of the impression for a 140° cone

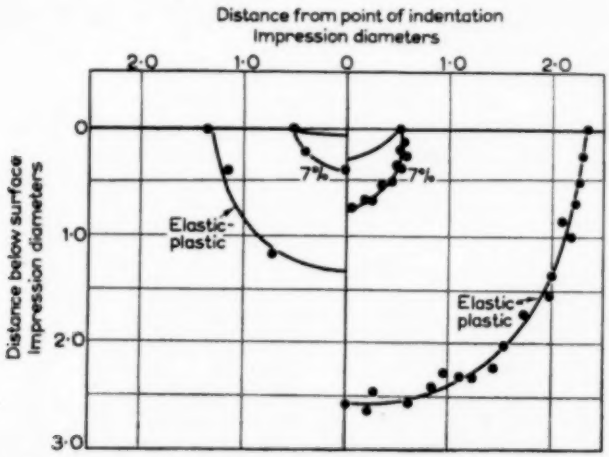

Fig. 2. Elastic-plastic and 7%-strain boundaries for nonstandard ball impressions. Left : $d_b/D = 0{\cdot}7$; Right : $d_b/D = 1{\cdot}25$.

indenter, which is about half the value found here. It is to be expected, however, that the surface deformed area would be less extensive in cold-worked than in annealed material, and the value found by the phase-contrast method for the present brass cold-worked 20% was, in fact, only about 0·9 d_p. This agrees well with DUGDALE's results, particularly when it is considered that the phase-contrast method of detecting the boundary of the deformed area is probably more sensitive than the method used by him.

(b) *Nonstandard Impressions.* The 7%-strain and elastic-plastic boundaries only were determined for the nonstandard ball impressions, the results being plotted in Fig. 2. These boundaries are similar to those for the standard impression, but proportionately extend to greater depths with increasing indenting load ; this is consistent with the change in the effective form of the indenter.

4. SPECIMENS OF FINITE THICKNESS

A specimen 3·280 mm in thickness was prepared as previously with both top

and bottom surfaces metallographically polished. Pyramidal impressions were made on one surface with progressively increasing loads, the specimen resting on a sheet of plate glass. The bottom surface was then inspected microscopically under phase-contrast illumination and the indenting conditions determined which just resulted in the development of slip lines on this surface underneath the impression. It may be assumed that the elastic-plastic boundary then just intersects the bottom surface, i.e. the specimen is of critical thickness (T_c). The conditions for $T_c = 3{\cdot}280$ mm were $P = 42{\cdot}5$ kg, $d_p = 1{\cdot}302$ mm, $T_c/d_p = 2{\cdot}5$ (or $T_c \simeq 17{\cdot}5$ times the depth of the impression).

The elastic-plastic boundary under the critical conditions was determined by the transverse sectioning technique, the result being given in Fig. 3 and compared with the corresponding boundary for an impression in a semi-infinite specimen. Bringing the bottom surface of the specimen close to the impression has caused the elastic-plastic boundary to extend considerably in depth but little laterally; this is as Hill (1950a) supposed.

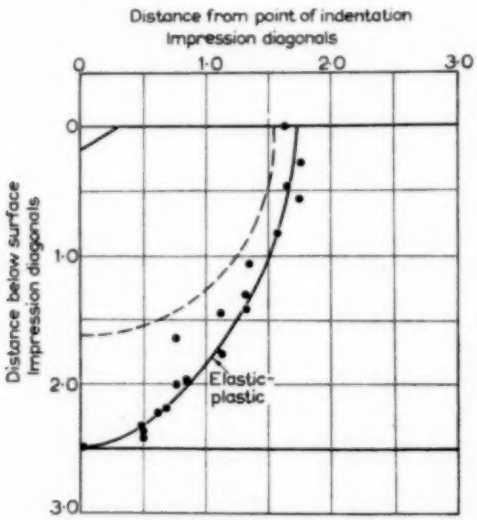

Fig. 3. Elastic-plastic boundary for pyramidal impression in a specimen of critical thickness. The broken line is the corresponding boundary for a specimen of semi-infinite thickness.

5. Impressions Close to Edge of Specimen

A rectangular specimen 1·25 cm in thickness was prepared with the top and one side face metallographically polished. Pyramidal impressions with the side of the impression parallel to the edge were then made in the top surface at progressively decreasing distances from the prepared side face. The side face was examined microscopically under phase-contrast illumination and the indenting conditions determined which just resulted in the development of slip lines in this surface adjacent to the impression. It may be assumed that the elastic-plastic boundary then just intersects the side face. An indenting load of 20 kg was used in this experiment, giving an impression with $d_p = 0{\cdot}897$ mm; the critical spacing impression centre to edge was then 1·570 mm, or $1{\cdot}75\, d_p$.

The elastic-plastic boundary for the critical impression was determined by examining successive levels parallel to the side face. The result is given in Fig. 4, and compared with the corresponding boundary for a semi-infinite specimen. The theoretical model developed by HILL (1950a) suggests that the elastic-plastic boundary in a specimen of this type might emerge at the side face at a point beneath the indented surface. Some evidence of this was found in the present work, but this evidence was not conclusive. It was observed that the slip lines developed at the side face with an impression at the critical spacing were more marked and more numerous in a zone somewhat beneath the top edge, although in all instances a few slip lines were present right up to the edge. The slip-line indications developed in the first level examined beneath the side face extended completely up to the indented surface. It can only be said, therefore, that the existence of a purely elastically deformed region at the corner of the specimen is possible within the limits indicated by the heavy broken line in Fig. 4.

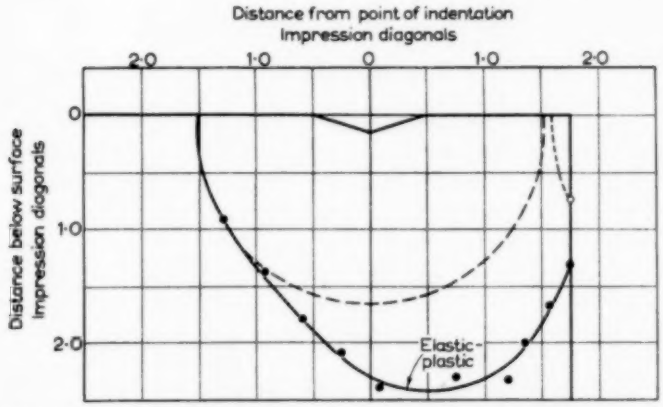

Fig. 4. Elastic-plastic boundary for pyramidal impression made at the critical edge spacing. The fine broken line is the corresponding boundary for a semi-infinite specimen.

The significant feature of this strain boundary, however, is that, as for the impression made in a specimen of finite thickness, the boundary has extended considerably in depth but only a small amount laterally. Moreover, the boundary extended in depth to about $2{\cdot}5\,d_p$, the same value as for the impression in the specimen of finite thickness (Section 4). This implies that the restraint normal to the indented surface is removed on one side of the impression almost as effectively when a side face is brought close as when the bottom face is brought close. The form of the boundary also suggests that the case of an impression in a specimen of critical width may not be exactly equivalent to the one considered above. Because of experimental difficulties, however, this point was not investigated.

6. Discussion of Results

Before the present results can be compared with the theoretical models it is necessary to consider the relationship between the boundaries described in the

two cases. The theoretical treatments are concerned with a boundary between material which has plastically deformed and material which has remained rigid. This boundary does not enclose the full plastic region, since there is a further zone in which the material is stressed to the yield point but remains rigid because it is prevented from deforming by the constraint of the non-plastic matrix (Hill 1949 and 1950b). This additional zone, which usually is not calculated in a theoretical treatment, corresponds in an actual material to a zone in which the plastic and elastic parts of the strain are of comparable magnitude. None of the boundaries determined in a material of the type investigated can correspond exactly to the boundary of the theoretical models. However, although there may be some doubts in the case of the elastic-plastic boundary where the elastic and plastic parts of the strain could be of comparable magnitude, there can be no doubt that the 1%-strain boundary determined in the present experiments encloses a deforming zone. It is at least reasonable, therefore, to compare the form of this and the experimental 7%-strain boundary with the boundary of the plastically-deformed zone of the theoretical models. When this comparison is made, it is apparent that there is quite a fundamental difference between the boundaries derived by the two methods.

For example, for a pyramidal impression in a semi-infinite specimen, it is basic to the theoretical treatment that the boundary passes through the tip of the impression, and it is suggested that in a real material the boundary might extend only slightly beneath the tip (Hill, Lee and Tupper 1947). A mechanism which might be described as a cutting type is supposed in which material is considered to be displaced sideways and upwards from the face of the wedge. The tendency is unmistakable, however, for the boundaries determined in the present experiments to extend as far, if not further, beneath the tip of the impression as they do laterally. The suggestion is that the forces immediately under the impression are largely compressive and that material is displaced to the surface around approximately hemispherical shells. In this event, the surface probably must be imagined to fold down about the edge of the impression during indentation, and this might be described roughly as a compression mechanism of indentation. It may be noted that the close similarity between the boundaries determined for pyramid and ball indenters, the changes in the form of the boundaries for ball impressions with increasing depth of indentation, and the form of the elastic-plastic boundary for pyramid impressions made close to the edge of the specimen all tend to support the mechanism suggested.

This difference in indenting mechanisms conceivably could be attributable to any one or all of at least three factors, namely :

(a) the considerable difference between the deformation characteristics of the material investigated and the theoretical plastic-rigid material ;

(b) a difference in indenting mechanism with change in wedge angle, the extreme cases being an acute-angled wedge which cuts and an almost flat punch which compresses with the change-over occurring at an angle less than 136° ; and

(c) a difference in indenting mechanism between a two-dimensional wedge and a three-dimensional pyramid.

It has been suggested by HILL (1950b, pp. 258-9) that the first factor may be of considerable importance in this regard, and the experiments of DUGDALE (1954) indicate that the second may also be of significance. However, these points obviously require further experimental investigation.

As for the practical application of the results, the following limits to indenting conditions for a diamond pyramid hardness test are indicated :

Minimum Impression Spacing, centre to edge of adjoining impression :	$2{\cdot}7\ d_p$
Minimum Spacing, centre of impression to edge of specimen :	$1{\cdot}8\ d_p$
Minimum Specimen Thickness :	$2{\cdot}5\ d_p$

These values represent, however, only the extreme theoretical limits to the factors concerned, and it is likely that considerably lower values would be satisfactory in practice. For example, it is probable that a detectable error would be introduced as a result of the close spacing of impressions only when the deformed zones in which significant work hardening has occurred overlap. In the material investigated, this zone would be inside the 1%-strain boundary. Moreover, the factors apply only to the particular material investigated. The extent of the elastic-plastic boundary, and hence the theoretical spacing factors, is likely to depend upon the yield point of the specimen material, as evidenced by the considerable reduction found in the present experiments in the extent of the surface deformed area after cold working the brass. The practical factors presumably will also depend upon the work-hardening characteristics of the material. For these reasons, it is not possible to compare the above factors with those determined experimentally by DUGDALE (1953, 1954, 1955).

It is likely, however, that the practical factors would always preserve the same relative proportions as those listed above. It is at present standard practice in hardness testing to use the one set of factors for all materials ; for diamond pyramid hardness testing, these factors are : $2{\cdot}5\ d_p$, $2{\cdot}5\ d_p$ and $1{\cdot}5\ d_p$, respectively, in the order given above. It would seem that the justification of these factors warrants critical investigation, and this is in hand.

ACKNOWLEDGMENTS

This paper is published with the permission of the Chief Scientist, Department of Supply, Australia. The helpful criticisms received from Dr. D. TABOR and Professor R. HILL are gratefully acknowledged.

REFERENCES

DUGDALE, D. S.	1953	*J. Mech. Phys. Solids* **2**, 14.
	1954	*J. Mech. Phys. Solids* **2**, 265.
	1955	*J. Mech. Phys. Solids* **3**, 197.
GREEN, A. P. and HUNDY, B. B.	1956	*J. Mech. Phys. Solids* **1**, 172.
HILL, R.	1949	*Qu. J. Appl. Math.* **2**, 40.
	1950a	*Phil. Mag.* **41**, 745.
	1950b	*The Mathematical Theory of Plasticity* (Clarendon Press, Oxford).

HILL, R., LEE, E. H. and TUPPER, S. J.	1947	*Proc. Roy. Soc.* A **188**, 273.
JACQUET, P. A.	1949	*Compt. rend.* **228**, 1027.
	1954	*Acta Met.* **2**, 752.
SAMUELS, L. E.	1952	*J. Inst. Metals* **81**, 471.
	1954	*J. Inst. Metals* **83**, 359.
	1956	*J. Inst. Metals* **85**, 51.
SAMUELS, L. E. and HATHERLY, M.	1955	*J. Inst. Metals* **84**, 84.
TABOR, D.	1951	*The Hardness of Metals* (Clarendon Press, Oxford).
WILLIAMS, G. H. and O'NEILL, H.	1956	*J. Iron Steel Inst.* **182**, 266.

Journal of the Mechanics and Physics of Solids, 1957, Vol. 5, pp. 135 to 142. Pergamon Press Ltd., London.

ELASTIC-PLASTIC BENDING OF A BUILT-IN CIRCULAR PLATE UNDER A UNIFORMLY DISTRIBUTED LOAD*

By Bekir Tekinalp
Brown University, Providence, Rhode Island

(*Received 2nd August*, 1956)

Summary

The paper contains an analysis of the bending moments and deflections of a uniformly loaded and built-in circular plate that is made of an incompressible elastic-plastic material obeying Tresca's yield condition and the associated flow rule. The analysis is simplified by assuming that any plate element is either entirely elastic or entirely plastic. This assumption is practically fulfilled for a sandwich plate : for a solid plate it represents a first approximation to the actual diagram of bending moment *versus* curvature.

1. Introduction

The serious theoretical objections that can be raised against all stress-strain laws of the total strain type† are now generally recognized. All the same, these laws are still widely used for reasons of mathematical expediency because the physically sound laws of the incremental strain type usually lead to more difficult mathematical problems than the physically unsound laws of the finite strain type.

Koiter (1953) and Prager (1953) remarked that the incremental laws become mathematically more tractable when piecewise linear yield conditions and the associated flow rules are used. Since then numerous problems concerning non-hardening rigid-plastic and work-hardening rigid-plastic plates and shells have been treated in this manner (see, for instance, Hopkins and Prager 1953, 1954, 1955 ; Prager 1955a, b, 1956 ; Boyce 1956 ; for plates : and Drucker 1958 ; Hodge 1954 ; Onat 1954 ; Onat and Prager 1954, 1955 ; and Freiberger 1956 ; for shells).

The present paper is concerned with the bending moments and deflections of a uniformly loaded, built-in, circular plate that is made of an incompressible non-hardening elastic-plastic material. The corresponding problem for a simply supported plate has been treated in an earlier paper (Tekinalp 1956). Following Haythornthwaite (1955), the analysis is simplified by assuming that any plate element is either entirely elastic or entirely plastic. This assumption is practically fulfilled for a sandwich plate. For a solid plate the adoption of this simplifying

* The results presented in this paper were obtained in the course of research sponsored at Brown University by the Ballistics Research Laboratories of Aberdeen Proving Ground (Contract DA-19-020-ORD-708).

† The author would like to use this opportunity of drawing attention to the terminology recently introduced by Finzi (1935) who uses the terms " holonomic " and " nonholonomic " to refer to total and incremental laws, in obvious analogy to the use of these terms in dynamics.

assumption means that the actual diagram of bending moment *versus* curvature is approximated by two straight lines corresponding to the fully elastic and fully plastic states.

2. NOTATIONS AND FUNDAMENTAL EQUATIONS

Using the polar co-ordinates r and ϕ in the middle plane of the plate, we denote the radial and circumferential bending moments and curvatures by M_r, M_ϕ and κ_r, κ_ϕ, respectively. On account of the assumed incompressibility of the plate material, the curvature-bending-moment relations in the elastic range are

$$\tfrac{1}{6} Eh^3 \kappa_r = 2M_r - M_\phi, \qquad \tfrac{1}{6} Eh^3 \kappa_\phi = 2M_\phi - M_r, \tag{1}$$

where E denotes Young's modulus and h the plate thickness. These relations are valid below the yield limit.

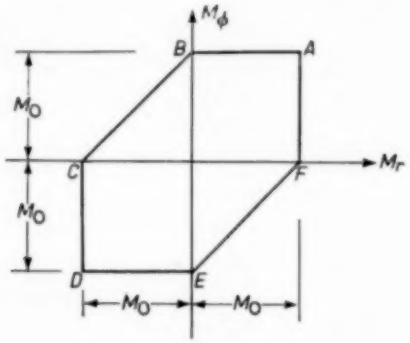

Fig. 1.

Under the assumptions stated in Section 1, the hexagonal yield locus shown in Fig. 1 indicates the yield limit for a generic plate element : any combination of bending moments M_r, M_ϕ represented by a " stress point " inside this hexagon stresses the plate element in a purely elastic manner, and only combinations represented by stress points on the hexagon can produce plastic flow. When plastic flow takes place under constant bending moments the increments of curvature $d\kappa_r$, $d\kappa_\phi$ occurring during this flow are purely plastic and obey the flow rule associated with the hexagonal yield locus of Fig. 1 (see, for instance, KOITER 1953 ; or PRAGER 1953). If the constant state of stress is represented by a point on the side AB of this yield locus,

$$d\kappa_r = 0, \qquad d\kappa_\phi > 0. \tag{2}$$

Similarly, if the constant state is represented by a point on the side BC,

$$d\kappa_\phi + d\kappa_r = 0, \qquad d\kappa_\phi - d\kappa_r > 0. \tag{3}$$

When the stress point moves along the yield locus during the plastic flow, the elastic response obtained by differentiating (1) must be added to the plastic response. For example, if the stress point moves along the side AB, the total increments of curvature satisfy

$$\tfrac{1}{6} Eh^3 \, d\kappa_r = 2dM_r, \qquad \tfrac{1}{6} Eh^3 \, d\kappa_\phi > - dM_r, \tag{4}$$

since $dM_\phi = 0$ when the stress point moves along AB. If, on the other hand, the stress point moves along the side BC, the total increments of curvature satisfy

$$\tfrac{1}{6} Eh^3 (d\kappa_\phi + d\kappa_r) = 2dM_r, \qquad \tfrac{1}{6} Eh^3 (d\kappa_\phi - d\kappa_r) > 0, \tag{5}$$

since $dM_r - dM_\phi = 0$ when the stress point moves along BC.

If the plate element has been stressed in a purely elastic manner until the stress point reaches the side AB, and if thereafter the stress point has never left this side, the first (4) can be integrated to furnish

$$\tfrac{1}{6} Eh^3 \kappa_r = 2M_r - M_0, \tag{6}$$

where the constant of integration has been chosen to provide a continuous variation of κ_r and κ_ϕ as the element passes from the elastic to the plastic state. Similarly, if the stress point has first reached the yield locus on BC and has since then stayed on this side, the first of (5) can be integrated to yield

$$\tfrac{1}{6} Eh^3 (\kappa_\phi + \kappa_r) = 2M_r + M_0. \tag{7}$$

The equations considered so far described the behaviour of the plate element; they must be supplemented by the equation of equilibrium,

$$(rM_r)' = M_\phi - \int_0^r prdr, \tag{8}$$

and the equation of compatibility,

$$\kappa_r - (r\kappa_\phi)' = 0, \tag{9}$$

where the prime denotes differentiation with respect to r, and $p = p(r)$ is the intensity of the distributed load. Equation (9) is obtained by eliminating the deflection w between the definitions of the curvatures:

$$\kappa_r = - w'', \qquad \kappa_\phi = - w'/r. \tag{10}$$

3. Built-in Circular Plate under Uniformly Distributed Load

Consider a built-in circular plate of the radius R under a uniformly distributed load of gradually increasing intensity p.

In the elastic range, expressions for the bending moments can be found by substituting the curvatures (1) into the equation of compatibility (9) and integrating the system consisting of the equation obtained in this manner and the equation of equilibrium (8). One finds

$$M_r = - \tfrac{7}{32} pr^2 + \frac{c_1}{r^2} + c_2, \qquad M_\phi = - \tfrac{5}{32} pr^2 - \frac{c_1}{r^2} + c_2, \tag{11}$$

where c_1 and c_2 are constants of integration. To determine these constants, we have boundary conditions, $M_r(0) - M_\phi(0) = 0$ and $w'(R) = 0$, where κ_ϕ must be evaluated by substituting the expressions (11) into the second of (1). One obtains

$$M_r = \frac{pR^2}{32}\left(3 - 7\,\frac{r^2}{R^2}\right), \qquad M_\phi = \frac{pR^2}{32}\left(3 - 5\,\frac{r^2}{R^2}\right). \tag{12}$$

Elimination of r between these two equations yields

$$7M_\phi - 5M_r = \tfrac{3}{16}\, pR^2. \tag{13}$$

Equation (13) shows that the stress points for a fixed value of the load intensity p and various values of the radius r form a straight segment such as PQ in Fig. 2. As p increases, starting from zero, the points P and Q, which correspond to $r = R$ and $r = 0$, respectively, move along the lines $0P_1$ and $0A$. The parametric equations of these lines are obtained by setting $r = R$ or $r = 0$ in (12).

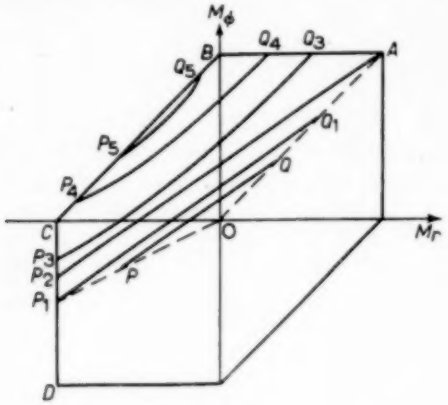

Fig. 2.

Following HODGE (1954), the segment PQ will be called the "stress profile" for the considered load intensity. In the elastic range, the stress profiles for various load intensities are parallel to each other. It is seen from Fig. 2 that the point P reaches the yield locus at P_1, while the corresponding point Q_1 is still inside the yield locus. This means that plastic deformation sets in at the built-in edge, while the plate centre is still elastic. The load intensity p_1 which marks the end of the elastic range is found by setting $M_r = -M_0$ in the first of (12):

$$p_1 = 8M_0/R^2. \tag{14}$$

As the load intensity increases beyond the value p_1, the plastic regime CD might spread from the edge into the interior of the plate. It is readily seen, however, that such an annulus in the regime CD is not possible. Indeed, with $M_r = -M_0$ and $p > p_1$, the equation of equilibrium (8) would require that the circumferential bending moment at the plate edge exceed $3M_0$ in violation of the yield condition. We conclude from this that only the plate edge enters regime CD, whereas adjacent plate elements remain elastic as the load intensity p_1 is reached and exceeded. As a consequence of this localized yielding along the plate edge, the slope w' ceases to vanish at $r = R$, and the boundary condition w' ceases to vanish at $r = R$, and the boundary condition $w'(R) = 0$ is replaced by $M_r(R) = -M_0$. With the boundary conditions $M_r(0) = M_\phi(0)$ and $M_r(R) = -M_0$, the elastic analysis of the plate furnishes

$$M_r = -M_0 + \frac{7pR^2}{32}\left(1 - \frac{r^2}{R^2}\right), \qquad M_\phi = -M_0 + \frac{pR^2}{32}\left(7 - 5\,\frac{r^2}{R^2}\right). \tag{15}$$

Elimination of r between these equations shows that the stress profile continues to be a straight-line segment with the slope $M_\phi/M_r = 5/7$. While the left endpoint of this segment, which corresponds to $r = R$, now moves along DC, the right endpoint, which corresponds to $r = 0$, continues to move along OA. The last stress profile of this type is $P_2 A$. The corresponding load intensity p_2 is found by setting $M_\phi(0) = M_0$ in the second of (15) and solving for the load intensity. Thus,

$$p_2 = \frac{64 M_0}{7R^2}. \tag{16}$$

As the load intensity continues to increase, the stress profile will assume some such shape as $P_3 Q_3 A$ in Fig. 2, the segment AQ_2 corresponding to a central plastic region, say $0 < r < \rho$, and the arc $Q_3 P_3$ to the surrounding elastic annulus $\rho < r < R$. In the central plastic region, the bending moment M_ϕ has the constant value $M_\phi = M_0$. Substituting this into (8) and integrating under the boundary condition $M_r(0) = M_0$, we obtain

$$M_r = M_0 - \tfrac{1}{6} pr^2, \qquad M_\phi = M_0 \text{ for } 0 \leqslant r \leqslant \rho. \tag{17}$$

For the elastic annulus, equations (11) are valid, but for the determination of the constants of integration we now have the conditions that M_r must have the value $-M_0$ at $r = R$, and M_r and M_ϕ be continuous at $r = \rho$. These three conditions yield

$$c_1 = \frac{-10 M_0 \rho^4/R^2}{16 + 5(1 - \rho^2/R^2)^2}, \tag{18}$$

$$c_2 = M_0 \left(1 + \frac{20\,\rho^2/R^2}{16 + 5(1 - \rho^2/R^2)^2}\right), \tag{19}$$

$$p = \frac{192 M_0/R^2}{16 + 5(1 - \rho^2/R^2)^2}. \tag{20}$$

This analysis remains valid until the left endpoint of the stress profile reaches the corner C of the yield hexagon in Fig. 2, at which time $M_\phi(R) = 0$. This condition yields the equation

$$\left(\frac{\rho}{R}\right)^4 + \tfrac{2}{3}\left(\frac{\rho}{R}\right)^2 - \tfrac{2}{3} = 0, \tag{21}$$

the relevant root of which is $\rho = 0{\cdot}7141R$. According to (20), the corresponding load intensity is

$$p_3 = 11{\cdot}16\, M_0/R^2. \tag{22}$$

This value is already very close to the load-carrying capacity of the plate, which HOPKINS and PRAGER (1953) found to be $p^* = 11{\cdot}26\, M_0/R^2$. Accordingly, the continuation of the analysis is hardly necessary for practical purposes ; it is sketched, however, to indicate the manner in which the elastic-plastic plate approaches the limiting state furnished by the simpler rigid-plastic analysis.

As the load intensity increases beyond the value (22), an annulus in the plastic regime BC will form along the edge. As regards the edge, itself, it might stay in regime C or move into regime BC. Assuming at first that the stress point for the edge moves along CB from C towards B, we have $dM_r > 0$. Relations (5) then

show that $d\kappa_\phi > 0$ and hence $dw' < 0$ by the second of (10). The yield hinge at the edge thus would continue to operate, but this requires the stress point for the edge to stay at C, contrary to our assumption. The stress profile immediately after the load (22) is exceeded must therefore have some such shape as CP_4Q_4A in Fig. 2.

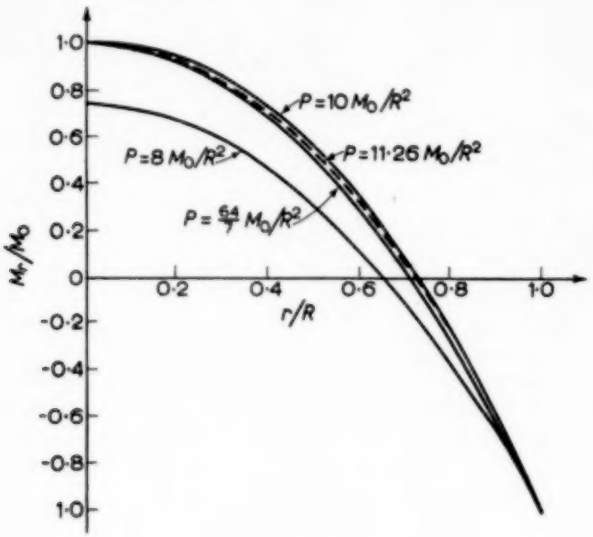

Fig. 3.

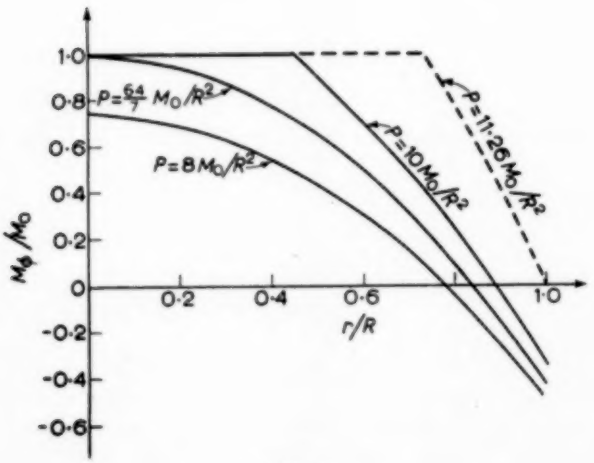

Fig. 4.

We now have three regions : a central plastic region $0 < r < \rho$ in regime AB, an elastic annulus $\rho < r < \sigma$, and a plastic annulus $\sigma < r < R$ in regime BC, the plastic edge $r = R$ being in regime C. Equations (17) are valid in the central region, and the bending moments in the elastic annulus have the form (11), where the constants of integration remain to be determined. Expressions for the bending

moments in the plastic annulus can be obtained by substituting the yield condition $M_\phi - M_r = M_0$ (i.e. the equation of the side BC of the yield hexagon) into the equilibrium condition (8) and integrating. One finds

$$\left.\begin{aligned} M_r &= M_0 \log r - \frac{pr^2}{4} + c_3, \\ M_\phi &= M_0 \left(1 + \log \frac{r}{R}\right) - \frac{pr^2}{4} + c_3 \end{aligned}\right\} \quad \text{for } \sigma \leqslant r \leqslant R, \tag{23}$$

where c_3 is a constant of integration.

The boundary condition $M_r(R) = -M_0$ and the conditions of continuity for M_r and M_ϕ at $r = \rho$ and $r = \sigma$ furnish five equations for c_1, c_2, c_3, ρ, and σ. We omit details and mention only that the point Q_4 of the stress profile reaches the corner B of the yield hexagon when $\rho = 0{\cdot}725R$ and $\sigma = 0{\cdot}942R$. The corresponding load intensity is found to be

$$p_4 = 11{\cdot}24\, M_0/R^2. \tag{24}$$

When the load intensity exceeds this value, the stress profile has some such shape as $CP_5 Q_5 BA$ in Fig. 2. The bending moments can again be determined by using (11), (17), and (23), the boundary condition $M_r(R) = -M_0$ and the conditions of continuity for the bending moments at the interfaces between the various regimes. We again omit all details and mention only that the elastic annulus disappears when $\rho = 0{\cdot}730R$. The corresponding load intensity is the load-carrying capacity

$$p^* = 11{\cdot}26\, M_0/R^2, \tag{25}$$

which Hopkins and Prager (1953) found by a rigid-plastic analysis.

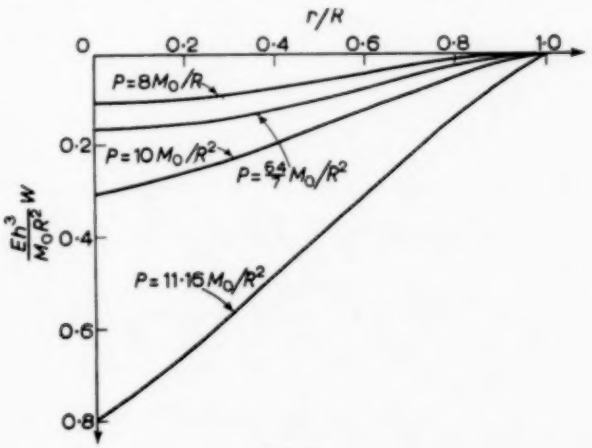

Fig. 5.

Fig. 3 and 4 show the development of the bending-moment distributions with increasing load intensity. After the bending moments and the interfaces between the various regimes have been determined for a given load, the deflections w can be found as follows. The second of (1) is used in the elastic regime, and (6) and

(7) in the plastic regimes AB and BC. The bending moments appearing on the right-hand sides of these equations have already been determined as functions of r; after the expressions (10) have been substituted into the left-hand sides, the equations are integrated under the conditions that w and w' must be continuous at the regime interfaces and w must vanish at the edge. This procedure is valid only as long as no plate element passes from one plastic regime into another, i.e. up to the load intensity (22). Fig. 5 shows the development of the deflections up to this load intensity. Note that the slope w' vanishes at $r = R$ only for $p \leqslant p_1$ and at $r = 0$ only for $p \leqslant p_2$. The last deflected shape that can be found by this method ($p = p_3$) is already very close to the conical shape furnished by the rigid-plastic analysis. Fig. 6 shows the variation of the load intensity with the central deflection $w(0)$.

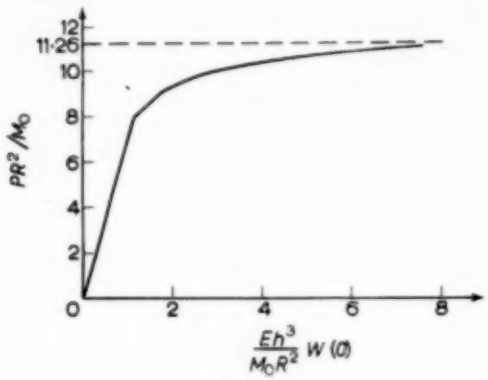

Fig. 6.

REFERENCES

BOYCE, W. E.	1956	To appear in *Q. Appl. Math.*
DRUCKER, D. C.	1953	Proc. Midwestern Conf. *Solid Mech.* (Urbana, Ill.), 158.
FINZI, L.	1955	*Rend. Acc. Lincei* **18**, 274.
FREIBERGER, W.	1956	To appear in *J. Appl. Mech.*
HAYTHORNTHWAITE, R. M.	1955	Proc. U.S. Nat. Congress *Appl. Mech.* 521 (ASME, New York, N.Y.).
HODGE, Jr., P. G.	1954	*J. Appl. Mech.* **21**, 336.
HOPKINS, H. G., and PRAGER, W.	1953	*J. Mech. Phys. Solids* **2**, 1.
	1954	*Z. ang. Math. Phys.* **5**, 317.
	1955	*J. Appl. Mech.* **22**, 372.
KOITER, W. T.	1953	Biezeno Anniversary Volume (H. Stam, Haarlem), 232.
ONAT, E. T.	1954	*Q. Appl. Math.* **13**, 63.
ONAT, E. T., and PRAGER, W.	1954	*Proc. Koninkl. Nederl. Ak. Wetens.* (B) **57**, 534.
	1955	*De Ingenieur* **67**, 0-46.
PRAGER, W.	1953	*J. Appl. Mech.* **20**, 317.
	1955a	*Bull. Techn. Suisse Romande.* **81**, 85.
	1955b	*De Ingenieur* **67**, 0.141.
	1956	To appear in *J. Appl. Mech.*
TEKINALP, B.	1956	Brown Univ. Report CH-6.

Journal of the Mechanics and Physics of Solids, 1957, Vol. 5, pp. 143 to 149. Pergamon Press Ltd., London.

ANALYSIS OF ELASTIC AND PLASTIC STRAINS OF A FACE-CENTRED CUBIC CRYSTAL*

By T. H. Lin
Department of Engineering, University of California

(*Received 22nd October*, 1956)

Summary

A method of analysis of both the elastic and plastic strains in a face-centred cubic crystal under a given path of strain is shown. The consideration of elastic strain shows the effect of the curve of critical shear stress vs. the sum of slips in the crystal, on the activation of the five active slip systems under a uniaxial strain. This method gives the sequence of active slip systems in the process of loading. This enables the calculation of the transition from one set of active slip systems to another for a crystal deformed under varying ratios of principal strains. The slip systems on active planes, on which sliding is taking place, are taken to harden little less than those on the other crystal planes. This differential hardening and the sequence of active slip systems serve to reduce the number of possible combinations of five active slip systems, so the rotation and the orientation of a crystal under deformation can be more closely determined.

1. Introduction

Single crystal tests have shown that under high stress, slips occur along certain crystallographic directions on crystal planes. For face-centred cubic crystals, there are four crystal planes and three slip directions at sixty degrees apart on each plane, so there are twelve slip systems. From single crystal tests, it has been found by Taylor and Elam (1923) that single slip depends on the resolved shear stress (the shear stress along the direction of slip on the crystal plane) and is independent of the normal pressure on the plane. The resolved shear stress to cause further slip is called the critical shear stress. Duplex slip in single crystal tests shows that the resolved shear stresses of the two active slip systems are equal and depend on the sum of the two slips in about the same way that the resolved shear stress depends on the amount of slip in single slipping as obtained from single crystal tests. This dependency of the resolved shear stress on the sum of slips does not differentiate one slip system from the other. Therefore the resolved shear stresses on the active slip systems in simultaneous multiple slipping is taken to be the same and the critical shear stress depends on the sum of slips in the crystal as in the case of duplex slip.

It is known that metals undergo considerable deformation without cracks, so that the crystals originally in contact remain so during deformation. An aggregate of crystals of all possible orientations can be deformed without gaps occurring at

*This research was supported by the United States Air Force through the Office of Scientific Research of the Air Research and Development Command, under the contract No. AF-18-600-1466 between OSR and the University of Detroit.

the grain boundaries, in an infinite number of ways. This actually takes place, however, in such a manner that it corresponds to minimum work, consistent with the given small strain of the aggregate. Any other combination of slips, which satisfies the condition of no cavity at the boundaries of the crystals, must involve a greater amount of work. The case, that the strains of all the individual crystals are homogeneous and are the same as that of the aggregate, has been worked out by Taylor (1938a, b). It gives the upper limit for the yield stress for the aggregate. This is shown in Taylor's noteworthy paper on " Plastic Distortion of Metals " (1938a). This upper limit has been shown to be very close to the empirical values. The error involved in the assumption of the same strain on all crystals seems to be small in the calculation of stress-strain curve of the aggregate. This assumption has been used by Taylor (1398a) and by Bishop and Hill (1951a, b), in the calculation of both the stress-strain curve and the texture (the distribution of preferred orientations of crystals) of the aggregate under a given strain. Bishop (1955) has shown this assumption is a good first approximation in those calculations. Hence the analysis of strain in a single crystal under an assigned macroscopic strain is rather important to the calculation of stress-strain curve and textures of polycrystalline aggregates.

2. Plastic Strains Produced by Five Systems of Slips

A given strain can be defined by six components. With the condition of no change of volume, the six components reduce to five independent components. For this strain to be produced by slips alone, five slip systems are required. There are twelve slip systems in a face-centred cubic crystal. For determining which five out of the twelve are operative, Taylor (1938a, b) has applied the principle of virtual work. The given strain in the crystal is produced by those five slip systems, which give the minimum sum of slips in the crystal. In order to determine these five active slip systems, different combinations of five out of twelve have to be calculated and then the one with the least sum of slips is taken to be the actual one taking place. This involves very lengthy calculations. At the same time, one objection has been raised by Bishop and Hill (1951a) that it is not proved that a combined stress could always be found to operate any geometrically possible set of shears without exceeding the critical shear stress in nonactive slip systems. To eliminate this objection, and to shorten the calculations, Bishop and Hill introduced the principle of maximum work. This principle states that, if a crystal is caused to deform plastically by an increment of strain de_{ij}, the work done by the required stress σ_{ij} is not less than that done by any other stress σ_{ij}^* not violating the yield condition, i.e., no system of slip has resolved shear stress greater than the critical shear stress. The actual σ_{ij} is the one giving maximum work for the de_{ij} and at the same time not violating the yield condition. By comparing the works done by different σ_{ij}'s, the actual σ_{ij} is determined. The elastic modulus is assumed to be infinitely large, so that the crystal remains rigid under increasing load until the resolved shear stresses in five slip systems have reached the critical value for sliding. Both Taylor's method and the method given by Bishop and Hill neglect elastic strains and do not give the sequence of the five active slip systems.

The elastic modulus in actual crystals is finite. Elastic strain is always present under loading. With uniform loading of an aggregate under increasing loads, all the crystals are taken to be stressed and strained equally and elastically until one crystal is stressed to the critical shear stress in one of its slip systems. The elastic modulus of individual crystals is assumed to be isotropic and of the same value as that of the aggregate.

3. Active Slip Systems Determined by Elastic Strains

Let us consider a simple crystal under uniaxial strain. As the imposed strain increases, the resolved shear strains in all slip systems in the crystal increase. The presence of elastic strain permits plastic slip in the slip system with highest resolved shear stress to take place as soon as the critical shear stress is reached in that system. Let this system first to slide be called system A. Due to work hardening, the critical shear stress in the different systems in the crystal increases with the amount of slip. After system A slides, the elastic strain in the crystal equals the imposed strain on the crystal minus the plastic strain due to slips. The amount of slip in system A is determined by the condition that the elastic resolved shear strain in system A always gives the critical shear stress corresponding to the amount of slip present in the crystal. The imposed strain and this slip in system A determine the elastic resolved shear strains and hence the resolved shear stresses in all the slip systems. Slip in system A proceeds with the increase of imposed strain on the crystal until a second slip system B has the same elastic resolved shear strain as system A. Then both systems A and B slide simultaneously. The incremental slips in A and B with the incremental imposed strain on the crystal are determined by the condition that in the two active slip systems A and B, the resolved elastic shear strains must be equal and follow the relation of strain hardening of the crystal as obtained from duplex slip tests. This process proceeds until the third system C has the same resolved shear stress as either of the systems A and B. In the same way, the fourth and the fifth active slip systems are found. Since there are only five independent components in the deviated strain, these five slip systems are sufficient to give the plastic part of the imposed strain on the crystal. So long as the direction and the ratios of the principal strains imposed on the crystal remain the same as in the case of uniaxial strain, the five slip systems do not change. When either the direction or the ratios of the principal strains or both vary, the condition that the elastic resolved shear strains in the active slip systems must be the same is satisfied either by varying the rates of incremental slips in the five systems or by changing the five slip systems. The former gives no change of the ratios of the deviated stress components but the latter gives different ratios of stress components.

The stress in a crystal can be split into two parts : one is the hydrostatic stress and the other the deviated stress. The deviated stress consists of five independent components which are completely determined by the five equal resolved shear stresses in the five active slip systems. As slips in these five systems increase, the critical shear stress increases for work hardening materials. The ratios of the components of the deviated stress tensor remain constant, while the magnitudes of these components increase proportionally. When the five slip systems change

in the process of loading, the stress tensor changes with the current slip systems and can be calculated. Therefore, from the history of strain imposed on a crystal, the history of the stress in the crystal can be completely determined.

4. Mathematical Formulation of the Theory

Let x_1, x_2, x_3 be the rectangular coordinates with one axis coinciding with the axis of the specimen y_1, y_2, y_3 the rectangular coordinate axes coinciding with the axes of the crystal, and z_{11}, z_{12}, z_{13}; z_{21}, z_{22}, z_{23} . . . . .; z_{n1}, z_{n2}, z_{n3}, the n-sets of rectangular axes of which each set has one axis along the normal of the crystal plane and another axis along one direction of slip on that plane.

Let R_{x-y} be the rotation matrix to convert x-coordinates into y-coordinates and R^*_{x-y}, the transpose of R_{x-y}:

$$x_i = R_{x-y}\, y_i, \qquad y_i = R^*_{x-y}\, x_i.$$

Let E, E', and E'' be the total deviated strain tensor, the elastic part and the plastic part of the deviated strain tensor respectively. Let T be the deviated stress tensor, γ the shear strain, and τ the shear stress.

The total strain is composed of elastic and plastic strains:

$$E = E' + E'', \tag{1}$$

$$T = 2GE', \tag{2}$$

where G is the elastic modulus of rigidity.

A given imposed aggregate strain E_x, in x-coordinates, can be transformed into a strain tensor E_y in y-coordiantes by

$$E_y = R^*_{x-y}\, E_x\, R_{x-y}. \tag{3}$$

Transferring this strain to z-coordinates to give the shear strain in a slip system,

$$E_{z_m} = R^*_{y-z_m}\, E_y\, R_{y-z_m} = R^*_{y-z_m}\, R^*_{x-y}\, E_x\, R_{x-y}\, R_{y-z_m}$$

where E_{z_m} is the strain tensor in z_m coordinates. This gives the shear strain on one slip system due to the imposed aggregate strain tensor E_x.

The twelve slip systems are not independent. The slip in one system releases or increases some shear strains in other systems. For a given slip in one slip system represented by E''_{z_m},

$$E''_y = R^*_{z_m-y}\, E''_{z_m}\, R_{z_m-y}. \tag{5}$$

The shear strain in any other slip system z_j due to this E''_{z_m} will be,

$$E''_{z_j} = R^*_{y-z_j}\, R^*_{z_m-y}\, E''_{z_m}\, R_{z_m-y}\, R_{y-z_j}. \tag{6}$$

If there are p slip systems with slip taken place, the strain tensor in z_j coordinates due to the p slip systems, is

$$E''_{z_j} = \sum_{m=1}^{p} R^*_{y-z_j}\, R^*_{z_m-y}\, E''_{z_m}\, R_{z_m-y}\, R_{y-z_j}, \tag{7}$$

$$\begin{aligned} E'_{z_j} &= E_{z_j} - E''_{z_j} \\ &= R^*_{y-z_j}\, R^*_{x-y}\, E_x\, R_{x-y}\, R_{y-z_j} - \sum_{m=1}^{p} R^*_{y-z_j}\, R^*_{z_m-y}\, E''_{z_m}\, R_{z_m-y}\, R_{y-z_j}. \end{aligned} \tag{8}$$

Equation (8) gives the elastic shear strains in the different slip systems.

Let γ_{ij}, γ'_{ij} and γ''_{ij} be the shear strains, the elastic and the plastic shear strains in the different slip systems of the crystal. Let there be n active slip systems and p slip systems having slips :

$$\gamma'_{(ij)_1} = \gamma'_{(ij)_2} = \gamma'_{(ij)_3} = \ldots\ldots\ldots = \gamma'_{(ij)_n} \tag{9}$$

The critical resolved shear stress along the directions of slip depends on the sum of slips,

$$\tau_{(ij)_1} = \tau_{(ij)_2} = \tau_{(ij)_n} = f\Big[\sum_{p=1}^{p} \big|\gamma''_{(ij)_p}\big|\Big] \tag{10}$$

where f is the functional relation between the critical shear stress and the sum of slips. Considering the incremental elastic shear strains in the active systems,

$$\Delta\tau_{(ij)} = G\Delta\gamma'_{(ij)_1} = f'\Big[\sum_{p=1}^{p} \big|\gamma''_{(ij)_p}\big|\Big] \sum_{p=1}^{p} \big|\Delta\gamma''_{(ij)_p}\big| \tag{11}$$

$$\Delta\gamma'_{(ij)_1} = \Delta\gamma'_{(ij)_2} = \ldots\ldots\ldots = \Delta\gamma'_{(ij)_n} = \frac{1}{G} f'\left[\Sigma\gamma''_{(ij)_p}\right] \Sigma\Delta\gamma''_{(ij)_p} \tag{12}$$

Let the components of the strain tensor E_y be e_{pq}. The total, i.e. the plastic plus the elastic shear strain in any of the slip systems, can be expressed as,

$$\left.\begin{aligned} \gamma_{ij} &= K_{ijpq}\, e_{pq}, \\ \gamma''_{ij} &= K_{ijlm}\, \gamma''_{lm}, \\ \gamma'_{ij} &= K_{ijpq}\, e_{pq} - K_{ijlm}\, \gamma''_{lm}, \end{aligned}\right\} \tag{13}$$

where γ''_{lm} are the slips in the different systems. The repetition of the subscripts denotes summation. K_{ijpq} and K_{ijlm} are constants found from (8).

At start, the plastic slip is zero, so the elastic strain γ'_{ij} is obtained from E_y or e_{pq} alone as shown in (13) until one system, say $\tau_{(ij)_1}$, reaches the critical value τ_0. Then this system starts to slide.

$$\begin{aligned} G\Delta\gamma'_{(ij)_1} &= G\left[K_{(ij)_1\, pq}\, \Delta e_{pq} - \Delta\gamma''_{(ij)_1}\right] \\ &= f'\left[\gamma''_{(ij)_1}\right] \Delta\gamma''_{(ij)_1}. \end{aligned} \tag{14}$$

From this, $\Delta\gamma'_{(ij)_1}$ and $\Delta\gamma''_{(ij)_1}$ can be expressed in terms of Δe_{pq}. From (8), all the incremental elastic shear strains in the twelve slip systems of the crystal can be found. Then the second active slip system can be determined. With slips taken place in more than one systems of slip, (14) becomes

$$\begin{aligned} G\Delta\gamma'_{ij} &= G\left[K_{ij\,pq}\, \Delta e_{pq} - K_{ijlm}\, \gamma''_{lm}\right] \\ &= f'\Big[\sum_{p=1}^{p} \big|\gamma''_{(lm)_p}\big|\Big] \sum_{n=1}^{n} \big|\Delta\gamma''_{(lm)_n}\big|. \end{aligned} \tag{15}$$

Similarly, the third, the fourth and the fifth active slip systems are obtained.

Equation (15) gives the same number of equations as the number of active slip systems, so the incremental slips $\Delta\gamma''_{lm}$'s can be solved in terms of Δe_{pq}. These $\Delta\gamma''_{lm}$'s determine the incremental elastic shear strains $\Delta\gamma'_{ij}$ in all slip systems and hence determine the subsequent active slip systems and the corresponding

deviated stress tensor. It is seen from (15) that the incremental slips in the active slip systems $\Delta\gamma''_{lm}$'s depend not only on the orientation of the crystal, but also on $f'\left[\sum_{1}^{p}\gamma''_{(lm)_p}\right]$, the slope of the curve of critical shear stress vs. sum of slips.

After five independent active slip systems have been activated, the critical shear stresses in these five systems remain equal, but increase in magnitude with the sum of slips. The components of the elastic deviated strains tensor and the deviated stress tensor increase proportionally and the ratios of the elastic shear strains in the different slip systems remain the same. Therefore, the portion of the curve from the start of slip to the start of the fifth slip system determines the final ratios of the components of the deviated stress tensor and the corresponding sets of five active slip systems. Hence this deviated stress tensor, giving five independent active slip systems in a crystal under a given strain, depends not only on the orentation of the crystal, the initial critical shear stress to start slip, the elastic modulus G, but also on the slope of the curve of the critical shear stress vs. the sum of slips. For different metals, this initial critical shear stress vs. sum of slips may vary and hence may give different sets of active slip systems with different deviated stress tensors and different rotations of crystal axes. Therefore, different metals of the same lattice structure (such as face-centred cubic) give different textures under the same strain, as observed in experiments. BISHOP (1955) has proposed that the different textures observed under similar straining conditions by metals of the same lattice type are due to the relative hardening of active and latent glide systems. With the consideration of elastic strain, it seems that other factors, as discussed, may also be the causes of these different textures.

At any stage of loading, the deviated stress, the deviated elastic strain and the plastic strain tensors are uniquely determined. However, when there are more than five active slip systems having attained critical shear stress, the possible combinations of five slip systems satisfying the stress and strain tensor may be many. Generally either six or eight slip systems in the crystal will attain critical shear stress and there are a number of possible combinations of five out of these six or eight systems. The stress tensor specifies the critical shear stress in the slip systems in a specific sense. The slip must be either non-negative or non-positive according to whether the critical shear stress is in a positive or negative sense. This condition greatly reduces the number of possible combinations. However, the remaining ones may still be quite a few. Each combination gives a different rotation of the crystal under a given strain. These multiple combinations give a range of rotations as calculated by BISHOP (1955).

When a single crystal specimen is distorted by sliding parallel to a given crystal plane along a given crystal axis, the longitudinal axis of the specimen moves relatively to the crystal axis towards the direction of slip. When the specimen axis reaches the position making equal angles with two slip planes, the resolved shear stresses on two slips systems, one on each plane, are equal. From single crystal tests by TAYLOR and ELAM (1925) it has been noticed that the specimen axis has a tendency to move beyond the position of giving equal stresses on the two planes, to cause the resolved shear stress in the new slip plane to be little larger than that in the original slip plane at the start of duplex slip. Therefore, in multi-plane slip, the critical shear stress on the planes slipped previously is

taken to be little less than that on the planes, which have not slid before. This serves to differentiate the systems on active planes from those on the latent planes to become active slip systems. By this consideration, the possible combinations of five active slip systems are further reduced. For example, suppose at certain stages of loading, four active slip systems are present in the crystal and these four systems are distributed as one on two planes (A and B) and two on third plane C. At a later stage of loading, another four systems attain critical stress simultaneously, and any one of them combining with the first four systems satisfies the stress tensor and the given strain. Suppose the last four systems are taken to be distributed with one on plane A, one on plane B, and the remaining two on plane D (the plane has not slid before). Either of the former two systems together with the first four gives a possible set of five active slip systems, but either of the two systems on plane D together with the first four systems is ruled out as a possible combination. By this consideration, the range of possible orientations of a crystal, subject to a given macroscopic strain, will be reduced. Hence, the deformation textures developed by assuming that each crystal undergoes the same strain can be calculated more closely.

Elastic strain plays an important role in the initiation of slip systems. It seems that it is necessary to consider the elastic strain in the study of the inelastic behaviour occurring from the start of slip in one of the crystals to the completion of five active slip systems in all the individual crystals.

Acknowledgment

The author wishes to express his thanks to Sir G. I. Taylor for his kind comments and suggestions.

References

Bishop, J. F. W. 1955 *J. Mech. Phys. Solids* **3**, 143.
Bishop, J. F. W. and Hill, R. 1951 *Phil. Mag.* **42** (a) 414 and (b) 1298.
Taylor, G. I. 1925 *Proc. Roy. Soc.* **A 108**, 643.
1938a *J. Inst. Metals* **62**, 307.
1938b *S. Timoshenko Anniversary Volume*, p. 218 (Macmillan).
Taylor, G. I. and Elam, C. F. 1925 *Proc. Roy. Soc.* **A 108**, 28.

Journal of the Mechanics and Physics of Solids, 1957, Vol. 5, pp. 150 and 151. Pergamon Press Ltd., London.

RESEARCH NOTE

On primary creep

N. J. Hoff
Polytechnic Institute of Brooklyn

(*Received* 31*st August*, 1956)

It is the purpose of this note to show that in the presence of variations in the properties of the individual crystals of a polycrystalline aggregate the assumption that only two mechanisms of deformation exist, namely one of linear elasticity and one of nonlinear steady (or secondary) creep, suffices to explain the existence of primary (or transient) creep. In the analysis two different neighbouring crystals will be represented by two parallel bars of equal length. The differences in the mechanical behaviour of the crystals may be due to a different orientation of their crystallographic axes or to different amounts of prior deformation during the manufacturing process. The deformation law for the first bar is taken as

$$\dot{\epsilon}_1 = (\dot{\sigma}_1/E_1) + (\sigma_1/\lambda)^n \tag{1}$$

and that for the second as

$$\dot{\epsilon}_2 = (\dot{\sigma}_2/E_2) + (\sigma_2/\mu)^m \tag{2}$$

where ϵ is the variable strain, σ the variable stress, E the constant modulus of elasticity, the dot denotes differentiation with respect to time, and λ, μ, m and n are constants.

The constant load P applied parallel to the axis of the bars is

$$P = \sigma_1 A_1 + \sigma_2 A_2 \tag{3}$$

where A_1 and A_2 are the cross-sectional areas of the two bars. The requirement of equal elongations can be written as

$$\dot{\epsilon}_1 = \dot{\epsilon}_2 \tag{4}$$

If the ratio of the force P_1 in the first bar to the total load P is denoted by r,

$$r = P_1/P \tag{5}$$

the stresses in the two bars can be expressed as

$$\sigma_1 = (P/A_1)\, r, \qquad \sigma_2 = (P/A_2)\,(1 - r). \tag{6}$$

Consideration of all the preceding equations leads to the differential equation

$$\dot{r} = (1/P)\,\frac{E_1 A_1 E_2 A_2}{E_1 A_1 + E_2 A_2}\left[(P/A_2\,\mu)^m (1 - r)^m - (P/A_1\,\lambda)^n r^n\right] \tag{7}$$

which can be integrated if m and n are given.

As an example one may take

$$E_1 = E_2 = E, \qquad A_1 = A_2 = A/2, \qquad m = 1, \qquad n = 2. \tag{8}$$

With these assumptions (7) reduces to

$$2\dot{r} = (E/\mu)(1 - r) - (E/\lambda)(2P/A\lambda)\, r^2. \tag{9}$$

The numerical values of the constants can be assumed as

$$E = 10^7 \text{ lb. in.}^{-2}, \qquad P/A = 5{,}000 \text{ lb. in.}^{-2},$$
$$\mu = 10^4 \text{ lb. in.}^{-2} \text{ hr}, \qquad \lambda = 10^4 \text{ lb. in.}^{-2} \text{ hr}^{1/2}. \tag{10}$$

With these values (9) becomes

$$2\dot{r} = 10^3 (1 - r - r^2) \tag{11}$$

If the initial condition is that the linearly elastic stress distribution must prevail at the moment of load application,

$$r = 0{\cdot}5 \qquad \text{when} \qquad t = 0, \tag{12}$$

and the integral of the differential equation is

$$t = 0{\cdot}894 \times 10^{-3} \left[\log \frac{1 + 0{\cdot}618\, r}{1 - 1{\cdot}618\, r} - 1{\cdot}924 \right] \tag{13}$$

where time is measured in hours. The stress σ_1 in the first bar, the strain $\epsilon = \epsilon_1 = \epsilon_2$ and the strain rate $\dot{\epsilon} = \dot{\epsilon}_1 = \dot{\epsilon}_2$ have been computed and are plotted against time in Fig. 1. From (13) the asymptotic value of r is 0·618.

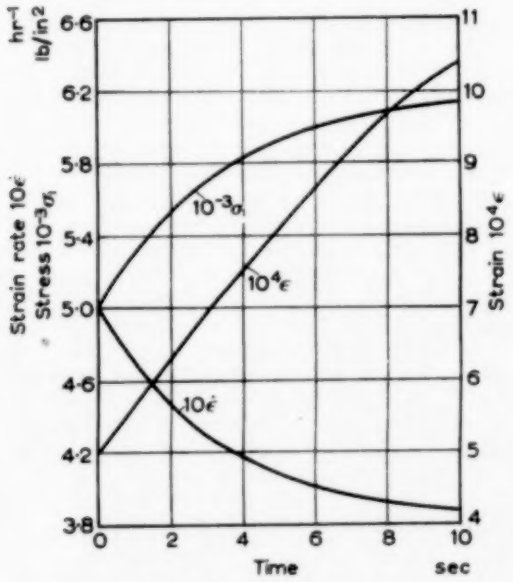

Fig. 1. History of stress and deformation.

As it was shown earlier (Andrade 1910 ; Hoff 1953) that tertiary creep can also be explained on the basis of secondary creep and the geometry of deformations, it appears that the mechanisms of elasticity and secondary creep can lead to all the three experimentally observed phases of the creep phenomenon. Unfortunately, the writer has insufficient knowledge of metal physics to judge how many other effects need be taken into account to describe creep completely.

References

Andrade, E. N. da C. 1910 *Proc. Roy. Soc.* **A84**, 1.
Hoff, N. J. 1953 *J. Appl. Mech.* **20**, 105.

BOOK REVIEW

A. PHILLIPS: **Introduction to Plasticity** Ronald Press Co., New York, 1956. pp. ix. + 230. $7.

THE greater part of this book, the first six chapters, is concerned with the elementary one dimensional theory of bending of beams. The calculation of fully plastic pure bending moments, collapse loads for beams under different types of loading, relations between bending moment and curvature for various hardening laws, bending under axial loading, and the calculation of beam deflections, are discussed in great detail for different sections with many formidable tables of collected formulae. Very few experimental data are presented in support of this theory. Brief mention is made of the plastic limit design of elementary structures, but no attempt is made to apply much of the beam theory to this problem, nor are the limitations of the simple methods of plastic design discussed. A serious basic error is made on page 3 where the symbol σ is defined as *nominal* stress, though it is used throughout the book to denote *true* stress, and the distinction between the two quantities is nowhere made clear.

The above topics are far too restricted to serve as an introduction to most of the basic ideas of plasticity theory but the remaining three chapters of the book make little amends for this. Here, a short account of general theory (15 pages) is followed by a more or less partial account of such topics as thick spherical shells under internal pressure, torsion, wire drawing, and plane plastic strain. References to the literature are inadequate, and the accounts given are inferior to those in existing books and papers, especially where the standard methods of treatment are not adopted. For example, the simple geometrical, stress, and velocity, properties of slip-line fields in plane plastic strain, and a clear idea of the method of upper and lower bounds, are quite lost in the tortuous mathematics of pp. 153-167. Also, here and in other parts of the book no attempt is made to relate the theory to practice so that the reader can gauge how closely it corresponds to physical reality, how far it can be relied on in practice, and in what respects it is likely, or has been definitely shown, to be a poor approximation for a real metal. The wire drawing theory presented is a poor approximation in the practical range and better approximations exist. On p. 158 it is not mentioned that the theory is relevant to the problem of indentation and can be applied, within certain limits, to a finite body. The practical purpose of the section on shearing stresses in bending of beams (pp. 193-196) is obscure, and, contrary to the author's statement, shearing stresses *can* exist in the plastic region (near constraining supports and concentrated loads). The validity of the analysis given is extremely doubtful and does not throw any light on the important practical problem (which has been treated by several writers, one of whom is quoted) of how shearing load can effect the yield-point bending moment.

The book has value as a reference work on the plastic bending of beams, but cannot be recommended as an introduction to plasticity.

A. P. GREEN

Journal of the Mechanics and Physics of Solids, 1957, Vol. 5, pp. 153 to 161. Pergamon Press Ltd., London

ON THE PROBLEM OF UNIQUENESS IN THE THEORY OF A RIGID-PLASTIC SOLID—III

By R. Hill
Department of Mathematics, University of Nottingham

(*Received* 10*th January*, 1957)

Summary

In previous papers in this series the question of how to select an actual mode of deformation from the set of virtual modes was answered when geometry changes can be disregarded. In the present paper that restriction is dropped. At the outset this calls for a reappraisal of what constitutes an adequate setting of the boundary-value problem when the future position of the surface is unknown in advance. A sufficient criterion for uniqueness is then established under quite general loading conditions. It is shown how to determine, in any given situation, a critical rate of workhardening above which the mode is certainly unique and below which it probably is not. The conventional tension, compression, and torsion tests are taken as illustrations.

1. Introduction

In the conventional formulation of the typical boundary-value problem for a rigid-plastic solid the velocity is given on a part S_v of the surface and the traction on the remainder S_F. This formulation does not generally lead to a unique solution. Not one deformation mode but an infinite set is compatible with the internal state of stress and with the velocity boundary conditions. The characterization and selection of the physically-possible mode(s) is the subject of this series of papers. The main thesis is that in a proper statement of the boundary value problem there should also be given the traction-rate on S_F.

In Part I (Hill 1956a) the analysis was restricted to situations where displacements of elements and changes in geometry can be disregarded, and it was shown that one continuous mode at most is compatible with the additional boundary-conditions when the material workhardens. In Part II (Hill 1956b) the specification of the warping function for hollow bars under torsion was taken as an illustration. In the present paper the restriction on geometry changes is dropped and the theory of Part I is generalized in this respect. Furthermore, when there is no workhardening, the extended analysis takes due account of discontinuous modes.

It now becomes necessary to reconsider the specification of the loading on S_F since the changes in shape and area of surface elements are themselves unknowns. For the most part it is supposed here that the change in the *load* vector on each infinitesimal element of S_F is assigned (irrespective of the change in its area); i.e., there is given, not the rate of change of the *true* traction, but the rate of change of the *nominal* traction based on the configuration at the initial instant. An

important special case is that of 'dead' loading. We consider also a type of loading that does not fall in this category, namely the application of a uniform fluid pressure over S_F.

2. Basis for Examination of Uniqueness

Let x_i be the position vector in a Cartesian frame of reference at time t, the moment under consideration. Let σ_{ij} be the *true* stress at time t and $\sigma_{ij} + \delta\sigma_{ij}$ the true stress in the same material element after an infinitesimal time δt, both tensors being associated with the same Cartesian axes. Let δs_{ij} be the increment in *nominal* stress in the same element in time δt, based on the dimensions at time t; that is, $\sigma_{ij} + \delta s_{ij}$ is at time $t + \delta t$ the jth component of the load per unit original area at time t, acting over a plane originally perpendicular to the ith direction (of course $s_{ij} \equiv \sigma_{ij}$ at time t). Let δu_i be the increment of displacement of the element. Then, since the plastic volume change is assumed zero,

$$\delta s_{ij} = \delta\sigma_{ij} - \sigma_{kj}\frac{\partial}{\partial x_k}\delta u_i$$

to first order, or, in terms of rates,

$$\dot{s}_{ij} = \dot{\sigma}_{ij} - \sigma_{kj}\frac{\partial v_i}{\partial x_k} \tag{1}$$

where v_i is velocity, the summation convention being adopted henceforward. Note that $\dot{s}_{ij}$ is not symmetric. If $\dot{g}_i$ is the rate of increase in body force per unit mass and ρ the density at time t,

$$\frac{\partial}{\partial x_i}\dot{s}_{ij} + \rho\dot{g}_j = 0 \tag{2}$$

for continuing equilibrium. The increment in nominal traction is $\delta F_j = l_i\,\delta s_{ij}$ and so

$$\dot{F}_j = l_i\,\dot{s}_{ij} \tag{3}$$

where l_i is the unit normal to the surface at time t.

If a distribution of traction-rate is prescribed over the whole of the surface S at time t (satisfying $\int \dot{\mathbf{F}}\,dS = 0$ for linear equilibrium), it might appear that the mode could in any event only be determined to within an arbitrary rigid-body motion since there are no geometrical constraints. However, this is not so as regards *spin* since the resulting movement would unbalance the given load-vectors by displacing their lines of action through varying amounts. In fact, the actual mode must satisfy the overall condition that the resultant couple of the surface tractions remains zero, namely

$$\frac{d}{dt}\int(\mathbf{r}\wedge\dot{\mathbf{F}})\,dS = 0$$

where $\mathbf{r}$ is the actual position-vector of a surface element. This becomes

$$\int(\mathbf{v}\wedge\mathbf{F})\,dS = -\int(\mathbf{r}\wedge\dot{\mathbf{F}})\,dS. \tag{4}$$

Since the right-hand side is known we have three scalar conditions on the mode; in general these will exclude the possibility of superimposing an arbitrary rigid-body spin.

Suppose that there could be more than one solution to the boundary-value problem set by given velocities on S_v, nominal tractions and traction-rates on S_F, and nominal body-force rates (the latter being assumed given irrespective of what the positional changes might be). Let the prefix Δ indicate the *difference* of any corresponding quantities in two solutions. Since (1), (2), (3) hold for both, their difference satisfies

$$\Delta \dot{s}_{ij} = \Delta \dot{\sigma}_{ij} - \sigma_{kj} \frac{\partial}{\partial x_k} \Delta v_i, \tag{5}$$

$$\frac{\partial}{\partial x_i} \Delta \dot{s}_{ij} = 0, \qquad \Delta \dot{\mathbf{F}}_j = l_i \, \Delta \dot{s}_{ij}, \tag{6}$$

in the zone where the existing stress is uniquely determined by the given boundary-values for traction and velocity at time t. Elsewhere, the stress is indeterminate by strict rigid-plastic theory, but the material is rigid (possibly consisting of separated parts) and its motion is usually completely determined by the geometrical constraints; therefore $\Delta v_i = 0$. Where this is not so we suppose that the existing stress is *given*, and then (5) applies there also.*

Using (6) and GREEN's theorem for integrals over the surface S and volume V:

$$\int \Delta \dot{\mathbf{F}} \, \Delta \mathbf{v} \, dS = \int \Delta \dot{s}_{ij} \frac{\partial}{\partial x_i} \Delta v_j \, dV.$$

But the left-hand integrand vanishes everywhere in view of the boundary conditions, while the right-hand integrand vanishes in any rigid zone whose motion is known in advance. Hence, by (5), if ϵ_{ij} denotes true strain-rate,

$$\int \left[\Delta \dot{\sigma}_{ij} \, \Delta \epsilon_{ij} - \sigma_{kj} \frac{\partial}{\partial x_k} (\Delta v_i) \frac{\partial}{\partial x_i} (\Delta v_j) \right] dV = 0 \tag{7}$$

where the integral really extends over the region where the existing stress is uniquely known or given, but may be extended formally over the whole body on the understanding that the symbol σ_{kj} is undefined in rigid zones whose motion is known ($\Delta v_i = 0$).

This equation is an appropriate basis for the examination of uniqueness in a rigid-plastic solid since the quantities involved are just those in the corresponding physical laws. Equation (7) differs from the basis in Part I by the second term, which arises from the previously neglected positional changes.

3. A Sufficient Condition for Uniqueness

For convenience the stress-strain relations are here briefly recapitulated; a full presentation is given in Part I (Section 2). The notation is simplified by regarding the stress and strain-rate tensors as 'vectors' $\boldsymbol{\sigma}$ and $\boldsymbol{\epsilon}$ in a 9-space; the juxtaposition of two vectors signifies their scalar product. Then, in an element currently stressed to its yield point,

* The actual mode, even when unique with this formulation, might nevertheless *depend* on the given stress state(s) in the rigid zone(s).

$$h\dot{\boldsymbol{\epsilon}} = \begin{cases} (\mathbf{n}\,\dot{\boldsymbol{\sigma}})\,\mathbf{n} & \text{when} \quad \mathbf{n}\dot{\boldsymbol{\sigma}} \geqslant 0 \qquad (8a) \\ 0 & \text{when} \quad \mathbf{n}\dot{\boldsymbol{\sigma}} \leqslant 0 \qquad (8b) \end{cases}$$

where h is a positive function depending on the workhardening, and $\mathbf{n}$ is the unit outward normal in stress space to the local yield surface; since volume changes are excluded, the latter must have generators parallel to the direction corresponding to a hydrostatic stress. When $h = 0$ (no hardening) (8) is replaced by

$$\dot{\boldsymbol{\epsilon}} = \begin{cases} \lambda\mathbf{n}, & \lambda \geqslant 0 \quad \text{and} \quad \mathbf{n}\dot{\boldsymbol{\sigma}} = 0 \qquad (9a) \\ 0, & \mathbf{n}\dot{\boldsymbol{\sigma}} \leqslant 0. \qquad (9b) \end{cases}$$

In an element stressed below its yield point, $\mathbf{n}\dot{\boldsymbol{\sigma}}$ can have any value and $\dot{\boldsymbol{\epsilon}}$ is zero.

Normally, when the rotation of an element is not negligible, an explicit equation involving stress-rate is ambiguous unless the appropriate convected component of stress-rate is specified. In particular this is necessary for anisotropic rigid-plastic material; however, since the proper specification is not known at the present time, anisotropy has to be excluded here. On the other hand, when the material is isotropic, as we now assume, the product $\mathbf{n}\dot{\boldsymbol{\sigma}}$ in (8) and (9) depends only on the stress invariants and their derivatives. Consequently stress-rate in (8) and (9) can have the meaning that it necessarily has in (7), namely the tensor formed from the time-derivatives of stress components associated always with fixed Cartesian axes.

We now show that, for $h \geqslant 0$,

$$\Delta\dot{\boldsymbol{\sigma}}\,\Delta\dot{\boldsymbol{\epsilon}} \geqslant h\,(\Delta\dot{\boldsymbol{\epsilon}})^2$$

at every point of the body. For the limited purposes of Part I it was sufficient to show merely that the left-hand side was non-negative; the proof of the present stronger inequality is on identical lines. Subscripts 1 and 2 refer to two solutions. Four regions have to be separately considered; in the first three, where one or both of $\dot{\boldsymbol{\epsilon}}_1$ and $\dot{\boldsymbol{\epsilon}}_2$ are nonzero, the existing stress is unique, at the yield point, and known in principle.

(i) $\dot{\boldsymbol{\epsilon}}_1 \neq 0$, $\dot{\boldsymbol{\epsilon}}_2 \neq 0$. L.h.s. $= h^{-1}\{\mathbf{n}\,(\dot{\boldsymbol{\sigma}}_2 - \dot{\boldsymbol{\sigma}}_1)\}^2 = h\,(\dot{\boldsymbol{\epsilon}}_2 - \dot{\boldsymbol{\epsilon}}_1)^2$

when $h \neq 0$, from (8a).

L.h.s. $= (\lambda_2 - \lambda_1)\,\mathbf{n}\,(\dot{\boldsymbol{\sigma}}_2 - \dot{\boldsymbol{\sigma}}_1) = 0 = h\,(\dot{\boldsymbol{\epsilon}}_2 - \dot{\boldsymbol{\epsilon}}_1)^2$

when $h = 0$, from (9a).

(ii) $\dot{\boldsymbol{\epsilon}}_1 \neq 0$, $\dot{\boldsymbol{\epsilon}}_2 = 0$. L.h.s. $= h\dot{\boldsymbol{\epsilon}}_1^{\,2} - h^{-1}\,(\mathbf{n}\dot{\boldsymbol{\sigma}}_1)(\mathbf{n}\dot{\boldsymbol{\sigma}}_2) \geqslant h\dot{\boldsymbol{\epsilon}}_1^{\,2} = h\,(\dot{\boldsymbol{\epsilon}}_2 - \dot{\boldsymbol{\epsilon}}_1)^2$

when $h \neq 0$, since $\mathbf{n}\dot{\boldsymbol{\sigma}}_1 > 0$ (8a), $\mathbf{n}\dot{\boldsymbol{\sigma}}_2 \leqslant 0$ (8b).

L.h.s. $= \lambda_1\,\mathbf{n}\,(\dot{\boldsymbol{\sigma}}_1 - \dot{\boldsymbol{\sigma}}_2) \geqslant 0 = h\,(\dot{\boldsymbol{\epsilon}}_2 - \dot{\boldsymbol{\epsilon}}_1)^2$

when $h = 0$, since $\mathbf{n}\dot{\boldsymbol{\sigma}}_1 = 0$ and $\lambda_1 > 0$ (9a), $\mathbf{n}\dot{\boldsymbol{\sigma}}_2 \leqslant 0$ (9b).

(iii) $\dot{\boldsymbol{\epsilon}}_1 = 0$, $\dot{\boldsymbol{\epsilon}}_2 \neq 0$. Similar to (ii).

(iv) $\dot{\boldsymbol{\epsilon}}_1 = 0$, $\dot{\boldsymbol{\epsilon}}_2 = 0$. L.h.s. $= 0 = h\,(\dot{\boldsymbol{\epsilon}}_1 - \dot{\boldsymbol{\epsilon}}_2)^2$ for all h.

The statement is thereby proved, and so

$$\int \Delta\boldsymbol{\sigma}\ \Delta\boldsymbol{\epsilon}\, dV > \int h\,(\Delta\boldsymbol{\epsilon})^2\, dV. \tag{10}$$

Suppose, now, that we were able to show, in a particular situation, that

$$\int \left(h\,\boldsymbol{\eta}^2 - \sigma_{kj}\frac{\partial w_i}{\partial x_k}\frac{\partial w_j}{\partial x_i}\right) dV > 0 \tag{11}$$

for all incompressible velocity fields $\mathbf{w}$ which vanish on S_v, while the corresponding strain-rate $\boldsymbol{\eta}$ is zero except in part or all of the uniquely-stressed zone where it is parallel to $\mathbf{n}$ (though not necessarily in the same sense). In other words, $\mathbf{w}$ satisfies the same conditions as the difference of two distinct virtual modes. If the traction-rate is given all over S, $\mathbf{w}$ is required also to satisfy $\int (\mathbf{w} \wedge \mathbf{F})\, dS = 0$ in view of (4).

On the supposition that there could be two distinct actual modes, their difference would constitute such a field, and so from (10) and (11)

$$\int \left(\Delta\dot{\boldsymbol{\sigma}}\ \Delta\boldsymbol{\epsilon} - \sigma_{kj}\frac{\partial}{\partial x_k}(\Delta v_i)\frac{\partial}{\partial x_i}(\Delta v_j)\right) dV > 0.$$

But this contradicts (7), and so the supposition is false and there can not be more than one physically-possible (continuous) mode. Equation (11) is therefore a *sufficient condition for uniqueness* (but the present analysis does not indicate when it is also necessary).

If the material hardens, the present framework is inadequate to discuss discontinuous velocity fields since the first term in (11) diverges at a discontinuity surface regarded as a vanishingly thin zone of unlimited shear strain-rate. If there is no hardening, however, this term vanishes identically while the second term gives a finite contribution ; in this case the analysis is adequate.

4. Critical Rate of Hardening

To assess the influence of the rate of hardening on uniqueness we substitute μh for h in (11), where μ is an arbitrary constant, and write

$$H = \int h\boldsymbol{\eta}^2\, dV. \qquad \Sigma = \int \sigma_{kj}\frac{\partial w_i}{\partial x_k}\frac{\partial w_j}{\partial x_i}\, dV. \tag{12}$$

H depends on the hardening distribution function and is essentially positive, while Σ depends on the existing stress and may have either sign. The condition (11) is satisfied when

$$\mu > \max\,(\Sigma/H), \tag{13}$$

the *algebraic* maximum being implied. When μ is less than or equal to this value there may be more than one physically-possible mode.

Three possibilities are worth distinguishing :

(a) $\Sigma > 0$ for at least one field $\mathbf{w}$. The critical value of μ is positive. This strongly suggests that in this case the indeterminacy for a non-hardening solid is real and is not removable by appeal to a limiting process in which μ is made vanishingly small.

(b) $\Sigma < 0$ for all (nonzero) fields $\mathbf{w}$. Equation (13) is certainly satisfied when $\mu \geqslant 0$. There is not more than one physically-possible continuous mode whatever the rate of hardening, and not more than one mode altogether (whether continuous or discontinuous) when there is no hardening. In this case the consideration of positional changes removes the apparent indeterminacy in a non-hardening solid.

(c) $\Sigma = 0$ for at least one (nonzero) field $\mathbf{w}$, and $\Sigma < 0$ for any others. Equation (13) is satisfied when $\mu > 0$ but not when $\mu = 0$. In this case consideration of positional changes does not in itself guarantee uniqueness in a non-hardening solid, and one may appeal to a limiting process where μ is made vanishingly small (cf. Part I, Section 4).

The question now arises: in a situation where the mode is unique, to what extent does it differ from the one characterized by the extremum principle in Part I (Section 3), where the effects of positional changes were neglected? In other words, when is the theory of Part I acceptable as an approximation? Another important question is the relation of the uniqueness condition (11) to the stability criterion for a rigid-plastic solid. We defer general answers, and here investigate some particular situations.

5. ILLUSTRATIONS

(i) *Uniaxial tension.* In a tension test on a specimen of uniform section the current state of stress is (ideally) a uniform tension σ, in the x_3 direction say. Then, whatever the yield surface, the strain-rate components in the $\mathbf{w}$ field satisfy

$$\frac{\partial w_1}{\partial x_1} = \frac{\partial w_2}{\partial x_2} = -\tfrac{1}{2}\frac{\partial w_3}{\partial x_3},$$

$$\frac{\partial w_1}{\partial x_2} + \frac{\partial w_2}{\partial x_1} = 0, \qquad \frac{\partial w_2}{\partial x_3} + \frac{\partial w_3}{\partial x_2} = 0, \qquad \frac{\partial w_3}{\partial x_1} + \frac{\partial w_1}{\partial x_3} = 0,$$

since the material is assumed isotropic. These have the general solution

$$w_1 = -\tfrac{1}{4}a\,(x_1^2 - x_2^2 + 2x_3^2) - \tfrac{1}{2}b\,x_1 x_2 - 2c\,x_1 x_3 - \tfrac{1}{2}dx_1$$

$$w_2 = -\tfrac{1}{2}a\,x_1 x_2 - \tfrac{1}{4}b\,(x_2^2 - x_1^2 + 2x_3^2) - 2c\,x_2 x_3 - \tfrac{1}{2}dx_2$$

$$w_3 = ax_1 x_3 + bx_2 x_3 + c\,(x_1^2 + x_2^2 + 2x_3^2) + dx_3$$

to within a rigid-body motion, where a, b, c, d are arbitrary constants; this solution is included in PRAGER's (1954) expressions for virtual modes associated with a uniform plastic state. The constants may have different values (in particular zero) in different regions provided $\mathbf{w}$ is made continuous across their interfaces by adding suitable rigid-body motions.

If h is also uniform the uniqueness criterion becomes

$$\frac{h}{\sigma} > \max\left\{\int\left[\left(\frac{\partial w_3}{\partial x_3}\right)^2 - \left(\frac{\partial w_3}{\partial x_1}\right)^2 - \left(\frac{\partial w_3}{\partial x_2}\right)^2\right]dV \Big/ \frac{3}{2}\int\left(\frac{\partial w_3}{\partial x_3}\right)^2 dV\right\}.$$

Irrespective of the boundary conditions on the ends and whatever the admissible functions $\mathbf{w}$, the inequality is certainly satisfied when $h/\sigma > \frac{3}{4}$.* From (8a) for

* It is likely that stronger inequalities could be found for certain boundary conditions and dimensions (particularly very short specimens).

uniaxial tension, for which $\mathbf{n} = \sqrt{(\frac{2}{3})}\,(-\frac{1}{2}, -\frac{1}{2}, 1)$ in principal-stress space, we find that $h = \frac{3}{2}d\sigma/de$ where e is the total logarithmic strain. Hence $d\sigma/de > \sigma$, so that the mode is unique when the slope of the tensile stress-strain curve exceeds the local yield stress. As is well known, at the critical value $d\sigma/de = \sigma$ the load attains its maximum and either a further general extension or local necking is possible in principle (at least when the specimen is sufficiently long).

(ii) *Compression of a strut.* A strut of uniform sectional area A is built in at one end and axially loaded at the other by an increasing load P. Apart possibly from a neighbourhood of the fixed end, the existing stress can be taken to be a uniaxial compression of amount P/A. If the strut is long and slender the contribution from this neighbourhood can be neglected and the uniqueness criterion becomes

$$\frac{h}{P/A} > \max \left\{ \int \left[\left(\frac{\partial w_3}{\partial x_1}\right)^2 + \left(\frac{\partial w_3}{\partial x_2}\right)^2 - \left(\frac{\partial w_3}{\partial x_3}\right)^2 \right] dV \Big/ \frac{3}{2} \int \left(\frac{\partial w_3}{\partial x_3}\right)^2 dV \right.$$

The admissible functions w_3 are as in (i), except near the fixed end. Since the other end is completely free, it seems safe to assume that we need only consider fields where the constants have the same values everywhere (i.e. we do not consider modes that would produce an inflexion in the strut). Furthermore, the above expressions for $\mathbf{w}$ satisfy, as they stand, the end-conditions $w_1 = w_2 = w_3 = \partial w_1/\partial x_3 = \partial w_2/\partial x_3 = 0$ at the origin when this is at the fixed end (here again a similar small approximation is made).

If the x_1, x_2 directions are those of the principal axes of section at the centroid, then

$$\frac{3h}{2P l^2} > \max \frac{\left(\frac{1}{3} - \frac{I_2}{Al^2}\right) a^2 + \left(\frac{1}{3} - \frac{I_1}{Al^2}\right) b^2 + \left(\frac{I_1 + I_2}{4Al^2} - \frac{1}{3}\right) c^2 - \frac{cd}{l} - \frac{d^2}{l^2}}{I_2 a^2 + I_1 b^2 + \frac{1}{3} Al^2 c^2 + Ad^2}$$

where l is the length of the strut, and I_1 and I_2 are the second moments of area about the x_1 and x_2 axes respectively. When the strut is so slender that $(I_1 + I_2)/Al^2 < 1$, the (approximate) greatest value of the expression is obtained with $c = d = 0$, and either $b = 0$ when $I_1 > I_2$, or $a = 0$ when $I_2 > I_1$, or any a/b when $I_1 = I_2$. In all cases this greatest value is $1/(3I)$ where I is the least moment of area, and the $\mathbf{w}$ field reduces to pure bending. With $h = \frac{3}{2}d\sigma/de$ as in (i), the uniqueness condition becomes

$$\frac{d\sigma}{de} > \frac{Pl^2}{3I}.$$

(iii) *Torsion.* Consider a twisted uniform prismatic bar at its initial yield point under the usual boundary condition. All virtual modes are of type

$$v_1 = -x_2 x_3, \qquad v_2 = x_1 x_3, \qquad v_3 \equiv v_3(x_1, x_2) \tag{14}$$

where x_3 is parallel to the generators (Part II, p. 4). Hence the $\mathbf{w}$ fields are of type

$$w_1 = 0, \qquad w_2 = 0, \qquad w_3 \equiv w_3(x_1, x_2)$$

while the only non-vanishing stress components are σ_{13} and σ_{23}. It is easily verified that the integrand of the functional Σ in (12) vanishes identically, so that the conclusions under (c) of Section 4 apply.

We can show, moreover, that the unique mode is characterized in this case by the extremum principle of Part I (Section 3). The starting point is

$$\int \dot{\mathbf{F}}\,(\mathbf{v}^* - \mathbf{v})\,dS = \int \dot{s}_{ij}\frac{\partial}{\partial x_i}(v_j^* - v_j)\,dV$$

$$= \int \dot{\sigma}\,(\epsilon^* - \epsilon)\,dV - \int \sigma_{kj}\frac{\partial v_i}{\partial x_k}\frac{\partial}{\partial x_i}(v_j^* - v_j)\,dV$$

from (4), where $(\mathbf{v}, \epsilon)$ is the actual mode and $(\mathbf{v}^*, \epsilon^*)$ a virtual mode. In view of (14) the integrand of the right-hand integral is equal to

$$x_3\left(\sigma_{13}\frac{\partial}{\partial x_2} - \sigma_{23}\frac{\partial}{\partial x_1}\right)(v_3^* - v_3) = 2x_3\left[\sigma_{13}(\epsilon_{23}^* - \epsilon_{23}) - \sigma_{23}(\epsilon_{13}^* - \epsilon_{13})\right],$$

again with the use of (14). But, since the material is isotropic and the stress is a pure shear,

$$\epsilon_{13}^*/\epsilon_{23}^* = \epsilon_{13}/\epsilon_{23} = \sigma_{13}/\sigma_{23},$$

and so the expression vanishes. Proceeding as in Part I we conclude that the same extremum principle holds, provided that the given traction-rate is interpreted as nominal and not actual.

In particular, if the lateral surface of the bar remains free and if the axial component of nominal traction remains zero on the ends then the actual mode minimizes $\int h\epsilon^{*2}\,dV$. This is precisely the result that was obtained in Part I when positional changes were neglected, and so the analysis of Part II (Sections 3 and 4) supplies the correct mode (though not necessarily the correct distribution of stress-rate).

6. Loading by Fluid Pressure

Instead of prescribing the variation of nominal traction on S_F, suppose that the actual traction is given to be a *uniform* normal pressure $p(t)$; that is, this part of the surface is immersed in an inviscid fluid. Then

$$\dot{\mathbf{F}}_j = pl_k\frac{\partial v_k}{\partial x_j} - l_j\,\dot{p}$$

and so, for the difference of two solutions,

$$\Delta\mathbf{F}_j = pl_k\frac{\partial}{\partial x_j}(\Delta v_k) \text{ on } S_F. \tag{15}$$

Hence

$$\int\left\{\Delta\dot{F}_j - pl_k\frac{\partial}{\partial x_j}(\Delta v_k)\right\}\Delta v_j\,dS = 0$$

since one of the factors in the integrand vanishes on S_F and the other on S_v. By (6) and GREEN's theorem,

$$\int\left[\Delta\dot{s}_{ij}\frac{\partial}{\partial x_i}(\Delta v_j) - p\frac{\partial}{\partial x_k}\left(\Delta v_j\frac{\partial}{\partial x_j}\Delta v_k\right)\right]dV = 0$$

since p is a constant. Using (5) and the incompressibility relation $\partial(\Delta v_k)/\partial x_k = 0$,

$$\int\left[\Delta\dot{\sigma}\,\Delta\epsilon - (\sigma_{kj} + p\delta_{kj})\frac{\partial}{\partial x_k}(\Delta v_i)\frac{\partial}{\partial x_i}(\Delta v_j)\right] dV = 0, \tag{16}$$

which takes the place of (7), under the same conditions.

Thus, a sufficient condition for uniqueness is

$$\int\left[h\eta^2 - (\sigma_{kj} + p\delta_{kj})\frac{\partial w_i}{\partial x_k}\frac{\partial w_j}{\partial x_i}\right] dV > 0 \tag{17}$$

in place of (11). But the set of virtual modes and the value of $\sigma_{kj} + p\delta_{kj}$ in the uniquely stressed zone are independent of p, since the addition of an all-round uniform surface pressure only alters the stress-state at the yield point by a uniform hydrostatic stress of the same amount. Consequently, if (17) were satisfied with one value of p, say zero, it would be with any other value.

For instance, in a tension test the critical rate of hardening would be that calculated in Section 5 (i) even if the lateral surface of the specimen were subjected to fluid pressure.

References

Hill, R. 1956 *J. Mech. Phys. Solids* (a) **4**, 247 ; (b) **5**, 1.

Prager, W. 1954 *Rev. Fac. Sci., Univ. Instanbul* **19**, 23.

Journal of the Mechanics and Physics of Solids, 1957, Vol. 5, pp 162 to 171 Pergamon Press Ltd., London

ENERGY ABSORBED BY ELASTIC WAVES DURING IMPACT

By S. C. Hunter
Armament Research and Development Establishment, Fort Halstead

(*Received 4th January*, 1957)

Summary

The absorption of vibrational energy in the form of elastic waves generated by a transient localized force acting normally to the free surface of a semi-infinite solid is calculated in terms of the Fourier components of the force. The result is applied to the Hertzian collision of a small body with the plane surface of a massive specimen. It is concluded that for impact velocities small compared with the propagation velocity of elastic waves in the specimen, a negligible proportion of the original kinetic energy of the small body is transferred to the specimen by the collision. The result is of some interest in justifying the validity of the Hertz theory for collisions between a small and a massive body.

While experimental evidence for the impact of steel ball bearings on massive glass specimens shows some measure of agreement with these theoretical conclusions, results obtained for steel specimens are somewhat at variance, the observed values of the coefficient of restitution (0·90-0·95) indicating absorption of 10 %-20 % of the initial kinetic energy of the ball. A possible explanation of this anomaly is the existence, at the high rates of strain involved in such collisions, of either anelastic or viscous (dissipative) forces in the steel.

1. Introduction

The contents of the present note were prompted by certain observations made during the course of a number of experiments devoted to investigating dynamic yield phenomena in steels by sclerescopic methods. In collisions between ball bearings and steel specimens it was observed that for impact velocities below the critical velocity required to initiate plastic deformation in the specimen,* the relation between the impact velocity V_0 and the duration of impact T closely followed the theoretical prediction of Hertz (Section 3) :

$$T = K V_0^{-1/5}$$

where K is a constant defined in terms of the elastic properties and geometry of the system. However, the observed velocity of recession V_1 subsequent to impact was always significantly less than V_0 :

$$V_1/V_0 \simeq 0{\cdot}90 - 0{\cdot}95$$

indicating an absorption of some of the kinetic energy originally available in the ball. One possible source for this energy loss appears to lie in the dissipation of energy in the specimen in the form of elastic vibrations occasioned by the transient

* For moderate size balls of order a few cm/sec, see e.g. Davies (1949).

nature of the collision. It is with the calculation of this energy loss that the present analysis is concerned.

In Section 2 an expression is derived for the energy of elastic vibration produced in a semi-infinite solid by a transient pressure pulse acting normally over a small area of the free surface. In particular the formula is applied to the pulse whose profile is defined to be the positive half cycle of a sinusoid. Section 3 is devoted to a brief exposition and discussion of the HERTZ theory of impact. Finally in Section 4 the theoretical conclusions to be drawn from applying the results of Section 2 to the HERTZIAN collision of a small and a massive body are compared with the available experimental evidence.

2. ENERGY ABSORPTION PRODUCED BY TRANSIENT PULSES

The problem of the response of an isotropic elastic semi-infinite medium to time dependent surface forces has been considered by LAMB (1904) and more recently by MILLER and PURSEY (1954, 1956).† All three papers are concerned primarily with periodic forces, although LAMB generalizes some of his results to cover the problem of transient pulses. The present analysis is based on a result given in M.P.I. for the normal displacement of the free surface of a semi-infinite body subjected to a uniform periodic surface pressure Pe^{iwt} acting over a circular area of radius a. With the help of this result we obtain by a FOURIER synthesis the mean surface displacement $\bar{u}$ over the circle for a pressure pulse of arbitrary profile $P(t)$. Finally the rate of doing work on the specimen is given by

$$\frac{dW}{dt} = \pi a^2 P(t) \frac{d\bar{u}}{dt} \tag{1}$$

and by integrating this expression we obtain for the total energy absorbed in the form of elastic vibrations :

$$W = \int_{-\infty}^{\infty} \frac{dW}{dt}\, dt = \int_{-\infty}^{\infty} \pi a^2 P(t) \frac{d\bar{u}}{dt}\, dt. \tag{2}$$

Equation (129) of M.P.I. gives for the normal surface displacement of a semi-infinite solid subjected to a uniform pressure Pe^{iwt} ($w > 0$) over the area $0 \leqslant r \leqslant a$

$$u(r, t, z = 0) = Pe^{iwt} k_2^2 \int_0^{\infty} \frac{(\xi^2 - k_1^2)^{1/2}\, a\, J_1(\xi a)\, J_0(\xi r)\, d\xi}{C_{44}\, F(\xi)}. \tag{3}$$

Here

$$k_2 = w/(C_{44}/\rho)^{1/2}, \qquad k_1 = w/(C_{11}/\rho)^{1/2} \tag{4}$$

and $F(\xi)$ is the function

$$F(\xi) = (2\xi^2 - k_2^2)^2 - 4\xi^2 [(\xi^2 - k_1^2)(\xi^2 - k_2^2)]^{1/2}. \tag{5}$$

The mean displacement over the area under pressure is

$$\begin{aligned} \bar{u} &= \frac{2}{a^2} \int_0^{\infty} urdr = Pe^{iwt} k_2 \int_0^{\infty} \frac{(\xi^2 - k_1^2)^{1/2} J_1^2(\xi a)\, d\xi}{C_{44}\, \xi F(\xi)} \\ &= \frac{2\gamma^2 a^2 Pe^{iwt}}{C_{44}} \int_0^{\infty} \frac{k_1 (\xi^2 - 1)^{1/2} J_1^2(\xi k_1 a)\, d\xi}{\xi k_1^2 a^2 F_0(\xi)} \end{aligned} \tag{6}$$

on changing the integration variable from ξ to $k_1\xi$. In (6) $F_0(\xi)$ is a dimensionless quantity depending only on ξ and POISSON's ratio σ :

† Referred to subsequently by the abbreviations M.P.I., and M.P.II. respectively.

$$F_0(\xi) = (2\xi^2 - \gamma^2)^2 - 4\xi^2 [(\xi^2 - 1)(\xi^2 - \gamma^2)]^{1/2} \tag{7}$$

and

$$\gamma = k_2/k_1 = (C_{11}/C_{44})^{1/2} = \{2(1-\sigma)/(1-2\sigma)\}^{1/2}. \tag{8}$$

The existence of branch points and poles of the integrand in (6) for values of ξ on the real axis leads to some ambiguity in the interpretation of the integral. The correct prescription for circumnavigating these singularities has been obtained in M.P.I., to which the reader is referred for further details.

It is convenient to re-write the integral (6) in terms of its real and imaginary parts, viz.

$$\bar{u} = \frac{2\gamma^2 a^2 P e^{iwt}}{C_{44}} (A(w) + iB(w)) \qquad (w > 0) \tag{9}$$

where

$$A + iB = k_1 \int_0^\infty \frac{(\xi^2 - 1)^{1/2} J_1^2(\xi k_1 a)\, d\xi}{\xi k_1^2 a^2 F_0(\xi)}. \tag{10}$$

Equation (9) is valid only for values of $w > 0$. To construct the solution corresponding to $w < 0$ we note from (10) that both A and B are odd functions of w. It follows that for $w < 0$ we must have

$$\bar{u} = \frac{2\gamma^2 a^2 P e^{iwt}}{C_{44}} [-A(w) + iB(w)] \qquad (w < 0) \tag{11}$$

in order to obtain real values of u for the real pressures $P\cos(wt)$ and $P\sin(wt)$.

For a pulse of arbitrary profile,

$$P(t) = \int_{-\infty}^{\infty} P(w) e^{iwt}\, dw, \tag{12}$$

the mean normal displacement of the free surface area subjected to pressure is given by (9), (11) and the superposition principle, in the form

$$\begin{aligned}\bar{u}(t) &= \frac{2\gamma^2 a^2}{C_{44}} \left\{ \int_0^\infty P(w) e^{iwt} [A + iB]\, dw + \int_{-\infty}^0 P(w) e^{iwt} [-A + iB]\, dw \right\} \\ &= \frac{2\gamma^2 a^2}{C_{44}} \int_0^\infty dw \left\{ P(w) e^{iwt} (A + iB) + P(-w) e^{-iwt} (A - iB) \right\}\end{aligned} \tag{13}$$

Substituting (12) and (13) into (1) yields

$$\frac{dW}{dt} = -\frac{2\pi a^4 \gamma^2 i}{C_{44}} \int_0^\infty dw \int_{-\infty}^\infty dw'\, P(w') \left\{ wP(w) e^{i(w'+w)t} (A + iB) - wP(-w) e^{i(w'-w)t} (A - iB) \right.$$

Integrating with respect to t, using the results

$$\int_{-\infty}^\infty e^{i(w'+w)t}\, dt = 2\pi\, \delta(w' + w), \qquad \int_{-\infty}^\infty e^{i(w'-w)t}\, dt = 2\pi\, \delta(w' - w),$$

and carrying out the resultant trivial integration with respect to w' yields

$$\begin{aligned}W &= -\frac{4\pi^2 a^4 \gamma^2}{C_{44}} i \int_0^\infty dw.\, wP(w) P(-w) \{(A + iB) - (A - iB)\} \\ &= \frac{8\pi^2 a^4 \gamma^2}{C_{44}} \int_0^\infty wB(w) |P(w)|^2\, dw\end{aligned} \tag{14}$$

since reality of $P(t)$ demands

$$P(w) = P^*(-w).$$

Further simplification ensues if the pulse $P(t)$ contains significant FOURIER components only

for those frequencies satisfying the inequality

$$k_1 a \equiv wa/(C_{11}/\rho)^{1/2} \ll 1 \tag{15}$$

For these frequencies, (10) approximates to

$$A + iB = \frac{wa}{4(C_{11}/\rho)^{1/2}} \int_0^\infty \frac{(\xi^2 - 1)^{1/2}\, \xi d\xi}{F_0(\xi)}$$

i.e.

$$B(w) = \frac{\beta w}{4(C_{11}/\rho)^{1/2}} \tag{16}$$

where β is a dimensionless quantity dependent only on the value of Poisson's ratio,

$$\beta = \text{imaginary part of} \int_0^\infty \frac{(\xi^2 - 1)^{1/2}\, \xi d\xi}{F_0(\xi)} \tag{17}$$

$$\left.\begin{array}{lll} \text{For} & \sigma = \frac{1}{4} & \beta = 0{\cdot}5374 \quad \text{(M.P.II)} \\ \text{while for} & \sigma = \frac{1}{3} \quad \text{we estimate} & \beta = 0{\cdot}415 \end{array}\right\} \tag{18}$$

Combining (14) and (16) gives

$$W = \beta \frac{2\pi^2 a^4 \gamma^2}{C_{44}(C_{11}/\rho)^{1/2}} \int_0^\infty w^2 |P(w)|^2\, dw \tag{19}$$

which is analogous to the expression (31) of M.P.II for the average rate of energy generating in the solid for a periodic force. Equation (19) may be re-written

$$W = \frac{8\beta(1+\sigma)}{\rho C_0^3} \left\{\frac{1-\sigma^2}{1-2\sigma}\right\}^{1/2} \int_0^\infty w^2 |f(w)|^2\, dw \tag{20}$$

where $C_0 = (E/\rho)^{1/2}$ is the velocity of longitudinal waves in a thin rod and where $f(w)$ is the Fourier component of the total force $f(t) = \pi a^2 P(t)$, i.e.

$$f(w) = (2\pi)^{-1} \int_{-\infty}^{\infty} f(t)\, e^{-iwt}\, dt = \pi a^2 P(w). \tag{21}$$

A simple application of (20) relevant to the elastic collision problem, is given by the pulse shape

$$\left.\begin{array}{ll} f(t) = M_0 \cos(w_0 t) & |t| \leqslant \pi/2w_0 \\ = 0 & |t| \geqslant \pi/2w_0 \end{array}\right\} \tag{22}$$

We have

$$f(w) = \frac{M_0}{2\pi} \int_{-\pi/2w_0}^{\pi/2w_0} \cos(w_0 t)\, e^{-iwt}\, dt$$

$$= \frac{M_0 w_0}{\pi} \frac{\cos(w\pi/2w_0)}{w_0^2 - w^2} \tag{23}$$

whence

$$W = \frac{8\beta(1+\sigma)}{\rho C_0^3} \left\{\frac{1-\sigma^2}{1-2\sigma}\right\}^{1/2} \frac{M_0^2 w_0}{\pi^2} \int_0^\infty \frac{z^2 \cos^2(\pi z/2)}{(z^2-1)^2}\, dz. \tag{24}$$

The integral may be evaluated by considering the real part of

$$\tfrac{1}{4} \int_C \frac{z^2 (e^{i\pi z} + 1)}{(z^2 - 1)^2}\, dz$$

where C is a closed contour defined by the entire real axis and the semi-circle at infinity in the first and second quadrant of the Z plane. The integral around the semi-circle vanishes while the

integrand possesses simple poles at the points $Z = \pm 1$ with residues

$$\text{Residue}\,(\pm 1) = -i\pi/4$$

Thus, by CAUCHY's theorem,

$$\int_0^\infty \frac{z^2 \cos^2(\pi z/2)}{(z^2-1)^2}\,dz = \frac{\pi i}{4}\left[-\frac{i\pi}{4} - \frac{i\pi}{4}\right] = \frac{\pi^2}{8}. \tag{25}$$

Inserting this value into (24), there results

$$W = \frac{\beta(1+\sigma)}{\rho C_0^3}\left(\frac{1-\sigma^2}{1-2\sigma}\right)^{1/2} M_0^2 u_0. \tag{26}$$

3. THE HERTZ THEORY OF IMPACT

The analysis of HERTZ (for a readily accessible account see LOVE (1944)) for the treatment of the collision of two elastic bodies proceeds from the assumption that the stress system in the vicinity of the region of contact may be determined from the stress equilibrium equations, i.e. with neglect of inertial or stress wave effects. In this manner, for example, the following equations are obtained for the description of the collision of a mass m_1 with the plane surface of a mass m :

$$\left.\begin{aligned} P(r,t) &= \frac{2(1-r^2/b^2)^{1/2} z}{\pi b g}, \qquad r \leqslant b \\ &= 0 \qquad\qquad\qquad\quad r > b \end{aligned}\right\} \tag{27}$$

$$b^2 = RZ. \tag{28}$$

Here Z is the distance of approach of the centres of mass of m and m_1 measured from origin at the initiation of contact, R is the radius of curvature of the mass m_1 in the region of contact,* and $P(r,t)$ is the normal distribution of stress over the contact circle of radius b. Finally, the constant g is defined by the elastic properties of the system; in an obvious notation

$$g = \left(\frac{1-\sigma^2}{E} + \frac{1-\sigma_1^2}{E_1}\right). \tag{29}$$

The total force between the two bodies is

$$f(t) = -2\pi \int_0^b P(r,t)\, r\,dr = -\frac{4bZ}{3g} = -\frac{4}{3g} R^{1/2} Z^{3/2} \tag{30}$$

on using (28) to eliminate b. Equating (30) to the rate of change of momentum of the two bodies yields a differential equation for Z

$$\left(\frac{mm_1}{m+m_1}\right)\ddot{Z} = -\frac{4}{3g} R^{1/2} Z^{3/2}$$

with solution

$$\frac{Z}{Z_0} = \phi(V_0 t/Z_0) \tag{31}$$

where $\phi(q)$ is defined by the inverse relation

* For simplicity m_1 is assumed to possess identical principal radii of curvature in the region of contact.

$$q = \int_0^{\phi} \frac{d\nu}{(1 - \nu^{5/2})^{1/2}}, \tag{32}$$

Z_0 is the maximum value of Z attained during the collision, viz.

$$Z_0 = \left(\tfrac{15}{16}\left[\frac{mm_1}{m + m_1}\right]g\right)^{2/5} R^{-1/5}\, V_0^{4/5} \tag{33}$$

and V_0 is the initial velocity of impact. Finally, the total duration of contact is given by

$$T = \frac{2Z_0}{V_0}\int_0^1 \frac{dq}{(1 - q^{5/2})^{1/2}} = 2{\cdot}94\, Z_0/V_0$$

$$= K V_0^{-1/5} \tag{34}$$

where

$$K = 2{\cdot}94\left(\tfrac{15}{16}\frac{mm_1}{m + m_1}g\right)^{2/5} R^{-1/5}. \tag{35}$$

It does not seem possible to express $\phi(q)$ explicitly in finite terms; a graphical solution of (32) obtained by numerical integration is displayed in the full curve of Fig. 1.

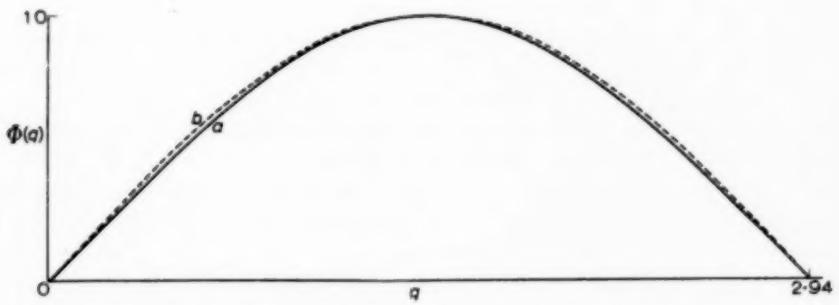

Fig. 1. Comparison of $\phi(q)$ with sine approximation. (a) $q = \int_0^{\phi} \frac{d\nu}{(1 - \nu^{5/2})^{1/2}}$ (b) $\phi = \sin(1{\cdot}068q)$.

It is of some importance to note that a particular consequence of the quasi-stationary nature of the HERTZ approximation is that the elastic energy of the two bodies acquired during the collision process is entirely reversible, the approach and recessional velocities of impact are identical and the restitution coefficient unity.

LOVE (1944) states the condition for the validity of the HERTZ approximation to be " that the duration of impact should be a large multiple of the gravest period of free vibration of either body which involves compression at the place in question." The physical basis for the LOVE criterion is that in order for a quasi-stationary approximation to hold, there must be sufficient time for the passage of large numbers of elastic waves back and forth along the relevant directions (i.e. those directions involving compression in the contact region) of the two bodies. For two bodies with dimensions and radii of curvature in the region of contact of comparable

order of magnitude, and for which the elastic moduli and densities are likewise similar, the LOVE criterion is reducible to a simple restriction on the velocity of impact,

$$(V_0/C_0)^{1/5} \ll 1, \tag{36}$$

providing an upper limit of order $3 \times 10^{-5}\, C_0$ on the acceptable values of V_0.

As appears subsequently, the LOVE criterion is unduly restrictive and the HERTZ theory of impact is readily extendable to the collision of a small body with a massive one. Experimental evidence for the validity of the HERTZ criterion in the latter case has been obtained from observations on the collision of steel ball bearings with the plane face of a massive steel specimen. The relation between impact velocity and duration of contact followed closely the theoretical prediction of equation (34) and (35), the constant K being evaluated in the limit $m \to \infty$, viz.

$$K = 2{\cdot}94 \left(\frac{15\, m_1}{16}\, g\right)^{2/5} R^{-1/5}$$

where m_1 is here the mass and R the radius of the ball bearing. The theoretical explanation of the agreement with the HERTZ theory under these circumstances follows from the realization that a quasi-stationary state of the massive specimen can arise from outgoing waves alone. This possibility has been demonstrated (HUNTER 1954) for the somewhat similar problem of the propagation of spherically-symmetric outgoing waves generated by transient pressure pulses at the internal cavity face of an infinite medium. For this problem the time required for the medium to respond quasi-statically to a step function pressure pulse is of order $2a/C_0$ where a is the cavity radius. Returning to the impact problem, we expect the corresponding time to be of order $t_1 = 2R/C_0$.

For a mass m_1 whose dimensions and radius of curvature are of comparable magnitude and whose density and elastic properties are not too dissimilar from those of the massive body, we have

$$\frac{t_1}{T} \sim (V_0/C_0)^{1/5}.$$

It follows that the response of the massive body is of a quasi-stationary nature provided the velocity of impact V_0 satisfies the restriction

$$(V_0/C_0)^{1/5} \ll 1. \tag{37}$$

Since this inequality also follows from applying the LOVE restriction to m_1, the HERTZ theory may be expected to provide an adequate description of collisions between small and massive bodies at moderate velocities.

This viewpoint is confirmed if we evaluate, in the HERTZ approximation, the loss in kinetic energy of m_1 due to the excitations of elastic vibrations in the massive body. The calculated energy loss is small, thus providing a justifiable first order correction to the unit value of the restitution coefficient given by the basic HERTZ theory.

To estimate the vibrational energy of the massive body subsequent to impact, we make use of the approximation afforded by Fig. 1. In this graph the full line shows the function $\phi(q)$ calculated by numerical integration of equation (32) while the dotted line is the approximation

$$\phi(q) \simeq \sin(1{\cdot}068\, q)$$

which we shall use in the subsequent calculations. Therefore from (31) and (32)

$$Z = Z_0 \sin(1{\cdot}068\ V_0 t/Z_0)$$

and the force between the two bodies is given by

$$\left.\begin{aligned} f(t) &= m_1 \ddot{Z} \\ &= -m_1 Z_0 w_0^2 \sin(w_0 t) \\ &= 0 \end{aligned}\right\} \quad \begin{aligned} &0 \leqslant t \leqslant \pi/w_0 \\ &t < 0, \quad t > \pi/w_0 \end{aligned} \tag{38}$$

where

$$w_0 = 1{\cdot}068\,(V_0/Z_0). \tag{39}$$

By moving the origin of time forward through $\pi/2w_0$, (38) may be re-written

$$\begin{aligned} f(t) &= -m_1 Z_0 w_0^2 \cos(w_0 t), && |t| \leqslant \pi/2w_0 \\ &= 0, && |t| > \pi/2w_0 \end{aligned}$$

which is precisely the pulse shape expressed by (22), with

$$M_0 \equiv -m_1 Z_0 w_0^2. \tag{40}$$

Thus, from (39), (40) and (26), the total elastic vibrational energy of the large mass is

$$W = \frac{(1{\cdot}068)^5 \beta(1+\sigma)}{\rho C_0^3} \left(\frac{1-\sigma^2}{1-2\sigma}\right)^{1/2} m_1^2 Z_0^{-3} V_0^5. \tag{41}$$

On substituting for Z_0 from (33) in the limit $m \to \infty$,
i.e.

$$Z_0 = \left\{\tfrac{5}{14} m_1 g\right\}^{2/5} R^{-1/5} V_0^{4/5}$$

there results

$$W = \frac{\tau m_1^{4/5} R^{3/5} g^{-6/5} V_0^{13/5}}{\rho C_0^3} \tag{42}$$

where

$$\tau(\sigma) = (1{\cdot}068)^5 (1+\sigma) \left(\frac{1-\sigma}{1-2\sigma}\right)^{1/2} (\tfrac{6}{15})^{6/5} \beta(\sigma). \tag{43}$$

It is convenient to express (41) as the ratio

$$\frac{W}{\tfrac{1}{2} m_1 V_0^2} \equiv \lambda = \frac{2\tau m_1^{-1/5} R^{3/5} g^{-6/5} V_0^{3/5}}{\rho C_0^3} \tag{44}$$

where $\tfrac{1}{2} m_1 V_0^2$ is the initial kinetic energy of m_1.

For the particular case where m_1 is a sphere of radius R, $m_1 = (4\pi/3) R^3 \rho_1$, we have

$$\lambda = \frac{2\tau (4\pi/3)^{-1/5} \rho_1^{-1/5} g^{-6/5} V_0^{3/5}}{\rho C_0^3} \tag{45}$$

which is independent of R.

With the values

$$E\,(\text{steel}) = 2 \times 10^{12}\ \text{dynes/cm}^2, \qquad E\,(\text{glass}) = 7 \times 10^{11}\ \text{dynes/cm}^2,$$

$$\sigma = \tfrac{1}{3}, \qquad \sigma = \tfrac{1}{4},$$

$$\rho = 7{\cdot}8\ \text{gms/cc}, \qquad \rho = 2{\cdot}6\ \text{gms/cc},$$

$$\tau(\tfrac{1}{3}) = 1{\cdot}35, \qquad \tau\,(\tfrac{1}{4}) = 1{\cdot}38,$$

we find for the collision of ball bearings with steel

$$\lambda = 1{\cdot}04\,(V_0/C_0)^{2/5}, \qquad C_0 = 5 \times 10^5\ \text{cm/sec}, \tag{46}$$

while for the collision of ball bearings with glass

$$\lambda = 1{\cdot}27\,(V_0/C_0)^{2/5}, \qquad C_0 = 5{\cdot}2 \times 10^5\ \text{cm/sec}. \tag{47}$$

It is apparent that for values of (V_0/C_0) satisfying (37), the ratio λ is very small compared to unity and the first order correction to the coefficient of restitution is given by

$$e = (1 - \lambda)^{1/2} \simeq (1 - \lambda/2). \tag{48}$$

The derivation of (44) ignores both the non-uniform stress distribution predicted by equation (27) and the variation of the circle of contact with time; in effect the distributed reaction of the small mass on the larger is replaced by a point force of equivalent strength. At large distances from the contact region, it seems unlikely that the nature of the stress system depends significantly on the precise distribution of normal stress over the contact circle. Since the formula (20) is alternatively derivable from a knowledge of the asymptotic form of the stress system at large distances from the source (c.f. the derivation of equations (28) and (31) of M.P.II), the point force assumption is probably adequate for the calculation of W.

4. Comparison with Experiment

The most recently published results on the collisions of ball bearings with massive bodies are those of Tillet (1954). In particular Tillet has studied the variation of the coefficient of restitution with both velocity of impact and thickness of specimen in the direction normal to impact. For thin specimens it was found that, apart from a small constant discrepancy, the experimental curve of e as a function of V_0 closely followed the theoretical predictions of Zener (1941) who evaluated the energy loss due to flexural vibrations originating in impact. As the thickness of the glass increases so does the restitution coefficient. For the limit where the thickness is sufficient to prevent the first reflected elastic wave returning to the contact area before the impact terminates, we are in the region where Zener's theory necessarily predicts a restitution coefficient of order unity, and where the present analysis becomes applicable. All experimental figures quoted subsequently were obtained under these conditions.

For the impact of ball bearings on glass Tillet quotes the values

$$e = 0{\cdot}985, \qquad V_0 = 90\ \text{cm/sec}, \tag{49}$$

together with the statement that the variation in e for a 300 cm/sec variation in V_0 is of order $\frac{1}{2}$ per cent. The values given by the present theory for a number of velocities V_0 are

$$\left.\begin{aligned} V_0 &= 10 \text{ cm/sec}, \qquad e = 0{\cdot}999 \\ V_0 &= 90 \text{ cm/sec}, \qquad e = 0{\cdot}996 \\ V_0 &= 300 \text{ cm/sec}, \qquad e = 0{\cdot}993 \end{aligned}\right\} \tag{50}$$

The experimental value of e at 90 cm/sec is significantly lower than the theoretical estimate. On the other hand the variation in e over the velocity range 10 cm/sec to 300 cm/sec is approximately 0·006 or of the order $\frac{1}{2}$ per cent quoted above.

For materials other than glass TILLET reports much lower experimental values of e. In particular for steel specimens at velocities sufficiently low to prevent permanent deformation (see footnote in Section 1),

$$e \simeq 0{\cdot}95 \qquad \text{with} \qquad V_0 \sim \text{few cm/sec}$$

whereas the value given by the present calculations is effectively unity. The major loss of energy observed in the collisions of steel on steel is clearly a consequence of some process other than that of elastic wave propagation. At the high rates of strain involved in such collisions the most likely source of energy loss lies in the inelastic or viscous (damping) forces present in the metal (e.g. ZENER 1948).

Crown copyright reserved. Reproduced with the permission of the Controller H.M.S.O.

REFERENCES

DAVIES, R. M.	1949	*Proc. Roy. Soc.* A **197**, 416.
HUNTER, S. C.	1954	Unpublished Ministry of Supply Report.
LAMB, H.	1904	*Phil. Trans. Roy. Soc.* A **203**, 1.
LOVE, A. E. H.	1944	*Mathematical Theory of Elasticity* p. 198 (C.U.P. 4th Edition).
MILLER, G. F. and PURSEY, H.	1954	*Proc. Roy. Soc.* A **223**, 521.
	1955	*Proc. Roy. Soc.* A **233**, 55.
TILLET, J. P. A.	1954	*Proc. Phys. Soc.* B **67**, 677.
ZENER, C.	1941	*Phys. Rev.* **59**, 669.
	1948	*Elasticity and Anelasticity of Metals* (Chicago University Press).

Journal of the Mechanics and Physics of Solids, 1957, Vol. 5, pp. 172 to 181. Pergamon Press Ltd., London

LOW TEMPERATURE BRITTLENESS*

By A. W. MAGNUSSON† and W. M. BALDWIN, JR.†

(*Received 14th January*, 1957)

SUMMARY

W, Cd, Sn, Mo, Fe and Cr become brittle at low temperatures and high strain rates. When the reciprocal of the absolute temperature for full brittleness is plotted vs. log strain-rate, or log time to fracture, straight lines are obtained. These curves extrapolated toward a roughly common value of strain rate, $\dot{\epsilon} \approx 10^{12}$ in./in./min, or time to fracture, $t \approx 10^{-13}$ min, at $1/T = 0$. STROH's theory estimates t (at $1/T = 0$) $\approx 10^{-17}$ min. Zinc is brittle at low temperatures and high strain rates, but the brittle boundary curve extrapolates to a higher strain rate, $\dot{\epsilon} \approx 10^{38}$ in./in./min, or shorter time to fracture, $t \approx 10^{-34}$ min, at $1/T = 0$. Hg, V, Ta. Zr and Ti (all non-face-centred cubic metals) are ductile down to liquid air temperatures and at strains rate equal to 19,000 in./in./min.

1. INTRODUCTION

SOME metals become brittle at low temperatures and at high strain rates (see Fig. 1); e.g., tungsten (JEFFRIES 1919, BECHTOLD and SHEWMON 1954, DAVIDENKOV and SHEVANDIN 1938), tin (KALISH and DUNKERLEY 1949), molybdenum (SYKES 1920, BECHTOLD 1954, BECHTOLD and SCOTT 1951, BECHTOLD 1953, RIPLING 1955), steel (JONES and WORLEY 1948, BROWN and BALDWIN 1954, VITMAN and STEPANOV 1939), chromium (WAIN and HENDERSON 1953, SULLY, BRANDES and

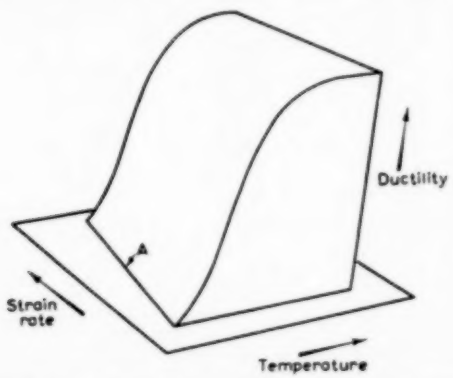

Fig. 1. Schematic diagram relating ductility, temperature and strain rate of a metal which shows low temperature brittleness.

* This paper is based upon a portion of a research programme conducted in the Department of Metallurgical Engineering, Case Institute of Technology, in cooperation with the Office of Naval Research. The data were used as the basis of a thesis submitted by Mr. MAGNUSSON in partial fulfilment for the degree of Master of Science.

† Research Assistant and Research Professor, respectively, Case Institute of Technology, Cleveland, Ohio.

Mitchell 1953, Goodwin, Gilbert, Schwartz and Greenridge 1953, Sully 1954, Wain, Henderson and Johnstone 1954, Johansen and Asai 1954), zinc (Goerens and Mailaender 1927, Ripling and Baldwin 1951), magnesium alloys (Ripling 1954a, Greenwood, Miller and Suiter 1954). In a few of these metals – steel (Morkovin 1944), zinc (Ripling and Baldwin 1951) – the boundary to the brittle zone (line *A* in Fig. 1) has been observed to follow a simple relationship : the line *A* becomes a straight line if the strain rates are plotted on a logarithmic scale and the temperatures are plotted to a reciprocal absolute temperature scale. This report adduces new data and assembles old data pertinent to this curiously regular behaviour.

2. Material and Procedure

Three body-centred cubic metals (tungsten, tantalum and vanadium), three close-packed hexagonal metals (zinc, cadmium and zirconium), one body-centred tetragonal metal (tin), and one rhombohedral metal (mercury) were subjected to tensile tests over a range of temperatures at various strain rates.

The tungsten was pressed and sintered into an ingot and swaged into $\frac{1}{8}$ in. rod from purified powder. Spectrographic analysis of a standard lot of similarly produced metal is : Al – 0·017 %, Co – 0·055 %, Fe – 0·006 %, Ni – 0·006 %, Cu – 0·001 %, Mo – 0·005 %, Si – 0·017 %.

The tantalum in purified powder form was sintered in a high vacuum, hammered, resintered, swaged, rolled into $\frac{1}{8}$ in. rod and annealed. A typical analysis of such material is : Fe – 0·03 %, C – 0·03 %, W and Co less than 0·05 %.

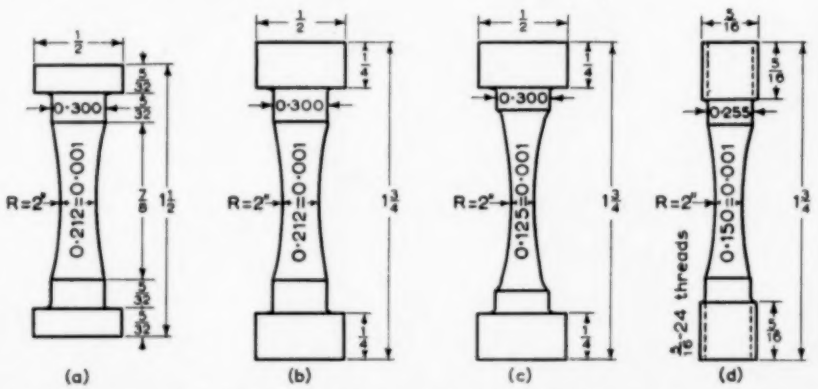

Fig. 2. Tensile specimens used in this investigation : (a) standard unnotched tensile specimen used for zinc, cadmium, tantalum and zirconium ; (b) modified tensile specimen used for tin ; (c) modified tensile specimen used for tungsten ; (d) modified tensile specimen used for vanadium.

The vanadium was arc melted, swaged, rolled into $\frac{1}{8}$ in. rod and annealed. The hydrogen content of this material was approximately 80 p.p.m.

The zirconium was high purity iodide grade. The crystal bar was arc-melted into an ingot, forged, hot rolled and then cold drawn to $\frac{1}{2}$ in. diameter rod. The typical range of impurities in such material is : Al – 30 to 60 p.p.m., C – 100 p.p.m., Fe – 400 to 600 p.p.m., Hf – 100 to 150 p.p.m., Ni – 25 to 60 p.p.m., O – less than 200 p.p.m., Si – 20 to 80 p.p.m., W – less than 100 p.p.m., Ti – 20 to 40 p.p.m.

The other metals – zinc, cadmium and tin – were of commercial high purity obtained as recrystallized $\frac{1}{2}$ in. diameter rods.

The mercury was frozen in liquid nitrogen.

Specimens of the type shown in Fig. 2 were subjected to tensile tests at four different strain rates : 0·05, 10, 100, and 19,000 in./in./min. The 0·05 and 10 in./in./min rates were obtained on a tensile testing machine ; the 100 in./in./min rate on a hydraulic type draw bench with a special fixture ; and the 19,000 in./in./min rate on a drop-hammer. Testing temperatures ranged from − 195°C to + 540°C. In the tests carried out at low strain rates (0·05 and 10 in./in./min) the specimens were held in a low-temperature box containing the cooling liquid, or in a furnace so that the temperature could be kept constant during the test period. At high strain rates (100 and 19,000 in./in./min) the specimens were transferred from the cold liquid or from the furnace and tested while surrounded by air at room temperature. The elapsed transfer and testing time was about four seconds.

The ductility is reported here as per cent reduction in area. Each value represents an average of six measurements of the initial and final diameters with an optical comparator.

From the ductility vs. test temperature plot for each strain rate the critical temperature at which the curve first levelled off at a brittle value was obtained and plotted in reciprocal absolute temperature co-ordinates against the logarithm of the strain rate. The critical temperatures are indicated by arrows in the reduction in area vs. test temperature curves.

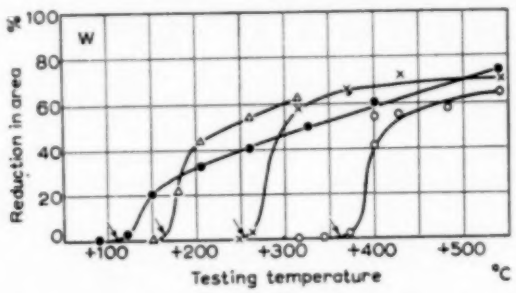

Fig. 3. The effect of temperature and strain rate on the ductility of tungsten. Strain rates : ● 0·05 in./in./min ; △ 10 in./in./min ; × 100 in./in./min ; ○ 19,000 in./in./min.

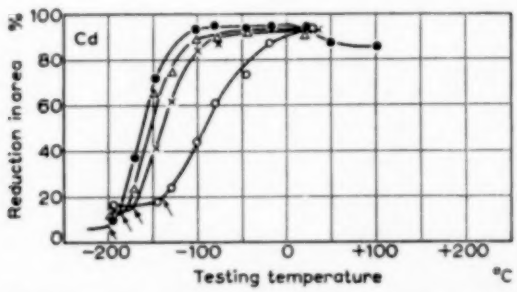

Fig. 4. The effect of temperature and strain rate on the ductility of cadmium. Strain rates : ● ~ 0·05 in./in./min ; △ ~ ~ 10 in./in./min ; × ~ ~ 100 in./in./min ; ○ ~ 19,000 in./in./min.

3. Results and Discussion

Ductility vs. temperature curves for tungsten, cadmium, tin, and zinc are given in Figs. 3 to 6. The temperature and strain rate at which these curves level off to brittle values (as indicated by the arrows in Figs. 3 to 6) are plotted in Arrhenius co-ordinates (log strain-rate vs. reciprocal absolute temperature) in Fig. 7. Good straight lines result. To make certain comparisons with theory later on, an alternate

ordinate scale has been provided : log time to fracture. Most of the brittle boundary points (the temperatures and strain rates indicated by the arrows in Figs. 3 to 6) occurred at fracture strains around ten per cent reduction in area. Theoretically,

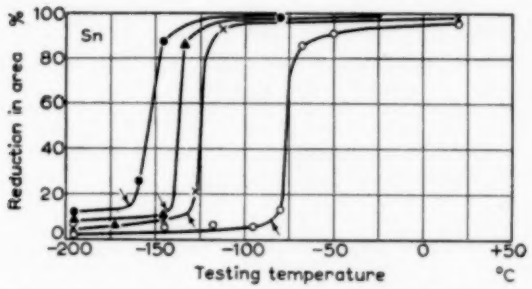

Fig. 5. The effect of temperature and strain rate on the ductility of body-centred tetragonal tin. Strain rates : ● ~ ~ 0·05 in./in./min ; ▲ ~ ~ 10 in./in./min ; × ~ ~ 100 in./in./min ; ○ ~ 19,000 in./in./min.

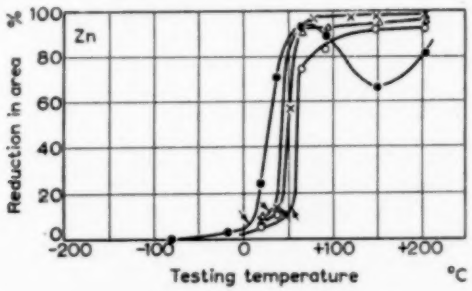

Fig. 6. The effect of testing temperature and strain rate on the ductility of zinc. Strain rates : ● – 0·05 in./in./min ; △ – 10 in./in./min ; × – 100 in./in./min ; ○ – 19,000 in./in./min.

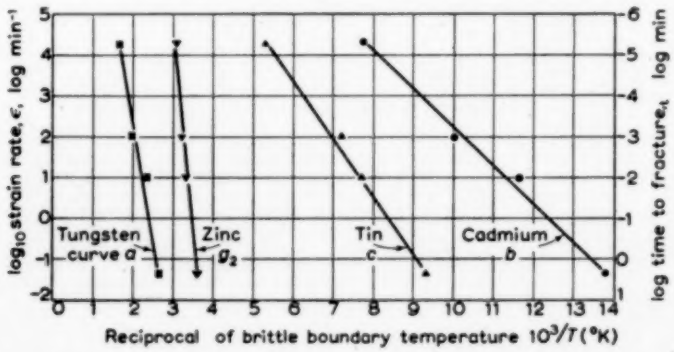

Fig. 7. Brittle boundaries plotted in Arrhenius co-ordinates. Code letters g_2, etc. explained in Table 1.

the conversion between strain rate, $\dot{\epsilon}$, and time to fracture, t, would thus run $t = 0{\cdot}1/\dot{\epsilon}$ and the alternative scale was so constructed. A few experimentally observed times to fracture on zinc pulled at a strain rate of 0·05 min^{-1} and at a

temperature where its ductility was close to ten per cent gave conversion factors running from 0·075 to 0·107.

Brittle boundaries may be constructed from data in the literature for molybdenum (for different grain sizes), steel (both unnotched tensile and unnotched bend tests), chromium (unnotched bend tests), and some magnesium alloys (Fig. 8 and Table 1). In all these cases the ductility vs. temperature curves show a sharp enough transition temperature that the brittle boundary can be chosen without ambiguity with the exception of one magnesium alloy. Here two ductility drops are found with falling temperature. In the present case the brittle boundary is taken at the base of the major ductility drop (points *BB* in Fig. 9).

Table 1. *Summary of information pertaining to Figs.* 7, 8 *and* 10

Metal	*Code Letter in Figs.* 7, 8, 10	*Testing Condition or Prior Treatment*	*Reference*	A, min^{-1}	B, *min*	U, *eV*
Tungsten	a	Swaged	This investigation	$10^{13\cdot5}$	$10^{-14\cdot5}$	1·00
Cadmium	b	Recrystallized	This investigation	$10^{11\cdot7}$	$10^{-12\cdot7}$	0·184
Tin	c	Recrystallized	This investigation	$10^{11\cdot8}$	$10^{-12\cdot8}$	0·30
Molybdenum	d_1	Hot rolled	Ripling (1954)	$10^{14\cdot4}$	$10^{-15\cdot4}$	0·60
Molybdenum	d_2	Recrystallized coarse-grained	Ripling (1954)	10^{11}	10^{-12}	0·80
Molybdenum	d_3	Recrystalilzed fine-grained	Ripling (1954)	$10^{10\cdot5}$	$10^{-11\cdot5}$	0·54
Molybdenum	d_4	Annealed	Bechtold (1954)	$10^{9\cdot3}$	$10^{-10\cdot3}$	0·46
SAE 1095 Steel	e_1	Annealed	Jones & Worley (1948)	$10^{13\cdot2}$	$10^{-14\cdot2}$	0·28
Rimmed Steel	e_2	Hot rolled	Jones & Worley (1948)	$10^{12\cdot7}$	$10^{-13\cdot7}$	0·22
SAE 1020 Steel	e_3	Spheroidized	Brown & Baldwin (1954)	$10^{12\cdot5}$	$10^{-13\cdot5}$	0·20
1035 Steel	e_4*	Hot rolled	Vitman & Stepanov (1939)	$10^{10\cdot7}$	$10^{-11\cdot7}$	0·26
1035 Steel	e_5*	Annealed	Vitman & Stepanov (1939)	$10^{11\cdot1}$	$10^{-12\cdot1}$	0·24
Chromium	f_1*	Annealed	Sully *et al.* (1953)	10^{12}	10^{-13}	0·94
Chromium	f_2*	Annealed	Johansen & Asai (1954)	$10^{11\cdot7}$	$10^{-12\cdot7}$	0·52
Zinc	g_1	Annealed	Ripling & Baldwin (1951)	10^{33}	10^{-34}	1·80
Zinc	g_2	Annealed	This investigation	10^{31}	10^{-32}	1·80
Magnesium Alloy	h_1	Annealed	Greenwood *et al.* (1954)	$10^{11\cdot5}$	$10^{-12\cdot5}$	1·26
AZ-31 Magnesium Alloy	h_2		Ripling (1954a)	$10^{10\cdot9}$	$10^{-10\cdot9}$	0·80

* Brittle boundary curves obtained with bend specimens; brittle boundary curves for other metals obtained with tensile specimens. Tensile strain rate $\dot{\epsilon}$ in outer fibre of bend test converted from rate of deflection $\dot{\eta}$ either by formula $\dot{\epsilon} = 6t\dot{\eta}/L^2$ (where t is specimen thickness and L specimen length for four-point loading) or by empirical formulas taken from replica tests for three-point loading.

All of the Arrhenius curves *with the exception of those for zinc* have one common feature: they extrapolate at $1/T = 0$ to a value of $\epsilon \approx 10^{12}$ min^{-1} or $t \approx 10^{-13}$ min. This is true not only from metal to metal but for a metal with different grain sizes (molybdenum), and for metals tested under different conditions (smooth tensile tests or bend tests on steel, bend tests on chromium, etc.). This is important: it means that in the Arrhenius equations which describe all these curves,

$$\dot{\epsilon} = A\, e^{-U/kT} \tag{1}$$

or

$$t = Be^{U/kT} \tag{2}$$

the constants A and B are roughly the same for all the metals, grain sizes, and test conditions assembled here. On the other hand the *slope* of the individual curves (which correspond to U in (1) or (2)) does change from metal to metal and under different test conditions. Table 1 lists the values of A, B, and U for all the curves of Figs. 7 and 8.

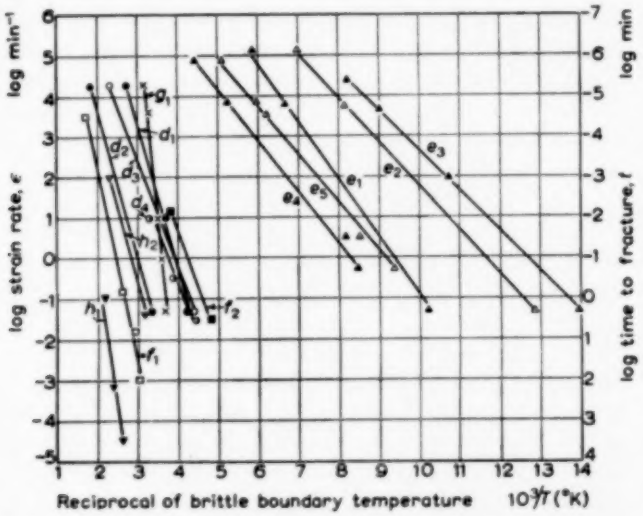

Fig. 8. Brittle boundaries plotted in Arrhenius co-ordinates. Code letters e_3, etc. explained in Table 1. ○ – Molybdenum ; △ – Steel ; □ – Chromium ; ▽ – Magnesium ; × – Zinc.

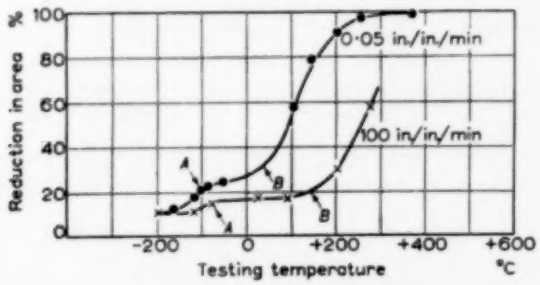

Fig. 9. The effect of testing temperature and strain rate on the ductility of a magnesium alloy showing two ductility drops (at AA and BB) as test temperature is lowered. AZ-31 Magnesium alloy (2·98% Al, 0·95% Zn, 0·45% Mn) Ripling (19).

The Arrhenius relationship between temperature and strain rate for the brittle boundary was first noticed by Morkovin (1944) in Vitman and Stepanov's (1939) data for steel. Yokobori (1952) and Stroh (1955) have given rationalizations of low temperature brittleness based on dislocation theory which lead to (2). Stroh, in particular, assumes a definite model and gains the advantage of being able to

calculate the constants B and U. He assumes that in a deforming metal dislocations pile up at some obstruction. The stress field surrounding this accumulation of dislocations tends to tear other near-by dislocations away from their anchoring solute atoms. They are torn away ultimately by the thermal fluctuations of atoms normally occurring in all metals at temperatures above absolute zero thus furthering the deformation of the metal, but this process requires a time given by

$$t = \frac{b}{\nu l} e^{U(s)/kT}.$$

Here b is the BURGERS vector of the anchored dislocation, l is its length, ν is a frequency factor, k is Boltzmann's constant. U is the activation energy involved in tearing the anchored dislocation away from its pinning atoms; it is a function of the stress which the dislocation pile-up throws onto the anchored dislocation. If in the meantime enough dislocations have continued to accumulate at the original obstruction the stress field surrounding the aggregation may crack the metal open.

In STROH's equation, $b/\nu l$ corresponds to B in (2) and would not be expected to change much from metal to metal or under different test conditions. STROH himself estimates that a fair value for ν is 10^{12} sec^{-1} while a fair value for l/b is about 10^3 giving 10^{-15} sec or about 10^{-17} min as a fair value of B. This is roughly ten thousand times smaller than the experimental value of B. It is doubtful whether B based on the time for fracture and $b/\nu l$ based on the time for a pile-up to build up to fracturing size should be compared. STROH's model undoubtedly should be looked upon as a *unit* process which is enacted (probably in some variety of forms) thousands and thousands of times throughout a metal before one of the tiny microcracks opened by a pile-up of dislocations grows or joins with other microcracks to form the macrocrack that finally breaks the metal and brings deformation to a halt.

Other comparisons between STROH's work and the present data should be made. STROH assumes a value of 0·6 eV for U for steel which accounts for the abnormally high value of 300°K for his transition temperature (strain rate unspecified). The experimental values of U for the five steels listed in Table 1 run between 0·20 to 0·28 eV. It will be noted, too, that the transition temperatures of these steels all run below 300°K depending, of course, on strain rate.

STROH proposes as a measure of the width of the transition range the temperature rise which will change p, where

$$p = \exp\left[-(\nu lt/b)\exp\left\{-U/kt\right\}\right]$$

from 0·9 to 0·1. At a given strain rate (t = constant), and with $A = \nu l/b$ relatively constant, the brittle boundary temperature (which may be associated with the temperature at which $p = 0{\cdot}9$) becomes proportional to U. Accordingly, the temperature rise ΔT necessary to change p from 0·9 to 0·1, i.e., the transition range, becomes proportional to the brittle boundary temperature. The transition ranges taken from the ductility vs. temperature curves (0·05 min^{-1} strain rate) in Figs. 3 to 6 and from similar curves (at the same strain rate) in the literature are plotted against the brittle boundary temperature in Fig. 10. No clear-cut trend is to be found.

The exceptional behaviour of zinc should be noted. To be sure, its brittle boundary is a straight line on log $\dot{\epsilon}$ and $1/T$ co-ordinates but it lies athwart the brittle boundaries of all the other metals, running off to a value of $t \approx 10^{-34}$ min at $1/T = 0$. This oddity must be truly characteristic of zinc for it has been observed before by RIPLING and BALDWIN (1951). It is difficult to rationalize ; the constant B in (2) – with which the value of 10^{-34} min must be identified – in a broad sense is a frequency factor made up of the product of the number of chances per unit

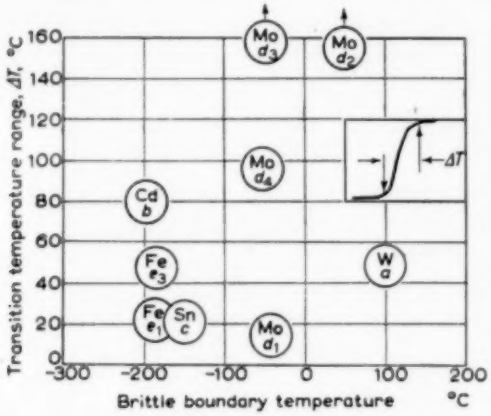

Fig. 10. Transition temperature range plotted against brittle boundary temperature. Code letters e_1, etc., explained in Table 1.

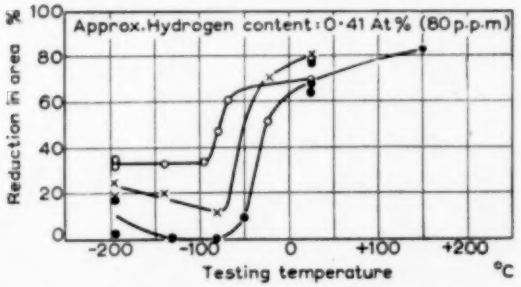

Fig. 11. The effect of testing temperature and strain rate on the ductility of vanadium containing hydrogen. Strain rates : ● ~ 0·05 in./in./min ; × ~ 100 in./in./min ; ○ ~ 19,000 in./in./min.

time the micromechanism responsible for this phenomenon can occur at a given site and the number of sites at which the micromechanism can take place. It is hard to imagine which of these reduces the value of B for zinc by a factor of 10^{-21} from that found for all the other metals of Figs. 7 and 8. The behaviour of zinc is all the more astonishing since cadmium – which has the same crystal structure with virtually the same proportions (c/a ratio) as zinc – behaves orthodoxly.

Lastly, there remains the question of the generality of the behaviour reported here. Although the magnesium alloys studied by GREENWOOD, SUITER and MILLER (1954) and RIPLING (1594) follow the general pattern set by tungsten, etc.,

RIPLING (1954a) points out that commercially pure magnesium behaves in a different manner. He suggests that the drop in ductility of unalloyed magnesium as temperature is lowered is complicated by recrystallization effects.

Vanadium, tantalum, zirconium, titanium, mercury showed no brittleness at all in tensile tests carried out as low as − 196°C and at speeds up to 19,000 in./in./min.* In other words, even though all the metals which showed brittleness in the present study were not face-centred cubic metals (tungsten, cadmium, tin, molybdenum, iron, chromium, and zinc), not all non-face-centred cubic metals (vanadium and tantalum being body-centred cubic, zirconium and titanium being hexagonal, and mercury being rhombohedral) were brittle at the low temperatures or high speeds used in this investigation.

ACKNOWLEDGMENTS

The authors wish to thank the General Electric Company, Cleveland Wire Works, for the tungsten; Fansteel Metallurgical Corporation for the tantalum; Union Carbide and Carbon Corporation, Niagara Works, for the vanadium; and Westinghouse Electric Corporation for the zirconium. E. B. EVANS, GEORGE CONDZER and other members of the Staff of the Department of Metallurgical Engineering, Case Institute of Technology, performed many kind services.

REFERENCES

BECHTOLD, J. H.	1953	*J. Metals* **5**, 1469.
	1954	*Trans. ASM* **46**, 1449.
	1955	*Acta Met.* **3**, 249.
BECHTOLD, J. H. and SCOTT, H.	1951	*J. Electrochem. Soc.* **98**, 495.
BECHTOLD, J. H. and SHEWMON, P. G.	1954	*Trans. ASM* **46**, 397.
BROWN, J. T. and BALDWIN, W. M., JR.	1954	*Trans. AIME* **200**, 298.
DAVIDENKOV, N. and SHEVANDIN, E.	1938	*J. Tech. Physics, USSR* **8**, 1507.
GOERENS, P. and MAILAENDER, R.	1927	*Forsch. Ver. Deut. Ing.* No. 295, 18.
GOODWIN, H. B., GILBERT, R. A., SCHWARTZ, C. M. and GREENRIDGE, C. T.	1953	*J. Electrochem. Soc.* **100**, 152.
GREENWOOD, J. N., MILLER, D. R. and SUITER, J. W.	1954	*Acta Met.* **2**, 250.
JEFFRIES, Z.	1919	*Trans. AIME*, 474.
JOHANSEN, H. and ASAI, G.	1954	*J. Electrochem. Soc.* **101**, 604.
JONES, P. G. and WORLEY, W. J.	1948	*Proc. ASTM* **48**, 648.
KALISH, H. S. and DUNKERLEY, F. J.	1949	*Trans. AIME* **180**, 637.

* We speak here of relatively pure metals. An example of the spurious effects that can be encountered otherwise is offered by vanadium containing about 80 p.p.m. of hydrogen. Ductility drops at low temperature (see Fig. 11). A careful inspection of the curves in Fig. 11 reveals that this is not a case of low temperature brittleness, however: the ductility after dropping with falling temperature then rises albeit slightly (cf. also ROBERTS and ROGERS (to be published)), while at the same time, *increased* test speed moves the " transition temperature " to *lower* temperatures. These features are the same as those found in hydrogen-containing steels (BROWN and BALDWIN (1954)) and are typical of hydrogen embrittlement.

No brittleness was found in commercially pure titanium down to − 196°C and strain rates of 19,000 in/in/min by RIPLING (1954), nor in tantalum at $T = -196$°C and $\dot{\epsilon} = 1{\cdot}68 \times 10^{-2}$ in/in/min by BECHTOLD (1955).

Morkovin, D.	1944	*Trans. ASM* **33**, 221.
Ripling, E. J.	1954	WADC, Technical Report 55-5.
	1954a	Frankford Arsenal Contract No. DA-33-019-ORD-1360, First Phase Report, Case Institute of Technology.
Ripling, E. J. and Baldwin, W. M., Jr.	1951	*Proc. ASTM*, **51**, 1023.
Roberts, B. W. and Rogers, H. C.	1957	*Trans. AIME* (to be published).
Stroh, A. N.	1955	*Phil. Mag.* **46**, 968.
Sully, A. H.	1954	*Creep of Metals* p. 131-151 (Academic Press).
Sully, A. H., Brandes, E. A. and Mitchell, K. W.	1953	*J. Inst. Metals* **81**, 585.
Sykes, W. P.	1920	*Trans. AIME* **64**, 780.
Vitman, F. F. and Stepanov, V. A.	1939	*J. Tech. Physics*, USSR, **9**, 1070.
Wain, H. L. and Henderson, F.	1953	*Proc. Phys. Soc.* **B66**, 515.
Wain, H. L., Henderson, F. and Johnstone, S. T. M.	1954	Commonwealth of Australia, Dept. of Supply. Research and Development Branch, A.R.L./-MET 1.
Yokobori, T.	1952	*J. Phys. Soc. Japan* **7**, 44.

Journal of the Mechanics and Physics of Solids, 1957, Vol. 5, pp. 182 to 192. Pergamon Press Ltd., London

FATIGUE TESTS ON NOTCHED MILD STEEL PLATES WITH MEASUREMENTS OF FATIGUE CRACKS

By N. E. Frost and D. S. Dugdale*
Mechanical Engineering Research Laboratory, East Kilbride

(*Received 6th December*, 1956)

Summary

Fatigue tests have been carried out on steel specimens of section 2·5 in. × 0·3 in. containing edge notches 0·2 in. deep and of various root radius. The growth of cracks from these notches was observed as the tests proceeded. Circumstances for obtaining no cracks, non-propagating cracks and complete failure were determined in terms of root radius, mean stress and stress range.

1. Introduction

The determination of the strength of a notched specimen tested under fatigue loading has been the subject of much published work. The subject is, of course, of the greatest practical importance in engineering, as all machine parts must necessarily contain fillets, keyways, oil-holes, etc. Experimentally, the greater number of recent researches on notch effects have been carried out with small cylindrical specimens containing circumferential notches tested in rotating bending. The main purpose of such work is to devise a sound method for predicting the fatigue strength of a notched specimen from a knowledge of the fatigue strength of un-notched specimens. For this purpose it is usual to employ the theoretical stress concentration factor K_t calculated from the geometry of the notch by assuming perfect elasticity.

Experimental results may be expressed by a strength reduction factor K_f derived from the usual S–N curves for plain and notched specimens. To do this it is necessary to compare either true fatigue limits or fatigue strengths at a conventional number of cycles, say 10 million. Due to the difficulty which has been found in reconciling, for any given notch, the theoretical value K_t with the experimentally determined value K_f, many relations, based on various hypotheses, have been suggested (Yen and Dolan 1952). Briefly, two features of the experimental results seem to cause difficulty. First, it is well known that K_f may be equal to but more generally is less than K_t, the difference between them increasing as K_t increases. Secondly, for geometrically similar specimens K_f approaches more nearly to K_t as the size of the specimen increases. It would appear desirable to keep separate the possible reasons for these two effects but in the past they have frequently been considered together.

*Now at University College, Swansea.

Current explanations of the discrepancy between K_f and K_t seem to fall into two groups. In the first group, it is supposed that plastic flow causes a redistribution of stress in the vicinity of the notch, so that the actual maximum stress is no longer equal to the theoretical elastic stress (FORREST 1956). The second group presupposes some kind of size-effect, which may include one or more of the following hypotheses :-

(a) The critical stress must be considered to act over a finite length or volume of material (NEUBER 1946).

(b) The small volume of material at the root of a notch can withstand higher stresses than the bulk material, before either fatigue failure or static yielding will occur (SHAW 1952).

(c) Strength is dependent on the maximum elastic stress gradient (SIEBEL and STIELER 1955).

(d) The smaller the volume of material the less likelihood of it containing flaws.

(e) Grains situated at the root of a notch are more effectively supported by their neighbours and can withstand higher stresses before cracking than grains situated on the surface of a parallel-sided specimen (VITOVEC 1953).

While the possible importance of these considerations in relation to the initial formation of a crack is fully acknowledged, emphasis is placed in the present work on studying the circumstances under which a crack once formed propagates to cause failure.

Recent investigations by FENNER *et al.* (1951), FROST (1955a), using cylindrical specimens with circumferential vee notches, have shown that when unbroken notched specimens which had been subjected to large numbers of stress reversals were examined, the material at the notch root was cracked, although the crack had not propagated to cause failure. It has also been shown (FROST 1955b) that in the case of zero mean load a critical notch severity existed at which these non-propagating cracks formed.

This means that when a series of fatigue tests have been carried out on notched specimens and a conventional S–N curve obtained, specimens usually denoted as " unbroken " may

(a) contain no crack at all, or

(b) contain a crack at the root of the notch which has failed to develop.

Therefore, for a complete understanding of the problem, observation of the material at the notch root is of the utmost importance.

With this requirement in mind, tests have been carried out on plate specimens containing edge notches. This allows continuous microscopic examination of the material at the notch root. Such an examination was not possible with the cylindrical type of specimens mentioned previously. ROS and EICHINGER (1950) carried out tests on plate specimens of mild steel and aluminium alloy with various edge notches. Their results on the former material show the same trend as those given in this paper; however, they did not examine the material at the notch root in detail, and so the arguments put forward by these authors to explain their results must be considered incomplete.

2. Experimental Details

The mild steel used was supplied in the form of plates 0·5 in. thick measuring 8 ft × 4 ft, hot-rolled and normalized. The chemical composition was: carbon 0·22%; sulphur 0·036%; phosphoros 0·022%; manganese 0·51%. Tensile tests on strips of section 1 in. × ½ in. cut from the normalized plate gave a yield stress of 19 tons/sq. in. and a tensile strength of 28 tons/sq. in. with an elongation of 45% measured on a 2 in. gauge length. Numerous polished and etched sections prepared in the course of the work showed that the microstructure was quite normal, and that no large inclusions were present.

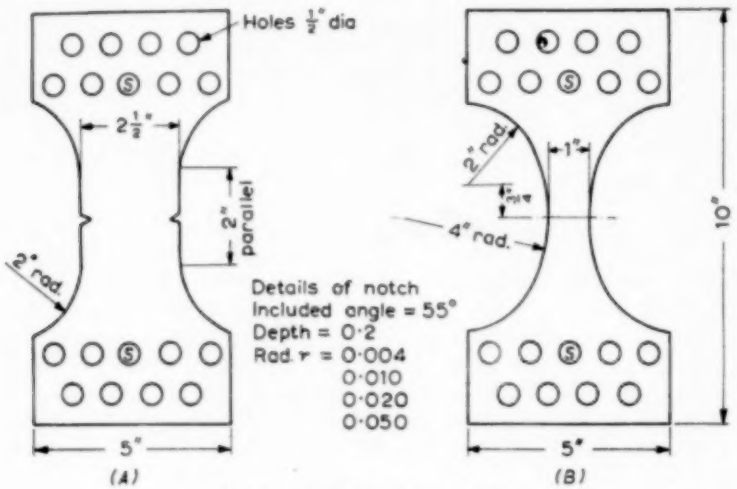

Fig. 1. Fatigue test specimens.

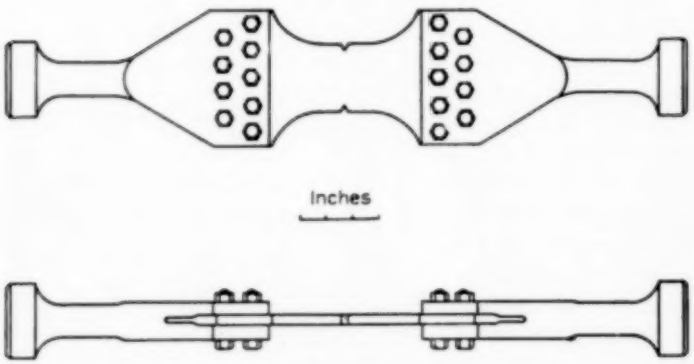

Fig. 2. Method of gripping plate specimens.

Fatigue specimens were cut from the plates such that their longitudinal direction coincided with the direction of rolling and were machined all over to give a thickness of 0·3 in. with grinding as a finishing operation. Previous experience of testing sheets under static and alternating loads suggested for the notched specimens the profile shown in Fig. 1 (a). The ends of the specimen were drilled for clamping in a Schenck-type fatigue machine by means of the fork-ends shown in Fig. 2. One hole at each end (marked *S* in Fig. 1) was bored to size to take a fitted bolt, the other holes being bored $\frac{1}{32}$ in. oversize. The clamps were fitted in the fatigue machine so that the specimen lay in the vertical plane. This allowed easy inspection of the notch roots. When

each specimen was inserted, care was taken that it slipped freely into the fork-ends with a clearance of the order of 0·002 in. These precautions ensured that no bending stresses were introduced into the specimen while it was being fixed in the machine. To check the stress distribution across the test section, Huggenberger extensometers were fitted to an unnotched specimen and a series of static loads applied. It was found that the stress did not vary more than $\pm$ 3 per cent from the average, across the central section.

A large radius was used for the profile of the plain specimen as shown in Fig. 1 (b). At the minimum section, the theoretical elastic stress concentration factor due to the radius was estimated at 1·08.

Vee-type notches were formed with a grinding wheel dressed to the required radius; they were 0·2 in. deep with an included angle of 55° and radii of 0·004, 0·010, 0·020 and 0·050 in. respectively. When all machining operations had been completed, the specimens were stress-relieved by heating them in vacuo for one hour at 650°C.

The usual procedure for fatigue-testing was followed. The Schenck machines ran at about 2,000 cycles per minute, the specimens being subjected to direct stress. Tests were carried out both with zero mean load and with various superimposed tensile and compressive mean loads.

To facilitate detection of a crack when it formed, the sides of the specimen were lightly polished with fine emery paper just before testing. The area around the root of each notch was strongly illuminated, and periodically examined (while the machine was running) by means of a small hand-microscope. The microscope gave a magnification of about 10, and had a graduated scale reading in millimetres. These arrangements were found to be quite satisfactory, and there was never any doubt about the true extent of the crack. All specimens remaining unbroken were cut up, and the section containing the notches was metallurgically mounted. When these sections were polished, and if necessary etched, they were examined under magnifications up to 500. Where it is stated that no crack was present, the statement is based on an examination of this kind. Confidence can be placed in this method for showing up a crack clearly even though it may be less than 0·001 in. long.

3. Elastic Stress Concentration Factors

Tests for developing machine parts usually require specimens that simulate these parts in shape. However, tests for investigating basic characteristics of stress-raisers demand a simple form of specimen which will allow a fairly reliable analysis of stress. For the present work, a plate type of specimen was favoured, both because the stress system is initially a simple one and because of the ease of observing the progress of a crack. When the depth of notch is small in relation to the width of specimen (i.e. when the notch is " shallow "), the stress concentration factor is decided by the depth and root-radius of the notch. While it is often preferable from a mathematical point of view to consider nominal stresses based on the full section, it is usually more acceptable to engineers to express results as stresses based on the reduced section. Theoretical stress concentration factors worked out on this basis as given by Inglis (1913), Neuber (1946), and Peterson (1953), are shown in Table 1.

Table 1.

Root radius (in.)	*Inglis*	*Neuber*	*Peterson*
0·004	12·7	12·2	12·5
0·010	8·3	7·8	8·2
0·020	6·1	5·8	6·1
0·050	4·2	3·7	4·0

4. Experimental Results

It is conventional to present results of fatigue tests in the form of S–N curves. For notched specimens, however, these curves do not give any information about whether or not cracks are present in specimens stressed below the fatigue limit, nor do they indicate the relative periods occupied by initiation and propagation of the crack that finally leads to fracture. As the main object of this work was to investigate the formation of cracks, it appeared that little would be gained by testing specimens at high stresses to obtain the usual S–N curve. Stresses were therefore restricted to values around the fatigue limit, and special attention was given to the effect of mean load.

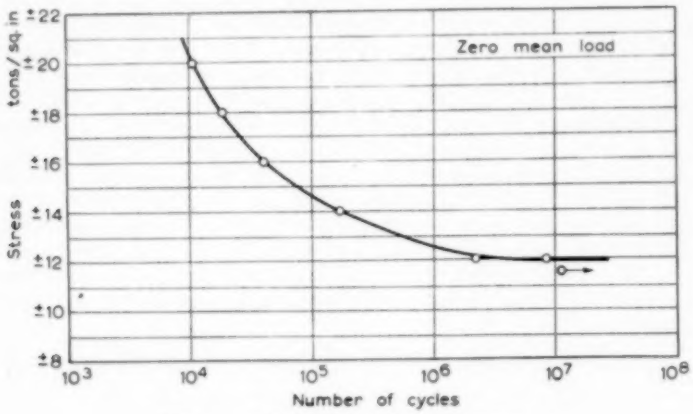

Fig. 3. S–N curve for plain specimens.

The results for the plain specimens, which were tested only under zero mean load, are plotted on Fig. 3. These give a nominal fatigue limit of $\pm$ 11·9 tons/sq. in. As this was obtained with a stress concentration of 1·08 present, it is considered that the true plain fatigue limit should be taken as $\pm$ 13 tons/sq. in.

The results for plates having notches of various severities are given in Table 2. Corresponding curves of the crack growth for some of the plates are shown in Figs. 4 and 5. The crack length shown is the average of the four measured lengths, one on each side of each notch. Only a selection of the curves obtained can be shown here but these are quite typical. Lengths of crack were measured only for the purpose of ascertaining whether or not the crack was growing, and not for the purpose of measuring rates of growth. The shape of specimen is not ideal for such work.

In a plain specimen subjected to a constant stress range above the fatigue limit, failure normally follows soon after the appearance of the first crack. However, if a mild steel specimen does not break within about 10 million cycles, it is unlikely that fracture will subsequently occur. This suggests that cracks will not appear in mild steel after about 10 million cycles, so this was taken as a suitable endurance for determining whether a crack was going to form or not at the root of the notch. When a crack was observed during the test, the test was prolonged to at least 15 million cycles. At the lower stresses, however, it was sometimes

found that although no cracks could be detected during the test, they were revealed on subsequent examination of mounted sections under high magnification.

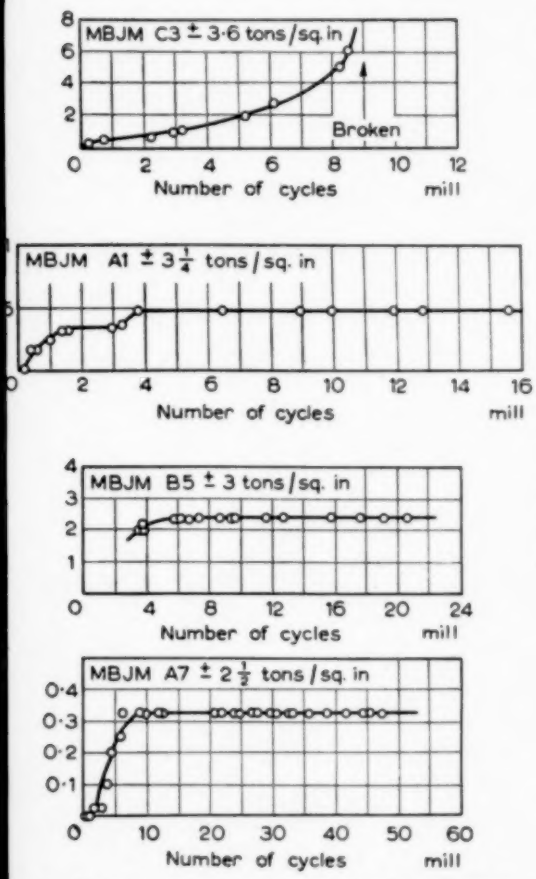

Fig. 4. Curves of crack growth notched mild steel plate 0·010 in. root radii.

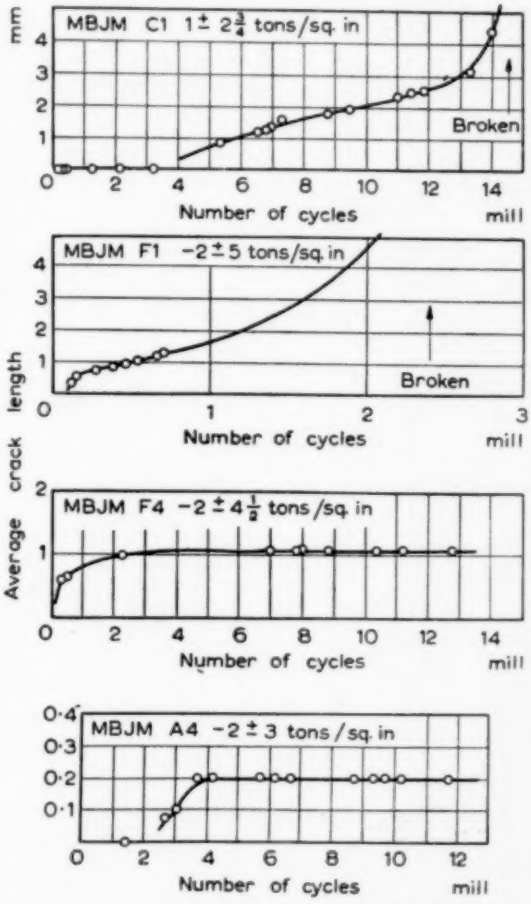

Fig. 5. Curves of crack growth notched mild steel plate 0·020 in. root radii.

5. Discussion

The previous work (Fenner *et al.* 1951, Frost 1955a, 1955b) concerned with non-propagating cracks had utilized cylindrical specimens. With such specimens proof that a particular crack is non-propagating cannot be absolute as microscopic examination of such a specimen results in its destruction. One of the main purposes of the present paper was to overcome this difficulty and present definite proof on this question.

The crack growth curves (Figs. 4 and 5) show clearly whether or not any particular crack is propagating. For example, one of the curves represents a test in which after 10×10^6 cycles the curve is absolutely flat up to 50×10^6 cycles. Fig. 6 shows micro-photographs of two such non-propagating cracks.

At stresses near the critical propagating stress the crack growth was not continuous but tended to proceed in jumps. Perhaps this is not surprising as any

Table 2. *Results of notched mild steel plates*

Specimen mark MBJM	*Applied nominal stresses, tons/sq. in.*	*Nominal maximum tensile stress in cycle tons/sq. in.*	*Cycles, millions*	*Remarks*
0·004 in. root radius				
MBJM A6	$2 \pm 1\frac{3}{4}$	$3\frac{3}{4}$	3·431	Broken
C2	$1 \pm 2{\cdot}3$	3·3	9·540	Broken
B7	$0 \pm 3\frac{1}{4}$	$3\frac{1}{4}$	9·146	Broken
C4	0 ± 3	3	16·056	Unbroken but cracked
H1	1 ± 2	3	10·358	Unbroken but cracked
H5	0 ± 2	2	13·229	Unbroken but cracked
G2	$0 \pm 1\frac{1}{2}$	$1\frac{1}{2}$	11·227	Uncracked
C7	$2 \pm 1\frac{1}{4}$	$3\frac{1}{4}$	13·900	Uncracked
C6	$0 \pm 1\frac{1}{4}$	$1\frac{1}{4}$	10·904	Uncracked
0·010 in. root radius				
MBJM B4	0 ± 5	5	0·224	Broken
G3	2 ± 3	5	3·660	Broken
F6	$2 \pm 2\frac{1}{2}$	$4\frac{1}{2}$	6·258	Broken
B8	0 ± 4	4	1·271	Broken
B9	0 ± 4	4	1·876	Broken
H6	2 ± 2	4	13·545	Broken
H4	$1 \pm 2\frac{3}{4}$	$3\frac{3}{4}$	12·023	Broken
C3	$0 \pm 3{\cdot}6$	3·6	9·023	Broken
G7	$1 \pm 2\frac{1}{2}$	$3\frac{1}{2}$	26·251	Unbroken but cracked
A1	$0 \pm 3\frac{1}{4}$	$3\frac{1}{4}$	15·529	Unbroken but cracked
B5	0 ± 3	3	20·560	Unbroken but cracked
G6	-1 ± 4	3	12·727	Unbroken but cracked
A7	$0 \pm 2\frac{1}{4}$	$2\frac{1}{4}$	47·346	Unbroken but cracked
B1	0 ± 2	2	20·670	Unbroken but cracked
B3	-1 ± 2	1	11·938	Uncracked
G4	$2 \pm 1\frac{3}{4}$	$3\frac{3}{4}$	16·075	Uncracked
F7	$1 \pm 1\frac{1}{4}$	$2\frac{1}{4}$	11·650	Uncracked
0·020 in. root radius				
MBJM C1	$1 \pm 2\frac{3}{4}$	$3\frac{3}{4}$	14·570	Broken
C5	$0 \pm 3\frac{1}{2}$	$3\frac{1}{2}$	7·058	Broken
A2	$0 \pm 3\frac{1}{4}$	$3\frac{1}{4}$	22·079	Broken
F1	-2 ± 5	3	2·407	Broken
A3	0 ± 3	3	15·613	Unbroken but cracked
A9	$0 \pm 2\frac{3}{4}$	$2\frac{3}{4}$	17·996	Unbroken but cracked
F4	$-2 \pm 4\frac{1}{2}$	$2\frac{1}{2}$	12·740	Unbroken but cracked
A4	-2 ± 3	1	11·757	Unbroken but cracked
F2	$1 \pm 2\frac{1}{2}$	$3\frac{1}{2}$	10·845	Uncracked
F8	$-2 \pm 2\frac{1}{2}$	$\frac{1}{2}$	10·320	Uncracked
A8	$0 \pm 2\frac{1}{4}$	$2\frac{1}{4}$	11·720	Uncracked
0·030 in. root radius				
G1	0 ± 5	5	0·784	Broken
E4	0 ± 4	4	7·799	Broken
H3	-4 ± 6	2	12·857	Broken
E1	-2 ± 5	3	18·659	Unbroken but cracked
F3	-4 ± 5	1	18·817	Unbroken but cracked
E5	$-2 \pm 3\frac{1}{2}$	$1\frac{1}{2}$	10·625	Uncracked
E2	$0 \pm 3\frac{1}{4}$	$3\frac{1}{4}$	11·538	Uncracked

small irregularity in the applied stresses or in the material might be sufficient here to either start or stop the growth.

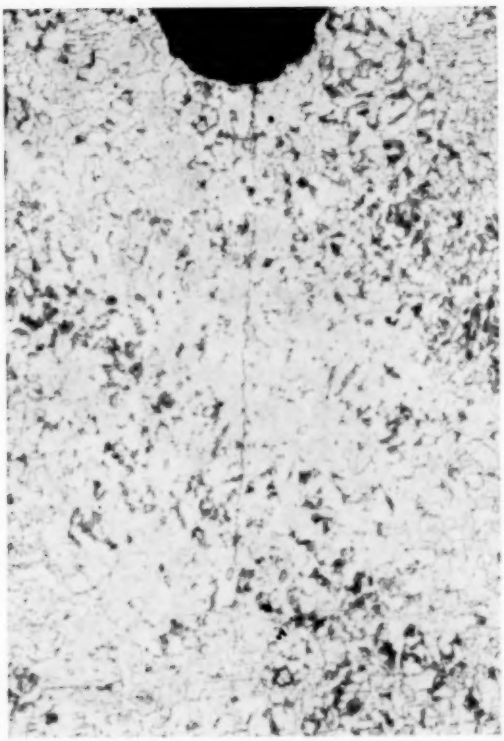

Fig. 6. (a) Specimen MBJM C4 × 100 ± 3 tons/sq. in. $16{\cdot}056 \times 10^6$ cycles.

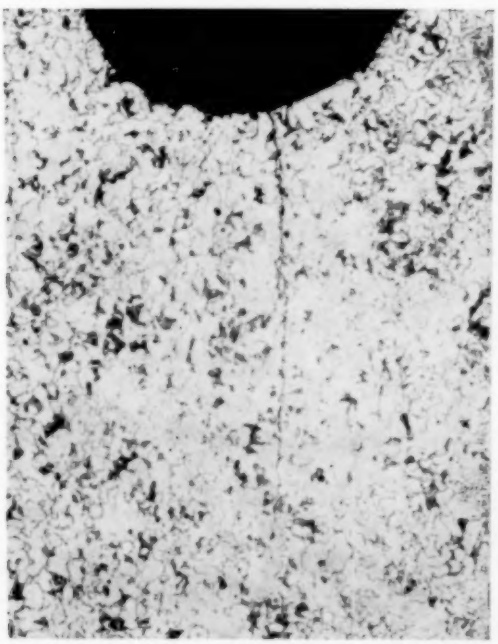

(b) Specimen MBJM G6 × 100 —1 ± 4 tons/sq. in. $12{\cdot}727 \times 10^6$ cycles.

The present work shows conclusively that it is possible for a crack to be quite stationary and not creeping slowly forward as suggested for instance by LESSELLS and JACQUES (1950).

The values of alternating stress, mean stress, and maximum tensile stress required to produce cracking and fracture are shown in Table 2 and Figs. 7 and 8. When a crack has been formed, a certain minimum nominal stress is required before the crack will extend to cause fracture. If the applied nominal stress is

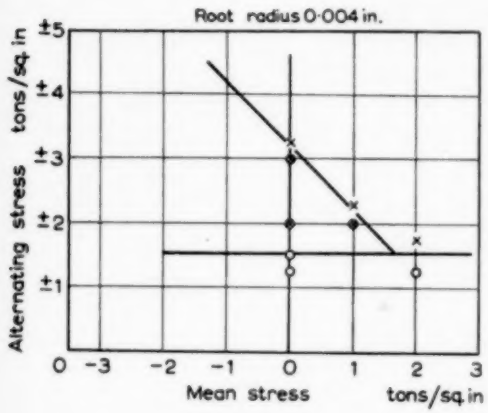

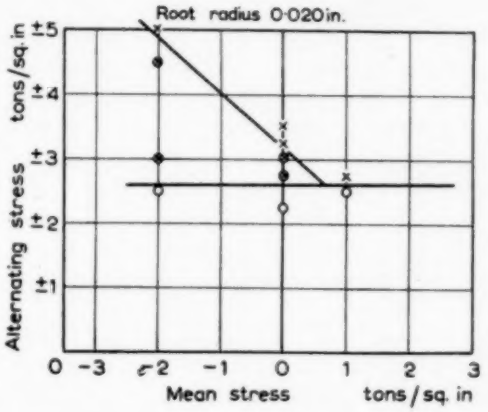

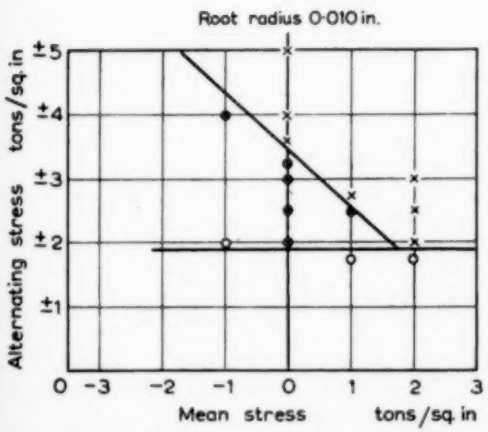

Fig. 7. Mild steel plate MBJM. Relation between alternating stress and mean stress. X broken; ⊕ Unbroken but cracked; ⊙ Uncracked.

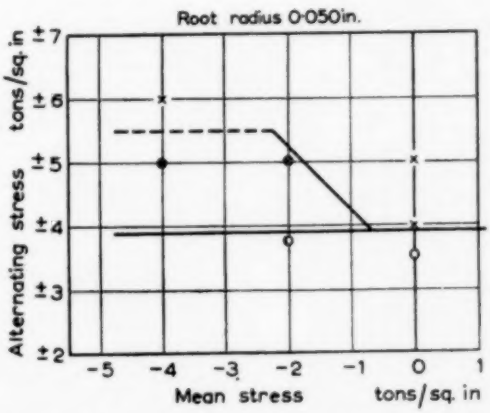

Fig. 8. Mild steel plate MBJM. Relation between alternating stress and mean stress. X Broken; ⊕ Unbroken but cracked; ○ Uncracked.

less than this, the crack will be non-propagating. The conditions governing initial cracking and subsequent spreading of the crack seem to be quite distinct. Dealing first with the condition for spreading a crack, the experimental results obtained over a range of mean stress $p = +2$ to -2 tons/sq. in., give the following equations for the required amplitude of alternating stress f:

Radius 0·004 in. $f = \pm (3{\cdot}20 - 1{\cdot}00p)$ tons/sq. in.

Radius 0·010 in. $f = \pm (3{\cdot}45 - 0{\cdot}90p)$ tons/sq. in.

Radius 0·020 in. $f = \pm (3{\cdot}20 - 0{\cdot}85p)$ tons/sq. in.

Radius 0·050 in. $f = \pm (3{\cdot}25 - 1{\cdot}00p)$ tons/sq. in.

In other words, within normal experimental errors, a fatigue crack will continue to grow when the greatest tensile stress in the cycle exceeds about $3\frac{1}{4}$ tons/sq. in. and this value is independent of the notch root radius. This empirical rule seems to break down when the mean compressive stress is too great, as shown by the dotted line in Fig. 8 for the notch of 0·050 in. root radius.

Turning now to the values of stress required to initiate a crack in the notch root, the horizontal lines drawn in Figs. 7 and 8 seem to be quite compatible with the experimental points. This means that over the range of mean stresses considered the initiation of the crack is governed by the value of the applied alternating stress. Hence the Figures show that the region where non-propagating cracks are formed is that bounded by the two full lines. It is interesting to note that for all radii except the 0·050 in. it is possible to form non-propagating cracks with zero mean load.

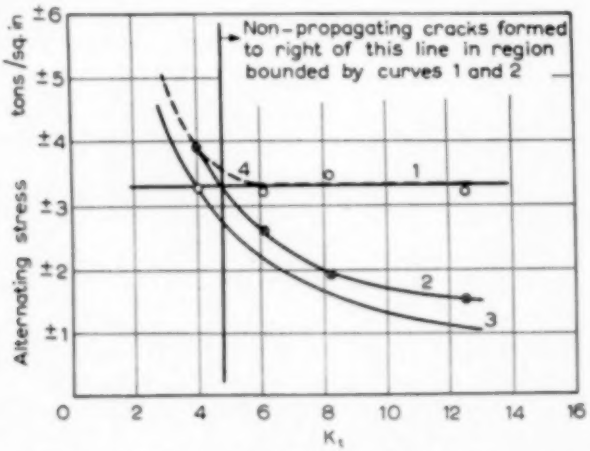

Fig. 9. Fatigue strength and K_t for zero mean load. (1) Stress to propagate crack; (2) Stress to initiate crack; (3) Theoretical curve ± 13 tons/sq. in./K_t; (4) Dotted line represents nominal fatigue limit based on broken specimens.

It may be useful in conclusion to discuss the results in relation to the conventional factors K_t and K_f'. Values for zero mean load shown in Figs. 7 and 8 are replotted in Fig. 9, the notch root radius being represented here by its appropriate K_t value. In this Figure, the horizontal line (1) represents the stress required to propagate a crack, curve (2) the experimental values of stress required to initiate a crack, curve (3) the theoretical stress to initiate a crack, obtained by dividing the fatigue limit for plain specimens by the theoretical stress concentration factor K_t, and curve (4) the conventional nominal fatigue limit. The point on curve (1)

for the 0·050 in. root radius notch is an extrapolated value, since at zero mean load a crack is not initiated until an alternating stress represented by the corresponding point on curve (2) is applied; once formed, however, the crack will propagate at the stress given by curve (1). To the left of the vertical line shown in Fig. 9 the initiation stress is higher than the propagating stress and a crack once formed must grow, while to the right of the line the propagating stress is higher than the initiation stress and non-propagating cracks can form at all stresses between curves (1) and (2).

Previous workers in this field have tried to obtain relations between K_t and K_f by comparing curves (3) and (4). Because there is such a wide divergence between the curves a large number of relations have been put forward based on the hypotheses mentioned in the Introduction. It is now obvious from Fig. 9 that such relations have but little meaning, unless considered in conjunction with such a figure. Curve (4) is composed of two parts: to the left of the vertical line it coincides with curve (2) and to the right of the vertical line with curve (1). Any relation involving the intrinsic fatigue properties can only be used to compare curves (3) and (2). It can be seen that these curves are of similar form and the small displacement between them may be due to plasticity and size effects.

The critical value of K_t (i.e. the value below which a non-propagating crack cannot be formed at zero mean load given by the vertical line shown in Fig. 9) is approximately equal to 5. This agrees with the results of tests on round bars with circumferencial notches carried out by Frost (1955b).

6. Conclusions

1. Observations have confirmed that cracks in mild steel can remain unchanged in length for many millions of stress cycles, i.e. that they can be truly non-propagating.

2. Consistent agreement was found between the minimum amplitude of alternating stress required to cause initial cracking at the notch root and the stress calculated conjointly from the plain specimen fatigue limit and the theoretical stress concentration factor.

3. The stress required to propagate a crack once it is formed was found to be independent of notch root radius. Over the range of mean stress examined, viz. 2 tons/sq. in. compression to 2 tons/sq. in. tension, cracks appeared to propagate whenever the maximum tensile stress of the cycle exceeded $3\frac{1}{4}$ tons/sq. in. These are nominal stresses based on the minimum cross-sectional area of specimen.

4. Many of the relations between K_f and K_t found in the literature cannot be expected to have a very wide range of validity. Indeed there can be no direct relation when non-propagating cracks are present.

Acknowledgments

The authors acknowledge the interest and advice of Mr. C. E. Phillips, Head of the Mechanics and Materials Division. The work has been carried out as part of the research programme of the Mechanical Engineering Research Board of the Department of Scientific and Industrial Research. The article is published by permission of the Director of Mechanical Engineering Research.

References

Fenner, A. J., Owen, N. B. and Phillips, C. E.	1951	*Engineering* **171**, 637.
Forrest, P. G.	1956	International Conference on Fatigue of Metals, *Inst. Mech. Engrs.*
Frost, N. E.	1955a	*Engineer* **200**, 464 and 501.
	1955b	D.S.I.R. MERL Report PM 184. To be published in *Aero. Quart.*
Inglis, C. E.	1916	*Trans. Inst. Naval Architects* **55**, 219.
Lessells, J. M. and Jacques, H. E.	1950	*Welding Journal* Research Supplement **15** 74s.
Neuber, H.	1946	*Theory of Notch Stresses* (J. S. Edwards, Ann Arbor, Michigan).
Peterson, R. E.	1953	*Stress Concentration Design Factors* Wiley, New York).
Ros, M. and Eichinger, A.	1950	Report No. 173, *E.M.P.A.*, Zurich.
Shaw, M. C.	1952	*J. Franklin Inst.* **254**, 109.
Siebel, E. and Stieler, M.	1955	*Z. Ver. Dtsch. Ing.* **97**, 121.
Vitovec, F. H.	1953	W.A.D.C. Technical Report 53-167.
Yen, C. S. and Dolan, T. J.	1952	University of Illinois Eng. Expt. Station, Bulletin Series No. 398.

Journal of the Mechanics and Physics of Solids, 1957, Vol. 5, pp. 193 to 201. Pergamon Press Ltd., London

PARTIAL SIDEWAYS EXTRUSION FROM A SMOOTH CONTAINER

By W. Johnson
Department of Engineering, University of Manchester

(*Received 14th December*, 1956)

Summary

Except in the case of simple sideways extrusion, die orifices are usually placed at right angles to the direction of the punch movement. Results are presented, covering a narrow range of reductions, of a theoretical investigation, into the effect of inclining the orifice at 60° to this direction and of varying its position along the inclined die face. Further results are given for the instances in which the orifice is variously inclined and with one of its edges coinciding with the container wall.

1. Introduction

The increasing extent to which the extrusion process is being used for the production of parts of unsymmetrical form justifies enquiry into the consequences on the extrusion pressure and flow geometry of unusual locations of the die with respect to the direction of motion of the punch.

This paper gives the results of a theoretical investigation into the plane strain extrusion of sheet (Fig. 1) through a die orifice whose plane is inclined obliquely at $\phi°$ to the walls of the smooth container. That the extruded product does not

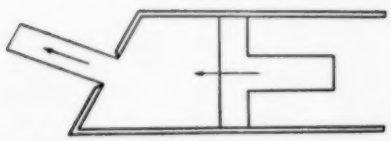

Fig. 1. Diagrammatic representation of a partial sideways extrusion.

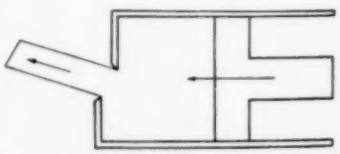

Fig. 2. Extrusion through a square staggered die which is similar to the case in Fig. 1.

emerge at right angles to the orifice depends upon both the relative magnitude of the orifice and its position, or eccentricity, with respect to the container walls. For the range of reductions 0·5 to 0·7 when $\phi = 60°$ an examination is made of the effect of both these factors on the pressure necessary for effecting extrusion and on the consequent speed and direction of the extruded sheet. This is the same problem in many respects as that of extrusion through square dies, the two halves being staggered as in Fig. 2.

GREEN (1955) has given the results of calculations of the pressure, p, versus nominal reduction r' for extrusion through eccentrically placed square dies, $\phi = 90°$ in Fig. 1, and for sideways extrusion $\phi = 0°$. The case examined below in which $\phi = 60°$, falls between the two given by GREEN, and is therefore referred to as " partial sideways extrusion."

2. STRESS AND VELOCITY FIELDS

The theoretical analysis of this problem follows the same pattern as that generally used in plane-strain problems. After making certain assumptions consistent with physical facts, a slip-line or stress field for the given geometrical boundary conditions is first constructed and the consequent velocity field – or hodograph – then drawn and examined. If the two fields are then compatible the solution is an acceptable one. From the first field the extrusion pressure, p (strictly $p/2k$, where k is the yield shear stress in plane strain) is calculated and from the second the resultant velocity of the emerging sheet is obtained. A full account of these techniques is available elsewhere (HILL 1950 and PRAGER 1953).

The details for performing the calculations are given below.

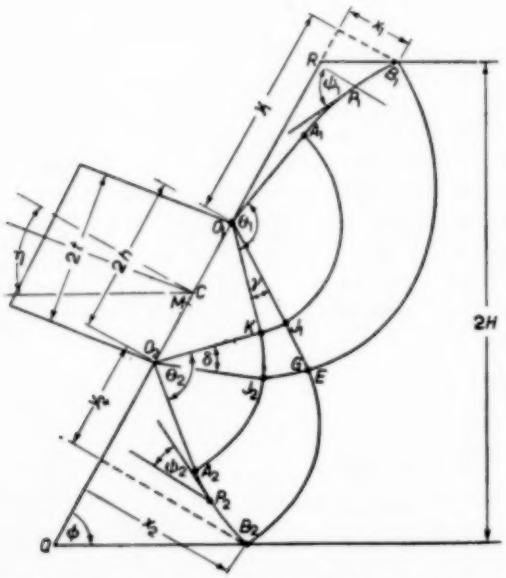

Fig. 3. Diagram defining the quantities required for making the calculation and showing the general shape of the stress field.

(a) *Slip-line field.* The slip-line field proposed for the situation is shown in Fig. 3. There are two regions of dead metal as with symmetrically placed square dies, but they are now of unequal extent; their shape is determined by the form of the field and appears to be a reasonable one to assume.

The field was drawn using a 5° equiangular net, starting from the assumption that there is zero force perpendicular to $O_1 O_2$. At B_1 and B_2, the slip lines meet the

walls at 45°, thus fulfilling the condition that the walls should be perfectly smooth. The actual task of drawing the field was unnecessary, one being available from investigations previously made on square dies (JOHNSON 1955) which was easily adaptable to the present case.

The stress calculations were based on the following expressions which were originally derived by use of the HENCKY equations. The quantities in the equations below will be obvious by reference to Figs. 3 and 5. Treating first the portion of the die face above the orifice, the hydrostatic pressure, p_p, calculated at each point on the dead metal surface is given by

$$p_p = k\,(1 + 4\theta_1 - \pi/2) - 2k\,\psi_1. \tag{1}$$

The total force on this face resolved parallel to the direction of motion of the punch is F_1, where

$$F_1/k = (x_1 \sin\phi + y_1 \cos\phi) + (1 + 4\theta_1 - \pi/2)\,(y_1 \sin\phi - x_1 \cos\phi)$$
$$- 2\,(\sin\phi \int_{O_1}^{B_1} \psi_1\, dy_1 - \cos\phi \int_{O_1}^{B_1} \psi_1\, dx_1). \tag{2}$$

Similarly, the total resolved force F_2 on the face of the lower dead metal zone is given by

$$F_2/k = (x_2 \sin\phi - y_2 \cos\phi) + (1 + 4\theta_2 - \pi/2)\,(y_2 \sin\phi + x_2 \cos\phi)$$
$$- 2\,(\cos\phi \int_{O_2}^{B_2} \psi_2\, dx_2 + \sin\phi \int_{O_2}^{B_2} \psi_2\, dy_2). \tag{3}$$

It follows that the extrusion pressure, p, is given by

$$p/2k = (F_1/k + F_2/k)/4H. \tag{4}$$

It will be observed that once the coordinates (x, y) and the integrals $\int\psi\, dx$ and $\int\psi\, dy$ have been determined, it is easy to complete calculations for different values of ϕ. Also, when $\phi = 90°$, equation (4), with the help of equations (2) and (3), reduces to that originally given by HILL (1948).

It is usual to define the reduction r' as

$$r' = 1 - 2h/2H. \tag{5}$$

where $2h$ is the distance directly across the orifice and $2H$ the original sheet thickness. However, having regard to the fact that the sheet does not emerge at right angles to the orifice and assuming it to be of thickness $2t$, the true reduction, r, is

$$r = 1 - 2t/2H \tag{6}$$

and r' is recognized as a nominal reduction. For the purpose of the calculations it is observed that

$$2H = (y_1 + y_2 + 2h) \sin\phi + (x_2 - x_1) \cos\phi \tag{7}$$

and

$$2t = 2h \sin(\phi + \eta) \tag{8}$$

where η is the angle of inclination of the emergent sheet to the direction of the punch travel.

A further variable in the analysis is the position of the orifice with respect to the die walls, or the eccentricity. This quantity is denoted by e and is defined as

$$e = \frac{CM}{\frac{1}{2}QR} = 1 - \frac{(h + y_2)\sin\phi + x_2\cos\phi}{H} \tag{9}$$

where M is the mid-point of QR and C is the mid-point of $O_1 O_2$ (Fig. 3). This eccentricity may be either negative or positive, according as the orifice centre C is above or below M. The sign of the eccentricity is important since a value of say $e = +0{\cdot}1$ has a quite different effect on the dependent variables from that of $e = -0{\cdot}1$; in GREEN's investigations of eccentricity in square dies, the symmetry in the stress field nullified the effects of the sign of the eccentricity.

(b) *Velocity field.* To the stress field for a given reduction there corresponds a hodograph, and for each value of r' in the stress field a hodograph was constructed. A typical example is shown in Figs. 4 and 5, which are scale diagrams for a reduction of about 0·72; corresponding points in the stress field and hodograph are similarly labelled. It is from the velocity diagram that both the final

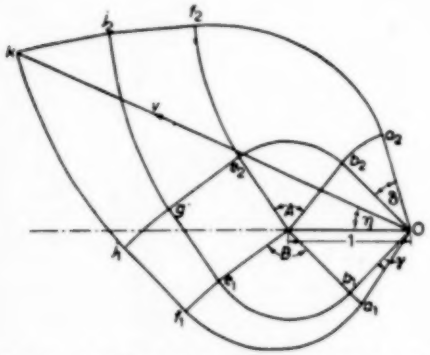

Fig. 4. A hodograph drawn to scale for $\phi = 60°$ and corresponding with the stress field and the geometry of the case in Fig. 5.
$A = 60° - \beta + \alpha$, $B = 120° + \beta - \alpha$.

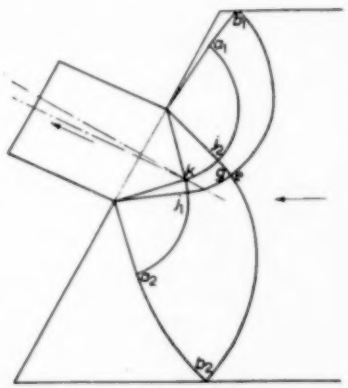

Fig. 5. A slip-line field of the type in Fig. 3 drawn to scale for $r' \sim 0{\cdot}72$ and $e \sim 0{\cdot}12$.

speed, v, and the angle of emergence of the extruded sheet η are found. Having found η, it is then possible to determine r in equation (6).

Further, having thus found r and η it is possible to check by comparison with the stress field diagram that the quantity of material emerging is equal to that being displaced by the punch. This latter check was made for each reduction, the disparity between the results of the slip-line field diagram and the hodograph seldom exceeding 1 per cent.

3. RESULTS

Figs. 6 (a) to (d) show the variation of v, e, η, r and $p/2k$ with r'; curves showing the variation of $p/2k$ with e for certain values of r were deduced. In Figs. 7 (a) to (d) four such curves, $r = 0{\cdot}55$, $0{\cdot}60$, $0{\cdot}65$ and $0{\cdot}70$, are shown. Fig. 8 gives the variation of $p/2k$ with r for different values of e.

The following observations are made in the light of the results of the calculations.

(1) Fig. 8 includes a curve showing $p/2k$ versus r for a square die. It is seen that, for a given reduction, $p/2k$ is always least for the square (unstaggered) die, no matter what the eccentricity of the oblique die.

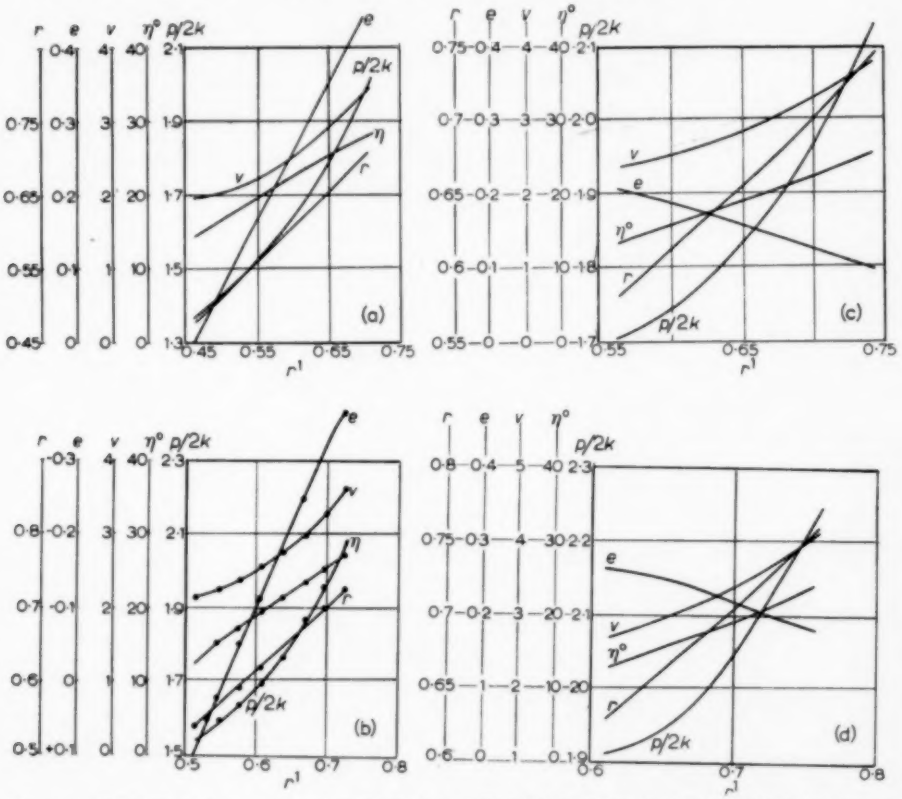

Fig. 6. Variation of v, e, η, r and $p/2k$ with r'. This information is obtained directly from a slip-line field and its corresponding hodograph.

(2) In Fig. 8 it is also seen that positive eccentricities have a much larger effect on the pressure than do negative eccentricities. The calculations show that the values of $p/2k$ for $e = -0{\cdot}2$ are hardly distinguishable from those for $e = -0{\cdot}1$.

(3) The observations in (2) are also well displayed in Fig. 7 where the curves for negative values of e are seen to be almost flat and little affected by the actual magnitude of e; on the other hand, when e is positive, alterations in it have comparatively large effects on the pressure.

(4) The direction of the emergent sheet lies between 13° and 28° to the punch travel direction in all cases; it does not emerge perpendicular to the orifice. There are insufficient points to produce curves showing how η varies with r for given values of e, but it is clear that as the reduction increases, η approaches

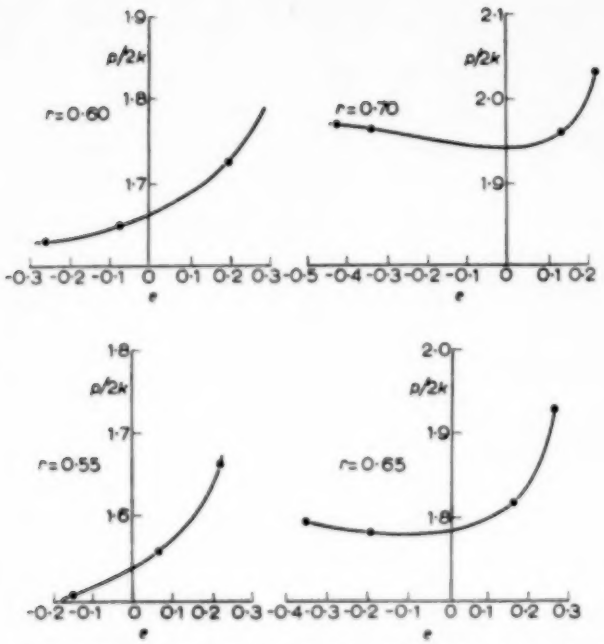

Fig. 7 Variation of $p/2k$ with e derived from Fig. 6 for given values of r.

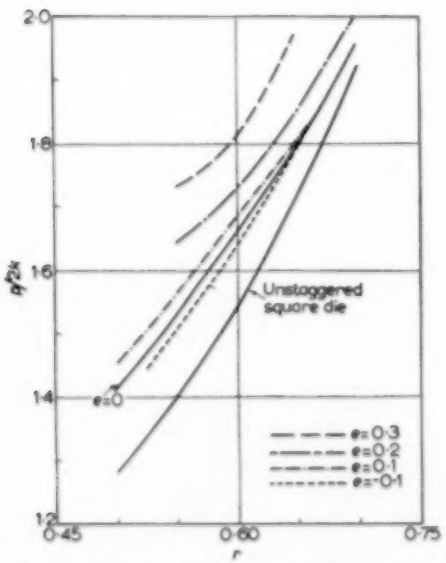

Fig. 8. Variation of $p/2k$ with r derived from Fig. 6 for given values of e.

30°, i.e. the extrusion direction increasingly approaches that of the normal to the plane of the orifice.

(5) For the range of reductions covered in this paper, the ratio r to r' or $2t$ to $2h$, is $\sin(\frac{1}{2}\pi + \eta)$. Thus, for the lower reductions when $r \sim 0{\cdot}55$ and $\eta \sim 14°$, this ratio is least and $\sim 0{\cdot}96$. For larger reductions the ratio approaches unity. While the disparity between r and r' is not of great importance as regards pressure calculations, it may be of major consequence when considering the finishing size of a product.

4. Die Face wholly on one side of Orifice

As a corollary to the above investigation we may consider extrusion through an orifice which is placed at the position of greatest negative eccentricity, that is when the whole of the die face is immediately below the orifice (Fig. 9).

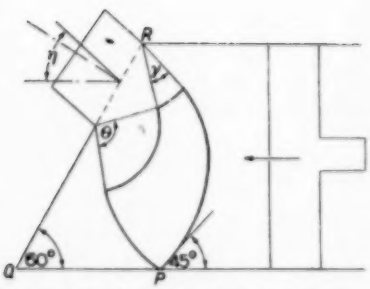

Fig. 9. Slip-line field when the die face is wholly on one side of the orifice.

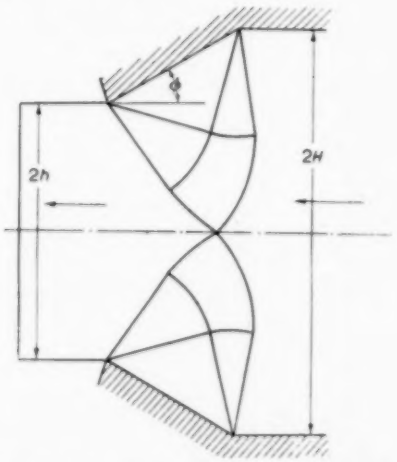

Fig. 10. Slip-line field for extrusion through wedge-shaped die when $r_w < 2\sin\phi/(1 + 2\sin\phi)$.

In this case the die face is presumed to carry a dead metal zone and the slip lines meet the lower smooth container wall at 45°, while the radii from the upper edge of the orifice are drawn such that $\gamma \leqslant 30°$. The slip-line field will be recognized as the lower part of that shown in Fig. 3, and accordingly it follows that the extrusion pressure is given by re-writing (4) as

$$p/2k = (F_2/k)/4H. \tag{10}$$

The quantity F_2/k is available from the previous calculations.

An alternative method exists, however, for determining $p/2k$ here and depends upon the formal similarity of the stress field in Fig. 9 to that for symmetrical extrusion through wedge-shaped dies of small reduction of semi-angle ϕ (Fig. 10). It is not difficult to show that, when the stress field is of the same shape for the two otherwise different physical situations of Figs. 9 and 10,

$$r_w(p/2k) = (p/2k)_w(1 - r_w) \tag{11}$$

where $(p/2k)_w$ refers to the extrusion pressure for the symmetrical wedge-shaped die, and $r_w = 1 - 2d/2D$. JOHNSON (1955) has presented in graphical form the results of calculations showing the variation of $(p/2k)_w$ with r_w for $10° \leqslant \phi \leqslant 90°$, and these may be converted via equation (11) to the present problem, with ϕ no longer restricted to 60°. It is to be noted that since

$$r' = 1 - r_w/\sin\phi \tag{12}$$

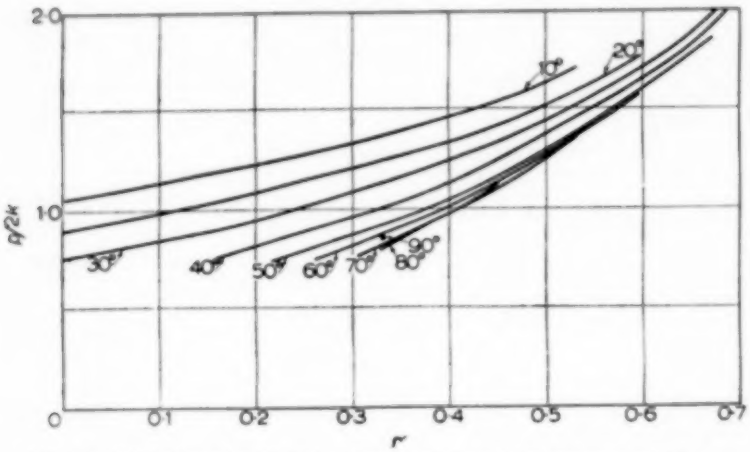

Fig. 11. Variation of $p/2k$ with r' for the stress field of the type in Fig. 9.

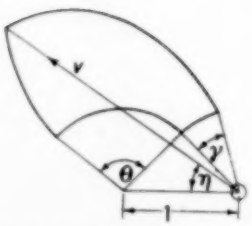

Fig. 12. Velocity field corresponding to stress field in Fig. 9.

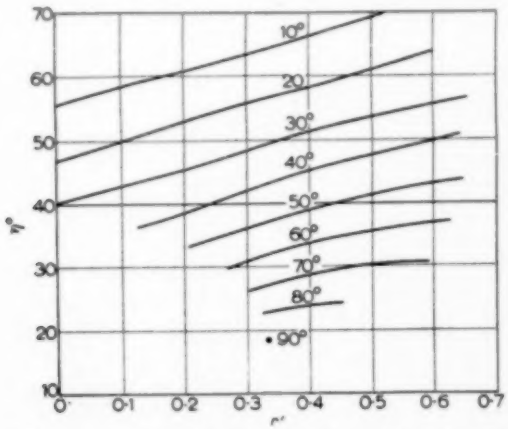

Fig. 13. Showing the variation of η with r' for the stress fields of the type in Fig. 9.

then, particularly for small values of ϕ, it is possible for r' to be zero or even negative. In Fig. 11 the variation of $p/2k$ with r' is given for values of $0 \leqslant r' \leqslant 0{\cdot}70$ for various values ϕ.

The form of the hodograph for this particular type of slip-line field is shown in Fig. 12 and is found to be identical in shape with its own stress field ; accordingly having drawn a stress field in the first place as in Fig. 9, it is a simple matter to take off the required direction η as angle QRP. In Fig. 13 the variation of η with r' for the particular values of ϕ are shown.

If values of r' are considered such that $0{\cdot}6 > r' > 0{\cdot}3$ and $50^\circ > \phi > 35^\circ$, it appears that the sheet emerges almost at right angles to the orifice, i.e. the inclination to the orifice normal is $\chi = (\eta + \phi) \sim 90^\circ$. For almost all the values of r' and ϕ dealt with, χ has no very significant effect in altering the ratio of r/r' from unity. Alternatively, $p/2k$ is insensitive to the changes in χ encountered in this particular type of problem and the difference between the ratio r/r' and unity would only be of importance in an industrial sizing operation, in which case other factors (principally friction) would also require to be considered.

Acknowledgments

The writer wishes to thank Professor J. Diamond for encouragement and interest in the work and B.I.S.R.A. for permission to publish results taken from the original report (Johnson 1956).

References

Green, A. P. 1955 *J. Mech. Phys. Solids* **3**, 189.
Hill, R. 1948 *J. Iron Steel Inst.* **158**, 177.
1950 *The Mathematical Theory of Plasticity* (Clarendon Press).
Johnson, W. 1955 *J. Mech. Phys. Solids* **3**, 177.
1956 *B.I.S.R.A. Report MW/G/86/56.*
Prager, W. 1953 *Trans. Roy. Inst. Stockholm* **65**.

Journal of the Mechanics and Physics of Solids, 1957, Vol. 5, pp. 202 to 214. Pergamon Press Ltd., London

THE PLANE STRAIN EXTRUSION OF SHORT SLUGS

By W. Johnson
Department of Engineering, University of Manchester

(*Received 20th February*, 1957)

Summary

In steady state extrusion the slug remaining to be extruded is required to be longer than the depth of the associated slip-line field; the same field applies when these two lengths are equal if a perfectly rough punch is assumed. This field may next be modified to accommodate shorter slug lengths and the method of doing so is described for the case of square dies. The results of calculations made are presented and show how the extrusion pressure varies with slug length.

Similar proposals are made for modifying the original stress fields of Hill and Tupper for the case of wedge-shaped dies and the calculated deformation of an initially square grid is compared with some experimental results. The possible application of these results to the final phase of the extrusion process as regards the phenomenon of piping and the pressure/punch-travel diagram is discussed.

1. Introduction

The analysis of plane-strain extrusion as a steady motion problem by the use of the theory of slip-line fields has been shown to be capable of providing reasonably good estimates of the pressure required for extrusion (Johnson 1956b) and of the deformation undergone by various parts of the sheet (Green 1955). Two-dimensional extrusion also illuminates various features of axi-symmetric extrusion and, empirically, is moderately successful for studying metal deformation and extrusion pressures in these cases (Purchase and Tupper 1953, Johnson 1955).

There are several respects, however, in which the theory of steady-state extrusion used in analysing experimental results is incomplete, and two of these will be examined in this paper. They are:

(1) that the theoretically predicted pressure takes no account of either slug length or the roughness of the punch.

(2) the fact that so far theory has not yet been related to the problem of piping or coring.

Besides these two points, problems of extrusion have hitherto been treated, in theory, as steady-state ones in which the slug is supposed to be more than long enough to contain the appropriate slip-line field; this field is assumed fixed in space and the velocity at a point in the plastic region does not vary with time. The treatment of the problem as a steady-state one ignores the effect of punch friction and requires the slug to be long. In certain practical cases these conditions may be of major importance, for slugs may have a length only a fraction of their diameter, (compare the analogous case of the manufacture of collapsible tubes), and punch face friction can vary greatly.

It has been observed that to obtain a " proper " extrusion, a certain minimum length of slug is essential (JOHNSON 1954), and slugs exceeding this minimum give autographic or punch load/punch travel diagrams which can be superposed once the pressure required to cause extrusion has been reached; the same dip or kink at the end of the diagram is repeated by each slug if its initial length exceeds this minimum length. For less than this minimum length, however, the form of the autographic diagram varies with the slug length. These facts are well illustrated in the case of axi-symmetric extrusion in Fig. 1 (CHANG 1950

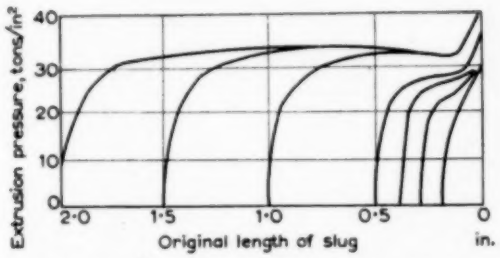

Fig. 1. Punch load – punch travel diagrams for the extrusion of aluminium cylindrical rods from slugs of initial length between 2·0 in. and 0·25 in.

and JOHNSON 1954). It follows that steady state extrusion exists when the slug length is greater than a certain amount and that an unsteady state occurs for slug lengths less than this amount. Thus, with short slugs, an alteration in the length-diameter ratio for a given reduction alters the shape of the plastically deforming region and so generates the unsteady state.

The occurrence of an unsteady state is also important in that the deformation induced at one instant affects that occurring in the next, since stress and velocity fields change continuously. This is important in relation to piping and coring, photographs of which are shown in Fig. 2. The nature of the flow of the metal is such as to cause material which was contiguous with the punch and near (*not on*) the axis of the slug to move away from it and create a void; in fact, two voids are created, one on each side of the axis, and the continued emphasis of this tendency with change in geometry of the slug leads to this pronounced and peculiar phenomenon known as piping. It would appear that the change from steady to unsteady flow marks the onset of piping; this is the stage at which the process often ceases to be of use industrially, and which, if it could be defined exactly for given conditions, would be of considerable value.

Thus, it would seem useful to investigate the unsteady state extrusion of short slugs and to consider its possible repercussions on the final stage of an extrusion operation.

2. Slip-line Field for Short Slugs and Square Dies

In Fig. 3 the slip-line field for an extrusion through square dies in which the reduction, r, exceeds 0·5 is shown. The angle at which the slip-lines meet the container wall takes account of the friction between it and the metal, and is 45°

if there is no friction at one extreme, and 0° and 90° at the other extreme of perfect roughness. For lesser values of the coefficient of friction the angles lie between these extremes. A region of dead metal on the die face is assumed as indicated. When the punch face XY is tangential to the slip-line field, the slip-lines inter-

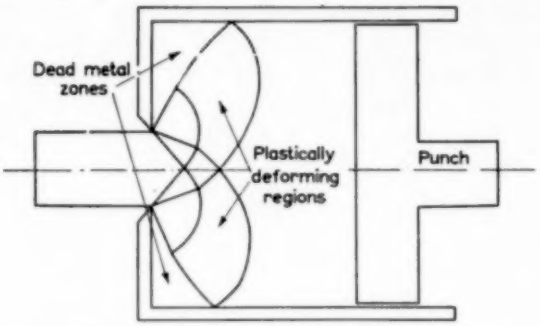

Fig. 3. Steady state slip-line field for a square die, $\tau > 0{\cdot}5$.

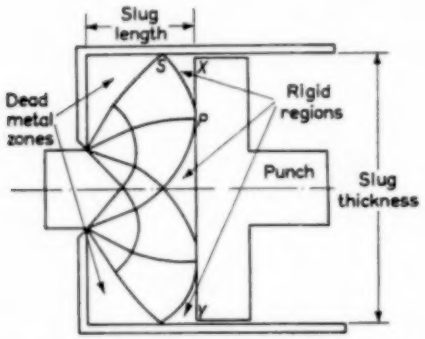

Fig. 4. The slip-line field of Fig. 4 for a case of unsteady state extrusion, assuming the use of a rough punch.

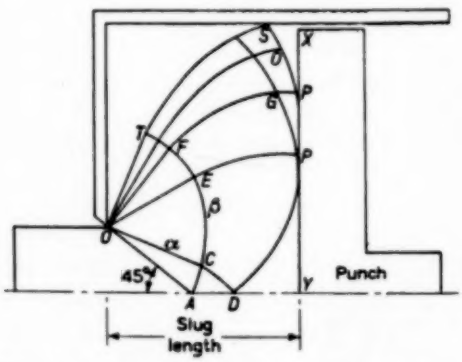

Fig. 5. An unsteady state slip-line field for $\tau > 0{\cdot}5$.

secting the punch normally and tangentially at P, a perfectly rough punch is presumed (see Fig. 4). This kind of field, as originally proposed by HILL (1948), was for steady-state extrusion, but as shown in Fig. 4 it is an incipient unsteady

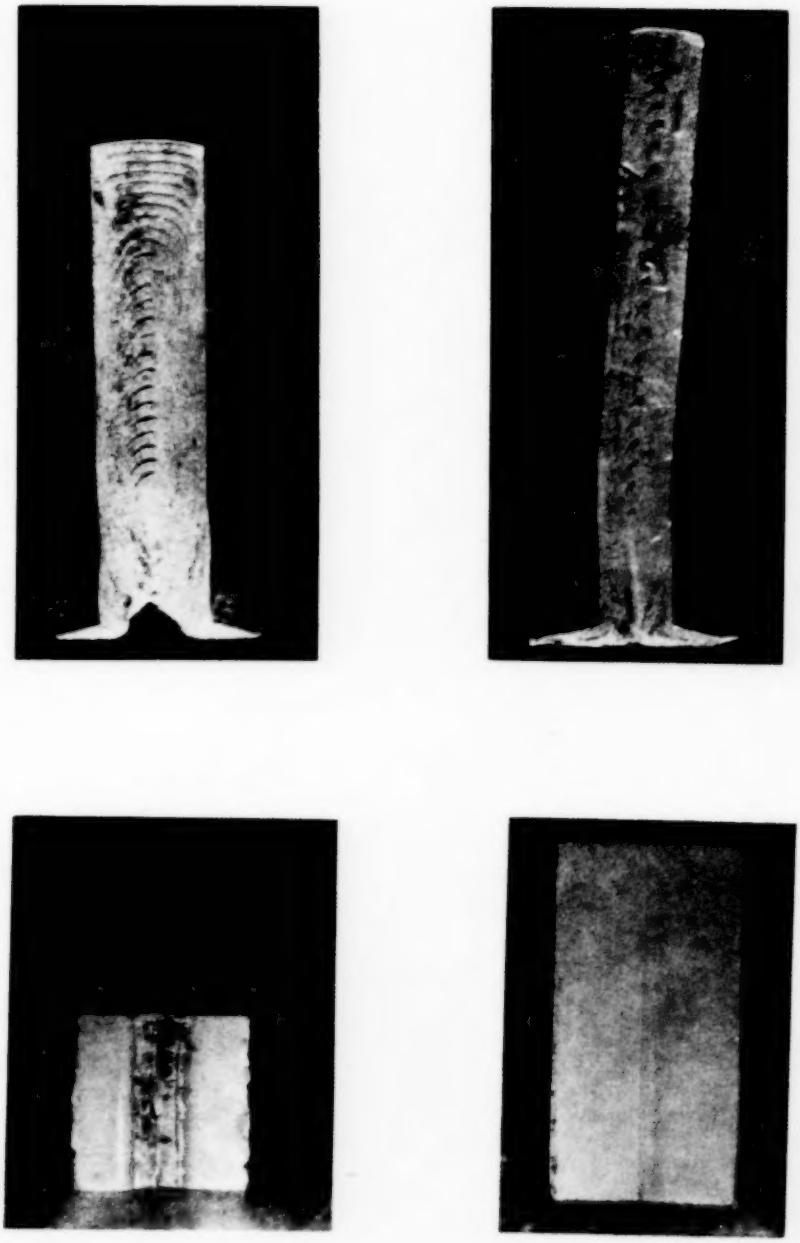

Fig. 2. Photographs showing coring in plane-strain specimens for different reductions for dies at semi-angle 75°.

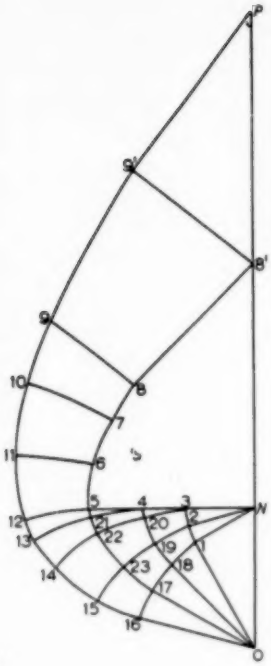

6a.

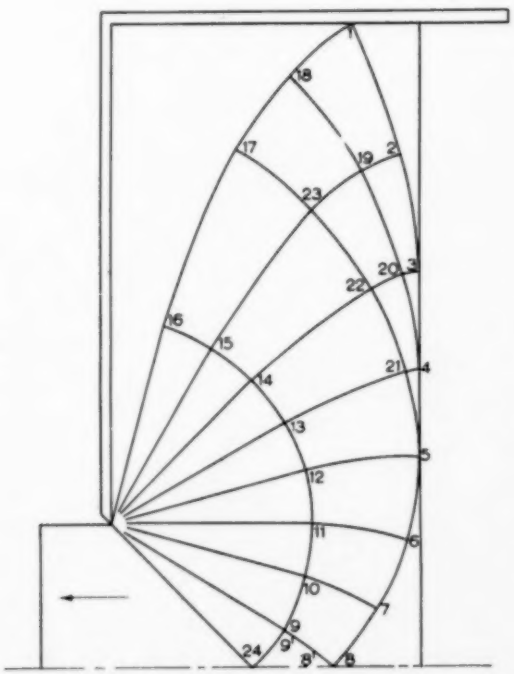

6b.

Fig. 6. Half slip-line fields for slugs of decreasing thickness (*b*), (*c*) and (*d*), and corresponding hodographs (*a*), (*b*), and (*c*), the reduction being the same in all three.

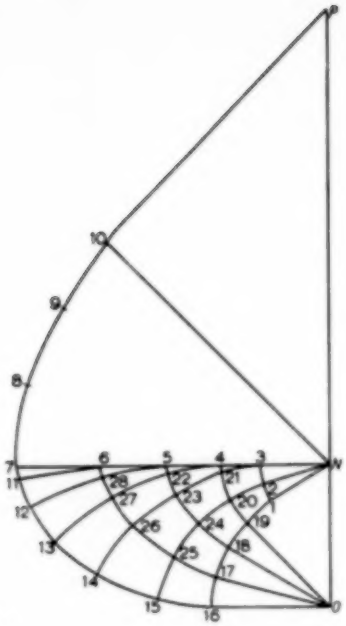
P
10
9
8
7
11
12
13
14
15
16
6
5
4
3
N
28
27
26
25
22
23
24
21
20
18
17
2
1
19
0

6c.

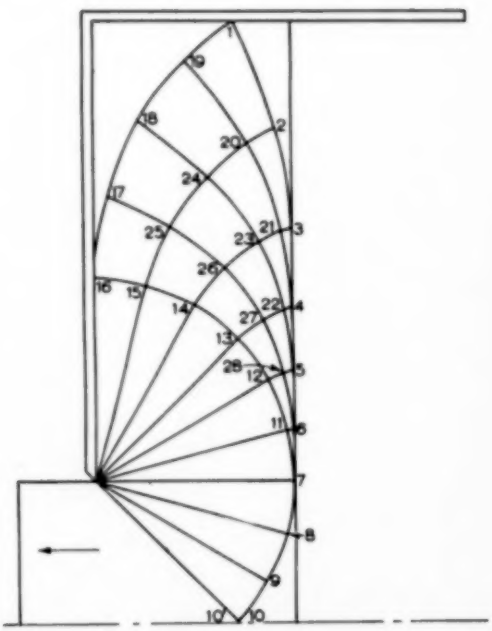
1
19
18
20
2
24
17
25
23
21
3
26
16
15
14
27
22
4
13
28
12
5
11
6
7
8
9
10
10

6d.

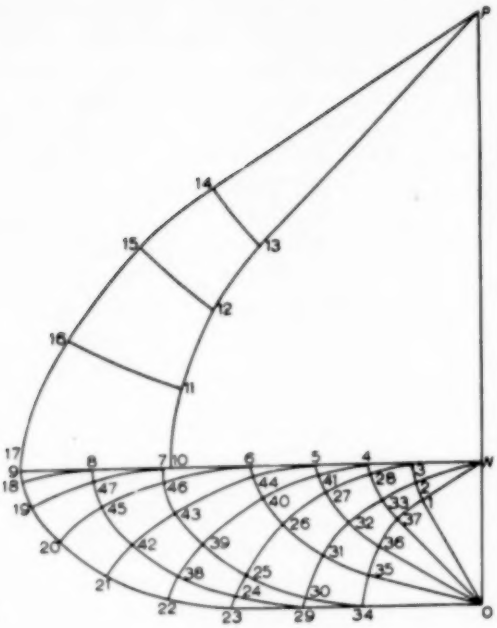
P
14
15
13
12
16
11
17
9
18
19
20
21
22
8
7
10
6
5
4
3
N
47
46
45
44
43
42
41
40
39
38
27
26
25
24
23
29
28
33
32
31
30
34
2
37
36
35
O

6e.

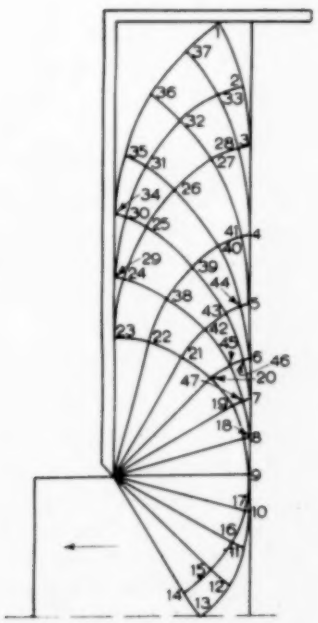
1
37
2
36
33
32
28
3
35
31
27
34
26
30
25
41
4
40
29
24
39
44
38
5
43
42
23
22
21
45
6
46
20
47
7
19
18
8
9
17
10
16
11
15
12
14
13

6f.

state field only applying instantaneously. The extrusion pressure when calculated applies only for the particular length-to-thickness ratio holding at each instant. When the slug length is reduced the slip-line field must be modified accordingly. It is emphasized that at this stage the continuous extrusion of a slug is *not* being considered; modification of the original field is being suggested for slugs of length (assuming constant thickness) less than that shown in Fig. 4. Considering Fig. 5, a centred fan radiates from O, and OA meets the centre line at 45°. OC is extended outwards also to meet the centre line at 45° at D. The field is now developed in the usual way as far as line OEP_1; from G the α-line (HILL'S convention) is extended to meet XY normally at P_2, so that between P_1 and P_2 all the slip-lines meet XY either at right angles or tangentially. The field is next continued outwards from $OFGP_2$ and a line such as P_2QS marks off a rigid block, while OTS defines the reduced extent of the dead metal zone. If the reduction and wall friction is the same for the cases shown in Fig. 4 and Fig. 5, it is to be noted that angle AOC reduces as the slug length decreases. For purposes of illustration a complete set of half-fields, drawn to scale for a reduction about 0·78, is shown in Fig. 6; Figs. 6 (b) and 5 are actually of the same form, and this type of field prevails until the length of the slug has decreased to length OA. The field for the same reduction is then altered to that shown in Fig. 6 (d). For even shorter lengths the field is that of Fig. 6 (f). Half of the hodographs corresponding to each type of slip-line field are shown in Figs. 6 (a), (c) and (e), conveniently rotated through 90°; for if the initial slug speed is numerically equal to the thickness of the emerging sheet, then the speed of the emerging sheet as given by the hodograph should be equal to the original slug thickness.

The types of field shown in Figs. 6 (b) and (d) require no comment about the friction between the die face and the metal, but, in order to treat the case of very thin slugs, OT may have to be allowed to lie along the die face; then shearing is occurring along the die face and the coefficient of friction between it and the metal is at least 0·176.

3. CALCULATION OF EXTRUSION PRESSURES

The variation in extrusion pressure with slug length for smooth and perfectly rough container walls was obtained as follows, using in all cases 15° equiangular nets.

In Fig. 5, if it is supposed that angle AOC is 15°, then the remainder of the field is completed as far as OEP_1, the slip-lines at P_1 being parallel and perpendicular to the slug axis. Next, XY is drawn perpendicular at P_1 to the slug centre line. The field is now extended as described in Section 2. For a rough container wall, extrusion pressure values corresponding to P_2 (i.e. of thickness twice P_2Y) will be for a reduction and a length to thickness ratio differing from those pertaining to P_1. For a selected value of angle OAC, and therefore of absolute length in the actual field drawn, using the HENCKY equations and summing the stresses over, say, $OFGP_2$, the extrusion pressure p can be obtained. For this value of angle AOC a plot of $p/2k$ against x, the length to thickness ratio, is made (k is the yield shear stress of the material in plane strain). An example is shown in Fig. 7 from which, for a particular reduction, corresponding values of $p/2k$ and x are obtained. The same procedure was repeated making angle OAC, 0°, 30°, 45°, etc., extracting

values $p/2k$ versus x for given reductions and then assembling them to determine the variation of $p/2k$ with x.

(i) *Rough container wall.* Terminating the slip-line field at P_1, P_2, etc. Fig. 5 pre-supposes a rough container wall. The " assembled values " referred to for reductions between 0·5 and 0·85 are shown in Fig. 8 ; the chain lines join together the points derived for the same individual values of angle AOC, while values on line NM are those appertaining to the steady-state problem.

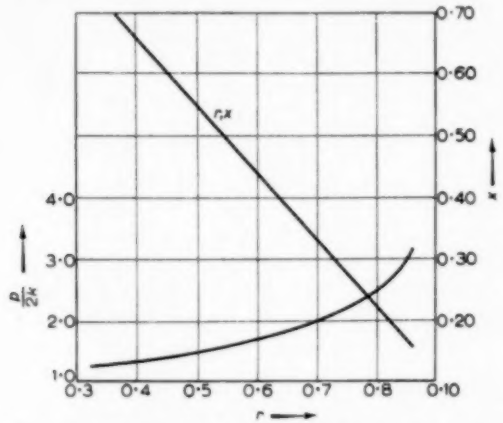

Fig. 7. An example of the calculated results obtained from one particular form of stress-field. The lower curve corresponds to r, $p/2k$.

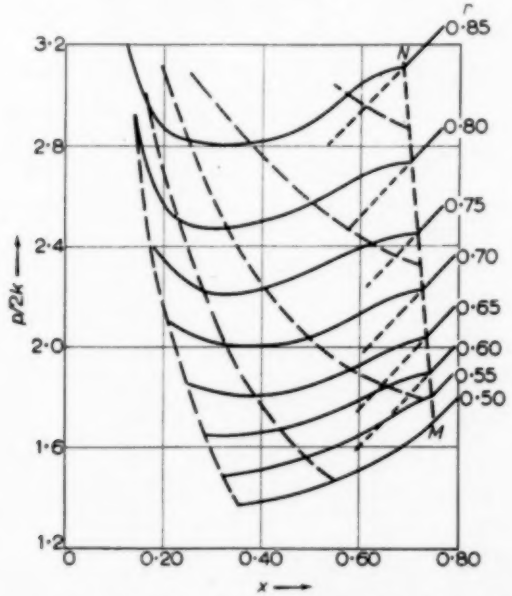

Fig. 8. Variation of $p/2k$ with r for a square die and rough container walls.

If, for a given value of r, x' denotes the steady state extrusion length represented by a point on NM, and if x is greater than x', then the parameter $p/2k$ will be

increased by an amount $(x - x')$ due to frictional drag on the slug, and hence all the characteristics to the right of NM rise at the same rate.

(ii) *Smooth container wall.* The slip-line field is terminated at points such as S (Fig. 4), where the slip-lines make 45° with the container wall. The curves of $p/2k$ against x are obtained by the same method as in (i), and the results are given in Fig. 9. Again, the steady-state extrusion pressures lie on NM.

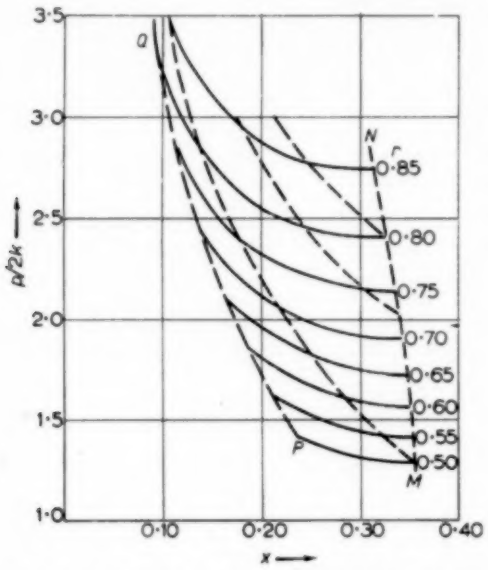

Fig. 9. Variation of $p/2k$ with r for a square die and smooth container walls.

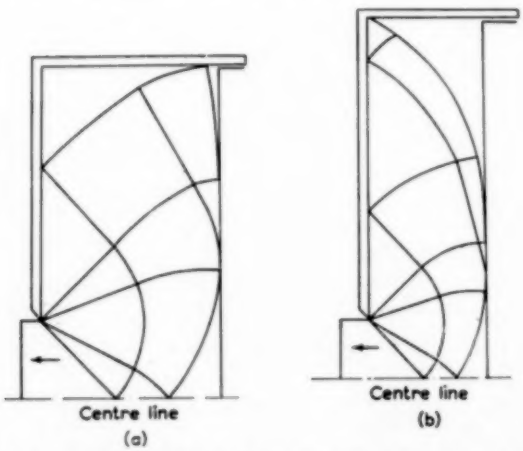

Fig. 10. Other possible types of slip-line field for : (a) die face smooth and container wall rough, (b) die face smooth and container wall smooth.

It is surprising to find that for a considerable range of thicknesses a sizeable and fairly rapid reduction in $p/2k$, to less than that associated with a steady state process, accompanies a reduction in slug thickness when the container walls are

rough. However, as Fig. 8 shows, this is less remarkable when it is considered that, even before the onset of the unsteady state, the pressure is falling at a constant rate as the punch advances, and that after NM it rises above the extrapolated line.

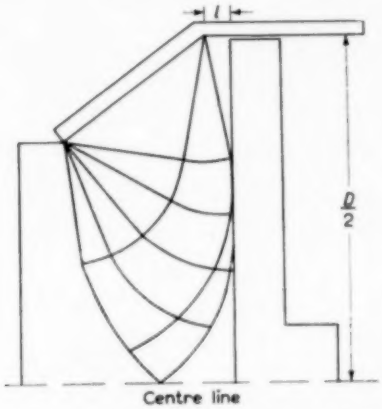

Fig. 11. A possible type of slip-line field for short slugs extruded through smooth wedge-shaped dies.

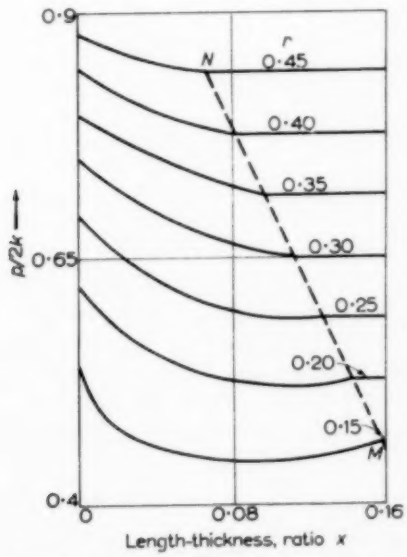

Fig. 12. Variation of $p/2k$ with x for extrusion through a smooth wedge-shaped die of semi-angle 45°

4. Other Types of Field

It is easy to adapt other known types of steady state stress field for square dies to this kind of problem (Johnson 1956a) and, in particular, two are shown in Figs. 10 (a) and 10 (b) for the cases in which the die face is perfectly smooth and the container wall either perfectly smooth or perfectly rough.

Considering the type of field initially suggested by HILL and TUPPER (1948) for smooth wedge-shaped dies of semi-angle α, and for which the reduction, r, is less than $2 \sin \alpha/(1 + 2 \sin \alpha)$, it will be clear how the field may be altered to allow for short slug lengths by reference to Fig. 11.

Using the piecemeal method described in the previous section for a smooth 45° die, values of $p/2k$ versus x for given values of r have been obtained by HINCHLEY (1956) and are shown in Fig. 12; in this instance $x = l/D$.

5. DEFORMATION OF A SQUARE GRID

If a square grid is marked on the face of a slug which is then extruded by a *small* amount, the grid will be deformed; two examples of the calculated deformation are shown in Figs. 13 (a) and 13 (b). It will be observed that the horizontal grid lines appear to diverge in a radial fashion from a point on the slug axis on emerging from the die orifice, and this is always observed in experiments with metal. In Fig. 14 a sequence of photographs of distorted grids obtained for increasing slug lengths is shown for a 45° die. This apparent radial divergence of horizontal grid lines is clearly evidence of unsteady state extrusion.

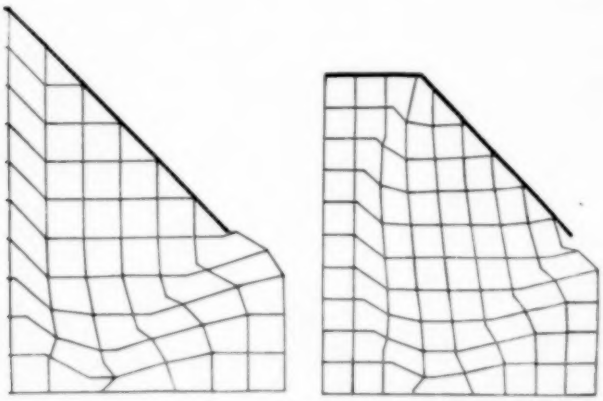

Fig. 13. Deformation undergone by slugs extruded by a small amount with (a) die face smooth, (b) die face rough.

6. PIPING OR CORING

An attempt to explain this phenomenon is made below. Consider two rows of particles A and B at a very small distance on either side of line PP (Fig. 15 (a)); let PP advance to take up position $P'P'$ tangential to slip-line CTD. Then row A will have been distorted to the form indicated diagrammatically in Fig. 15 (b) and row B will still be a straight line. Imagine row A to be the last line of particles of the slug and row B to be the first line (or face) of those of the punch. Row B by its nature cannot distort, and in the limit the two rows are contiguous; but the consequence of their belonging to different bodies is that (1) row A over length H_2 proceeds ahead of the punch, and (2) over length H_1 the particles endeavour to invade the punch face. While (2) is prevented, (1) is possible and results in the

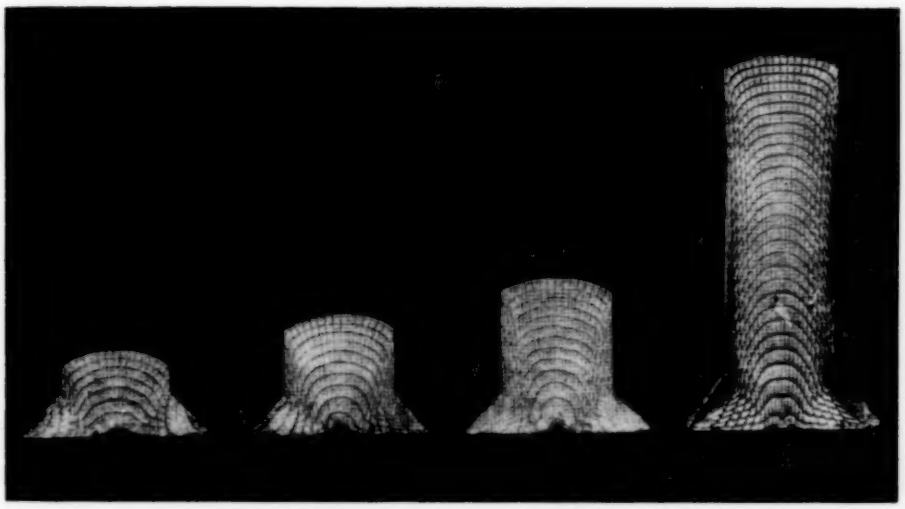

Fig. 14. Deformation developed by extruding increasing lengths of slugs through lubricated wedge-shaped dies.

formation of a void. The formation of a void in the remaining length of a slug partially extruded would be known as " coring " or " piping " ; its formation can be explained as above by reference to the calculable deformation occuring in plane-strain in an ideal material.

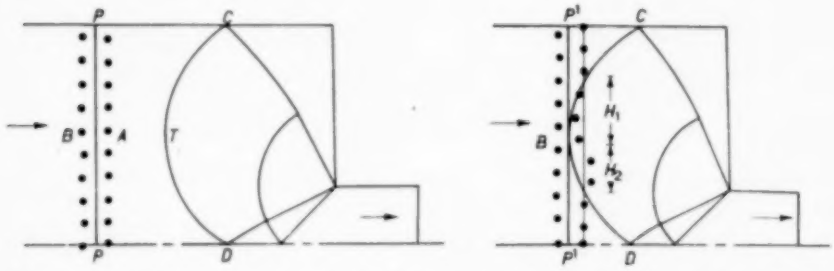

Fig. 15. Slip-line field for $r > 0{\cdot}5$, (a) steady state extrusion, (b) the same field just accommodated in the remaining slug length, to illustrate the development of coring.

The increased speed of flow as the distorted particles approach the axis enlarges this gap and thus piping becomes more pronounced. It will be seen that the tendency will be for a rigid block, roughly triangular in section, to be sheared off as the " bellying " over H_2 increases. This, indeed sometimes occurs in experiments with aluminium, it being possible to remove a thin sliver of metal if the extrusion is arrested when just sufficient piping has occurred. Careful examination of the longest extrusion in Fig. 14 reveals two small voids, one on either side of the slug axis, as well as the unusual but sometimes theoretically required cusp on the axis.

It becomes clear that over length H_2 the pressure on the pad must be nil (or nearly so), while over length H_1 the tendency will be for the pressure to increase. It can be shown theoretically that the ostensible penetration over length H_1 is always less than the gap opened up over H_2 ; when the slip-line DTC meets the container wall normally, the depth over H_1 is zero. One consequence of the inability of the row A to penetrate the punch over length H_1 is that this unaccommodated volume must displace neighbouring material and in fact distort the " horizontal " grid lines next to the punch face so that they present the appearance of bending in towards the axis. This is a feature often observed in photographs of slugs which have been extruded to an " excessive " degree.

7. The Autographic Diagram for Long Slugs

By a long slug is meant one which is long enough to be the subject of a steady state extrusion. If a long slug is extruded with a rough punch, then when the remaining slug length is just sufficient to contain the slip-line field, the value $p/2k$ is given by a point on NM of Figs. 8 or 9. At about this point piping commences and the extrusion is no longer a steady state one. Assuming the correctness of the discussion in Section 6, two voids develop over a certain length of the punch and the slug, being extruded, remains rectangular no longer. There are now two principal factors affecting the extrusion load (or nominal extrusion

pressure) : the changing slug geometry and the punch face roughness. However, if it is assumed that the effect of the voids on the geometry of the short slug is negligible, parameter $p/2k$ should vary with the remaining slug length-to-diameter ratio x in the typical manner of Figs. 8 and 9. This is to say that with a rough punch the curves given in these Figures are to some degree the end portions of the typical autographic diagrams in Fig. 1.

ACKNOWLEDGMENTS

The author wishes to express his thanks to Mr. A. P. GREEN for criticisms of certain sections of the paper, Mr. P. HINCHLEY for providing Figs. 12, 13 and 14 and B.I.S.R.A. for permission to publish some of the results taken from the original report (JOHNSON 1955).

REFERENCES

CHANG, T. M. 1950 *D.S.I.R., M.E.R.O. Report MF/MS* 41.
GREEN, A. P. 1955 *J. Mech. Phys. Solids* **3**, 189.
HILL, R. 1948 *J. Iron Steel Inst.* **158**, 177.
HILL, R. and TUPPER, S. J. 1948 *J. Iron Steel Inst.* **159**, 353.
HINCHLEY, P. 1956 Thesis for B.Eng. Hons. Degree, Sheffield University.
JOHNSON, W. 1954 *B.I.S.R.A. Report MW/E/55/54.*
1955 *B.I.S.R.A. Report MW/E/51/55.*
1956a *J. Mech. Phys. Solids* **4**, 191.
1956b *J. Mech. Phys. Solids* **4**, 269.
PURCHASE, N. W. and TUPPER, S. J. 1953 *J. Mech. Phys. Solids* **1**, 234.

Journal of the Mechanics and Physics of Solids, 1957, Vol. 5, pp. 215 to 222. Pergamon Press Ltd., London

AN EXPERIMENTAL INVESTIGATION OF THE YIELD CRITERION AND THE STRESS-STRAIN LAW

By G. Lianis and H. Ford
City and Guilds College, London

(*Received* 21*st January*, 1957)

Summary

The theory of notched strips loaded in tension under conditions of plane stress is used to verify the yield criterion and the stress-strain law in the plastic region. A new method to obtain ideally plastic material is employed. The experimental results compare favourably with the von Mises criterion and the Prandtl-Reuss flow rule.

1. Introduction

In order to verify the yield criterion and the stress-strain law of a metal under a complex state of stress two methods have been used in the past ; (a) Thin walled tubes subjected to internal pressure and axial tension ; (b) Thin wall tubes loaded in tension and torsion, and bending and torsion (Siebel 1953). These methods enable the stress system to be exactly defined from measurement of overall loads because of the symmetry and the thinness of the tube. Such tests require complicated apparatus, and it is difficult to produce thin-walled tubes to close tolerances.

It is desirable therefore to produce an arbitrary uniform state of combined stress by some different method which should involve simple apparatus, easily and accurately made specimens and simple technique. Hill has suggested such a method in his theory of localized necking (Hill 1953) in strips loaded in simple tension under conditions of plane stress. Hundy and Green (1954) used Hill's theory for aluminium and copper, but the material had a rounded stress-strain curve and considerable work-hardening. It was difficult therefore, to extrapolate the load-extension curve to find the yield load accurately, and only the stress-strain law has been investigated in their experiments.

2. Theory of the Method

A thin uniform rectangular strip subjected to axial load is deformed plastically under conditions of plane stress. The distortion can be restricted in a narrow straight zone by cutting on the wide faces two opposed grooves having an oblique direction with respect to the axis of the strip (Fig. 1).

By measuring the angle θ of the inclination of the groove, and the angle ψ of the relative velocity v of the two parts on either sides of the grooves the flow rule can be deduced. By measuring also the axial load the yield surface can be

found experimentally. It is quite difficult however, to cut accurately the grooves in such a thin strip. This difficulty is avoided in the alternative method proposed by Hill, in which the same constraint on the distortion is obtainable by notching the strip unsymmetrically (Fig. 2).

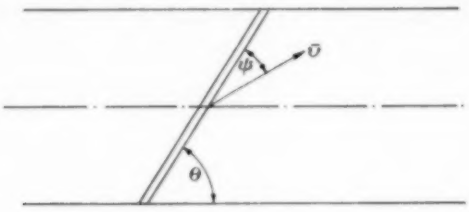

Fig. 1.

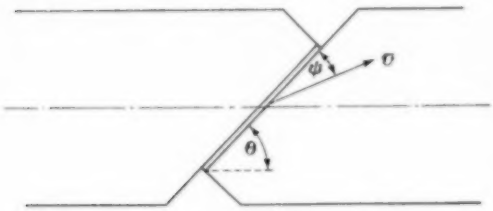

Fig. 2.

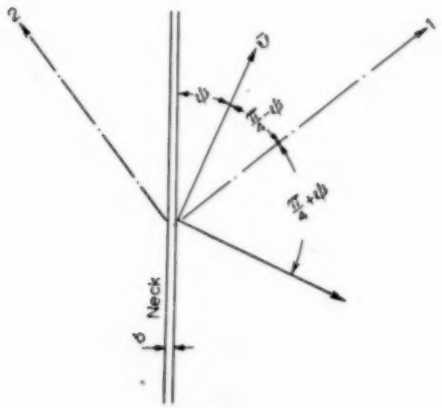

Fig. 3.

If the notches are deep and sharp and the thickness sufficiently small plastic flow is localized in a narrow straight neck joining the roots of the notches. Before the neck is far developed the deformation and stress system is similar to those given by the theory of localized necking.

This latter method can be used only for metals having very small rate of hardening. With metals such as annealed copper the rate of hardening is so great that the distortion is diffuse.

In the present experimental work commercially pure aluminium rolled at the temperature of liquid air has been used since it behaves nearly as an ideal plastic metal (HUTCHINSON 1948).

The neck is one of the two characteristics for the velocity components. It coincides at every point with a direction of zero rate of extension, the other direction being the normal to the relative velocity **v** (Fig. 3). The local breadth b of the neck and the strip thickness are sufficiently small compared with the length and radius of curvature of the trace of the neck.

Using the symbols shown in Fig. 3 the following relations due to HILL can be found :

$$\left.\begin{aligned} \dot{e} &= \frac{v}{2b}(1+\sin\psi) \\ \dot{e}_2 &= \frac{-v}{2b}(1-\sin\psi) \\ \dot{e}_3 &= \frac{-v}{b}\sin\psi \end{aligned}\right\} \tag{1}$$

$$\sin\psi = \frac{\dot{e}_1+\dot{e}_2}{\dot{e}_1-\dot{e}_2} = \left(\frac{\partial f}{\partial\sigma_1}+\frac{\partial f}{\partial\sigma_2}\right)\Big/\left(\frac{\partial f}{\partial\sigma_1}-\frac{\partial f}{\partial\sigma_2}\right) \tag{2}$$

where $f(\sigma_1, \sigma_2) = 0$ is the yield function and plastic potential, σ_1 and σ_2 being the principal stresses in the zone of the neck ($\sigma_1 \geqslant \sigma_2 \geqslant \sigma_3$).

LODE's variable for the strain increment is therefore

$$\nu = \frac{2\dot{e}_2-\dot{e}_1-\dot{e}_3}{\dot{e}_1-\dot{e}_3} = -\frac{3(1-\sin\psi)}{(1+3\sin\psi)} \tag{3}$$

and takes values between 0 (pure shear) and -1 (uniaxial tension) as ψ varies between 90° and $\sin^{-1}\frac{1}{3} = 19°\,30'$. Assuming that the load F is uniformly distributed along the length l of the neck, by considering the normal and shearing stress it can be shown that

$$\left.\begin{aligned} F\sin\theta/hl &= \tfrac{1}{2}(\sigma_1+\sigma_2)+\tfrac{1}{2}(\sigma_1-\sigma_2)\sin\psi, \\ F\cos\theta/hl &= \tfrac{1}{2}(\sigma_1-\sigma_2)\cos\psi. \end{aligned}\right\} \tag{4}$$

Hence

$$\frac{\sigma_1}{\sin(\theta-\psi)+\cos\theta} = \frac{\sigma_2}{\sin(\theta-\psi)-\cos\theta} = \frac{F}{hl\cos\psi}. \tag{5}$$

The length of the vector in the deviatoric stress space is (HILL 1950. p. 18)

$$\sqrt{\tfrac{2}{3}}(\sigma_1^2-\sigma_1\sigma_2+\sigma_2^2)^{\frac{1}{2}} = \sqrt{\tfrac{2}{3}}\frac{F}{hl\cos\psi}[\sin^2(\theta-\psi)+3\cos^2\theta]^{\frac{1}{2}} \tag{6}$$

The LODE's variable for the stress is

$$\mu = \frac{2\sigma_2-\sigma_1-\sigma_3}{\sigma_1-\sigma_2} = -\frac{3\cos\theta-\sin(\theta-\psi)}{\cos\theta-\sin(\theta-\psi)} \tag{7}$$

and the inclination of the stress vector to the direction representing pure shear is $\tan^{-1}(-\mu/3)$. If the yield locus has a six-fold symmetry it is only necessary to

find points over a 30° segment of the deviatoric plane between $\mu = 0$ and $\mu = 1$.

The above solution, consisting of a deformation mode, has been shown by Bishop (1953) to be the exact solution when the two notches are symmetrically placed about the axes. Bishop's calculation also gives a general idea of the critical depth of the notches for the unsymmetric case to ensure that plastic distortion is, in fact, limited to the neck and does not extend into the surface of the notch. On these grounds, and the evidence of the experimental results described below, it is clear that Hill.'s solution is the exact solution of the problem for unsymmetrical notches.

3. Simple Tension Tests

If a strip of commercially pure aluminium is rolled down at the temperature of liquid air it acquires the properties of a nearly perfectly plastic metal. The strips were put in a thermos flask full of liquid air to lower their temperature. After the thermal equilibrium has been established the strips were put quickly in a 4″ × 6″ rolling mill and given a series of successive reductions. They were then left until they acquired the room temperature.

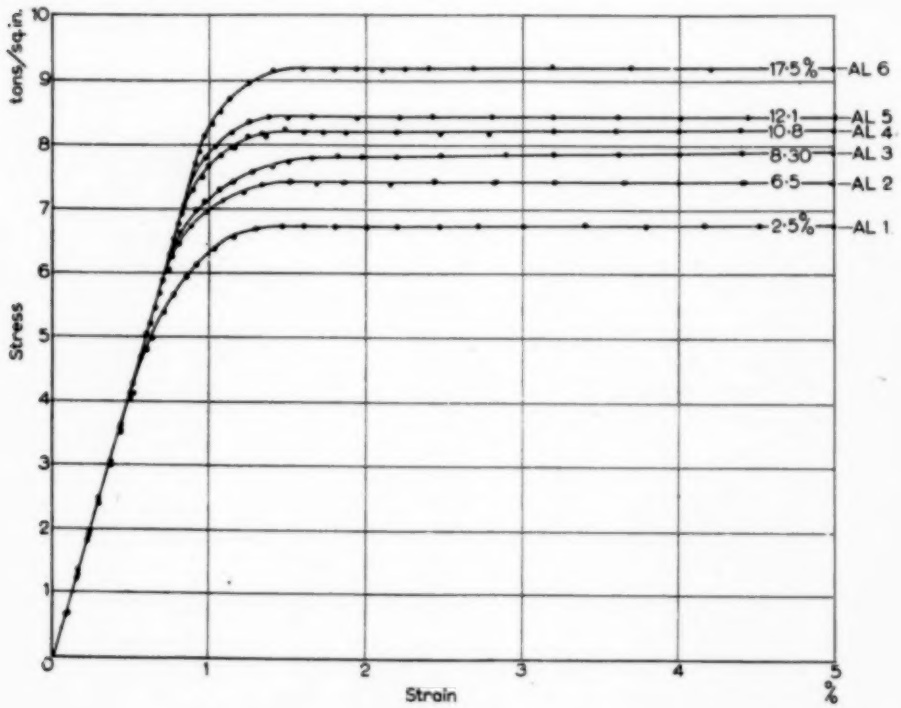

Fig. 4.

Standard 2 inch gauge length test pieces were used, the elongation being measured by a Lindley extensometer. Owing to the flat stress-strain curve, a neck forms quickly and it was necessary to re-machine the test piece to a uniform thickness, and reload to obtain strains of the order of 4%. The stress-strain curves plotted

in Fig. 4 are satisfactorily flat with a small rounded transition region (numbers in parentheses show the percentage reduction by rolling).

4. Preparation of the Specimens

Aluminium strips 3″ wide rolled down from the thicknesses shown in Table I at the temperature of liquid air by about 20% reduction were cut to the general dimensions shown in Fig. 5.

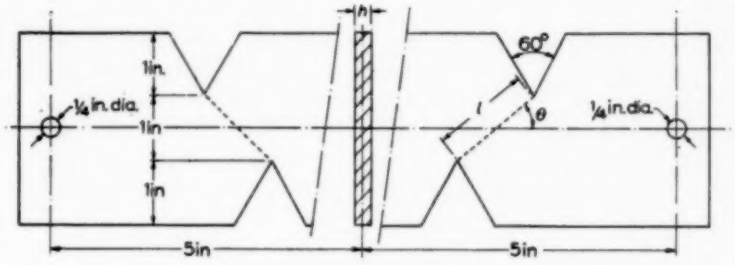

Fig. 5.

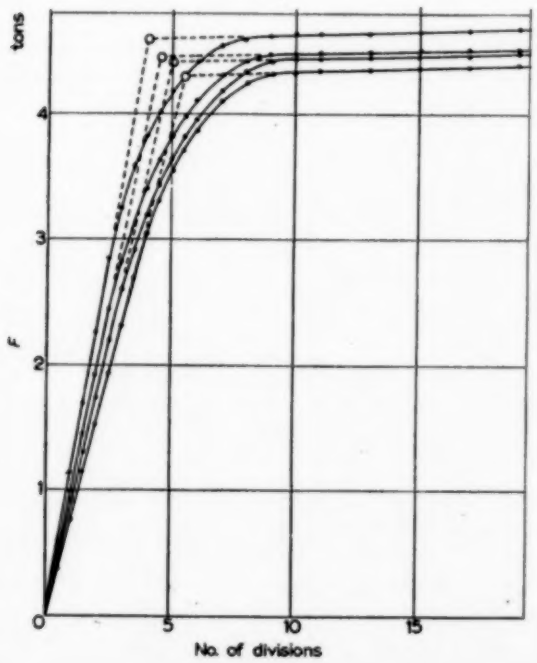

Fig. 6.

A double pair of similar notches were cut to avoid unsymmetrical loading due to the rotation of the two parts after the formation of the neck. The angle θ was measured by a travelling microscope.

To measure the angle ψ of the relative velocity v with respect to the neck the following method due to Hundy and Green, (1954) has been employed. The theoretical value of ψ from the relation $\tan\theta = 4\tan\psi$ (being true for $\mu = \nu$) was first estimated. A fan of straight lines were scribed with a razor blade at angles dispersed at 1° intervals around this estimated angle. The two parts of each line do not lie in the same direction after the neck has been formed unless they coincide with the direction of v. Using a travelling microscope the lateral displacement of each part relative to its continuation can be measured, and by interpolation the angle ψ of the direction which would correspond with v can be found.

With a polished strip surface and very fine lines the angle ψ can be measured with an accuracy of $\pm 0{\cdot}5°$. The specimens were loaded in a Hounsfield tensometer. Loads in steps of 0·05 tons were applied and the extension measured by a Huggenburger extensometer. The desired angle ψ is that corresponding to the onset of necking. To minimize any error due to finite deformation all specimens were measured to give the smallest possible amount of necking.

5. Discussion of the Experimental Results

The load versus axial extension has been plotted for seventeen specimens tested. By extrapolating back the flat part of the curve to meet the elastic line the yield load corresponding to the onset of necking can be found (see Fig. 6 for a typical result). The yield stress found from a simple tensile test has the value of $Y = 7{\cdot}42$ tons/sq. in. The experimental results are shown in Table I and Figs. 7 and 8.

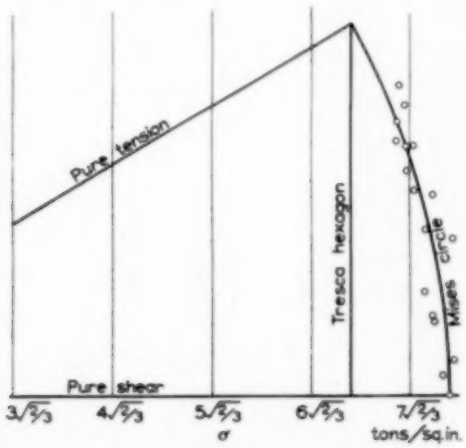

Fig. 7.

They compare favourably with the von Mises yield criterion. The experimental points lie close to a circular yield locus, the discrepancies being less than $\pm 3\%$ and equally scattered on either side (Fig. 7). The experimental points also lie close to the straight line $\mu = \nu$ (Fig. 8).

This differs from the results obtained by Taylor and Quinney (1936) who found a certain deviation from the $\mu = \nu$ rule. Similar results fitting to the equality

of LODE's variable have been found in HUNDY and GREEN's (1954) experiments, and by SIEBEL (1953).

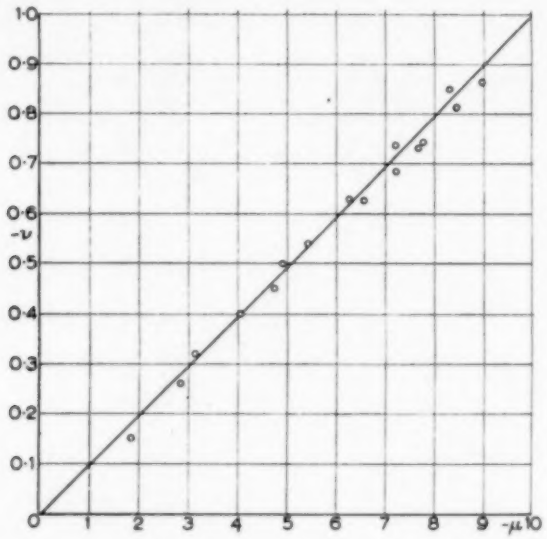

Fig. 8.

6. TESTS FOR HOMOGENEITY OF STRESSES AND ANISOTROPY

In HILL's theory it is assumed that the stresses are uniformly distributed across the neck. To check this assumption the following test was performed. A specimen in which the two necks were formed simultaneously was loaded to just below the yield load. The specimen was assumed therefore to remain elastic during loading, and the stresses proportional to the local deformation. Using a Johansson extensometer with a $\frac{1}{8}$ inch gauge length, measurements of the axial deformation were taken in various positions on either side of the necks. Within the measurable accuracy of a division the stress system was uniformly distributed across the neck. Fig. 9 shows the measurements in number of scale divisions of the extensometer.

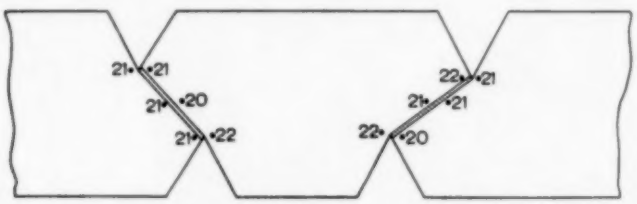

Fig. 9.

Small specimens cut from a test piece at four different angles with respect to the rolling direction were tested in simple tension to check for anisotropy. The yield stress Y for the four directions taken is :

0° to the rolling direction $Y = 8{\cdot}5$ tons/sq. in.

30° „ „ „ „ $Y = 8{\cdot}55$ „

45° „ „ „ „ $Y = 8{\cdot}45$ „

90° „ „ „ „ $Y = 8{\cdot}65$ „

It is therefore presumed that no appreciable anisotropy was introduced by the rolling.

References

Bishop, J. F. W.	1953	*J. Mech. Phys. Solids* **2**, 53.
Hill, R.	1950	*Mathematical Theory of Plasticity* p. 18 (Clarendon Press).
	1952	*J. Mech. Phys. Solids* **1**, 19.
Hutchinson, T. S.	1948	*Nature* **162**, 374.
Hundy, B. B. and Green, A. B.	1954	*J. Mech. Phys. Solids* **1**, 16.
Siebel, M. P. L.	1953	*J. Mech. Phys. Solids* **3**, 189.

BOOK REVIEWS

Progress in Metal Physics. Edited by B. CHALMERS and R. KING, Pergamon Press, London and New York, 1956. Vol. 6. viii + 354 pp., 70s.

METALLURGISTS, solid-state physicists, and physical chemists, will all find something to interest them in this volume of the now-familiar series on Progress in Metal Physics ; for, of the six articles in the book, two deal with essentially metallurgical topics – creep and steel transformations ; two with physical topics – electrical resistivity and mosaic structure ; and two with chemical topics – whisker growth and the mechanism of evaporation.

Diagrams showing the variation of energy bands with interatomic spacing are familiar in books on the electronic structure of solids, but until recently they have been purely theoretical constructions. However, in the last few years research into effects of high pressures has opened the way to the determination of these diagrams experimentally from effects of pressure on electrical resistivity. In his article which deals with this work A. W. LAWSON describes many interesting new effects that have been discovered, such as overlap of electrons into higher Brillouin zones, electronic rearrangements in the shell structures of the atoms, changes of crystal structure, and the conversion of semi-conductors into metals. The second article, by H. K. HARDY, is an account of another topical subject – the growth of metal whiskers. Although recent work on these was stimulated in the first place by a purely practical problem, whiskers have proved so remarkable in their mode of growth and their mechanical properties that they are now being studied intensively in many laboratories. HARDY'S interesting article traces the history of filamentary growths of metals back some hundreds of years, describes the various circumstances of growth, and outlines the recent theories.

The two metallurgical articles deal with more traditional topics. Writing on the austenite-pearlite reaction in steel, R. F. MEHL and W. C. HAGEL discuss the metallography, the thermodynamics, and the kinetics, of the reaction thoroughly from a highly critical standpoint that does not hide the difficulties facing atomistic theories in this field. A. H. SULLY adopts a more indulgent attitude towards theory in his article on the process of creep in metals, but the main feature of the article is a clear and well-balanced survey of the numerous and bewilderingly diverse observations made in recent years on cell formation, kinking, and grain boundary movements, during creep.

Evaporation is a basically simpler process than either creep or the decomposition of austenite and, accordingly, atomistic theories fare much better here. Thus O. KNACKE and I. N. STRANSKI are able in their article to give a satisfying account of the evaporation process in which the statistical-mechanical theory is closely linked to experimental observation; the discussion of the atomic structure at the surface of an evaporating crystal is particularly interesting. In the final article, P. B. HIRSCH describes the experimental study of mosaic structures in metal crystals clearly, comprehensively and authoritatively. The reader is left in no doubt that many methods for determining the distributions and densities of dislocations in crystals are now available, and all that seems to be missing from this field is a unifying theory of the various sub-structures observed.

One is grateful to the authors for having taken the time and trouble to prepare such comprehensive and authoritative reviews. The pity is that the inevitable high price of the book may prevent it from occupying the place where it so rightly belongs, on the bookshelf of every research physical metallurgist.

A. H. COTTRELL

K. SWAINGER : **Analysis of Deformation III – Fluidity.** Chapman and Hall, Ltd., 1956. xxvii + 266 pp., 65s.

DR. SWAINGER is an inveterate iconoclast, of by now universal repute. He goes on his way as assured as ever that everyone else is wrong and only he is right, notwithstanding complete failure

to impress informed scientific opinion, even after many years of determined onslaught. In turn he has proposed sweeping (one could say outrageous) modifications in the accepted mechanics of solids and fluids (elastic, plastic, or viscous). His more obvious errors of fact and opinion have been repeatedly pointed out. But his publishers continue to be remarkably indulgent and so yet another volume must be reviewed (and still another is promised).

His objection to classical hydrodynamics is basic. He proposes to leave out the nonlinear term $(\mathbf{v} \cdot \text{grad})\,\mathbf{v}$ from Euler's kinematic formula for acceleration, however large the velocity (Bernoulli's theorem of course goes by the board); see pp. 45, 61-62, 71-73, and especially the candid footnote on p. 73 which contains the remark that Euler misapplied Newton's theory on force and acceleration. Naturally this proposal would make the subject delightfully easy, even if somewhat other-worldly. Dr. SWAINGER's argument is, need it be said, incomprehensible; so far as one can tell, he has been motivated simply by a feeling that there *ought* to be a steady viscous flow $u = cx$, $v = -\frac{1}{2}cy$, $w = -\frac{1}{2}cz$ under uniform uniaxial stress, however large the constant c is.

But this is not all. He also maintains that the Saint-Venant compatibility relations in elasticity between the strains, and their analogues in viscous flow between the strain-rates, are insufficiently restrictive. For example, in a plane elastic state the Airy stress function should satisfy $\nabla^2\phi =$ constant, and not only $\nabla^4\phi = 0$ (pp. 68 and 115); in other words, $\sigma_x + \sigma_y$ should be constant. How Dr. SWAINGER would deal with the innumerable cases where it is not, or how he thinks his equation for ϕ is compatible with the possibility of arbitrarily prescribing the boundary values of both ϕ and its normal derivative (seeing that $\nabla^4\phi = 0$ itself then has only one solution), he does not (in the nature of things) tell us. (I refer him to TIMOSHENKO and GOODIER, *Elasticity*, pp. 190-1.)

Many solutions to plastic problems are wrong, roundly asserts Dr. SWAINGER (pp. 187-8), because the strain-rates do not satisfy even the Saint-Venant compatibility relations – at least according to *his* calculations (which he withholds). This contention is ludicrous in the extreme since (even in the example he quotes, viz. the compression of a block between rough plates) *explicit* expressions for the velocities are stated as part and parcel of the accepted solution, and so the corresponding strain-rates could not fail to satisfy the compatibility relations. A different method of debunking conventional theory appears on p. 190, in relation to the expansion of a cylinder by pressure. Here he does not bother to start with the accepted plastic state of stress, but takes a quite different one of his own, then computes from this the corresponding strain-rates (with a scale-factor also of his own choosing) and finds they do not satisfy the compatibility relations!

R. HILL

I. S. SOKOLNIKOFF: **Mathematical Theory of Elasticity.** 2nd Ed. McGraw-Hill Book Co., 1956. xi + 476 pp., 71s. 6d.

THIS new edition of a well-known standard work has been greatly expanded in all parts, but principally by the addition of chapters on two- and three-dimensional problems. In the treatment of plane problems the complex variable approach is adopted and is taken to a fairly advanced stage; there are numerous references to recent important Russian work. The chapter on problems in three dimensions, is by comparison, somewhat sketchy and disconnected; the emphasis is on solution by combinations of special functions, and the alternative method of the Green's function receives less than its proper share.

The first three chapters, dealing with basic ideas, have been polished up to a pitch of perfection. (Perhaps one may regret the exclusion of a proof from thermodynamics that the matrix of elastic coefficients is symmetric in the general case). On the other hand, the exercises left to the student reader have received little further consideration; they remain surprisingly unimaginative and are but slight variants of the text (incidentally questions 8–11 on p. 396 properly belong to the early chapters). The final chapter, on variation methods, has also been added to, but is still not too well systematized; it also suffers from a circuitous and unedifying proof of the continued inequality linking the two basic extremum principles.

However, these are minor complaints by comparison with the excellent features of the book, particularly the clear exposition and the very valuable bibliography.

R. HILL

Solid State Physics, Vol. II. Edited by F. SEITZ and D. TURNBULL, Academic Books Ltd., London, 1956. 468 pp., £4. $12.

THERE is a great need for review articles on the many different topics which comprise solid state physics, for the flow of research papers over the last few years has been enormous. Professors SEITZ and TURNBULL, the editors of this new series, have set out to meet this need, and have asked many of the most eminent workers in the field to contribute suitable articles. The first two volumes, containing altogether eleven articles, have now appeared. The series as a whole is expected to amount to about twelve volumes, to be published initially at the rate of two per year. Thus, in quite a short period, a set of articles covering the main topics in solid state physics will become available. It is the editorial policy to publish the articles as soon as possible after they have been written, thereby reducing the delays in publication. While it is desirable to have up-to-date reviews there is the disadvantage that it is not always possible to group related topics in the same volume. The prospective purchaser is therefore likely to find, unless he has very wide interests indeed, that in order to obtain the articles which most interest him he will have to buy several volumes, thereby acquiring as well a number of reviews in which he has little interest. At £4 per volume many physicists will think twice before doing this, and for this reason only it is not possible to recommend the purchase of these volumes to those who have adequate library facilities and limited finances. The difficulty would, of course, be overcome if it were possible to obtain individual articles, but there is at present no suggestion that this may become possible.

Most of the articles in the first volume dealt with theoretical aspects of the solid state, for the reason that theoretical physicists seem to be able to produce review articles more rapidly than do experimentalists.

The second volume has less theoretical bias, and begins with an article by G. E. PAKE on nuclear magnetic resonance. In this the ideas and methods of nuclear resonance are so simply and carefully explained that it is only when one comes to the second article, by W. D. KNIGHT, that one realizes that the solid state has hardly been mentioned. KNIGHT's article, based on his thesis, describes the way in which information about electronic paramagnetism can be obtained from nuclear resonance in metals. While this is an undoubtedly important use of nuclear resonance in the solid state it is by no means the only one, and it is to be hoped that an article of wider scope will be forthcoming. Next comes a most interesting account of neutron diffraction in solids by C. G. SHULL and WOLLAN. Here is a new experimental tool which has already yielded valuable results and which promises even greater things. Anyone who is wondering whether neutron diffraction can help with their particular problem would do well to consult this article. After an elementary introduction, J. DE LAUNAY considers the general problem of lattice dynamics, and the distribution of the frequencies of the lattice vibrations for various crystal lattices is dealt with at some length. The final article, by F. SEITZ and J. S. KOEHLER, deals with the subject of the displacement of atoms during irradiation, mainly by charged particles. The mechanisms by which the incoming particles give energy to the lattice, the nature of the damage which results, and the effect on the physical properties are all considered. Although radiation damage is of considerable technical importance this aspect is not stressed, the main emphasis being on the fundamental nature of the processes involved.

To sum up, this volume contains a rather peculiar mixture of topics but their value is considerable, for very little of the information can be found outside the original papers.

K. W. H. STEVENS

Solid State Physics, Vol. III. Edited by F. SEITZ and D. TURNBULL. Academic Books Ltd., London, 1956. 388 pp., £4. $12.00.

THE third volume of *Solid State Physics*, published, as promised, approximately six months after volume II, continues the good work of providing up-to-date reviews of the various topics which comprise solid state physics. It is increasingly obvious that this series is going to be of immense value.

As in the earlier volumes no attempt is made to correlate the articles, but this is of much less consequence now, for the existing gaps are rapidly being filled. For example, H. Y. FAN's article

in volume I, on silicon and germanium, together with H. WELKER and H. WEISS' article on the Group III-Group V semiconductors in the present volume cover the major part of the semiconductor field. The latter review has been very carefully prepared and the authors clearly feel that experimental results are most readily assimilated when they are displayed in graphs. In an article of 78 pages there are 65 figures ! Then follows an account of the *Continuum Theory of Lattice Defects*, in which J. D. ESHELBY describes, in a straightforward and lucid way, how the usual elasticity theory can be modified to deal with some of the consequences of lattice defects, by representing them as suitably chosen centres of internal stress. LESTER GUTTMAN'S article on *Order-Disorder Phenomena in Metals* sounds as if it might overlap considerably with T. MUTO and Y. TAGAKI'S *Theory of Order-Disorder Transitions in Alloys* in volume I. The overlap is not in fact very great, being mainly in the introductory parts, and Dr. GUTTMAN finds much to describe which does not appear in the other article, particularly the thermodynamic and kinetic aspects of order-disorder transformations. The next review, by one of the joint editors, D. TURNBULL, is entitled *Phase Changes*, and covers, in a more general way, some of the thermodynamics given in the previous article. In addition it deals with the nucleation of phase changes and shows that the whole phenomenon is well understood in its broad outline and that good progress is being made in its more detailed study. The article by F. A. KRÖGER and H. L. VINK, *Relations between the Concentrations of Imperfections in Crystalline Solids*, uses mainly the law of mass action to determine the equilibrium concentrations of imperfections, beginning with quite simple examples and passing on to much more involved situations. The general impression is that this topic is more complicated than difficult. The final article, by C. KITTEL and J. K. GALT, describes *Ferromagnetic Domain Theory*, and is an extension of an earlier review by Professor KITTEL. It will be even more valuable.

All the articles are well written and very comprehensive, with many references. One really feels that every author has given all he has, and although this means that to assimilate all the information in any one article is by no means an easy task, if one wants to become an expert in solid state physics these are the articles to read.

K. W. H. STEVENS

E. W. ELCOCK : **Order-Disorder Phenomena.** A Methuen Monograph on Physical Subjects. 1956. 162 pp., 11s. 6d.

ALTHOUGH a good deal is known about the physical properties of alloys we are still far from having a complete understanding of their behaviour. The whole subject thus presents many challenging problems, and in this monograph Dr. ELCOCK gives an account of the progress which has been made in the study of order-disorder phenomena. Two distinct approaches have been made, and both are discussed in some detail. The first, which relies primarily on experimental observations, seeks to correlate the changes in physical properties of alloys, some of which are very striking, with changes in their degree of ordering. Very little mathematics is needed for this. The second uses the methods of statistical mechanics in a discussion of the thermodynamic properties of the order-disorder change, using a model in which the atoms are regarded as structureless billiard balls.

The presentation is clear and free from errors and provides a concise and stimulating account of order-disorder phenomena in alloys in thermoydnamic equilibrium. There is also a brief account of the allied phenomena of magnetic ordering in non-metallic substances. The author is clearly aware of the need for further experimental and theoretical work, and his choice of material and his discussion of it is such that the existing limitations in our understanding are always apparent. Probably the most valuable part of the book is that which deals with the correlations between the physical properties and the use of order parameters. The average reader may well feel that the reward for working through the statistical theory is insufficient, for this uses the methods of theoretical physics and will probably only begin to have a general appeal when it begins to produce quantitative results and suggest new experiments.

K. W. H. STEVENS

International Symposium on the Nondestructive Testing of Materials and Structures. Reunion internationale des laboratoires d'essais et de recherches sur les materiaux et les constructions, Paris, January, 1954. Published by The Secretariat-General, RILEM., 12 Rue Brancion, Paris XV^{e}. (2 Vols.)

The complete report of this symposium includes the text of the 41 notes and papers presented, and a verbatim report of the resulting discussions.

The report is published in two volumes, in the first of which papers are devoted to the determination of the mechanical properties of various materials (chiefly concretes), by means of resonant vibrations or " speed of pulse transmission " measurements, and a second into which the subject matter of the first overflows, but which includes nondestructive testing by indentation methods and the use of X-ray and nuclear-radiation techniques.

Nondestructive testing of a structure, or of a material, is obviously of great value if it leads to the determination of the magnitude of the applied loads, or the stress condition, at which failure will occur. Contributors to the discussion do not seem to be agreed that any single criterion of the worth of a concrete exists, but the majority feel that vibration methods allow of the determination of the dynamic modulus of elasticity, and hope that the allowable compressive stress may be obtained, thereafter, from a relationship determined independently. There is considerable divergence of opinion as to the form this relationship takes, although it seems to be accepted that such a relationship does exist for a particular type of concrete (i.e. with identical aggregate, cement and mix proportions) and a particular shape of compression specimen.

This need for individual calibration is emphasized by authors who report the results of indentation tests, but here the final goal is further obscured by the fact (to which attention is drawn by both authors and contributors to the discussion) that schlerometer and ball indentation tests results are affected only by the state of the outermost material.

All authors seem to be agreed that considerable experience of each particular type of test, and of each particular piece of apparatus, is necessary before results can be interpreted in the form of crushing strength.

At this stage, the reviewer feels that he could not recommend with confidence the use of any one such item of test equipment in the field. The sensation of bewilderment is heightened by the poor translation of many of the papers – the quaintness of the English frequently distracts attention from, and occasionally obscures, the point under discussion.

R. C. Coates

BOOKS RECEIVED

FREUDENTHAL, A. M. (edited by). *Fatigue in Aircraft Structures.* (New York: Academic Press, 1956) $12.00.

JAEGER, J. C. *Elasticity, Fracture and Flow.* pp. 152 (London : Methuen, 1956) 10s. 6d.

FRIEDEL, J. *Les Dislocations.* pp. 314 (Paris : Gauthier-Villars, 1956).

HENISCH, H. K. *Rectifying Semi-Conductor Contacts.* pp. 372 (London : Clarendon Press, 1957) 70s.

EIRICH, F. R. (edited by). *Rheology—Theory and Applications.* pp. 761 (New York : Academic Press, 1956) $20.00.

NEAL, B. G. *Plastic Methods of Structural Analysis.* pp. 353 (London : Chapman & Hall, 1956) 45s.

GRAMMEL, R. (edited by). *Verformung und Fliessen des Festkörpers.* pp. 324 (Germany : Springer-Verlag, 1956). 65s. 8d.

Journal of the Mechanics and Physics of Solids, 1957, Vol. 5, pp. 229 to 241. Pergamon Press Ltd., London

ON UNIQUENESS AND STABILITY IN THE THEORY OF FINITE ELASTIC STRAIN

By R. Hill
Department of Mathematics, University of Nottingham

(*Received* 18*th March*, 1957)

Summary

It is shown that there is a direct relation between the criterion for stability of an elastic solid in a state of finite strain and the criterion for a unique solution to the associated boundary-value problem set by given velocities and nominal traction-rates on its surface. The criteria are obtained in a particularly simple form through a convenient choice of stress and strain variables. A suggestive connexion exists between the structure of the criteria and the idea of functional convexity in relation to the strain-energy density ; this concept is explained in detail. Finally, the stability limit is characterized by eigenfunctions, or adjacent positions of equilibrium.

1. Introduction and Basic Equations

Although the theory of finite elastic strain has been carried to a point where solutions can be generated for boundary-value problems of considerable generality, nevertheless there appears to be no criterion for deciding when a solution is or is not unique. Such a criterion is established in the present paper, and is further shown to be closely related to the condition that a state of finite strain should be stable under dead loading. The paper is self-contained, and every effort has been made to simplify the presentation for non-specialists.*

Several choices of the stress and strain variables are practicable and have been accorded varying degrees of emphasis by writers on the subject. The form of the field equations used here is certainly well known but nevertheless does not appear to have been previously recognized as ideally suited for the treatment of *general* questions concerning uniqueness, stability and allied matters.

Let s_{ij} denote the unsymmetric ' nominal stress ' tensor associated with rectangular Cartesian axes ; that is, $s_{ij}\,dS$ is the j th component of the force currently acting on the plane element which, in the unstrained state, was perpendicular to the i th axis and of infinitesimal area dS. The force currently acting on a plane element whose vectorial area was $l_i\,dS$ in the unstrained state has components $F_j\,dS$ where

$$F_j = l_i\,s_{ij} \tag{1}$$

is the nominal traction (the summation convention being adopted). When the co-ordinates a_i in the unstrained state are taken as the independent variables the

*Of whom I am certainly one. The literature on finite elastic strain suggests that the specialists rarely try to make their subject appear other than recondite.

equations of linear equilibrium are

$$\frac{\partial s_{ij}}{\partial a_i} + \rho_0 g_j = 0 \tag{2}$$

where ρ_0 is the original density and g_j the body force per unit mass.

If u_j denotes the total displacement of an element from its position in the unstrained state, the virtual work of the current surface and body forces on any deformed piece of material of arbitrary initial volume V is

$$\int F_j\,\delta u_j\,dS + \int \rho_0 g_j\,\delta u_j\,dV = \int l_i\,s_{ij}\,\delta u_j\,dS + \int \rho_0 g_j\,du_j\,dV \qquad \text{from (1)}$$

$$= \int \left[\frac{\partial}{\partial a_i}(s_{ij}\,\delta u_j) + \rho_0 g_j\,\delta u_j\right] dV \qquad \text{by Green's theorem}$$

$$= \int s_{ij}\,\frac{\partial}{\partial a_i}(\delta u_j)\,dV \qquad \text{from (2)}$$

The incremental work of distortion per unit original volume is therefore $s_{ij}\,\delta(\partial u_j/\partial a_i)$. For an ideal elastic solid under either isothermal or adiabatic conditions it is postulated (or it may be plausibly argued from thermodynamics – TRUESDELL 1952, pp. 168-171) that this work is equal to a perfect differential δE, where E is a positive single-valued function of state called the strain-energy density. Then, if the material is compressible (so that the virtual displacement gradients are independent), there follows Kirchhoff's formula

$$s_{ij} = \frac{\partial E}{\partial(\partial u_j/\partial a_i)}. \tag{3}$$

We shall also need the differential form of this:

$$\left.\begin{aligned} ds_{ij} &= c_{ijkl}\,d\left(\frac{\partial u_l}{\partial a_k}\right) \\ \text{where}\qquad c_{ijkl} &= \frac{\partial^2 E}{\partial(\partial u_j/\partial a_i)\,\partial(\partial u_l/\partial a_k)}. \end{aligned}\right\} \tag{4}$$

Clearly, the matrix of coefficients is symmetrical in that

$$c_{klij} = c_{ijkl}. \tag{5}$$

In terms of rates (4) becomes

$$\dot{s}_{ij} = c_{ijkl}\frac{\partial v_l}{\partial a_k} \tag{6}$$

where v_j is the velocity of the element initially at a_j.

E is not a *general* function of the 9 displacement gradients but rather of the 6 independent components of some symmetric tensor depending only on the distortion, say the Lagrangian components (e.g., SOKOLNIKOFF 1956, section 11)

$$e_{ij} = \tfrac{1}{2}\left(\frac{\partial u_i}{\partial a_j} + \frac{\partial u_j}{\partial a_i} + \frac{\partial u_k}{\partial a_i}\frac{\partial u_k}{\partial a_j}\right). \tag{7}$$

Then, if $x_j = a_j + u_j$ is the final position of an element,

$$s_{ij} = \frac{\partial x_j}{\partial a_k} \frac{\partial E}{\partial e_{ik}} \tag{8}$$

from (3) and (7), when E is symmetrized in the 9 strain components and these are treated as independent in the differentiation. The 'true stress' tensor σ_{ij}, based on the current dimensions, is given by

$$\frac{\rho_0}{\rho} \sigma_{ij} = \frac{\partial x_i}{\partial a_l} s_{lj} = \frac{\partial x_i}{\partial a_l} \frac{\partial x_j}{\partial a_k} \frac{\partial E}{\partial e_{lk}} \tag{9}$$

where ρ is the final density (MURNAGHAN 1937). This is symmetric in i and j, and so moment equilibrium is automatically ensured by the form (8). In this respect (3) is not in itself fully explicit and it is to be understood that E, regarded as a function of the displacement gradients, is restricted so that $\sigma_{ij} = \sigma_{ji}$; that is, E satisfies

$$\left(\delta_{il} + \frac{\partial u_i}{\partial a_l}\right) \frac{\partial E}{\partial (\partial u_j/\partial a_l)} = \left(\delta_{jl} + \frac{\partial u_j}{\partial a_l}\right) \frac{\partial E}{\partial (\partial u_i/\partial a_l)}$$

where δ_{ij} is the Kronecker delta (cf. TRUESDELL 1952, § 37).

At the present time it is not known with certainty whether the function E should be subject to any further general restrictions, irrespective of particular material properties; indeed, TRUESDELL (1956) regards this as the main outstanding problem in the theory of finite elastic strain. When the material is isotropic certain plausible restrictions have been proposed by TRUESDELL (1952, pp. 181-2) and by BAKER and ERICKSEN (1954), but no use is made of them here.

2. Convexity and Uniqueness

Although the idea of a convex function is described here in the context of the theory of finite elastic strain, it is of considerably wider significance. Not only is it the basis of a unified treatment of uniqueness theorems and extremum principles in many existing branches of the mechanics of solids and fluids, but it affords a simple and automatic procedure for formulating and proving such theorems where possible in new branches as they arise (HILL 1956).

A differentiable continuous function f of n variables $\theta_i (i = 1, \ldots n)$ is said to be *convex* if

$$f(\theta_1', \ldots \theta_n') - f(\theta_1, \ldots \theta_n) - (\theta_i' - \theta_i) \frac{\partial f}{\partial \theta_i} \geqslant 0$$

for any two sets of values θ_i, θ_i' (summation convention)*. We may write this shortly as

$$\Delta f - \frac{\partial f}{\partial \theta_i} \Delta\theta_i \geqslant 0 \tag{10}$$

where the prefix Δ denotes the difference between the respective values of the associated quantity. If the function is visualized as a surface in $(f, \theta_1, \ldots \theta_n)$

*This is the appropriate definition for present purposes; it differs from that preferred by analysts, viz:

$$\tfrac{1}{2}\{f(\theta_i) + f(\theta_i')\} \geqslant f\left(\frac{\theta_i + \theta_i'}{2}\right)$$

but it is easily shown to be equivalent (and is obviously so geometrically).

space, (10) is the condition that the entire surface should lie on one side only of *any* tangent plane. The function is said to be ***strictly convex*** if the inequality sign holds except when all $\Delta\theta_i = 0$. In the definition (10) θ_i and θ_i' are interchangeable; by adding the two equations so obtained :—

$$\Delta\left(\frac{\partial f}{\partial \theta_i}\right)\Delta\theta_i \geqslant 0 \tag{11}$$

where the inequality holds when f is strictly convex unless all $\Delta\theta_i = 0$.

When the first derivatives of f are continuous and the second derivatives sectionally continuous, a necessary and sufficient condition for strict convexity is that the Hessian matrix $(\partial^2 f/\partial\theta_i\,\partial\theta_j)$ should be positive-definite for any values of the independent variables. In terms of the associated quadratic form :

$$\frac{\partial^2 f}{\partial\theta_i\,\partial\theta_j}\,\xi_i\,\xi_j > 0 \qquad \text{unless all} \qquad \xi_i\text{'s} = 0. \tag{12}$$

From the TAYLOR expansion of f this condition is clearly implied by (10) when $\Delta\theta_i$ is sufficiently small; we may say that this is the condition for *local* convexity. Conversely, it is intuitive that a surface which is locally convex at every point is also strictly convex in its entirety.

There follows a sketch of the proof. We introduce the function of $\theta_1', \ldots \theta_n'$,

$$\phi(\theta_i') = \Delta f - \frac{\partial f}{\partial \theta_i}\Delta\theta_i$$

regarding $\theta_1, \ldots \theta_n$ as fixed. Consider the curve obtained by a plane section of the ϕ surface in an arbitrary direction $l_1 : l_2 : \ldots l_n$ through the point θ_i, i.e.

$$\Delta\theta_1/l_1 = \ldots = \Delta\theta_n/l_n = s$$

where s is a variable parameter. Then, in this section,

$$\frac{d\phi}{ds} = l_i\,\Delta\left(\frac{\partial f}{\partial\theta_i}\right) = 0 \qquad \text{when } s = 0,$$

$$\frac{d^2\phi}{ds^2} = l_i\,l_j\,\frac{\partial^2 f}{\partial\theta_i\,\partial\theta_j} > 0 \qquad \text{for all } s.$$

Since $\phi = 0$ when $s = 0$ these equations evidently imply $\phi > 0$ in the section, and similarly everywhere on the ϕ surface.

Consider, now, the boundary-value problem set by given total displacements on a part S_u of the surface S and by given nominal tractions on the remainder S_F, together with given body forces in V. The field equations (1), (2) and (3) have exactly the structure admitting a uniqueness theorem and extremum principle of the type previously mentioned. Suppose there could be two distinct solutions of the elastic field equations and denote their difference by Δu_i. Then, from (1), (2) and (3),

$$\int \Delta F_j\,\Delta u_j\,dS = \int \Delta\left\{\frac{\partial E}{\partial\,(\partial u_j/\partial a_i)}\right\}\Delta\left(\frac{\partial u_j}{\partial a_i}\right)dV$$

by a transformation similar to that detailed in deriving the virtual work identity (Section 1). If, now, E were a strictly convex function of the displacement gradients

(when the displacements do not differ merely by a rigid-body movement), the above volume integral would be positive by (11) if the two solutions involve different strains. But the integrand in the surface integral vanishes everywhere since $\Delta F_j = 0$ on S_F and $\Delta u_j = 0$ on S_u. Consequently there could not be more than one solution (the boundary conditions exclude a superimposed rigid-body movement). Again, from (10) and the same transformation,

$$\int \Delta E \, dV > \int F_j \, \Delta u_j \, dS_F + \int \rho_0 g_j \, \Delta u_j \, dV$$

where Δu_j now stands for $u_j^* - u_j$, u_j being the actual displacement and u_j^* any geometrically possible one. Thus, in moving from the actual configuration to any other allowed by the constraints, the increase in strain energy exceeds the work done by prescribed dead loads; i.e., the system is always stable under such loads.

It is clear, then, that to stipulate that E should be strictly convex for all strains would be too severe a restriction, in view of the behaviour of actual materials. Indeed, the fundamental question is perhaps not really whether the solution is unique under boundary conditions producing a *finite* distortion, but rather whether it is unique under an *infinitesimal* change in boundary conditions following a previous given finite distortion. Let, then, the nominal traction-rate $\dot{F}_j$ be prescribed over S_F, the velocity v_j over S_v, and the body-force rate in V; these rates are quasi-static, being measured in terms of the variation of some parameter other than time. Suppose there could be two distinct solutions and denote their difference by $\Delta \dot{s}_{ij}$, Δv_j. Then

$$\frac{\partial}{\partial a_i} \Delta \dot{s}_{ij} = 0 \text{ in } V, \qquad l_i \, \Delta \dot{s}_{ij} = 0 \text{ on } S_F, \qquad \Delta v_j = 0 \text{ on } S_v.$$

By the same transformation as before, and using (6),

$$0 = \int \Delta \dot{F}_j \, \Delta v_j \, dS = \int \Delta \dot{s}_{ij} \frac{\partial}{\partial a_i} (\Delta v_j) \, dV = \int c_{ijkl} \frac{\partial}{\partial a_i} (\Delta v_j) \frac{\partial}{\partial a_k} (\Delta v_l) \, dV.$$

If, therefore,

$$\int c_{ijkl} \frac{\partial}{\partial a_i} (\Delta v_j) \frac{\partial}{\partial a_k} (\Delta v_l) \, dV > 0 \tag{13}$$

for *all* fields Δv_j which vanish on S_v and are not identically zero, the original supposition would lead to a contradiction and so there could not be more than one solution. The solution would also be unique if the opposite inequality always held in (13). Since the current state is then unstable (as will be shown later) this case is of no practical importance.

It is worth noting that when (13) is satisfied we have the following extremum principle:

$$\int c_{ijkl} \frac{\partial v_j^*}{\partial a_i} \frac{\partial v_l^*}{\partial a_k} \, dV - 2 \int \dot{F}_j \, v_j^* \, dS_F > \int c_{ijkl} \frac{\partial v_j}{\partial a_i} \frac{\partial v_l}{\partial a_k} \, dV - 2 \int \dot{F}_j \, v_j \, dS_F$$

$$= \int \dot{F}_j \, v_j \, dS_v - \int \dot{F}_j \, v_j \, dS_F$$

where v_j is the actual solution and v_j^* any other continuous differentiable field taking the prescribed values on S_v. For, in view of (5), the difference between the two sides of the equation is just (13) with $v_j^* - v_j$ in place of Δv_j.

When the velocity is given over the whole of S it can be shown that (13) is equivalent to a restriction on E examined by ERICKSEN and TOUPIN (1956), namely that the second variation of $\int E\,dV$ should be positive for all variations in the velocity field that vanish on S. The uniqueness proof of ERICKSEN and TOUPIN is closely related to the present one but does not have the basic structure specially emphasized here for its connexion with the subsequent investigation of stability, nor does their method give prominence to the form (13). When the solid is isotropic and undeformed in the given state, E being quadratic as in the classical linear theory, ERICKSEN and TOUPIN show that their condition – and therefore (13) – is satisfied when the LAMÉ constants are such that $\lambda + 2\mu > 0$, $\mu > 0$. This is a noteworthy result, being stronger for these special boundary conditions than the familiar Kirchhoff uniqueness theorem which depends on (14) below, or $3\lambda + 2\mu > 0$, $\mu > 0$ (ERICKSEN and TOUPIN do not draw attention to this aspect of their analysis).

An obviously *sufficient* condition for (13) is that, at each point of the body, the quadratic form associated with the tensor c_{ijkl} should be positive-definite, i.e.

$$c_{ijkl}\,\xi_{ij}\,\xi_{kl} > 0 \qquad \text{unless all} \qquad \xi_{ij} = 0. \tag{14}$$

Recalling the definition (4) we see by comparison with (12) that (14) is equivalent to requiring the E surface to be *locally* convex at those values of the displacement gradients associated with the given state. Complementary extremum principles associated with this uniqueness theorem can be immediately derived by the systematic process of HILL (1956).

However, my intention was not to suggest restrictions on E that would allow a definite uniqueness theorem in specified circumstances, but simply to obtain a sufficiency *criterion* in the significant form (13). This test is of course incomplete in that it cannot *disprove* uniqueness (no immediate conclusion can be drawn when the right-hand integral vanishes or has different signs for some values of the variables – this is taken up again in section 4).

3. STABILITY AND UNIQUENESS

We take as fundamental the definition and dynamic test of stability due to DIRICHLET and KELVIN. An equilibrium state is said to be stable if, in the motion following an arbitrary disturbance, the amplitude of the additional displacement is always vanishingly small when the disturbance itself is. If, on the other hand, the amplitude is finite for some one type of disturbance, however small this might be, the state is said to be unstable. Evidently, a sufficient condition for stability is that in any (infinitesimal) geometrically-possible displacement from the position of equilibrium the internal energy stored or dissipated should exceed the work done on the system by the external loads (their variation with changes in position or shape of the body must be specified). For, by the principle of conservation of energy, the system can then move from the equilibrium position only as far as the

point where this excess becomes equal to the kinetic energy communicated by the disturbance; since the displacement amplitude must therefore vanish with the disturbance the system is stable. That this condition is also necessary (at any rate for an elastic system under conservative forces) follows from the classical linear theory of vibrations, where it is shown that, when the condition is not satisfied, the assumption that an arbitrary infinitesimal disturbance produces only an infinitesimal motion leads to a contradiction*.

Attention is confined to the case when the applied loading is 'dead,' i.e. the current nominal tractions and body forces do not vary during an arbitrary displacement δu_j from the equilibrium position. The functional whose sign is to be considered is then

$$\int \delta E \, dV - \int F_j \, \delta u_j \, dS_F - \int \rho_0 g_j \, \delta u_j \, dV = \int \left(\delta E - s_{ij} \frac{\partial}{\partial a_i} \delta u_j \right) dV$$

by the usual transformation, since $\delta u_j = 0$ on S_u when the geometrical constraints are maintained during the motion. For sufficiently small δu_j the functional becomes (with neglect of higher order terms)

$$\tfrac{1}{2} \int \delta s_{ij} \frac{\partial}{\partial a_i} (\delta u_j) \, dV$$

in view of the dependence (3) between stress and displacement gradient. Thus, from (4), the condition for stability is that

$$\int c_{ijkl} \frac{\partial}{\partial a_i} (\delta u_j) \frac{\partial}{\partial a_k} (\delta u_l) \, dV > 0 \tag{15}$$

for all fields δu_j which vanish on S_u and are not identically zero (it no longer matters that δu_j should be small since a proportionality factor in (15) makes no difference). It will be convenient to speak of a state as being at the *stability limit* if the functional in (15) is merely non-negative (being actually zero for one or more δu_j fields).

The restrictions placed by (13) and (15) on the c_{ijkl} distribution are identical, the interpretations of Δv_j and δu_j being now immaterial. For an elastic solid, then, questions of stability and incremental uniqueness are intimately related; in particular, the incremental boundary-value problem has a unique solution when the state is stable, but not necessarily when it is not stable. The general connexion does not seem to have been proved before in this context, though it is familiar enough for a conservative system with a finite number of degrees of freedom†. Even the fundamentals of the continuum theory of elastic stability itself have in my opinion only recently received an entirely satisfactory and consistent analysis, i.e. on the basis of (3) or an equivalent (Pearson 1956)‡. The condition (15) is Pearson's equation (10) reduced to a form that shows immediately the connexion with the investigation of uniqueness.

*Namely, unbounded time-factors associated with complex roots of the frequency determinant.

†See, for instance, Lyttleton (1953) where it is shown that questions of stability and uniqueness both turn on the matrix $\partial^2 V / \partial q_i \, \partial q_j$ and its associated quadratic form, $V(q_1, \ldots, q_n)$ being the potential energy, in direct analogy with (4), (13) and (15).

‡Pearson's work on stability is referred to again later. I take this opportunity to acknowledge my indebtedness to his definitive paper.

A stability problem is usually formulated in relation to a 'linear series' of equilibrium states (POINCARÉ's terminology). This series is obtained by the continuous variation of a single parameter, λ say, in the boundary-conditions (e.g. the resultant thrust on the end of a strut). It is then asked what value of λ corresponds to the stability limit (POINCARÉ's 'point of bifurcation' of a linear series* – we shall prove this equivalence in Section 4). In general the dependence of the tensor c_{ijkl} on λ will not be simple. If, however, the shape of the body is such that the total strain at the stability limit is small, (15) becomes approximately

$$\int (c_{ijkl})_{\lambda=0} \frac{\partial}{\partial a_i}(\delta u_j) \frac{\partial}{\partial a_k}(\delta u_l)\, dV + \lambda \int \left(\frac{\partial c_{ijkl}}{\partial \lambda}\right)_{\lambda=0} \frac{\partial}{\partial a_i}(\delta u_j) \frac{\partial}{\partial a_k}(\delta u_l)\, dV > 0$$

when λ is chosen so that it is initially zero. The first integral is twice the strain energy for small departures from the unstrained state and is positive-definite; the second integral depends on the final stress and may have either sign (a more explicit form of it appears later in (22)). The problem is thereby reduced to a conventional eigenvalue problem, the critical value of λ being obtainable as an extremum of a Rayleigh quotient of two functionals. The connexion with existing treatments of stability is discussed later in Section 5.

4. EIGENSTATES

It has been seen that, when the current state of strain is such that condition (13) is not satisfied, the incremental boundary-value problem does not necessarily have a unique solution. We now characterize more precisely those states where it is *certain* that more than one solution exists.

The equations to be satisfied by a solution are

$$\frac{\partial \dot{s}_{ij}}{\partial a_i} + \rho_0 \dot{g}_j = 0 \quad \text{and} \quad \dot{s}_{ij} = c_{ijkl} \frac{\partial v_l}{\partial a_k} \quad \text{in} \quad V,$$

$$l_i \dot{s}_{ij} \text{ given on } S_F, \qquad v_j \text{ given on } S_v.$$

The difference of any two solutions evidently satisfies exactly the same equations as would a possible instantaneous motion under *dead* loading, namely

$$\left.\begin{aligned} \frac{\partial}{\partial a_i}\left(c_{ijkl}\frac{\partial v_l}{\partial a_k}\right) = 0 \quad \text{in} \quad V, \\ l_i\, c_{ijkl}\frac{\partial v_l}{\partial a_k} = 0 \quad \text{on} \quad S_F, \qquad v_j = 0 \text{ on } S_v. \end{aligned}\right\} \tag{16}$$

Since the equations and boundary conditions are both homogeneous the solution is usually identically zero and the solution of the general boundary-value problem definitely unique. However, for certain c_{ijkl} distributions (the eigenstates), (16) admits non-vanishing solutions (the eigenfunctions) and then the solution of the general boundary-value problem is definitely not unique. From this standpoint (13) appears as a condition ensuring that a given state does not admit an eigenfunction. For, if there could be an eigenfunction v_j,

*KOITER (1945) examines the stabilities of the *bifurcated* series just beyond the point of bifurcation, in the case when the total pre-strain is small.

$$\int c_{ijkl} \frac{\partial v_j}{\partial a_i} \frac{\partial v_l}{\partial a_k} \, dV = \int l_i v_j c_{ijkl} \frac{\partial v_l}{\partial a_k} \, dS - \int v_j \frac{\partial}{\partial a_i} \left(c_{ijkl} \frac{\partial v_l}{\partial a_k} \right) dV = 0$$

from (16), contradicting (13) which was stipulated for all functions (this is of course virtually just a repetition of the original proof of sufficiency).

The eigenfunctions have the property of rendering stationary the functional

$$\tfrac{1}{2} \int c_{ijkl} \frac{\partial v_j}{\partial a_i} \frac{\partial v_l}{\partial a_k} \, dV \tag{17}$$

in the class of continuous differentiable functions which vanish on S_v. The first variation of this functional is

$$\int c_{ijkl} \frac{\partial v_l}{\partial a_k} \frac{\partial}{\partial a_i} (\delta v_j) \, dV$$

using the symmetry property (5), and by transformation this becomes

$$\int l_i c_{ijkl} \frac{\partial v_l}{\partial a_k} \, \delta v_j \, dS_F - \int \delta v_j \frac{\partial}{\partial a_i} \left(c_{ijkl} \frac{\partial v_l}{\partial a_k} \right) dV.$$

For arbitrary variations δv_j this vanishes trivially for all c_{ijkl} states when $v_j \equiv 0$, but non-trivially only in eigenstates, v_j being the corresponding eigenfunction (16). The stationary value of (17) is zero, as we saw previously.

If in (16) v_j and $\dot{s}_{ij}$ are interpreted, not as rates, but as infinitesimal changes in displacement and stress, we can say (though not with strict accuracy) that the eigenfunctions (containing an arbitrary factor) define 'adjacent equilibrium positions' under the given dead loads. Moreover, by reference to the functional in (15), we recognize that the stationary property proved for (17) is just a restatement of the principle of virtual work for a conservative system in equilibrium (c.f. Section 1); viz., the total potential energy is stationary in the adjacent positions of equilibrium as well as in the actual configuration. The proof of this alternative characterization of the eigenfunctions was also indicated by PEARSON (1956, p. 143), but in other variables and with less economy.

Since the body, when in an eigenstate, would remain in equilibrium if slightly displaced in the manner of the eigenfunction, we can say that the stability is neutral with respect to *such* displacements (neglecting, as in the last paragraph, higher order terms in the expansion of the potential energy). For other displacements, however, the stability functional (15) will usually take different signs; in that event the state is *unstable* on the whole, i.e. with respect to *arbitrary* disturbances. Equally, any other (ordinary) state is unstable if the functional (15) takes different signs (though it also must vanish in certain neighbouring positions it is not stationary in these since the state is not an eigenstate and these positions are not in equilibrium).

The only eigenstates of practical significance are those that can be reached during progressive loading from zero through a sequence of stable states. By continuity, the stability functional for such eigenstates is *invariably positive* except when the incremental displacement coincides with the eigenfunction. Other eigenstates are embedded in ranges of unstable states and cannot be reached in practice (or at any rate only articially with the help of passive constraints)*.

*That the adjacent-equilibrium technique is not an adequate substitute for the dynamic criterion of stability and is insufficient in itself to decide the unstable ranges, even in conservative systems and still less elsewhere, has been especially emphasized by ZIEGLER (1956) in an admirably clear and attractive exposition.

5. ALTERNATIVE FORMULATION

For the actual determination of the eigenstate corresponding to the stability limit it may no longer be more convenient to work with the equations in the form (16) since these do not separate out the relative roles of the current stress and the elastic moduli. Instead of (6) one may use relations between the x_j components of *true* stress-rate $\dot{\sigma}_{ij}$, based on the current dimensions and following a given element, and the velocity gradients with respect to x_j. According to a formula of CAUCHY's (TRUESDELL 1952, p. 219; PEARSON 1956, equation (30)), obtainable from (6), (7) and (9),

$$\left.\begin{aligned} \dot{\sigma}_{ij} &= \frac{\dot{\rho}}{\rho}\sigma_{ij} + \sigma_{ik}\frac{\partial v_j}{\partial x_k} + \sigma_{jk}\frac{\partial v_i}{\partial x_k} + \gamma_{ijkl}\epsilon_{kl} \\ \text{where} \quad \epsilon_{kl} &= \tfrac{1}{2}\left(\frac{\partial v_k}{\partial x_l} + \frac{\partial v_l}{\partial x_k}\right), \qquad \gamma_{ijkl} = \frac{\rho}{\rho_0}\frac{\partial^2 E}{\partial e_{pq}\,\partial e_{rs}}\left(\frac{\partial x_i}{\partial a_p}\frac{\partial x_j}{\partial a_q}\frac{\partial x_k}{\partial a_r}\frac{\partial x_l}{\partial a_s}\right). \end{aligned}\right\} \tag{18}$$

The tensor γ_{ijkl} is symmetric with respect to interchange of i and j, k and l, ij and kl; since it depends directly on the derivatives of E with respect to the Lagrangian strains its components have the character of elastic moduli. The term containing it has therefore the magnitude of modulus $\times$ strain-rate; the three other terms, however, have the combined magnitude of stress $\times$ velocity gradient (it has to be remembered that the rate of rotation, and hence the velocity gradient, can be large compared with the rate of strain).

Writers on stability who do not take (3), (8) or (9) as a basis have adopted various relations between the stress-rate and velocity gradient tensors (e.g. JEFFREYS 1942, PRAGER 1947, GOODIER and PLASS 1952). From the very fact that their relations differ from (18) (when converted into these variables, where necessary) and are therefore incompatible with the definition (3) of an elastic solid, their derivations cannot be expected to carry conviction (criticisms of detail have been listed by PEARSON). And indeed, when incremental relations are postulated without connexion with a pre-existing unstrained state, an element of arbitrariness immediately enters in the very definition of stress-rate itself, in regard to its convected component. On this account such postulated relations are a priori likely to differ from (18) by terms of type stress $\times$ strain-rate, and this is precisely what we find in the cases cited. Actually, such terms make no significant difference in the analysis of elastic stability in metals since the total possible strain is small compared with unity and the stresses therefore small in relation to the moduli; hence the discrepant terms are negligible compared with the final one involving the moduli. But the differences *are* important in rubber-like materials at large strains where the stresses and moduli are comparable; the use of (6) or (18) is then compulsory.

As a more elegant alternative to (18) one may introduce the nominal stress-rate $(\dot{s}_{ij})_f$ following an element and based now on the given *final* configuration*. This is related to the true stress-rate by

$$(\dot{s}_{ij})_f = \dot{\sigma}_{ij} - \frac{\dot{\rho}}{\rho}\sigma_{ij} - \sigma_{jk}\frac{\partial v_i}{\partial x_k}. \tag{19}$$

*This has also been found effective in an investigation of uniqueness in a plastic solid (HILL 1957).

From (18) and (19) :
$$(\dot{s}_{ij})_f = \sigma_{ik} \frac{\partial v_j}{\partial x_k} + \gamma_{ijkl}\, \epsilon_{kl}. \tag{20}$$

This simple relation seems not to have been noticed before. It is to be coupled with the equations of equilibrium (whose form is now immediate)

$$\frac{\partial}{\partial x_i} (\dot{s}_{ij})_f + \rho \dot{g}_j = 0 \tag{21}$$

together with prescribed values of velocity and nominal traction-rate over the final surface and body-force rates in the final volume.

Transformation of the stability functional to the new variables gives

$$\int \left(\sigma_{ik} \frac{\partial v_j}{\partial x_i} \frac{\partial v_j}{\partial x_k} + \gamma_{ijkl}\, \epsilon_{ij}\, \epsilon_{kl} \right) dV_f \tag{22}$$

taken over the final volume V_f. This is equivalent to PEARSON's (10) and also particularizes to his (13) when the total distortion is so small that $\gamma_{ijkl} \sim c_{ijkl} \sim$ the matrix of elastic constants in the unstrained state. Alternatively, (22) could be derived at once from (20) and the second-order approximation

$$\tfrac{1}{2} \int (\delta s_{ij})_f \frac{\partial}{\partial x_i} (\delta u_j)\, dV_f$$

for the increment in potential energy.

6. Incompressible Solid

When the solid is incompressible the analysis has to be modified and becomes less elegant. The general conclusions are unaltered, save in obvious details.*

The strain-energy density can of course only be measured for strains that produce no change in volume and are therefore subject to the restriction

$$\left| \frac{\partial x_j}{\partial a_i} \right| = 1 \qquad \text{or} \qquad |\delta_{ij} + 2e_{ij}| = 1. \tag{23}$$

Let E now denote a function equal to the strain-energy density for incompressible strains but arbitrarily defined for all other (virtual) strains. Then $s_{ij}\, \delta\, (\partial u_j / \partial a_i) = \delta E$ for arbitrary variations of the displacement gradients in accord with (23) or an equivalent. Hence, if σ is a Lagrangian multiplier,

$$s_{ij} = \frac{\partial E}{\partial\, (\partial u_j / \partial a_i)} + \sigma \frac{\partial a_i}{\partial x_j}, \tag{24}$$

since
$$\frac{\partial a_i}{\partial x_j}\, \delta \left(\frac{\partial u_j}{\partial a_i} \right) = \frac{\partial}{\partial x_j}\, \delta u_j = 0$$

for variations producing no change in volume. From the first part of (9),

$$\sigma_{ij} = \frac{\partial x_i}{\partial a_l} \frac{\partial x_j}{\partial a_k} \frac{\partial E}{\partial e_{lk}} + \sigma \delta_{ij}. \tag{25}$$

The relation between σ and the stress is found in principle by eliminating the

*For instance, uniqueness can only be proved to within a uniform hydrostatic stress when $S_F = 0$.

displacement gradients from (23) and (24) or (25), and must evidently reflect the arbitrariness in the choice of E.

Consider, for example, the RIVLIN material (1948)

$$E = \mu e_{ii} = \mu \left(\frac{\partial u_i}{\partial a_i} + \tfrac{1}{2} \frac{\partial u_k}{\partial a_i} \frac{\partial u_k}{\partial a_i} \right) \tag{26}$$

where μ is a constant. For small strains $E(e_{ij})$ reduces to the classical quadratic expression for an incompressible solid, and μ is identified with the rigidity modulus. Generally, from (26) and the first of (23),

$$|\sigma_{ij} - \sigma \delta_{ij}| = \mu^3. \tag{27}$$

When this cubic for σ has three real roots the algebraically greatest must be taken.

A short calculation shows that the functional (13) or (15) becomes

$$\int \left(e_{ijkl} \frac{\partial v_j}{\partial a_i} \frac{\partial v_l}{\partial a_k} - \sigma \frac{\partial v_i}{\partial x_j} \frac{\partial v_j}{\partial x_i} \right) dV \tag{28}$$

where v_i, written instead of Δv_i or δu_i, is any incompressible velocity field vanishing on S_v. In (19) the second term now disappears, while (20) is replaced by

$$(\dot{s}_{ij})_f = \dot{\sigma} \delta_{ij} - 2\sigma \epsilon_{ij} + \sigma_{ik} \frac{\partial v_j}{\partial x_k} + \gamma_{ijkl} \epsilon_{kl} \tag{29}$$

which is obtainable from (19) and (25). Hence, in place of (22), the stability functional is

$$\int \left(- 2\sigma \epsilon_{ij}^2 + \sigma_{ik} \frac{\partial v_j}{\partial x_i} \frac{\partial v_j}{\partial x_k} + \gamma_{ijkl} \epsilon_{ij} \epsilon_{kl} \right) dV. \tag{30}$$

The application of (30) greatly simplifies for the RIVLIN material since $\gamma_{ijkl} \equiv 0$ from (18) and (26). As an illustration consider the condition for stability under dead-loading corresponding to a current all-round tension stress t, the body being undeformed and of arbitrary shape. From (27) $\sigma = t - \mu$ and so (30) can be put in the form

$$\int \left[(2\mu - t) \epsilon_{ij}^2 + \tfrac{1}{4} t \left(\frac{\partial v_j}{\partial x_i} - \frac{\partial v_i}{\partial x_j} \right)^2 \right] dV.$$

The stability limit is plainly $t = 2\mu$ since the integrand is always positive when $t < 2\mu$ and is zero when $t = 2\mu$ for any uniform straining field $v_1 = x_1$, $v_2 = a x_2$, $v_3 = -(1 + a) x_3$, a arbitrary*. The existence of an eigenstate at $t = 2\mu = 2\sigma$ can also be seen immediately from (29) and (21) (with $\dot{g}_j = 0$), which admit the above eigenfields in conjunction with $(\dot{s}_{ij})_f = 0$ and $\dot{\sigma} = 0$.

A more realistic stored-energy function, at least for rubber, is that suggested by MOONEY:

$$E = \alpha e_{ii} + \beta e_{ij} e_{ij}$$

where α, β are constants; the rigidity modulus for small strains is now $\alpha + 2\beta$. In the undeformed state $\gamma_{ijkl} = 2\beta \delta_{ik} \delta_{jl}$ and so the last term in the integrand of (30) is $2\beta \epsilon_{ij}^2$; moreover $\sigma = t - \alpha$. The subsequent analysis is therefore similar to that for the RIVLIN material, the stability limit being $t = 2(\alpha + \beta)$.

*This conflicts with RIVLIN's conclusion (1948, p. 491) that the undeformed state is stable unless t/μ lies between 1 and 3 ($\frac{1}{3}$).

References

Baker, M. and Ericksen, J. L.	1954	*J. Wash. Acad. Sci.* **44**, 33.
Ericksen, J. L. and Toupin, R. A.	1956	*Canad. J. Math.* **8**, 432.
Goodier, J. N. and Plass, H. J.	1952	*Qu. Appl. Math.* **9**, 371.
Hill, R.	1956	*J. Mech. Phys. Solids* **5**, 66.
	1957	*J. Mech. Phys. Solids* **5**, 153.
Jeffreys, H.	1942	*Proc. Camb. Phil. Soc.* **38**, 125.
Koiter, W. T.	1945	*Over de Stabiliteit van het Elastisch Evenwicht* (Thesis, Delft).
Lyttleton, R. A.	1953	*The Stability of Rotating Liquid Masses* pp. 6-13. (Cambridge University Press).
Murnaghan, F. D.	1937	*Amer. J. Math.* **59**, 235.
Pearson, C. E.	1956	*Qu. Appl. Math.* **14**, 133.
Prager, W.	1947	*Qu. Appl. Math.* **4**, 378.
Rivlin, R. S.	1948	*Phil. Trans. Roy. Soc. A* **240**, 459 and 491.
Sokolnikoff, I. S.	1956	*Mathematical Theory of Elasticity* (Second Edition, McGraw-Hill, New York).
Truesdell, C.	1952	*J. Rat. Mech. Anal.* **1**, 125 and **2**, 593.
	1956	*Z. Ang. Math. Mech.* **36**, 97.
Ziegler, H.	1956	*Advances in Applied Mechanics IV* pp. 351-403. (Academic Press, New York).

Journal of the Mechanics and Physics of Solids, 1957, Vol. 5, pp. 242 to 260. Pergamon Press Ltd., London

A GENERAL THEORY OF PIECEWISE LINEAR PLASTICITY BASED ON MAXIMUM SHEAR*

By P. G. Hodge, Jr.
Polytechnic Institute of Brooklyn

(*Received 11th March*, 1957)

Summary

A theory of plasticity is developed for a material which is initially isotropic and satisfies the maximum shear stress initial yield condition. It is shown that the most general piecewise linear theory depends upon 5 material constants. These include the initial yield stress, the rate of hardening, and three constants which describe the effect of hardening upon the condition for further yielding.

A restricted type of problem is then considered in which all stress points continue to load on each face with which they come in contact. For such a problem the flow law can be explicitly integrated. Further, the classical principles of minimum potential and complementary energy are shown to be valid for this integrated law.

The analysis is carried out in three dimensional terms, and the particular case of plane stress is also considered. The general theory is compared with various particular theories which have been proposed in the literature.

1. Introduction

There are two criteria which are important in assessing the validity of a mathematical theory of a physical phenomenon. On the one hand, the theory must be accurate, i.e. it must realistically describe the physical phenomenon. Secondly, the theory must be usable, i.e. it must be suitable for making predictions. Obviously, these two goals are not sharply defined. Accuracy and usability are only relative terms; the judgment of the scientist must determine the degree to which they are achieved. As modern technology extends into more complex fields of physical behaviour, these two aims of a theory diverge. It becomes more and more difficult to devise theories which satisfy the demands for both accuracy and usefulness. Thus, a theory which was satisfactory on both counts a generation ago may be insufficient on either or both grounds today. Ultimately, a new theory of a physical phenomenon can gain acceptance only if it is both sufficiently accurate and useful. However, the initial formulation of such a theory generally proceeds with one goal or the other in the forefront. Although in some respects it is more natural to start with the physical phenomenon in all its complexities, there are certain advantages to the opposing viewpoint.

In the present paper, certain assumptions concerning the behaviour of materials in the strain-hardening plastic range will be made on the basis of mathematical convenience. The consequences of these assumptions will be investigated, and the

*The results presented in this paper were obtained in the course of research sponsored by the Office of Naval Research

results will be a consistent theory of plasticity. Further, the theory will be reasonably simple, so that predictions can be based upon it. Whether or not the theory is also accurate is beyond the scope of the paper. Certainly this aspect must be investigated experimentally before the theory can be used with confidence. However, it will be shown that the theory includes as special cases various particular theories which have been proposed in the literature, so that there is at least a reasonable basis for giving it serious consideration.

The basic mathematical idea behind the proposed theory is the concept of piecewise linearity. This concept is as old as plasticity itself, since the yield condition proposed by TRESCA in 1868 is a piecewise linear one. However, it was only as recent as 1953, with the appearance of papers by KOITER (1953 a, b), PRAGER (1953), and HODGE (1953b), that the subject was first exploited in any detail. All of this work was done under the assumption that the material strain hardened in an isotropic manner or not at all. In 1955 SANDERS (1955) presented a significant paper in which he discussed piecewise linear plasticity from a general viewpoint. His essential contribution was to consider the loading mechanism at the intersection of two or more linear loading surfaces as a combination of the individual mechanisms. Various combinations of loading and unloading must, of course, be considered. The nature of the combinations of loading was left completely unspecified, so that in a sense SANDERS' work is the background of a theory, rather than an actual theory of plasticity.

The next significant development was the formulation by PRAGER (1955) of a particular theory of non-isotropic hardening of initially isotropic materials. This paper also was the first to recognize explicitly an important basic advantage to piecewise linear theory, namely, the partial independence of the final state upon the loading path. Later, PRAGER (1956) applied the theory to an example in circular plate theory. Meanwhile HODGE (1956 a, b ; 1957 a, b) had been further investigating isotropic hardening and had also constructed a combined theory which contained PRAGER's theory and isotropic hardening as special cases.

The present paper is concerned with a general approach to the problem of piecewise linear plasticity. Certain basic assumptions and definitions will be made in section 2, and the most general theory consistent with these assumptions will be derived in the next section. The flow law for each plastic régime will be explicitly given, and criteria will be provided by which the various plastic régimes may be distinguished. In section 4 a restricted theory, based on the general theory, will be developed. For this restricted theory, the flow laws may be integrated to yield direct relations between stress and strain. Also, as will be shown in section 5, the classical principles of minimum potential and minimum complementary energy are valid for this restricted theory. Finally, the paper will close with a discussion of the limitations of the theory and its relation to previous theories discussed in the references cited.

2. Basic Assumption

As in most theories of plasticity, it is assumed that the total strain at any time can be divided into an elastic or recoverable part, and a plastic or permanent part. For simplicity of exposition, the plastic strains only will be considered.

Since elastic strains are assumed to be governed by Hooke's law, they can easily be added to the analysis if desired.

Since the proposed theory is based upon the condition of maximum shear it is assumed that there are no strains so long as the maximum shear stress is less than one half the yield stress Y in simple tension. Thus, in Fig. 1, the material

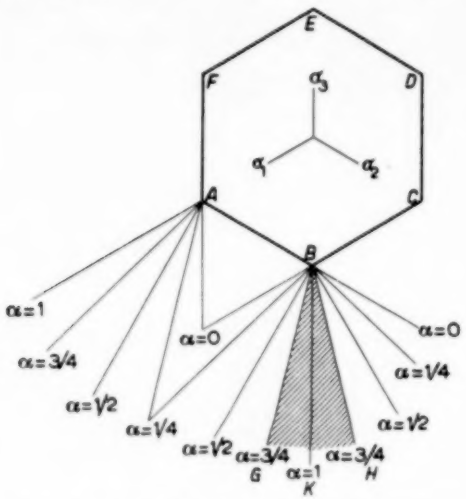

Fig. 1. Initial yield domain and motion of corners.

is rigid so long as the stress point remains in the interior of the hexagon $ABCDEF$.

For a stress point which moves outside of the hexagon $ABCDEF$, plastic straining will occur. It is assumed that this falls within the general frame-work of the plastic potential flow law (Bishop and Hill 1951, Drucker 1952, and Mises 1928), which states that the flow vector whose components are the principal strain rates must be normal to the yield surface on each face, and must lie between the limiting normals at each corner.

Within the limits already set, it still remains to determine the magnitude of the strain rate vector for each face and corner and the effect of strain hardening on the motion of the hexagon. In determining these relations, it will be assumed that the material is initially isotropic, and that all relations are piecewise linear. Initial isotropy does not preclude the introduction of anisotropic behaviour due to plastic flow. However, it does imply that once the flow laws have been established for one side and one corner of the hexagon in Fig. 1, they can be immediately adapted to the other sides and corners by suitable permutations of the principal stresses and strain rates.

The assumption of piecewise linearity states that in each plastic regime (i.e. side or corner) there exist linear relationships between the stress rates and strain rates whose coefficients are material constants independent of the strain history of the material. In addition, the effect of strain hardening upon the behaviour of the yield condition itself is also linear.

Finally, it will be assumed that the material is incompressible, and that the hydrostatic pressure has no effect upon the plastic behaviour.

3. Development of Theory

The flow law for a side of the hexagon will be considered first. On the side AB the conditions of normality and incompressibility require that

$$\dot{\epsilon}_2 = 0, \qquad \dot{\epsilon}_1 + \dot{\epsilon}_3 = 0. \tag{3.1}$$

The most general linear relationship available under the restrictions of (3.1) will express the strain rate $\dot{\epsilon}_1$ as a linear combination of the three principal stress rates. Such a relation may be conveniently written

$$\dot{\epsilon}_1 = A(\dot{\sigma}_1 - \dot{\sigma}_3) + B(\dot{\sigma}_2 - \dot{\sigma}_3) + C(\dot{\sigma}_1 + \dot{\sigma}_2 + \dot{\sigma}_3). \tag{3.2}$$

Since the plastic behaviour is independent of the hydrostatic pressure, C must equal zero, and the flow law on side AB may be written

$$\begin{aligned} \dot{\epsilon}_1 &= A(\dot{\sigma}_1 - \dot{\sigma}_3) + B(\dot{\sigma}_2 - \dot{\sigma}_3), \qquad \dot{\epsilon}_2 = 0, \\ \dot{\epsilon}_3 &= A(\dot{\sigma}_3 - \dot{\sigma}_1) + B(\dot{\sigma}_3 - \dot{\sigma}_2), \qquad \text{on } AB. \end{aligned} \tag{3.3}$$

Now, since the side ED is diametrically opposite the side AB, the flow law for ED is obtained from (3.3) by multiplying through by -1:

$$\begin{aligned} -\dot{\epsilon}_1 &= A(\dot{\sigma}_3 - \dot{\sigma}_1) + B(\dot{\sigma}_3 - \dot{\sigma}_2), \qquad -\dot{\epsilon}_2 = 0, \\ -\dot{\epsilon}_3 &= A(\dot{\sigma}_1 - \dot{\sigma}_3) + B(\dot{\sigma}_2 - \dot{\sigma}_3), \qquad \text{on } ED. \end{aligned} \tag{3.4}$$

On the other hand, on side ED the roles of σ_1 and σ_3 are reversed from what they are on AB, while the two sides are symmetrically located with respect to σ_2. Therefore, the flow law for ED may also be obtained by interchanging the subscripts 1 and 3 in (3.3):

$$\begin{aligned} \dot{\epsilon}_3 &= A(\dot{\sigma}_3 - \dot{\sigma}_1) + B(\dot{\sigma}_2 - \dot{\sigma}_1), \qquad \dot{\epsilon}_2 = 0, \\ \dot{\epsilon}_1 &= A(\dot{\sigma}_1 - \dot{\sigma}_3) + B(\dot{\sigma}_1 - \dot{\sigma}_2), \qquad \text{on } ED. \end{aligned} \tag{3.5}$$

Since (3.4) and (3.5) must express the same result regardless of how the stress point moves on side ED, the constant B must equal zero. Finally, since A is different from zero, a new constant may be defined by

$$c = 1/A, \tag{3.6}$$

and the flow law written

$$c\dot{\epsilon}_1 = \dot{\sigma}_1 - \dot{\sigma}_3, \qquad \dot{\epsilon}_2 = 0, \qquad c\dot{\epsilon}_3 = \dot{\sigma}_3 - \dot{\sigma}_1 \text{ on } AB. \tag{3.7}$$

Similar results are valid for the other five sides of the hexagon. The results are shown in Table 1a. Due to the initial isotropy, the constant c is the same in each case.

At a typical corner B the conditions of normality and incompressibility require only that

$$\dot{\epsilon}_1 + \dot{\epsilon}_2 + \dot{\epsilon}_3 = 0, \tag{3.8}$$

so that two independent relations of the type in (3.2) may hold, where constants are to be determined anew. As on the side, C must equal zero. Further, the relations must reflect the symmetry of the corner B with respect to the σ_1 and σ_2 axes. Therefore, the flow laws may be written

TABLE 1a. *Flow laws for side régimes*

Régime		*AB*	*BC*	*CD*	*DE*	*EF*	*FA*
Flow law		$\dot{\sigma}_1 - \dot{\sigma}_3 = c\dot{\epsilon}_1$	$\dot{\sigma}_2 - \dot{\sigma}_3 = c\dot{\epsilon}_2$	$\dot{\sigma}_2 - \dot{\sigma}_1 = c\dot{\epsilon}_2$	$\dot{\sigma}_3 - \dot{\sigma}_1 = c\dot{\epsilon}_3$	$\dot{\sigma}_3 - \dot{\sigma}_2 = c\dot{\epsilon}_3$	$\dot{\sigma}_1 - \dot{\sigma}_2 = c\dot{\epsilon}_1$
Strain rates	$\dot{\epsilon}_1$	$\dot{\epsilon}_m$	0	$-\dot{\epsilon}_m$	$-\dot{\epsilon}_m$	0	$\dot{\epsilon}_m$
	$\dot{\epsilon}_2$	0	$\dot{\epsilon}_m$	$\dot{\epsilon}_m$	0	$-\dot{\epsilon}_m$	$-\dot{\epsilon}_m$
	$\dot{\epsilon}_3$	$-\dot{\epsilon}_m$	$-\dot{\epsilon}_m$	0	$\dot{\epsilon}_m$	$\dot{\epsilon}_m$	0
Side motions	*AB*	$\dot{\sigma}_1 - \dot{\sigma}_3 = c\dot{\epsilon}_1$	$\dot{\sigma}_1 - \dot{\sigma}_3 = \alpha c\dot{\epsilon}_2$	$\dot{\sigma}_1 - \dot{\sigma}_3 = \beta c\dot{\epsilon}_2$	$\dot{\sigma}_1 - \dot{\sigma}_3 = \gamma c\dot{\epsilon}_3$	$\dot{\sigma}_1 - \dot{\sigma}_3 = \beta c\dot{\epsilon}_3$	$\dot{\sigma}_1 - \dot{\sigma}_3 = \alpha c\dot{\epsilon}_1$
	BC	$\dot{\sigma}_2 - \dot{\sigma}_3 = \alpha c\dot{\epsilon}_1$	$\dot{\sigma}_2 - \dot{\sigma}_3 = c\dot{\epsilon}_2$	$\dot{\sigma}_2 - \dot{\sigma}_3 = \alpha c\dot{\epsilon}_2$	$\dot{\sigma}_2 - \dot{\sigma}_3 = \beta c\dot{\epsilon}_3$	$\dot{\sigma}_2 - \dot{\sigma}_3 = \gamma c\dot{\epsilon}_3$	$\dot{\sigma}_2 - \dot{\sigma}_3 = \beta c\dot{\epsilon}_1$
	CD	$\dot{\sigma}_2 - \dot{\sigma}_1 = \beta c\dot{\epsilon}_1$	$\dot{\sigma}_2 - \dot{\sigma}_1 = \alpha c\dot{\epsilon}_2$	$\dot{\sigma}_2 - \dot{\sigma}_1 = c\dot{\epsilon}_2$	$\dot{\sigma}_2 - \dot{\sigma}_1 = \alpha c\dot{\epsilon}_3$	$\dot{\sigma}_2 - \dot{\sigma}_1 = \beta c\dot{\epsilon}_3$	$\dot{\sigma}_2 - \dot{\sigma}_1 = \gamma c\dot{\epsilon}_1$
	DE	$\dot{\sigma}_3 - \dot{\sigma}_1 = \gamma c\dot{\epsilon}_1$	$\dot{\sigma}_3 - \dot{\sigma}_1 = \beta c\dot{\epsilon}_2$	$\dot{\sigma}_3 - \dot{\sigma}_1 = \alpha c\dot{\epsilon}_2$	$\dot{\sigma}_3 - \dot{\sigma}_1 = c\dot{\epsilon}_3$	$\dot{\sigma}_3 - \dot{\sigma}_1 = \alpha c\dot{\epsilon}_3$	$\dot{\sigma}_3 - \dot{\sigma}_1 = \beta c\dot{\epsilon}_1$
	EF	$\dot{\sigma}_3 - \dot{\sigma}_2 = \beta c\dot{\epsilon}_1$	$\dot{\sigma}_3 - \dot{\sigma}_2 = \gamma c\dot{\epsilon}_2$	$\dot{\sigma}_3 - \dot{\sigma}_2 = \beta c\dot{\epsilon}_2$	$\dot{\sigma}_3 - \dot{\sigma}_2 = \alpha c\dot{\epsilon}_3$	$\dot{\sigma}_3 - \dot{\sigma}_2 = c\dot{\epsilon}_3$	$\dot{\sigma}_3 - \dot{\sigma}_2 = \alpha c\dot{\epsilon}_1$
	FA	$\dot{\sigma}_1 - \dot{\sigma}_2 = \alpha c\dot{\epsilon}_1$	$\dot{\sigma}_1 - \dot{\sigma}_2 = \beta c\dot{\epsilon}_2$	$\dot{\sigma}_1 - \dot{\sigma}_2 = \gamma c\dot{\epsilon}_2$	$\dot{\sigma}_1 - \dot{\sigma}_2 = \beta c\dot{\epsilon}_3$	$\dot{\sigma}_1 - \dot{\sigma}_2 = \alpha c\dot{\epsilon}_3$	$\dot{\sigma}_1 - \dot{\sigma}_2 = c\dot{\epsilon}_1$

TABLE 1b. *Flow laws for corner régimes*

Régime		*A*	*B*	*C*	*D*	*E*	*F*
Flow laws		$\dot{\sigma}_2 - \dot{\sigma}_1 = c(\dot{\epsilon}_2 + \alpha\dot{\epsilon}_3)$ $\dot{\sigma}_3 - \dot{\sigma}_1 = c(\dot{\epsilon}_3 + \alpha\dot{\epsilon}_2)$	$\dot{\sigma}_2 - \dot{\sigma}_3 = c(\dot{\epsilon}_2 + \alpha\dot{\epsilon}_1)$ $\dot{\sigma}_1 - \dot{\sigma}_3 = c(\dot{\epsilon}_1 + \alpha\dot{\epsilon}_2)$	$\dot{\sigma}_3 - \dot{\sigma}_2 = c(\dot{\epsilon}_3 + \alpha\dot{\epsilon}_1)$ $\dot{\sigma}_1 - \dot{\sigma}_2 = c(\dot{\epsilon}_1 + \alpha\dot{\epsilon}_3)$	$\dot{\sigma}_2 - \dot{\sigma}_1 = c(\dot{\epsilon}_2 + \alpha\dot{\epsilon}_3)$ $\dot{\sigma}_3 - \dot{\sigma}_1 = c(\dot{\epsilon}_3 + \alpha\dot{\epsilon}_2)$	$\dot{\sigma}_2 - \dot{\sigma}_3 = c(\dot{\epsilon}_2 + \alpha\dot{\epsilon}_1)$ $\dot{\sigma}_1 - \dot{\sigma}_3 = c(\dot{\epsilon}_1 + \alpha\dot{\epsilon}_2)$	$\dot{\sigma}_3 - \dot{\sigma}_2 = c(\dot{\epsilon}_3 + \alpha\dot{\epsilon}_1)$ $\dot{\sigma}_1 - \dot{\sigma}_2 = c(\dot{\epsilon}_1 + \alpha\dot{\epsilon}_3)$
Strain rates	$\dot{\epsilon}_1$	$\dot{\epsilon}_m$	> 0	< 0	$-\dot{\epsilon}_m$	< 0	> 0
	$\dot{\epsilon}_2$	< 0	> 0	$\dot{\epsilon}_m$	> 0	< 0	$-\dot{\epsilon}_m$
	$\dot{\epsilon}_3$	< 0	$-\dot{\epsilon}_m$	< 0	> 0	$\dot{\epsilon}_m$	> 0
Side motions	*AB*	$\dot{\sigma}_3 - \dot{\sigma}_1 = c(\alpha\dot{\epsilon}_2 + \dot{\epsilon}_3)$	$\dot{\sigma}_1 - \dot{\sigma}_3 = c(\dot{\epsilon}_1 + \alpha\dot{\epsilon}_2)$	$\dot{\sigma}_3 - \dot{\sigma}_1 = c(\alpha\dot{\epsilon}_3 + \beta\dot{\epsilon}_1)$	$\dot{\sigma}_1 - \dot{\sigma}_3 = c(\beta\dot{\epsilon}_2 + \gamma\dot{\epsilon}_3)$	$\dot{\sigma}_3 - \dot{\sigma}_1 = c(\gamma\dot{\epsilon}_1 + \beta\dot{\epsilon}_2)$	$\dot{\sigma}_1 - \dot{\sigma}_3 = c(\beta\dot{\epsilon}_3 + \alpha\dot{\epsilon}_1)$
	BC	$\dot{\sigma}_3 - \dot{\sigma}_2 = c(\beta\dot{\epsilon}_2 + \alpha\dot{\epsilon}_3)$	$\dot{\sigma}_2 - \dot{\sigma}_3 = c(\alpha\dot{\epsilon}_1 + \dot{\epsilon}_2)$	$\dot{\sigma}_3 - \dot{\sigma}_2 = c(\dot{\epsilon}_3 + \alpha\dot{\epsilon}_1)$	$\dot{\sigma}_2 - \dot{\sigma}_3 = c(\alpha\dot{\epsilon}_2 + \beta\dot{\epsilon}_3)$	$\dot{\sigma}_3 - \dot{\sigma}_2 = c(\beta\dot{\epsilon}_1 + \gamma\dot{\epsilon}_2)$	$\dot{\sigma}_2 - \dot{\sigma}_3 = c(\gamma\dot{\epsilon}_3 + \beta\dot{\epsilon}_1)$
	CD	$\dot{\sigma}_1 - \dot{\sigma}_2 = c(\gamma\dot{\epsilon}_2 + \beta\dot{\epsilon}_3)$	$\dot{\sigma}_2 - \dot{\sigma}_1 = c(\beta\dot{\epsilon}_1 + \alpha\dot{\epsilon}_2)$	$\dot{\sigma}_1 - \dot{\sigma}_2 = c(\alpha\dot{\epsilon}_3 + \dot{\epsilon}_1)$	$\dot{\sigma}_2 - \dot{\sigma}_1 = c(\dot{\epsilon}_2 + \alpha\dot{\epsilon}_3)$	$\dot{\sigma}_1 - \dot{\sigma}_2 = c(\alpha\dot{\epsilon}_1 + \beta\dot{\epsilon}_2)$	$\dot{\sigma}_2 - \dot{\sigma}_1 = c(\beta\dot{\epsilon}_3 + \gamma\dot{\epsilon}_1)$
	DE	$\dot{\sigma}_1 - \dot{\sigma}_3 = c(\beta\dot{\epsilon}_2 + \gamma\dot{\epsilon}_3)$	$\dot{\sigma}_3 - \dot{\sigma}_1 = c(\gamma\dot{\epsilon}_1 + \beta\dot{\epsilon}_2)$	$\dot{\sigma}_1 - \dot{\sigma}_3 = c(\beta\dot{\epsilon}_3 + \alpha\dot{\epsilon}_1)$	$\dot{\sigma}_3 - \dot{\sigma}_1 = c(\alpha\dot{\epsilon}_2 + \dot{\epsilon}_3)$	$\dot{\sigma}_1 - \dot{\sigma}_3 = c(\dot{\epsilon}_1 + \alpha\dot{\epsilon}_2)$	$\dot{\sigma}_3 - \dot{\sigma}_1 = c(\alpha\dot{\epsilon}_3 + \beta\dot{\epsilon}_1)$
	EF	$\dot{\sigma}_2 - \dot{\sigma}_3 = c(\alpha\dot{\epsilon}_2 + \beta\dot{\epsilon}_3)$	$\dot{\sigma}_3 - \dot{\sigma}_2 = c(\beta\dot{\epsilon}_1 + \gamma\dot{\epsilon}_2)$	$\dot{\sigma}_2 - \dot{\sigma}_3 = c(\gamma\dot{\epsilon}_3 + \beta\dot{\epsilon}_1)$	$\dot{\sigma}_3 - \dot{\sigma}_2 = c(\beta\dot{\epsilon}_2 + \alpha\dot{\epsilon}_3)$	$\dot{\sigma}_2 - \dot{\sigma}_3 = c(\alpha\dot{\epsilon}_1 + \dot{\epsilon}_2)$	$\dot{\sigma}_3 - \dot{\sigma}_2 = c(\dot{\epsilon}_3 + \alpha\dot{\epsilon}_1)$
	FA	$\dot{\sigma}_2 - \dot{\sigma}_1 = c(\dot{\epsilon}_2 + \alpha\dot{\epsilon}_3)$	$\dot{\sigma}_1 - \dot{\sigma}_2 = c(\dot{\epsilon}\alpha_1 + \beta\dot{\epsilon}_2)$	$\dot{\sigma}_2 - \dot{\sigma}_1 = c(\beta\dot{\epsilon}_3 + \gamma\dot{\epsilon}_1)$	$\dot{\sigma}_1 - \dot{\sigma}_2 = c(\gamma\dot{\epsilon}_2 + \beta\dot{\epsilon}_3)$	$\dot{\sigma}_2 - \dot{\sigma}_1 = c(\beta\dot{\epsilon}_1 + \alpha\dot{\epsilon}_2)$	$\dot{\sigma}_1 - \dot{\sigma}_2 = c(\alpha\dot{\epsilon}_3 + \dot{\epsilon}_1)$

$$\dot{\epsilon}_1 = A\,(\dot{\sigma}_1 - \dot{\sigma}_3) + B\,(\dot{\sigma}_2 - \dot{\sigma}_3),$$

$$\dot{\epsilon}_2 = B\,(\dot{\sigma}_1 - \dot{\sigma}_3) + A\,(\dot{\sigma}_2 - \dot{\sigma}_3), \qquad \text{on } B. \tag{3.9}$$

Except for the degenerate case when $A^2 = B^2$, which will be treated later, (3.9) can be inverted to yield

$$\dot{\sigma}_1 - \dot{\sigma}_3 = D\,(\dot{\epsilon}_1 + \alpha\dot{\epsilon}_2), \qquad \dot{\sigma}_2 - \dot{\sigma}_3 = D\,(\dot{\epsilon}_2 + \alpha\dot{\epsilon}_1), \qquad \text{on } B \tag{3.10}$$

where the new constants D and α are defined by

$$D = A/(A^2 - B^2), \qquad \alpha = -B/A. \tag{3.11}$$

The constant D can be related to the constant c in (3.7) by considering the transition case of a stress point which moves with the point B regarded as a point on AB. In such a case (3.7) and (3.10) must be simultaneously valid so that

$$\dot{\sigma}_1 - \dot{\sigma}_3 = c\dot{\epsilon}_1 = D\,(\dot{\epsilon}_1 + \alpha\,.\,0), \tag{3.12}$$

$$\dot{\sigma}_2 - \dot{\sigma}_3 = D\,\alpha\dot{\epsilon}_1 = \alpha\,(\dot{\sigma}_1 - \dot{\sigma}_3). \tag{3.13}$$

Equation (3.12) establishes that

$$D = c, \tag{3.14}$$

so that the flow law in corner B is given by

$$\dot{\sigma}_1 - \dot{\sigma}_3 = c\,(\dot{\epsilon}_1 + \alpha\dot{\epsilon}_2), \qquad \dot{\sigma}_2 - \dot{\sigma}_3 = c\,(\dot{\epsilon}_2 + \alpha\dot{\epsilon}_1) \qquad \text{on } B. \tag{3.15}$$

Similar laws are valid for the other five corners. The results are summarized in Table 1b.

Equation (3.13) describes the motion of the corner B under a stress point which remains at the transition between AB and B. Similar relations are available for the interaction of B with BC, A with AB, etc. Typical results are shown in Fig. 1.

Equation (3.13) also serves to answer the question as to whether a stress point at B is to be considered in the corner or on the side. It follows from (3.13) that it will be on the side AB if

$$\dot{\sigma}_2 - \dot{\sigma}_3 < \alpha\,(\dot{\sigma}_1 - \dot{\sigma}_3). \tag{3.16}$$

Similarly, it will be on the side BC if

$$\dot{\sigma}_1 - \dot{\sigma}_3 < \alpha\,(\dot{\sigma}_2 - \dot{\sigma}_3). \tag{3.17}$$

Finally, it will remain in the corner if

$$\dot{\sigma}_2 - \dot{\sigma}_3 > \alpha\,(\dot{\sigma}_1 - \dot{\sigma}_3),$$

$$\dot{\sigma}_1 - \dot{\sigma}_3 > \alpha\,(\dot{\sigma}_2 - \dot{\sigma}_3). \tag{3.18}$$

For example, if $\alpha = \frac{3}{4}$, it follows from Fig. 1 that if the stress point moves from B into the shaded wedge GBH, then it will remain in contact with the corner and be governed by (3.15). On the other hand, if the stress point moves in the region ABG, it will be governed by (3.7). In the former case the corner will move with the stress point; in the latter case the corner will move along BG.

Fig. 1 immediately indicates restrictions on the admissible values of the constant α. First, α must be equal or less than one since otherwise the stress point could

move to the right of BK and be in régime AB or to the left of BK and be in régime BC – a result which is patently absurd. Next, it follows that if the stresses can increase significantly above the initial yield stress, that α cannot be less than $\frac{1}{2}$. For example, if $\alpha = \frac{1}{4}$, then side AB will disappear when the stress point advances to the point J on side BC. Further motion would then be governed simultaneously by the laws for corners A and B which is impossible. Therefore, the parameter α must satisfy.

$$\tfrac{1}{2} \leqslant \alpha \leqslant 1. \tag{3.19}$$

Equations (3.10) were obtained from (3.9) under the assumption that $B^2 \neq A^2$. In view of (3.11), $B = \pm A$ corresponds to $\alpha = \mp 1$. It follows from (3.19) that only the case $\alpha = +1$ ($B = -A$) needs to be considered. In this case (3.15) becomes

$$\dot{\sigma}_1 - \dot{\sigma}_3 = c\,(\dot{\epsilon}_1 + \dot{\epsilon}_2) = \dot{\sigma}_2 - \dot{\sigma}_3 \text{ on } B. \tag{3.20}$$

This is consistent with Fig. 1, which indicates that the stress point must move along the line BK if it is to stay in the corner B. Since Equation (3.20) cannot be solved for the strain rates, it appears that it is Equations (3.9) which have no meaning when $B = -A$, and that (3.15) can be used for all values of α satisfying (3.19).

As plastic straining takes place, the original yield hexagon $ABCDEF$ must change so as always to include the current stress point. Within the assumptions of piecewise linearity each side of the hexagon is free to translate independently. Rotations, the formation of new sides, or the disappearance of sides are not allowed. It follows that at any time the current yield condition will be a hexagon, but that it may no longer be regular, centred at the origin, or of the same size.

If the stress point moves along the side AB, the strain rate is characterized by the single quantity $\dot{\epsilon}_1$. If this is regarded as known, then the first of (3.7) can be taken as characterizing the motion of side AB:

$$\dot{\sigma}_1 - \dot{\sigma}_3 = c\dot{\epsilon}_1, \qquad \text{motion of } AB. \tag{3.21}$$

The motion of the corner B is determined by (3.13) for stress points on AB. Since the side BC can move only parallel to itself, this is then determined:

$$\dot{\sigma}_2 - \dot{\sigma}_3 = \alpha c\dot{\epsilon}_1, \qquad \text{motion of } BC. \tag{3.22}$$

Similarly, the motion of the corner A and hence of the side FA is given by

$$\dot{\sigma}_1 - \dot{\sigma}_2 = \alpha c\dot{\epsilon}_1, \qquad \text{motion of } FA. \tag{3.23}$$

Since the motion of side CD is independent of that of the other sides, a new parameter must be introduced. If the relative magnitude of this motion is denoted by β, the relation

$$\dot{\sigma}_2 - \dot{\sigma}_1 = \beta c\dot{\epsilon}_1, \qquad \text{on } CD, \tag{3.24}$$

is obtained. By symmetry, the motion of EF must be the same as that of CD, so that

$$\dot{\sigma}_3 - \dot{\sigma}_2 = \beta c\dot{\epsilon}_1, \qquad \text{on } EF. \tag{3.25}$$

Finally, the motion of the remaining side DE may be written in terms of an additional parameter γ:

$$\dot{\sigma}_3 - \dot{\sigma}_1 = \gamma c\dot{\epsilon}_1, \qquad \text{on } DE. \tag{3.26}$$

The assumption that the hexagon must remain a hexagon imposes certain restrictions upon the admissible values of β and γ. Thus the rate of motion of the intersection of sides CD and EF in the direction of the outward normal to the side AB must be less than the motion of ED in the same direction, or else side ED would disappear. Similarly, the motion of ED in that direction must be less than that of the corners C or F if the sides CD and EF are to remain. Similar arguments show that the motion of corners C and F must be less than that of side AB, which, in turn must be less than the intersection of sides BC and FA.

The component of motion in the direction of the outward normal to AB is given by $\dot{\sigma}_1 - \dot{\sigma}_3$. For each of the intersections and lines considered, this is easily found from Table 1. For example, if the stress point is on side AB, the intersection of sides CD and EF must satisfy.

$$\dot{\sigma}_2 - \dot{\sigma}_1 = \beta c\dot{\epsilon}_1, \qquad \dot{\sigma}_3 - \dot{\sigma}_2 = \beta c\dot{\epsilon}_1\,; \tag{3.27}$$

hence

$$\dot{\sigma}_1 - \dot{\sigma}_3 = -2\beta c\dot{\epsilon}_1, \qquad \text{intersection of } CD,\ EF. \tag{3.28}$$

The following results are obtained in a similar manner :

$$\begin{aligned}
&\dot{\sigma}_1 - \dot{\sigma}_3 = -\gamma c\dot{\epsilon}_1, && \text{side } DE\,;\\
&\dot{\sigma}_1 - \dot{\sigma}_3 = (\alpha - \beta)\, c\dot{\epsilon}_1, && \text{corners } C \text{ or } F\,;\\
&\dot{\sigma}_1 - \dot{\sigma}_3 = c\dot{\epsilon}_1, && \text{side } AB\\
&\dot{\sigma}_1 - \dot{\sigma}_3 = 2\alpha c\dot{\epsilon}_1, && \text{intersection of } BC,\ FA.
\end{aligned} \tag{3.29}$$

If there is to be no overtaking, then the following inequalities must hold on α, β and γ.

$$-2\beta \leqslant -\gamma \leqslant \alpha - \beta \leqslant 1 \leqslant 2\alpha \tag{3.30}$$

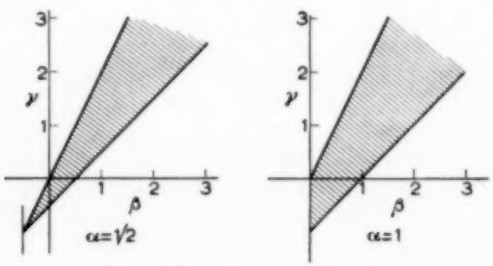

Fig. 2. Admissible values of α, β, γ.

In addition, α must satisfy (3.19). The shaded region in Fig. 2 indicates values of β and γ which satisfy (3.30) for typical values of α. It is readily verified that a consideration of motion in other directions or of stress points on other régimes does not lead to any further restrictions on α, β, or γ.

4. Theory of Regular Progression

As long as a stress point remains on a particular side or corner. the flow laws

in Table 1 can be integrated to obtain direct relations between stress and strain. These integrated laws will contain the stress and strains at which the stress point first entered the plastic regime in question as initial conditions. Therefore, as the stress point moves from one régime to another, a piecewise ' deformation theory ' of plasticity, which contains the transition stresses and strains as unknowns is obtained.

A particularly simple theory is obtained when the stress point either remains on a given side or corner, or moves from a side to an adjacent corner. This condition may be characterized as complete loading, in that once the loading mechanism of a side is activated it is never stopped. From this view-point, the loading mechanism at a corner is to be thought of as a combination of the mechanisms of either side. Stress points which move in this fashion are said to progress regularly.

TABLE 2. *Stress strain law for regular progression*

Régime	*General stress-strain law*	*Strains* ϵ_1	ϵ_2	ϵ_3	*Plane stress stress-strain law*
A	$\sigma_2 - \sigma_1 + Y = c(\epsilon_2 + \alpha\epsilon_3)$ $\sigma_3 - \sigma_1 + Y = c(\epsilon_3 + \alpha\epsilon_2)$	ϵ_m	−	−	$\sigma_1 - Y = c[\epsilon_1 + (1-\alpha)\epsilon_2]$ $\sigma_2 = c(1-\alpha)(\epsilon_1 + 2\epsilon_2)$
AB	$\sigma_1 - \sigma_3 - Y = c\epsilon_1$	ϵ_m	0	$-\epsilon_m$	$\sigma_1 - Y = c\epsilon_1$
B	$\sigma_2 - \sigma_3 - Y = c(\epsilon_2 + \alpha\epsilon_1)$ $\sigma_1 - \sigma_3 - Y = c(\epsilon_1 + \alpha\epsilon_2)$	+	+	$-\epsilon_m$	$\sigma_1 - Y = c(\epsilon_1 + \alpha\epsilon_2)$ $\sigma_2 - Y = c(\epsilon_2 + \alpha\epsilon_1)$
BC	$\sigma_2 - \sigma_3 - Y = c\epsilon_2$	0	ϵ_m	$-\epsilon_m$	$\sigma_2 - Y = c\epsilon_2$
C	$\sigma_3 - \sigma_2 + Y = c(\epsilon_3 + \alpha\epsilon_1)$ $\sigma_1 - \sigma_2 + Y = c(\epsilon_1 + \alpha\epsilon_3)$	−	ϵ_m	−	$\sigma_1 = c(1-\alpha)(2\epsilon_1 + \epsilon_2)$ $\sigma_2 - Y = c[(1-\alpha)\epsilon_1 + \epsilon_2]$
CD	$\sigma_2 - \sigma_1 - Y = c\epsilon_2$	$-\epsilon_m$	ϵ_m	0	$\sigma_2 - \sigma_1 - Y = c\epsilon_2$
D	$\sigma_2 - \sigma_1 - Y = c(\epsilon_2 + \alpha\epsilon_3)$ $\sigma_3 - \sigma_1 - Y = c(\epsilon_3 + \alpha\epsilon_2)$	$-\epsilon_m$	+	+	$\sigma_1 + Y = c[\epsilon_1 + (1-\alpha)\epsilon_2]$ $\sigma_2 = c(1-\alpha)(\epsilon_1 + 2\epsilon_2)$
DE	$\sigma_3 - \sigma_1 - Y = c\epsilon_3$	$-\epsilon_m$	0	ϵ_m	$\sigma_1 + Y = c\epsilon_1$
E	$\sigma_2 - \sigma_3 + Y = c(\epsilon_2 + \alpha\epsilon_1)$ $\sigma_1 - \sigma_3 + Y = c(\epsilon_1 + \alpha\epsilon_2)$	−	−	ϵ_m	$\sigma_1 + Y = c(\epsilon_1 + \alpha\epsilon_2)$ $\sigma_2 + Y = c(\epsilon_2 + \alpha\epsilon_1)$
EF	$\sigma_3 - \sigma_2 - Y = c\epsilon_3$	0	$-\epsilon_m$	ϵ_m	$\sigma_2 + Y = c\epsilon_2$
F	$\sigma_3 - \sigma_2 - Y = c(\epsilon_3 + \alpha\epsilon_1)$ $\sigma_1 - \sigma_2 - Y = c(\epsilon_1 + \alpha\epsilon_3)$	+	$-\epsilon_m$	+	$\sigma_1 = c(1-\alpha)(2\epsilon_1 + \epsilon_2)$ $\sigma_2 + Y = c[(1-\alpha)\epsilon_1 + \epsilon_2]$
FA	$\sigma_1 - \sigma_2 - Y = c\epsilon_1$	ϵ_m	$-\epsilon_m$	0	$\sigma_1 - \sigma_2 - Y = c\epsilon_1$

The case of a stress point which enters side AB is considered first. When the stress point first enters régime AB the strains are zero and the stresses satisfy.

$$\sigma_1 - \sigma_3 = Y. \tag{4.1}$$

Therefore the correct integrals of (3.7) are

$$c\epsilon_1 = \sigma_1 - \sigma_3 - Y, \qquad \epsilon_2 = 0, \qquad c\epsilon_3 = \sigma_3 - \sigma_1 + Y. \tag{4.2}$$

Similar results hold for each side, as indicated in Table 2.

For a stress point which enters the corner B directly the initial conditions are

$$\epsilon_1 = \epsilon_2 = \epsilon_3 = 0, \qquad \sigma_1 - \sigma_3 = Y, \qquad \sigma_2 - \sigma_3 = Y. \tag{4.3}$$

Therefore, the correct integrals of (3.15) are

$$\begin{aligned} \sigma_1 - \sigma_3 - Y &= c\,(\epsilon_1 + \alpha\epsilon_2), \\ \sigma_2 - \sigma_3 - Y &= c\,(\epsilon_2 + \alpha\epsilon_1). \end{aligned} \tag{4.4}$$

Finally, a stress point which enters side AB and then moves to corner B is considered. Equations (4.2) hold while it is in régime AB. Therefore, if the subscript 0 is used to denote the transition conditions between AB and B, these must satisfy

$$c\epsilon_{10} = \sigma_{10} - \sigma_{30} - Y, \qquad \epsilon_{20} = 0, \qquad c\epsilon_{30} = \sigma_{30} - \sigma_{10} + Y. \tag{4.5}$$

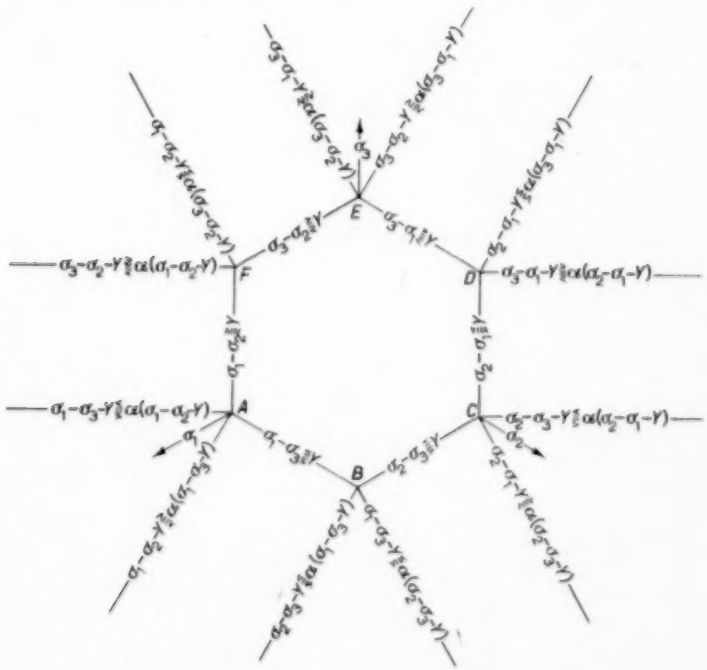

Fig. 3. Régimes for regular progression.

The correct integrals of (3.15) for régime B are now given by

$$\begin{aligned} \sigma_1 - \sigma_3 - (\sigma_{10} - \sigma_{30}) &= c\,(\epsilon_1 + \alpha\epsilon_2) - c\,(\epsilon_{10} + \alpha\epsilon_{20}), \\ \sigma_2 - \sigma_3 - (\sigma_{20} - \sigma_{30}) &= c\,(\epsilon_2 + \alpha\epsilon_1) - c\,(\epsilon_{20} + \alpha\epsilon_{10}). \end{aligned} \tag{4.6}$$

However, it follows from (4.5) that equations (4.6) are identical with (4.4).

Therefore, these latter apply whether the stress points enters régime B directly or by way of an adjacent side. Similar results hold for each corner and are listed in Table 2.

If the stress point is required to progress regularly, then the motion of the distant sides of the hexagon is immaterial ; hence the constants β and γ are of no interest. However, the motion of adjacent sides and corners is relevant since they are needed to check the assumption of regular progression and since they may determine whether a stress point remains on a side or moves into a corner. These motions can also be integrated. For example (3.13) becomes

$$\sigma_2 - \sigma_3 - Y = \alpha\,(\sigma_1 - \sigma_3 - Y) \tag{4.7}$$

for the motion of corner B when the stress point is on AB.

Equation (4.7) represents the dividing line between the side AB and the corner B. If the left side of (4.7) is less than the right side, then the stress point is on the side AB ; if it is greater, the stress point is in the corner B. Thus the condi-

Fig. 4. Régimes for regular progression in plane-strain.

tion that the stress point remain in a particular régime is governed by a set of inequalities representing the boundary of that régime. These results are conveniently summarized in Fig. 3.

Several applications of plasticity theory have been made in the field of plane stress. The theory of plane stress may be obtained from the three dimensional theory by setting $\sigma_3 = 0$. At the same time it is convenient to eliminate ϵ_3 with the incompressibility condition

$$\epsilon_3 = -(\epsilon_1 + \epsilon_2). \tag{4.8}$$

The results are summarized in Table 2 and Fig. 4.

5. Minimum Principles

The theorem of minimum complementary elastic energy states that among all statically admissible stress states the actual one minimizes the total complementary energy. Statically admissible stress states are those which satisfy the boundary conditions on stress and are in internal equilibrium. If the definition of statically admissible stress states is further restricted to require that all stress points progress regularly, then the same theorem is true for piecewise linear plasticity.

Similarly, the theorem of minimum potential elastic energy states that among all geometrically admissible displacement fields the actual one minimizes the total potential energy. A geometrically admissible displacement field is any one which satisfies the geometrical constraints of the problem. For this principle to be valid in piecewise linear plasticity it is necessary to impose two additional requirements on a geometrically admissible stress state. It must be incompressible, and it must be such that a regularly progressing stress state can be associated with it by means of Table 1. However, this associated stress will not, in general, be in equilibrium or satisfy stress boundary conditions.

In the most convenient form of stating these principles it is assumed that the boundary S of a volume V of material under consideration may be divided into regions of two types. On a displacement surface S_D, either the displacements are prescribed or the corresponding traction is zero. In either event, the work done upon two geometrically admissible displacement fields by any set of tractions $\mathbf{T}$ which satisfy the boundary conditions on tractions is the same. On a traction surface S_T, either the tractions are prescribed, or the corresponding displacement is zero. Thus the work done by any two statically admissible sets of tractions upon a geometrically admissible displacement field is the same.

With this terminology, the principle of minimum potential energy states that the actual state minimizes

$$\Pi \equiv \int_V U dv - \int_{S_T} \mathbf{T} \cdot \mathbf{u}\, dS - \int_V \mathbf{f} \cdot \mathbf{u}\, dv. \tag{5.1}$$

among all geometrically admissible displacement fields. Similarly, the principle of minimum complementary energy asserts the minimization of

$$\Pi_c \equiv \int_V U_c\, dV - \int_{S_D} \mathbf{T} \cdot \mathbf{u}\, dS \tag{5.2}$$

among all statically admissible states by the actual state. In (5.1) and (5.2) U and U_c represent the internal potential and complementary potential energy densities:

$$U = \int (\sigma_1\, d\epsilon_1 + \sigma_2\, d\epsilon_2 + \sigma_3\, d\epsilon_3), \tag{5.3}$$

$$U_c = \int (\epsilon_1\, d\sigma_1 + \epsilon_2\, d\sigma_2 + \epsilon_3\, d\sigma_3). \tag{5.4}$$

$\mathbf{T}$ is the traction vector, $\mathbf{u}$ the displacement vector, and $\mathbf{f}$ the body force vector.

The minimum principles may also be stated in the form of inequalities. Thus, if Π^* represents the total potential associated with a geometrically admissible displacement field $\mathbf{u}^*$, and if Π_c° represents the total complementary potential associated with a statically admissible stress field, then the minimum principles state that

$$\Delta\Pi \equiv \Pi^* - \Pi = \int_V (U^* - U)\, dv - \int_{S_T} \mathbf{T} \cdot (\mathbf{u}^* - \mathbf{u})\, dS - \int_V \mathbf{f} \cdot (\mathbf{u}^* - \mathbf{u})\, dv \geqslant 0, \tag{5.5}$$

and

$$\Delta\Pi_c \equiv \Pi_c^\circ - \Pi_c = \int_V (U_c^\circ - U_c)\, dv - \int_{S_D} (\mathbf{T}^\circ - \mathbf{T}) \cdot \mathbf{u}\, dS \geqslant 0. \tag{5.6}$$

In (5.5), the surface integral may be extended over the entire surface, since $\mathbf{T} \cdot (\mathbf{u}^* - \mathbf{u}) = 0$ on S_D by definition. The principle of virtual work can then be employed to transform the entire expression into the volume integral

$$\Delta\Pi = \int_V \left[U^* - U - \sigma_1 (\epsilon_1 - \epsilon_1^*) - \sigma_2 (\epsilon_2 - \epsilon_2^*) - \sigma_3 (\epsilon_3 - \epsilon_3^*)\right] dv. \tag{5.7}$$

Similarly, (5.6) can be transformed to

$$\Delta\Pi_c = \int_V \left[U_c^\circ - U_c - \epsilon_1 (\sigma_1 - \sigma_1^\circ) - \epsilon_2 (\sigma_2 - \sigma_2^\circ) - \epsilon_3 (\sigma_3 - \sigma_3^\circ)\right] dv. \tag{5.8}$$

The evaluation of the integrals (5.3) and (5.4) must be carried out separately for each plastic régime. However, it may readily be verified from Table 2 that the resulting expressions can be written in the form

$$U = \tfrac{1}{2} (\sigma_1 \epsilon_1 + \sigma_2 \epsilon_2 + \sigma_3 \epsilon_3 + Y\epsilon_m), \tag{5.9}$$

$$U_c = \tfrac{1}{2} (\sigma_1 \epsilon_1 + \sigma_2 \epsilon_2 + \sigma_3 \epsilon_3 - Y\epsilon_m), \tag{5.10}$$

for each régime, ϵ_m being the largest absolute principal stress. Finally, then, the expressions for $\Delta\Pi$ and $\Delta\Pi_c$ may be written

$$2\Delta\Pi = \int_V (I_1^* + I_2)\, dv, \tag{5.11}$$

$$2\Delta\Pi_c = \int_V (I_1 + I_2^\circ)\, dv, \tag{5.12}$$

where

$$I_1^* = (\sigma_1^* - 2\sigma_1)\, \epsilon_1^* + (\sigma_2^* - 2\sigma_2)\, \epsilon_2^* + (\sigma_3^* - 2\sigma_3)\, \epsilon_3^* + Y\epsilon_m^*, \tag{5.13}$$

$$I_2 = \sigma_1 \epsilon_1 + \sigma_2 \epsilon_2 + \sigma_3 \epsilon_3 - Y\epsilon_m, \tag{5.14}$$

$$I_1 = (\sigma_1 - 2\sigma_1^\circ)\, \epsilon_1 + (\sigma_2 - 2\sigma_2^\circ)\, \epsilon_2 + (\sigma_3 - 2\sigma_3^\circ)\, \epsilon_3 + Y\epsilon_m, \tag{5.15}$$

$$I_2^\circ = \sigma_1^\circ \epsilon_1^\circ + \sigma_2^\circ \epsilon_2^\circ + \sigma_3^\circ \epsilon_3^\circ - Y\epsilon_m^\circ. \tag{5.16}$$

The proof of the minimum principles is carried out in the usual fashion by showing that the integrands in (5.11) and (5.12) are non-negative. The procedure is somewhat complicated by the fact that the actual state may be in any of 13 régimes (6 sides, 6 corners, or the interior)

in different parts of the body, while the admissible state may independently be in any of the same 13 régimes. Thus there are a total of 169 possible cases to consider. However, due to symmetry, it is necessary to evaluate only 19 of these explicitly.

The principle of minimum potential energy will be proved first. The geometrically admissible state may be in the interior (rigid) régime, on a side, or on a corner. Without loss of generality these latter may be taken to be AB or B, and the following values are obtained for I_1^* :

$$\text{in interior,} \qquad I_1^* = 0\,; \tag{5.17}$$

$$\text{on } AB, \qquad I_1^* = \left[c\epsilon_m^* - 2(\sigma_1 - \sigma_3 - Y)\right]\epsilon_m^*\,; \tag{5.18}$$

$$\text{on } B, \qquad I_1^* = c(\epsilon_1^{*2} + 2\alpha\epsilon_1^*\epsilon_2^* + \epsilon_2^{*2}) - 2\left[(\sigma_1 - \sigma_3 - Y)\epsilon_1^* + (\sigma_2 - \sigma_3 - Y)\epsilon_2^*\right]. \tag{5.19}$$

For each of these three possibilities for the admissible state, the following locations for the actual state must be considered explicitly, all other possibilities being handled by symmetry. If the admissible state is in the interior, the actual state may be in the interior, on AB, or on B. If the admissible state is on AB the actual state may in the interior, on AB, on B, on BC, on C, on CD, on D, or on DE. Finally, if the admissible state is on B, the actual state may be in the interior, on B, on BC, on C, on CD, on D, on DE, or on E.

As a typical example of the manipulations involved, let the admissible state be on AB and the actual state on BC. Then

$$I_2 = (\sigma_2 - \sigma_3 - Y)\epsilon_m \tag{5.20}$$

so that

$$I_1^* + I_2 = \left[c\epsilon_m^* - 2(\sigma_1 - \sigma_3 - Y)\right]\epsilon_m^* + (\sigma_2 - \sigma_3 - Y)\epsilon_m. \tag{5.21}$$

Now, ϵ_m^* is positive, and it follows from Fig. 3 that

$$\sigma_1 - \sigma_3 - Y \leqslant \alpha(\sigma_2 - \sigma_3 - Y) \tag{5.22}$$

in régime BC. Therefore

$$I_1^* + I_2 \geqslant \left[c\epsilon_m^* - 2\alpha(\sigma_2 - \sigma_3 - Y)\right]\epsilon_m^* + (\sigma_2 - \sigma_3 - Y)\epsilon_m. \tag{5.23}$$

Further, it follows from Table 2 that

$$\sigma_2 - \sigma_3 - Y = c\epsilon_m \tag{5.24}$$

in régime BC so that

$$I_1^* + I_2 \geqslant c(\epsilon_m^{*2} - 2\alpha\epsilon_m\epsilon_m^* + \epsilon_m^2). \tag{5.25}$$

Since $\alpha \leqslant 1$, this last expression is positive definite so that $I_1 + I_2^*$ is non-negative in this case.

As a second example, take the admissible state on AB and the actual state on C. Then

$$\begin{aligned} I_1^* + I_2 &= \left[c\epsilon_m^* - 2(\sigma_1 - \sigma_3 - Y)\right]\epsilon_m^* \\ &\quad + (\sigma_1 - \sigma_2 - Y)\epsilon_1 + (\sigma_3 - \sigma_2 + Y)\epsilon_3 \\ &= \left[c\epsilon_m^* - 2c(\epsilon_1 + \alpha\epsilon_3) - 2c(\epsilon_3 + \alpha\epsilon_1) + 2Y\right]\epsilon_m^* \\ &\quad + c(\epsilon_1 + \alpha\epsilon_3)\epsilon_1 + (\epsilon_3 + \alpha\epsilon_1)\epsilon_3. \end{aligned} \tag{5.26}$$

Since ϵ_m^* is positive, this expression will be greater than the same expression with the term $2Y\epsilon_m^*$ omitted. After some manipulation this latter can be written

$$\begin{aligned} I_1^* + I_2 &\geqslant \left[\epsilon_m^* + (1 - \alpha)(\epsilon_3 - \epsilon_1)\right]^2 + \alpha(2 - \alpha)(\epsilon_1^2 + \epsilon_3^2) \\ &\quad + (4a - 1 - a^2)\epsilon_1\epsilon_3. \end{aligned} \tag{5.27}$$

Since $\frac{1}{2} \leqslant \alpha \leqslant 1$, each term of this last expression is non-negative.

Similar techniques may be used for each of the other 17 possible combinations, and in each case it is possible to write a lower bound on $I_1^* + I_2$ in a form which is obviously non-negative, considering the limitations on α and the signs of the principle strains. Such a representation

is shown in Table 3. Since the integrand is non-negative for all possible combinations, $\Delta\Pi$ is non-negative, Q.E.D.

The validity of the principle of minimum complementary energy can now be established by direct analogy. It follows from (5.13)–(5.16) that if the geometrically admissible state is replaced by the actual one and the actual state by a statically admissible state, then the integrand for $\Delta\Pi$ is replaced by that for $\Delta\Pi_c$. Since the proof of $\Delta\Pi$ being positive depended

TABLE 3. *Positive lower bounds on integrand for $\Delta\Pi$ in different régimes*

Stress point		$(1/c)(I_1^* + I_2) \geqslant$
Adm.	*Act.*	
Int.	*Int.*	0
Int.	*AB*	ϵ_m^2
Int.	*B*	$(\epsilon_1^2 + 2\alpha\epsilon_1\epsilon_2 + \epsilon_2^2)$
AB	*Int.*	$\epsilon_m^{*2} - (2/c)(\sigma_1 - \sigma_3 - Y)\epsilon_m^*$
AB	*AB*	$(\epsilon_m^* - \epsilon_m)^2$
AB	*B*	$(\epsilon_m^* - \epsilon_1 - \alpha\epsilon_2)^2 + (1-\alpha^2)\epsilon_2^2$
AB	*BC*	$(\epsilon_m^* - \epsilon_m)^2 + 2(1-\alpha)\epsilon_m\epsilon_m^*$
AB	*C*	$[\epsilon_m^* + (1-\alpha)(\epsilon_3 - \epsilon_1)]^2 + \alpha(2-\alpha)(\epsilon_1^2 + \epsilon_3^2) + (4\alpha - 1 - \alpha^2)\epsilon_1\epsilon_3$
AB	*CD*	$(\epsilon_m^* + \alpha\epsilon_m)^2 + (1-\alpha^2)\epsilon_m^2$
AB	*D*	$\epsilon_m^{*2} + 2(\epsilon_3 + \alpha\epsilon_2)\epsilon_m^* + \epsilon_2^2 + 2\alpha\epsilon_2\epsilon_3 + \epsilon_3^2$
AB	*DE*	$(\epsilon_m^* + \epsilon_m)^2$
B	*Int.*	$\epsilon_1^{*2} + 2\alpha\epsilon_1^*\epsilon_2^* + \epsilon_2^{*2} - (2/c)[(\sigma_1 - \sigma_3 - Y)\epsilon_1^* + (\sigma_2 - \sigma_3 - Y)\epsilon_2^*]$
B	*B*	$[(\epsilon_1^* - \epsilon_1) + \alpha(\epsilon_2^* - \epsilon_2)]^2 + (1-\alpha^2)(\epsilon_2^* - \epsilon_2)^2$
B	*BC*	$(\epsilon_2^* - \epsilon_m + \alpha\epsilon_1^*)^2 + (1-\alpha^2)\epsilon_1^{*2}$
B	*C*	$[\epsilon_2^* + \epsilon_3 + (1-\alpha)\epsilon_1^* + \alpha\epsilon_1]^2 + (1-\alpha^2)(\epsilon_1^* - \epsilon_1)^2 + (2\alpha - 1)(\epsilon_1^{*2} + 2\epsilon_1^*\epsilon_2^*)$
B	*CD*	$\epsilon_1^{*2} + 2\alpha\epsilon_1^*\epsilon_2^* + (\epsilon_2^* - \alpha\epsilon_m)^2 + (1-\alpha^2)\epsilon_m^2$
B	*D*	$(\epsilon_3 + \epsilon_1^*)^2 + (\epsilon_2 - \epsilon_2^*)^2 + 2\alpha(\epsilon_3\epsilon_2 + \epsilon_1^*\epsilon_2 + \epsilon_1^*\epsilon_2^* + \epsilon_2\epsilon_2^*) + 2(1-\alpha)\epsilon_3\epsilon_2^*$
B	*DE*	$\epsilon_1^{*2} + 2\alpha\epsilon_1^*\epsilon_2^* + \epsilon_2^{*2} + \epsilon_m^2$
B	*E*	$\epsilon_1^{*2} + 2\alpha\epsilon_1^*\epsilon_2^* + \epsilon_2^{*2} + \epsilon_1^2 + 2\alpha\epsilon_1\epsilon_2 + \epsilon_2^2$

only upon the properties of the stress strain law and did not depend upon equilibrium or boundary conditions, the same correspondence can be made in each step of the proof ; hence the conclusion $\Delta\Pi_c \geqslant O$ must hold, Q.E.D.

As in the theory of elasticity, the two principles may be obtained to yield upper and lower bounds on the energies. Indeed, it follows from (5.1) and (5.2) that for the actual state

$$\Pi + \Pi_c = \int_V (U + U_c)\,dv - \int_S \mathbf{T}\cdot\mathbf{u}\,dS - \int_V \mathbf{f}\cdot\mathbf{u}\,dv. \tag{5.28}$$

Application of the principle of virtual work then yields

$$\Pi + \Pi_c = \int_V [(U + U_c) - (\sigma_1\epsilon_1 + \sigma_2\epsilon_2 + \sigma_3\epsilon_3)]\,dv. \tag{5.29}$$

Finally, it follows from (5.9) and (5.10) that

$$\Pi + \Pi_c = 0. \tag{5.30}$$

Therefore, with relation to any geometrically admissible and statically admissible states the following continued inequalities are valid :

$$-\Pi_c^\circ \leqslant -\Pi_c = \Pi \leqslant \Pi^*, \tag{5.31}$$

$$-\Pi^* \leqslant -\Pi = \Pi_c \leqslant \Pi_c^\circ. \tag{5.32}$$

6. Conclusions

Although the theory presented here is obtained from a general viewpoint, its limitations must still be recognized. In the first place, it follows from the method of formulation that the theory can be useful only in those problems in which the principal directions of stress and strain coincide and remain fixed throughout the loading process. Such problems include all one-dimensional stress problems (trusses, beams, frames, arches, etc.) and certain radially symmetric problems (circular tubes, circular plates, axially symmetric shells, etc.). However, it may be possible to extend some of the essential ideas to more general problems.

Even within this limitation of application, there is no assurance that any real material will satisfy the conditions of the theory. As mentioned in the Introduction, this can only be determined by experiment. However, it should be pointed out that in the present state of mathematical knowledge the theory may be useful as an approximation even if its agreement with experiment is less than perfect; a more accurate theory might prove mathematically intractable.

The relationship of previous specific theories of piecewise linear plasticity to the present general one is easily established. In the first place, the flow law for a side of the yield condition (3.7) involves only the hardening coefficient c, and so it must be the same for all theories. The differences will occur in the flow laws on the corner regimes, and in the effect of hardening upon the yield condition.

The theory of Prager (1955, 1956) is based on a kinematic model in which the yield condition is regarded as a rigid frame which is free to translate but not rotate. The stress point is regarded as a smooth pin which will move the yield frame whenever it presses against it. This theory implies that distances between all sides of the yield condition will remain fixed as the straining continues, so that the continued inequalities (3.30) must all be equalities. Therefore, according to the kinematic theory,

$$\alpha = \tfrac{1}{2}, \qquad \beta = -\tfrac{1}{2}, \qquad \gamma = -1. \tag{6.1}$$

The theory of isotropic hardening implies that the yield hexagon remains similar in shape and is always centred at the origin. It then follows immediately from their definitions that

$$\alpha = \beta = \gamma = 1 \tag{6.2}$$

for isotropic hardening.

The combined theory proposed by Hodge (1957 a, b) lets α be arbitrary and regards the hardening as a linear combination of kinematic and isotropic. It follows that β and γ must be linear functions of α consistent with (6.1) and (6.2). Thus

$$\beta = 3\alpha - 2, \qquad \gamma = 4\alpha - 3 \tag{6.3}$$

for combined hardening.

It might also be noted that the slip theory of Batdorf and Budiansky (1949) does not fall within the framework of piecewise linear plasticity, since according to this theory the sides of the yield hexagon may rotate and new sides may form.

Several applications of the special cases mentioned have been made in recent years. Radially symmetric thin sheets have been treated by Prager (1953), Hodge (1953b) and Hodge and Sankaranarayanan (1950). Hodge and

ROMANO (1956) and HODGE and NARDO (1957) have solved problems involving circular shells. Finally, the bending of circular plates has been investigated by PRAGER (1956), BOYCE (1956), and HODGE (1957 a, b). All of these problems are based upon plane stress, and it is of some interest to look more closely at this aspect.

According to isotropic hardening, with the constants given by (16.2), it makes no difference whether plane stress is considered directly or as a special case of three dimensional theory. However, if PRAGER's kinematic model is taken as the starting point, there is a definite distinction. The division lines between régimes in Fig. 4 have been drawn to scale for the case $\alpha = \frac{1}{2}$. Therefore, if the stress point starts in corner C and moves according to $\dot{\sigma}_2 = 10\,\dot{\sigma}_1$, say, it will remain in the corner régime. However, if the kinematic model is applied directly to the non-equilateral hexagon of Fig. 4, such a motion would obviously slide the peg along side BC. The explanation of this apparent paradox is that the hexagon is not a two dimensional frame, but rather a non-right section of an equilateral hexagonal cylinder. When the stress point is on side BC, it is pushing the cylinder not only in the direction of the σ_2 axis, but also in the direction of the $-\sigma_3$ axis. The result is that the intersection of the corner C with the plane $\sigma_3 = 0$ does not move along the σ_2 axis but along the line CM in Fig. 4.

With the exception of one example by HODGE (1957 b), all of the quoted examples using the kinematic law (16.1) or the combined law (16.3) have been based on the direct application of kinematic hardening to two dimensional model. This leads to a somewhat simpler analysis in the problems treated, and only experiment can tell whether the results are useful. However, the analysis is not consistent with a three dimensional viewpoint, and hence may be considered suspect.

Applications of the minimum principles have been made only by HODGE (1957b), HODGE and ROMANO (1956) and HODGE and NARDO (1947). The situation here is quite different from in the theory of elasticity. In piecewise linear plasticity, the minimum principles are valid only if both the actual and admissible stress points all progress regularly. The latter can be controlled, but since the exact solution is unknown it may conceivably involve non-regular progressions. It follows that applications of the minimum principles must be made with extreme caution. However, despite their mathematical shortcomings they may still be of engineering value in attacking otherwise intractable problems.

In conclusion then, the theory of piecewise linear plasticity presented in the present paper may offer an approach to plasticity problems which is sufficiently general to incorporate significant physical phenomena and sufficiently simple to be mathematically tractable. It is hoped that both of these aspects may be further investigated in the future.

REFERENCES

BATDORF, S. B. and BUDIANSKY, B.	1949	*NACA Tech. Note* 1871.
BISHOP, J.F.W. and HILL, R.	1951	*Phil. Mag.* **42**, 327.
BOYCE, W.	1956	*Qu. Appl. Math.* **14**, 277.
DRUCKER, D. C.	1952	*Proc. First U.S. Nat. Cong. Appl. Mech.*

HODGE, P. G., JR.	1953a	*J. Appl. Mech.* **20**, 183.
	1953b	*J. Appl. Mech.* **20**, 530.
	1956a	*Proc. Colloquium on Deformation and Flow of Solids* 147.
	1956b	*J. Rat. Mech. Anal.* **6**, 917.
	1957a	*J. Appl. Mech.* To be published.
	1957b	*Proc. Ninth Int. Cong. Appl. Mech.* To be published.
HODGE, P. G., JR. and ROMANO, F.	1956	*J. Mech. Phys. Solids* **4**, 145.
HODGE, P. G., JR. and NARDO, S. V.	1957	*J. Appl. Mech.* To be published.
HODGE, P. G., JR. and SANKARANARAYANAN, R.	1957	*J. Math. Phys.* To be published.
KOITER, W. T.	1953a	*Biezeno Ann. Vol.* 232.
	1953b	*Qu. Appl. Math.* **11**, 350.
VON MISES, R.	1928	*Z. Ang. Math. Mech.* **8**, 161.
PRAGER, W.	1953	*J. Appl. Mech.* **20**, 317.
	1955	*The theory of plasticity – a survey of recent achievements* James Clayton Lecture, Instn. Mech. Engrs. London.
	1956	*J. Appl. Mech.* **23**, 493.
SANDERS, J. L., JR.	1955	*Proc. Second U.S. Nat. Congr. Appl. Mech.* 455.
TRESCA, H.	1868	*Mém. Pres. Acad. Sci., Paris.* **118**, 733.

Journal of the Mechanics and Physics of Solids, 1957, Vol. 5, pp. 261 to 266. Pergamon Press Ltd., London

PURE BENDING OF PRETWISTED RECTANGULAR PLATES

By L. MAUNDER* and E. REISSNER†

(*Received* 11*th January*, 1957)

SUMMARY

AN EXPLICIT solution is obtained to the problem of pure elastic bending of a pretwisted rectangular plate. The results are generalizations of known simple solutions for plane stress and for transverse bending of flat plates. They may have application to turbine and compressor blades and to aircraft propellers.

1. INTRODUCTION

WE CONSIDER in the following a pretwisted rectangular plate, or shallow hyperbolic paraboloidal shell, with two opposite edges free of stress and the other pair of edges acted upon by bending couples (Fig. 1). It is assumed that the pretwisted plate is

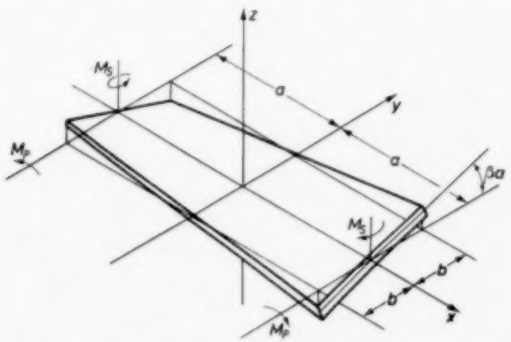

Fig. 1. The pretwisted plate.

unstressed prior to the application of the bending couples. An exact solution to the problem is to be obtained within the framework of the linear theory of thin shallow elastic shells. It will be shown that the results obtained in this way differ from the predictions of elementary beam theory and of the theory of transverse bending of flat plates. The physical cause of the differences can be described as an interaction which occurs between pretwist and lateral contractions induced by

* Postgraduate School of Applied Dynamics, University of Edinburgh.
† Massachusetts Institute of Technology.

bending: this interaction is not taken into account in the application of either beam or plate theory.

2. Formulation of the Problem

We assume that the undeflected middle surface of the shell is represented by

$$z = \beta xy \tag{1}$$

where β is the pretwist per unit length, and that the edges of the shell are defined by $x = \pm a$ and $y = \pm b$.

The differential equations for stresses and deflections of a plate which is pretwisted without stress in accordance with equation (1) and which is free of surface loads are known to be of the form (REISSNER 1955)

$$\left.\begin{aligned} \nabla^2 \nabla^2 F &= 2Eh\beta w_{,xy} \\ D\nabla^2 \nabla^2 w &= -2\beta F_{,xy} \end{aligned}\right\} \tag{2}$$

where F is an Airy stress function, w is the transverse deflection of the plate, h is the plate thickness, E is Young's modulus, $D = Eh^3/12(1-\nu^2)$, ν is Poisson's ratio, and commas indicate differentiation. These equations follow by suitable specialization from more general equations for shallow shells which have been given by MARGUERRE (1938).

Stress resultants and couples are given in terms of F and w as follows,

$$N_{xx} = F_{,yy}; \qquad N_{yy} = F_{,xx}; \qquad N_{xy} = -F_{,xy} \tag{3}$$

$$\left.\begin{aligned} M_{xx} &= -D(w_{,xx} + \nu w_{,yy}); \qquad M_{yy} = -D(w_{,yy} + \nu w_{,xx}) \\ M_{xy} &= -(1-\nu) D w_{,xy} \end{aligned}\right\} \tag{4}$$

$$\left.\begin{aligned} V_x &= -D[w_{,xxx} + (2-\nu) w_{,xyy}] + \beta y N_{xx} + \beta x N_{xy} \\ V_y &= -D[w_{,yyy} + (2-\nu) w_{,yxx}] + \beta y N_{xy} + \beta x N_{yy} \end{aligned}\right\} \tag{5}$$

In addition to the stress resultants there are concentrated transverse corner forces of magnitude $\pm 2M_{xy}$. The resultants N are tangential to the middle surface of the shell and, to the degree of approximation which is involved in the theory, are also parallel to the x-, y-plane. The resultants V are perpendicular to the x-, y-plane.

Midsurface strains are given in terms of midsurface displacements u, v, w in the coordinate directions and in terms of stress resultants as follows,

$$\begin{aligned} Eh\epsilon_x &= Eh(u_{,x} + \beta y w_{,x}) = N_{xx} - \nu N_{yy} \\ Eh\epsilon_y &= Eh(v_{,y} + \beta x w_{,y}) = N_{yy} - \nu N_{xx} \\ Gh\gamma_{xy} &= Gh(u_{,y} + v_{,x} + \beta y w_{,y} + \beta x w_{,x}) = N_{xy} \end{aligned} \tag{6}$$

The differential equations (2) are to be solved in conjunction with the following system of boundary conditions,

$$y = \pm b: \qquad N_{yy} = N_{xy} = V_y = M_{yy} = 0 \tag{7}$$

$$x = \pm a \qquad \left\{ \begin{array}{r} \displaystyle\int_{-b}^{+b} N_{xx}\, dy = \int_{-b}^{+b} N_{xy}\, dy = 0 \\ \displaystyle\int_{-b}^{+b} V_x\, dy - 2\left[M_{xy}\right]_{-b}^{+b} = 0 \\ \displaystyle\int_{-b}^{+b} N_{xx} \cdot y dy = M_s \\ \displaystyle\int_{-b}^{+b} M_{xx}\, dy + \int_{-b}^{+b} N_{xx} \cdot z\, dy = M_p \\ \displaystyle\int_{-b}^{+b} (V_x \cdot y - z \cdot N_{xy})\, dy - 2\left[yM_{xy}\right]_{-b}^{+b} = 0 \end{array} \right\} \tag{8}$$

and the solution is to express the stresses and displacements in the interior of the pretwisted plate in terms of the sheet bending moment M_s and the plate bending moment M_p.

3. Solution of the Problem

The solution of the problem is obtained by what amounts to experimentation with generalizations of the known solution for $\beta = 0$. Under these circumstances it is simplest to state the solution in its final form, whence it may be verified that all conditions stated in equations (2), (7) and (8) are satisfied.

It is found that

$$w = -\frac{M_p}{4b\,(1-\nu^2)\,D} \cdot (x^2 - \nu y^2) + \frac{\beta M_s}{12b\,(1-\nu^2)\,D} \cdot (x^3 - 3\nu\, xy^2) \tag{9}$$

$$F = \frac{M_s}{4}\left[\left(1 + \frac{4\nu}{5} \cdot \frac{b^4}{h^2} \cdot \beta^2\right)\frac{y^3}{b^3} - \frac{2\nu}{5} \cdot \frac{b^4}{h^2} \cdot \beta^2 \cdot \frac{y^5}{b^5}\right]. \tag{10}$$

Therewith stress resultants and couples are given by the following expressions,

$$N_{xx} = \frac{3M_s}{2b^2}\left[\left(1 + \frac{4\nu}{5} \cdot \frac{b^4}{h^2} \cdot \beta^2\right)\frac{y}{b} - \frac{4\nu}{3} \cdot \frac{b^4}{h^2} \cdot \beta^2 \cdot \frac{y^3}{b^3}\right], \quad N_{yy} = 0, \quad N_{xy} = 0 \tag{11}$$

$$M_{xx} = \frac{M_p}{2b} - \frac{\beta M_s}{2b} \cdot x, \quad M_{yy} = 0, \quad M_{xy} = \frac{\beta M_s}{2b} \cdot \frac{\nu y}{1+\nu} \tag{12}$$

$$V_x = -\frac{\beta M_s}{2b} \cdot \frac{1-\nu}{1+\nu} + \frac{3\beta M_s}{2b}\left[\left(1 + \frac{4\nu}{5} \cdot \frac{b^4}{h^2} \cdot \beta^2\right)\frac{y^2}{b^2} - \frac{4\nu}{3} \cdot \frac{b^4}{h^2} \cdot \beta^2 \cdot \frac{y^4}{b^4}\right], \; V_y = 0. \tag{13}$$

It is readily seen that (9) and (10) satisfy the differential equations (2). Furthermore, (11), (12) and (13) indicate directly that the boundary conditions (7) are satisfied. The first, second and last of the boundary conditions (8) are also verified without calculation. The remaining three conditions in (8) are verified by substitution and integration.

We note that the stresses and deflections w due to the plate bending moment M_p are, to the degree of approximation associated with the theory of shallow shells, unaffected by the pretwist of the plate. Stresses and deflections w due to sheet

bending moment M_s are, however, affected by pretwist. In order to see the possible order of magnitude of this effect, we consider cases for which $b \ll a$, in order to be able to appeal to St. Venant's principle. Since $w_{,x} = \beta y$ and $w_{,y} = \beta x$, there occurs as a limitation on the validity of the results the condition $(\beta a)^2 < 1$. For practical purposes this may be replaced by

$$\beta a < \tfrac{1}{4} \tag{14}$$

which means that the results obtained are meaningful as long as

$$\frac{b^4}{h^2} \cdot \beta^2 \lesssim \tfrac{1}{16} \cdot \frac{b^4}{a^2 h^2}. \tag{15}$$

Expression (15) shows that the parameter $b^4\beta^2/h^2$ may be of order unity, or even large compared with unity, provided that for given small b^2/a^2, the ratio b^2/h^2 is large enough.

4. Stresses and Deflections

In view of the fact that the moment M_p causes deflections w which are independent of β and moreover does not cause inplane stress resultants N_{xx}, it is apparent that the results of interest concern the effect on stresses and deflections of the moment M_s. Of particular interest in connection with applications is the result for the sheet stresses N_{xx}/h. We note that the presence of the y^3-term in expression (11) may be responsible for a considerable reduction of the maximum value of this stress due to pretwist. It is found that for given $b^4\beta^2/h^2$ the largest values of N_{xx}/h are given by the following formulae,

$$\left.\begin{aligned} &\frac{b^4}{h^2} \cdot \beta^2 \leqslant \frac{5}{16\nu}, \qquad \frac{y}{b} = 1 \\ &\frac{(N_{xx})_{\max}}{h} = \frac{bM_s}{I}\left(1 - \frac{8\nu}{15} \cdot \frac{b^4}{h^2} \cdot \beta^2\right) \end{aligned}\right\} \tag{16a}$$

$$\left.\begin{aligned} &\frac{5}{16\nu} \leqslant \frac{b^4}{h^2} \cdot \beta^2, \qquad \frac{y}{b} = \left(\frac{1}{5} + \frac{1}{4\nu} \cdot \frac{h^2}{b^4} \cdot \frac{1}{\beta^2}\right)^{1/2} \\ &\frac{(N_{xx})_{\max}}{h} = \frac{bM_s}{I} \cdot \frac{\left(1 + \dfrac{4\nu}{5} \cdot \dfrac{b^4}{h^2} \cdot \beta^2\right)^{3/2}}{3\left(\nu \cdot \dfrac{b^4}{h^2} \cdot \beta^2\right)^{1/2}} \end{aligned}\right\} \tag{16b}$$

where $I = 2hb^3/3$. Fig. 2 shows that the numerical effect of pretwist may be of appreciable magnitude.

The component curvature k_y of the deflected centreline of the plate is also of interest. This quantity is the value of the second derivative $v_{,xx}$ for $y = 0$, and from it component deflections of the centreline may be obtained by integration. Since $N_{xy} = 0$, the last of the stress-strain relations (6) yields

$$k_y = -\left[u_{,yx} + \beta\left(yw_{,y} + xw_{,x}\right)_{,x}\right]_{y=0}. \tag{17}$$

We take $u_{,yx}$ from the first of equations (6), and with $N_{yy} = 0$ as given by the second of equations (11), we find that

$$k_y = -\left[\frac{N_{xx'y}}{Eh}\right]_{y=0} + \left[\beta\,(y\,w_{,x})_{,y} - \beta\,(yw_{,y} + xw_{,x})_{,x}\right]_{y=0}$$

$$= -\left[\frac{N_{xx'y}}{Eh}\right]_{y=0} - \left[\beta\,xw_{,xx}\right]_{y=0}. \tag{18}$$

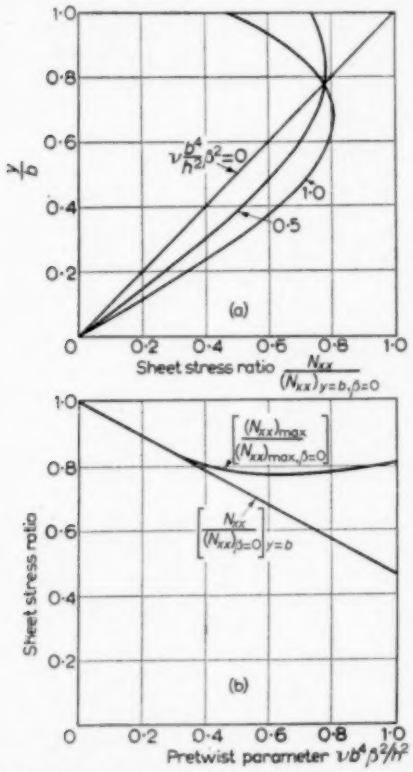

Fig. 2. Effect of pretwist on sheet stresses. (a) Stress distributions; (b) Maximum values.

Therewith it follows from equations (9) and (11) that

$$k_y = -\frac{3M_s}{2Ehb^3}\left(1 + \frac{4\nu}{5}\cdot\frac{b^4}{h^2}\cdot\beta^2\right) - \frac{\beta^2 M_s}{12b\,(1-\nu^2)\,D}\cdot 6x^2 + \frac{\beta x M_p}{2b\,(1-\nu^2)\,D}. \tag{19}$$

For present purposes it is sufficient to consider $M_p = 0$, with the result that

$$k_y = -\frac{M_s}{EI}\left(1 + \frac{4\nu}{5}\cdot\frac{b^4}{h^2}\cdot\beta^2 + 4\cdot\frac{b^4}{h^2}\cdot\beta^2\cdot\frac{x^2}{b^2}\right). \tag{20}$$

Two modifications of the corresponding result for $\beta = 0$ are noted. One is due to lateral contraction and is independent of location along the span of the plate. The other increases quadratically with distance from the origin and may be shown to be due to the rotation of the principal axes of the cross-section. Taking account of this rotation, the latter effect may be predicted by elementary beam theory. The

former effect is not predicted by beam theory. It shows that the component curvature of the centreline in the direction of one of the principal axes of the cross-section is larger than the value predicted by beam theory in the ratio $\left(1 + \frac{4\nu}{5} \cdot \frac{b^4}{h^2} \cdot \beta^2\right) : 1$.

REFERENCES

MARGUERRE, K.	1938	*Proc. Fifth Int. Cong. Appl. Mech.* pp. 93-101.
REISSNER, E.	1955	*J. Boston Soc. Civ. Engrs.* **42**, 120.

Journal of the Mechanics and Physics of Solids, 1957, Vol. 5, pp. 267 to 280. Pergamon Press Ltd., London

ON THE MULTIPLE HOLE EXTRUSION OF SHEETS OF EQUAL THICKNESS

By L. C. Dodeja† and W. Johnson*

(*Received 20th February*, 1957)

Summary

Slip-line fields are proposed and pressures are calculated for the extrusion of sheet through a square die containing one, two, or three orifices, when the container walls are perfectly smooth or rough. Experimental determinations of the parameter $p/2k$ for pure lead, tellurium lead and pure tin, are compared with those predicted. The actual rate of flow of material through each orifice for the three-hole die is also compared with that predicted.

1. Introduction

Plane-strain solutions of the problem of the extrusion of a non-hardening plastic-rigid material through a square die symmetrically placed at the end of a parallel-sided container, were first given by Hill (1948). Later, Green (1955) extended and modified these solutions to take account of dies which were unsymmetrically placed. In this paper, use is made of these solutions to analyse the problem which arises when the die has more than one aperture. It will be seen that the solutions proposed, which are for a particular range of reductions, are essentially a recombination of Hill's original ones. They assume that regions of dead metal are deposited across the face of the die, and the experimental evidence presented below confirms this, at least qualitatively. In the theoretical work, no account is taken of temperature effects, and the calculations are confined to the two extreme conditions of lubrication. In other respects too, e.g. stresses carried by rigid regions and the influence of the proximity of the punch to the plastic stress fields, the solutions do not completely analyse the situation. But these points appear to be of little consequence when viewed against a background of real materials with uncertain physical and metallurgical conditions.

This paper, though presented as a piece of self-contained work, was carried out as part of a programme concerned with the extrusion of circular rods through a multiple-hole die because it was hoped that it would provide some basic ideas assisting the understanding of multi-rod extrusion, in the same way that single-hole sheet extrusion is an aid to thinking about single rod extrusion. However, as a small amount of sheet is extruded commercially, the findings of the investigation should be of value industrially as well as in assessing the validity of the assumptions and theories.

†Department of Engineering, University of Sheffield.
*Department of Engineering, University of Manchester.

An examination of the manner of deformation of the lead and tin specimens generally substantiated the truth of the theoretical assumptions. The measurements of pressure, when compared with those theoretically predicted, are always of the correct order, but there is a discrepancy between theory and practice which increases with the reduction and the number of sheets produced; it cannot be claimed that the resolution of this disparity is entirely satisfactory.

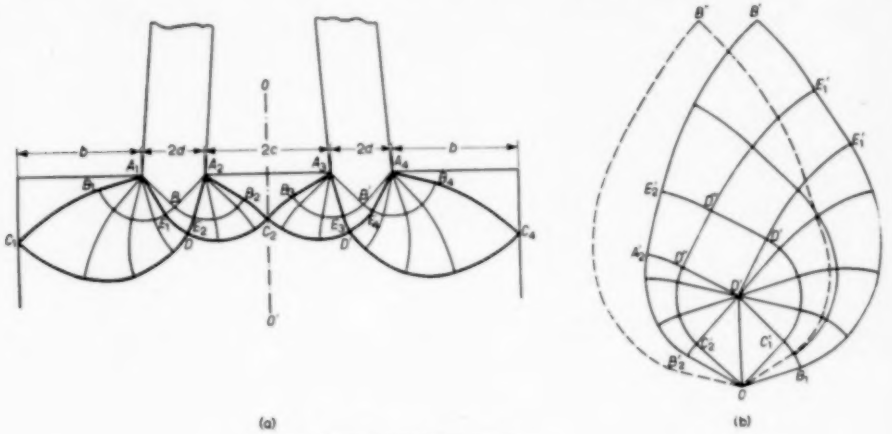

Fig. 1. (a) Slip-line field and (b) hodograph for extrusion through two holes when $r = 0{\cdot}75$ and $\epsilon = 0{\cdot}33$, the container walls being smooth. Assumption: slip-lines meet interplane at 45°.

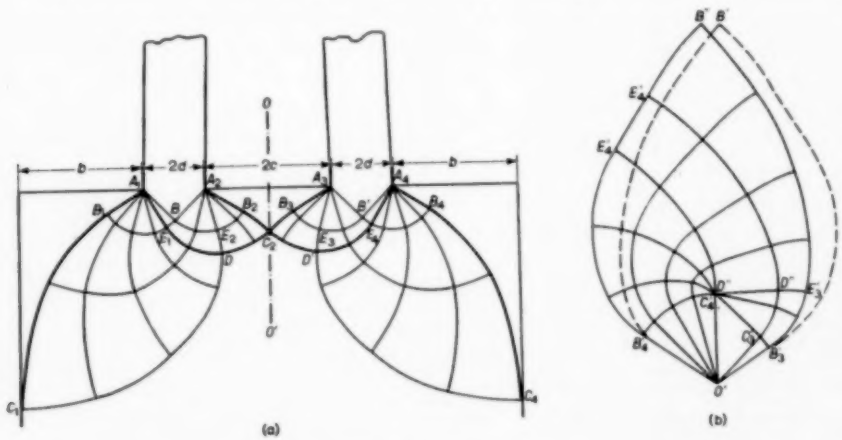

Fig. 2. (a) Slip-line field and (b) hodograph for extrusion through two holes when $r = 0{\cdot}75$ and $\epsilon = 0{\cdot}33$, the container walls being rough. Assumption: slip-lines meet interplane at 45°.

2. Extrusion Through Two Holes

In Figs. 1 and 2, $2d$ denotes the width of the die aperture and $2l$ the width of the container; the meaning of other symbols will be obvious by reference to the

figures. The total nominal fractional reduction is given by $r = (l - 2d)/l$, and it is described as a nominal reduction because the sheets emerge at an angle to the perpendicular to the plane of the orifice. Since this angle is small, however, there is very little difference between the nominal and the true reduction, and so the term nominal will henceforth be dropped (JOHNSON 1957). The eccentricity of the orifices may be denoted by $\epsilon = c/(b + c)$; ϵ is zero when the two orifices merge into one, and is unity when they touch the container walls.

(i) *Smooth container walls*

The form of slip-line field assumed is shown in Fig. 1 (a); it consists of two symmetrical halves, either of which corresponds to the known cases of single-hole extrusion through an eccentrically placed orifice. Implicit in this field is the assumption that all slip-lines intersect at 45° on the centre line OO'; this is essential in order that the yield criterion for material in the neighbourhood of C_2, in the dead metal zone $A_2 A_3 C_2$, shall not be exceeded. Fig. 1 (a) is drawn to scale for a reduction of 0·75 and Fig. 1 (b) is the corresponding hodograph, also drawn to scale. It will be observed that it is predicted that the two emergent sheets will be inclined towards one another.

The slip-line $A_1 B_1 C_1$ and a similar slip-line near the other wall corresponds in symmetrical single-hole extrusion to a reduction $r_1 = b/(b + d)$. Similarly, for the slip-lines $A_2 B_2 C_2$ and $A_3 B_3 C_2$, there corresponds in symmetrical single-hole extrusion a reduction $r_2 = c/(c + d)$. If the pressure corresponding to r_1 and r_2 are respectively p_1 and p_2, and if the total uniform pressure required over the punch is p for the total reduction r, then

$$p \,.\, 2l = 2\{p_1 (b + d) + p_2 (c + d)\}. \tag{1}$$

Since

$$r_1 = 2r(1 - \epsilon)/\{1 + r(1 - 2\epsilon)\}$$

and

$$r_2 = 2r(1 - \epsilon)/\{1 - r(1 - 2\epsilon)\}$$

then, in place of (1),

$$2p = (p_1 + p_2) + r(p_2 - p_1)(2\epsilon - 1). \tag{2}$$

This solution holds only if b and $c > d$. When b or $c > d$ the slip-line field has to be more complex (GREEN 1955). Now, for single sheet extrusion, smooth container walls and a symmetrically placed die, the relationship between $p/2k$ and r when $0{\cdot}93 \leqslant r \leqslant 0{\cdot}5$ may be expressed empirically (JOHNSON 1954) by the equation

$$p/2k = 0{\cdot}47 + 1{\cdot}2 \ln\{1/(1 - r)\}. \tag{3}$$

The corresponding expression when the container walls are perfectly rough is

$$p/2k = 0{\cdot}82 + 1{\cdot}2 \ln\{1/(1 - r)\}. \tag{4}$$

It follows, using (3), that

$$p_1/2k = 0{\cdot}47 + 1{\cdot}2 \ln\left\{\frac{1 + r(1 - 2\epsilon)}{1 - r}\right\} \tag{5}$$

and

$$p_2/2k = 0{\cdot}47 + 1{\cdot}2 \ln \left\{ \frac{1 - r(1 - 2\epsilon)}{1 - r} \right\}. \tag{6}$$

Substituting (5) and (6) in (2), and simplifying, it is found that

$$p/2k = 0{\cdot}47 + 1{\cdot}2 \ln \{1/(1 - r)\} + \Delta p/2k \tag{7}$$

where $\Delta p/2k = 0{\cdot}6 \ln \{1 - r^2(1 - 2\epsilon)^2\} +$

$$0{\cdot}6r(1 - 2\epsilon) \ln \left\{ \frac{1 + r(1 - 2\epsilon)}{1 - r(1 - 2\epsilon)} \right\}. \tag{8}$$

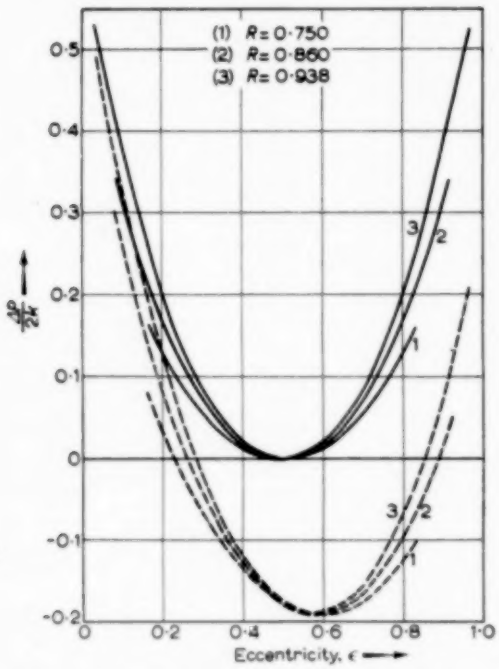

Fig. 3. Variation of $\Delta p/2k$ with ϵ for extrusion through two holes, $r = 0{\cdot}75$ and $\epsilon = 0{\cdot}33$. Assumption : slip-lines meet interplanes at 45°. ——— Smooth container walls. – – – – Rough container walls.

(ii) *Rough container walls*

Scale diagrams of both the stress field and the hodograph for $r = 0{\cdot}75$ are shown in Fig. 2. The stress field here holds only if $c > d$. Using (4), the expression for the extrusion pressure similar to (7) and (8), is

$$p/2k = 0{\cdot}82 + 1{\cdot}2 \ln \{1/(1 - r)\} + \Delta p/2k \tag{9}$$

where

$$\begin{aligned} \Delta p/2k = {} & 0{\cdot}6 \{1 + r(1 - 2\epsilon)\} \ln \{1 + r(1 - 2\epsilon)\} \\ & + 0{\cdot}6 \{1 - r(1 - 2\epsilon)\} \ln \{1 - r(1 - 2\epsilon)\} \\ & - 0{\cdot}175 \{1 - r(1 - 2\epsilon)\}. \end{aligned} \tag{10}$$

(iii) *Variation of $\Delta p/2k$ with eccentricity*

Calculations of the variation of $\Delta p/2k$ with orifice eccentricity for reductions of 0·75, 0·86, and 0·938 have been made and are shown in Fig. 3 for rough and smooth container walls respectively. From this Figure it will be observed that $\Delta p/2k$ is positive for all values of r for any given value of ϵ. There is also a value of ϵ for which $\Delta p/2k$ is least, and hence for which $p/2k$ is a minimum. This best value of ϵ is immediately evident in Fig. 3, but if calculated by differentiating equations (8) and (10), it is found that for smooth walls $\epsilon = 0{\cdot}5$ for all values of r, while for rough walls, $\epsilon = 0{\cdot}5 + 0{\cdot}0725/r$.

3. Extrusion Through Three Holes

The analysis of this situation is very similar to that of the previous section. Employing the same notation, and by reference to Fig. 3 from which the meaning of the various symbols will be obvious, it follows that the total reduction $r = (b + 2c)/(b + 2c + 3d)$. The central hole is symmetrically placed but the eccentricity of the side holes is $\epsilon = 2c/(b + 2c)$, so that when $c = 0$, $\epsilon = 0$, and all three holes merge into one ; when $\epsilon = 1$, the two side holes touch the container walls, b becoming zero.

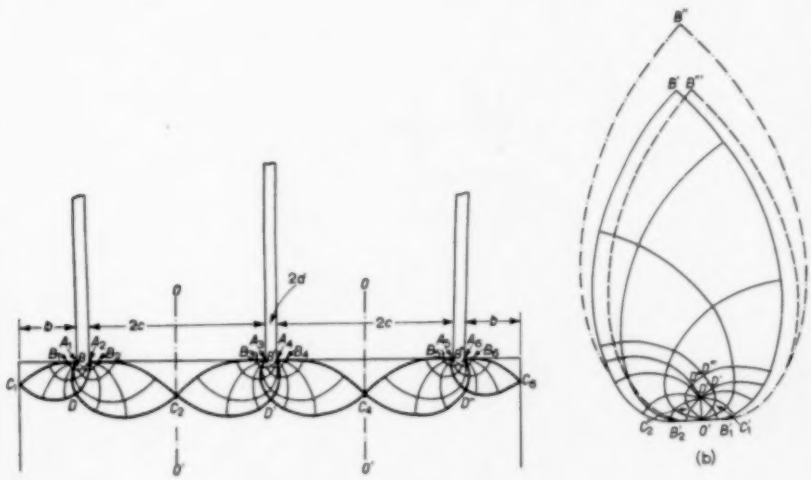

(c)

Smooth container walls

Fig. 4. (a) Slip-line field and (b) hodograph for extrusion through three holes when $r = 0{\cdot}938$ and $\epsilon = 0{\cdot}755$, the container walls being smooth.

(i) *Smooth container walls*

The form of slip-line field assumed and the consequent hodograph for a reduction of 0·938 are shown in Fig. 4, there being four regions of dead metal. The slip-line

$A_1 B_1 C_1$, and a similar one near the other wall, correspond in symmetrical single-hole extrusion to a reduction of $r_1 = 3r(1-\epsilon)/\{1 + r(2-3\epsilon)\}$. Slip-line $A_2 B_2 C_2$, and similar slip-lines bounding the two intermediate dead-metal zones, correspond similarly to a symmetrical single hole extrusion of reduction $r_2 = 3r\epsilon/\{2 - r(2-3\epsilon)\}$. If p_1 and p_2 are the pressures relating to reductions r_1 and r_2, and if p is the resultant uniform pressure required on the punch to extrude through three holes of total reduction r with two holes disposed eccentrically by amount ϵ, then

$$pl = p_1(b+d) + 2p_2(c+d). \tag{11}$$

Since

$$b = rl(1-\epsilon), \qquad c = rl\epsilon/2 \qquad \text{and} \qquad d = l(1-r)/3$$

(11) becomes

$$3p = (p_1 + 2p_2) + r(2-3\epsilon)(p_1 - p_2), \tag{12}$$

the solution holding only if $b > d$. After some manipulation it follows that

$$p/2k = 0{\cdot}47 + 1{\cdot}2 \ln\{1/(1-r)\} + \Delta p/2k \tag{13}$$

where

$$\Delta p/2k = 0{\cdot}4\{1 + r(2-3\epsilon)\} \ln\{1 + r(2-3\epsilon)\} + 0{\cdot}4\{2 - r(2-3\epsilon)\} \ln\{1 - r(2-3\epsilon)/2)\}, \tag{14}$$

use being made of (3) and (12).

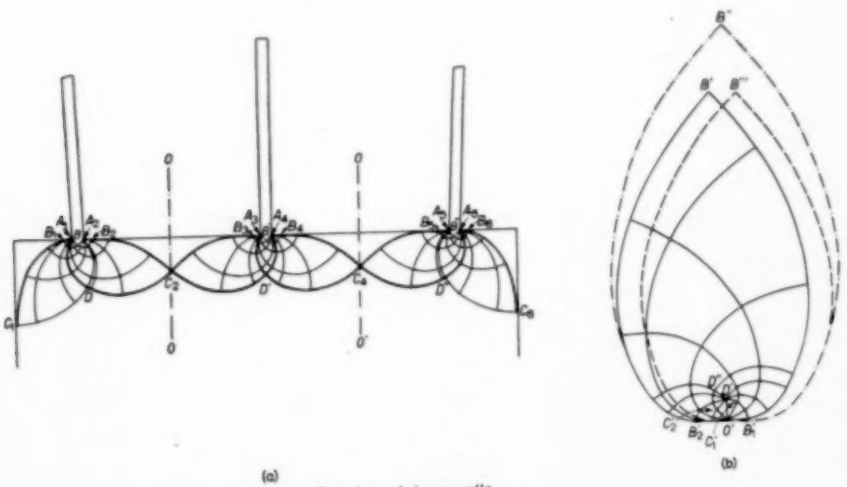

Fig. 5. (a) Slip-line field and (b) hodograph for extrusion through three holes when $r = 0{\cdot}938$ and $\epsilon = 0{\cdot}755$, the container walls being rough. Assumption : slip-lines meet interplanes at 45°.

(ii) *Rough container walls*

Scale diagrams of both the stress and velocity fields for a reduction of 0·938 are shown in Fig. 5. This solution is valid only if $c > d$. The expression for the

extrusion pressure, similar to those of (13) and (14) above, is

$$p/2k = 0{\cdot}82 + 1{\cdot}2 \ln \{1/(1-r)\} + \Delta p/2k \tag{15}$$

where

$$\begin{aligned}\Delta p/2k = {} & 0{\cdot}4\{1 + r(2 - 3\epsilon)\} \ln \{1 + r(2 - 3\epsilon)\} \\ & + 0{\cdot}8\{1 - r(2 - 3\epsilon)/2\} \ln \{1\ r - (2 - 3\epsilon)/2\} \\ & - 0{\cdot}7\{1 - r(2 - 3\epsilon)/2\}/3. \end{aligned} \tag{16}$$

(iii) *Variation of $\Delta p/2k$ with eccentricity*

This is shown in Fig. 6 for cases (i) and (ii) above, and observations similar to those for the case of two hole extrusion may be made. The best position for the

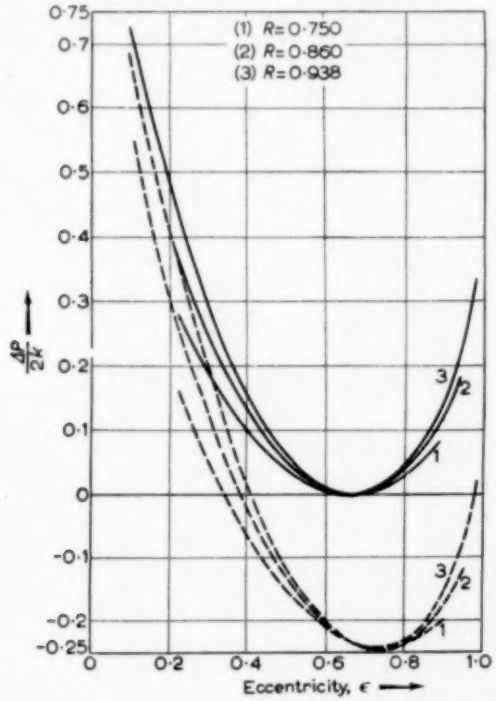

Fig. 6. Variation of $\Delta p/2k$ with ϵ for extrusion through three holes. Assumption : slip-lines meet interplanes at 45°. ——— Smooth container walls. – – – Rough container walls.

orifices, least total pressure being the criterion, can again be found analytically and is, for smooth container walls, $\epsilon = 0{\cdot}667$ (symmetrical disposition) for all values of r, and $\epsilon = 0{\cdot}667 + (0{\cdot}061/r)$ for rough container walls.

4. Experimental Work

(i) *Apparatus*

The plane strain extrusion apparatus used in this work was the same in most respects as that used in performing experiments in the extrusion of single sheet,

and has already been described (Johnson 1956). To make the alterations to that apparatus it was necessary to alter the chamber side pieces to take the various die pieces which would make two and three sheet extrusion possible.

The inner container, made of four segments joined by light steel dowels, is a press-fit into the container ; the overall interference is such as to require a load of 6 to 7 tons for pressing it into the outer container. To change from one-hole extrusion to two-hole, and later, three-hole extrusion, the inner container was pressed out and the side-pieces were replaced by another set of side-pieces having one or two slots at the top. The reconstituted container was then pressed back into the outer container. Into the slots in the chamber side-pieces die pieces were fitted which made possible different reductions and different dispositions of holes. Complete details concerning this can be found elsewhere (Dodeja 1956). Three different die retaining plates were used, depending on the number of sheets extruded.

From the point of view of ease and accuracy of manufacture, a thickness of $\frac{1}{2}$ inch for the die pieces was considered adequate. The overall accuracy in the size of the die pieces and their location in the slots in the side-pieces was thought to be about 0·0005 inch. All the die pieces were located using a light drive fit. A land was ground on the bottom of the container side-pieces and on the top of the side die pieces to achieve the best location. The die pieces were finally secured in place by the retaining plate which was fastened to the outer container with cup-headed screws.

(ii) *Specimens*

Pure lead and tellurium lead was available in the form of 1 inch by 1 inch square bar. All the lead specimens were therefore made in two segments 0·95 in. × 1·0 in. × 1·25 in. thick, and inserted into the container side by side. The specimens were finish-sized by pressing between a pair of smooth plates in a vice.

All lead specimens were annealed for 30 min in an oil bath over boiling water. Pure tin, available in the form of 1 in. × 1 in. extruded bar, was made into specimens of the appropriate size in the same manner as the lead, being annealed for 60 min in an oil bath over boiling water.

(iii) *Procedure*

For each extrusion test the container, the pressure-pad, all die pieces and the specimen were first cleaned with carbon tetrachloride. For lubricated extrusion the container walls were uniformly smeared with graphite-in-tallow. The cleaned die-pieces were driven into position, not allowing any lubricant on the die-faces, to assist in the establishment of dead metal zones. The die-pieces were then secured in position with the aid of the die-retaining plate. The specimen was also uniformly smeared with graphite-in-tallow, taking care not to have any lubricant on the bottom face, which would be in contact with the die-faces. The lubricated pressure-pad was then forced in along with the punch and the apparatus centred on the press platens. The test was then started, the average speed being adjusted to 0·1 in. per minute. The load readings were taken every 0·05 in. of punch travel and extrusion continued until the load, after indicating the true extrusion load and falling rapidly, started to rise again. This usually left about 0·05 in. to 0·025 in. of unextruded metal in the container. The test was then stopped, the apparatus removed from the press, the die-retaining plate unscrewed, and the extrusion pressed out along with the die-pieces and the pressure-pad.

Exactly the same procedure was followed for unlubricated extrusions except that the container and the specimen were left unlubricated. The two 1 inch sides of the specimen were, however, very carefully and lightly lubricated to conform to the assumptions of plane-strain theory. The pressure-pad was also lightly lubricated to mitigate the drag due to ' flashing.' Repeat tests gave loads to within 4% of one another. The extrusions for the study of metal deformation were also carried out in the same manner, except that the punch travel was restricted so as to obtain well-proportioned photographs of the steady-state deformation of the grid. The grid used and stamped on the common face of the composite slug was a square one of side 1/20 in.

5. Experimental Results and Discussion

(i) *Stress-strain curves*

True stress, log-strain curves, as calculated from the compression tests on the

individual materials, made following the method described by JOHNSON (1956), are shown in Fig. 7. Comparison of these curves with those previously obtained for pure lead and tellurium lead (JOHNSON 1956) show them to have mean yield stresses, $\bar{\sigma}$, some 10% different. This is not a surprising feature in lead since the inclusion of slight impurities and small differences in the working of the materials usually have large effects.

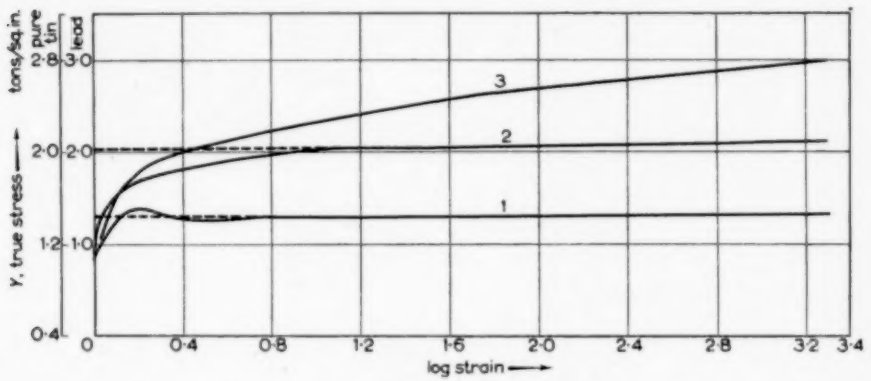

Fig. 7. Stress-strain curves for (1) pure lead, (2) tellurium lead, (3) pure tin.

The value of $2k$ for use in deriving the experimental value of $p/2k$ for each particular test was calculated, and the values are tabulated and shown in Table 1.

TABLE 1

Reduction	*Condition at walls*	*Mean equivalent strain*	*Pure lead*		*Tellurium lead*		*Pure tin*	
r		ϵ	$\bar{Y}$	$2k$	$\bar{Y}$	$2k$	$\bar{Y}$	$2k$
0·75	Smooth	2·13	1·305	1·51	2·045	2·36	2·41	2·78
	Rough	2·475	1·31	1·51	2·05	2·365	2·45	2·82
0·86	Smooth	2·835	1·31	1·51	2·055	2·375	2·49	2·875
	Rough	3·165	1·31	1·51	2·065	2·385	2·52	2·915
0·938	Smooth	3·82	1·315	1·52	2·07	2·39	2·60	3·00
	Rough	4·18	1·32	1·52	2·095	2·42	2·63	3·04

(ii) *Autographic diagrams*

The records of the variation of punch load with punch travel are shown in Figs. 8, 9 and 10, the true extrusion load being that prevailing at the coring point which is clearly indicated on each particular diagram (JOHNSON 1956).

From an examination of these diagrams it will be seen that there is a fair degree of consistency regarding the fraction of the slug length which remains when the coring point is reached, regardless of the kind of metal. The coring point occurs

later the larger the number of holes for a given total reduction. This follows, of course, from the fact that the size of the deformation zone reduces in proportion to the absolute size of the hole. The depths of the plastic zone as indicated by theory or the remaining slug lengths at which coring occurs when the reduction

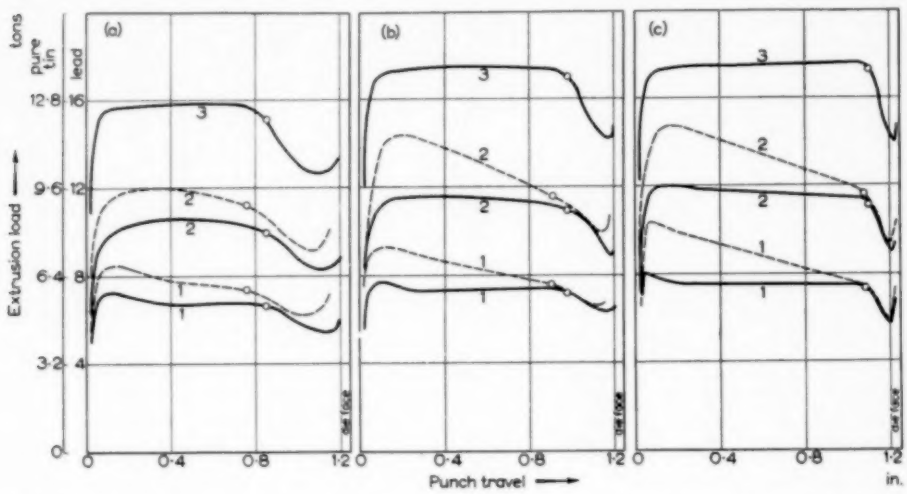

Fig. 8. Autographic diagrams for $r = 0{\cdot}75$, (a) 1 hole, (b) 2 hole, (c) 3 hole. (1) Pure lead, (2) tellurium lead, (3) pure tin. ——— Lubricated extrusion. - - - - Unlubricated extrusion. ⊙ Coring point.

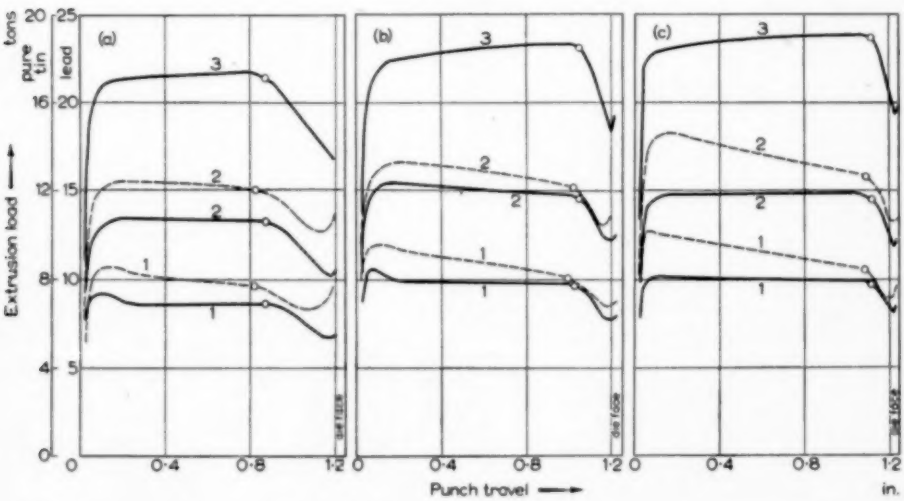

Fig. 9. Autographic diagrams for $r = 0{\cdot}86$. ——— Lubricated extrusion. - - - - Unlubricated extrusion. ⊙ Coring point.

is 0·75, are for a lubricated slug 1 inch thick, 0·33 in., 0·165 in., and 0·11 in., the corresponding lengths indicated by the appropriate positions of the coring points on the autographic diagrams are 0·4 in., 0·275 in., and 0·175 in., respectively.

These latter figures are only approximate, but they would be expected to exceed the theoretical ones, since the effect of friction and strain-hardening is to increase

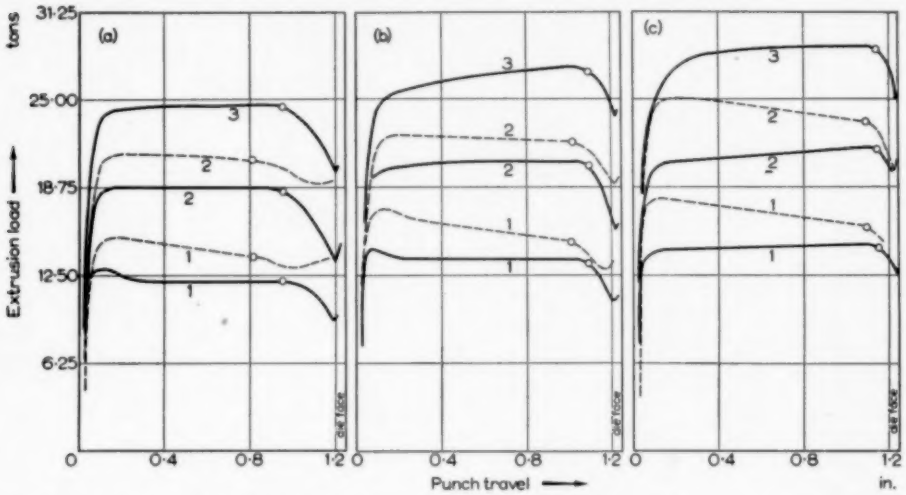

Fig. 10. Autographic diagrams for $r = 0{\cdot}938$. ——— Lubricated extrusion. - - - - Unlubricated extrusion. ○ Coring point.

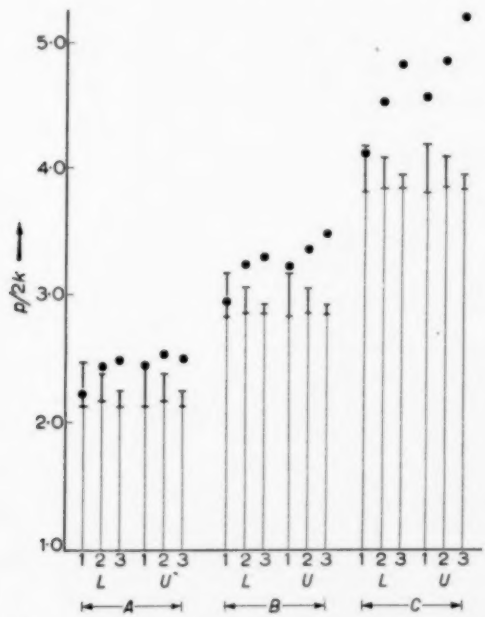

Fig. 11. Comparison of experimental and theoretical values. ——— Range of theoretical values. ● Experimental value. *A*, $r = 0{\cdot}75$; *B*, $r = 0{\cdot}86$; *C*, $r = 0{\cdot}938$. *L* — Lubricated. *U* — Unlubricated.

the depth of the region of large deformation. Collateral with the reduction in this depth is an increase in the rapidity of onset of coring.

TABLE 2

L – lubricated extrusion *U* – unlubricated extrusion. *n* – number of holes in die.

Extrusion die details				*Pure lead*			*Tellurium lead*			*Pure tin*			*Average experimental value of*	*Theoretical value of p/2k*	
r		*n*	*ε*	*P*	*p*	*p/2k*	*P*	*p*	*p/2k*	*P*	*p*	*p/2k*	*p/2k*	*L*	*U*
0·75	L	1	0	6·4	3·37	2·23	9·75	5·14	2·18	11·8	6·21	2·23	2·21	2·13	2·475
	L	2	0·333	6·95	3·66	2·42	10·70	5·64	2·39	13·4	7·05	2·54	2·45	2·17	2·38
	L	3	0·667	7·05	3·71	2·46	11·0	5·79	2·45	13·7	7·21	2·60	2·50	2·13	2·24
	U	1	0	7·10	3·74	2·47	11·0	5·79	2·45				2·46	2·13	2·475
	U	2	0·333	7·30	3·84	2·54	11·35	5·98	2·53				2·53	2·17	2·38
	U	3	0·667	7·20	3·79	2·51	11·3	5·95	2·51				2·51	2·13	2·24
0·86	L	1	0	8·4	4·42	2·92	13·0	6·84	2·88	16·7	8·79	3·06	2·95	2·835	3·165
	L	2	0·382	9·3	4·89	3·24	14·3	7·54	3·17	18·0	9·48	3·30	3·24	2·86	3·05
	L	3	0·764	9·6	5·05	3·34	14·3	7·54	3·17	18·5	9·74	3·39	3·30	2·85	2·92
	U	1	0	9·4	4·95	3·27	14·8	7·79	3·20				3·23	2·835	3·165
	U	2	0·382	9·7	5·1	3·37	15·0	7·90	3·33				3·35	2·86	3·05
	U	3	0·764	10·2	5·37	3·55	15·5	8·16	3·42				3·48	2·85	2·92
0·93	L	1	0	11·8	6·21	4·09	18·2	9·59	4·01	24·2	12·83	4·24	4·11	3·82	4·18
	L	2	0·378	13·0	6·84	4·5	20·0	10·52	4·41	26·7	14·05	4·68	4·53	3·85	4·08
	L	3	0·755	14·0	7·37	4·85	21·0	11·05	4·63	28·25	14·88	4·96	4·81	3·84	3·94
	U	1	0	13·6	7·16	4·71	20·4	10·73	4·44				4·57	3·82	4·18
	U	2	0·378	14·5	7·64	5·0	21·7	11·42	4·72				4·86	3·85	4·08
	U	3	0·755	15·5	8·16	5·35	23·0	12·11	5·01				5·18	3·84	3·94

For each test the load is taken from the autographic diagram and the pressure derived ; these are given in Table 2. The appropriate values of k being known from Table 1, $p/2k$ can be readily calculated and the individual values of $p/2k$ for each material and at each reduction are given in Table 2. Finally, an average value for all three materials (only two in the unlubricated cases) for otherwise given conditions is found, and may be compared with the possible range of theoretical values (see Table 2). In Fig. 11, the experimental and theoretical results are compared graphically. The heavy vertical bars show the possible theoretical range, from perfectly smooth to perfectly rough container walls, of values of $p/2k$ for each particular instance, and the circles indicate the average of the experimental values.

(iii) *Discussion of results*

As will be seen by reference to Fig. 11, theory underestimates the expected experimental values for the two and three hole dies, though the discrepancy in absolute value is not excessive ; it is greatest, however, in respect of the consistent trends observable in connection with the number of holes. Theoretically, as the number of symmetrically placed holes is increased, the tendency should be for $p/2k$ to approach the value of that for one hole of the same reduction with smooth container walls. But the results of the experiments suggest a contrary conclusion, for $p/2k$ is seen to increase in proportion to the number of holes ; this tendency is emphasized as the reduction increases. Since the evidence from a study of the velocity of emission of the various sheets (see next sub-section) indicates the general correctness of the theoretical assumptions, it is not clear how this feature may be explained. But the increasing disparity in the absolute values of $p/2k$ for theory and experiment with increasing reduction may be explicable by reference to the behaviour of the apparatus at high pressures. Flashing occurs in an extrusion operation when material is extruded backwards between the punch (or pressure-pad) and the container wall, and it may well be imagined that the consequential frictional drag on the punch will be large. The flashing occurs when at a certain pressure the elastic increase in the internal dimensions of the container (which has been press fitted and so is initially subjected to considerable hoop stress), due to the compression of the slug by the punch, exceeds the elastic expansion of the punch face (or pressure-pad) due to the compressive load it is transmitting; the difference in these two expansions eventually provides a gap through which metal is forced. Flashing can often be recognized as occurring in so-called well-lubricated direct extrusions, when the portion of the autographic diagram before the coring point shows an increasing load. Careful inspection of the autographic diagrams in Figs. 9 and 10, for the three-hole extrusion, show precisely this feature – a slowly rising load-line which contrasts with the decreasing load-line at the smaller reduction. It follows from this that in unlubricated tests the flashing can only reveal itself in a characteristic which has a smaller rate of decrease than that which might otherwise be expected.

(iv) *Flow patterns and tests*

A square grid of lines was stamped on the inner side of one of the two blocks comprising the slug, and an amount of extrusion effected which was sufficient to ensure that the steady-state had been reached. Comparing them with the hodograph

predictions, qualitative agreement concerning the tendency of the emerging sheets to coverage or diverge from one another was observed. The dead metal zones also appeared where they were expected, and there was qualitative agreement concerning their extent.

It was possible to test the validity of some of the assumptions made in the construction of the stress fields for the three-hole dies by measuring the length of extrusion through each orifice. If the effect of the angle of obliquity at emergence (which is small) is neglected, then, compared with the speed of the two side sheets, the central sheet should emerge (a), for the 0·75 reduction, at the same speed; (b), for the 0·86 reduction, 17% faster, and (c), for the 0·938 reduction, 20% faster. On making the actual experimental comparison, it was found that the central sheet was for (a) slower by about 4%, for (b) 12% faster, and for (c) 17% faster. Thus it appears there is an error of approximately 4%, and the assumptions must be nearly correct.

Acknowledgments

The authors wish to express their especial thanks to Mr. J. Thomas and the workshop staff of Sheffield University for the very careful attention given to the manufacture and setting of the dies used in the experimental work.

References

Dodeja, L. C.	1956	*Thesis for degree of M.Eng., University of Sheffield.*
Green, A. P.	1955	*J. Mech. Phys. Solids* **3**, 189.
Hill, R.	1948	*J. Iron Steel Inst.* **158**, 177.
	1950	*Mathematical Theory of Plasticity* (Clarendon Press, Oxford).
Johnson, W.	1954	*B.I.S.R.A. Report MW/E/55/54.*
	1956	*J. Mech. Phys. Solids.* **4**, 269.
	1957	*J. Mech. Phys. Solids.* **5**, 3 193, 202.

Journal of the Mechanics and Physics of Solids, 1957, Vol. 5, pp. 281 to 295. Pergamon Press Ltd., London

THE COLD EXTRUSION OF CIRCULAR RODS THROUGH SQUARE MULTIPLE HOLE DIES

By L. C. Dodeja† and W. Johnson*

(*Received* 24 *April* 1957)

Summary

Experiments were carried out to determine the pressure necessary to cold extrude pure lead, tellurium lead, pure tin and super-pure aluminium through 90° dies containing up to four holes arranged in different patterns. It is shown that, with the aid of a stress strain curve for each material and knowing the reduction and lubrication conditions, this pressure is predictable to a fair degree of accuracy by assuming a simple expression for extrusion through a single hole die and by utilizing some of the empirical knowledge gained from the experiments described.

The paper concludes with a summary of the observations on the nature of the flow of the metal during its passage through the holes of the die. Some experimental results affording a comparison between plane-strain and axisymmetric pressures and flow patterns are also presented.

1. Introduction

Extrusion through multiple hole dies has been a common industrial practice for some time and is finding increased application in connection with the less familiar metals (U.S.A.E.C. 1956). It is employed however, for the production of small sections and because it is a means of substantially increasing production rates. There appears to be little published work concerning the differences in pressure required to extrude through a number of holes, or regarding the nature of the flow of the metal during such a process. While reference is often made to difficulties associated with differences in the rate of extrusion through the individual holes in a die, there has been little enquiry into multiple hole extrusion in respect of either empirical investigations or of rationalized observations.

There are apparently only two previous references to multi-hole extrusion. Pearson (1955) states that " with lead a three-hole die called for only 10 per cent and a four-hole die for 22 per cent more pressure than a single hole die of the same total area." Watkins, Ashcroft and McKenzie (1954) have performed preliminary experiments on the extrusion of 1 in. diameter, 1 in. long, lubricated slugs of chemical lead, through one, two and three-hole dies at 0·86 reduction. (The precise disposition of the holes is not given.) They report pressure increases for both the two and three-hole dies above that of the single hole die of the same total reduction. These latter pressures were however the maximum ones occurring near the commencement of the extrusion and in the case mentioned by Pearson

†Department of Engineering, University of Sheffield.
*Department of Engineering, University of Manchester.

it is not clear what pressure on the autographic diagram is referred to nor to what reduction the results apply. Also in both instances the experimental results are of restricted value since they refer only to lead where the amount of strain hardening is small.

In this work the extrusion pressure for three different fairly large total reductions has been obtained for dies containing one and two holes symmetrically placed and for three and four hole dies arranged in-line (i.e. along a diameter) or symmetrically disposed about the die centre line, i.e. radially. The experiments were carried out on pure lead and tellurium lead (the yield stress increases slightly if at all with strain), pure tin and super-pure aluminium (typical examples of materials having well-rounded stress-strain curves).

The treatment of the experimental results is novel and they have been interpreted as follows. For plane-strain extrusions it is possible to calculate theoretically the the necessary extrusion pressures for a number of holes (compare Dodeja and Johnson 1957), but this is not yet the case for single or multiple rod extrusion (Hill 1950). While reasonable estimates can however be made by boldly assuming that the same relationship between pressure and reduction prevails for single rod as for single sheet extrusion, it has been found possible to improve the correlation between experiment and prediction by establishing an empirical relationship between the pressure and reduction for cylindrical extrusions based on experiments with pure lead for single hole dies (Johnson 1957, 1957a). This relationship, which provides a parameter for a given reduction and lubrication condition, can be shown to apply for all materials with a surprising degree of correctness.

These parameters obtained for a one-hole extrusion can be utilized in analysing the results for multi-hole extrusion, and through them a measure of the effect of the disposition of the holes on the extrusion pressure, reasonably free from the complicating effects of strain-hardening, can be evaluated.

The method is explained at length in section 4 below and is, essentially, an extension of the method formerly used in dealing with plane-strain extrusions (Johnson 1956). It must be acknowledged however, that the method is characterized more by success than by theoretical rigour.

Photographs are presented showing how the metal is deformed to give the different rods and in some instances the non-uniformity of deformation as between the different rods is well exemplifield.

The paper concludes by comparing the present results with those of the comparable cases in plane-strain extrusions already presented (Dodeja and Johnson 1957). It is shown that the patterns of metal flow display substantially the same features in both cases and that the pressures for a given total reduction are for all practical purposes remarkably close if the eccentricity of the orifices is about the same in both instances.

2. Experimental

Apparatus and tools. The extrusion apparatus used for the experiments was originally designed by T. M. Chang and is illustrated in Fig. 1. The extrusion container is a compound cylinder of 1 in. bore along which the punch travels and into which the compression disc and the extrusion slug are initially inserted. The outer cylinder was made from a piece of gun barrel and the inner sleeve from high speed steel. The load was applied to the punch through a spherical head which

thereby ensured axial loading. The lower end of the container is closed by a threaded plug which acts also as a die holder, see Fig. 2.

The dies used were square ones made of suitably heat treated B.K.V. steel of $1\frac{1}{8}$ in. diameter and $\frac{3}{4}$ in. thick ; they were made to be a good push fit into the recess in the die holder ; thus this

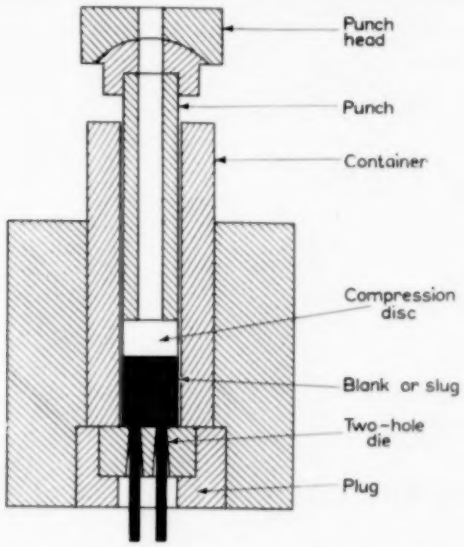

Fig. 1. Apparatus for extrusion of cylindrical rod.

TABLE 1

r	*Die*	D in.	t in.
0·75	*A*	$D_1 = 0{\cdot}5000$	——
	B	$D_2 = 0{\cdot}3535$	$t_2 = 0{\cdot}250$
	C	$D_3 = 0{\cdot}2887$	$t_3 = 0{\cdot}0625$
	E	$D_5 = 0{\cdot}2887$	$t_5 = 0{\cdot}3125$
0·86	*A*	$D_1 = 0{\cdot}3750$	——
	B	$D_2 = 0{\cdot}2644$	$t_2 = 0{\cdot}3125$
	C	$D_3 = 0{\cdot}2159$	$t_3 = 0{\cdot}1250$
	D	$D_4 = 0{\cdot}1870$	$t_4 = 0{\cdot}0625$
	E	$D_5 = 0{\cdot}2159$	$t_5 = 0{\cdot}2500$
	F	$D_6 = 0{\cdot}1870$	$t_6 = 0{\cdot}5000$
0·938	*A*	$D_1 = 0{\cdot}2500$	——
	B	$D_2 = 0{\cdot}1767$	$t_2 = 0{\cdot}3750$
	C	$D_3 = 0{\cdot}1443$	$t_3 = 0{\cdot}1875$
	D	$D_4 = 0{\cdot}1250$	$t_4 = 0{\cdot}1250$
	E	$D_5 = 0{\cdot}1443$	$t_5 = 0{\cdot}2500$
	F	$D_6 = 0{\cdot}1250$	$t_6 = 0{\cdot}3750$

accurately located the position of the holes. Details of the hole sizes and their disposition are given in Table 1 and Fig. 3. All the holes lie symmetrically within the circle of 1 in. diameter outlined by the chamber inner diameter. In all 16 dies were used and three total fractional reductions in area were investigated, $r = 0{\cdot}75$, 0·86, and 0·938.

Compression tests. These tests were performed on the materials extruded, two specimens of each being compressed to a logarithmic strain of about 3·4. The tests were carried out at the same speed as the extrusion, i.e. 0·1 in. per min. The procedure followed was the same as that previously used (Johnson 1956).

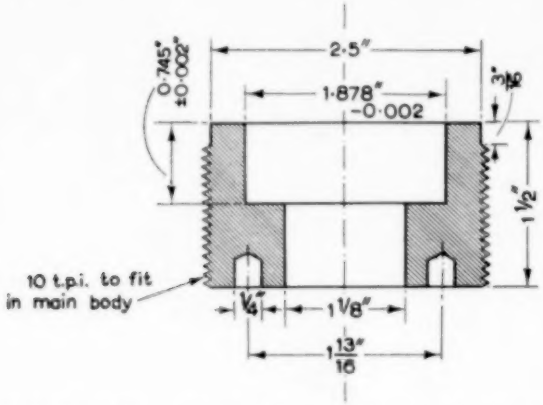

Fig. 2. Die-holder – threaded plug for axisymmetric extrusion.

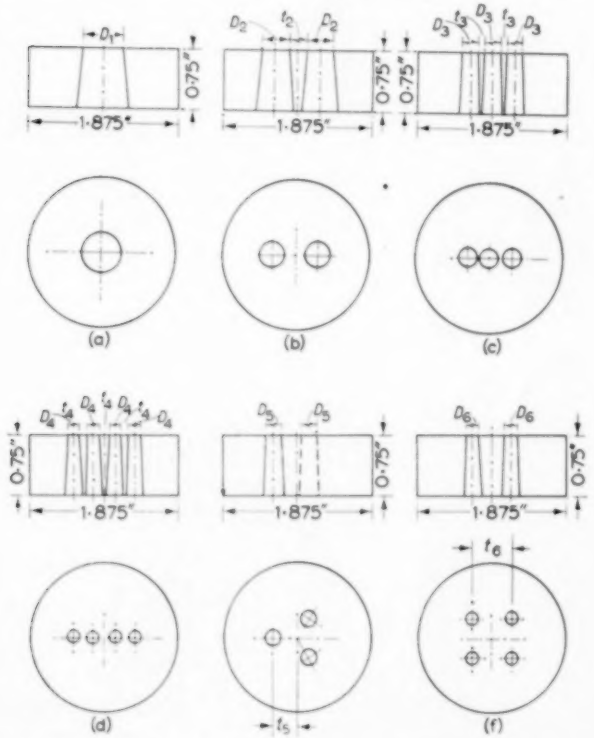

Fig. 3. Disposition and dimensions of the holes in the various dies.

Materials extruded. The materials used were (a) pure lead, (b) tellurium lead, (c) pure tin and (d) super-pure aluminium.

All the lead specimens were annealed for 30 min over boiling water and the tin specimens similarly treated for 60 min. No heat treatment was given to the aluminium.

Specimens. These consisted of cylindrical blocks 1 in. diameter and 1·3 in. long supplied originally in the form of extruded rod of 1 in. diameter.

Test procedure. Before commencing a test the specimen, container, die and pressure pad face were cleansed with carbon tetrachloride. The lubricant used, if any, was graphite-in-tallow. The loads were recorded at intervals of 0·05 in. of punch travel for distances of about 1·1 in. the testing machine crosshead having been set to advance at a constant rate of 0·1 in. per min.

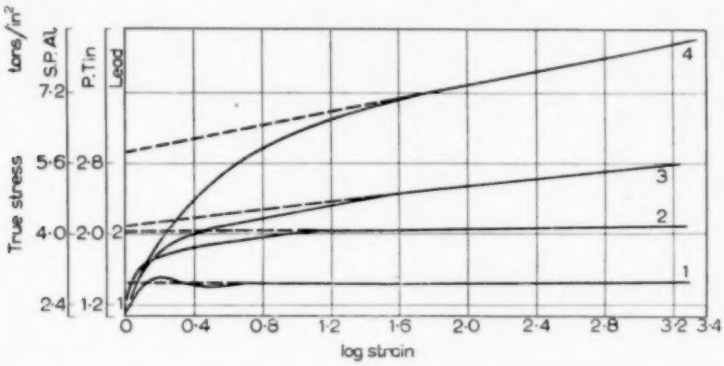

Fig. 4. True stress – logarithmic strain curves for
(1) Pure lead (2) Tellurium lead
(3) Pure tin (4) Super-pure aluminium
———— Experimental – – – – – – Extrapolation

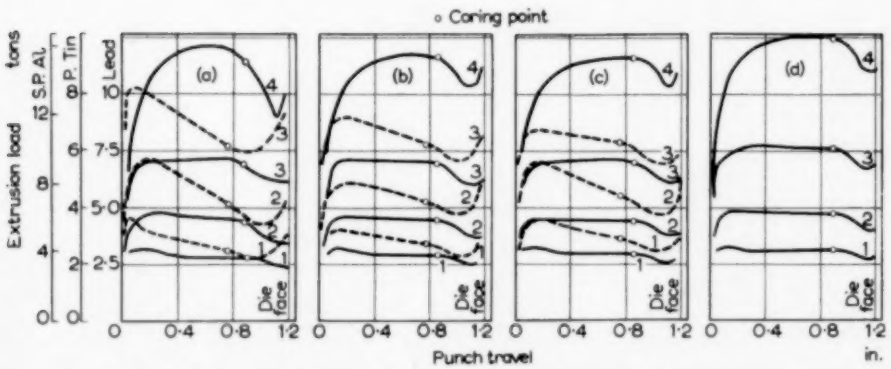

Fig. 5. Autographic diagrams for a reduction of 0·75 for dies containing,
(a) 1 Hole (b) 2 Holes
(c) 3 Holes-in-line (d) 3 Holes set radially
———— Lubricated extrusion – – – – – – Unlubricated extrusion
(1) Pure lead (2) Tellurium lead
(3) Pure tin (4) Super-pure aluminium
O Coring point.

3. Results

Stress-strain curves. True stress (Y)-logarithmic strain curves as calculated from the compression tests for all materials are shown in Fig. 4 : the curves for

the two tests made on each material were almost identical. It must be added that a reasonable extrapolation of the curves has had to be made beyond the recorded strain of 3·4 in order to analyse results.

Comparison of these curves with those previously obtained (Johnson 1956), shows good agreement for super-pure aluminium, but stress increases of about + 10 per cent for the same strain occurred for both kinds of lead.

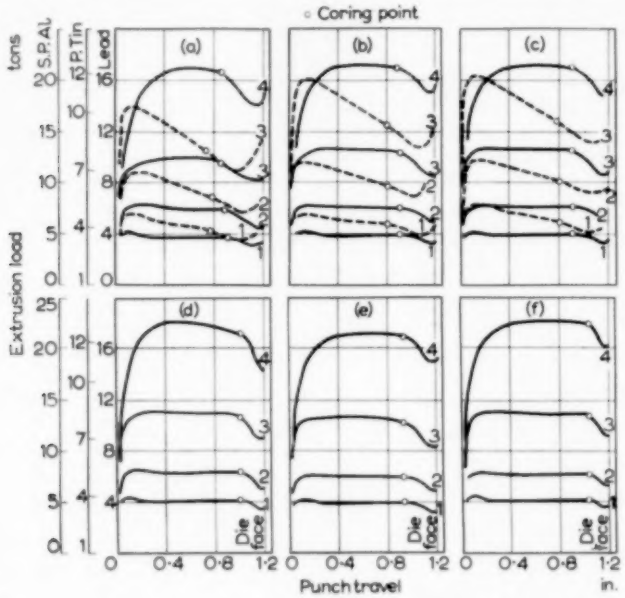

Fig. 6. Autographic diagrams for a reduction of 0·86 for dies containing.

(a) 1 Hole (b) 2 Holes (c) 3 Holes-in-line
(d) 3 Holes set radially (e) 4 Holes-in-line
(f) 4 Holes set on-square

——— Lubricated extrusion – – – – – – Unlubricated extrusion

(1) Pure lead (2) Tellurium lead
(3) Pure tin (4) Super-pure aluminium

○ Coring point.

Autographic diagrams. This diagram is a record of the variation of punch load, P, with punch travel, and from it the 'true' extrusion pressure $p = P/A_0$ is deduced; A_0 is the original cross sectional area of the specimen. (The point at which this is taken is clearly marked on the various diagrams reproduced below). All the autographic diagrams are given in Figs. 5 to 7 inclusive. Repeat tests performed on lubricated and unlubricated specimens in respect of pressure generally agreed to be better than 3 per cent for the former and 6 per cent for the latter.

Flow patterns. It is interesting and useful for such purposes as indicating hardness variations and residual stress distribution in extrusions to gain some insight into how metal in the parent slug attains its final position in the extruded product. Two different methods of examination were used. In the first method, the usual practice was followed of forming two semi-cylindrical slugs stamping a square grid on the axial plane of one of them and then extruding the composite slug;

in the second method, two slugs approximately $\frac{3}{4}$ in. long were placed one behind the other in the container and then partly extruded. These methods will also be obvious from an examination of Figs. 9 to 13.

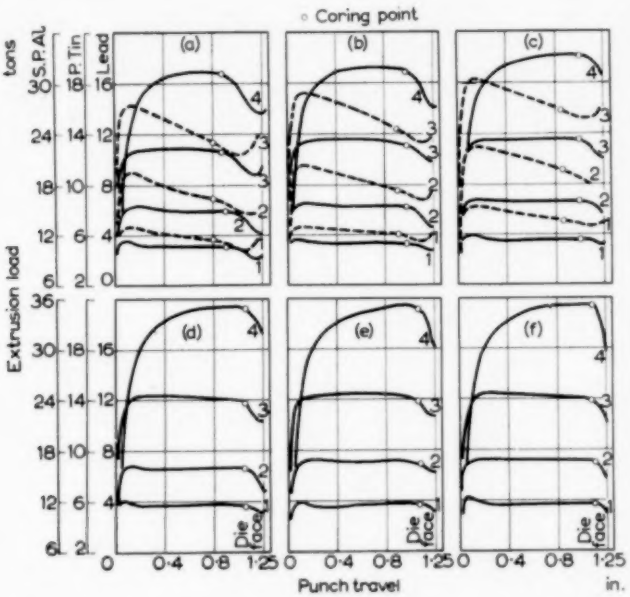

Fig. 7. Autographic diagrams for a reduction of 0·938.

(a) 1 Hole (b) 2 Holes

(c) 3 Holes-in-line (d) Holes set radially

———— Lubricated extrusion - - - - - - Unlubricated extrusion

(1) Pure lead (2) Tellurium lead

(3) Pure tin (4) Super-pure aluminium

○ Coring point.

4. Interpretation of Experimental Data

Autographic diagrams. Autographic diagrams may be analysed by considering them to be composed of three principal phases, a primary coining phase, a secondary steady-state phase and a tertiary unsteady-state phase (Johnson 1957a, b). The load at the point of demarcation between the steady- and unsteady-state phases is that at which the extrusion pressure is no longer applied over the whole of the pressure pad. This point, called the coring point, is clearly marked on the autographic diagrams below, though its position is less obvious the more rounded is the strain-hardening characteristic of the extruded metal. The extrusion punch load is taken as that applying at the coring point and for each experiment it is read off from the autographic diagram and recorded in Tables 2, 3, and 4. The residual slug length at which coring occurs has been assumed to be independent of the metal for a given test. This, seen to be nearly true by inspecting the autographic diagrams, is also useful in helping to make consistent readings of the extrusion load in the case of tin and aluminium.

On allowing for the strain-hardening characteristic of a material. First, consider an ideal non-hardening material of which the yield shear stress in plane strain is k. Then, theoretically, the pressure, p, for extrusion through symmetrically placed square dies may be calculated and the results expressed empirically in the form

$$p/2k = a + b \ln \{1/(1 - r)\}. \tag{1}$$

where a and b are determinable constants.

Now $k = Y/2$ or $\sqrt{3}\,Y/3$, according as the material yields following the criterion of Tresca or von Mises respectively, Y being the uniaxial yield stress in compression or tension, both of which are assumed equal. Thus, (1) may be re-written

$$p = Y [a' + b' \ln \{1/(1 - r)\}]. \tag{2}$$

It may now be conjectured that, in a similar way,

$$p = Y[a'' + b'' \ln \{1/(1 - r)\}] \tag{3}$$

for the extrusion of single circular rods, a'' and b'' being different however from a' and b'. The constants a'' and b'' are not theoretically determinable for axisymmetric extrusion as has been stated above, but the form of (3) has been well justified by Purchase and Tupper (1953).

Since (2) can be interpreted as stating that the extrusion pressure is given by the product of the uniaxial yield stress and a mean value of the total logarithmic strain, so may equation (3). However, two points then arise :

(i) How to determine values of a'' and b'' in the absence of a theory, and

(ii) The meaning or value to be given to Y when dealing with strain-hardening materials.

(i) If, when experiments are performed using a non-hardening material, the value of p is measured for various reductions and if Y can be determined from simple compression tests, then a'' and b'' may then be established inductively. This method of determining a'' and b'' has incidentally an advantage over that of determining them theoretically. The latter can only be of greatest value when the f. tional boundary conditions are known precisely and in experiments this is rarely, if ever, the case. Thus, to some extent, a'' and b'' as found experimentally will take into account the imprecisely known frictional conditions.

Pure lead, which is self-annealing at room temperature, simulates a non-hardening material (as is evident from Fig. 4) and from experiments using it one can obtain values of p/Y for the two boundary conditions of typical good lubrication and no lubrication. Now, it has been shown that for extrusion through square dies at speeds of about 0·1 in. per min, the best values for a'' and b'' are as given in (4) for work lubricated with graphite-in-tallow (Johnson 1957a), when $0{\cdot}5 \leqslant r \leqslant 0{\cdot}94$,

$$p/Y = 0{\cdot}8 + 1{\cdot}5 \ln \{1/(1 - r)\}, \tag{4}$$

and for unlubricated work by (5) (Dodeja 1956) where $0{\cdot}75 \leqslant r \leqslant 0{\cdot}94$,

$$p/Y = 0{\cdot}6 + 1{\cdot}8 \ln \{1/(1 - r)\}. \tag{5}$$

These expressions are thought to be correct to within about 7 per cent, and are verifiable by reference to the single-hole results in Tables 2, 3 and 4.

(ii) It has been maintained that the right hand side of equations (4) and (5)

TABLE 2
(For $r = 0{\cdot}75$)

	Pure lead			*Tel. lead*			*Pure tin*			*S.P. aluminium*			*Empirical value of* $p/\bar{Y}$	*Average experimental value of* $p/\bar{Y}$	*Percentage increase in* $p/\bar{Y}$ *on that for 1 hole die*	*E*
$\bar{Y}$ tons/in^2	1·31			2·04			2·41			6·82						
Lubricated	*P*	*p*	$p/\bar{Y}$	*P*	*p*	$p/\bar{Y}$	*P*	*p*	$p/\bar{Y}$	*P*	*p*	$p/\bar{Y}$				
1 Hole	2·80	3·57	2·74	4·35	5·54	2·72	5·50	7·00	2·90	15·25	19·42	2·85	2·89	2·80		
2 Hole	2·85	3·63	2·77	4·40	5·61	2·75	5·55	7·07	2·93	15·50	19·75	2·90		2·84	1·4	0·854
3 Hole in-line	2·90	3·69	2·82	4·40	5·61	2·75	5·60	7·14	2·96	15·45	19·68	2·89		2·86	2·1	0·535
3 Hole radial	3·10	3·95	3·02	4·70	5·99	2·94	6·05	7·71	3·20	16·60	21·15	3·10		3·06	9·0	0·796
Unlubricated																
$\bar{Y}$ tons/in^2	1·31			2·04			2·42									
1 Hole	3·10	3·95	3·01	5·15	6·56	3·21	6·15	7·84	3·25				3·04	3·16	—	—
2 Hole	3·35	4·27	3·27	5·20	6·63	6·25	6·25	7·96	3·31					3·28	3·8	0·854
3 Hole in-line	3·55	4·52	3·46	5·45	6·94	3·40	6·39	8·03	3·33					3·40	7·6	0·535

TABLE 3
(For $r = 0{\cdot}86$)

	Pure lead			*Tel. lead*			*Pure tin*			*S.P. aluminium*			*Empirical value of* $p/\overline{Y}$	*Average experimental value of* $p/\overline{Y}$	*Percentage increase in* $p/\overline{Y}$ *on that for 1 hole die*	E
$\overline{Y}$ tons/in^2	1·31			2·04			2·48			7·07						
Lubricated	P	p	$p/\overline{Y}$	P	p	$p/\overline{Y}$	P	p	$p/\overline{Y}$	P	p	$p/\overline{Y}$				
1 Hole	3·80	4·84	3·70	5·90	7·52	3·66	7·40	9·43	3·79	20·75	26·4	3·72	3·77	3·72		
2 Hole	4·00	5·09	3·89	6·05	7·71	3·75	7·90	10·07	4·05	21·25	27·05	3·81		3·86	3·8	0·664
3 Hole in-line	3·95	5·03	3·84	6·05	7·71	3·75	7·90	10·07	4·05	21·25	27·05	3·81		3·86	3·8	0·710
3 Hole radial	4·10	5·22	3·99	6·30	8·02	3·91	8·05	10·26	4·13	21·40	27·25	3·85		3·97	6·7	0·500
4 Hole in-line	3·95	5·03	3·89	6·00	7·64	3·72	7·80	9·94	4·00	21·20	27·0	3·81		3·89	4·5	—
4 Hole on-square	4·15	5·29	4·03	6·20	7·90	3·85	8·15	10·38	4·17	22·25	28·35	4·00		4·01	7·8	0·831
Unlubricated																
$\overline{Y}$ in tons/in^2	1·31			2·05			2·50									
1 Hole	4·25	5·42	4·13	6·85	8·73	4·24	8·05	10·26	4·09				4·08	4·15		
2 Hole	4·80	6·12	4·66	7·80	9·94	4·81	9·30	11·85	4·73					4·74	14·2	0·664
3 Hole in-line	4·90	6·24	4·76	8·10	10·31	5·00	9·50	12·10	4·82					4·86	17·1	0·710

TABLE 4
(FOR $r = 0{\cdot}938$)

	Pure lead			*Tel. lead*			*Pure tin*			*S.P. aluminium*			*Empirical value of* $p/\bar{Y}$	*Average experimental value of* $p/\bar{Y}$	*Percentage increase in* $p/\bar{Y}$ *on that for 1 hole die*	*E*
$\bar{Y}$ tons/in^2	1·31			2·04			2·53			7·35						
Lubricated	*P*	*p*	$p/\bar{Y}$	*P*	*p*	$p/\bar{Y}$	*P*	*p*	$p/\bar{Y}$	*P*	*p*	$p/\bar{Y}$				
1 Hole	5·15	6·55	5·00	7·95	10·1	4·97	16·8	13·8	5·43	31·0	39·5	5·33	4·97	5·18		
2 Hole	5·30	6·75	5·15	8·20	10·43	5·14	11·45	14·60	5·74	31·8	40·5	5·50		5·39	3·9	0·580
3 Hole in-line	5·50	7·01	5·35	8·60	10·95	5·39	11·55	14·70	5·78	32·1	40·9	5·56		5·52	6·5	0·661
3 Hole radial	5·70	7·25	5·53	8·70	11·10	5·46	12·00	15·30	6·02	35·0	44·6	6·07		5·77	11·5	0·500
4 Hole in-line	5·75	7·32	5·58	9·20	11·71	5·76	12·30	15·65	6·16	35·1	44·7	6·08		5·90	13·9	—
4 Hole on-square	5·70	7·25	5·53	9·10	11·60	5·70	12·00	15·30	6·02	35·1	44·7	6·07		5·83	12·6	0·540
Unlubricated																
$\bar{Y}$ tons/in^2	1·32			2·05			2·58									
1 Hole	5·65	7·20	5·46	8·90	11·32	5·57	11·35	14·46	5·58				5·51	5·54		
2 Hole	6·05	7·71	5·85	9·55	12·18	6·00	12·40	15·79	6·10					5·98	8·0	0·580
3 Hole in-line	7·05	8·98	6·82	11·0	14·01	6·89	13·90	17·70	6·85					6·85	23·6	0·661

represent the mean logarithmic strain during a cylindrical rod extrusion and accordingly it is proposed, as in the procedure followed when investigating plane-strain extrusion, that the value to be substituted for Y, henceforth $\overline{Y}$, when the stress-strain curve is rounded, should be the mean value of the true stress over the range of logarithmic strain 0 to $a'' + b'' \ln \{1/(1 - r)\}$.

This approach is admittedly approximate but it offers a successful means of handling experimental results. The method has been used in analysing the results for each material for each single-hole extrusion, and the experimental values of $p/\overline{Y}$ have been compared with those predicted by the empirical equations (4) and (5). The general agreement between them is seen to be reasonably close. For multi-hole extrusion the procedure followed is that, for the same frictional boundary conditions and the same total reduction for any number of holes, the assumed value of $\overline{Y}$ is that for a single-hole extrusion having the same value of r based on the quantity p/Y given by (4) or (5). The procedure may be clarified with some actual values. Consider lubricated extrusion of pure tin through three equal diameter holes set radially, the reduction r being 0·938. From equation (4) $p/\overline{Y}$ is found to be 4·97. $\overline{Y}$ is the mean ordinate in Fig. 4 over the range 0 to 4·97, which is easily determined to be 2·53 tons/in^2. The measured punch pressure, p, is 15·3 tons/in^2 and hence the experimental value of the parameter $p/\overline{Y}$ for the radial three hole die is $15{\cdot}3/2{\cdot}53 = 6{\cdot}02$, for this particular case.

5. Discussion and Summary of Experimental Results for Pressure

In Tables 2 to 4 for all the materials, each reduction and all types of die, the quantity $p/\overline{Y}$ is given ; from these values certain general conclusions can be made (only of course over the range of reductions and for the particular eccentricity of holes in the experiments). The average value of $p/\overline{Y}$ for all materials for a given reduction and configuration of holes serves as a reasonably good measure of the effect of a particular disposition of holes almost independent of the material used.

The definition of orifice eccentricity will be clear from Fig. 8.

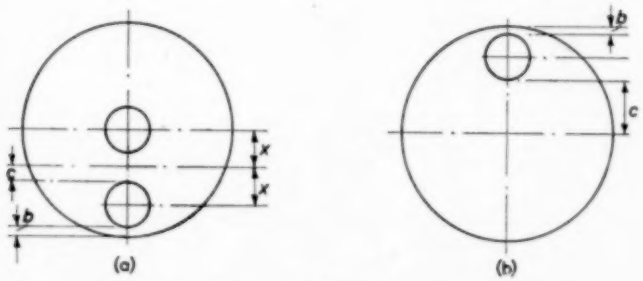

Fig. 8. Definition of orifice eccentricity
for (a) 3-Holes-in-line die, $E = 2c/(b + 2c)$, and for (b) 2-Holes, 3-holes-radial and 4-Hole square die, $E = c/(b + c)$.

(i) Parameter $p/\overline{Y}$ is primarily dependent on total reduction and only secondarily on the disposition of the holes.

(ii) The disposition of the holes as reflected in $p/\overline{Y}$ assumes
(a) decreasing importance as the degree of lubrication improves,
(b) increasing importance with increase in reduction.

(iii) For a given reduction $p/\overline{Y}$ increases as the number of holes increases; for a given number of holes an in-line setting generally produces lower values of $p/\overline{Y}$ than does a triangular or square distribution.

(iv) For lubricated extrusion through multi-hole dies up to and including four holes, $p/\overline{Y}$ is more than for one hole by less than 13 per cent; if unlubricated, the corresponding figure for a three-hole die is about 25 per cent.

The effect of the various factors involved, except that due to eccentricity, can best be obtained by studying the penultimate three columns of the three Tables.

It is clear that extrusion pressure increases with the number of holes; and since a multi-hole die is essentially a particular case of a re-entrant die, the conclusion is, the larger the degree of re-entrance the larger the pressure (other things being equal). This observation is reinforced by the results of unpublished work on the extrusion of *I*-section shapes – a re-entrant form which has been found to require larger pressure than do the convex forms of equal reduction.

6. Flow Pattern Tests

Photographs of some of the numerous tests are presented in Figs. 9 to 13 inclusive and comments and observations made on them are summarized below.

(i) Fig. 9 shows, in relief, the metal flow and the size and shape of the dead metal zones for four of the multi-hole dies when performing a lubricated extrusion. The portions and manner in which the initial slug divides itself in order to form particular rods is indicated in the Figures; these pictures are otherwise self-explanatory.

(ii) In Fig. 10 the flow marks on the rear end of particular slugs are seen, and they are probably representative of the method by which material from different parts of the slug flows transversely to the individual holes. Piping, in conformity with the number and location of the rods extruded, is seen to have taken place.

(iii) One of the most interesting observations that may be made relates to the effect of lubrication on the speed of flow through holes of the same area, for in-line dies when the disposition of the holes is a balanced one about the die centre line. From Figs. 11 (a) (iv), 11 (b) (iv), 12 (a) (iii) and (v), 12 (b) (iii) and (v) and 13 (i) and (iii), it is observed that lubrication results in a higher rate of extrusion through the holes nearest to the container wall; if no lubricant is applied to the slug in the first instance (see Figs. 13 (ii) and (iv) this phenomenon is reversed and the rate of extrusion through the inner holes is greatest or, through the holes nearest the container wall, is least.

(iv) In Figs. 11 (a) (iv) and 11 (b) (iv) it is clearly seen that the individual elements of the central rod at given distances from its centre line are similarly distorted. The pattern of deformation in the outside rods is, however, quite asymmetrical, being fairly uniformly worked on the outer halves of the rods but much more heavily deformed on the inside halves. This asymmetrical distribution of deformation is also evident in Figs. 11 (a) (ii) and 11 (b) (ii).

(v) From Figs. 11, 12 and 13, an indication of the extent and the number and shape of the dead metal zones created is apparent as is the extent of the region of deformation just before passage through the various holes.

7. Comparison of Axisymmetric and Plane-Strain Extrusions

A precise and straightforward comparison of extrusion pressures for these two cases cannot be made except in the cases of single sheet and single rod extrusion. By reference to the authors' previous paper (1957), Table 5 may be drawn up.

Table 5

		Pressures in tons/in²								
r		*Pure lead*			*Tel. lead*			*Pure tin*		
		P . S	*A*	*d*	*P . S*	*A*	*d*	*P . S*	*A*	*d*
0·75	*L*	3·37	3·57	12	5·14	5·54	8	6·21	7·09	13
	U	3·74	3·95	6	5·79	6·56	13	—	7·84	—
0·86	*L*	4·42	4·84	10	6·84	7·52	10	8·79	9·43	7
	U	4·95	5·42	9	7·79	8·73	12	—	10·26	—
0·938	*L*	6·21	6·55	5	9·59	10·1	5	12·83	13·8	8
	U	7·16	7·20	1	10·73	11·32	5	—	14·46	—

L = Lubricated tests *U* = Unlubricated tests
P . S = Plane-strain *A* = Axisymmetric
(*d* = 100 (1-Plane-strain pressure/axisymmetric pressure)).

It is clear that the plane-strain pressure is always less than the axisymmetric pressure, and that the disparity decreases with increasing reduction and is not significantly affected by the lubrication conditions.

Another observation is that the pressure increases as the number of holes increases for both cases. In this respect the present experimental results corroborate those for plane-strain, for which there was an unexplained discrepancy between theory and experiment.

Again, direct comparison of metal flow patterns is not possible but it is worthwhile reproducing some of those available from the plane-strain work in Figs. 14 to 17 ; these serve to emphasize the basic similarity of flow for both processes. There was no consistent degree of non-parallelism between emergent circular rods as there is between sheets.

Acknowledgments

The authors wish to express their especial thanks to Mr. J. Thomas and his workshop staff for their careful workmanship in manufacturing the dies used,

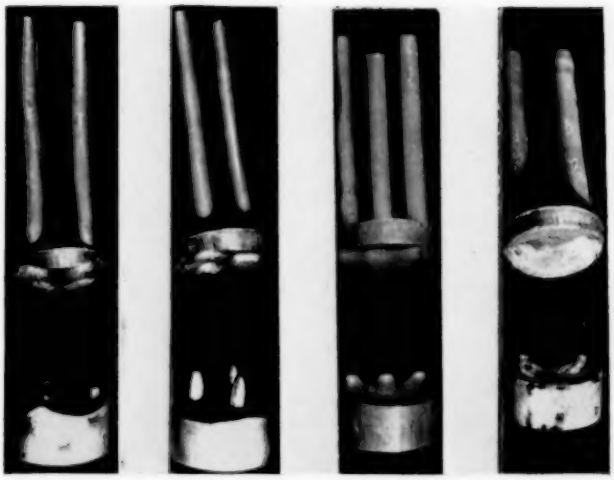

Fig. 9. Flow and dead metal zones in extruding through multi-hole dies ; lubricated aluminium at a reduction of 0·86.

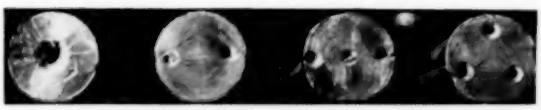

Fig. 10. Directions of flow and coring pattern at rear end of slugs of lubricated aluminium.

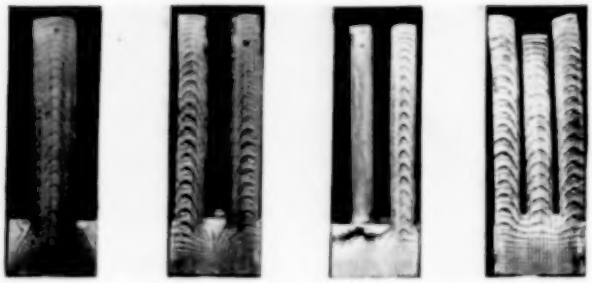

(i) (ii) (iii) (iv)

Fig. 11 (a)

(i) (ii) (iii) (iv)

Fig. 11 (b)

Fig. 11. Pattern of flow when $\epsilon = 0{\cdot}75$ for (a) lubricated aluminium, (b) lubricated tellurium lead.

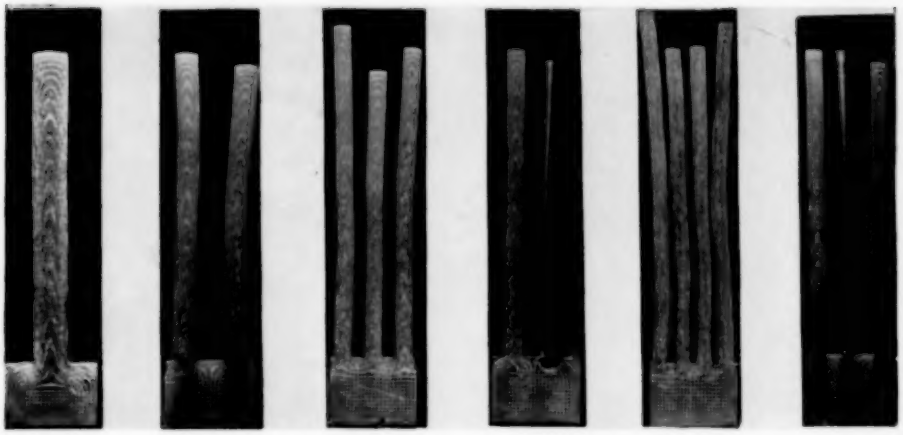

(i) (ii) (iii) (iv) (v) (vi)

Fig. 12 (a)

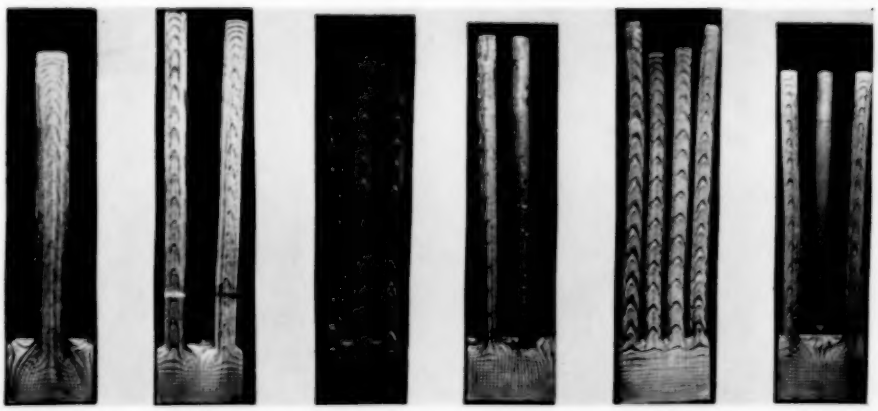

(i) (ii) (iii) (iv) (v) (iv)

Fig. 12 (b)

Fig. 12. Pattern of flow when $r = 0{\cdot}86$ for (a) lubricated tellurium lead, (b) lubricated aluminium.

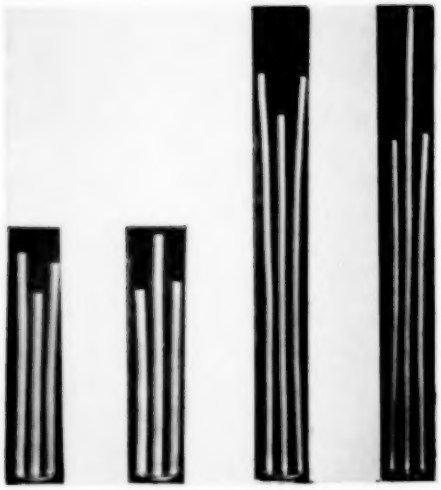

(i) (ii) (iii) (iv)

Fig. 13. Effect of lubrication on rate of metal flow through different holes : (i) and (iii) lubricated (ii) and (iv) unlubricated slugs.
For (i) and (ii) $r = 0{\cdot}75$, and for (iii) and (iv) $r = 0{\cdot}86$.

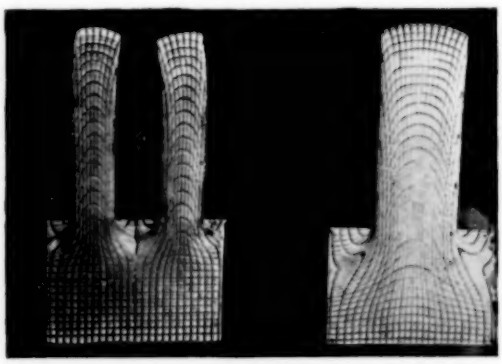

(i) (ii)

Fig. 14. Pattern of flow for two instances in which $r = 0{\cdot}5$; lubricated aluminium: plane-strain.

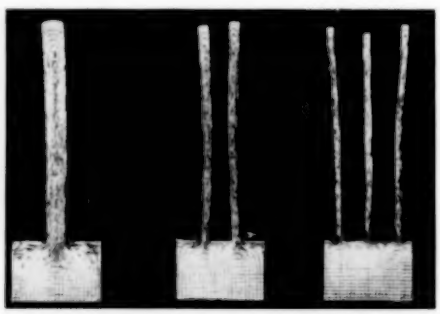

(i) (ii) (iii)

Fig. 15. Pattern of flow for instances in which $r = 0{\cdot}75$; lubricated tellurium lead: plane-strain.

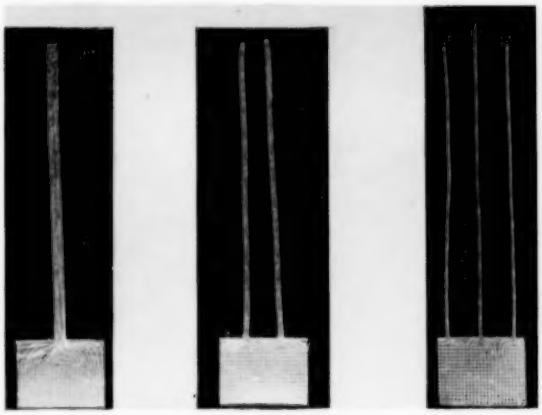

(i) (ii) (iii)

Fig. 16. Pattern of flow for instances in which $r = 0{\cdot}86$; lubricated aluminium: plane-strain.

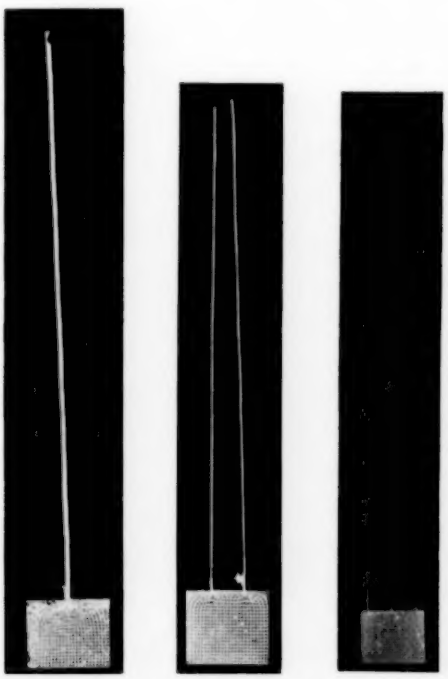

(i) (ii) (iii)

Fig. 17. Pattern of flow for instances in which $r = 0{\cdot}938$; lubricated aluminium: plane-strain.

and British Iron and Steel Research Association under whose aegis some of this work was originally performed.

References

Dodeja, L. C.	1956	*Thesis for degree of M. Eng.*, University of Sheffield.
Dodeja, L. C. and Johnson, W.	1957	*J. Mech. Phys. Solids* **5**, 267.
Hill, R.	1950	*Mathematical Theory of Plasticity* (Clarendon Press, Oxford).
Johnson, W.	1956	*J. Mech. Phys. Solids* **4**, 269-289.
	1957a	*J. Inst. Metals* **85**, 403.
	1957b	*J. Mech. Phys. Solids* **5**, 203.
Johnson, W. and Dodeja, L. C.	1956	*B.I.S.R.A. Report MW/G/56/56.*
Pearson, C. E.	1955	*Extrusion of Metals* (Chapman and Hall, London).
Purchase, N. W. and Tupper, S. J.	1953	*J. Mech. Phys. Solids* **1**, 277.
Watkins, Ashcroft and and McKenzie	1954	*D.S.I.R., M.E.R.O., Report MF/MS* 102.
U.S.A.E.C.	1956	*General Properties of Materials, Reactor Handbook* Vol. 3. p. 81.

Journal of the Mechanics and Physics of Solids, 1957, Vol. 5, pp. 296 to 301. Pergamon Press Ltd., London

PLASTIC BENDING OF A RING SECTOR BY END COUPLES

By W. M. Shepherd and F. A. Gaydon
Department of Theoretical Mechanics, University of Bristol

(*Received* 7 *May* 1957)

Summary

Exact values of the end couples necessary to produce incipient plastic flow in a thin plate in the form of a ring sector, bent in its own plane, are determined. Both the Mises and Tresca yield criteria and their associated flow rules are used.

1. Introduction

In this paper Hill's maximum work principle is applied to the problem of the incipient plastic flow in plane stress in a uniform, isotropic, thin, plane plate of plastic-rigid material in the shape of a ring sector, when the curved edges are free and the plate is in equilibrium under the action of couples applied, in the plane of the plate, to the straight edges.

With cylindrical polar co-ordinates r, θ, z the plate is supposed bounded by the circular arcs $r = a$, $r = b$, the radii $\theta = 0$, $\theta = \Omega$, and the planes $z = \pm h$. The tractions acting on each straight end are equivalent to a couple as shown in Fig. 1.

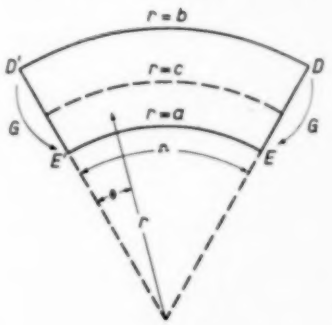

Fig. 1.

The object of this investigation is to find the couple under certain loading conditions. These conditions are (i) the ends, $\theta = 0$ and $\theta = \Omega$, are constrained to remain plane and (ii) either (a) the couple is applied by means of normal forces or (b) the ends are constrained so that no relative radial motion is possible. In both cases, for realistic dimensions, the magnitude of the couple is exactly determined. The problem is dealt with first using the Mises yield condition and secondly using the Tresca yield condition, in each case with the corresponding flow rule.

2. Extremum Principles

Hill (1951) has established extremum principles for a plastic-rigid material. These are now summarized and adapted to this problem (c.f. Bishop 1953).

I. A lower bound to the work-rate of the external forces at the yield point is

obtained from the rate of working of those surface-tractions given by any equilibrium distribution of stress extending throughout the body and satisfying the stress-boundary conditions and the yield criterion.

II. An upper bound to the work-rate of the external forces at the yield point is obtained from any velocity mode (having zero divergence) satisfying the velocity boundary conditions.

If in a plastically-deforming region the stress-field assumed in I can be associated with a velocity field satisfying the conditions in II then the lower and upper bounds to the work rate will be equal. HILL (1951) has shown that such a stress field is the actual yield-point state of stress wherever deformation is occurring, though the associated deformation mode may not be the actual mode.

Suppose that N, T are the actual normal and tangential surface tractions over the ends of the ring-sector, and u_r, u_θ are the actual velocities. Then the work-rate of the actual external forces is

$$\int (Nu_\theta + Tu_r)\, dS,$$

where the integral is taken over the ends of the ring-sector. The actual yield-point couple G can only be derived from this work-rate if u_θ/r is constant over each end *and* either (a) T is zero or (b) u_r is constant over each end.

3. Stress Field – Mises Criterion

In this section a stress state σ_r, σ_θ, $\tau_{r\theta}$ is found which satisfies the conditions laid down in section 2 (I). This stress state, subject to the existence of an associated velocity mode, will give the couple required to initiate plastic flow under either of the conditions (a) or (b) of section 2. It is convenient to postulate that the assumed stresses are independent of θ and that $\tau_{r\theta} = 0$.

The Mises yield criterion then takes the form

$$\sigma_r^2 - \sigma_r \sigma_\theta + \sigma_\theta^2 = 3k^2. \tag{1}$$

The equilibrium conditions reduce to the single equation

$$r \frac{d\sigma_r}{dr} = \sigma_\theta - \sigma_r. \tag{2}$$

Denote the radius at the neutral surface by $r = c$. In the region $a \leqslant r < c$ the yield condition is satisfied if the stresses are given in terms of a parameter α by the equations

$$\sigma_r = -2k \sin \alpha, \qquad \sigma_\theta = -2k \sin (\alpha + \pi/3). \tag{3}$$

The equilibrium equation, with the boundary condition $\sigma_r = 0$ when $r = a$, gives the relation between r and α:

$$2r^2/a^2 = \sqrt{3} \sec (\alpha + \pi/6) \exp (\sqrt{3}\, \alpha). \tag{4}$$

When $r = c$, $\alpha = \gamma$ giving

$$2c^2/a^2 = \sqrt{3} \sec (\gamma + \pi/6) \exp (\sqrt{3}\, \gamma). \tag{5}$$

In the region $c < r \leqslant b$ the stresses again satisfy equations (1) and (2) and the appropriate forms in terms of a parameter β are

$$\sigma_r = -2k \sin \beta, \qquad \sigma_\theta = -2k \sin (\beta - \pi/3), \tag{6}$$

where

$$2r^2/b^2 = \sqrt{3} \sec (\beta - \pi/6) \exp (-\sqrt{3}\,\beta). \tag{7}$$

Since σ_r is continuous across the neutral surface, $\beta = \gamma$ when $r = c$ and

$$2c^2/b^2 = \sqrt{3} \sec (\gamma - \pi/6) \exp (-\sqrt{3}\,\gamma). \tag{8}$$

Equations (5) and (8) show that γ is related to b/a by

$$b^2/a^2 = \cos (\gamma - \pi/6) \sec (\gamma + \pi/6) \exp (2\sqrt{3}\,\gamma).$$

Since the plate is in equilibrium, the tractions at each end must be statically equivalent to a couple G which is given by

$$G = 2hk \int_a^b r\sigma_\theta \, dr = 2hk \left\{ \int_a^c r\sigma_\theta \, dr + \int_c^b r\sigma_\theta \, dr \right\} = 2hk\,(I_1 + I_2),$$

where

$$2I_1 = 2c^2 \sin (\gamma + \pi/3) - \sqrt{3}\,a^2 - \sqrt{3}\,a^2 \int_0^\gamma \sec (\alpha + \pi/6) \cos (\alpha + \pi/3) \exp (\sqrt{3}\,\alpha)\, d\alpha,$$

$$2I_2 = 2c^2 \sin (\pi/3 - \gamma) - \sqrt{3}\,b^2 + \sqrt{3}\,b^2 \int_0^\gamma \sec (\beta - \pi/6) \cos (\beta - \pi/3) \exp (-\sqrt{3}\,\beta)\, d\beta.$$

The integrals I_1 and I_2 were evaluated numerically for a range of values of γ and it was found that the resulting values of G were very nearly proportional to $(b - a)^2$. On further investigation and after considerable algebraic manipulation it was found that

$$\frac{G}{2hk\,(b-a)^2} = \frac{\sqrt{3}}{4}\left\{1 - \frac{\gamma^2}{36} - \frac{\gamma^4}{216} - \frac{131\,\gamma^6}{36288} \cdots\right\}.$$

A more convenient form of this result is

$$\frac{G}{2hk} = \frac{\sqrt{3}}{4}\, t^2 \left\{1 - \frac{1}{192}\,\frac{t^2}{R^2} - \frac{5}{6144}\cdot\frac{t^4}{R^4} - \frac{1}{6670}\cdot\frac{t^6}{R^6} \cdots\right\},$$

where $t = b - a$ and R = mean radius $= \frac{1}{2}(a + b)$. In this series the coefficients are exact except that of t^6/R^6 where 6670 is the denominator to the nearest integer. For all reasonable dimensions the first two terms of the series are sufficient.

4. The Velocity Field – Mises Criterion

Suppose that the characteristics, through the point C $(c, \frac{1}{2}\,\Omega)$ in the neutral surface, of the stress system in section 3 are CA, CA' in the region $b \geqslant r > c$, and CB, CB' in the region $c > r \geqslant a$ (Fig. 3). These characteristics are defined

by the stress-free arcs AA', BB' respectively. The associated stress states are those given in (3) and (6), respectively.

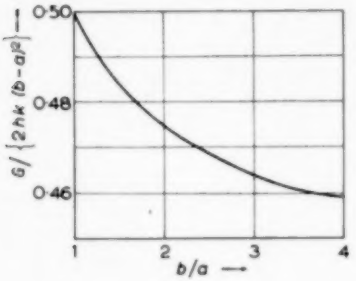

Fig. 2.

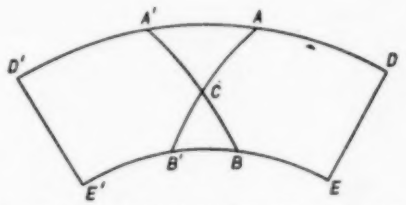

Fig. 3. Characteristics for the Mises criterion.

In the region $a \leqslant r < c$ the characteristics are inclined to the radial direction at an angle $\frac{1}{4}\pi + \frac{1}{2}\psi$ (Hill 1950, p. 300) where

$$3 \sin \psi = \frac{\sigma_r + \sigma_\theta}{\sigma_r - \sigma_\theta}.$$

It follows from (3) that

$$\sqrt{3} \sin \psi = -\tan(\alpha + \pi/6), \tag{9}$$

and since $rd\theta/dr = \tan(\frac{1}{4}\pi + \frac{1}{2}\psi)$ for one set of characteristics it may be deduced after substitution for r from (4), and integrating, that

$$\theta = \tfrac{1}{2}\psi - \tan^{-1}(2 \tan \psi) + \text{constant}. \tag{10}$$

Equations (9), (4), (10) relate r and θ. Similarly, the corresponding equations for the region $c < r \leqslant b$ are

$$\sqrt{3} \sin \psi = \tan(\pi/6 - \beta),$$

together with (7) and

$$\theta = -\tfrac{1}{2}\psi + \tan^{-1}(2 \tan \psi) + \text{constant}.$$

The complementary set of characteristics in each case are the reflections of those given above in the line $\theta = \Omega/2$. The characteristics are real if $\gamma \leqslant \pi/6$ which corresponds to $b/a \leqslant \sqrt{2} \exp(\pi/2\sqrt{3}) \doteq 3{\cdot}345$. They are therefore real for what may be considered all realistic shapes of ring sector.

What is important, for the present purposes, is that the two sets of characteristics are not orthogonal. Consider the velocity mode in which the part $ADEBC$ rotates about C as a rigid body while the part $A'D'E'B'C$ remains at rest. Such a mode determines the component velocity in ACA' at points of the arc AC, in the direction of the characteristics of the set of which $A'C$ is a member. Since the two families are not orthogonal the resulting velocity distribution in ACA' cannot be compatible with the rigid body motions of $ADEBC$ and $A'D'E'B'C$ without necking along CA, CA', and (by a similar argument) along CB, CB', (see Hill 1952). If the couple G is such as to increase the curvature, then the necking along CA, CA' is positive or of the thinning type, while that along

CB, CB' is negative or of the thickening type. It will be realised that *in this case* negative necking could not continue to develop but would be followed by the establishment of a succession of similar negative necks along neighbouring characteristics, resulting in a continuous thickening on the compression side.

This velocity mode satisfies the incompressibility equation, and the boundary conditions for the cases (a) and (b) of section 2. Moreover, it contains only permissible discontinuities and is compatible with the stress field of equations (3), (6). It follows that equation (13) gives the exact value for the couple G.

5. Stress Field – Tresca Criterion

The boundary conditions are the same as in section 3 but the yield condition is different. In $a \leqslant r < c$, σ_r and σ_θ have the same sign so that the Tresca yield condition is

$$\sigma_\theta = -2k. \tag{11}$$

The equilibrium equation with the boundary condition on $r = a$ gives

$$\sigma_r = -2k\,(1 - a/r). \tag{12}$$

In $c < r \leqslant b$, σ_r and σ_θ have opposite signs so that the Tresca yield condition is

$$\sigma_\theta - \sigma_r = 2k.$$

The equilibrium equation with the boundary condition on $r = b$ gives

$$\sigma_r = 2k \log (r/b), \qquad \sigma_\theta = 2k\left[1 + \log (r/b)\right]. \tag{13}$$

The continuity of σ_r at $r = c$ then gives the relation between a, b, c:

$$\log (c/b) + 1 - a/c = 0. \tag{14}$$

On evaluating the integral $\int_a^b r\,\sigma_\theta\,dr$ and using (14) it is found that the couple G is given by

$$G = hk\,(2a^2 - 2ac + b^2 - c^2). \tag{15}$$

The values of the couple corresponding to a number of values of b/a are given in the table.

Table

b/a	1·104	1·216	1·468	1·762	2·110	2·523	3·019
$G/2hk\,(b-a)^2$	0·496	0·492	0·485	0·479	0·473	0·468	0·464

This relation is also shown in the graph in Fig. 2. It is easily verified that as $b/a \to 1$, $G/2hk\,(b-a)^2 \to 0{\cdot}5$.

6. Velocity Field – Tresca Criterion

When the Tresca criterion is used, a stress state satisfying the conditions of

Section 2 (I) is given in equations (11), (12), (13). There is only one stress characteristic from C $(c, \frac{1}{2}\Omega)$ in the region $a \leqslant r < c$, for the maximum shear stress is out of the plane (σ_z is the algebraically greatest stress). In the region $b \geqslant r > c$, $|\sigma_\theta - \sigma_r| = 2k$ and there are two characteristics from C, CA and CA' (Fig. 4). These are everywhere inclined at an angle $\frac{1}{4}\pi$ to the radial direction and the two families are consequently orthogonal (Hill 1950, p. 303). If the associated flow rule is used in conjunction with the Tresca yield criterion (see Prager 1953), the strain rates ϵ_r, ϵ_θ, ϵ_z are in the ratios $0 : 1 : -1$ along CB and in the ratios $-1 : 1 : 0$ in ACA'. It follows that the velocity characteristics are the same as the stress characteristics. Now consider the velocity mode in which, as before, $ADEBC$ rotates about C as a rigid body. This mode determines the normal velocities on the arc CA and since these are zero on CA' the velocity field in ACA' is determined. On the other hand, the mode determines the discontinuity in normal velocity over CB, this line being the trace of an incipient negative neck (see Hill 1952). This velocity mode satisfies the necessary conditions as before and is compatible with the stress field given by (11), (12) and (13). The exact yield couple is therefore that given by (15).

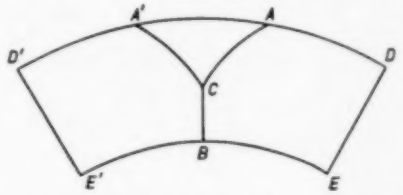

Fig. 4. Characteristics for the Tresca criterion.

Acknowledgment

The authors wish to thank Prof. R. Hill for some helpful suggestions as to the presentation of these results.

References

Bishop, J. F. W. 1953 *J. Mech. Phys. Solids* **2**, 43.
Hill, R. 1950 *Mathematical Theory of Plasticity* (Clarendon Press, Oxford).
1951 *Phil. Mag.* **42**, 868.
1952 *J. Mech. Phys. Solids* **1**, 19.
Prager, W. 1953 *J. Appl. Mech.* **20**, 317.

Journal of the Mechanics and Physics of Solids, 1957, Vol. 5, pp. 302 to 307. Pergamon Press Ltd., London

ON THE PROBLEM OF UNIQUENESS IN THE THEORY OF A RIGID-PLASTIC SOLID—IV

By R. Hill
Department of Mathematics, University of Nottingham

(*Received* 18 *July* 1957)

Summary

In Part III of this series a sufficient condition, in terms of the rate of workhardening, was obtained for the uniqueness of the deformation mode in a properly formulated boundary-value problem. The unique mode is now characterized by an extremum property in the set of virtual modes. This is a generalization of one obtained in Part I, in that it takes due account of changes in geometry.

1. Conjectured Extremum Principle

In Part III of this series (Hill 1956, 1957) a sufficient condition was established for the uniqueness of a continuous solution to the boundary-value problem set by traction $\mathbf{F}$ and nominal traction-rate $\dot{\mathbf{F}}$ on a part S_F of the surface and velocity $\mathbf{v}$ on the remainder S_v. The condition is that

$$U(\mathbf{w}) = \tfrac{1}{2}\int\left(h\eta^2 - \sigma_{kj}\frac{\partial w_i}{\partial x_k}\frac{\partial w_j}{\partial x_i}\right)dV > 0 \tag{1}$$

for every velocity field $\mathbf{w}$ expressible as the difference of a pair of virtual modes in the set defined by $\mathbf{F}$ on S_F and $\mathbf{v}$ on S_v. h is a measure of the rate of hardening, $\boldsymbol{\eta}$ is the strain-rate corresponding to $\mathbf{w}$, σ_{kj} is the existing stress and is uniquely known in the deformable zone and is supposed given in any rigid zone whose motion is unknown in advance. The condition (1) on the ' uniqueness functional ' U can be regarded as defining a critical rate of hardening above which the actual mode is certainly unique and below which it probably is not (Part III, section 4). It is a sufficient condition for the reason that $U(\mathbf{w}) \leqslant 0$ if there were a field $\mathbf{w}$ which is the difference between two distinct actual modes; the equality holds when neither mode involves flow in a region where unloading takes place in the other (equations (7) and (10), Part III).

When the effects of changes in geometry can be disregarded, the unique mode is characterized by an extremum property (Part I, section 3a). The proof is closely allied structurally with that of uniqueness, from which the functional can be guessed beforehand by analogy with similar theorems in related branches of solid mechanics. Equally, when geometry changes are allowed for, the form (1) immediately suggests the probable modified functional, namely

$$U(\mathbf{v}^*) - \int \dot{\mathbf{F}}\,\mathbf{v}^*\,dS_F, \tag{2}$$

the admissible functions being the set of virtual modes, with velocity $\mathbf{v}^*$ and strain-rate $\boldsymbol{\epsilon}^*$ (cf. equation (4) of Part I). The proof that the actual mode does minimize (2), whenever (1) is satisfied, is not obvious, despite the help of analogies, and is the main purpose of the present paper.

It is noteworthy that the condition (1) for certain uniqueness in no way depends on what traction-rate is specified on S_F. By contrast, the property (2) makes explicit the dependence on traction-rate of the actual mode itself.

2. Proof

The natural starting point is

$$\int \dot{\mathbf{F}}\,(\mathbf{v}^* - \mathbf{v})\,dS = \int \dot{\boldsymbol{\sigma}}\,(\boldsymbol{\epsilon}^* - \boldsymbol{\epsilon})\,dV - \int \sigma_{kj}\frac{\partial v_i}{\partial x_k}\frac{\partial}{\partial x_i}(v_j^* - v_j)\,dV$$

where unstarred quantities refer to the actual mode and starred quantities to any distinct virtual mode. This follows from (1), (2), and (3) of Part III by the usual transformation†.

To the right-hand side of this equation we add the positive quantity $U(\mathbf{v}^* - \mathbf{v})$. Then

$$\int \dot{\mathbf{F}}\,(\mathbf{v}^* - \mathbf{v})\,dS < \int \left\{\dot{\boldsymbol{\sigma}}\,(\boldsymbol{\epsilon}^* - \boldsymbol{\epsilon}) + \tfrac{1}{2}h\,(\boldsymbol{\epsilon}^* - \boldsymbol{\epsilon})^2\right\} dV$$

$$- \tfrac{1}{2}\int \sigma_{kj}\frac{\partial}{\partial x_k}(v_i^* + v_i)\frac{\partial}{\partial x_i}(v_j^* - v_j)\,dV. \qquad (3)$$

Now, at every point in the body,

$$\dot{\boldsymbol{\sigma}}\,(\boldsymbol{\epsilon}^* - \boldsymbol{\epsilon}) + \tfrac{1}{2}h\,(\boldsymbol{\epsilon}^* - \boldsymbol{\epsilon})^2 \leqslant \tfrac{1}{2}h\,(\boldsymbol{\epsilon}^{*2} - \boldsymbol{\epsilon}^2) \qquad (4)$$

for $h \geqslant 0$; the inequality arises only in elements which are unloading in the actual mode but deforming in the virtual one. This is a stronger inequality than was needed in Part I (section 3a) but is easily proved on similar lines (it parallels the stronger inequality needed in the proof of the uniqueness theorem in Part III). Combining (3) and (4):

$$\int \dot{\mathbf{F}}\,(\mathbf{v}^* - \mathbf{v})\,dS < \tfrac{1}{2}\int h\,(\boldsymbol{\epsilon}^{*2} - \boldsymbol{\epsilon}^2)\,dV$$

$$- \tfrac{1}{2}\int \sigma_{kj}\frac{\partial}{\partial x_k}(v_i^* + v_i)\frac{\partial}{\partial x_i}(v_j^* - v_j)\,dV. \qquad (5)$$

The right-hand integrand in (5) is equal to

$$\sigma_{kj}\left(\frac{\partial v_i^*}{\partial x_k}\frac{\partial v_j^*}{\partial x_i} - \frac{\partial v_i}{\partial x_k}\frac{\partial v_j}{\partial x_i}\right)$$

since

$$\sigma_{kj}\left(\frac{\partial v_i}{\partial x_k}\frac{\partial v_j^*}{\partial x_i} - \frac{\partial v_i^*}{\partial x_k}\frac{\partial v_j}{\partial x_i}\right) = 0 \qquad (6)$$

for any two modes when the material is isotropic. To show this we first split the tensor $\partial v_i/\partial x_j$ into its symmetric and antisymmetric parts:

†The term in rate of body-force is omitted for brevity. It is always analogous to the traction-rate term and enters any equation in a precisely similar way.

$$\epsilon_{ij} = \tfrac{1}{2}\left(\frac{\partial v_i}{\partial x_j} + \frac{\partial v_j}{\partial x_i}\right), \qquad \alpha_{ij} = \tfrac{1}{2}\left(\frac{\partial v_i}{\partial x_j} - \frac{\partial v_j}{\partial x_i}\right).$$

The expression in (6) reduces to

$$2\sigma_{kj}\,(\epsilon_{ik}\,\alpha_{ji}{}^{*} - \epsilon_{ik}{}^{*}\,\alpha_{ji}),$$

the other triple products vanishing in pairs on account of the symmetry and antisymmetry properties of their factors (as may easily be seen by the standard method of interchanging dummy suffixes). The remaining triple products are invariants and may be evaluated from the components associated with any convenient set of axes. Take these to be the common principal axes of the stress and strain-rate tensors (the material being isotropic). The tensors $\epsilon_{ik}\,\sigma_{kj}$ and $\epsilon^{*}_{ik}\,\sigma_{kj}$ are then diagonal, while $\alpha_{jl}{}^{*}$ and α_{jl} retain their antisymmetry. Consequently, the sum of the diagonal components of each of the tensors $\epsilon_{ik}\,\sigma_{kj}\,\alpha_{jl}{}^{*}$ and $\epsilon_{ik}{}^{*}\,\sigma_{kj}\,\alpha_{jl}$ vanishes, proving (6).

Finally, combining (5) and (6) and re-arranging,

$$U(\mathbf{v}^{*}) - \int \dot{\mathbf{F}}\,\mathbf{v}^{*}\,dS_F > U(\mathbf{v}) - \int \dot{\mathbf{F}}\,\mathbf{v}\,dS_F$$

remembering that $\mathbf{v}^{*} = \mathbf{v}$ on S_v. For the actual mode

$$U(\mathbf{v}) = \tfrac{1}{2}\int \dot{\mathbf{F}}\,\mathbf{v}\,dS,$$

and so

$$U(\mathbf{v}^{*}) - \int \dot{\mathbf{F}}\,\mathbf{v}^{*}\,dS_F > \tfrac{1}{2}\left\{\int \dot{\mathbf{F}}\,\mathbf{v}\,dS_v - \int \dot{\mathbf{F}}\,\mathbf{v}\,dS_F\right\}. \tag{7}$$

It is to be observed that the integral of $\dot{\mathbf{F}}\mathbf{v}$ over S_v is also uniquely determined by the boundary conditions that fixed the mode, even though the $\mathbf{F}$ distribution itself is not (being dependent on the 'acceleration' $\dot{\mathbf{v}}$ on S_v; see Part I, section 1).

The following points should be noted:

(i) The present analysis takes cognizance of discontinuous modes when $h = 0$. The σ_{kj} term in U gives a finite contribution at a velocity discontinuity, this being regarded as a vanishingly thin layer of indefinitely large shear strain-rate (see the next Section for an illustration). When $h \neq 0$, on the other hand, the analysis is not adequate to deal with discontinuous modes since the contribution from the h term in U diverges.

(ii) The expression (2) has an *analytic* minimum when no unloading occurs in the rigid zone of the actual mode. For (4) becomes an equality, while the inequality (3) rests on the *second-order* quantity $U(\delta\mathbf{v})$, where $\mathbf{v} + \delta\mathbf{v}$ is a virtual mode differing infinitesimally from the actual one. But when unloading actually occurs in part of the rigid zone, and when there is a neighbouring virtual mode involving flow in that part, (4) is an inequality resting on the *first-order* quantity $(\mathbf{n}\dot{\boldsymbol{\sigma}})\,(\mathbf{n}\,\delta\,\boldsymbol{\epsilon})$ for that mode, and so the extremum is not analytic with respect to arbitrary variations.

For the same reasons, even when (1) is *not* satisfied, (2) has a *stationary* value in any actual mode which does not involve partial unloading.

(iii) When $S_v = 0$, or $\mathbf{v} = 0$ on S_v, there is generally no disposable factor of proportionality with a given field $\mathbf{v}^*$ since $\int (\mathbf{v}^* \wedge \mathbf{F})\, dS$ has a given value depending on the specified traction-rate, namely $-\int (\mathbf{r} \wedge \dot{\mathbf{F}})\, dS$ (Part III, section 2). (This value is, however, necessarily zero for continuing overall equilibrium when changes in geometry are neglected, and then a disposable factor can be chosen as in (6) of Part I). Also, when traction-rates are specified all over the surface, flow may or may not ensue. The necessary and sufficient condition that it ceases, when $h \neq 0$, is that the traction-rate should satisfy

$$\int \dot{\mathbf{F}}\, \mathbf{v}^*\, dS + \int \sigma_{kj} \frac{\partial v_i^*}{\partial x_k} \frac{\partial v_j^*}{\partial x_i}\, dV \leqslant 0$$

for all virtual modes; this is an obvious generalization of (8) in Part I. When $h = 0$, the *permissible* traction-rate must be so restricted; the *strict* inequality is then a sufficient, but not necessary, condition for flow to cease.

(iv) When the loading on S_F is by *fluid pressure*, a similar extremum principle holds, with

$$\tfrac{1}{2} \int \left\{ h\dot{\epsilon}^{*2} - (\sigma_{kj} + p\delta_{kj}) \frac{\partial v_i^*}{\partial x_k} \frac{\partial v_j^*}{\partial v_i} \right\} dV + \int \dot{p} l_j v_j^*\, dS_F \qquad (8)$$

in place of (2), where p is the existing pressure and l_j the unit outward normal. The proof is very similar, with $\sigma_{kj} + p\,\delta_{kj}$ throughout in place of σ_{kj}, and starting with the transformation of

$$\int \left(\dot{\mathbf{F}}_j - p l_k \frac{\partial v_k}{\partial x_j} \right) (v_j^* - v_j)\, dS$$

as indicated by the analysis in Part III (section 6). The functional does not depend on the current value of the pressure since $\sigma_{kj} + p\delta_{kj}$ is independent of p, being equal to the yield-point stress under zero pressure on S_F and the same velocity on S_v. The actual mode depends only on the rate of change of pressure, and not on its current value.

(v) No attempt is made here to classify the cases when the actual mode with the property (7) happens to coincide with that obtained when geometry changes are disregarded (as in Part I). However, one such situation is obviously when the term

$$\int \sigma_{kj} \frac{\partial v_i^*}{\partial x_k} \frac{\partial v_j^*}{\partial x_i}\, dV$$

has the same value for all virtual modes, so that its variation vanishes. In particular, this occurs in torsion, as can be verified without difficulty, in agreement with the result already proved by a slightly different method in Part III (section 5 (iii)).

3. Alternative Expression for Functional

For some purposes it may be useful to separate the contributions of strain and rotation in the term in (1) and (2) that arises from the geometry changes.

We have the identity

$$\sigma_{kj}\frac{\partial v_i}{\partial x_k}\frac{\partial v_j}{\partial x_i} \equiv \sigma_{kj}\,(\epsilon_{ik}\,\epsilon_{ji} + \alpha_{ik}\,\alpha_{ji}) \tag{9}$$

since

$$\sigma_{kj}\,(\epsilon_{ik}\,\alpha_{ji} + \epsilon_{ji}\,\alpha_{ik}) \equiv 0$$

by interchange of suffixes (without calling on the isotropy property which makes the terms vanish separately, as in section 2). Hence

$$U(\mathbf{v}) = \tfrac{1}{2}\int (h\epsilon_{ij}\,\epsilon_{ij} - \sigma_{kj}\,\epsilon_{ik}\,\epsilon_{ji})\,dV - \tfrac{1}{2}\int \sigma_{kj}\,\alpha_{ik}\,\alpha_{ji}\,dV. \tag{10}$$

Now introduce the principal values $(\sigma_1, \sigma_2, \sigma_3)$ and $(\epsilon_1, \epsilon_2, \epsilon_3)$ of the stress and strain-rate tensors. Let $(\omega_1, \omega_2, \omega_3)$ be the components of the spin, $\frac{1}{2}$ curl $\mathbf{v}$, referred to the local principal axes at each point, so that the corresponding elements of α_{ij} are

$$\alpha_{ij} = \begin{pmatrix} 0 & -\omega_3 & \omega_2 \\ \omega_3 & 0 & -\omega_1 \\ -\omega_2 & \omega_1 & 0 \end{pmatrix}.$$

The functional becomes

$$U(\mathbf{v}) = \tfrac{1}{2}\int \Sigma\left\{(h-\sigma_1)\,\epsilon_1^2\right\}dV + \tfrac{1}{2}\int \Sigma\left\{\sigma_1\,(\omega_2^2+\omega_3^2)\right\}dV. \tag{11}$$

In particular, if the existing stress is a uniform uniaxial tension $\sigma_1 = \sigma$, $\sigma_2 = \sigma_3 = 0$, then $\epsilon_1 = \epsilon$, $\epsilon_2 = \epsilon_3 = -\frac{1}{2}\epsilon$. The first integrand in (11) is $(\frac{3}{2}h - \sigma)\,\epsilon^2$ and so U is certainly positive, irrespective of the possible spin functions, when $h > 2\sigma/3$ (as already derived in Part III, section 5 (i)).

In *plane strain*, where $\omega_1 = \omega_2 = 0$, $\epsilon_3 = 0$, $\epsilon_1 = -\epsilon_2 = \gamma$ (the maximum shear strain-rate, tensor definition), and $\sigma_3 = \frac{1}{2}(\sigma_1 + \sigma_2) = -p$ (the conventional notation), we have

$$U = \iint \left\{(h+p)\,\gamma^2 - p\omega^2\right\}dx_1\,dx_2. \tag{12}$$

When $h = 0$ the contribution to U from a curvilinear element of area bounded by neighbouring pairs of α and β slip-lines is

$$p\,(dv + ud\phi)_\alpha\,(du - vd\phi)_\beta$$

where (u, v) are the (α, β) velocity components, ϕ the anticlockwise orientation of the slip-lines, and the subscripts refer to the slip-lines along which the differentials are taken. In particular, if there is a discontinuity in u across an α–line, of constant amount $[u]$ in the positive direction of the β–lines, the contribution is

$$p\,[u]\,(dv + \bar{u}d\phi)_\alpha \tag{13}$$

where $\bar{u}$ is the arithmetic mean of the values of u on either side of the discontinuity. Similarly, for a discontinuity of amount $[v]$ across a β-line, the contribution is

$$p\,[v]\,(du - \bar{v}d\phi)_\beta. \tag{14}$$

References

HILL, R. 1956 *J. Mech. Phys. Solids* **4**, 247 ; *Ibid.* **5**, 1.
1957 *J. Mech. Phys. Solids.* **5**, 153.

BOOK REVIEW

Fatigue in Aircraft Structures. Edited by A. M. FREUDENTHAL. Proceedings of the International Conference held at Columbia University, January, 1956. Academic Press Inc., New York. 456 pp. $12.

THE declared intention of this conference was to stimulate the exchange of information between physicists and physical metallurgists, test engineers, and design engineers, and the papers are presented in three groups roughly corresponding to these divisions. The first section, dealing with fundamental aspects of fatigue, contains reports of interesting work on the phenomena of slip and dislocations by WOOD, FORSYTH, THOMPSON and others. The emphasis is on experimental observations of a fundamental nature, and conclusions are drawn regarding the events preceding the formation of a fatigue crack. A paper by PHILLIPS on the propagation of fatigue cracks under repeated loading takes us logically to the next section of the book, dealing with the collection and interpretation of fatigue test data. The statistical aspect of this problem is given a prominent place, WEIBULL and FREUDENTHAL being among the contributors. The final section, dealing with the philosophy and practice of fatigue design in aircraft, is more obviously valuable to the design engineer than to the physicist, but makes interesting background reading for anyone concerned with the fatigue problem. As a whole the book progresses logically from the fundamental studies of the early chapters to the very practical, though somewhat empirical, recommendations to designers contained in SCHLEICHER's penultimate chapter. Much of the material has been published elsewhere, but the collection into one volume, with reports on the discussion following each paper, gives a book useful to all workers in the fatigue field.

F. SHERRATT

BOOKS RECEIVED

GRIFFITH, R. H. and MARSH, J. D. F. *Contact Catalysis.* 299 pages. (Clarendon Press, Oxford University Press, 1957) 50s.

DELAHAY, PAUL. *Instrumental Analysis.* 384 pages. (The Macmillan Co., New York and London, 1957) 55s. 6d.

FAST, J. D., VAN BUERON, H. G. and PHILIBERT, J. (Edited by). *La Diffusion dans les Metaux.* 124 pages. (Bibliotheque Technique Philips, distributed in Great Britain and Eire by Cleaver-Hume Press Ltd., 1957) 37s. 6d.

END OF VOL.